

Bulletin 137



New Mexico Bureau of Mines & Mineral Resources

A DIVISION OF
NEW MEXICO INSTITUTE OF MINING & TECHNOLOGY

Field guide to geologic excursions in New Mexico and adjacent areas of Texas and Colorado

Prepared for the Geological Society of America
Rocky Mountain and South-Central Sections Annual Meeting,
Albuquerque, New Mexico, 21-24 April 1991

Edited by Betsy Julian¹ and Jiri Zidek²

¹Department of Geological Sciences, University of Texas at El Paso, El Paso, Texas 79968;

²New Mexico Bureau of Mines & Mineral Resources, Socorro, New Mexico 87801

NEW MEXICO INSTITUTE OF MINING & TECHNOLOGY

Laurence H. Lattman, *President*

NEW MEXICO BUREAU OF MINES & MINERAL RESOURCES

Frank E. Kottlowski, *Director and State Geologist*

James M. Robertson, *Associate Director*

BOARD OF REGENTS

Ex Officio

Bruce King, *Governor of New Mexico*

Alan Morgan, *Superintendent of Public Instruction*

Appointed

Steve Torres, *President, 1967-1997, Albuquerque*

Carol A. Rymer, M.D., *President-Designate, 1989-1995, Albuquerque*

Lt. Gen. Leo Marquez, *Secretary/Treasurer, 1989-1995, Albuquerque*

Robert O. Anderson, *1987-1993, Roswell*

Charles Zimmerman, *1991-1997, Socorro*

BUREAU STAFF

Full Time

ORIN J. ANDERSON, *Geologist*
RUBEN ARCHULETA, *Metallurgical Lab. Tech.*
AUGUSTUS K. ARMSTRONG, *USGS Geologist*
GEORGE S. AUSTIN, *Senior Industrial Minerals Geologist*
AL BACA, *Maintenance Carpenter II*
JAMES M. BARKER, *Industrial Minerals Geologist*
MARGARET W. BARROLL, *Post-Doctoral Fellow*
PAUL W. BAUER, *Field Economic Geologist*
ROBERT A. BIEBERMAN, *Emeritus Sr. Petroleum Geologist*
LYNN A. BRANDVOLD, *Senior Chemist*
RON BROADHEAD, *Petrol. Geologist, Head, Petroleum Section*
MONTE M. BROWN, *Cartographic Drafter II*
KATHRYN E. CAMPBELL, *Cartographic Drafter II*
STEVEN M. LATHER, *Field Economic Geologist*
RICHARD CHAMBERLIN, *Economic Geologist*
CHARLES E. CHAPIN, *Senior Geologist*
RICHARD R. CHAVEZ, *Assistant Head, Petroleum Section*
RUBEN A. CRESPIN, *Garage Supervisor*

Lois M. DEVLIN, *Director, Bus./Pub. Office*
ROBERT W. EVELETH, *Senior Mining Engineer*
Lois GOLLMER, *Staff Secretary*
IBRAHIM GUNDILER, *Metallurgist*
WILLIAM C. HANEBERG, *Engineering Geologist*
JOHN W. HAWLEY, *Senior Env. Geologist*
CAROL A. HJELLMING, *Assistant Editor*
GRETCHEN K. HOFFMAN, *Coal Geologist*
GLEN JONES, *Computer Scientist/Geologist*
ANN LANNING, *Administrative Secretary*
ANNABELLE LOPEZ, *Petroleum Records Clerk*
THERESA L. LOPEZ, *Receptionist/Staff Secretary*
DAVID W. LOVE, *Environmental Geologist*
JANE A. CALVERT LOVE, *Editor*
WILLIAM MCINTOSH, *Research Geologist*
CHRISTOPHER G. MCKEE, *X-ray Facility Manager*
VIRGINIA MCLEMORE, *Geologist*
LYNNE McNeil, *Technical Secretary*

NORMA J. MEEKS, *Senior Pub./Bus. Office Clerk*
BARBARA R. POPP, *Chemical Lab. Tech. II*
MARSHALL A. REITER, *Senior Geophysicist*
JACQUES R. RENAULT, *Senior Geologist*
JAMES M. ROBERTSON, *Senior Economic Geologist*
JANETTE THOMAS, *Cartographic Drafter II*
SAMUEL THOMPSON III, *Senior Petrol. Geologist*
REBECCA J. TITUS, *Cartographic Supervisor*
JUDY M. VAIZA, *Executive Secretary*
MANUEL J. VASQUEZ, *Mechanic I*
JEANNE M. VERPLOEGH, *Chemical Lab. Tech. II*
ROBERT H. WEBER, *Emeritus Senior Geologist*
SUSAN J. WELCH, *Assistant Editor*
NEIL H. WHITEHEAD, III, *Petroleum Geologist*
MARC L. WILSON, *Mineralogist*
DONALD WOLBERG, *Vertebrate Paleontologist*
MICHAEL W. WOOLDRIDGE, *Scientific Illustrator*
JIRI ZIDEK, *Chief Editor—Geologist*

Research Associates

CHRISTINA L. BALK, *NMT*
WILLIAM L. CHENOWETH, *Grand function, CO*
PAIGE W. CHRISTIANSEN, *Kitty Hawk, NC*
RUSSELL E. CLEMONS, *NMSU*
WILLIAM A. COBBAN, *USGS*
AUREAL T. CROSS, *Mich. St. Univ.*
MARIAN GALUSHA, *Amer. Mus. Nat. Hist.*
LELAND H. GILE, *Las Cruces*

JEFFREY A. GRAMBLING, *UNM*
JOSEPH HARTMAN, *Univ. Minn.*
DONALD E. HATTIN, *Ind. Univ.*
ALONZO D. JACKA, *Texas Tech. Univ.*
DAVID B. JOHNSON, *NMT*
WILLIAM E. KING, *NMSU*
DAVID V. LEMONE, *UTEP*

HOWARD B. NICKELSON, *Carlsbad*
LLOYD C. PRAY, *Univ. Wisc.*
ALLAN R. SANFORD, *NMT*
JOHN H. SCHILLING, *Reno, NV*
WILLIAM R. SEAGER, *NMSU*
RICHARD H. TEDFORD, *Amer. Mus. Nat. Hist.*
JORGE C. TOVAR R., *Petroleos Mexicanos*

Graduate Students

WILLIAM BECK
JENNIFER BORYTA

ROBERT KING

ERNEST SCHARKAN, JR.
DAVID SIVILS

Plus about 30 undergraduate assistants

Original Printing

Preface

This volume contains 10 field guides to trips scheduled to take place before, during, and after the joint annual meeting of the GSA Rocky Mountain and South-Central Sections in Albuquerque, New Mexico, on 21-24 April 1991. Most of the field guides combine road logs and technical papers, but *Geomorphic and neotectonic evolution along the margin of the Colorado Plateau and Rio Grande rift, northern New Mexico*, by Gonzalez and Dethier, is a technical paper with field-trip stops and topics of discussion only briefly listed in an appendix. The detailed road log to this paper is *Open file Report no. 374*, available from the New Mexico Bureau of Mines & Mineral Resources, Socorro, New Mexico 87801, tel. (505) 835-5147.

The field guides are arranged in the order in which the trips were announced (*GSA News & Information*, v. 12, no. 10, October 1990); however, three of those announced are not included. One is *Educational geology of the Albuquerque area*, a pre-meeting, one-day trip open only to schoolteachers, for which no field guide has been submitted. The other two are post-meeting trips, *Geology of the Valles caldera and Jemez volcanic field* (one day) and *Cenozoic magmatism and tectonics of the southeastern Colorado Plateau, New Mexico* (three days), for which field guides have already appeared in the *New Mexico Bureau of Mines & Mineral Resources Memoir 46* (1989), and the field-trip participants thus can be supplied with reprints from that publication.

Fifty-five authors have contributed to the volume. Because of the large number of authors, their geographic separation, and the short time from submittal to publication (two field guides were made available to us only in mid-February!), it has not been possible to completely standardize the format and to improve on the quality of some of the figures and tables. However, we have done everything possible to turn out a good-quality publication, and we hope our effort will be viewed with the understanding that we had to work *fast*.

We would like to take this opportunity to thank the authors for their contributions and the University of New Mexico Printing Services for an outstanding performance in all phases of production of this volume.

Betsy Julian
Jiri Zidek

Contents

Examples of modern rift volcanism and Proterozoic anorogenic magmatism:	
The Potrillo volcanic field of southern New Mexico and the Franklin Mountains of west Texas.	
<i>E. Y. Anthony, C. G. Barnes, W. Chen, J. M. Hoffer, G. R. Keller, K. M. Marsaglia, V. T. McLemore, J. M. Seeley, M. A. Seward, W. M. Shannon, and W. F. Thomann</i>	1
Introduction.	1
Day 1: The Proterozoic section in the Franklin Mountains [road log].	1
<i>C. G. Barnes, K. M. Marsaglia, J. M. Seeley, M. A. Seward, W. M. Shannon, and W. F. Thomann</i>	1
Geology of the middle Proterozoic Thunderbird Group, Franklin Mountains, El Paso, Texas.	3
<i>W. F. Thomann</i>	3
Petrology of the middle Proterozoic Mundy Breccia, Franklin Mountains, Texas.	5
<i>W. F. Thomann</i>	5
Summary of geochemistry and petrology of Proterozoic granitic rocks, Franklin Mountains, west Texas.	7
<i>W. M. Shannon and C. G. Barnes</i>	7
Day 2: The Potrillo volcanic field.	12
<i>J. M. Hoffer, W. Chen, V. T. McLemore, and E. Y. Anthony</i>	12
[Road log].	12
Geochemistry of late Cenozoic lavas of southern New Mexico.	18
Day 3: Las Cruces to Albuquerque.	20
 Open-system magmatic evolution of the Summer Coon and Del Norte volcanoes, Conejos Formation, San Juan Mountains volcanic field, Colorado.	
<i>D. F. Parker, D. A. Grau, and C. D. Thomas</i>	21
Introduction.	21
Field trip [Stops 1-7].	23
Acknowledgments.	28
References.	28
 Geomorphic and neotectonic evolution along the margin of the Colorado Plateau and Rio Grande rift, northern New Mexico.	
<i>M. A. Gonzalez and D. P. Dethier</i>	29
Introduction.	29
Geologic setting and previous investigations.	29
Geomorphic features and late Cenozoic drainage evolution.	29
Pre-Quaternary surfaces and the Puye aggradation episode.	33
Quaternary surfaces and periods of aggradation and incision.	34
Climate change and development of surfaces.	36
Neotectonic analysis of faults of the Abiquiu embayment.	38
Conclusions and future work.	43
Acknowledgments.	43
References.	43
Appendix: Field-trip stops and topics of discussion.	45
 Correlation of Triassic strata of the Colorado Plateau and southern High Plains, New Mexico.	
<i>S. J. Lucas</i>	47
Introduction.	47
Colorado Plateau edge: Lucero uplift to Chama basin.	47
Rio Grande rift: Hagan basin.	49
Eastern edge of Basin and Range: Lamy area.	52
Southern High Plains: Santa Rosa to Tucumcari.	52
Paleogeographic significance.	52
Field-trip stops [1-4].	54
Acknowledgments.	54
References.	54

Tectonics, intrusive rocks, and mineralization of the San Pedro-Ortiz porphyry belt, north-central New Mexico.	<i>S. R. Maynard, L. A. Woodward, and D. L. Giles</i>	57
Introduction.		57
Tectonic setting of the San Pedro-Ortiz porphyry belt.	<i>L. A. Woodward</i>	57
Road log: Day 1, Stop 1.		60
Tijeras Canyon, Sandia Mountains, and Tijeras graben.	<i>L. A. Woodward</i>	60
Road log: Day 1, Stops 2-5.		61
Geologic outline of the Cerrillos mining district, Cerrillos porphyry copper deposit, and associated mineralization.	<i>D. L. Giles</i>	62
Geology and gold mineralization of the Ortiz Mountains.	<i>S. R. Maynard</i>	65
Introduction.		65
Igneous rocks.		65
Structural geology.		66
Gold mineralization.		67
Road log: Day 2.		67
Combined references.		69
Proterozoic tectonic history of the Manzano Mountains, central New Mexico.	<i>A. G. Thompson, J. A. Grambling, and R. D. Dallmeyer</i>	71
Introduction.		71
Highlights en-route to Stop 1.		71
Stop 1: Overview of Monte Largo shear zone.		72
Stop 2: Monte Largo Canyon shear zone.		72
Highlights en-route to Stop 3.		73
Stop 3: Southern margin of the Priest pluton.		73
General geology of the central and southern Manzano Mountains.		73
Conclusions.		76
References.		77
Late Pennsylvanian stratigraphy and paleontology of the Kinney Brick Quarry, Manzanita Mountains, New Mexico.	<i>S. G. Lucas and P. Huber</i>	79
Introduction.		79
Previous research.		79
Stratigraphy and age.		80
Fossil assemblages.		81
Depositional environments.		84
Access to the Kinney Brick Quarry.		85
Acknowledgments.		85
References.		85
Appendix: Measured stratigraphic section.		86
A tale of two volcanoclastic aprons: Field guide to the sedimentology and physical volcanology of the Oligocene Espinaso Formation and Miocene Peralta Tuff, north-central New Mexico	<i>G. A. Smith, D. Larsen, S. S. Harlan, W. C. McIntosh, D. W. Erskine, and S. Taylor</i>	87
Geologic background to excursions to the Espinaso Formation and Peralta Tuff.	<i>G. A. Smith</i>	87
Stratigraphy and sedimentology of Espinaso Ridge [Stop 1].	<i>G. A. Smith</i>	89
Stratigraphy and sedimentology of the Espinaso Formation in the Cerrillos area (Stops 2 and 3).	<i>D. Larsen and S. Taylor</i>	90
Paleomagnetic constraints on the temperature of emplacement of two volcanic breccias in the Oligocene Espinaso Formation, New Mexico: A progress report.	<i>S. S. Harlan</i>	93
The composition of Ortiz porphyry belt extrusives as recorded in the Espinaso Formation.	<i>G. A. Smith and D. W. Erskine</i>	96

Stratigraphy, sedimentology, and volcanology of the Peralta Tuff Member of the Bearhead Rhyolite (Stops 4, 5, and 6)	<i>G. A. Smith</i>	97
Preliminary ⁴⁰ Ar/ ³⁹ Ar age determinations and paleomagnetic results from the Peralta Tuff Member, Bearhead Rhyolite, Ten Rocks area, Jemez Mountains, New Mexico.	<i>W. C. McIntosh and S. S. Harlan</i>	101
Combined references.		103
Quaternary and Neogene landscape evolution: A transect across the Colorado Plateau and Basin and Range provinces in west-central New Mexico.	<i>J. W. Hawley and D. W. Love</i>	105
Introduction.		105
Day 1: Grants, Gallup, and Zuni Mountain loop.		109
Stop 1-1 (optional): Forest ecosystems of the Zuni Mountain area: Impact of timber management practices.		111
Stop 1-2 (optional): Western Puerco River basin from Fort Wingate Centennial Monument.		111
Stop 1-3a: Alluvial fills of the Puerco River valley-Gallup Hogback area, and impacts of the 1979 uranium tailings spill north of Church Rock.		111
Stop 1-3b: Older alluvial deposits near South Fork and mainstem Puerco River confluence.		113
Stop 1-4: Bidahochi Formation.		114
Stop 1-5 (optional): Arroyo processes and valley-fill sequences: The impacts of Holocene climatic changes, and land and water management practices.		115
Stop 1-6: Southern El Malpais area of Zuni-Bandera volcanic field from Oso Ridge cinder cone.		116
Stop 1-7: Northern El Malpais area of the Zuni-Bandera field from the McCartys flow.		118
Day 2: Grants to Estancia basin.		120
Day 2, Part 1: Grants to Mountainair.		121
Stop 2-1: Geomorphic and tectonic evolution of the lower Rio San Jose drainage basin.		121
Stop 2-2: Los Lunas volcano.		123
Stop 2-3: Rio Puerco.		125
Stop 2-4 (optional): Hydrogeologic investigations of Sierra Ladrones Formation.		126
Stop 2-5: Overview of southeastern Albuquerque basin and Sevilleta National Wildlife Refuge area.		128
Vegetation history of the Sevilleta LTER.	<i>J. L. Betancourt, R. M. Turner, and S. Tharnstrom</i>	128
Day 2, Part 2: Lake Estancia basin tour.		130
Stop E-1: Lake Estancia shorelines.		130
Stop E-2: Lake Estancia stratigraphic record.		131
Day 3, Part 1: Continuation of Estancia basin tour.		132
Stop E-3: Lake Estancia glacial-maximum shoreline deposits.		132
Day 3, Part 2: Albuquerque-Rio Rancho urban-area tour.		134
Stop A-1: Elena Gallegos Park and Sandia Mountain piedmont.		136
Stop A-2: North Edith section of Lambert (1968) and environmental geology of the eastern valley-border area.		138
Stop A-3: Ceja del Rio Puerco and Sand Hill fault zone.		141
Stop A-4: Albuquerque Volcanoes and Volcano Cliffs.		143
References.		144
Laminated ice bodies in collapsed lava tubes at El Malpais National Monument, central New Mexico.	<i>L. Thompson, E. Mosley-Thompson, J. L. Betancourt, D. W. Love, A. Wilson, G. Leonard, and R. S. Anderson</i>	149
Late Cenozoic geomorphic and tectonic evolution of the Rio San Jose and tributary drainages within the Basin and Range/Colorado Plateau transition zone in west-central New Mexico.	<i>P. G. Drake, C. D. Harrington, S. G. Wells, F. V. Perry, and A. W. Laughlin</i>	149
Geologic overview and Pliocene-Quaternary history of the Albuquerque basin, central New Mexico.	<i>R. P. Lozinsky, J. W. Hawley, and D. W. Love</i>	157
Cuspate-lobate folds along a sedimentary contact, Los Lunas volcano, New Mexico.	<i>W. C. Haneberg</i>	162
Hydrogeologic investigations of upper Sierra Ladrones Formation.	<i>R. C. Lohmann, J. M. Davis, D. W. Love, and F. Phillips</i>	164
Effect of climatic change on Estancia Valley, New Mexico: Sedimentation and landscape evolution in a closed-drainage basin.	<i>B. D. Allen</i>	166
Summary of recent work on the geomorphology of the Rio Puerco.	<i>P. J. Slavin</i>	171

Lower and Middle Pennsylvanian stratigraphic relations, type Derryan region, southern New Mexico and westernmost Texas	<i>W. W. Clopine, W. L. Manger, P. K. Sutherland, and D. A. Kaiser</i>	173
Introduction		173
Geologic setting		173
Lithostratigraphy		174
Biostratigraphy		174
Regional correlations		175
Stop descriptions		175
Stop 1: Type Derryan section, Sierra County, New Mexico		175
Stop 2: Bishop Cap section, Doña Ana County, New Mexico		176
Stop 3: Vinton Canyon section, El Paso County, Texas		179
References		181
Lower and Middle Pennsylvanian fusulinid biostratigraphy in south-central New Mexico and westernmost Texas: A brief review	<i>W. W. Clopine</i>	181
Morrowan brachiopods from the type "Derryan" Series (Pennsylvanian), southern New Mexico	<i>P. K. Sutherland</i>	186
Morrowan-Atokan (Pennsylvanian) conodont biofacies, south-central New Mexico and westernmost Texas	<i>D. A. Kaiser and W. L. Manger</i>	188

Examples of modern rift volcanism and Proterozoic anorogenic magmatism: The Potrillo volcanic field of southern New Mexico and the Franklin Mountains of west Texas

E. Y. Anthony¹, C. G. Barnes¹, W. Chen¹, J. M. Hoffer¹, G. R. Keller¹, K. M. Marsaglia¹, V. T. McLemore^{1/4}, J. M. Seeley¹, M. A. Seward¹, W. M. Shannon¹, and W. F. Thomann¹

¹Department of Geological Sciences, University of Texas at El Paso, El Paso, Texas 79968; ²Department of Geology, Texas Tech University, Lubbock, Texas 79409;

³Department of Geosciences, Texas A&I University, Kingsville, Texas 78363; ⁴New Mexico Bureau of Mines & Mineral Resources, Socorro, New Mexico 87801

Introduction

This article describes a three-day field trip which originates in El Paso, Texas, and terminates in Albuquerque, New Mexico. The first day we will present an overview of the present-day Rio Grande rift and also examine the Proterozoic sedimentary section in the Franklin Mountains, the 1.1 Ga Red Bluff Granite which intrudes it, and coeval trachyte lavas and rhyolitic ignimbrites in the Thunderbird Group. The purpose of these stops is to provoke discussion of tectonic models for this sequence within the context of

regional Proterozoic geology. The second two days will focus on features of the Rio Grande rift. We will visit the Quaternary Potrillo volcanic field, with stops at a classic shield volcano — the Aden Crater — and two maars, including Kilbourne Hole. The second night will be spent in Las Cruces. The third day we will travel to Albuquerque, stopping to examine the tectonic style and geologic features along the way.

Day 1: The Proterozoic section in the Franklin Mountains

C. G. Barnes, K. M. Marsaglia, J. M. Seeley, M. A. Seward, W. M. Shannon, and W. F. Thomann

The focus of Day 1 is an overview of Proterozoic sections exposed in the Franklin Mountains, Texas (Figs. 1, 2), and a general introduction to the Rio Grande rift (see IGC guidebook for Day 3, Callender et al., 1989). To access this region, take the northbound US-54 exit from I-10. Note that US-54 becomes FM 3255 (the North—South Freeway). From US-54 (FM 3255) take the Loop 375 (Woodrow Bean Trans-Mountain Road) exit, and follow road log below. Please use caution when examining the unstable roadcuts and outcrops along Loop 375.

Mileage

0.0 Start at intersection of Loop 375 (Woodrow Bean Trans-Mountain Road) and FM 3255 (North—South Freeway). Proceed west on Loop 375 past Wilderness Park Museum to Stop 1.

0.9 **Stop 1:** Roadside next to Indian Spring Canyon. To the east lies the Hueco bolson, an extensional basin filled with over 3 km of Cenozoic sediments (see Stop 3, IGC guidebook). The low knob to the north is a relatively fresh exposure of the main phase of the Red Bluff Granite (Nelson, 1940), which is a coarse-grained biotite—amphibole granite. Hike due north for 0.5 mi, then proceed west, up dirt road 0.5 mi into Indian Spring Canyon. The entrance of Indian Spring Canyon is underlain by biotitearfvedsonite granite. It occurs as a sill hosted by the Red Bluff Granite and crops out continuously for approximately 1 mi. The biotite—arfvedsonite granite is locally banded or layered (i.e. line rock). Apophyses from this sill extend southeast to Trans-

Mountain Road and northwest to an abandoned tinmine locality.

1.5 **Stop 2:** First roadcut on Loop 375 West. This outcrop consists of blocks of Castner Marble (see description below) and metabasalt (geochemically distinct from the Mundy Breccia; Thomann and Hoffer, 1985) that are hosted and intensely injected by a medium-grained to pegmatitic leucocratic biotite granite (Harbour, 1972). A block of the porphyritic quartz syenite (with Lanoria Quartzite still attached) is exposed on the northeastern end of the outcrop. The lack of internal stratigraphic order suggests that these blocks are stope blocks. In addition, questionable sedimentary structures (mud cracks) within the xenolith of Castner Marble at the west end of the roadcut suggest that this block may be overturned. The leucocratic biotite granite is probably a late phase of the Red Bluff Granite (see Shannon and Barnes, this volume). Dikes of biotite—arfvedsonite granite cut all other rock types.

2.5 **Stop 3:** Pull off into parking area just before third roadcut on Loop 375 West. At this location, Proterozoic metasediments (Castner Marble and Lanoria Quartzite) and metavolcanics (Mundy Breccia and diabase sills) comprise a roof pendant within the Red Bluff Granite complex. The intrusive contact between the Red Bluff Granite complex and this large xenolith is well-exposed on the slope to the north. The light-gray, bedded unit is the oldest formation, the Castner Marble, which consists of thinly laminated to thickly bedded, medium- to coarse-grained marble with alternating layers of

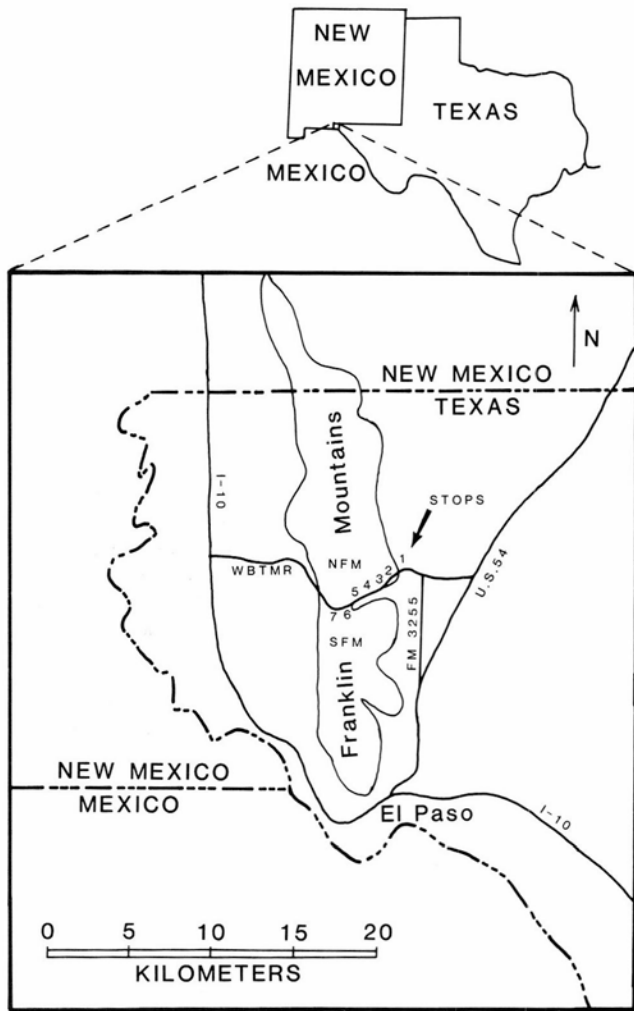


FIGURE 1—Index map showing field-trip stops for Day 1. WBTRM = Woodrow Bean Trans-Mountain Road, NFM = North Franklin Mountain, SFM = South Franklin Mountain. Modified from Thomann and Hoffer (1989).

hornfels. Also exposed on this slope are diabase sills within the Castner Marble, and the Mundy Breccia which unconformably overlies the Castner Marble and pinches out just below the ridge crest. The cliff-forming unit above the Mundy Breccia is the lowermost member of the Lanoria Quartzite (L1, see Stop 5). In the valley to the right, algal stromatolitic mounds and *Conophyton*-type stromatolites have been described in a lower block of the Castner Marble (Toomey and Babcock, 1983). The Castner Marble is exposed along the roadcut to the left of the parking area. Hoffer (1976) described two metamorphic facies in the Castner Marble: (1) hornblende-hornfels facies and (2) K-feldspar—cordierite-hornfels facies, which places the conditions of metamorphism at approximately 515°C and 1000 bars of pressure. A distinctive skarn zone in the Castner Marble is exposed at the eastern edge of this roadcut. Further up section, an enigmatic breccia pipe (or clastic dike?) cuts across the Castner Marble. The amount of hornfels (meta-shale), soft-sediment deformation and edgewise, intraformational conglomerates increases towards the top of the formation (Denison and Hetherington, 1969;

Hoffer, 1976; LeMone, 1982; LeMone and Cornell, 1988; Thomann and Hoffer, 1989). Along this roadcut the Castner Marble/Mundy Breccia contact is poorly exposed, but outcrops just north of the roadcut show the disrupted nature of this contact (see Thomann, this volume, for further discussion of the Mundy Breccia).

- 2.8 **Stop 4:** Fourth roadcut on Loop 375 West. The granitic sill exposed at this location has been informally named porphyritic microgranite (McAnulty, 1967). We suggest that this terminology should be abandoned (see Shannon and Barnes, this volume). The sill was emplaced into the lower member of the Lanoria Quartzite and has chilled margins 1-5 m thick. The center of the sill is a porphyritic biotite—amphibole quartz syenite and is probably cumulate. The chilled margins are granitic porphyry. Numerous Proterozoic basaltic dikes cut the sill.
- 3.1 **Stop 5:** West end of fourth roadcut on Loop 375 West. Exposures of the middle Proterozoic Lanoria Formation can be seen to the north. This formation consists of approximately 750 m of quartzitic sandstones, siltstones, and mudstones which have been intruded and contact-metamorphosed by granites of the Red Bluff Granite complex to at least the albite-epidote-hornfels facies. Due to the low degree of metamorphism, sedimentary structures and textures are relatively well preserved. Harbour (1960) divided the formation into three unnamed members based primarily on topographic constraints (Fig. 2), whereas Seeley (in preparation) subdivides these three members into six members (L1 through L6; Fig. 2) based on lithology and depositional environment. According to Seeley (in preparation), these rocks were deposited in shallow, subtidal-shelf to estuarine environments (members L1, L3 and L5: inner shelf; members L2 and L4: outer shelf; member L6: estuarine lagoon behind a protective tidal shoal). The members of the Lanoria represent pulses of transgression and regression across a gently sub-

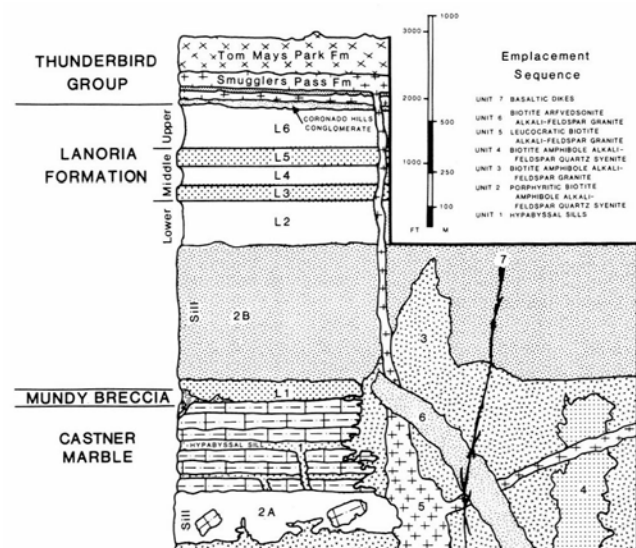


FIGURE 2—A schematic interpretation of Proterozoic stratigraphy exposed along Woodrow Bean Trans-Mountain Road (Fig. 1). This figure has been modified from LeMone (1989). See Stop 5 for discussion of Lanoria Formation subdivisions (L1–L6), and the articles by Thomann and by Shannon and Barnes (below) for further discussion of igneous rocks.

siding platform. Facies distributions and paleocurrent data suggest that the platform sloped northward and that the shelf gradient was relatively low. At this stop, the gray L2 member of the Lanoria Formation is exposed on the lower (gentle) slope, and the overlying middle members (L3 through L5; white quartzite beds and a gray, fine-grained unit) form the cliff along the ridge.

4.3 Stop 6: Carefully cross over gravel median and enter large parking lot on opposite side of road. Massive outcrops of the Thunderbird Group (Thomann, 1980, 1981) can be seen up ahead in roadcuts along Smugglers Pass. From parking area, proceed south along marked hiking trail into canyon, where the three formations of the Thunderbird Group are well exposed. The Coronado Hills Conglomerate is the basal unit that forms prominent, relatively steep cliffs. Units of the Smugglers Pass Formation occur above the basal conglomerate and include a lowermost melanocratic porphyritic trachyte that grades into a lighter-colored (pink) porphyritic trachyte, followed by a relatively thick, light-colored tuffaceous sandstone that is also a cliff-former. A thin porphyritic trachyte overlies this sandstone. The thickest and uppermost formation, the Tom Mays Park Formation, is a recrystallized, metamorphosed ignimbrite (originally a crystal[quartz, K-feldspar]-vitric tuff). In outcrop and hand specimen, the Tom Mays Park Formation superficially resembles a porphyritic rhyolite, but thin-section examination reveals its true pyroclastic nature. Despite contact metamorphism from intrusions of the Red Bluff Granite complex, all igneous and sedimentary textures and structures are well preserved at this locality and throughout the Franklin Mountains.

5.1 Stop 7: Carefully cross over gravel median and continue west on Loop 375 through Smugglers Pass. Carefully cross back over gravel median and enter large parking lot on opposite side of road for scenic overview of Mesilla basin (see Stops 4 and 5, IGC guidebook).

References

- Callender, J. F., Hawley, J. W., and Keller, G. R., 1989, Rio Grande rift: 28th International Geological Congress, Guidebook to Field Trip T318, 37 pp.
- Denison, R. E., and Hetherington, E. A., 1969, Basement rocks in far west Texas and south-central New Mexico: New Mexico Bureau of Mines & Mineral Resources, Circular 104: 1-16.
- Harbour, R. L., 1972, Geology of the northern Franklin Mountains, Texas and New Mexico: U.S. Geological Survey, Bulletin 1298: 129 pp.
- Hoffer, R. L., 1976, Contact metamorphism of the Precambrian Castner Marble, Franklin Mountains, El Paso County, Texas: Unpublished MS thesis, University of Texas at El Paso, 77 pp.
- LeMone, D. V., 1982, Stratigraphy of the Franklin Mountains, El Paso County, Texas and Doña Ana County, New Mexico: El Paso Geological Society, Symposium on the Franklin Mountains, pp. 42-72.
- LeMone, D. V., 1989, Stratigraphy and structure of the Franklin Mountains, west Texas; *in* Structure and stratigraphy of Trans-Pecos Texas: 28th International Geological Congress, Field Trip Guidebook T317: 55-64.
- LeMone, D. V., and Cornell, W. C., 1988, Franklin Mountains, Texas and New Mexico: El Paso Geological Society and American Association of Petroleum Geologists, Stratigraphy Field Guide, 43 pp.
- McAnulty, W. N., Jr., 1967, Geology of the Fusselman Canyon area, Franklin Mountains, El Paso County, Texas: Unpublished MS thesis, University of Texas at Austin, 79 pp.
- Nelson, L. A., 1940, Paleozoic stratigraphy of Franklin Mountains, west Texas; *in* DeFord, R. K., and Lloyd, E. R. (eds.), West Texas—New Mexico Symposium: American Association of Petroleum Geologists, Bulletin, 24(1): 157-172.
- Seeley, J. M. (in preparation), Stratigraphy, petrology, and depositional environment of the Middle Proterozoic Lanoria Formation, Franklin Mountains, El Paso County, Texas: Unpublished MS thesis, Texas A&I University, Kingsville.
- Thomann, W. F., 1980, Petrology and geochemistry of the Precambrian Thunderbird Formation, Franklin Mountains, El Paso County, Texas: Unpublished PhD dissertation, University of Texas at El Paso, 162 pp.
- Thomann, W. F., 1981, Ignimbrites, trachytes, and sedimentary rocks of the Precambrian Thunderbird Group, Franklin Mountains, El Paso, Texas: Geological Society of America, Bulletin, 92: 92-100.
- Thomann, W. F., and Hoffer, J. M., 1985, Petrology and geochemistry of the Precambrian Mundy Breccia, Franklin Mountains, Texas: Texas Journal of Science, 36: 267-281.
- Thomann, W. F., and Hoffer, R. L., 1989, Stratigraphy, sedimentary structures and petrology of the Middle Proterozoic Castner Marble, Franklin Mountains, far west Texas: University of Wyoming, Contributions to Geology, 27: 33-39.
- Toomey, D. F., and Babcock, J. A., 1983, Precambrian and Paleozoic algal carbonates, west Texas and southern New Mexico: Colorado School of Mines, Professional Contribution 11: 345 pp.

Geology of the middle Proterozoic Thunderbird Group, Franklin Mountains, El Paso, Texas

William F. Thomann

Introduction

The middle Proterozoic Thunderbird Group occurs in the Franklin Mountains, north of El Paso, Texas. The Franklins are a north—south-trending, fault-block range located in the southeastern part of the Basin and Range province. West-dipping middle Proterozoic through Paleozoic age strata are well exposed along the steep, east-facing scarps of the range. Continuous outcrops of the Thunderbird Group extend from Mundy's Gap, located just east of Franklin Mountains State Park (formerly Tom Mays Memorial Park), to South Franklin Mountain. The Thunderbird Group is the youngest of a stratigraphic succession of middle Proterozoic rocks. This succession consists of, from oldest to youngest, the Castner Marble (Denison and Hetherington, 1969; Hoffer, 1976; Thomann and Hoffer, 1989), formerly called Castner Lime

stone (Harbour, 1960, 1972), the Mundy Breccia (Harbour, 1960, 1972; Thomann and Hoffer, 1985), the Lanoria Quartzite (Richardson, 1909), and the Thunderbird Group (Thomann, 1980, 1981). The Red Bluff Granite complex intruded all of the middle Proterozoic sedimentary and volcanic rocks. Precambrian(?) diabase dikes subsequently intruded all of these. Isotopic dating of the volcanics of the Thunderbird Group, and of the granites, indicates an age of —950 Ma (Denison and Hetherington, 1969). Denison and Hetherington (1969) stated that the granites and volcanics were contemporaneous (comagmatic?) because they fit a single isochron. More recent age determinations by Norman et al. (1987) and Copeland and Bowring (1988) indicate the granites are about 1.1 Ga.

Despite devitrification of all glass and subsequent contact

metamorphism, relict igneous and sedimentary textures are well preserved in units of the Thunderbird Group. Thus, the Thunderbird Group provides evidence on the origin of these middle Proterozoic igneous and sedimentary rocks in the Franklin Mountains.

The Thunderbird Group

The Thunderbird Group is divided into three formations based upon distinct lithologies and consists of the lower Coronado Hills Conglomerate, the middle Smugglers Pass Formation composed of volcanic and sedimentary rocks, and the upper Tom Mays Park Formation composed almost entirely of rhyolitic ignimbrites. The term "ignimbrite," as defined by Sparks et al. (1973), refers to a pyroclastic rock originally composed of pumice and glass shards, regardless of degree of welding. The type locality of the Thunderbird Group is in the Franklin Mountains, —914 m northeast of Smugglers Pass in Fusselman Canyon at latitude 31°53'06" and longitude 106°29'34".

Coronado Hills Conglomerate

The Coronado Hills Conglomerate consists of well-rounded cobbles and pebbles of quartzite, quartz—sericite siltstone, shale, chert, jasper, ignimbrite, porphyritic trachyte, and rare marble and granite in a recrystallized matrix composed of sand-sized quartz, alkali-feldspar, devitrified pumice, and glass shards. Most of the sedimentary clasts were presumably derived from erosion of the Lanoria Quartzite and Castner Marble, whereas the volcanic and granite clasts were derived from erosion of older but unknown source rocks. Thickness of the conglomerate ranges from 11 to 27 m. Structures such as horizontal bedding, scour fills, and cross-bedding are visible in outcrops throughout this formation.

Smugglers Pass Formation

Melanocratic porphyritic trachyte member—A melanocratic porphyritic trachyte, up to 46 m thick, is the lowermost unit of the Smugglers Pass Formation. The dark-gray to olive-black groundmass is due to the presence of abundant, very fine-grained amphibole. Some other trachytes, however, contain abundant, very fine-grained chlorite and opaque minerals which are indistinguishable from amphibole except in thin-section. Phenocrysts are predominantly albitized microcline perthites with very minor amounts of plagioclase; some perthites have albite rims. Glomerophenocrysts of anhedral feldspars are common; a few possess albite rims. The few plagioclase phenocrysts are altered entirely to an assemblage of albite + epidote ± calcite. Hence, the original plagioclase composition is not known. The albite + epidote ± calcite assemblage is found in no other rock type throughout the Thunderbird Group.

Porphyritic trachyte member—The porphyritic trachyte is up to 61 m thick. Two facies are present. The grayish-red trachytes are similar to the melanocratic trachytes except for the absence of very fine-grained amphibole in the groundmass. The presence of abundant, fine-grained opaques in some trachytes produces a dark-red groundmass. Albitized microcline perthite is the predominant phenocryst and some of these grains occur as glomerophenocrysts of randomly oriented feldspars. Albite rims some grains and glomerophenocrysts of microcline perthite. Quartz and albite phenocrysts are rare. Relict zoning is present in a few of the least altered (albitized) microcline-perthite phenocrysts. Groundmass minerals are a very fine-grained, equi-

granular assemblage of albite, K-feldspar, and some quartz.

Tuffaceous sandstone and conglomerate member—The tuffaceous sandstones and conglomerates are up to 27 m thick. The tuffaceous sandstones and the matrix of the tuffaceous conglomerates consist of detrital particles of quartz, pumice, and lithic fragments, and minor amounts of perthite, albitized perthite, and magnetite. Quartz grains are angular to well rounded; feldspar, lithic, and pumice grains are angular to subrounded. The framework of the tuffaceous conglomerates is composed of rounded boulders, cobbles, and pebbles of trachyte, silicified ignimbrite, and minor amounts of quartzite. Primary sedimentary structures visible in outcrops include horizontal bedding and low-angle cross-bedding.

Silicified ignimbrite member—The silicified ignimbrites vary in thickness from one to about 6 m. Microclineperthite phenocrysts and rare quartz phenocrysts occur within a dark-gray groundmass that is partly to completely replaced by silica. In thin-section, compacted pumice and glass shards draped partly around phenocrysts indicate that these tuffs are densely welded. All original glass devitrified to a very fine-grained assemblage of quartz and alkali-feldspar. Groundmass minerals consist of microphenocrysts of microcline perthite and minor amounts of primary (volcanic) quartz. A few ash-fall deposits occur throughout the silicified ignimbrites. These ash deposits are no more than several centimeters thick and are locally silicified.

Tom Mays Park Formation

Ignimbrites—The ignimbrites of the Tom Mays Park Formation attain a maximum thickness of 168 m. An erosional surface at the top of the formation indicates that it was originally thicker. Individual flow units have not been recognized due to the uniform texture of the groundmass throughout the formation. The uniform texture was produced in part by devitrification of glass and in part by subsequent contact metamorphism caused by intrusions of the Red Bluff Granite complex.

In thin-section, textural alterations in the groundmass vary from those ignimbrites which retained original outlines of glass shards and pumice to those which contain little or no evidence of shards and pumice. The least altered ignimbrites retained not only evidence of the pyroclastic origin of these rocks but also evidence of dense welding, even though the glass recrystallized to a very fine-grained assemblage of alkali-feldspar, quartz, and opaques. Most of the ignimbrites in the formation contain little or no evidence of shards and pumice because of textural and mineralogical changes in the groundmass.

Pumice occurs as compacted lenses and irregularly shaped shreds consisting of a fine-grained equigranular assemblage of quartz and alkali-feldspar. The coarser-grained texture and lighter color of the pumice relative to the groundmass permit detection of pumice in even highly recrystallized ignimbrites. The longest dimension of compacted pumice is less than 20 times the length of the smallest dimension measured perpendicular to bedding. According to Ross and Smith (1961), this suggests flattening due to compaction and not elongation due to stretching.

Almost all ignimbrites are crystal-vitric tuffs. Phenocrysts consist of quartz and alkali-feldspar, and some quartz phenocrysts exhibit resorption with either rounded edges and/or embayed features. Most feldspar phenocrysts are too altered to identify the type of feldspar. In the least altered

ignimbrites, however, the feldspar phenocrysts are microcline perthites. In most other ignimbrites, the feldspars are highly albitized along rims, cracks, and cleavages. The groundmass consists of a very fine-grained, equigranular assemblage of microcline perthite, quartz, and albite.

Porphyritic rhyolites—Porphyritic rhyolites occur as widely scattered dikes which intrude the ignimbrites of the Tom Mays Park Formation. In volume, the dikes are insignificant compared to the rhyolitic ignimbrites in this formation. There are *no* rhyolite lava flows recognized anywhere within the Tom Mays Park Formation. The porphyritic rhyolites contain quartz and alkali-feldspar phenocrysts in a fine-grained groundmass of quartz, microcline perthite, and albite.

Contact metamorphism

Elevated temperatures accompanying granite intrusions of the Red Bluff Granite complex metamorphosed rocks of the Thunderbird Group to the albite—epidote-hornfels facies. Absence of penetrative deformation and the preservation of igneous and sedimentary textures indicate that lithostatic pressure was low. Evidence of metamorphic grade is based on thin-section identification of diagnostic metamorphic-mineral assemblages in particular rock types of the Thunderbird. The melanocratic porphyritic trachyte provides the most critical evidence of metamorphic grade. This trachyte contains coexisting albite + epidote + chlorite + sericite ± calcite. Coexisting metamorphic minerals in the other rock types of the Thunderbird Group are chlorite + albite + sericite, an assemblage which is not strictly diagnostic of the albite—epidote-hornfels facies.

Conclusions

Recognition of ignimbrites in the middle Proterozoic rocks of the Franklin Mountains, Texas, confirms the suggestions made by Sellards et al. (1932) and Harbour (1960, 1972) concerning the possible pyroclastic origin of the volcanic rocks generally referred to as "rhyolite porphyry." The ignimbrites of the Tom Mays Park Formation in the Thunderbird Group resemble, in outcrop and hand specimen, a rhyolite porphyry. Detailed petrographic analysis is required to recognize the pyroclastic origin.

The Franklin Mountains provide a unique setting in the study of the middle Proterozoic rocks that compose the Thunderbird Group. The formations of the Thunderbird Group are the only late middle Proterozoic metavolcanic and volcanoclastic rocks in the west Texas area which (1) are well exposed in a continuous sequence, (2) are virtually undeformed, and (3) possess well preserved volcanic and sedimentary textures.

The nearest outcrops of rhyolitic volcanics of age and lithology similar to the Thunderbird Group are located at Pump Station Hills, Hudspeth County, Texas, —70 mi (113

km) east of El Paso, Texas. Rb/Sr ages based on feldspar and whole-rock analyses for a "rhyolite porphyry" are 996 Ma and 959 Ma, respectively (Wasserburg et al., 1962). U—Pb ages of zircons extracted from a "rhyolite porphyry" are older, ranging from 1005 to 1175 Ma (Wasserburg et al., 1962). Thin-section examination of the "rhyolite" and "rhyolite porphyry" reveals mineralogy and texture almost identical to the altered ignimbrites of the Tom Mays Park Formation in the Thunderbird Group. Thus, the volcanics at the Pump Station Hills appear to be correlative to the volcanics in the Franklin Mountains.

References

- Copeland, P., and Bowring, S., 1988, U—Pb zircon and $^{40}\text{Ar}/^{39}\text{Ar}$ ages from Proterozoic rocks, west Texas (abs.): Geological Society of America, Abstracts with Programs, 20: 95-96.
- Denison, R. E., and Hetherington, E. A., Jr., 1969, Basement rocks in far west Texas and south-central New Mexico: New Mexico Bureau of Mines & Mineral Resources, Circular 104: 1-16.
- Harbour, R. L., 1960, Precambrian rocks at North Franklin Mountain, Texas: American Association of Petroleum Geologists, Bulletin, 44: 1785-1792.
- Harbour, R. L., 1972, Geology of the Northern Franklin Mountains, Texas and New Mexico: U.S. Geological Survey, Bulletin 1298, 129 pp.
- Hoffer, R. L., 1976, Contact metamorphism of the Precambrian Castner Marble, Franklin Mountains, El Paso County, Texas: Unpublished MS thesis, University of Texas at El Paso, 77 pp.
- Muehlberger, W. R., Denison, R. E., and Lidiak, E. G., 1967, Basement rocks in continental interior of United States: American Association of Petroleum Geologists, Bulletin, 51: 2351-2380.
- Norman, D. I., Condie, K. C., Smithy, R. W., and Thomann, W. F., 1987, Geochemical and Sr and Nd isotopic constraints on the origin of the late Proterozoic volcanics and associated tin-bearing granites from the Franklin Mountains, west Texas: Canadian Journal of Earth Sciences, 24: 830-839.
- Richardson, G. B., 1909, Descriptions of the El Paso quadrangle, Texas: U.S. Geological Survey, Atlas, Folio 166, 11 pp.
- Ross, C. S., and Smith, R. L., 1961, Ash flow tuffs: Their origin, geologic relations, and identification: U.S. Geological Survey, Professional Paper 366, 81 pp.
- Sellards, E. H., Adkins, W. S., and Plummer, F. B., 1932, The geology of Texas: University of Texas Bureau of Economic Geology Bulletin, Publication 3232: 1-44.
- Sparks, R. S. J., Self, S., and Walker, G. P. L., 1973, Products of ignimbrite eruptions: Geology, 1: 115-118.
- Thomann, W. F., 1980, Petrology and geochemistry of the Precambrian Thunderbird Formation, Franklin Mountains, El Paso County, Texas: Unpublished PhD dissertation, University of Texas at El Paso, 162 pp.
- Thomann, W. F., 1981, Ignimbrites, trachytes, and sedimentary rocks of the Precambrian Thunderbird Group, Franklin Mountains, El Paso, Texas: Geological Society of America, Bulletin, 92: 94-100.
- Thomann, W. F., and Hoffer, J. M., 1985, Petrology and geochemistry of the Precambrian Mundy Breccia, Franklin Mountains, Texas: Texas Journal of Science, 36: 267-281.
- Thomann, W. F., and Hoffer, R. L., 1989, Stratigraphy, sedimentary structures, and petrology of the Middle Proterozoic Castner Marble, Franklin Mountains, far West Texas: University of Wyoming, Contributions to Geology, 27: 33-39.
- Wasserburg, G., Wetherill, W. W., Silver, L. T., and Flawn, P. T., 1962, A study of the ages of the Precambrian of Texas: Journal of Geophysical Research, 67(10): 4021-4047.

Petrology of the middle Proterozoic Mundy Breccia, Franklin Mountains, Texas

William F. Thomann

Introduction

The Mundy Breccia is one of four Proterozoic stratigraphic units exposed in the Franklin Mountains. These include, from oldest to youngest, the Castner Marble (Hof

fer, 1976; Thomann and Hoffer, 1989), Mundy Breccia (Harbour, 1960, 1972; Thomann and Hoffer, 1985), Lanoria Quartzite (Richardson, 1909), and Thunderbird Group (Thomann, 1980, 1981). The middle Proterozoic Mundy

Breccia crops out on the east side of the Franklin Mountains at four isolated outcrops; the largest one is located adjacent to and north of the Trans-Mountain Road. The Mundy Breccia has not been studied in any detail and previous workers described only briefly its petrography, but they suggested possible origins: volcanic agglomerate (Harbour, 1960, 1972), weathered basalt lava flow or sill (Harbour, 1960, 1972), basalt flow breccia (McAnulty, 1967), and surface or submarine flow breccia (Denison and Hetherington, 1969). Contact metamorphism of all Proterozoic sedimentary and volcanic rocks in the Franklin Mountains resulted in mineralogical alteration with virtually no change in original textures and structures. Heat derived from intrusive granites of the Red Bluff Granite complex (Ray, 1982; McCutcheon, 1982) metamorphosed all Precambrian stratigraphic units, with the highest-grade metamorphic rocks occurring at and near the intrusive margins and the lowest-grade metamorphic rocks located well away from the granite contacts (Harbour, 1960, 1972; McAnulty, 1967; Dye, 1970; Hoffer, 1976; Denison and Hetherington, 1969; Thomann, 1980, 1981; Thomann and Hoffer, 1989).

Stratigraphy

The Mundy Breccia varies in thickness from zero to 64 m at the largest outcrop north of the Trans-Mountain Road and trends approximately north—south with an average dip of 27° west. The breccia lies unconformably on the Castner Marble along a contact marked by a 3 to 20 cm skarn zone. This zone formed as a result of thermal metamorphism from intrusive granites. Chemical reactions that occurred between the basalt and marble resulted in the formation of an equilibrium mineral assemblage of primarily calc-silicates (Hoffer, 1976).

The breccia filled-in channels and also produced depressions by differential loading as it flowed onto the semiconsolidated carbonate sediments. Evidence of disrupted bedding in the upper portion of the Castner Marble includes load casts, intraformational breccias, imbricate structures, and folds. Along strike, the upper contact of the Mundy Breccia with the Lanoria Quartzite is sharp and uniform. The upper contact is an erosional surface and, therefore, the original thickness of the breccia is not known.

The framework of the Mundy Breccia consists almost entirely of angular to subrounded basalt clasts ranging in size from granule to boulder. The fabric varies considerably, both vertically and laterally, from a clast-supported framework with little matrix to a very open framework with clasts supported by matrix. There is no evidence of superposed mudflows.

The breccia is unsorted and unstratified. Spheroidally weathered clasts in various stages of decomposition constitute the matrix of the upper 4.5 m of the breccia. These weathered clasts provide evidence of weathering, and probable erosion, prior to burial by overlying sediments of the Lanoria Formation. The intensity of weathering diminishes gradually beneath the quartzite—breccia contact; the lower basalt fragments retain their original angular to subrounded shapes.

Denison and Hetherington (1969) interpreted the Mundy Breccia as a mudflow breccia but they, as well as other authors, could not determine whether the breccia was a surface or submarine flow. The Mundy Breccia has characteristics of a mudflow breccia that includes granule- to boulder-sized fragments derived from weathering and ero-

sion of a basalt. More recently, Thomann and Hoffer (1985) concluded that the Mundy Breccia is an epiclastic volcanic breccia.

Petrography

Basalt clasts in the Mundy Breccia are predominantly aphanitic; a few are amygdaloidal. Thin-sections of the clasts reveal a metamorphic mineralogy in the basalts with well preserved relict intersertal (glassy) textures seen in only a few samples. The very fine-grained nature of much of the groundmass in the clasts and matrix prevents an accurate point-count determination of percentages of metamorphic minerals.

Cobble- and boulder-size clasts exhibit the best preserved relict intersertal (and/or amygdaloidal) textures. In these basalts, plagioclase crystals retain their original lath shapes, although they altered to albite and/or sericite. Microphenocrysts now composed of fine-grained actinolite, minor biotite, plagioclase, and less commonly sericite, are pseudomorphic after olivine and pyroxene. Former glass (tachylite?) altered to a very fine-grained aggregate of feldspar (albite?), sericite, magnetite, tremolite, actinolite, biotite, and lesser amounts of epidote, clinozoisite, and chlorite. In some samples, fine-grained magnetite is so abundant that extensive portions of a thin-section are opaque to transmitted light. Those basalts with the rarer amygdaloidal texture have vesicles filled with very fine-grained muscovite, biotite, and minor amounts of coarser-grained quartz and feldspar. The well preserved textures and the relatively low concentrations of olivine and pyroxene (as shown by pseudomorphs) suggest that these rocks are tholeiitic olivine basalts. The remaining basalts show a wide range of textural variations from those with some traces of former relict igneous textures (i.e. lath shapes of former plagioclase) to those so thoroughly recrystallized that no evidence of former textures remains. The relative amounts of metamorphic minerals vary considerably from one sample to the next throughout the breccia. Generally, in the intensely recrystallized and usually coarser-grained metabasalts, the predominant replacement minerals are actinolite, biotite, epidote, and/or clinozoisite.

Matrix minerals in the Mundy Breccia include actinolite, tremolite, biotite, epidote, magnetite, albite, chlorite, clinozoisite, muscovite, quartz, microcline, and some zoned tourmaline. Small patches, streaks, lenses, or fracture fillings of actinolite, biotite, epidote, quartz, and magnetite are coarse enough to identify in some hand specimens by the unaided eye or hand lens. Locally, some portions of the matrix are composed predominantly of quartz with muscovite, biotite, albite, actinolite, microcline, and magnetite in subordinate amounts. However, there is no uniformity in the distribution of mineral assemblages found throughout the matrix in the Mundy Breccia.

The mineralogy and texture of the spheroidally weathered basalt in the upper 4.5 m of the breccia are similar to the underlying metabasalts. Although original minerals are no longer present, relict textures of the weathered rinds are well preserved, with a typical clast showing various stages of decomposition from the core of the unweathered clast to the outermost weathered rind. The rinds vary in thickness from a few millimeters up to 1 cm and consist of fine-grained actinolite, biotite, albite, and magnetite.

Near the biotite granite and dikes in the northern part of the outcrop area, the Mundy Breccia has been texturally and mineralogically altered by alkali metasomatism. Alter-

ation of basalts involved conversion of plagioclase laths to microcline and replacement of groundmass by muscovite, biotite, and microcline. No evidence of intersertal or amygdaloidal textures is seen in these rocks. The skarn zone at the contact of the Mundy Breccia with the Castner Marble consists mostly of massive garnet (andradite) and scapolite with minor amounts of calcite, biotite, magnetite, diopside(?), and actinolite. Isolated euhedral garnets attain sizes up to 5 cm.

Equilibrium mineral assemblages indicate the Mundy Breccia experienced at least low-grade metamorphism. Total pressure at the time of metamorphism was at least 0.3 kb based on Harbour's (1972) estimates of the stratigraphic thickness of Precambrian rocks overlying the Mundy Breccia.

Conclusions

The source of basalt that now makes up the clasts in the Mundy Breccia could be from two basalt dikes that lie unconformably below the breccia. However, it is not possible to tell if the breccia formed from erosion of a lava flow or from shallow emplacement of a sill. Intersertal and amygdaloidal textures are common in lava flows as well as high-level synvolcanic sills and dikes (Best, 1982). The lack of sorting and stratification in the Mundy Breccia suggests that the breccia moved as a thick, viscous mudflow capable of carrying clay- to boulder-size clasts. There is no evidence to indicate if the Mundy Breccia is a single- or multiple-flow unit, or whether the breccia traveled as subaerial or subaqueous flow. Deposition of the breccia onto carbonate sediments resulted in disruption of layering, folding, and development of intraformational breccias. The breccia was subsequently exposed to weathering for some length of time, as shown by spheroidally weathered clasts at various stages of decomposition in the upper portion of the volcanic mud-flow breccia. In addition to weathered, sand-sized and smaller basalt particles, the matrix was probably a mud composed of minerals such as clay and Fe-oxides derived from weathering of the basalt. Locally, quartz, perhaps a result of later silicification, was abundant enough to cement the framework and matrix. Deposition of sediments of the Lanoria Formation, and sediments and volcanic rocks of the Thun

derbird Group on top of the Mundy Breccia, was followed by a period of plutonic igneous activity with intrusion of several phases of the Red Bluff Granite complex. Emplacement of the high-level granite plutons resulted in stopping of roof rocks and contact metamorphism of all pre-existing rocks.

References

- Best, M. G., 1982, *Fundamentals of igneous and metamorphic petrology*: W. H. Freeman & Co., New York, 656 pp.
- Denison, R. E., and Hetherington, E. A., Jr., 1969, *Basement rocks in far west Texas and south-central New Mexico*: New Mexico Bureau of Mines & Mineral Resources, Circular 104: 1-16.
- Dye, J. L., 1970, *Geology of the Precambrian rocks in the southern Franklin Mountains, El Paso County, Texas*: Unpublished MS thesis, University of Texas at El Paso, 81 pp.
- Harbour, R. L., 1960, *Precambrian rocks at North Franklin Mountain, Texas*: American Association of Petroleum Geologists, Bulletin, 44: 1785-1792.
- Harbour, R. L., 1972, *Geology of the northern Franklin Mountains, Texas and New Mexico*: U.S. Geological Survey, Bulletin 1298, 129 pp.
- Hoffer, R. L., 1976, *Contact metamorphism of the Precambrian Castner Marble, Franklin Mountains, El Paso County, Texas*: Unpublished MS thesis, University of Texas at El Paso, 77 pp.
- McAnulty, W. N., Jr., 1967, *Geology of the Fusselman Canyon area, Franklin Mountains, El Paso County, Texas*: Unpublished MS thesis, University of Texas at Austin, 79 pp.
- McCutcheon, T. J., 1982, *Petrology and geochemistry of the Precambrian Red Bluff Granite complex, northern Franklin Mountains, El Paso County, Texas*: Unpublished MS thesis, University of Texas at El Paso, 177 pp.
- Ray, D. R., 1982, *Geology of the Precambrian Red Bluff Granite complex, Fusselman Canyon area, Franklin Mountains, El Paso County, Texas*: Unpublished MS thesis, University of Texas at El Paso, 297 pp.
- Richardson, G. B., 1909, *Description of the El Paso quadrangle, Texas*: U.S. Geological Survey, Geological Atlas, Folio 166, 11 pp.
- Thomann, W. F., 1980, *Petrology and geochemistry of the Precambrian Thunderbird Formation, Franklin Mountains, El Paso County, Texas*: Unpublished PhD dissertation, University of Texas at El Paso, 162 pp.
- Thomann, W. F., 1981, *Ignimbrites, trachytes, and sedimentary rocks of the Precambrian Thunderbird Group, Franklin Mountains, El Paso, Texas*: Geological Society of America, Bulletin, 92: 92-100.
- Thomann, W. F., and Hoffer, J. M., 1985, *Petrology and geochemistry of the Precambrian Mundy Breccia, Franklin Mountains, Texas*: Texas Journal of Science, 36: 267-281.
- Thomann, W. F., and Hoffer, J. M., 1989, *Stratigraphy, sedimentary structures, and petrology of the Middle Proterozoic Castner Marble, Franklin Mountains, far west Texas*: University of Wyoming, Contributions to Geology 27: 33-39.

Summary of the geochemistry and petrology of Proterozoic granitic rocks, Franklin Mountains, west Texas

W. M. Shannon and C. G. Barnes

Introduction

Middle Proterozoic granitic and associated volcanic rocks are exposed for a distance of 25 km along the Franklin Mountains, a westward-tilted Basin and Range fault block (Richardson, 1909; Harbour, 1972; Lovejoy, 1975) that extends northward from the center of El Paso, Texas (Fig. 1). The granitic rocks intruded a Proterozoic metamorphic sequence (calc-silicates, basaltic breccia, and clastic rocks; Harbour, 1960) and presumably cogenetic felsic volcanic rocks (Thunderbird Group; Thomann, 1981).

The granitic rocks yield radiometric ages in the range 1.03-1.15 Ga (Wasserburg et al., 1962; Muehlberger et al., 1966; Denison and Hetherington, 1969; Norman et al., 1987;

Copeland and Bowring, 1988). Coeval felsic activity occurred in Colorado (Pikes Peak; Hedge, 1970) and central Texas (Enchanted Rock; Walker, 1988), and mafic activity occurred in west Texas (Nellie layered mafic intrusions; Hoover et al., 1985; Keller et al., 1989).

The granitic rocks have been inferred to be anorogenic (A-type) granite with a probable crustal source (Anderson, 1983) or to be the product of fractionation of tholeiitic magma typical of continental convergent margin and associated back-arc tectonic environments (Condie, 1982; Norman et al., 1987). One of the objectives of our research is to clarify the tectonic setting of these rocks by gaining a more complete understanding of their petrogenetic history.

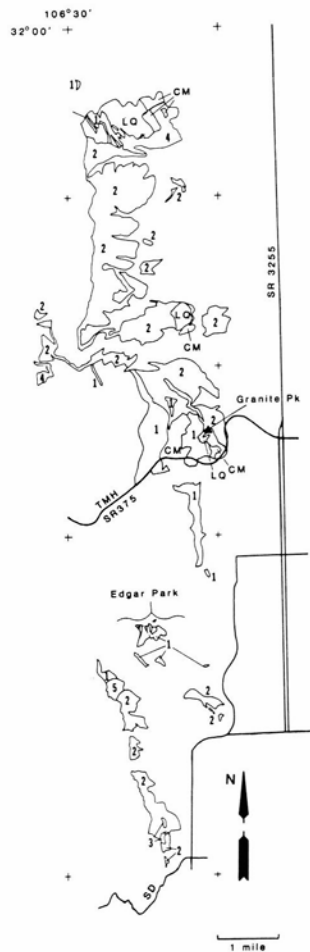


FIGURE 1—Location map. **1**, Amphibole–biotite–alkali-feldspar–quartz syenite and porphyritic alkali-feldspar granite (Stage 1); **2**, amphibole–biotite–alkali-feldspar granite (Stage 2); **3**, amphibole–biotite–alkali-feldspar–quartz syenite (Stage 3); **4**, biotite–alkali-feldspar granite (Stage 4); **5**, arfvedsonite granite (Stage 5). CM = Castner Marble, LQ = Lanoria Quartzite, SR = State Highway, SD = Scenic Drive. Modified after Dye, 1970; Harbour, 1972; Ray, 1982; and McCutcheon, 1982.

Field setting and petrography

The sequence of intrusion of the granitic rocks is listed below, from oldest to youngest (also see stratigraphic section in Anthony et al., this volume).

Stage 1 is composed of porphyritic biotite–amphibole–alkali-feldspar–quartz syenite (Fusselman Canyon sill) and porphyritic alkali-feldspar granite (sill in Edgar Park Quarry). The sill exposed in Fusselman Canyon intruded the lower member of the Lanoria Quartzite, and is up to 660 m thick. The central part is alkali-feldspar–quartz syenite with hypidiomorphic granular texture and abundant glomerocrysts of perthitic alkali-feldspar from 0.25 to 3.0 cm across. Ferrohedenbergite (Fe-rich clinopyroxene) occurs as anhedral inclusions in the alkali-feldspar and as cores in amphibole. Quartz phenocrysts reach as much as 2 mm in diameter. Amphibole, biotite, quartz, alkali-feldspar, ilmenite, apatite, and zircon are interstitial. The margins of the sill are 1–5 m thick and consist of porphyritic granite with euhedral quartz and alkali-feldspar phenocrysts as much as 10 mm across. Within 1 m of the contact, amphibole and biotite increase in grain size and abundance. Fluorite occurs as

inclusions in the amphibole and interstitially (with clusters of acicular biotite). Zircon is a microphenocryst phase.

The porphyritic alkali-feldspar granite sill that crops out in the vicinity of Edgar Park Quarry is also intruded into the Lanoria Quartzite. The sill has porphyritic hypidiomorphic granular texture with euhedral quartz and alkali-feldspar phenocrysts. Biotite and amphibole clusters occur in the groundmass. The biotite and amphibole are intergrown with fluorite and subhedral oxides. Zircon microphenocrysts are also present.

Stage 2, the main intrusive phase, is biotite–amphibole–alkali-feldspar granite. It forms about 80% of the Franklin Mountain granitic rocks (Fig. 1). It is hypidiomorphic granular and contains perthitic alkali-feldspar with cores of subhedral plagioclase (as calcic as An₃₆) or albite. Plagioclase, quartz, and zircon are interstitial, as are intergrowths of amphibole with biotite, albite, quartz, zircon, and fluorite. Ilmenite occurs as lamellar zones in biotite and as discrete subhedral grains in amphibole. Prismatic apatite occurs as inclusions in amphibole and biotite. Magnetite is sparse and its abundance increases as the ratio of amphibole to biotite decreases.

Stage 3 consists of biotite–amphibole–alkali-feldspar–quartz syenite. It is abundant in the southern end of the Franklin Mountains (Fig. 1). Stage-3 rocks are similar in texture and mineralogy to the Stage-2 granite and contain deuteric grunerite(? , after fayalite?). Quartz-syenite dikes contain alkali-feldspar phenocrysts with plagioclase cores (An₂₃ to An₃₁). In these dikes, poikilitic amphibole and biotite enclose alkali-feldspar and acicular apatite. Zircon forms abundant euhedral prisms as well as acicular crystals in the groundmass.

Stage-4 leucocratic biotite–alkali-feldspar granite underlies Granite Peak on the northeastern edge of Fusselman Canyon (Fig. 1). It is also well exposed in Tom Mays Park, where it intrudes volcanic rocks of the Thunderbird Group. It consists of an hypidiomorphic granular arrangement of quartz and alkali-feldspar with interstitial biotite, fluorite, ilmenite, and magnetite. Alkali-feldspar phenocrysts are present locally.

Stage 5 consists of biotite–arfvedsonite–alkali-feldspar granite. This rock type has two textural varieties: one is porphyritic and the other is equigranular. In the porphyritic variety, subhedral quartz and alkali-feldspar (now microcline) are phenocryst phases and arfvedsonite, astrophyllite, fluorite, and zircon form glomerocrysts. The matrix is a fine-grained hypidiomorphic granular arrangement of quartz, albite, and microcline. Some quartz and microcline crystals are broken and have poikilitic overgrowths with inclusions of matrix quartz and alkali-feldspars. Groundmass zircon is poikilitic; opaque oxides are rare.

Some dikes and sills of the arfvedsonite granite are banded (i.e. line rock). The bands consist of flow-foliated laths of arfvedsonite. Streaks within the layers have poikilitic arfvedsonite, biotite, quartz, and zircon. The upper contact of some sills is pegmatitic, with well-developed comb layering.

An abandoned tin-mining site is located north of Mundy Springs. East–west-trending pegmatitic ore veins cut Stage-2 granite. The margins of these veins are leucocratic ferriuscovite–topaz–alkali-feldspar granite. The rock is fine-grained, hypidiomorphic granular, and forms sharp intrusive contacts with the host granite. Perthitic alkali-feldspar, quartz, ferriuscovite, and topaz occur with accessory fluorite, zircon, ilmenite, and magnetite.

Mineral compositions

Alkali-feldspar compositions range from $Ab_{58}An_4Or_{38}$ in the quartz syenites to $Ab_{54}An_1Or_{45}$ in the most voluminous alkali-feldspar granites. Plagioclase cores in alkali-feldspar phenocrysts are $Ab_{66}An_{32}Or_2$ in the quartz syenites and $Ab_{62}An_{36}Or_2$ in the main-phase granite.

Biotite $Fe/(Fe + Mg)$ ranges from 0.9 to 1.0 (annite); the ratio increases from quartz syenite to main-phase granite. Mn content remains approximately constant and Ti content decreases with increasing $Fe/(Fe + Mg)$. Biotite in the arfvedsonite granite is Al-deficient and contains excess Si. In general, Cl fills about 10% of the hydroxyl site but fluorine was rarely detected. However, the ratio $F/(F + Cl + H_2O)$ ranges from 0.5 to 0.75 in annite in the arfvedsonite granite (and in ferriuscovite in the topaz granite).

Amphibole compositions (Fig. 2) range from ferroedenite to ferroactinolite when the Fe^{+3}/Fe^{+2} ratio is calculated according to Speer and Kimble (1981). This ratio ranges from 0.03 to 0.17. Edenite substitution appears to be the dominant mechanism of compositional variation, but Ti Tschermak's substitution is significant in amphiboles from the least siliceous quartz syenites. Ti content decreases and Mn content increases as $Fe/(Fe + Mg)$ increases. The ratio of halogens to hydroxyl in ferroedenite is about 0.25 and the fluorine content of the ferroedenitic amphiboles decreases with increasing $Fe/(Fe + Mg)$ and $Mn/(Mn + Ti)$. In addition to the magmatic amphiboles, interstitial deuteric grunerite is locally present.

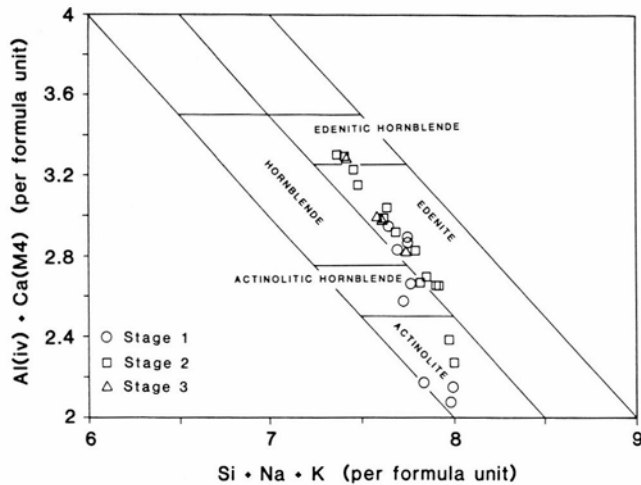


FIGURE 2—Amphibole classification (Giret et al., 1980).

Major-element, trace-element, and isotopic compositions

The chemical compositions of these rocks are typical of metaluminous alkali granites (e.g. Fig. 3, Table 1). Major- and trace-element trends are continuous from quartz syenite to granite and plot along linear trends. Si, Cs, Rb, Be, Hf, Y, Th, and the rare-earth elements (REE) increase in this sequence, whereas Zr, Ti, P, Fe, Mg, $Mg/(Fe + Mg)$, Mn, Sc, Al, K, Na, Ba, and Sr decrease. Table 1 shows that the rocks have high contents of high-field-strength elements (Zr, Hf, Nb, and Ta), total alkalis, and REE.

REE-element patterns are approximately parallel and total REE abundance increases from the quartz syenite to the granitic compositions (Fig. 4). The Eu anomaly increases with differentiation. Although the main-phase granite is texturally variable, its REE concentrations are all similar. The

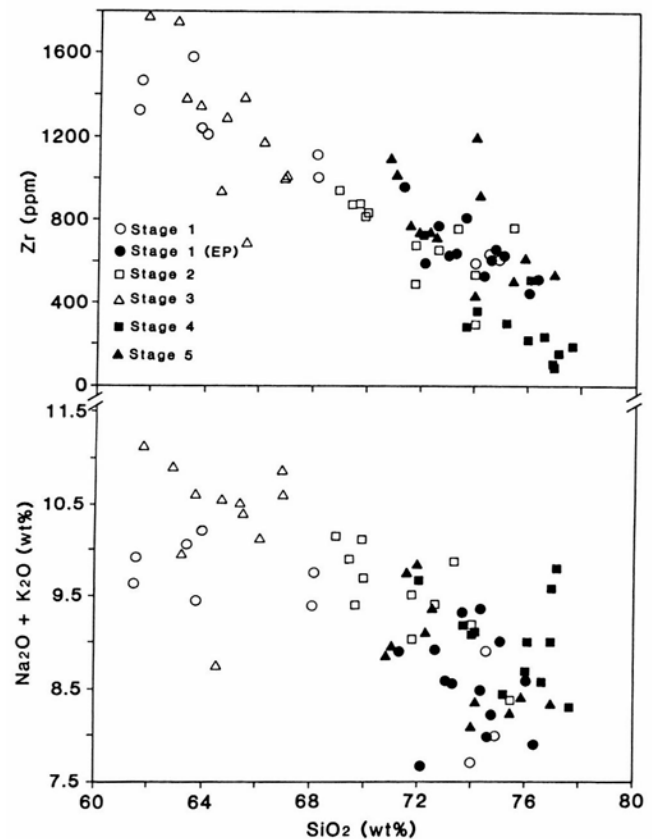


FIGURE 3—A, SiO_2 versus $Na_2O + K_2O$. B, SiO_2 versus Zr.

TABLE 1—Chemical composition of Proterozoic granitic rocks.

Sample	FHTM2A	FM170	FM107	FM157	FM133	FM538	FM519	FMK1
Stage	1 (FC)	1 (FC)	1 (EP)	2	2	3	3	5
SiO ₂	63.97	74.86	74.73	69.96	73.31	62.89	64.66	74.14
TiO ₂	0.63	0.24	0.23	0.22	0.20	0.54	0.58	0.14
Al ₂ O ₃	14.54	11.94	11.98	13.71	13.07	16.19	15.08	9.34
Fe ₂ O ₃	1.45	0.58	0.81	1.29	1.41	1.75	1.47	2.59
FeO	5.57	2.55	2.34	2.22	0.95	4.41	4.44	3.24
MnO	0.17	0.05	0.07	0.12	0.04	0.19	0.17	0.09
MgO	0.23	0.18	0.16	0.09	0.04	0.31	0.41	0.05
CaO	2.20	0.76	0.70	0.98	0.69	2.28	2.03	0.60
Na ₂ O	4.72	3.74	3.16	4.47	4.31	5.49	5.03	4.01
K ₂ O	5.50	4.25	5.06	5.23	5.57	5.41	5.52	4.33
P ₂ O ₅	0.09	0.02	0.03	0.02	0.02	0.09	0.12	0.01
LOI	0.34	1.04	0.99	0.77	0.71	0.44	0.39	0.26
Total	99.42	100.22	100.25	99.09	100.32	100.01	99.92	98.81
Delta 180xygen (per mil)								
Rock	7.8		9.56			8.1	8.69	7.98
Quartz	8.9						8.9	8.6
Sr	82.2	25	37.5	28.2	22.2	121	67.5	21.5
Ba	932	262	268	337	176	1534	978	24.3
Rb	153	113	166	200	300	138	196	707
Cs	2.6	0.9	0.4		2.9	1.8	1.6	2.8
Sc	7.36	1.27	1.25	2.53	2.2	15.5	15.7	0.493
U	5	2	2	2	2	3	3	3
Cr	6	DL	0	6	2	14	4	2
Cu	9	5	3	10	7	5	8	6
Zn	160	130	190	168	125	182	192	856
Se	3.3	5	5.4		8.2	4.7	6.2	19.7
Y	103	166	154	164	203	121	141	405
Zr	1210	617	661	834	761	1748	1287	917
Hf	29.8	20.2	20.3		24.3	41.8	31.7	36.8
Nb	59	75	74	68	99	86	94	258
Ta	2.8	3.9	4.1		6.3	3.6	4.8	12.3
Th	11.3	30.1	30.4		35.3	14.9	16.7	37.2
U	2.8	7.3	6.7		7.2	4.1	4.1	11.4
La	97.6	133.4	133.1		216.6	76.6	127.5	198.6
Ce	220.2	336.8	327.2		462.1	185.9	290.8	567.5
Nd	113	153.9	148.1		192.5	105.8	149.3	259.7
Sm	22.93	30.55	29.59		37.27	23.16	30.54	68.98
Eu	3.83	1.54	1.64		1.87	5.03	4.29	1.48
Gd	19.98	29.52	32.03		36.12	21.69	25.46	77.27
Tb	2.92	4.64	4.88		5.66	4.05	4.58	14.85
Yb	12.97	17.01	17.58		20.69	14.06	16.65	34.86
Lu	2.01	2.31	2.46		2.86	2.23	2.54	5.28

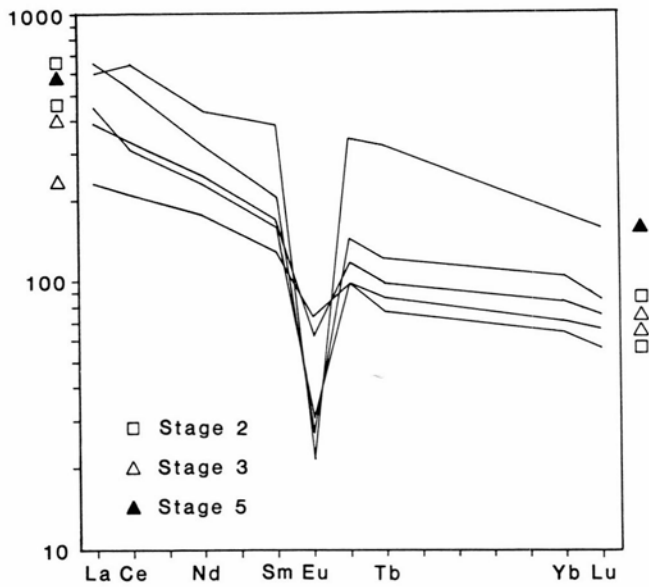


FIGURE 4—Rare-earth-element patterns.

REE patterns of the Fusselman Canyon quartz syenite are identical to those of the early granitic sill near Edgar Park Quarry (Table 1), an indication that the two sills may represent a single intrusive event.

The quartz syenites have whole-rock $\delta^{18}\text{O}$ values of about 8‰ and quartz values of about 9‰. $\delta^{18}\text{O}$ of the main granite is about 7‰ (whole rock) and 8‰ (quartz). These values suggest that hydrothermal alteration did not lower the whole-rock $\delta^{18}\text{O}$ value. The initial $87\text{Sr}/86\text{Sr}$ for the Franklin Mountain granites is about 0.7034 (Norman et al., 1987). This value is slightly higher than that of the uniform reservoir at 1.14 Ga (0.7032). END for the granites and late alkali-basalt dikes ranges from +3.8 to +1.4 at 1.14 Ga (Patchett and Ruiz, 1989; Norman et al., 1987).

Conditions of emplacement

A pseudoternary plot of normative albite, quartz, and orthoclase indicates that the rocks differentiated from the Ab—Or join toward the 0.5 kbar water-saturated minimum (Fig. 5). This is consistent with pressure of emplacement estimated on the basis of stratigraphic reconstruction of about 1 kbar. Low-pressure emplacement was preceded by partial crystallization in a deeper magma chamber because the compositional fields for the bulk of the quartz syenites and granites lie in a zone that is compatible with crystallization at pressures closer to 3 kbar. This inference is consistent with the subsolvus nature of the rocks (plagioclase cores in

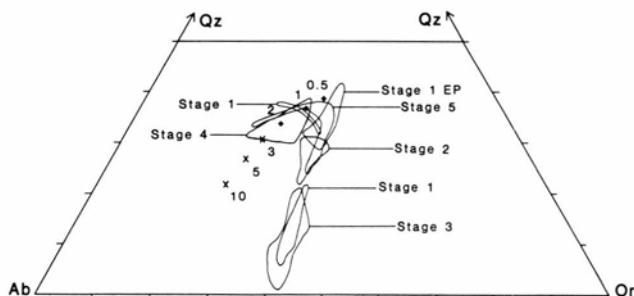


FIGURE 5—Normative albite-quartz-orthoclase (Ab—Qz—Or) diagram, experimental ternary minima after Barker et al. (1975). Compositional fields refer to stages of Franklin Mountain granites and syenites.

alkali-feldspar crystals) which indicate partial crystallization at pressures higher than that of intrusion (Nekvasil, 1990).

Several lines of evidence suggest that the oxidation state $f(\text{O}_2)$ in the syenitic and granitic magmas was low. These include the extreme $\text{Fe}/(\text{Fe} + \text{Mg})$ of mafic minerals and whole rocks, the mineral assemblage ferrohedenbergite + ferroedenite + annite + ilmenite, and the presence of arfvedsonite as a magmatic phase (Wones, 1981, 1989). The hedenbergite + ilmenite assemblage may be represented by the reaction: $3 \text{ sphene} + 2 \text{ magnetite} + 3 \text{ quartz} = 3 \text{ ferrohedenbergite} + 3 \text{ ilmenite} + \text{O}_2$. Rocks on the hedenbergite + ilmenite side of the buffer require an oxygen fugacity at or below the fayalite—quartz—magnetite buffer (Wones, 1989).

The presence of fluorite as a late magmatic phase in most rock types, as well as the moderate fluorine content of late-stage ferromagnesian minerals, indicates that both fluorine and water were dissolved in the magmas. However, the lack of abundant pegmatitic rocks suggests that fluid saturation was probably reached at near-solidus conditions.

Discussion

Mineralogical and isotopic data suggest that magmas parental to the Franklin Mountain granitic suite were derived from a source that was relatively reduced, had mantle-like Sr and Nd-isotopic compositions, but oxygen-isotope compositions that were slightly elevated relative to the normal mantle. Trace-element abundances indicate that the parental magma was derived from a source that was enriched in high-field-strength elements or that a more mafic HFSE-rich magma underwent protracted fractionation to produce the trace-element enrichments observed in the granitic suite. We prefer the latter explanation (i.e. an alkali-basaltic parent) because of the difficulty of attaining such high HFSE concentrations in a metaluminous magma by partial melting. This difficulty is caused by the fact that in a crustal-source region, the HFSE are held in refractory accessory phases that have low solubility in metaluminous magmas. Sparse, late-stage, SiO_2 -undersaturated mafic alkalic dikes cut the granitic rocks and indicate that such compositions were present.

Major- and trace-element variations suggest that differentiation among the granitic rocks could have occurred by progressive removal of alkali-feldspar, ferroedenite, annite, ilmenite, apatite, and zircon (Fig. 6). In addition, the Rb/Y ratio of the suite is nearly constant (Fig. 7), as would be expected if fractional crystallization was the dominant process. Fractional crystallization cannot explain the higher ^{18}O value of the syenitic rocks relative to the granites. This higher value indicates that the granitic rocks cannot be related to the syenites by the simple process of fractional crystallization. In spite of this isotopic discrepancy, we tested the possibility that a mafic syenitic magma was parental to the granitic compositions.

Major-element mass-balance calculations (Bryan et al., 1969) were used to model fractional crystallization of mafic quartz-syenitic magma to make successively more differentiated granitic daughter magmas. Alkali-feldspar, ferrohedenbergite, ferroedenite, annite, ilmenite, and apatite were the minerals removed in the models. The results of the calculations are combined with trace-element data in Fig. 6. Trace-element variations (as a function of calculated fraction of liquid remaining; F) indicate that fractional crystallization can produce the range of granitic compositions observed.

- LeMone, D. V. (eds.), Border stratigraphy symposium: New Mexico Bureau of Mines & Mineral Resources, Circular 104: 1-16.
- Dye, J. C., 1970, Geology of the Precambrian rocks in the Southern Franklin Mountains, El Paso County, Texas: Unpublished MS thesis, University of Texas at El Paso, 81 pp.
- Giret, A., Bonin B., and Leger, J. M., 1980, Amphibole compositional trends in oversaturated and undersaturated alkaline plutonic ring complexes: *Canadian Mineralogist*, 18: 481-495.
- Harbour, R. L., 1960, Precambrian rocks at North Franklin Mountain, Texas: *American Association of Petroleum Geologists, Bulletin*, 44: 1785-1792.
- Harbour, R. L., 1972, Geology of the northern Franklin Mountains, Texas and New Mexico: U.S. Geological Survey, Bulletin 1298: 129 pp.
- Hedge, C. E., 1970, Whole rock Rb-Sr age of the Pikes Peak batholith, Colorado: U.S. Geological Survey, Professional Paper 700-B: 86-89.
- Hoover, J. D., Keller, G. R., and Hills, J. M., 1985, The Nellie intrusion: a basic stratiform intrusion in the Central basin platform in west Texas: *EOS*, 66: 1136.
- Keller, G. R., Hills, J. M., Baker, M. R., and Wallin, E. T., 1989, The Nellie intrusion: a basic stratiform intrusion in the Central basin platform in west Texas: *Geology*, 17: 1049-1052.
- Lovejoy, E. M. P., 1975, An interpretation of the structural geology of the Franklin Mountains, Texas; *in* Seager, W. R., Clemons, R. E., and Callender, J. F. (eds.), *Las Cruces country: New Mexico Geological Society, Guidebook 26*: 261-268.
- McAnulty, W. N., Jr., 1967, Geology of the Fusselman Canyon area, Franklin Mountains, El Paso County, Texas: Unpublished MS thesis, University of Texas at Austin, 79 pp.
- McCutcheon, T. J., 1982, Petrology and geochemistry of the Precambrian Red Bluff Granite complex, Fusselman Canyon area, Franklin Mountains, El Paso County, Texas: Unpublished MS thesis, University of Texas at El Paso, 177 pp.
- Muehlberger, W. R., Hedge, C. E., Denison, R. E., and Marvin, R. F., 1966, Geochronology of the midcontinent region, United States: Part 3, Southern area: *Journal of Geophysical Research*, 71: 5409-5426.
- Nekvasil, H., 1990, Reaction relations in the granite system: Implications for trachytic and syenitic magmas: *American Mineralogist*, 75: 560571.
- Nelson, L. A., 1940, Paleozoic stratigraphy of Franklin Mountains, west Texas; *in* De Ford, R. K., and Lloyd, E. R. (eds.), *West Texas-New Mexico Symposium: American Association of Petroleum Geologists, Bulletin*, 24: 157-172.
- Norman, D. I., Condie, K. C., Smithy, R. W., and Thomann, W. F., 1987, Geochemical and Sr and Nd isotopic constraints on the origin of the late Proterozoic volcanics and associated tin-bearing granites from the Franklin Mountains, west Texas: *Canadian Journal of Earth Sciences*, 24: 830-839.
- Patchett, P. J., and Ruiz, J., 1989, Nd isotopes and the origin of Grenville-age rocks in Texas: Implications for Proterozoic evolution of the United States mid-continent region: *Journal of Geology*, 97: 685-695.
- Ray, R. D., 1982, Geology of the Precambrian Red Bluff Granite complex, Fusselman Canyon area, Franklin Mountains, El Paso County, Texas: Unpublished MS thesis, University of Texas at El Paso, 295 pp.
- Richardson, G. B., 1909, Descriptions of the El Paso quadrangle, Texas: U.S. Geological Survey, Atlas, Folio 166, 11 pp.
- Strecheisen, A., 1974, Classification and nomenclature of plutonic rocks: Recommendations of the IUGS Subcommittee on the Systematics of Igneous Rocks: *Geologischen Rundschau*, 63: 773-786.
- Taylor, H. P., Jr., and Sheppard, S. M. F., 1986, Igneous rocks: I. Processes of isotopic fractionation and isotope systematics; *in* Valley, J. W., Taylor, H. P., Jr., and O'Neil, J. R. (eds.), *Stable isotopes in high temperature geological processes: Mineralogical Society of America, Reviews in Mineralogy*, 16: 227-271.
- Thomann, W. F., 1981, Ignimbrites, trachytes and sedimentary rocks of the Precambrian Thunderbird Group, Franklin Mountains, El Paso, Texas: *Geological Society of America, Bulletin*, 92: 94-100.
- Walker, N. W., 1988, U-Pb zircon evidence for 1305-1231 Ma crust in the Llano uplift, central Texas (abs.): *Geological Society of America, Abstracts with Programs*, 20: A205.
- Wasserburg, G. J., Wetherill, G. W., Silver, L. T., and Flawn, P. T., 1962, A study of the ages of the Precambrian of Texas: *Journal of Geophysical Research*, 67: 4021-4047.
- Wones, D. R., 1981, Mafic silicates as indicators of intensive variables in granite magmas: *Mining Geology*, 31: 191-212.
- Wones, D. R., 1989, Significance of the assemblage titanite + magnetite + quartz in granitic rocks: *American Mineralogist*, 74: 744-749.

Day 2: The Potrillo volcanic field

J. M. Hoffer, W. Chen, V. T. McLemore, and E. Y. Anthony

Driving distance and time: 135.5 mi, 8 hrs, 4 stops.
Road-log starting point: Intersection of Mesa and Doniphan, just west of I-10 (Mesa exit) in northwest El Paso.

Mileage

- 0.0 Stoplight at Mesa and Doniphan, straight ahead on Texas Farm Road 260 (Country Club road). **0.6** 0.6
Stoplight; continue straight. **0.4**
- 1.0 Stoplight; continue straight. **0.5**
- 1.5 Cross Rio Grande. **0.5**
- 2.0 Stop sign; enter New Mexico on NM-184, straight ahead. **0.6**
- 2.6 Stop sign; turn right onto NM-273. **1.5**
- 4.1 Prepared food plant on right. **0.2**
- 4.3 Turn left onto Airport Road. **0.2**
- 4.5 Santa Teresa School on right. **2.3**
- 6.8 Turn left. **0.4**
- 7.2 Stop sign; cross railroad tracks and bear right on A-17, continue parallel to railroad tracks on the La Mesa surface. The La Mesa surface represents the upper surface of the Rio Grande rift basin-fill deposits; here it is a dune sand composed of sub-rounded, clear to iron-coated quartz grains (70%)

and subordinate opaques, zircon, tourmaline, and pyroxene (Hoffer, 1976). **0.8**

8.0 Turn left on A-03. **0.8**

8.8 Cattle guard. **5.9**

14.7 Turn left and then right onto the old railroad bed of the El Paso and Southwestern Railroad, continue west. **3.0**

17.7 Cattle guard. **1.4**

19.1 East Potrillo Mountains at 2:00-3:00. These mountains (Fig. 1) exhibit Laramide, early Tertiary, and late Tertiary deformation, and contain Permian, Lower Cretaceous, and Cenozoic strata (Seager and Mack, 1986). **2.6**

21.7 Cattle guard. **5.1**

26.8 Cattle guard. **0.4**

27.1 West Potrillo Mountains at 12:00-2:00; Mt. Riley and Mt. Cox at 2:00; and East Potrillo Mountains at 2:00-3:00. The West Potrillo Mountains (Fig. 1) are a broad topographic high covered by late Tertiary and Quaternary alkaline lavas. The Potrillo volcanic field as a whole is of an alkaline nature and varies, with differentiation, from basanites through alkali basalts to trachybasalts (Table 1, Fig. 2). The plateau rises 120 to 240 m above the La

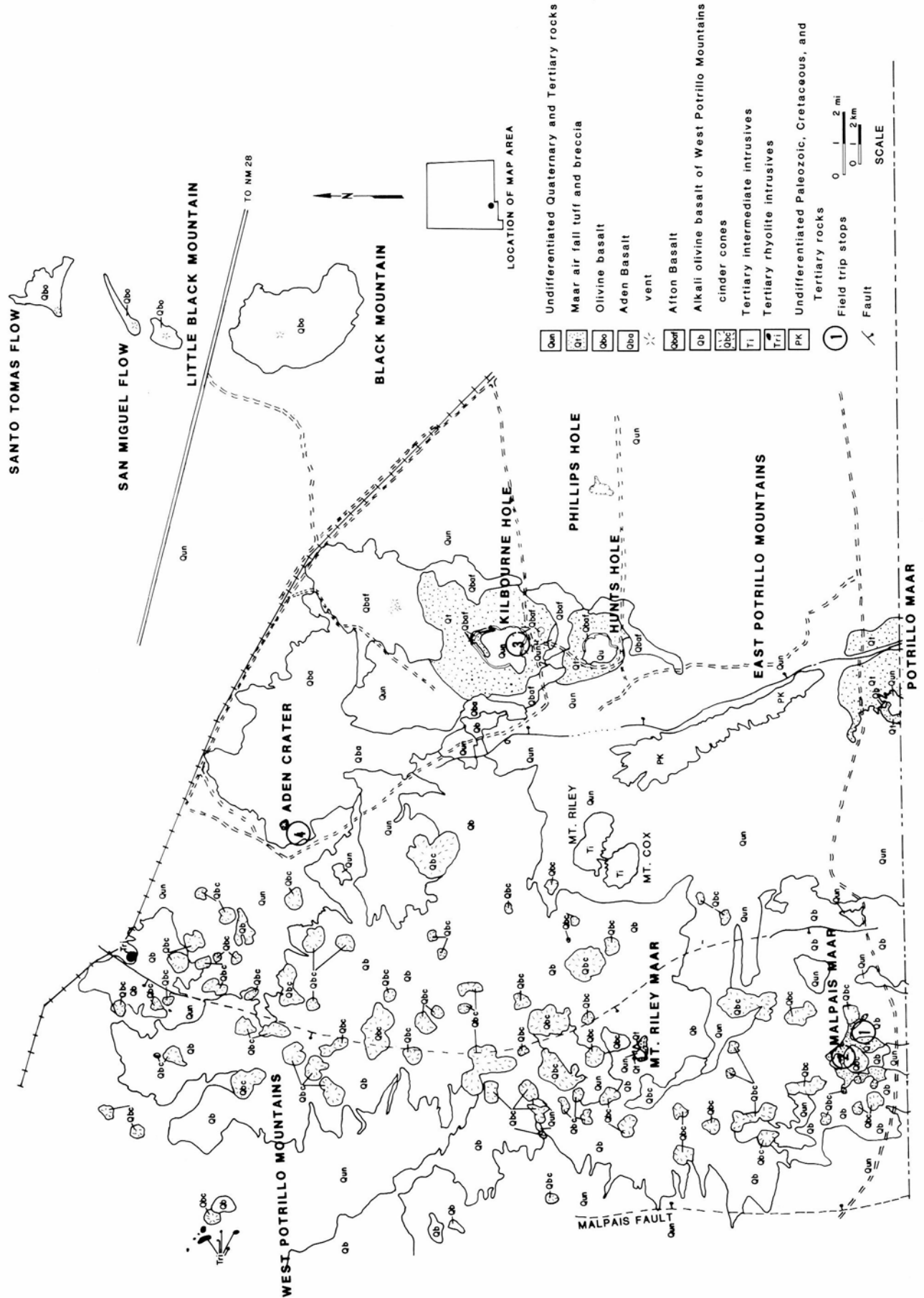


FIGURE 1—Geologic map of the Potrillo Mountains. Simplified from Seager et al. (1987) and Seager (in press).

TABLE 1—Composition of lavas from southern New Mexico.

	Potrillo Volcanic Field							
	22 ADEN	8/26 AFTON	21 AFTON	8/24 MAAR	13 MAAR	20 MAAR	16 POST	8/23 POST
SiO ₂	46.06	44.74	44.87	44.23	44.65	44.49	47.73	47.35
TiO ₂	2.17	2.13	2.08	2.19	2.17	2.17	2.08	2.08
Al ₂ O ₃	15.09	14.54	14.46	13.79	13.82	13.76	16.52	16.24
Fe ₂ O ₃	10.40	10.91	11.29	11.90	11.89	11.82	10.36	10.38
MnO	0.17	0.19	0.19	0.19	0.19	0.20	0.16	0.17
MgO	10.33	10.93	10.99	12.59	12.54	12.57	7.86	8.15
CaO	9.63	10.84	10.81	9.39	9.32	9.38	9.49	9.28
Na ₂ O	3.53	3.32	2.97	3.48	3.38	3.35	4.01	4.07
K ₂ O	1.74	1.63	1.59	1.59	1.61	1.55	1.67	1.67
P ₂ O ₅	0.50	0.47	0.47	0.45	0.46	0.46	0.53	0.52
LOI	0.02	0.47	0.07	0.43	0.39	0.33	0.05	0.53
Sum	99.64	100.16	99.76	100.23	100.41	100.07	100.45	100.43
or**	8.5	8.5	8.1	8.7	8.3	8.2	7.5	8.1
ab	15.3	9.9	9.9	13.7	9.8	13.3	22.9	23.6
an	22.6	21.6	22.2	17.4	19.5	19.0	22.9	22.6
ne	5.5	10.0	6.6	9.7	9.5	7.9	4.1	6.8
cpx	19.5	24.9	24.3	22.2	21.8	21.8	19.4	18.2
cpx	0.0	0.0	0.0	0.0	0.0	0.0	0.0	0.0
ol	18.4	16.6	18.4	19.7	20.7	20.4	13.4	13.2
nt	2.6	2.6	2.7	2.7	2.8	2.7	2.4	2.4
il	4.2	3.9	4.0	4.2	4.3	4.1	4.0	4.0
ap	0.7	0.8	0.7	0.9	0.7	0.7	0.7	0.8
Rb (ppm)	32	34	33	34	35	34	36	36
Sr	623	578	577	582	581	574	640	637
Zr	178	177	175	194	202	198	214	215
Nb	50	48	48	49	50	49	50	50
Phenocrysts								
ol	10	11		7	12		7	8
cpx	-	-	-	-	-	-	-	-
pl	9	2		1	3		7	4
Groundmass								
ol	1	1		11	9		3	3
cpx	35	38		11	22		31	26
pl	20	20		19	15		22	35
gl	15	18		21	29		20	12
ox	10	9		9	7		10	12

Major- and trace-element analyses by XRF.
 CIPW normative minerals calculated with FeO/Fe₂O₃ = 0.90.
 Modal analyses based on 350 counts. ol = olivine, cpx = clinopyroxene,
 pl = plagioclase, gl = glass, and ox = oxide.

Mesa surface and is dotted by numerous volcanoes that reach elevations of nearly 1675 m (Hoffer and Sheffield, 1981). Mantle and crustal xenoliths and xenocrysts are common in the flows and maars of the area and include spinel peridotite, amphibole, and plagioclase (Ortiz, 1979). Abundant crystals of feldspar occur as loose crystals or as inclusions in bombs associated with the older cones. The crystals are anhedral to euhedral, white to colorless, and range from several millimeters to nearly 5 cm in diameter. They range in composition from anorthoclase to plagioclase (Hoffer and Hoffer, 1973).

Cinder cones are the most abundant volcanoes in the range; over 150 cones have been mapped (Hof-

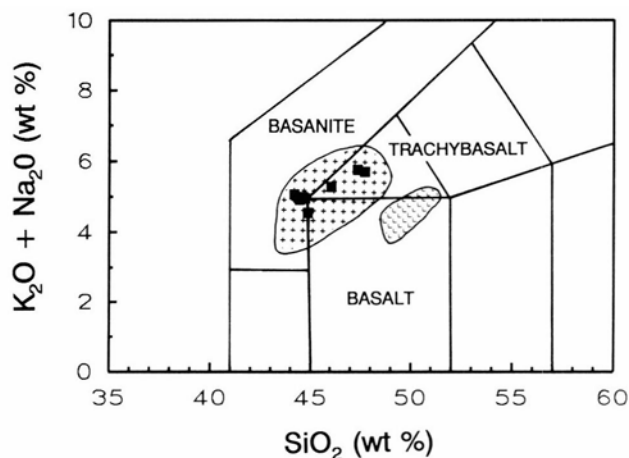


FIGURE 2—SiO₂ (wt%) versus K₂O + Na₂O (wt%). Analyses from the Potrillo volcanic field (Table 1) are shown as the square symbols. The field designated by the cross-pattern represents the range in composition for nepheline-normative lavas throughout southern New Mexico (Anthony et al., in review). The field designated by the "V" pattern represents hypersthene-normative lavas from the same area. Note that all lavas from the Potrillo volcanic field fall within the nepheline-normative group. Chemical field designations from LeBas et al. (1986).

fer, 1976). They range from 60 to 150 m in height and 300 to 900 m in diameter. They appear to be of at least two ages, with the younger cones large and steep-sided, with slopes from 20 to 25°, and older cones more subdued, with slopes from 10 to 20°. Two maars, Mt. Riley (not to be confused with the trachydacite Mt. Riley, see mileage 72.5) and Malpais, occur in the West Potrillo Mountains. They have been described by Bersch (1977) and Page (1975), respectively. **0.4**

27.6 Caliche outcrops mark location of northwest-trending fault. **4.9**

32.5 Road to right leads to Mt. Riley ranch; continue straight. **0.5**

33.0 Caliche outcrops mark location of north-striking fault. **0.5**

33.5 Basalt lava flows of the West Potrillo Mountains at 1:00-3:00. **0.9**

34.4 A-4 to the left; continue straight. **3.9**

38.3 Camel Mountain, a local landmark at 12:00. **0.7** 39.0 Cattle guard; Guzman Lookout, a young cinder cone at 1:30. **0.7**

39.7 Turn right onto dirt road and drive north to Malpais maar. Caution, drive slowly as the road is rough. **1.4**

41.1 **Stop I:** Leave cars and walk about 100 yards down the arroyo to examine the air-fall and base-surge deposits on the east side of Malpais maar (Fig. 3). Eruption began at Malpais maar with deposition of up to 15 m of bedded debris over the surrounding area. Thickest accumulations of tuffs are located where the base-surge clouds encountered nearby cinder cones and were forced to move upslope. The deposits wrap gently around this topography, dipping away from the cone summits at 5 to 20°. The style of eruption later changed to lava fountaining and tephra production, with construction of a cinder cone and flow complex within the crater. Late-stage activity included extrusion of parasitic lava flows and intrusion of dikes into the bedded-tuff sequence. The dikes are concentrated along the maar rim. A small, maar-type vent is found along the strike continuation of one of the dikes (Page, 1975). Sedi-

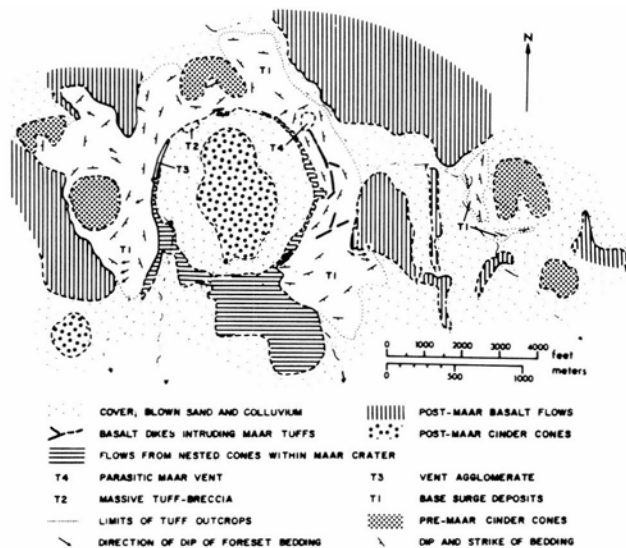


FIGURE 3—Geologic map of Malpais maar.

mentary structures, typical of base-surge deposits (Crowe and Fisher, 1973), are present throughout the bedded-tuff sequence. These structures include: (1) long wavelength, low amplitude, undulatory bedding (plane-parallel lamination); (2) asymmetrical, ripple-like to dune-like bed forms; (3) small-to large-scale crosslamination; and (4) bedding-sag deformation under bombs and blocks. The maar rim is nearly circular, approximately 1250 m in diameter, and is perhaps 10 to 15 m in height, although the lower contact is not exposed. Inward-dipping beds are exposed at three locations along the maar rim, dipping 30 to 35° towards the center of the crater. Outer-flank beds near the rim dip 5 to 20° away from the vent. Farther from the rim, bedding in the tuffs generally conforms to subdued pre-tuff topography, although crosslamination in ripple and dune bedforms indicate a consistent, radial transport for the base-surge clouds. **1.0**

- 42.1 **Stop II:** Cinder quarry in the crater of Malpais maar. Return to cars and retrace route to A-17. **2.4**
 44.5 Turn left on A-17 and travel east. **6.9**
 51.4 Mt. Riley ranch road on left; continue straight. **5.8**
 57.2 Cattle guard. **1.5**
 58.7 Turn left on A-08. **3.3**
 62.0 Site of abandoned marble quarry at the base of the East Potrillo Mountains at 9:00. **2.0**
 64.0 Cattle guard. **2.8**
 66.8 Turn right onto A-14. **1.6**
 68.4 Turn left and travel north to Hunt's Hole. 0.2 68.6 Turn left and travel around the south end of Hunt's Hole. **0.1**
 68.7 View of Hunt's Hole. Hunt's Hole is the smallest of three circular maar volcanoes in the westernmost part of the La Mesa surface. The other maars are

Kilbourne Hole located 3.4 km north of Hunt's Hole, and Potrillo maar 16.5 km to the south. The three maars are aligned north-south along the inferred down-to-the-west Fitzgerald fault; this fault is not exposed in the maars or on the La Mesa surface but is expressed by a line of topographic depressions. Hunt's Hole is excavated in mudstone and sandstone of the Pleistocene Santa Fe Group and an overlying basalt flow which represents the south end of the Aden-Afton volcanic centers. The age of the maar-forming event is probably less than 50,000 yrs based on the small degree of dissection and lack of weathering of the base-surge tuffs (Stuart, 1981). **1.0**

69.7 Cattle guard. **0.9**

70.6 Small spatter cone at 12:00. **1.8**

72.4 **Stop III:** Kilbourne Hole overlook (lunch stop). Kilbourne Hole (Fig. 4) is a maar 3.3 km long and 2 km wide. The floor of the depression is 250 to 90 m below the surface of the surrounding desert and is bordered by a 20 to 170 ft rim. Recent work by Seager (1987) indicates that an important process in the formation of the present crater is caldera-like collapse at the end of the volcanic cycle. Evidence for this interpretation includes: (1) the presence of large downfaulted masses of the tuff-ring material located at the base of the inner crater wall and beneath the crater floor, and (2) the small volume of pyroclastic material in the maar rim and on the La Mesa plains as compared to the volume of the crater. Age estimates of the maar range from 180,000 yrs (Seager et al., 1984) based on a K-Ar date on post-maar lavas at Potrillo maar, to 24,000 yrs based on the amount of pedogenic-carbonate development in soils of the Kilbourne rim ejecta (Gile, 1987). In addition, a fission-track date on apatite obtained

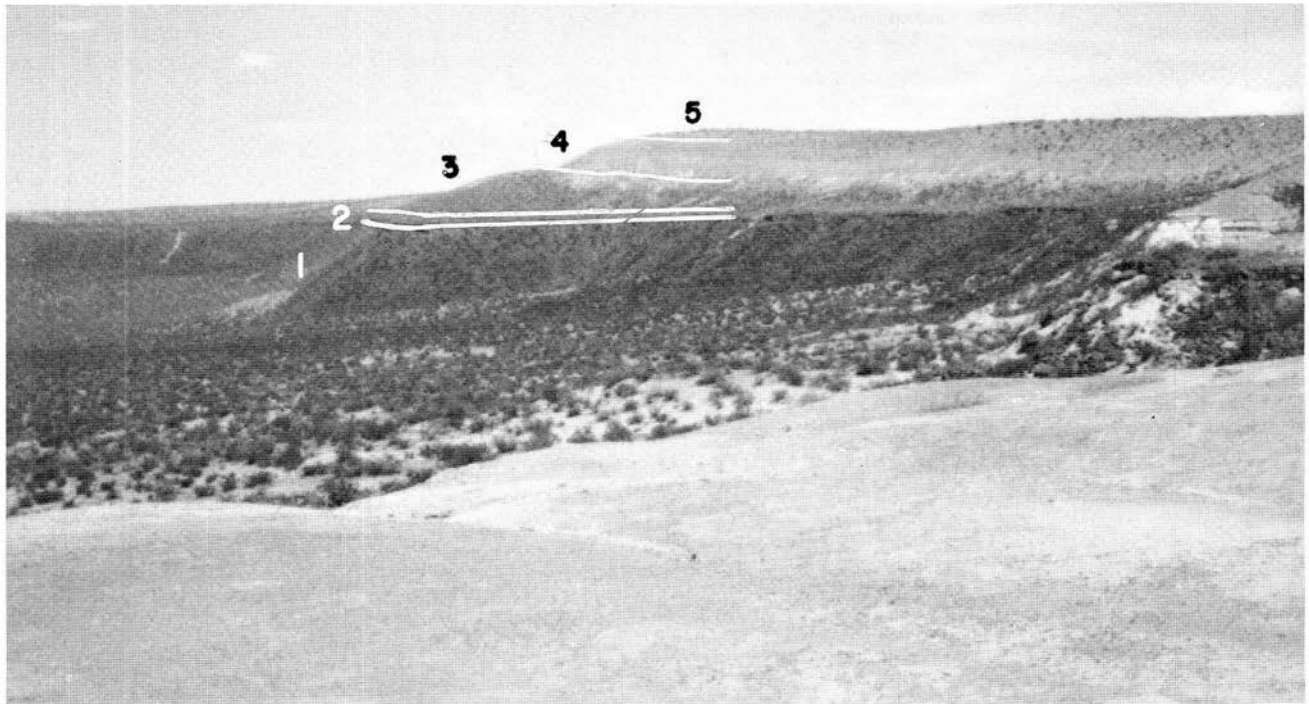


FIGURE 4—Kilbourne Hole, view to the north. The section consists of: (1) Santa Fe Group, covered by talus from lava flow; (2) lava flow; (3) coarse ejecta mantling rim deposits; (4) rim deposits of air-fall and base-surge origin; (5) Holocene blow sand.

from the outer surface of a basalt bomb yields an age of 80,000 yrs (V. Harder, pers. comm. 1988).

0.1

72.5 Return to main road; bear right toward Mt. Riley. Mt. Riley and Mt. Cox are two peaks from a single pluton. Mt. Riley, to the northeast, is the larger and reaches an elevation of 5915 ft (1804 m). The pluton is a steep-sided, domal intrusion of dense trachydacite (nomenclature of LeBas et al., 1986) of probable Tertiary age. It intrudes Cretaceous(?) sedimentary rocks and Tertiary volcanic and sedimentary rocks, and is composed of 58% plagioclase (andesine), 20% potassium feldspar, 14% quartz, 7% biotite and hornblende, and 1% magnetite (Millican, 1971). It contains 65.2% SiO₂ and 7.9% K₂O + Na₂O. **1.6**

74.1 Turn right. **2.0**

76.1 A-12 to the right; continue straight. **1.0**

77.1 Abandoned ranch on right. **0.2**

77.3 Gardner cones (Afton flows) at 12:00. **0.6**

77.9 Cinder cone of the West Potrillo field (two tanks on top of the cone) at 12:00. **1.1**

79.8 Cross flows of the West Potrillo field. **0.4**

79.4 Gate; continue straight. **0.4**

79.8 Turn left at gate. **0.1**

79.9 Turn right at gate. **0.9**

80.8 Road is on the flows of the West Potrillo field, Aden flows on the right at 12:00-5:00. **1.5**

82.3 Gate. **3.1**

85.4 Beyond water tank, Aden Crater at 2:00. **0.3**

85.7 Gate; bear right and pass through a second gate and then left. **1.8**

87.5 Turn right toward Aden Crater. **0.6**

88.1 **Stop IV:** Aden Crater, which lies on top of the Aden flows and along the Aden rift. It is thought that the Aden flows were emplaced along fissures associated with the Robledo fault and that the crater was built from younger central eruptions. It is classified as a small shield volcano or lava cone (DeHon, 1965). The base of the cone is approximately 4.5 km in diameter and composed of thin pahoehoe lava flows which slope gently outward from the summit at 35° (Hoffer, 1976). The cone rises about 50 m above the surrounding terrane and covers an area of approximately 15 km², with an estimated minimum lava volume of 0.3 km³ (Kahn, 1987). The age of the crater is probably less than 100,000 yrs based on surface freshness and soil development (tile, 1987).

The formation of Aden Crater involved the following sequence of events. A series of thin basaltic flows issued from a central vent and spread out radially, building a small shield volcano. This period of quiet activity was followed by a more explosive gas phase in which spatter was ejected, constructing a spatter rampart around the outer rim of the crater. The magma, after degassing, issued once again from the vent and formed a lava lake which was contained by the spatter rim. At several locations, lava breached the rim and flowed down the flank of the volcano. The low viscosity of the lava is indicated by the fact that several overflowing lava tongues and tubes are only 12-24 cm wide, but flowed 40-50 m down the side of the volcano.

At the close of this effusive period of activity, a portion of the ponded lava drained back down the vent and the lava lake solidified and collapsed over the vent. After solidification of the lava lake, which produced tension cracks parallel to the spatter rim, a period of minor fountaining occurred in the central crater and on the southeast flank of the cone producing a series of spatter cones. Final activity was confined to a fumarole on the east rim of the crater (Hoffer, 1990).

Geologic tour of Aden Crater

Distance: roundtrip = 2.5 km, time = 3 hrs, 5 stops.

Total
Distance

- 0 Parking area, northwest flank of Aden Crater (Fig. 5). **360 m**
- 0.36 km Walk up the slope of the volcano toward the south-southeast to view a series of spatter cones at Stop 1. Spatter cones are generally steep-sided, small volcanic cones which are composed of ejected clots or globs of magma that were still somewhat fluid when they accumulated. Note the taffy-like appearance on the outer surface of the fragments. Note also the alignment of the cones toward the southwest along a probable fracture or fissure zone on the flank of Aden. **300 m**
- 0.66 km Climb up over the spatter rim and across the floor of Aden Crater to the large spatter cone at Stop 2. The floor of Aden was formed by a series of basaltic lava flows that flooded the interior crater and were dammed by the spatter rim. The depth of this former lava lake is unknown, but a hole drilled into the lake in 1970 by NASA penetrated over 30 m of lava. The spatter cone of this stop sits on top of the lava lake and was one of the latest events in the development of Aden. On the west side of the cone (Fig. 5) note that a portion of the crater rim has slid some distance down the

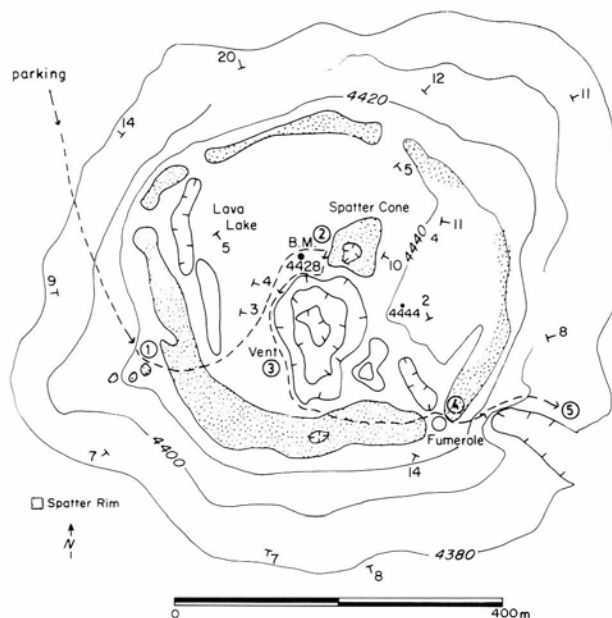


FIGURE 5—Index map and Stops 1-5, Aden Crater.

slope. The grooved and flattened surface upslope from the slide block indicates that the rim had not yet completely solidified when the slide occurred. **180 m**

0.84 km Walk south and then southwest around the west side of the crater vent to Stop 3. This is the location of the primary vent of the volcano; it measures approximately 160 by 100 m and is over 17 m deep. The present configuration of the vent is due to collapse which occurred at the close of the period of lava-lake formation. During its active phase, the vent alternated between fountaining and quiet effusion of basaltic lava. Note, across the vent to the southwest, the moderate-size hill covered with red to reddish-brown spatter. This spatter probably accumulated downwind during fountaining episodes of the vent. **270 m**

1.10 km Continue south from the vent and then follow the crude trail on the spatter rim of the crater to the fumarole at Stop 4. The Aden fumarole is situated in the southeast rim of the crater. The fumarole opening is approximately 2 m in diameter at the surface and is 33 m deep. In 1928, the well preserved remains of a ground sloth (*Nothrotheriops*) were discovered at the bottom of the fumarole. C¹⁴ data on the sloth bones indicate an age of 11,080 ± 200 yrs. **300 m**

1.40 km Walk east down the flank of the volcano to view the collapsed portion of a lava tube at Stop 5. The collapsed portion of the lava tube measures 230 m long, 60 m wide, and 9 m deep. A small spatter mound has been constructed at the southeast rim of the tube. This lava tube can be traced under the rim of Aden, just north of the fumarole, into the floor of the crater where numerous collapse depressions and tube cross-sections exist.

End of Aden Crater walking tour. Return by walking the lower slopes of the volcano, approximately 1.1 km. **0.6**

88.7 Return to main road and turn right. **4.2**

92.9 Turn right on A-17 and travel parallel to railroad tracks. **0.5**

93.4 Cattle guard. **4.5**

97.9 Cattle guard. **2.5**

100.4 Cross basal flows of the Afton flows. **0.5**

100.9 Turn left, cross railroad tracks and bear left. **0.2**

101.1 Cattle guard. **0.1**

101.2 Turn right onto B-4. **2.1**

103.3 Pass ranch. **0.1**

103.4 Bear left and continue straight. **1.3**

104.7 Government installation on right. **0.7**

105.4 Cattle guard. **2.4**

107.8 Turn right onto B-8. **1.0**

108.8 Cattle guard and start of pavement. **0.4**

109.2 Cattle guard, El Paso Natural Gas pumping station on left. **1.7**

110.9 Cattle guard. **1.1**

112.0 Little Black Mountain cinder cone at 9:00. **1.7**

113.7 Turn off to Black Mountain on right.

Four eruptive centers, extending north-south approximately 38 km², occur along the eastern margin of the La Mesa surface. They are, from north to south, Santo Tomas, San Miguel, Little Black Mountain, and Black Mountain. Black Mountain

and Santo Tomas both display multiple eruptions.

The Black Mountain area consists of eight volcanic cones and at least six flows (Hoffer, 1971). In the center of the area are four cinder cones, the largest being the Black Mountain cone. It is symmetrical in outline, with a diameter of 700 m and a height of 30 m.

Cinder-spatter cones are located north and south of Black Mountain. These cones possess a low-sloping base of cinder and spatter and are capped by a rim of agglutinated spatter. The layers of spatter and dribble dip steeply inward toward the center of the cone. The cones range from 30 to 80 m in diameter and from 5 to 14 m in height. **2.5**

116.2 Cattle guard. **1.9** 118.1

Cattle guard. **0.4** 118.5 Cross

bridge. **0.8** 119.3 Intersection of

NM-28 and B-8; turn left onto NM-

28, which is part of the Don Juan de Oñate trail, a

historic route commemorating Don Juan de Oñate's

travels through New Mexico. Cotton, alfalfa, hay,

and chili are grown in the fields along NM-28. **0.3**

119.6 Sierra Vista nursery and greenhouses on the left.

Organ Mountains at 1:00-2:00. On Day 3 we will

drive along the foothills of this mountain range.

1.8

121.4 Road junction with County Road 189 at stop sign.

Turn left to remain on NM-28. **1.1**

122.5 Bend in road. Little Black Mountain at 10:00. **0.3**

122.8 Edge of La Mesa, one of numerous small farming communities on NM-28. La Mesa is Spanish for "table" and was named for the nearby Black Mesa lava flow. **2.6**

125.4 La Clinica de Familia on the right. Colorful murals such as this are common on public buildings in Old Mexico. Edge of San Miguel. **0.6**

126.0 Junction with County Road 192. Continue straight on NM-28 through San Miguel. **0.2**

126.2 San Miguel Catholic Church on the left is built with boulders from the San Miguel and Santo Tomas flows to the west. **0.3**

126.5 North end of San Miguel. San Miguel lava flow is at 9:00. This flow has been dated by K/Ar as 490,000 ± 30,000 yrs (Seager et al., 1984). However, recent sedimentologic studies by Gile (1990) suggest that the age is approximately 200,000 yrs. The Santo Tomas flow, consisting of a cinder cone and three associated flows (Hoffer, 1971), is at 10:00- 11:30. **0.5**

127.0 MP 20. Entering Stahmann Farms, one of the world's largest pecan groves which markets the Del Cerro pecans. Stahmann Farms end at the Rio Grande, although many smaller, privately owned groves continue along NM-28. **3.0**

130.0 MP 23. Crossing the Rio Grande. Picacho Peak and the Robledo Mountains at 11:00. On Day 3 we will discuss the geology of the Robledo Mountains (Hawley, 1978). **3.1**

133.1 Entering San Pablo. **1.6**

134.7 Junction with County Road 373. Continue straight on NM-28. **0.8**

135.5 Road junction. Turn left onto Calle de Parian into La Mesilla (Spanish for "Little Table"). La Mesilla was built on a small mesa above the Rio Grande in

1850 and has been a state monument since 1957. The Butterfield Overland Trail passed through La Mesilla and famous historic characters such as Billy the Kid visited the town. Today a plaza surrounded by the church and numerous shops and restaurants draw tourists from throughout the world.

End of road log.

Geochemistry of late Cenozoic lavas of southern New Mexico

Introduction

Late Cenozoic mafic lavas from southern New Mexico fall into two chemical groups: (a) low-silica, nepheline-normative basanites, alkali basalts, and trachybasalts, and (b) higher-silica, hypersthene-normative subalkali basalts (Fig. 2). Both types have similar ages and both are found in the axis of the rift as well as on its flanks. In any individual

volcanic field the lavas will belong predominantly to one chemical group or to the other. For instance, the Jornada del Muerto, Animas, and Carrizozo fields belong to the hypersthene-normative group, and the Geronimo, Elephant Butte, and Palomas fields belong to the nepheline-normative group (Anthony et al., in review). The Potrillo volcanic field is of the nepheline-normative type, with lavas from various parts of the field ranging from basanites through alkali basalts to trachybasalts (Table 1, Fig. 2).

Inter-field chemical variations

The hypersthene-normative group of lavas is characterized by lower concentrations of the incompatible elements Rb, Sr, Zr, Nb, and TiO_2 (Figs. 6a, 7a). Although the factors responsible for generating the two chemical groups, e.g. volatile contents, degree of partial melting, and depth of magma generation, are still under investigation, the data at hand suggest that variable degrees of partial melting may have played a significant role. Higher concentrations of incompatible elements (particularly Nb and Sr) in the nepheline-normative lavas are consistent with their genesis by lesser degrees of partial melting. Also, as noted by Luhr et

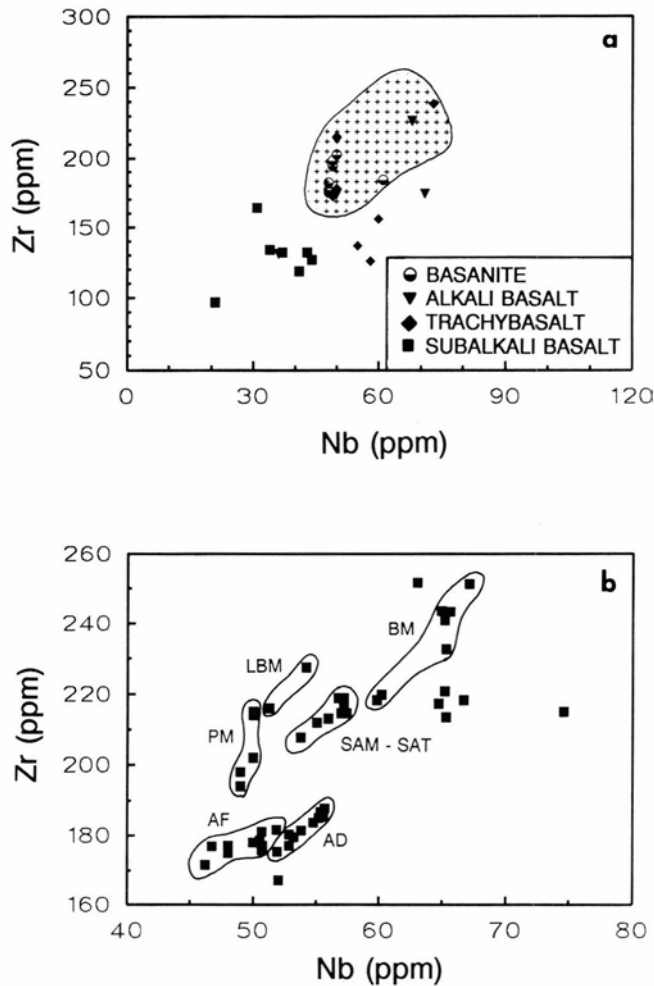


FIGURE 6—Zr versus Nb in ppm. **a**, Hypersthene-normative lavas (i.e. the subalkali basalts) have lower concentrations of both Zr and Nb compared to the nepheline normative lavas (i.e. the basanites, alkali basalts, and trachybasalts). The field designated by crosses represents the range of compositions found in the Potrillo volcanic field. **b**, Compositions of lavas from the Potrillo volcanic field (Table 2). In approximate stratigraphic order the volcanic centers are: AF = Afton flows; Ad = Aden flows; PM = Potrillo maar; LBM = Little Black Mountain; SAM - SAT = San Miguel and Santo Tomas; BM = Black Mountain. Unlabelled points represent samples from the West Potrillo Mountains.

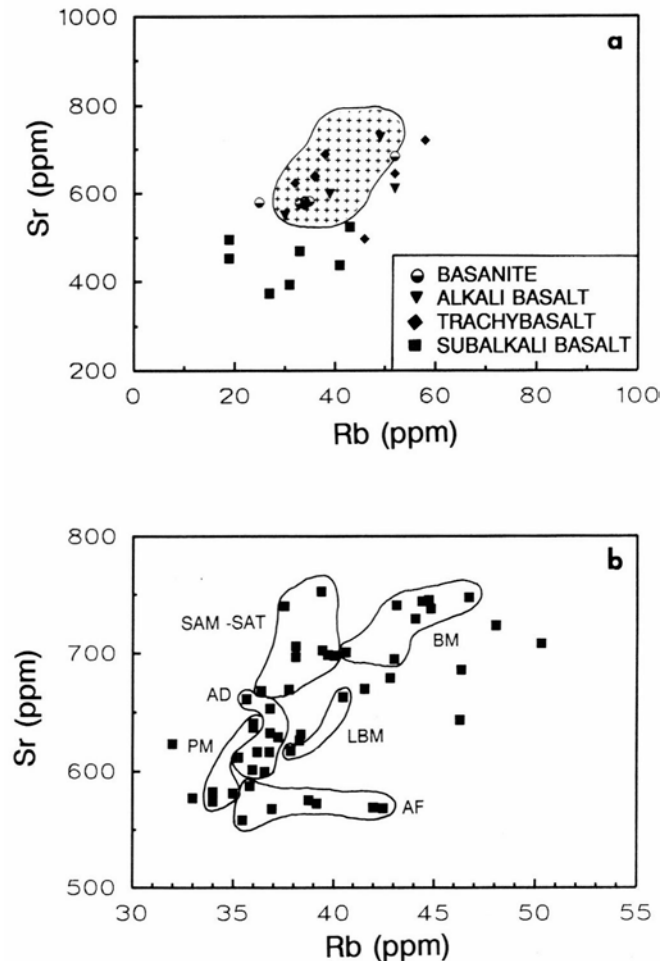


FIGURE 7—Sr versus Rb in ppm. **a**, Hypersthene-normative lavas (i.e. the subalkali basalts) have lower concentrations of these elements compared to the nepheline-normative lavas (i.e. the basanites, alkali basalts, and trachybasalts). The field designated by crosses represents the range of compositions found in the Potrillo volcanic field. **b**, Compositions of lavas from the Potrillo volcanic field. Sample designations as in Fig. 6b.

al. (1989) for similar lavas from San Luis Potosi, Mexico, of the various hypotheses for generating undersaturated lavas, incremental partial melting best explains the observed correlation between silica undersaturation and incompatible-element enrichment.

Intra-field chemical variations

Magmas of both the nepheline and hypersthene groups appear to have resided temporarily in low-pressure reservoirs. Lavas of both groups share a similar phenocryst population of olivine and plagioclase with minor clinopyroxene. These phases are near liquidus at pressures less than approximately 10 kb, corresponding to depths at or above the Moho (30 to 35 km) in this region (Keller et al., 1990). Further, within a volcanic field, the incompatible elements Zr, Nb, Sr, and Rb increase up-section, suggesting sufficient residence time for crystal fractionation and/or crustal assimilation. This increase in incompatible elements up-section has been documented for lavas from the Jornada del Muerto field (a hypersthene-normative field) and the Potrillo volcanic field (Table 2, Figs. 6b, 7b). The shallow level of ponding is consistent with barometric determinations for crustal and mantle xenoliths transported with the magmas during their final ascent.

TABLE 2—XRF analyses of trace-element concentrations (ppm).

	Malpais Maar					West Potrillo Mountains				
	M-1-1	M-1-2	M-2-2	M-3-1	M-4	4300-5-1	WPM-6	WPM-7	WPM-8	WPM-10
Rb	45	48	38	50	38	50	46	46	72	43
Sr	745	723	696	708	631	1075	685	643	959	679
Y	26	26	25	28	25	27	26	27	31	28
Zr	217	221	167	218	177	215	213	252	301	204
Nb	65	65	52	67	57	75	65	63	89	59

	Aden flows									
	AD-1	Ad-1-H	Ad-1-A	Ad-2	Ad-2-A	Ad-3	Ad-3-A	Ad-4	Ad-5	Ad-6
Rb	37	37	38	37	35	36	37	36	36	37
Sr	629	632	626	616	612	661	653	601	616	600
Y	26	26	26	26	25	28	25	27	25	26
Zr	185	188	184	181	180	185	187	177	180	175
Nb	55	56	55	54	53	56	55	53	53	52

	Afton flows						
	AF-1	AF-2-X	AF-2	AF-2-A	AF-3	AF-4	AF-5
Rb	39	42	42	39	37	35	36
Sr	575	569	568	572	568	558	587
Y	28	27	28	27	29	26	28
Zr	182	176	177	178	181	172	177
Nb	52	51	51	51	51	46	47

	Black Mountain							Little Black Mtn	
	BM-1	BM-2	BM-3	BM-4	BM-5	BM-5-A	BM-5-H	LBM-1	LBM-2
Rb	41	44	43	47	45	44	43	38	41
Sr	700	744	695	747	737	729	740	618	662
Y	30	31	29	33	32	31	31	29	30
Zr	220	232	218	251	243	241	243	216	227
Nb	60	65	60	67	65	65	66	51	54

	Santo Tomas						San Miguel		
	SAT-2	SAT-3	SAT-4	SAT-4-A	SAT-4-H	SAT-5	SAM-1	SAM-X	SAM-A
Rb	38	36	39	38	38	42	40	39	40
Sr	669	668	753	740	705	670	698	702	698
Y	29	29	29	28	28	28	30	29	29
Zr	212	213	215	215	215	204	219	218	219
Nb	55	56	57	57	57	54	57	57	57

X Duplicate sample from same hand specimen.

A Sample cleaned in 10% HCl.

H Sample cleaned in warm 10% HCl.

XRF facility, for his expert and patient analysis. This manuscript benefited from the comments of Nancy McMillan, New Mexico State University, and Jacques Renault, New Mexico Bureau of Mines & Mineral Resources.

References

- Anthony, E. Y., Hoffer, J. M., and Waggoner, W. K. (in review), Compositional diversity in late Cenozoic lavas in the Rio Grande rift and Basin and Range province, southern New Mexico.
- Bersch, M. G., 1977, Petrography and geology of the southern West Potrillo Basalt Field, Dona Ana County, New Mexico: Unpublished MS thesis, University of Texas at El Paso, 60 pp.
- Crowe, B. M., and Fisher, R. V., 1973, Sedimentary structures in base-surge deposits with special reference to cross-bedding, Ubehebe Craters, Death Valley, California: Geological Society of America, Bulletin, 94: 663-682.
- DeHon, R. A., 1965, Maare of La Mesa: New Mexico Geological Society, Guidebook 16: 204-209.
- Gile, L. H., 1990, Chronology of lava and associated soils near San Miguel, New Mexico: Quaternary Research, 33: 37-50.
- Gile, L. H., 1987, A pedogenic chronology for Kilbourne Hole, southern New Mexico. Soil Science Society of America, Journal 51: 746-760.
- Hawley, J. W. (compiler), 1978, Guidebook to Rio Grande rift in New Mexico and Colorado: New Mexico Bureau of Mines & Mineral Resources, Circular 163: 241 pp.
- Hoffer, J. M., 1990, Geologic tour of Aden Crater: El Paso Geological Society, Guidebook to the Fall 1990 Field Trip, 42 pp.
- Hoffer, J. M., 1976, Geology of Potrillo basalt field, south-central New Mexico: New Mexico Bureau of Mines & Mineral Resources, Circular 149: 30 pp.
- Hoffer, J. M., 1971, Mineralogy and petrology of the Santo Tomas—Black Mountain basalt field, Potrillo volcanics, south-central New Mexico: Geological Society of America, Bulletin, 82: 603-611.
- Hoffer, J. M., and Hoffer, R. L., 1973, Composition and structural state of feldspar inclusions from alkali olivine basalt, Potrillo basalt, southern New Mexico: Geological Society of America, Bulletin, 84: 2139-2142.
- Hoffer, J. M., and Sheffield, T. M., 1981, Geology of the West Potrillo Mountains, south-central New Mexico: El Paso Geological Society, Guidebook, pp. 79-82.
- Kahn, P. A., 1987, Geology of Aden Crater, Dona Ana County, New Mexico: Unpublished MS thesis, University of Texas at El Paso, 90 pp.
- Keller, G. R., Morgan, P., and Seager, W. R., 1990, Crustal structure, gravity anomalies, and heat flow in the southern Rio Grande rift and their relationship to extensional tectonics: Tectonophysics, 174: 21-37.
- LeBas, M. J., Le Maitre, R. W., Streckeisen, A., and Zanettin, B., 1986, A chemical classification of volcanic rocks based on the total alkali-silica diagram: Journal of Petrology, 27: 745-750.
- Luhr, J. F., Aranda-Gomez, J. J., and Pier, J. G., 1989, Spinel—lherzolite-bearing Quaternary volcanic center in San Luis Potosi, Mexico. I. Geology, mineralogy and petrology: Journal of Geophysical Research, 94: 7916-7940.
- Millican, R. S., 1971, Geology and petrography of the Tertiary Riley—Cox Pluton, Doña Ana County, New Mexico: Unpublished MS thesis, University of Texas at El Paso, 87 pp.
- Ortiz, T. S., 1979, Megacrysts and mafic and ultramafic inclusions of the southern West Potrillo Basalt Field, Dona Ana County, New Mexico: Unpublished MS thesis, University of Texas at El Paso, 95 pp.
- Page, R. O., 1975, Malpais Maar volcano: New Mexico Geological Society, Guidebook 26: 135-137.
- Seager, W. R., 1987, Caldera-like collapse at Kilbourne Hole maar, New Mexico: New Mexico Geology, 9: 69-73.
- Seager, W. R. (in press), Geology of southwest quarter of Las Cruces and northwest El Paso 1° x 2° sheets, New Mexico: New Mexico Bureau of Mines & Mineral Resources, Geologic Map 60, scale 1:125,000.
- Seager, W. R., and Mack, G. H., 1986, Summary of geology of East Potrillo Mountains area: El Paso Geological Society, Guidebook, pp. 158-159.
- Seager, W. R., Hawley, J. W., Kottlowski, F. E., and Kelley, S. A., 1987, Geology of east half of Las Cruces and northeast El Paso 1° X2° 2° sheets, New Mexico: New Mexico Bureau of Mines & Mineral Resources, Geologic Map 57, scale 1:125,000.
- Seager, W. R., Shafiqullah, M., Hawley, J. W., and Marvin, R. F., 1984, New K—Ar dates from basalts and the evolution of the southern Rio Grande rift: Geological Society of America, Bulletin, 95: 87-99.
- Stuart, C. J., 1981, Hunt's Hole Maar volcano, Doña Ana County, south-central New Mexico: El Paso Geological Society, Guidebook, pp. 64-72.

Acknowledgments

Chemical compositions reported herein were obtained by XRF analysis at the New Mexico Bureau of Mines & Mineral Resources. We thank Chris McGee, manager of the

Day 3: Las Cruces to Albuquerque**G. R. Keller and V. T. McLemore**

The third day of the trip will follow the itinerary set forth in the following guidebook: Callender, J. F., Hawley, J. W., and Keller, G. R., 1989, Rio Grande rift: 28th International Geological Congress, Guidebook to Field Trip T318, 37 pp. A copy of this guidebook will be provided as

part of the registration package. In addition to discussions by the field-trip leaders, Richard W. Harrison and Richard P. Lozinsky will help with the stops in the Truth or Consequences area, and Lee R. Russell and Richard P. Lozinsky will help with stops in the Albuquerque basin.

Open-system magmatic evolution of the Summer Coon and Del Norte volcanoes, Conejos Formation, San Juan Mountains volcanic field, Colorado

Don F. Parker, D. Anne Grau, and Charles D. Thomas

Department of Geology, Baylor University, Waco, Texas 76798-7354

Introduction

Many modern petrologic investigations have emphasized open-system behavior in magmatic systems, where crystal fractionation, assimilation of country rock, and magma mixing provide genetic relations between end members of igneous suites (Hildreth et al., 1986; Dungan et al., 1986; Smith and Leeman, 1987). Petrologists have, of course, recognized these controls for many years, but usually were only able to document fractional crystallization because of limitations of technique. Today, electron-probe microanalysis of minerals, trace-element analysis, and isotopic studies of rocks aid petrologists in identifying, respectively, out-of-range phenocrysts in mixed rocks and the geochemical and isotopic signatures of assimilated country rock in magmas.

This study tests the applicability of open-system behavior to the evolution of igneous rocks of the Summer Coon and Del Norte volcanoes. Field evidence for open-system behavior, including compositional banding of lava, mafic enclaves, and inclusions of basement gneiss in dikes and lavas are examined, and major- and trace-element data bearing on the question of assimilation of crustal rocks are presented. The first description of the Del Norte volcano is given, and data from previous studies of the Summer Coon volcano are amplified.

Geologic setting

The San Juan volcanic field (SJVf) was formed during the mid-Cenozoic as part of a broad continental arc associated with shallow subduction of oceanic lithosphere along the southwestern margin of North America (Lipman et al., 1971; Cross and Pilger, 1978). The SJVf is an erosional remnant of a larger field that covered much of south-central Colorado and northern New Mexico (Steven, 1975). Subduction-related magmatism spanning the interval from 35 to 30 Ma produced a coalescing assemblage of composite volcanoes of largely andesitic composition, which is overlain by thick ash-flow tuffs erupted from caldera sources during the period 30-26 Ma (Lipman et al., 1970; Lipman, 1989). Volcanism associated with development of the Rio Grande rift began 26 Ma ago and has continued to the present. The San Luis Valley, formed by an asymmetric graben associated with the Rio Grande rift, lies east of the SJVf.

Summer Coon and Del Norte volcanoes

The Summer Coon and Del Norte volcanoes belong to the older episode of intermediate volcanism that is represented in the eastern SJVf by the Conejos Formation (Fig. 1). The Summer Coon volcano (SCV) is a highly dissected

composite cone 12 km in diameter, with a well-exposed, extensive radial dike swarm (Lipman, 1968, 1976; Mertzman, 1971; Noblett and Loeffler, 1987). Igneous rocks associated with the SCV span the compositional spectrum from high-potassium basaltic andesite to rhyolite (Fig. 2). The Del Norte volcano (DNV) is a highly eroded silicic shield composed of thick lava flows, which span a relatively narrow range of compositions from high-potassium silicic andesite to dacite.

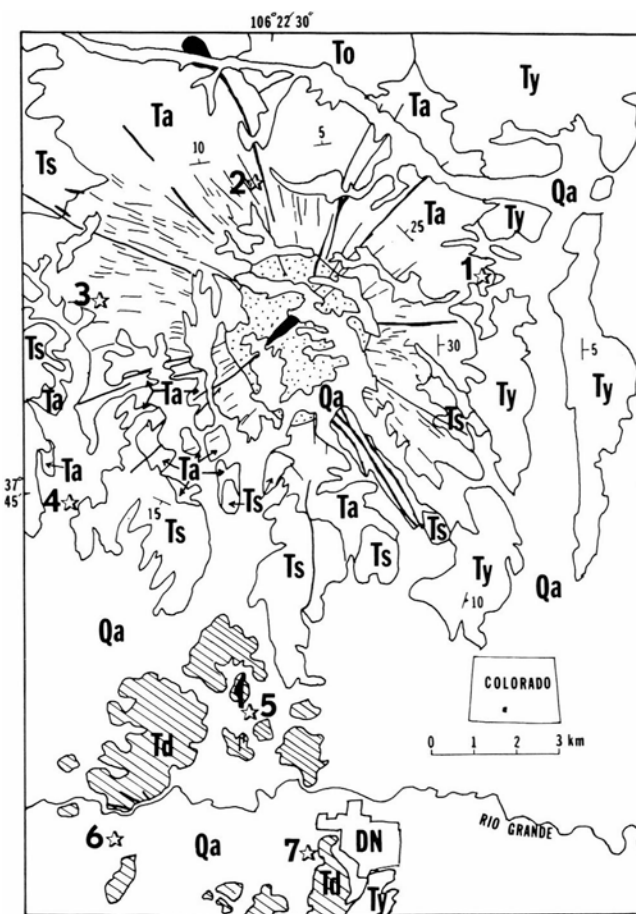


FIGURE 1—Geologic sketch map of the Summer Coon and Del Norte volcanoes (after Zielinski and Lipman, 1976). To = undifferentiated older Conejos rocks; Td = Del Norte volcanic rocks; Ta = cone unit of Summer Coon volcano; Ts = late silicic units of Summer Coon volcano; Ty = younger volcanic rocks (largely ash-flow tuffs); Qa = Quaternary alluvium and colluvium. Major dikes are shown by black lines. The central intrusive complex of the Summer Coon volcano is stippled. The town of Del Norte (DN on map) is located along the south-central margin of the map. Field-trip stops are numbered and denoted by stars.

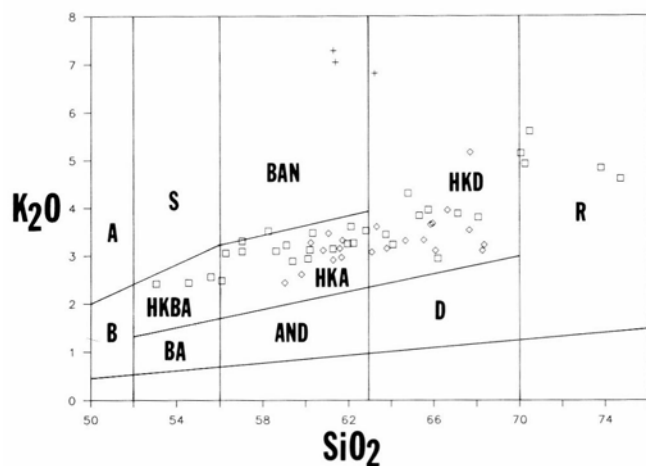


FIGURE 2—Classification of Summer Coon (open squares) and Del Norte (open diamonds) igneous rocks according to the K_2O - SiO_2 scheme of Peccerillo and Taylor (1976). Biotite-gneiss inclusions (crosses) are shown for reference. B = basalt; HKBA = high-potassium basaltic andesite; HKA = high-potassium andesite; HKD = high-potassium dacite; R = rhyolite; BA = basaltic andesite; AND = andesite; D = dacite; A = absarokite; S = shoshonite; BAN = banakite. The unlabeled fields along the base of the diagram represent low-potassium basalt through rhyolite.

The oldest eruptive unit of the SCV is the Tsa unit of Lipman (1976) (Ta in Fig. 1). It is largely composed of thick, coarse volcanic breccias that are mostly debris-avalanche and lahar deposits formed in association with explosive eruptions. Lava flows are locally common within the Ta unit, but are subordinate in volume to the breccias. Rock compositions range from basaltic andesite to dacite, with andesite most abundant. The Ta unit is overlain by packages of silicic lavas (Ts in Fig. 1), mostly on the southern flank of the volcano, erupted in the sequence rhyolite—dacite (Thomas, 1988; Parker and Thomas, 1988). Eruptions at SCV were fed from a large radial dike swarm. Dike compositions mirror the compositions of flows. Basaltic-andesite and andesite dikes are mostly thin (0.5-3 m thick), whereas dacite and rhyolite dikes can be much thicker. A central region of fine- to coarse-grained intrusions probably originally underlay the summit region of the composite cone (Mertzman, 1971).

Whole-rock chemistry and mineralogy

Chemical analyses of igneous rocks from the SCV have previously been given in Mertzman (1971) and Zielenki and Lipman (1976). Conclusions of this report are based on 60 new whole-rock major- and trace-element analyses completed at Baylor University. Broadly, the igneous rocks constitute a suite ranging from high-potassium basaltic andesite to rhyolite, with an average composition of silicic andesite (Figs. 2, 3). These results are similar to those reported by Mertzman (1971) for the SCV and by Lipman et al. (1978) for early intermediate-composition rocks of the entire SJVF. Harker diagrams (not illustrated) show linear correlations between oxides of major elements and silica, with only the alkali oxides showing appreciable enrichment.

Major-phenocryst chemistry of SCV rocks is summarized in Figs. 3 and 4. Plagioclase (pc), magnetite (mt), and apatite occur in all samples, and zircon occurs in most samples. Olivine (ol) occurs only in basaltic andesite and some andesite. Clinopyroxene (cpx) is abundant in basaltic andesite and occurs with orthopyroxene (opx) in andesite.

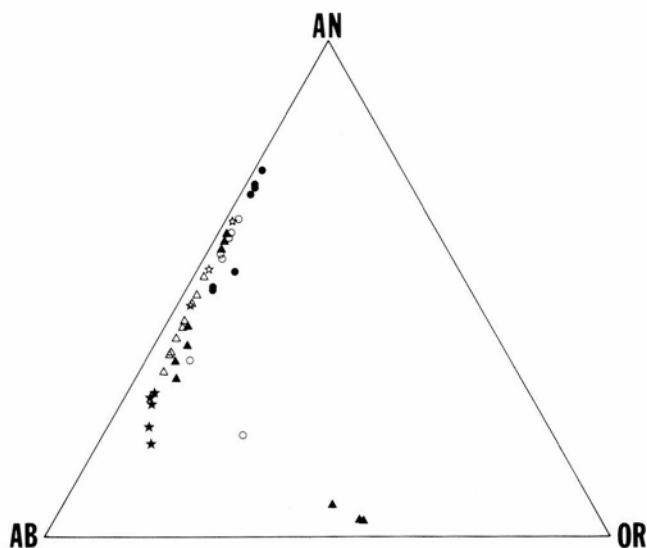


FIGURE 3—Feldspar compositions plotted in an-ab-or triangle. Filled circles = basaltic andesite; empty circles = andesite; filled triangles = silicic andesite; empty triangles = dacite; filled stars = rhyolite. Empty stars = hornblende andesite of Del Norte volcano.

Some dacites have opx. The only alkali-feldspar grains discovered are suspected to be disaggregated crystals from inclusions of hypabyssal intrusions in a highly porphyritic silicic-andesite lava. DNV rocks are similar, but contain abundant hornblende (hbl) in all rocks, including andesite, where it occurs in-lieu of pyroxene. Hornblende is only abundant in dacite and some rhyolite of the SCV. Biotite (bi) is common in the most evolved rocks of both volcanoes.

Summary of trip itinerary

This field trip consists of seven stops. The first four stops are concerned with the Summer Coon volcano (SCV). The stops provide a representative look at the different geologic units constituting the SCV (Fig. 5). Stop 1 examines intermediate lava flows of the Ta unit. Stop 2 emphasizes dikes, especially an andesite dike with abundant, large gneiss inclusions. Stop 3 focuses upon the breccias within the Ta unit, and Stop 4 examines late silicic flows of the SCV. After lunch, the last three stops concern the Del Norte volcano (DNV). Stop 5 examines the large dacitic dike of Indian Head. Stop 6 is an overview of a silicic eruptive center on the west flank of the DNV, and Stop 7 examines intermediate lava and a dacite dome on Lookout Mountain, just outside of Del Norte, Colorado. The general theme of all the stops will be to underline field evidence for open-system behavior in these volcanoes.

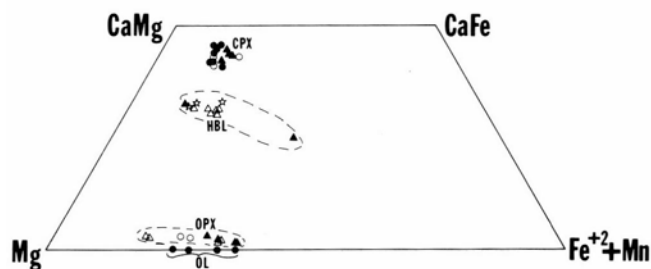


FIGURE 4—Clinopyroxene (cpx), orthopyroxene (opx), olivine (ol), and hornblende (hbl) plotted in pyroxene quadrilateral. Symbols as in Fig. 3.

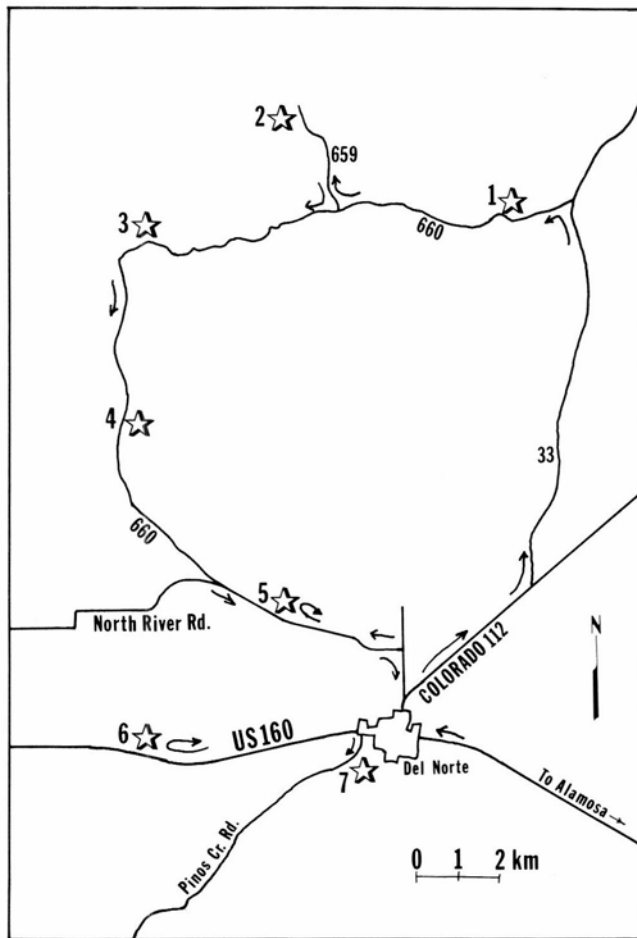


FIGURE 5—Road map for stops (numbered and indicated by stars). Lunch will be in Del Norte between Stops 4 and 5.

Field trip

Directions to Stop 1

The trip starts at the intersection of US-285 and US-160 in downtown Alamosa, Colorado. Proceed west on US-160 through Monte Vista, Colorado, to Del Norte, Colorado (about 30 mi). In Del Norte, turn north on CO-112 and proceed approximately 3.2 mi to the intersection with the La Garita Road (Rio Grande County 33) (Fig. 5). Turn left onto the La Garita Road, which becomes unpaved. The road enters a strike valley between west-facing cuestas formed by, respectively, the Fish Canyon Tuff to the west and the Carpenter Ridge Tuff to the east (both lumped in Ty of Fig. 1). These tuffs were erupted from calderas in the central San Juan Mountains. Continue north on the La Garita Road to the intersection with Forest Service Road 660 (about 6 mi from the intersection with CO-112). Turn left on Forest Road 660 (also known as Road A32) and proceed about 1 mi to Stop 1, which is located along the eastern extremity of the Summer Coon volcano where a small stream valley emerges from the eroded remnants of the volcano.

Stop 1

The Ta unit of Fig. 1 is dominated by coarse, crudely layered, poorly sorted breccia deposits, which largely formed by mass-wasting processes on the flanks of the SCV (Fig. 6). Lava flows, however, are locally abundant in the Ta unit,

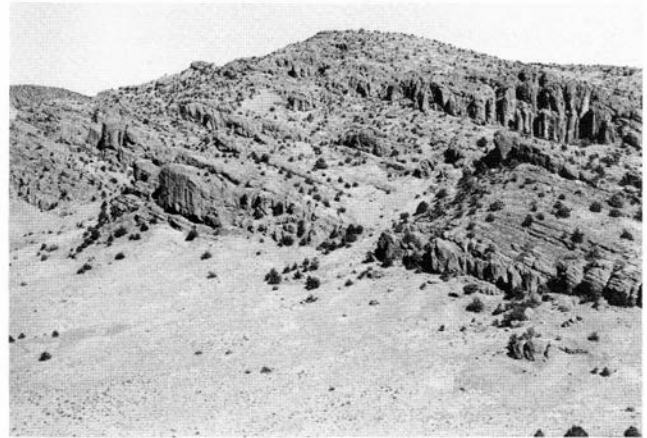


FIGURE 6—Typical exposure of main-cone unit (Ta) of Summer Coon volcano (view north from Forest Service Road 660 west of Stop 1).

and Stop 1 contains an unusual concentration of these lava flows in the upper part of the Ta unit.

At least three dark, vesicular andesite lavas are overlain by two flows of silicic andesite. The andesite lavas (Analysis A, Table 1) crop out in the small hill next to the road, and in streamcuts, and possess highly scoriaceous flow tops. Silicic-andesite lava (Analysis B, Table 1) forms cliffs along the northern margin of the streambed. The two silicic-andesite flows are similar chemically and mineralogically and could be lobes from a single eruption. The upper silicic flow is 15–20 m thick, overlies andesitic breccia, and is capped by a thin flow breccia. Well-developed foliation is parallel to the 12° dip of the unit near the base, but steepens upward into ramp structures.

Andesite lavas, such as exposed at this stop, show textural and mineralogical evidence for magma mixing and assimilation of crustal rocks. Evidence for magma mixing includes out-of-range phenocrysts, compositional banding of lavas, and mafic enclaves with acicular hornblende interpreted to be quickly chilled lumps of mafic magma mixed with andesite magma (Bacon, 1986). Out-of-range phenocrysts include olivine mantled by cpx and highly resorbed opx mantled by cpx in andesite (Fig. 7). Normally, neither of nor opx would be present in a mafic andesite. Evidence

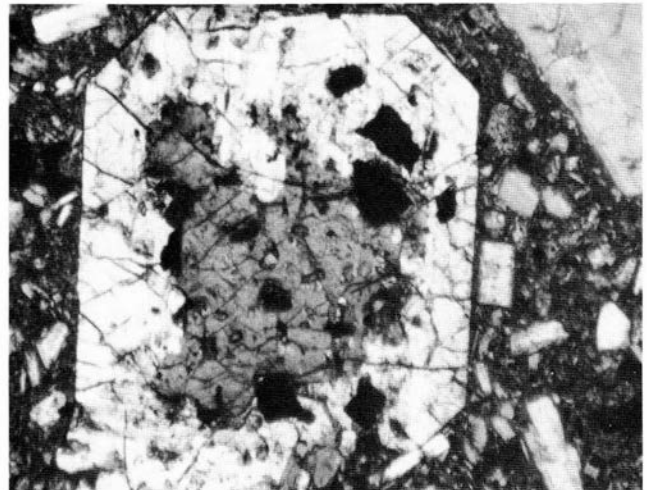


FIGURE 7—Photomicrograph of clinopyroxene grain (approximately 1 mm in diameter) with an amoeboid orthopyroxene core and magnetite inclusions in an ejected andesite block (crossed nicols).

TABLE 1—Whole-rock analyses, Summer Coon and Del Norte volcanoes.

Analysis Stop Sample	A 1 89662	B 1 87703	C 2 90602	D 2 90601	E 2 83408	F 3 87709	G 3 88604	H 4 85913	I 5 89657	J 6 90830	K 6 90813	L 7 87712	M 7 90610
SiO ₂	58.24	62.21	60.18	63.21	65.72	61.94	55.57	74.70	64.66	66.63	67.69	61.59	67.65
TiO ₂	1.16	0.87	1.03	0.68	0.65	0.84	1.27	0.18	0.76	0.52	0.41	0.87	0.52
Al ₂ O ₃	16.00	15.98	17.09	18.56	15.56	17.12	16.11	14.38	14.93	16.18	16.18	15.98	15.24
FeO*	7.33	5.23	6.64	2.88	3.69	5.14	7.77	0.14	4.89	3.58	1.96	5.70	3.09
MnO	0.12	0.09	0.12	0.02	0.06	0.12	0.09	0.03	0.07	0.08	0.00	0.11	0.05
MgO	3.50	3.09	2.12	1.65	2.87	2.47	5.87	0.39	3.61	1.22	0.65	3.31	1.99
CaO	6.11	5.05	5.45	1.51	3.51	4.94	6.54	1.00	3.96	3.26	3.75	5.52	3.35
Na ₂ O	3.57	3.83	3.68	4.46	3.67	3.86	3.43	4.50	3.59	4.42	4.07	3.37	4.41
K ₂ O	3.52	3.27	3.12	6.82	3.96	3.25	2.56	4.61	3.32	3.96	5.17	3.16	3.54
P ₂ O ₅	0.45	0.39	0.56	0.22	0.32	0.33	0.80	0.07	0.23	0.17	0.11	0.40	0.16
TOTAL	100.61	99.50	101.20	100.77	100.28	99.29	98.08	100.14	103.16	100.11	101.34	98.23	100.37
Trace elements (ppm)													
RB	46	54	52	95	64	60	45	88	50	54	65	51	60
SR	918	819	885	408	647	812	762	290	755	705	626	762	731
ZR	181	200			182	347	216	180	187			180	
BA	1216	1238	1199	1710	1302	1320	1006	1531	1349	1446	1510	1185	1435
NB	7.0	7.0			7.0	7.1	9.2	14.0	4.8			4.1	
K (WT.%)	2.92	2.71	2.59	5.66	3.29	2.70	2.12	3.83	2.75	3.28	4.29	2.62	2.94
K/RB	639	500	495	594	515	447	474	436	546	609	659	515	491

*Total FE reported as FeO

- | | |
|-----------------------------|------------------------------|
| A. Andesite lava. | H. Rhyolite lava. |
| B. Silicic Andesite lava. | I. Dacite Intrusion. |
| C. Andesite Dike. | J. Dacite lava. |
| D. Biotite Gneiss Xenolith. | K. Dacite lava. |
| E. Dacite Dike. | L. Hornblende Andesite lava. |
| F. Andesite Dike. | M. Dacite Dome. |
| G. Basaltic Andesite Block. | |

All analyses by XRF, Baylor University. Analyses normalized to 100% on a volatile-free basis, except for original totals.

for assimilation includes small inclusions in lava of granite and granite gneiss, some of which have been partly assimilated judging from their amoeboid shapes, and large xenoliths of biotite gneiss in an andesite dike. These features will be examined and discussed at various stops on our trip.

Stop 2

From Stop 1, proceed west on FS Road 660 approximately 3.1 mi to the junction with FS Road 659, which is a spur leading to the La Ventana area. Travel north on FS-659 about 1.7 mi and park near La Ventana, a natural arch formed by weathering of a large dacitic dike. Walk west-northwest about 200 m from La Ventana to the biotitegneiss-xenolith locality.

Stop 2A consists of an andesite dike 2 m in diameter (Analysis C, Table 1), which contains angular to rounded inclusions of biotite gneiss (Analysis D, Table 1) up to 1 m in diameter (Fig. 8). The andesite contains *pc*, *cpx*, *opx*, and *mt* microphenocrysts and, other than the xenoliths, is unremarkable. The inclusions are composed of alkali feldspar, plagioclase, biotite and minor opaque minerals. No quartz was observed, although one sample was quartz-normative. The other two analyzed samples had minor normative nepheline. Most of the alkali feldspar is now sanidine due to heating from the andesite, although appreciable microcline remains. Several of the inclusions contain small rounded blebs of brown glass (in some devitrified), indicating incipient melting of the inclusions. The andesitic magma certainly was hot enough to melt the gneiss. A temperature of $1030 \pm 50^\circ\text{C}$ was estimated from coexisting pyroxene compositions from a similar Summer Coon andesite (Parker and Thomas, 1988).

Previous workers have documented the importance of assimilation of locally heterogeneous crust to the evolution of the Conejos magma series (Colucci et al., 1989; Lipman et al., 1978). Crustal influences can be modeled through the use of incompatible-element ratios (Davidson et al.,

1987). In particular, the K/Rb ratio for Conejos rocks is a good measure, because both are very incompatible in the magmas, and no mineral, except plagioclase to a small



FIGURE 8—Contact of biotite-gneiss xenolith with andesite of dike exposed in float, Stop 2. Other xenoliths are subrounded. Knife is 8 cm long.

degree and hornblende, seems capable of fractionating K relative to Rb. Hornblende, although abundant in silicic andesite of the DNV, is absent from andesite and basaltic andesite of the SCV. The K/Rb ratio should, therefore, remain constant in a sequence dominated by fractional crystallization, or, possibly, might decrease somewhat.

Fig. 9 shows K/Rb ratios of SCV and DNV rocks plotted against Rb as an index of differentiation. The overall trend could be interpreted as a result of simple fractional crystallization, or coupled assimilation—fractional crystallization, with typical high Rb, low K/Rb crustal assimilate. Many andesites, however, and some dacites from SCV and DNV have K/Rb values higher than those of basaltic andesite. In fact, most andesite analyses fall along mixing lines between basaltic andesite and a field represented by the three analyzed gneiss inclusions. This suggests evolution of the SCV and DNV magmatic suites by a two-fold process: (1) assimilation of crustal material represented by the gneiss inclusions (about 25 wt% is indicated by comparison of Rb and Ba values), then (2) fractional crystallization to yield the more evolved dacites and rhyolites. This model, of course, does not preclude an earlier episode of deep crustal assimilation by basalt to create basaltic andesite. We hope to further test the proposed model by additional geochemical work.

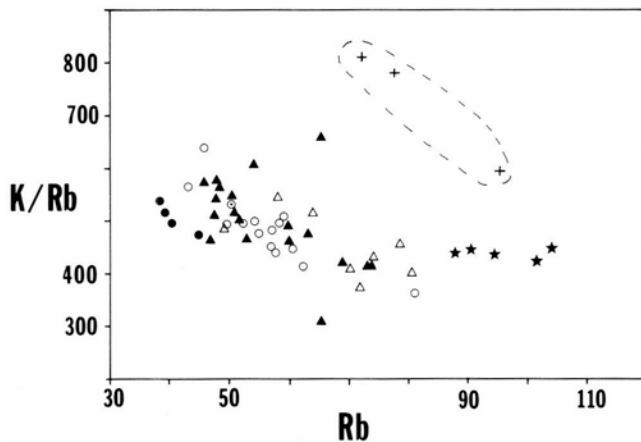


FIGURE 9—K/Rb versus Rb plot, Summer Coon and Del Norte rocks. Silicic andesite and dacite of Del Norte volcano indicated by filled triangles. Summer Coon rocks: basaltic andesite = filled circles; andesite = open circles; dacite = open triangles; rhyolite = stars; biotite-gneiss xenoliths = crosses. The andesite dike (Analysis C, Table 1) with the gneiss xenoliths is indicated by a circle with a dot at its center. See text for discussion.

Stop 2B will allow examination of the large dacite dike that forms La Ventana. This dike is about 6 m thick and contains pc, hbl, bi, opx, cpx, and mt phenocrysts. The margins of the dike have horizontal columnar joints. Pieces of a vitrophyre from this dike can be found along the eastern flank of the dike. Unfortunately, we have not located the source of the vitrophyre. A two-pyroxene model estimate for the temperature of the dacite dike was $970 \pm 50^\circ\text{C}$.

Return back to FS Road 660, then turn right (west). Proceed west on FS Road 660 approximately 5 mi to the crest of a low divide to reach Stop 3.

Stop 3

Stop 3 will allow the examination of typical exposures of the Ta unit of Fig. 1, and a small andesitic dike (Analysis F, Table 1). Coarse breccias, probably largely debris-ava-



FIGURE 10—Probable lahar deposit in Ta unit, Stop 3. Note reverse grading of angular blocks.

lanche and lahar deposits resulting from mass wasting off the steep flanks of the composite cone of the SCV following explosive eruptions, are well exposed at Stop 3. Many beds show inverse grading of clasts (Fig. 10). Clasts within the beds include strongly compositionally banded rock, bread-crust bombs, and radially jointed blocks (Fig. 11). The latter indicate that many of the clasts were still hot when incorporated in the lahars. The clasts range in composition from basaltic andesite (Analysis G, Table 1) to low-silica dacite.

Proceed west on Forest Road 660 less than 0.5 mi to the junction with the Old Women Creek Road. Turn left (south) and go approximately 2.8 mi to Stop 4. Pull to the side of the road next to a faded brown signpost.



FIGURE 11—Radially jointed block 2 m in diameter in Ta unit, Stop 3.

Stop 4

Late in its eruptive history, the SCV produced silicic lava flows (Ts in Fig. 1), particularly along its southern margin. At this stop, we will examine rhyolitic and dacitic lavas belonging to the Tsr and Tsd units of Lipman (1976). In this section, partly brecciated and silicified, cream-colored, sparsely porphyritic rhyolite is overlain by platy, dark-brown, porphyritic dacite. The rhyolite ranges up to 150 m in thickness and contains only pc, bi, and mt phenocrysts. A chemical analysis (Analysis H, Table 1) from this locality shows 74.7 wt% SiO₂. Lipman (1976) reported a range from 71 to 73%, and Zielinski and Lipman (1976) published an analysis from this locality with 71.1% SiO₂. The overlying dacite lava, unfortunately, is not suited for analysis, but a similar sample taken northeast and updip from Stop 4 had 63.7% SiO₂.

One of the major differences between the SCV and the DNV is the presence of a minor rhyolite component in the SCV but not in the DNV. Zielinski and Lipman (1976) presented trace-element data that supported a fractional crystallization origin of rhyolite from andesite for the SCV. Parker and Thomas (1988) came to similar conclusions, and also proposed that these final eruptions from SCV were the products of a compositionally zoned magma chamber below SCV, in which rhyolite overlay denser, highly porphyritic dacitic magma. We are currently investigating the origin of rhyolite at SCV in more detail.

Continue southeast on FS Road 660 to the junction with the North River Road. Turn left (east) and go about 3.7 mi to the junction of the North River Road with CO-112. Go south (right) 0.2 mi to the Del Norte Centennial Park for lunch. After lunch, return to the North River Road and proceed approximately 3 mi from the intersection with CO-112 to Stop 5, the Indian Head dike.

Stop 5

This report is the first formal description of the Del Norte volcano (Grau, 1989). Lipman (1976) mentioned a volcano near Del Norte as a source for some of the Tcv units on his map. Previously, Mertzman (1971) mapped the Del Norte rocks as part of the Summer Coon volcano.

The Del Norte volcano (DNV) is a small silicic shield volcano with a diameter of about 6 km. At one time it probably resembled the larger, much younger, and better preserved San Antonio volcano of the Taos Plateau. The DNV is composed largely of thick hornblende-andesite and hornblende-dacite lava flows (many of them 100-200 m thick). Coarse breccias underlie flows; these breccias are in part autobreccias and in part debris-avalanche and lahar deposits. Lavas were erupted from a central dike swarm, much of which is covered today by alluvium from the Rio Grande (Fig. 1).

Stops 5, 6, and 7 examine vent areas of the DNV. Stop 5 examines the Indian Head dike (Analysis I, Table 1), a north-south dike which fed a shallow intrusion and probable dacite dome along the north margin of the DNV (Fig. 12). Several silicic dikes in the SCV and DNV have bulbous extensions or terminations. These dike flarings have been interpreted by Moats and Fink (1987) as the result of decreased lithostatic load on the dikes along the margins of the volcanoes.

No contact between the dike and country rock is visible near the highway. However, the western margin of the dike is brecciated and some of the clasts are vitrophyric, sug-

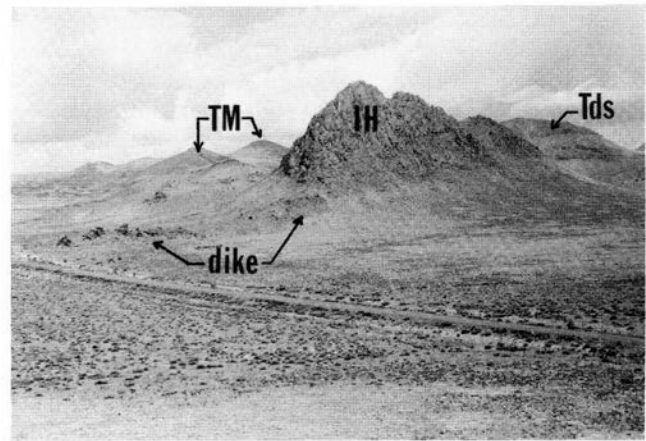


FIGURE 12—Indian Head intrusion (IH) and associated feeder dike, Stop 5, view NW. The Twin Mountains (TM) of the neighboring Baughman Creek center (Lipman, 1976) are visible in the distance to the left of Indian Head. Shield andesite and dacite lavas (Tds) of the DNV form the low hills to the right of Indian Head and in the left middle distance.

gesting proximity to the wall. The dike contains a number of inclusions of hornblende andesite, hypabyssal igneous rocks, and hornblende-rich metamorphic rocks.

Return to the town of Del Norte via the North River Road and CO-112. Turn right (west) onto US-160 at the intersection with CO-112. Go west about 3.7 mi and stop on the northern shoulder of the highway about 100 m past a roadcut in saddle.

Stop 6

Stop 6 is an overview of a dacite eruptive center along the western margin of the DNV (Fig. 13). The majority of

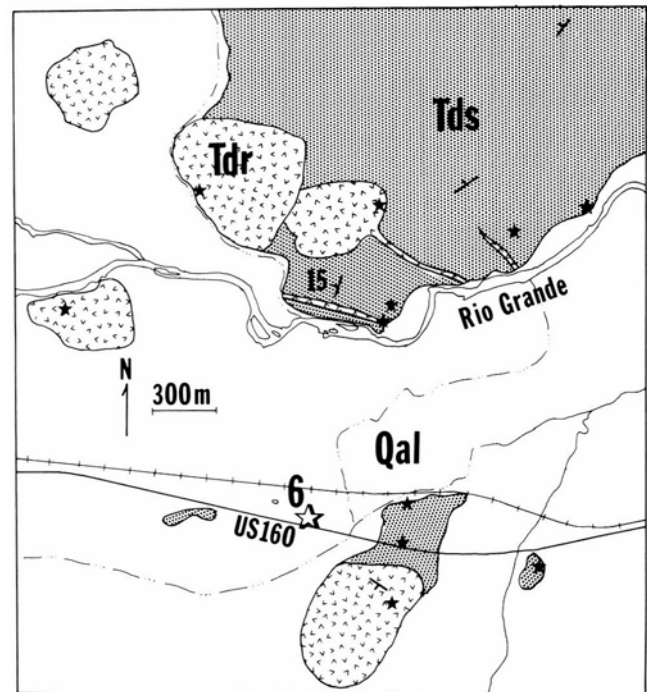


FIGURE 13—Sketch map of Stop 6 area. Silicic-dacite dikes cut the Del Norte shield lavas (Tds) and fed lava flows (Tdr = Tertiary Del Norte "rhyodacite"). The term "rhyodacite" is used to distinguish these lavas from the lower-silica dacites of the Del Norte shield. Stop 6 locality is indicated by the large empty star on US-160. Analyzed sample localities indicated by filled stars.

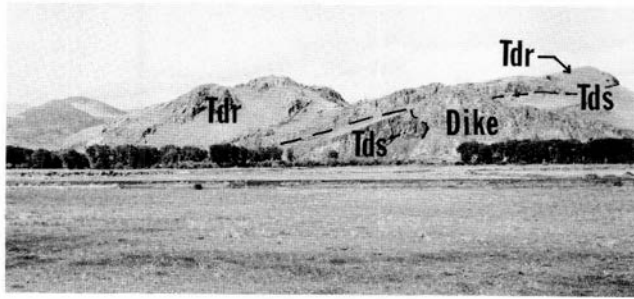


FIGURE 14—Large silicic-dacite dike cutting Tds unit. View north from Stop 6. The hills in the background are underlain by silicic-dacite lava (Tdr). The Rio Grande floodplain is in the foreground.

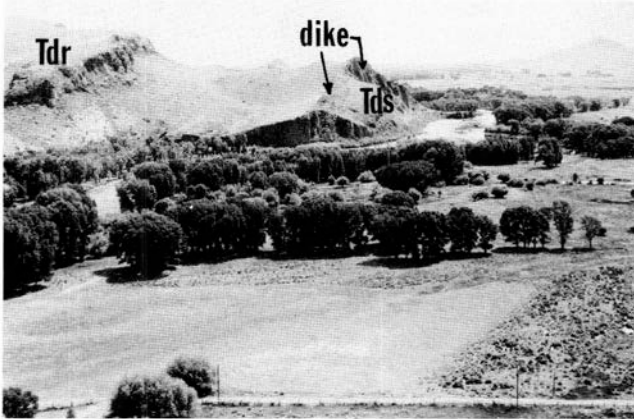


FIGURE 15—Strike view (looking east) of the silicic-dacite dike of Fig. 14.

the shield of the DNV (Tds in Fig. 13) is composed of hornblende andesite and dacite (SiO_2 range 58-65 wt%). The Tds unit forms a northwest-dipping cuesta north of the highway in Fig. 13. Three west-northwest-striking silicic dikes cut the Tds unit in exposures along the north bank of the Rio Grande. These three dikes appear to be radial to a common center south of the words "Rio Grande" in Fig. 13. All of these probably fed flows, but only the central dike can be traced upwards into a silicic-dacite lava (68.3 wt% SiO_2). The southwesternmost dike (about 10 m thick) can easily be seen from US-160 (Figs. 14, 15). These lavas and dikes are the most evolved rocks in the DNV (Analyses J and K, Table 1). The discovery of these dikes and other eruptive centers such as Lookout Mountain establishes the DNV as an independent eruptive center separate from the slightly younger SCV.

Return to Del Norte via US-160. At the western margin of Del Norte, turn south onto the Pinos Creek Road. Proceed 0.25 mi to Stop 7A. Park in the abandoned sand quarry on the southeast side of road.

Stop 7A

The Tds unit of the DNV is characterized by thick (usually more than 100 m) flows of silicic andesite and dacite (Fig. 16) that appear to have flowed several kilometers. This stop examines a hornblende-andesite lava (Analysis L, Table 1) of the Tds unit that shows evidence for mixing with a more mafic magma (Fig. 17). The flow at this stop overlies a flow breccia several meters thick, which in turn rests upon a breccia of probable laharic origin.

This flow contains streaks over 1 m long and several centimeters thick of vesicular, aphanitic mafic rock mingled

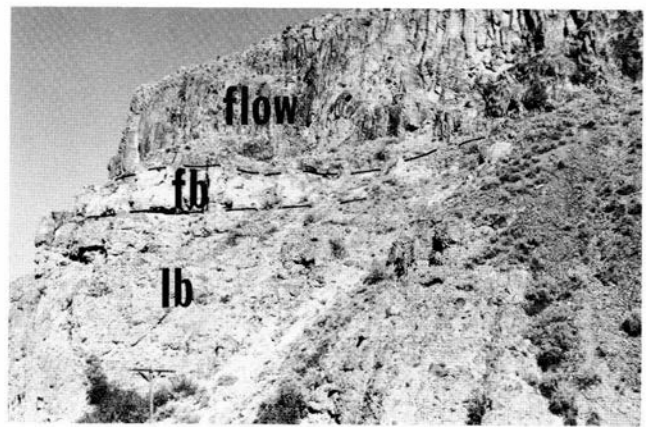


FIGURE 16—Thick silicic-andesite flow of Tds unit in exposure adjacent to Rio Grande. Massive cliff-forming flow (more than 100 m thick) overlies light-colored flow breccia (fb) (about 10 m thick), which in turn overlies laharic breccias (lb) that form lower half of exposure.

with the hornblende andesite (Fig. 18). We interpret these streaks as smeared-out mafic enclaves. Also present are subrounded inclusions up to 6 cm in diameter of plagioclase-hornblende rock, some with acicular hornblende, as well as rounded inclusions of granite or granite gneiss. The inclusions with acicular hornblende or other evidence for quick cooling may also represent mafic enclaves. If the process of mingling of magmas illustrated by the lava at this stop had proceeded further, most of the evidence for mixing would have disappeared. We suggest that some of the compositional banding present in andesitic rocks of the SCV could have resulted from such mixing.

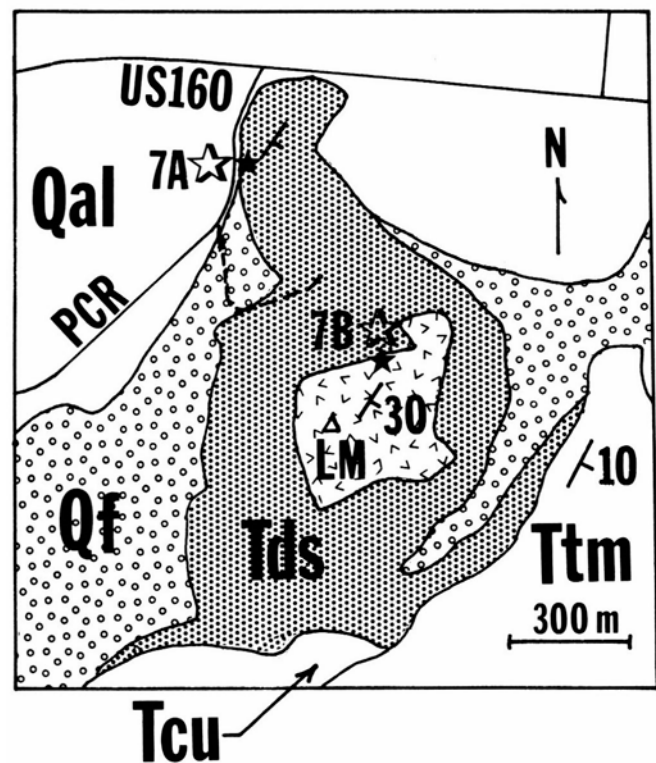


FIGURE 17—Sketch map of Stop 7. Tds = Del Norte shield; Tcu = upper andesite of Lipman (1976); Ttm = Treasure Mountain Tuff; LM = Lookout Mountain dome; Qf = Quaternary alluvial-fan and colluvium deposits. Stops 7A and 7B are indicated by empty stars. The summit of Lookout Mountain is indicated by a small, empty triangle above the letters "LM."

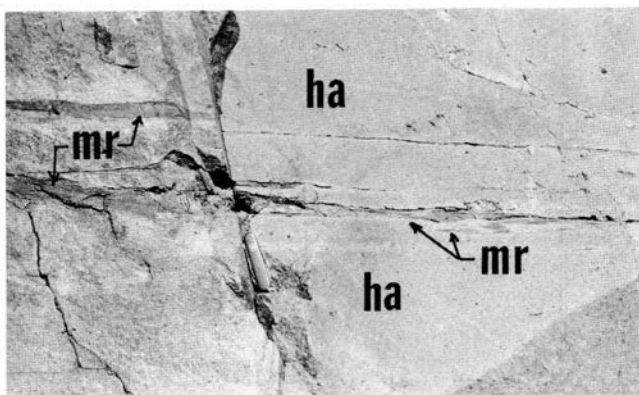


FIGURE 18—Mingled microscoriaceous mafic rock (mr) in hornblende-andesite lava (ha), Stop 7A. Knife is about 8 cm long.

Stop 7B

Return to the vehicles and drive up the gravel road to park next to a Del Norte water reservoir. Walk about 250 m southeast along a footpath.

Lookout Mountain (with the large white "D" on it) is the erosional remnant of a dacite dome of the DNV (Analysis M, Table 1) (Fig. 19) similar chemically to the silicic-dacite flows and dikes of Stops 5 and 6. The base of the dome is marked by a prominent vitrophyre several meters thick, which dips to the southeast at 30°. The crest of Lookout Mountain contains ramp structures indicating flow from the southeast (Fig. 19). The probable vent for the dome is along the southeastern margin of Lookout Mountain. The dome appears to have cut upwards through the Tds unit at a shallow angle (before tilting associated with the development of the San Luis graben steepened the dip). Its original extent was most likely not very different from the present outcrop.

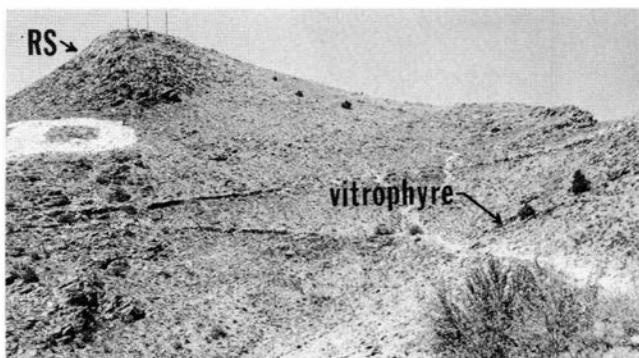


FIGURE 19—Silicic-dacite dome, Lookout Mountain. Note 30° dip of basal vitrophyre to left (southeast), and ramp structures (RS) in exposures just below the summit, indicating flow to the upper right.

Acknowledgments

This work was supported by the Department of Geology, Baylor University, and the University Research Council of Baylor University. The senior author benefited from a Summer Sabbatical from Baylor University awarded to pursue this research. We would also like to thank the landowners of the area for permission to work on their properties. We are indebted to many former Baylor University students for their help in collecting and processing samples, and especially to Richard Furner, Gary Henderson, and Greg Elkins. The excellent mapping by Peter Lipman served as a base for much of this project.

References

- Bacon, C. R., 1986, Magmatic inclusions in silicic and intermediate volcanic rocks: *Journal of Geophysical Research*, v. 91, pp. 6091-6112.
- Colucci, M. T., Dungan, M. A., Lipman, P. W., and Moorbath, S., 1989, Petrology and isotope geochemistry of the Conejos Formation, SE San Juan volcanic field: implications for multiple parent magmas and crustal interactions (abs.): *New Mexico Bureau of Mines & Mineral Resources, Bulletin 131*, p. 57.
- Cross, T. A., and Pilger, R. H., Jr., 1978, Constraints on absolute motion and plate interaction inferred from Cenozoic igneous activity in the western United States: *American Journal of Science*, v. 278, pp. 865-902.
- Davidson, J. P., Dungan, M. A., Ferguson, K. N., and Colucci, M. T., 1987, Crust—magma interaction and the evolution of arc magmas: the San Pedro—Pellado volcanic complex, southern Chilean Andes: *Geology*, v. 15, pp. 443-446.
- Dungan, M. A., Lindstrom, M. M., McMillan, N. J., Moorbath, S., Hoefs, J., and Haskin, L. A., 1986, Open system magmatic evolution of the Taos Plateau Volcanic Field, northern New Mexico, I. The petrology and geochemistry of the Servilleta Basalt: *Journal of Geophysical Research*, v. 91, pp. 5999-6028.
- Grau, D. A., 1989, Comparative petrologic evolutions of the Del Norte and Summer Coon volcanoes, eastern San Juan Mountains, Colorado: Unpublished BS thesis, Baylor University, Waco, Texas, 115 pp.
- Hildreth, W., Grove, T. L., and Dungan, M. A., 1986, Introduction to special section on open magmatic systems: *Journal of Geophysical Research*, v. 91, pp. 5887-5889.
- Lipman, P. W., 1968, Geology of the Summer Coon volcanic center, eastern San Juan Mountains, Colorado: *Colorado School of Mines Quarterly*, v. 63, pp. 211-236.
- Lipman, P. W., 1976, Geologic map of the Del Norte area, eastern San Juan Mountains, Colorado: U.S. Geological Survey, Miscellaneous Investigations Series Map I-952.
- Lipman, P. W., 1989, Oligocene—Miocene San Juan volcanic field, Colorado; in Chapin, C. E., and Zidek, J. (eds.), *Field excursions to volcanic terranes in the western United States, Volume I: Southern Rocky Mountain region*: New Mexico Bureau of Mines & Mineral Resources, Memoir 46, pp. 303-305.
- Lipman, P. W., Prostka, H. J., and Christiansen, R. L., 1971, Cenozoic volcanism and plate-tectonic evolution of the western United States, I. Early and middle Cenozoic: *Royal Society of London, Philosophical Transactions*, v. 271, pp. 217-248.
- Lipman, P. W., Steven, T. A., and Mehnert, H. H., 1970, Volcanic history of the San Juan Mountains, Colorado, as indicated by potassium—argon dating: *Geological Society of America, Bulletin*, v. 81, pp. 2329-2352.
- Lipman, P. W., Doe, B. R., Hedge, C. E., and Steven, T. A., 1978, Petrologic evolution of the San Juan volcanic field, southwestern Colorado: Pb and Sr isotope evidence: *Geological Society of America, Bulletin*, v. 89, pp. 59-82.
- Mertzman, S. A., Jr., 1971, The Summer Coon volcano, eastern San Juan Mountains, Colorado; in James, H. L. (ed.), *Guidebook of the San Luis Basin, Colorado*: New Mexico Geological Society, Guidebook 22, pp. 265-272.
- Moats, W., and Fink, J., 1987, Geometry of dikes at Summer Coon volcano, south-central Colorado (abs.): *Geological Society of America, Abstracts with Programs*, v. 19, no. 7, p. 775.
- Noblett, J. B., and Loeffler, B. M., 1987, The geology of Summer Coon volcano near Del Norte, Colorado; in Beus, S. S. (ed.), *Rocky Mountain Section of the Geological Society of America, Field Guide*, v. 2, pp. 349-352.
- Parker, D. F., and Thomas, C. D., 1988, Petrologic evolution of the Summer Coon volcano, San Juan Mountains, Colorado (abs.): *Geological Society of America, Abstracts with Programs*, v. 20, no. 7, p. A71.
- Peccerillo, A., and Taylor, S. R., 1976, Geochemistry of Eocene calc-alkaline volcanic rocks from the Kastamonu area, northern Turkey: *Contributions to Mineralogy and Petrology*, v. 58, pp. 63-81.
- Smith, D. R., and Leeman, W. P., 1987, Petrogenesis of Mount St. Helens dacitic magmas: *Journal of Geophysical Research*, v. 92, pp. 10313-10334.
- Steven, T. A., 1975, Middle Tertiary volcanic field in the southern Rocky Mountains: *Geological Society of America, Memoir 144*, pp. 75-94.
- Thomas, C. D., 1988, Petrologic evolution of the Summer Coon volcano, San Juan Mountains, southwestern Colorado: Unpublished BS thesis, Baylor University, Waco, Texas, 89 pp.
- Zielinski, R. A., and Lipman, P. W., 1976, Trace-element variations at Summer Coon volcano, San Juan Mountains, Colorado, and the origin of continental-interior andesite: *Geological Society of America, Bulletin*, v. 87, pp. 1477-1485.

Geomorphic and neotectonic evolution along the margin of the Colorado Plateau and Rio Grande rift, northern New Mexico

Mark A. Gonzalez¹ and David P. Dethier²

¹Department of Geology, University of New Mexico, Albuquerque, New Mexico 87131; ²Department of Geology, Williams College, Williamstown, Massachusetts 01267

Introduction

A number of investigators have examined fluvial systems as a means of deciphering the geologic evolution of the Rio Grande rift (e.g. Bryan, 1938; Bryan and McCann, 1936, 1938; Wright, 1946; Ruhe, 1967; Lambert, 1968; Bachman and Mehnert, 1978; Hawley, 1978; Kelley, 1979; Manley, 1979a, b; Kelson, 1986a, b; Kelson and Wells, 1987; Wells et al., 1987; Dethier and Harrington, 1987; Dethier et al., 1988). Ironically, the geomorphology of the lower Rio Chama, the largest tributary of the upper Rio Grande, has not been examined in detail. The lower reach of the Rio Chama seems especially suited for geomorphic analysis for several reasons. First, the valley of the Rio Chama and tributary arroyos expose extensive remnants of geomorphic surfaces, providing valuable spatial constraints on former base-level positions in this portion of the Rio Grande rift. Second, some investigators (C. E. Stearns, pers. comm. 1987, 1990; S. G. Wells, pers. comm. 1987) believe the Rio Chama may be the ancestral headwaters of the Rio Grande system, antedating the reach of the Rio Grande found upstream of the Rio Chama/Rio Grande confluence. The upper reach of the Rio Grande is believed to be geologically young, having formed since the mid-Pleistocene (Wells et al., 1987). Third, the fortuitous juxtaposition of geomorphic features and radiometrically dated volcanic material provides temporal constraints on the evolution of this portion of the Rio Grande rift. Finally, the Rio Chama has experienced climatic, tectonic, and volcanic perturbations, all of which appear to have left a geomorphic signature on the landscape.

The purpose of this excursion along the margin of the Rio Grande rift and Colorado Plateau of northern New Mexico is two-fold: (1) to examine evidence of the long-term (approximately 8 my) evolution of the Rio Chama/Rio Grande drainage system; and (2) to inspect neotectonic features that chronicle the timing, magnitude, and kinematics of movements on rift-margin structures.

Geologic setting and previous investigations

The Rio Grande rift extends from central Colorado through New Mexico and south to west Texas and Chihuahua, Mexico, a distance of over 1000 km. The southern portion of the rift is morphologically indistinct from the Basin and Range province, while the central and northern portions, which are bounded to the west by the Colorado Plateau and southern Rocky Mountains, are distinct morphotectonic basins (Baldrige et al., 1984). The central rift in New Mexico consists of three asymmetric half-grabens (San Luis, Espanola, and Albuquerque–Belen basins; Fig. 1).

Important structural features of the Espanola basin include mountain-front bounding faults to the east along the Sangre de Cristo Mountains (Cabot, 1938; Menges, 1988; Vernon and Riecker, 1989), the intra-basin NNE–SSW-trending Embudo fault (Muehlberger, 1979; Aldrich, 1986; Aldrich

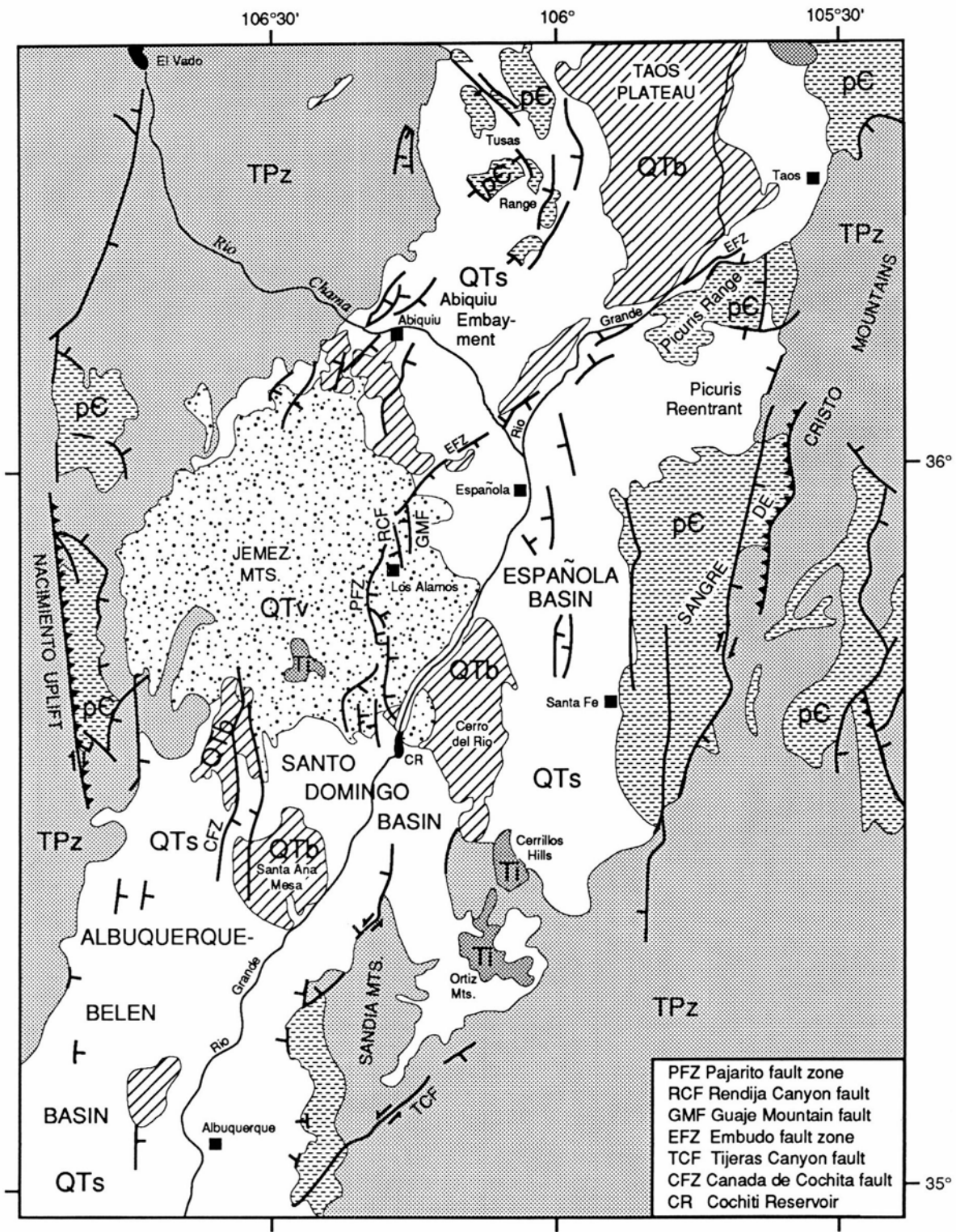
and Laughlin, 1984; also called the Santa Clara fault in Harrington and Aldrich, 1984), the intra-basin Velarde graben which parallels and is bounded in part by the Embudo fault zone (Manley, 1976a, 1979a), the N–S-trending Pajarito fault zone (Los Alamos fault of Kelley, 1979) which is the contemporary western boundary of the Espanola basin (Gardner and House, 1987; Gardner and Goff, 1984; Golombek, 1983), and N–S-trending ancient rift-margin fault zones such as the Canada de Cochiti fault zone (Gardner and Goff, 1984) and the Cannes fault zone (mapped by Manley, 1982; Figs. 1, 2).

Recently completed seismic profiles and gravity measurements (Biehler et al., in press; W. S. Baldrige, pers. comm. 1990; unpublished data from SAGE project—Summer of Applied Geophysical Experience) have supplemented previous geophysical studies (e.g. Cordell, 1978, 1979, and references therein), enhancing our understanding of the subsurface geology of the Espanola basin. Geophysical evidence suggests that the deepest parts of the Espanola basin are the NE–SW-trending Velarde graben (Fig. 1) southeast of the Embudo fault zone, where Tertiary rift-fill sediment and Paleozoic/Mesozoic sedimentary rocks are perhaps 23 km (about 7000–10,000 ft) thick, and the eastern side of the Pajarito fault zone (Biehler et al., in press). In contrast, the north side of the Embudo fault zone has only 1 km thickness (less than 3500 ft) of rift-fill sediments (W. S. Baldrige, pers. comm. 1990; unpublished seismic data from the 1990 SAGE course). The distinct change in sediment thickness across the Embudo fault suggests that the Espanola basin is structurally segmented, and we refer to the shallow northwestern part of the basin as the Abiquiu embayment.

The rift-fill sediment and paleontology have been studied by numerous investigators. Two seminal works, which provide comprehensive bibliographies, are the work by Galusha and Blick (1971) and the recent publication by Ingersoll et al. (1990). Fig. 3 provides a schematic view of the stratigraphy along the Rio Chama and Rio Grande valleys from Ghost Ranch to White Rock Canyon. Upper Paleozoic and Mesozoic sedimentary strata are found on the Colorado Plateau, and Eocene through Quaternary rift-fill sediment and volcanic rock dominate the strata of the Rio Grande rift.

Geomorphic features and late Cenozoic drainage evolution

Evidence for two periods of aggradation, three periods of valley incision, and the formation of four pre-Quaternary and as many as 10 Quaternary surfaces occurs along the margin of the Colorado Plateau, Abiquiu embayment, and eastern flank of the Jemez Mountains. We refer to the periods of aggradation and incision as: (1) the period of late Miocene through Pliocene incision; (2) the Puye aggradational period (Pliocene); (3) the pre-Bandelier incisional period (about 1.7 to 1.5 Ma), (4) the Bandelier aggradational period (1.5–



- QTs Miocene (24 Ma) and younger sedimentary rocks with Quaternary alluvium along streams and fan deposits near mountain fronts.
- QTv Miocene (24 Ma) and younger, silicic to intermediate, volcanic rocks and volcanoclastic deposits.
- QTb Miocene (24 Ma) and younger tholeiitic and alkali basalts.
- Ti Tertiary Intrusions.
- TPz Oligocene and older Phanerozoic sedimentary rocks.
- pC Pre-Cambrian crystalline rocks.
- Thrust fault with barbs on upthrown side.
- High-angle fault with ticks on downthrown side
- Fault with transcurrent motion

FIGURE 1—Generalized geologic map of the central Rio Grande rift of northern New Mexico (modified from Baldrige et al., 1983).

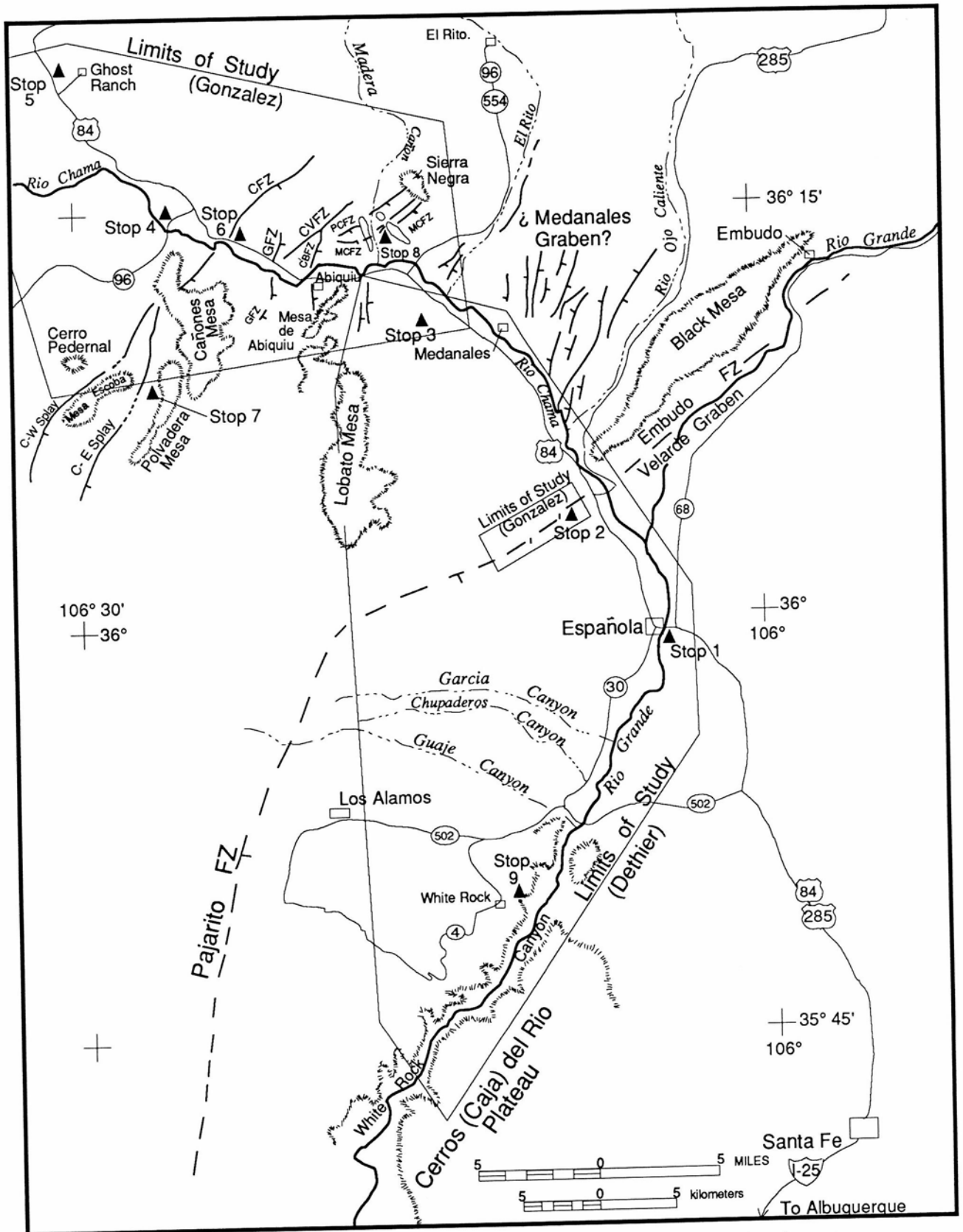


FIGURE 2—Roadways, field-trip stops, and physiography of the Española basin and Abiquiu embayment.

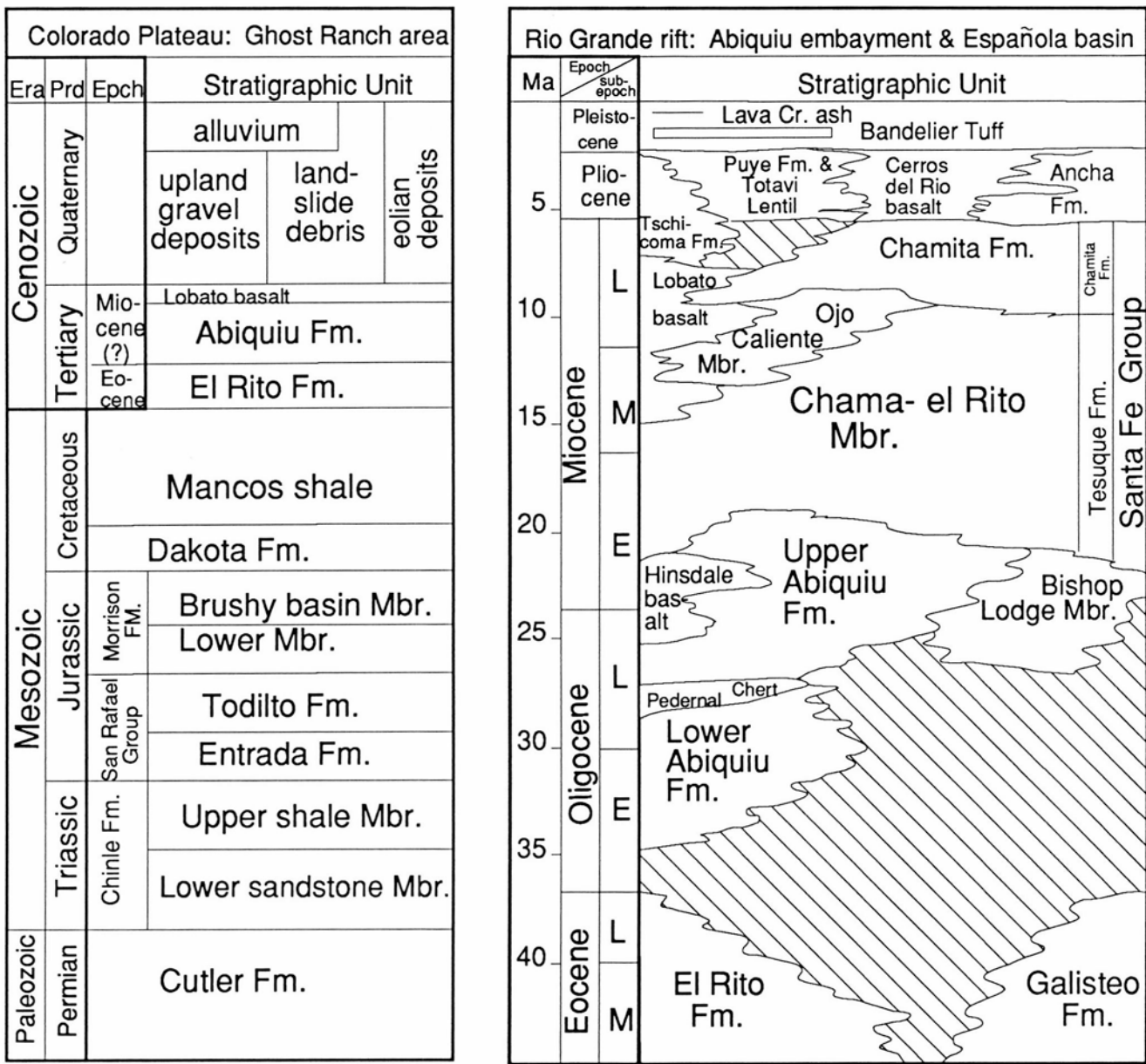


FIGURE 3—Stratigraphic columns of the southeast margin of the Colorado Plateau (after Smith et al., 1961), the Abiquiu embayment, and the eastern and northern flank of the Jemez Mountains of the Española basin (after Ingersoll et al., 1990; Gardner and Goff, 1984; Aldrich and Dethier, 1990).

1.1 Ma); and (5) the post-Bandelier incisional period (from 1.1 Ma to the present). In the following section we describe the evidence constraining the timing, spatial occurrence, and physical characteristics of the periods of aggradation and incision, as well as of the pre-Quaternary and Quaternary surfaces along approximately 90 km of the Rio Chama and Rio Grande valleys.

For correlation of surfaces, we rely primarily on the height of the surface above the axial-stream channel, as well as the radiometric ages of underlying or overlying (for buried surfaces) deposits where available. Irregular patterns of erosion and burial of soil horizons by slope wash and eolian mantles, and the polygenetic character of many surface remnants preclude the widespread use of soil stratigraphy and morphology for purposes of correlating surfaces.

Also, we assume that basalt flows that cap flat-lying mesas flowed down ancestral valley floors, which were at or near the base level of the ancestral axial stream. Then we assume

that the vertical change in the elevation of the surface (relative to axial-stream base level) is due to tectonism. Problems using basalt flows to locate paleobase-level elevations and then infer subsequent tectonic deformation include: (1) flows may be of considerably different age between mesas. Furthermore, age uncertainties for some radiometric dates cover a large enough time interval for considerable landscape changes to occur, irrespective of tectonism. (2) If the flows occupied tributary canyons, then the height above the axial-stream base level is still unknown. And (3) initial formation of the surfaces may greatly antedate the flows that bury them. Nevertheless, the position of these flows offers the best proxy for base level and, where dated, the most reliable numerical age constraint for the surfaces they bury. In the absence of better spatial and temporal constraints we will develop our interpretation of drainage and tectonic evolution, fully acknowledging the limitations of our approach.

Pre-Quaternary surfaces and the Puye aggradation episode

The oldest geomorphic surface preserved in the study area is T1. The T1 surface is late Miocene in age and is buried by the 8 Ma Lobato basalt flows which cap high mesas both in the Colorado Plateau and on the western edge of the Abiquiu embayment (Fig. 4A, Table 1). The T1 surface occurs in the Colorado Plateau below the 7.8 ± 0.7 Ma (Manley and Mehnert, 1981; Table 1) Lobato basalt flow that caps Cerro Pedernal and is underlain by alluvium which caps the upper Abiquiu Formation (see stratigraphic column of Church and Hack, 1939). Cerro Pedernal is 9862 ft (3006 m) above sea level and the contact between the buried T1 surface and overlying basalt flow is at approximately 9700 ft (2960 m) elevation, or, more importantly, at approximately 3630 ft (1110 m) above the present-day Rio Chama (Fig. 4A).

In the Abiquiu embayment, the T1 surface is preserved beneath basalt flows on parts of Cañones Mesa, Mesa Escoba (7.9 ± 0.5 Ma; Manley and Mehnert, 1981), and the northern end of Polvadera Mesa (7.8 ± 0.5 Ma; Manley and Mehnert, 1981; Figs. 2, 4A). Throughout the Abiquiu embayment, the T1 surface is at approximately 7900 ft (2400 m) elevation, or 1760 ft (540 m) above the present-day Rio Chama (Fig. 4A). We believe the difference in the height of the T1 surface from the Colorado Plateau to the Abiquiu

TABLE 1—Radiometric ages cited.

Unit/Feature	Radiometric Age	Reference
Lobato basalt flows:		
Cerro Pedernal	7.8 ± 0.7 Ma	Manley and Mehnert, 1981
Mesa Escoba	7.9 ± 0.5 Ma	Manley and Mehnert, 1981
Polvadera Mesa	7.8 ± 0.5 Ma	Manley and Mehnert, 1981
Sierra Negra	4.8 ± 0.1 Ma	Baldrige et al., 1980
El Alto basalt flows:		
Mesa de Abiquiu	3.2 ± 0.1 Ma	Baldrige et al., 1980
Cañones Mesa	2.8 ± 0.7 Ma	Manley and Mehnert, 1981
Cañones Mesa	2.8 ± 0.5 Ma	Manley and Mehnert, 1981
Cañones Mesa	3.1 ± 1.0 Ma	Manley and Mehnert, 1981
Servilleta basalt flow:		
Black Mesa	2.78 ± 0.44 Ma	Manley, 1976b
Cerros del Rio lava flows:		
Over Puye Fm.	2.6 ± 0.4 Ma	Manley, 1976b
Over Ancha Fm.	1.96 ± 0.06 Ma	Manley, 1976b
Beneath Goal	1.8 ± 0.2 Ma	Dethier, in press
Rim of Caja del Rio	2.3 ± 0.1 Ma	Dethier, in press
Tephra:		
Uppermost part of Puye Fm.	1.75 ± 0.08 Ma	Spell in Waresback and Turbeville, 1990
Lower Bandelier Tuff	1.50 ± 0.01 Ma	Spell et al., 1989
Upper Bandelier Tuff	1.13 ± 0.01 Ma	Spell et al., 1989

embayment is due to tectonism. Evidence for this is presented below.

T2 is an early Pliocene surface found at only one locality in the study area, near Sierra Negra (Figs. 2, 4B). Sierra Negra is a volcanic vent at 8052 ft (2454 m) elevation, from which issued a 4.8 ± 0.1 Ma (UAKA-77-93; Baldrige et al., 1980) basalt flow. The basalt flow descends from the vent down a hillslope towards the southeast, entering an ancestral stream channel at 7700 ft (2350 m) elevation. Within the paleochannel, a fluvial gravel deposit occurs beneath the flow (Wilson, 1977; Fig. 4B). The contact between the buried alluvium and the basalt is at approximately

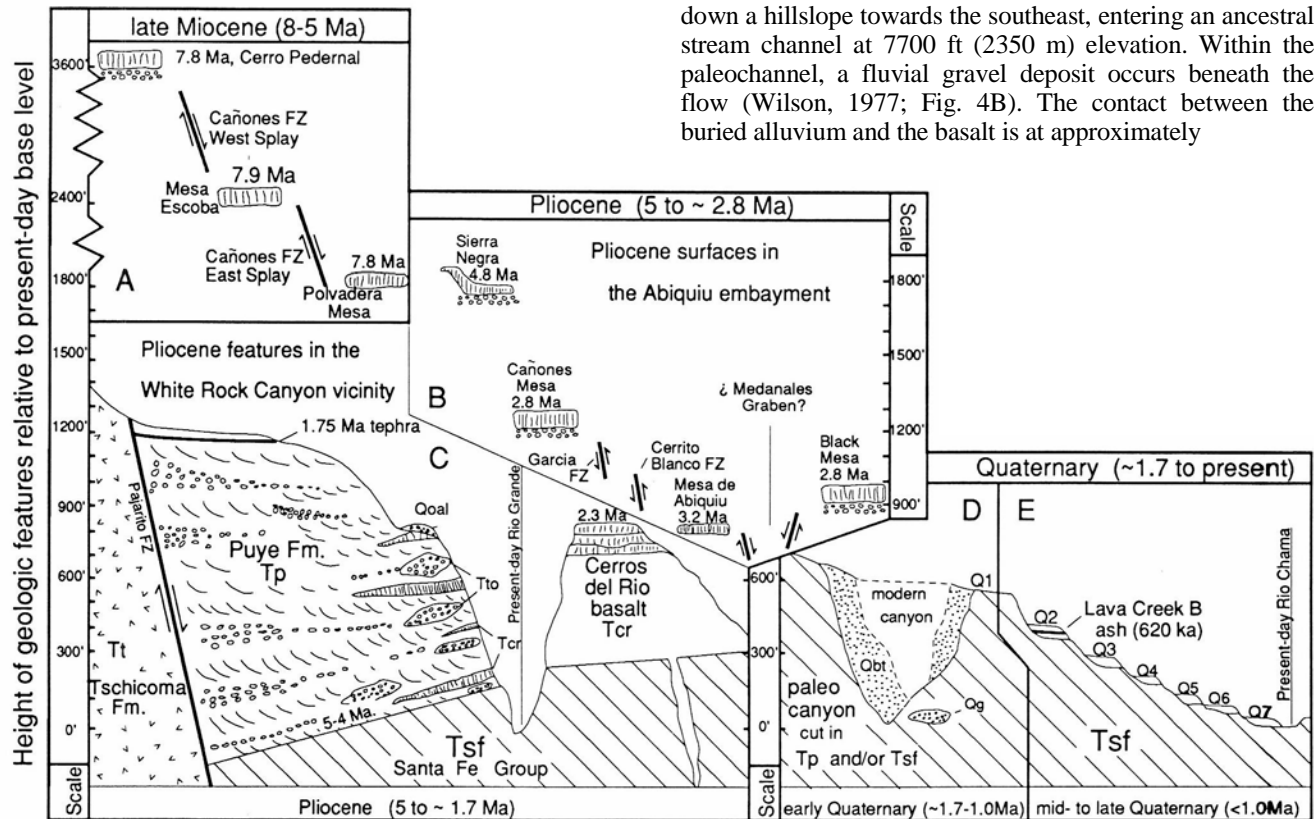


FIGURE 4—Schematic diagram illustrating the position (relative to present-day axial-stream base level) of late Cenozoic features found along the margin of the Rio Grande rift from Ghost Ranch to White Rock Canyon. Panel A depicts features formed during the late Miocene and subsequently offset by faulting. Note the break in scale for panel A. Panels B and C depict geologic features formed during the Pliocene and subsequently offset by faulting and tilting. Panel B highlights paleobase-level features in the Abiquiu embayment, while panel C illustrates base-level fall, the Pliocene burial of the T3 surface by the Puye aggradation episode, and west-tilting of rift-fill sediment in the Española basin by Pliocene (and Quaternary) faulting along the Pajarito fault zone. The contrast between relative base-level stability in panel B and overall Pliocene aggradation in panel C illustrates the control of intra-basin tectonism (i.e. the Embudo fault zone) on the geomorphic evolution of the Española basin. Panel D shows early Quaternary geomorphic evolution in the study area, specifically the pre-Bandelier incision episode to form paleocanyons, the Bandelier aggradational episode to back-fill the paleocanyons, and the post-Bandelier incision episode, which re-excavated canyons to form the present-day system of drainages along the Jemez Mountains, and formed the flight of mid- to late Quaternary terraces (Q1 to Q7-Q9) found along the axial and tributary drainages.

7650 ft (2330 m) elevation, or 1750 ft (530 m) above the Rio Chama channel (Fig. 4B). Unfortunately, since so little of the 4.8 Ma tributary channel is preserved and the exact location of the ancestral Rio Chama is unknown, we cannot determine the elevation of the axial-stream base level at 4.8 Ma other than to conclude that it must have been lower than the tributary-valley floor [7650 ft (2330 m) elevation].

T3 is a buried Pliocene surface formed prior to the deposition of the Puye Formation (Figs. 3, 4C). The importance of identifying the buried T3 surface is three-fold: first, to call attention to a Pliocene aggradational episode; second, to support an argument that the Embudo and Pajarito fault zones were actively moving (with down-to-the-south and -east motion, respectively) during the Pliocene; and third, to illustrate the role of intra-basin tectonism on the formation and preservation of geomorphic features. It has been recognized only south of the Embudo fault zone, and may be entirely absent in the Abiquiu embayment and on the Colorado Plateau where we have found no evidence of Pliocene aggradation.

Pliocene aggradation is recorded by the formation of large fan complexes on both the east and west sides of the Española basin. On the east side the Ancha Formation consists of sediment derived from the Sangre de Cristo Mountains. A Cerros del Rio basalt flow (1.96 ± 0.06 Ma; Manley, 1976b) that covers part of the upper Ancha Formation constrains fan formation to the Pliocene. The Puye Formation was deposited during the Pliocene on the west side of the Española basin (Fig. 4C). The Puye Formation is a volcano-genic, rift-margin fan complex derived from the Jemez Mountains volcanic pile primarily during and after the deposition of the Tschicoma Formation (7-3 Ma; Gardner and Goff, 1984; Waresback, 1986; Waresback and Turbeville, 1990). The Totavi Lentil (a member of the Puye Formation named by Griggs, 1964) consists of mid-Pliocene Rio Grande (or Chama) axial-stream deposits. The Puye Formation interfingers with Cerros del Rio basalt flows (Fig. 4C). Radiometric ages from the Cerros del Rio basalt provide temporal constraints on the timing of aggradation of the Puye and Ancha fans.

Between the Embudo fault zone and White Rock Canyon, the base of the Puye Formation (i.e. the buried T3 surface) is in places about 100 ft (30 m) above the Rio Grande (e.g. Ancho Canyon; Dethier, in press; Fig. 4C). Just 2-3 mi (35 km) upstream along some of the tributaries (e.g. Guaje Canyon, Chupaderos Canyon, Garcia Canyon, etc.), the base of the Puye Formation lies below the level of tributary-stream valley floors, either because the basal Puye is back-tilted by down-to-the-east motion on the Pajarito fault zone or because the Puye fan was deposited on a lower-gradient surface than is that of modern canyons draining the Pajarito Plateau (Griggs, 1964; also see cross-section B-B' of Smith et al., 1970; Fig. 4C).

In contrast, the Puye Formation (and the upper Santa Fe Group) is considerably higher throughout the Abiquiu embayment north of the Embudo fault zone (contrast cross-section A-A' with B-B' of Bailey et al., 1970). Also, the Puye Formation is thin north of the Embudo fault zone [less than 100 ft (30 m) thick as compared to 1000 ft (300 m) or more in places south of the Embudo fault]. Furthermore, only isolated remnants of the Puye Formation are found north of the Embudo fault zone, suggesting that the locus of deposition lay to the south, and little aggradation occurred in the Abiquiu embayment during the Pliocene. The striking

contrast between large-scale fan aggradation south of the fault (see Fig. 4C) and general base-level stability northwest of the Embudo fault zone (see Fig. 4B) during the Pliocene may suggest tectonic activity on the Embudo and Pajarito faults beginning in the Pliocene.

The T4 surface may mark an extended period of Pliocene base-level stability in the Abiquiu embayment. The T4 surface has been preserved by 3.2-2.8 Ma El Alto basalt flows on Cañones Mesa and Mesa de Abiquiu, and the 2.8 Ma Servilleta basalt flows that cap Black Mesa (Fig. 4B). We believe these basalt flows coursed down Pliocene stream valleys at or near an ancestral base level of the Rio Chama/ Rio Grande for the following reasons.

(1) All the flows have low surface gradients which decline toward, or parallel to, the axial drainage. The flow capping Mesa de Abiquiu (3.2 ± 0.1 ; UAKA-77-85; Baldrige et al., 1980) has a gradient of 2.2% in its upper reach before decreasing to 0.7% in its terminal reach. The Black Mesa flow has a surface gradient of approximately 1.6% in its southern end, which presumably followed the ancestral Rio Grande channel.

(2) Well-rounded stream gravel (in-situ and in float) is present below several of the flows. For example, Manley (1976a, pp. 43-45) reports finding axial-stream gravel beneath the Servilleta basalt flow (2.78 ± 0.44 ; Manley, 1976b) that caps Black Mesa. She states that the "composition, imbrication, and rounding of the gravels beneath the Servilleta Fm. on Black Mesa indicate the presence of an axial river with source areas in the Sangre de Cristo Mountains and north of the Española basin" (Manley, 1976a, p. 45). Also, we have noted a considerable quantity of well-rounded cobbles in the scree accumulated at and below the base of the basalt flow on Cañones Mesa. The clast lithologies are diagnostic of Rio Chama axial-stream deposits (i.e. Precambrian quartzites, crossbedded quartzites, and quartzitic conglomerates). Since no axial-stream deposits rest above the El Alto basalt flow, we argue that the flow capping lower Cañones Mesa has buried a former channel of the Rio Chama.

(3) The width of the flows is comparable to the width of the present-day drainages.

Quaternary surfaces and periods of aggradation and incision

Pre-Bandelier valley incision is recorded primarily along the northern and eastern flanks of the Jemez Mountains. Incision began after deposition of the Puye Formation [sometime after 1.75 Ma, based on the age of a rhyolite plinian deposit in the uppermost part of the Puye Formation (1.75 ± 0.08 Ma; Spell, unpublished data reported by Waresback and Turbeville, 1990)]. Incision ended before 1.50 Ma (± 0.01 Ma; Spell et al., 1989), when lower Bandelier Tuff sediment began to accumulate on the floors of existing canyons (Fig. 4D). During this interval of approximately 200,000 years, streams draining the eastern and northern flanks of the Jemez Mountains cut canyons which in places were as deep or deeper than present-day canyons (Dransfield and Gardner, 1986; Fig. 4D).

The pre-Bandelier canyons were quickly back-filled with Bandelier pyroclastic ejecta from 1.5 to 1.13 (± 0.01) Ma (Spell et al., 1989; Fig. 4D). During this aggradation, the deeply dissected pre-Bandelier landscape was quickly transformed to a low-relief, gently sloping ($2-3^\circ$) surface (Dransfield and Gardner, 1985). Furthermore, minor incision may have also occurred during general aggradation between dep-

osition of the lower and upper members of the Bandelier Tuff as the drainage systems of the Pajarito Plateau began to re-establish themselves.

A mid- to late Quaternary period of incision followed the period of Bandelier aggradation and resulted in re-excavation of canyons and deposits in the Abiquiu embayment and Española basin (Fig. 4E). Post-Bandelier incision appears to have continued since 1.1 Ma except for minor base-level stands or aggradational periods that were sufficiently long to allow Quaternary surfaces (on pediments, strath and fill terraces) to form.

Ten Quaternary-age surfaces are recognized in the study area (Fig. 4E). Seven Quaternary surfaces appear with regularity throughout the Colorado Plateau and Abiquiu embayment. We tentatively label these Q1–Q7, oldest to youngest. In addition, there are three Quaternary surfaces that predate Q1 (here tentatively labeled Qg, Qoal, and undesignated) (Fig. 4C, D). We describe and summarize the ages (where possible) of the Quaternary surfaces in Table 2.

Attempts to correlate the surfaces throughout the study area are difficult due to the spatial variation in the elevation at which these surfaces occur and due to the limited utility of other correlative tools (e.g. soil morphology). Variation of the number of surfaces and their height above modern-day river grade may result from:

(1) Continued tectonic movement on faults following formation of the surfaces.

(2) Changes in the modern-stream and paleostream gradients due to lithologic control on stream incision.

(3) Variability due to polygenetic surface evolution. For example, many surface remnants north of the Rio Chama in the Plaza Colorado and Plaza Blanca land grants (Stop 8) are topographically isolated buttes which now experience no surface runoff from adjacent highlands. In contrast, many surfaces south of the Rio Chama are contiguous with the flanks of the Jemez Mountains, thereby receiving runoff from the adjacent highlands. Eolian processes may be relatively more important on the surfaces located on buttes, while overland flow may be an important surface-modifying process on surfaces which receive runoff from adjacent highlands.

(4) The possibility that surfaces diverge or converge in either the downstream or upstream direction due to changes in sediment load and transport ability (Harvey et al., 1988).

(5) Measurement errors and investigator biases—one of us differentiating surfaces more finely than the other.

The sedimentary deposit associated with unit Qoal is a stratigraphic enigma. It consists of Rio Grande axial gravel found on top of a 1.8 Ma (Dethier, submitted; Table 1) Cerros del Rio basalt flow near the White Rock Canyon overlook (Stop 9; Fig. 4C). The perplexing question is whether this gravel was deposited near the end of Puye aggradation and prior to pre-Bandelier valley incision, in which case it could be considered a part of the Puye Formation, or in the mid-Quaternary following Bandelier aggradation (1.5–1.1 Ma; Spell et al., 1989). Mineralogic and/or chemical analyses of the interstitial material within the deposit may resolve the question of age.

Deposits of unit Qg comprise a single exposure of gravel which is buried by the Guaje pumice (Fig. 4D), the basal bed of the Bandelier Tuff, indicating the gravel is at least 1.5 Ma old (Table 2). This gravel has been previously recognized by Hawley (1978). It demarcates a stream-channel position before Bandelier aggradation commenced 1.5 Ma.

Unit Q1 is a high erosion surface cut on the Bandelier Tuff along the northern and eastern flanks of the Jemez Mountains. In the Colorado Plateau and in parts of the Abiquiu embayment the Q1 unit forms a terrace strath underlain by an axial-gravel deposit 1–5 m thick. The age of the Q1 surface is less than 1.1 Ma and greater than 0.62 Ma based on stratigraphic relationships with the Bandelier Tuff and Lava Creek B ash (Table 2; Fig. 4D, E). In the Colorado Plateau, the height of the Q1 surface is usually 465 ± 30 ft (140 ± 10 m) above stream grade. Further downstream within the western half of the Abiquiu embayment, the Q1 surface is usually 430 ft (130 m) above grade. Downstream from the Embudo fault zone, Dethier et al. (1988) mapped the Q1 surface at approximately 500 ft (150 m) above the present-day stream gradient. Much of this variation in surface elevation may be due to lithologic variations between the Colorado Plateau and the Rio Grande rift, and the river's ability to cut through the different lithologies. Also, there is an elevation uncertainty whenever projecting remnants of a sloping surface. In addition, Quaternary fault movements could be responsible for variation in surface heights (as appears to be the case at Stop 8).

Unit Q2 is often recognized in the field by the presence of reworked Lava Creek B ash (620 ka) just above the axial-stream gravel deposits (Figs. 4E, 5; Dethier et al., 1988). The ash provides a valuable mid-Quaternary isochron for region-wide correlation (Table 3). As yet, our investigations

TABLE 2—Age information for Quaternary surfaces.

Surface ¹	Elevation of gravel ² above axial channel, in feet	Age	Dating Method
Pre-Bandelier	~760	~1500 ka	Gravel capped by lower Bandelier tephra. Single exposure
Unnamed	~565	1500–620 ka	Stratigraphic
Q1	~500 ³	1500–620 ka	Stratigraphic; best exposed in SE of Mesa de Abiquiu
Q2	410	≥620 ka	See below
	360	620 ka	Lava Creek B tephra layer
Q3 ²	305	350–300 ka	Amino acid ratio
Q3 ²	250	~300–220 ka	Amino acid ratio
Q4	140	150–80 ka	Amino acid ratio; see also Dethier et al. (1988)
Q5	75	80–26 ka	Amino acid ratios; ¹⁴ C age
Q6	40–0	19 ka–modern	¹⁴ C age

¹ Refers to erosion surface cut across Quaternary deposits—see Dethier et al., 1988.

² ±40 feet; erosion surfaces are frequently cut across more than one buried sequence.

³ Only piedmont gravel present.

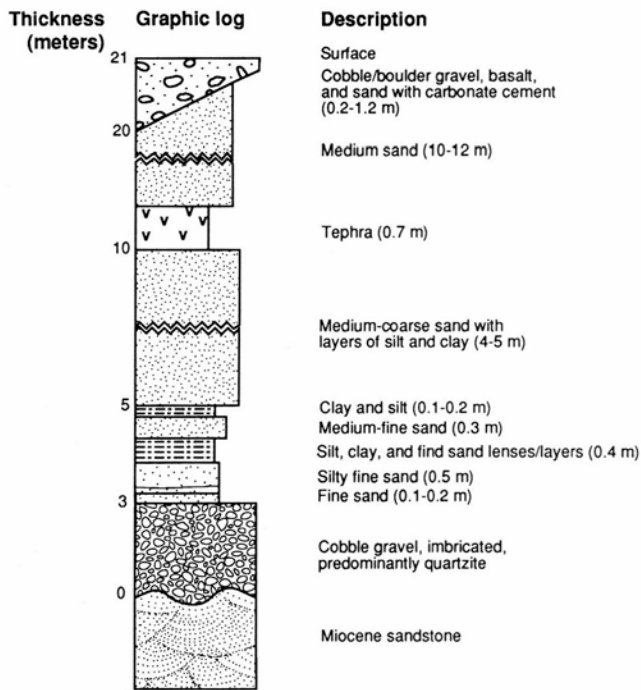


FIGURE 5—Schematic diagram of a typical stratigraphic sequence of deposits underlying mid- to late Quaternary surfaces in the Abiquiu embayment. This particular example includes the intercalated Lava Creek B tephra found in the deposits beneath Q2. Gastropods are found in about the same part of the stratigraphic sequence at other localities.

have failed to locate any ash deposits along the margin of the Colorado Plateau. Nevertheless, widespread occurrence of surface remnants at a consistent height above the present-day axial stream allows the Q2 surface to be traced fairly confidently from the rift onto the Colorado Plateau. In the Colorado Plateau, the Q2 surface lies 405 ± 25 ft (120 ± 10 m) above stream grade. In the Abiquiu embayment, the Q2 surface is generally 350 ± 25 ft (110 m) above stream grade; and near the Embudo fault, the Q2 surface is about 410360 ft (120-110 m) above grade (Table 2, Fig. 4E).

The remaining Quaternary surfaces are formed on dep

TABLE 3—Comparison of major-element chemistry of glass from the Rio Chama tephra to the chemistry of some other widespread tephra layers by means of electron microprobe (from Dethier et al., 1990).¹

Tephra	SiO ₂ ²	Al ₂ O	Fe ₂ O ₃	MgO	MnO	CaO	TiO ₂	Na ₂ O	K ₂ O	Total
Rio Chama ³ ash bed	76.63 0.09	12.30 0.04	1.56 0.04	0.02 0.01	0.03 >0.01	0.53 0.01	0.12 0.01	3.54 0.05	4.97 0.02	93.11 0.25
Lava Creek B ⁴ ash bed	76.60 0.32	12.41 0.19	1.57 0.05	0.02 0.01	0.03 0.02	0.54 0.02	0.11 0.01	3.57 0.10	5.16 0.15	94.28 0.33
Huckleberry Ridge ash bed ⁴	76.45 0.24	12.33 0.12	1.76 0.07	0.02 0.01	0.04 0.01	0.61 0.05	0.13 0.01	3.49 0.14	3.16 0.15	94.55 0.51
Bandelier Tuff Upper	72.70	12.80	1.47	0.05	0.08	0.33	0.08	3.08	5.36	95.95
Bandelier Tuff Lower	73.60	11.90	1.40	0.10	0.07	0.24	0.04	4.36	4.61	96.32
Bishop ash bed	77.55 0.20	12.64 0.22	0.74 0.03	0.04 0.01	0.03 0.01	0.45 0.03	0.06 0.01	3.70 0.18	4.78 0.24	94.02 0.75
A.E. ⁵	1.3%	2.2%	6.4%	6.6%	15.0%	6.2%	17.4%	3.9%	4.2%	

¹ From Sarna-Wojcicki et al. (1987), except for Bandelier Tuff, which is from Gardner et al. (1986). Values given are in weight-percent oxide, recalculated to 100% on a fluid-free basis. Original oxide totals before recalculation are given to indicate the approximate degree of hydration of glass. Approximately 15 individual shards were analyzed for each sample, except for Bandelier Tuff. C. E. Meyer, analyst.

² Values in percent $\pm 1\sigma$, except for Bandelier analyses, which do not include 1σ values.

³ Mean of samples from 4 sites.

⁴ Average of 7 samples.

⁵ Average analytical error, calculated from average of concentrations of the shard population (except Bandelier Tuff), expressed as a percentage obtained by dividing the average standard deviation for each element by the average concentration of that element, multiplied by 100.

ositional insets at elevations between the Q2 surface and the modern channel (Fig. 6). We believe each successive surface is younger than the surfaces above. Table 2 summarizes the data that limit the ages of these mid- to late Pleistocene surfaces.

Climate change and development of surfaces

Geology at several stops on this field trip demonstrates that the Rio Chama has been cutting down since pre-Bandelier time and that incision has been interrupted periodically by intervals of relatively stable base level. Uplift of both the Colorado Plateau and the Rio Grande rift may have helped to drive incision by the Rio Chama. However, climate change must have also contributed to downcutting and has likely mediated periods of rapid base-level change. The

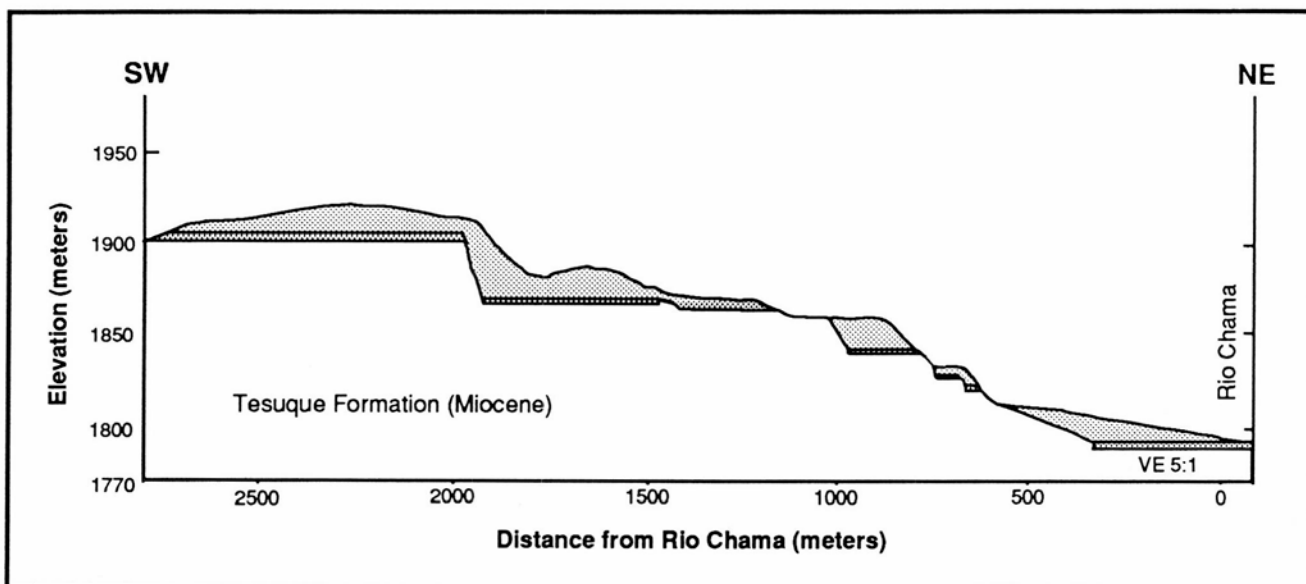


FIGURE 6—Cross-sectional diagram of the Rio Chama valley. The diagram depicts the relative position of mid- to late Quaternary surfaces and their underlying deposits.

change from relatively equitable climate to alternating glacial and interglacial periods at about 2.0 Ma probably increased the total flow in the Rio Chama system and the magnitude and duration of peak flows during the snowmelt period. Climate change also would have affected vegetation cover, sediment availability, and bed material, variables that help to control the balance between aggradation, lateral planation, and incision. We have not collected data that give us direct information about these variables; however, we hypothesize that much of the incision recorded along the Rio Chama is a result of higher peak discharge since mid-Pleistocene time. As the Rio Chama incised through Miocene bedrock, at least nine similar stratigraphic sequences were deposited at elevations ranging from 15 to 170 m above

present grade (Fig. 6). A flight of these surfaces is well preserved in three unnamed arroyos located south of the junction of US-84 and NM-554 (NM-96 on older maps; Fig. 7). Stop 3 traverses the Quaternary surfaces, which are underlain by axial-stream and valley-margin fan deposits. The typical sedimentary sequence of deposits underlying mid- to late Quaternary surfaces comprises: (1) a basal cobble gravel deposited by the ancestral Rio Chama on a bedrock surface; (2) 2-4 m of silty sand and sand deposited as overbank and alluvial-fan deposits; and (3) 5-40 m of medium sand to cobble gravel deposited by alluvial fans (Fig. 5). This typical sedimentary sequence is best preserved within the Rio Grande rift, south and west of the Rio Chama, where the tributaries draining the Jemez Mountains provided the

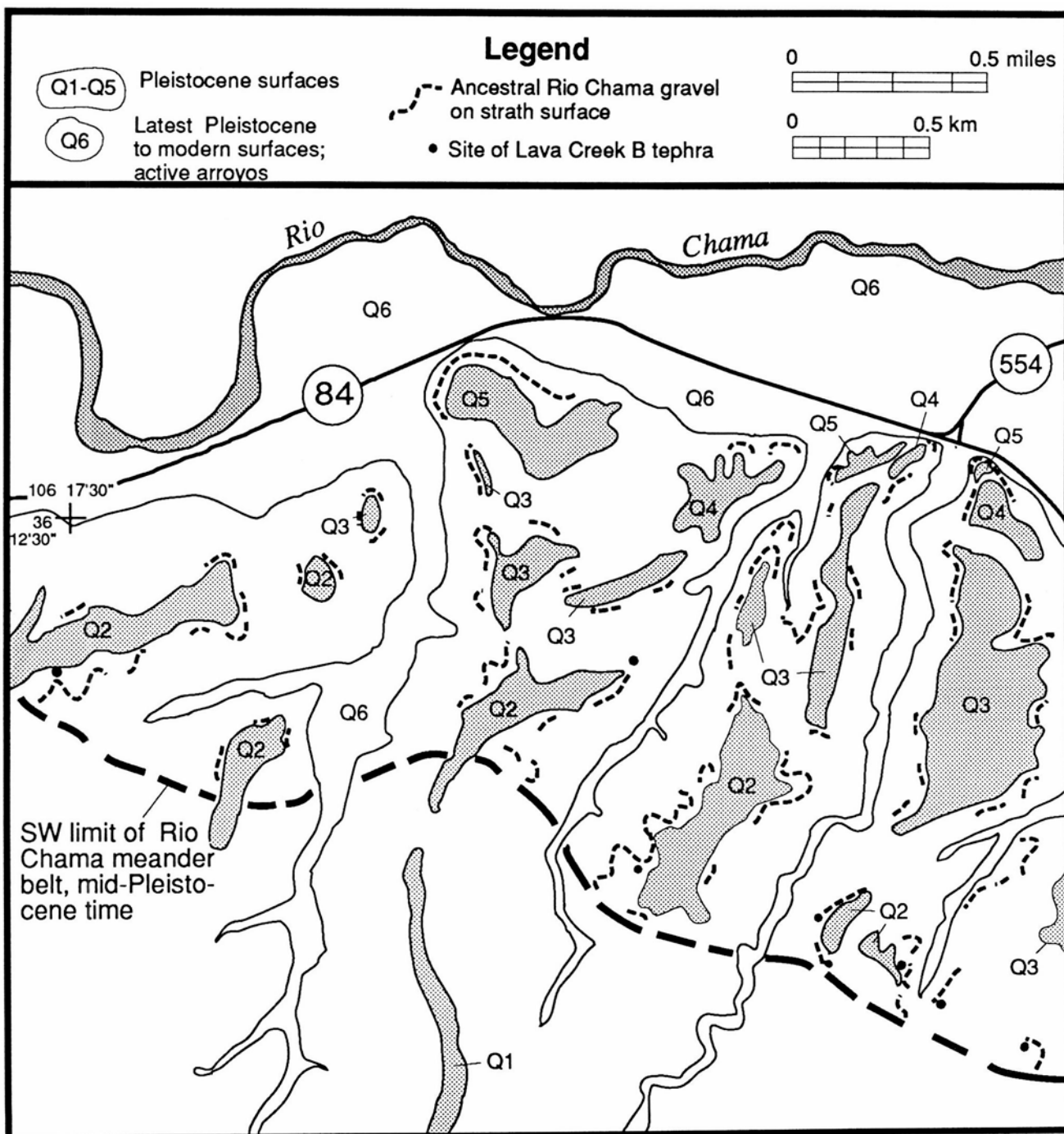


FIGURE 7—Sketch map of the mid- to late Quaternary surface remnants, ancestral Rio Chama axial-stream gravel deposits, and Lava Creek B tephra sites. The map area is in the northeast quarter of the Abiquiu, 1:24,000 scale, topographic map.

coarse alluvial-fan materials that cap and preserve the fine-grained overbank deposits. North of the Rio Chama and throughout most of the Colorado Plateau margin, the sedimentary sequence usually consists of the basal cobble axial-stream gravel with an eolian mantle of 0-2 m thick preserved in places.

Lava Creek B ash and, at many localities, fossil gastropods are preserved in the middle layer of this sequence (Fig. 5). Field relations suggest that alluvial fans prograded across the ancestral Rio Chama floodplain during episodes when the Rio Chama meander belt narrowed and shifted to the north and east. Subsequent lateral planation and downcutting by the ancestral Rio Chama broadened the meander belt and deepened the valley before alluvial fans again advanced across the valley. Love et al. (1987) used mapping and subsurface evidence to demonstrate that near Española, alluvial-fan progradation and narrowing of the meander belt began in the latest Pleistocene (at approximately 15 ka) and may have continued through the early Holocene. If this pattern of deposition and those described by Gile et al. (1981) in the Desert Project area of southern New Mexico are reasonable analogs for the Chama valley, then the repeated, inset sequences of ancestral Rio Chama sediment probably are related to episodic climate change. As a working hypothesis, we suggest that fan construction occurs during the transition from cool, moist to warm, dry climate, that axial-river incision occurs during the early or middle part of glacial pluvial cycles, and that minor aggradation and incision or lateral planation dominate most of the time.

We can use the deposits exposed at Stop 1 (near the Española High School) and two radiocarbon dates to constrain the timing of incision during the most recent period of climate change. At about 26 ka the Rio Chama flowed about 15 m above what Love et al. (1987) mapped as the latest Pleistocene level. Amino-acid ratios in higher elevation deposits (D. P. Dethier, unpublished data 1988) suggest that since the early Wisconsinan the Rio Chama had flowed within 10 m of its elevation at 26 ka. An apparently brief period of alluvial-fan aggradation occurred after 26 ka, and we interpret dune activity at 19 ka (Stop 1; Fig. 8) as evidence that the Rio Chama meander belt had widened following the downcutting that occurred between 26 and 19

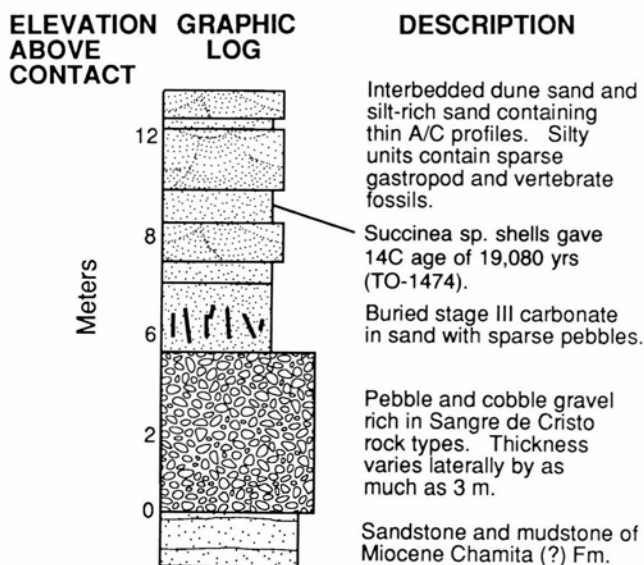


FIGURE 8—Stratigraphic sequence in late Pleistocene deposits near the Española High School (Stop 1).

ka. Strong eolian activity marked the transition from a pluvial to a more arid climate (see also Wells et al., 1990) that resulted in alluvial-fan construction from after 19 ka to the early Holocene(?). We infer from these data that incision by the axial channel most likely occurred close to the beginning of the pluvial period.

Neotectonic analysis of faults of the Abiquiu embayment

The Abiquiu embayment is a geophysically distinct segment of the Rio Grande rift (Biehler et al., in press), separated from the Colorado Plateau by NNE-trending normal faults and from the remainder of the Española basin by the ENE-trending Embudo fault zone. The Embudo fault zone appears to be a transfer fault as defined by Gibbs (1984; alternatively referred to as an intracontinental transform fault by Muehlberger, 1979). The Embudo fault zone accommodates differences in crustal extension on each side of the fault (Aldrich, 1986) and transfers motion between rift grabens (Española and San Luis basins). The Abiquiu embayment, northwest of the Embudo fault zone, is shallower than the rest of the Española basin. The thickness of Tertiary rift-fill sediment and Paleozoic/Mesozoic sedimentary rocks above the Precambrian basement is approximately 1 km (3000 ft; unpublished seismic profiles produced by SAGE in the summer of 1990; W. S. Baldrige, pers. comm. 1990). In contrast, the Española basin southeast of the Embudo fault zone has 2-3 km (7000-10,000 ft) of strata above the Precambrian basement (Biehler et al., in press).

Seven fault zones along the margin of the Rio Grande rift and within the Abiquiu embayment have been examined. The objectives are: (1) to determine the geometry of the fault zones; and (2) to find kinematic indicators along fault zones. The purposes are to determine the timing, magnitude, and rate of faulting along this rift margin and then to relate the local features to the regional tectonic forces affecting the evolution of the central Rio Grande rift in northern New Mexico. These faults within the Abiquiu embayment are informally named (from west to east) the Cañones, Garcia, Cerrito de la Ventana, Cerrito Blanco, Plaza Colorado, Madera Cañon, and Embudo fault zones (see Fig. 2 for locations). Over 450 fault-plane attitudes (main, antithetic, and cross faults; R1 and R2 planes to main, antithetic, and cross faults) and 300 fault-plane lineations (slickensides, striations, oriented mineral growths, and aligned particles) have been collected. The structural data for six of the fault zones, where data are sufficient to define trends, are depicted graphically in stereonets (Fig. 9A—L) and tabulated numerically in Table 4. In the following paragraphs, we report preliminary results of our ongoing fault-plane analyses.

Cannes fault zone

The Cannes fault zone (mapped by Manley, 1982) is the westernmost rift-bounding structure in the Abiquiu embayment. We informally divide the Cannes fault zone into a west splay (Gonzales fault of Kelley, 1979), east splay (Cañones fault of Kelley, 1979) and main splay (Cobre fault? of Kelley, 1979). The main splay of the Cañones fault zone crosses the Rio Chama valley and US-84 approximately 5 mi (8 km) west of Abiquiu (Stop 6; Fig. 2). At this locality the Cañones fault zone has at least 400 ft (120 m) of strati-graphic offset, juxtaposing upper Paleozoic and Mesozoic strata (Cutler and Chinle Formations) on the west against Eocene to early Miocene rift-fill sediments (El Rito and

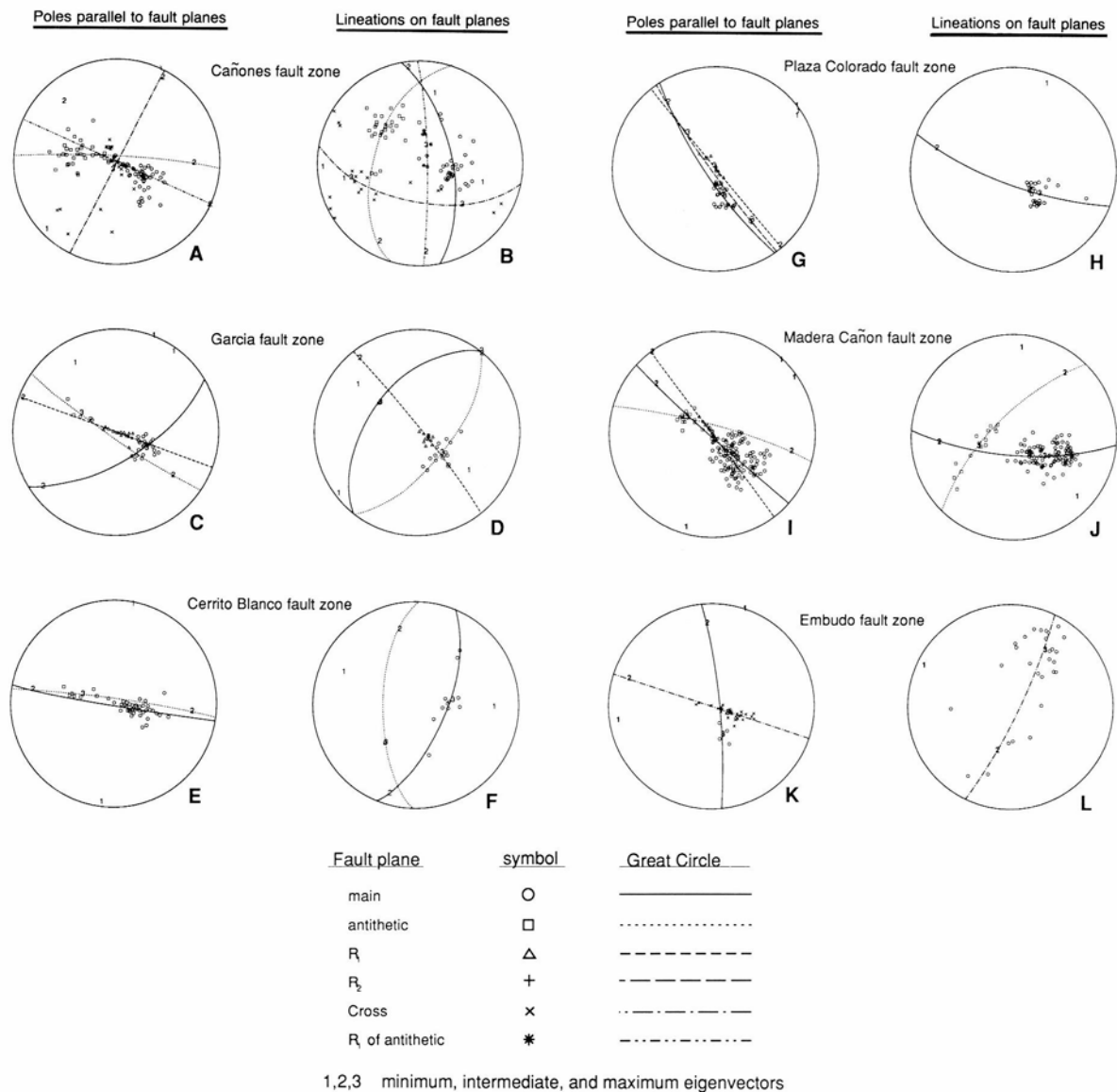


FIGURE 9A-L.—Stereonets of structural data from faults found within the bounding the Abiquiu embayment.

lower Abiquiu Formations; Fig. 3) on the east. This estimate of stratigraphic throw at the surface is in good agreement with subsurface seismic imaging of the fault done by the 1990 SAGE field class (W. S. Baldrige, pers. comm. 1990, and unpublished seismic data).

The average rake of lineations on the main fault of the Cañones fault zone is 79° NNE, indicating that the fault zone has formed primarily through dip-slip movement, along with a small component of left-lateral slip on the main fault. [Note: average rake angle is always acute. Rake angle = (tan of angle between fault-plane strike and lineation trend)/(cos of the dip angle of the fault plane).]

Vertical motion along the Cañones fault zone appears to increase to the south where the fault zone bifurcates into the west and east splays. We use the deformation of the T1 surface preserved beneath the late Miocene basalt flows on Cerro Pedernal, Mesa Escoba, and Polvadera Mesa to estimate that there is approximately 1870 ft (570 m) of vertical offset across the east and west splays of the Cañones fault zone (Figs. 2, 4A). The amount of throw is calculated relative to the present-day Rio Chama gradient, which we assume is comparable to the late Miocene gradient of the

Rio Chama. The long-term vertical slip rate across the Cañones fault zone is approximately 0.007-0.008 cm/yr (600 m/ 8 my). This long-term rate is a minimum slip rate since we cannot constrain when after 8 Ma motion began and when motion ceased (if it has) along this fault zone.

Sedimentary units, traditionally thought of as rift-fill sediment (i.e. the Eocene El Rio Formation and late Oligocene to early Miocene Abiquiu Tuff of Smith, 1938; Fig. 3) are found both east and west of the Cannes fault zone. Interpretation of this spatial pattern by previous workers suggested that the early rift-filling sedimentation (El Rito and Abiquiu Formations of Smith, 1938) took place on the broadly warped eastern limb of the Nacimiento uplift (a Laramide structure on the eastern edge of the Colorado Plateau) and the west margin of the Española basin before late Miocene and Pliocene faulting created a morphologically distinct rift basin (May, 1980, 1984; Baltz, 1978; summary of Wood and Northrop, 1946, and Smith et al., 1970).

Garcia and Cerrito Blanco fault zones

The Garcia and Cerrito Blanco fault zones lie several kilometers east of the Cañones fault zone. Both fault zones

TABLE 4—Structure-data summary, eigenvector values.

Fault zone	Fault plane	Number of data	Poles perpendicular to fault planes						K Ratio	C Ratio	Pattern	
			Vec-tor	Trend	Plunge	Eigen-values						
Cañones	Main	50	1	226	6	0.56	3.61±0.18	4.45±0.03	Strongly dev. cluster			
			2	318	22	1.47						
			3	122	67	47.97						
	Anti-thetic	39	1	183	5	0.76	2.56±0.14	3.85±0.05		Mod. dev. cluster		
			2	90	28	2.25						
			3	282	62	35.98						
	Cross	21	1	117	0.8	0.90	1.29±0.14	2.93±0.06			Mod. dev. clstr. w/ girdle	
			2	26	8	3.23						
			3	213	82	16.86						
	R ₁ of anti-thetic	6	1	24	0.5	0.00	1.03±0.07	10.34±0.16				Str. dev. grdl. and cluster
			2	114	0.8	0.03						
			3	261	89	5.97						
Garcia	Main	25	1	328	23	0.22	42.43±24.85	4.69±0.04	Str. dev. uniaxial cluster			
			2	233	12	0.25						
			3	117	64	24.52						
	Anti-thetic	5	1	34	5	0.01	1.33±0.21	6.33±0.17		Str. dev. cluster w/ girdle		
			2	127	31	0.13						
			3	296	58	4.86						
	R ₁	20	1	20	0.2	0.03	1.82±0.14	6.61±0.15			Str. dev. clstr. w/ girdle	
			2	290	4	0.28						
			3	113	86	19.70						
Cerrito Blanco	Main	37	1	10	2	0.26	2.39±0.13	4.94±0.06	Strongly dev. cluster			
			2	279	20	1.09						
			3	105	70	35.65						
	Anti-thetic	8	1	188	4	0.02	1.02±0.10	6.22±0.15		Str. dev. grdl. and cluster		
			2	96	26	0.33						
			3	285	63	7.66						
Plaza Colorado	Main	29	1	56	8	0.12	1.55±0.08	5.46±0.05	Str. dev. clstr. w/ girdle			
			2	323	21	1.01						
			3	165	68	27.87						
	R ₁	11	1	51	0.1	0.07	1.12±0.07	7.46±0.14		Str. dev. girdle and cluster		
			2	141	3	0.21						
			3	318	87	10.78						
	R ₂	3	1	54	4	0.00	0.71±0.08	11.71±0.29			Str. dev. girdle w/ cluster	
			2	147	38	0.02						
			3	319	51	2.98						
Madera Cañon	Main	112	1	42	2	2.83	6.48±0.19	3.61±0.01	Mod. dev. cluster			
			2	311	27	4.59						
			3	136	62	104.58						
	Anti-thetic	16	1	195	6	0.09	11.94±5.33	5.21±0.10		Strongly dev. girdle		
			2	102	23	0.13						
			3	300	66	15.78						
	R ₁	22	1	53	0.5	0.03	1.26±0.06	6.53±0.09			Str. dev. clstr. w/ girdle	
			2	323	0.9	0.56						
			3	172	89	21.41						
Embudo	Cross	32	1	18	0.6	0.07	1.19±0.05	6.05±0.06	Str. dev. girdle and cluster			
			2	288	16	1.14						
			3	110	74	30.78						
	Main	6	1	262	7	0.10	3.02±0.60	6.42±0.13		Strongly dev. cluster		
			2	355	24	0.05						
			3	158	65	5.94						

TABLE 4 continued

Fault zone	Fault plane	Number of data	Lineations on fault planes						
			Vec-tor	Trend	Plunge	Eigen-values	K Ratio	C Ratio	Pattern
Cañones	Main	30	1	259	25	0.82	4.16±0.58	3.51±0.05	Mod. dev. cluster
			2	352	7	1.62			
			3	96	64	27.56			
	Anti-thetic	27	1	107	38	0.69	3.79±0.51	3.59±0.06	Mod. dev. cluster
			2	207	13	1.46			
			3	313	49	24.85			
	Cross	20	1	10	31	1.34	0.67±0.08	2.30±0.07	Mod. dev. girdle w/ cluster
			2	134	43	5.30			
			3	258	31	13.36			
	R ₁ of anti-thetic	6	1	268	5	0.01	0.89±0.09	6.63±0.24	Str. dev. girdle w/ cluster
			2	176	14	0.25			
			3	16	75	5.74			
Garcia	Main	17	1	307	27	0.12	2.52±0.26	4.93±0.08	Strongly dev. cluster
			2	38	1	0.48			
			3	130	63	16.40			
	Anti-thetic	1	1	127	38	0.00	N.A.	N.A.	N.A.
			2	37	0	0.00			
			3	307	52	1.00			
	R ₁	10	1	231	3	0.02	5.03±0.99	6.36±0.11	Strongly dev. cluster
			2	322	9	0.05			
			3	123	80	9.93			
Cerrito Blanco	Main	11	1	292	24	0.06	0.62±0.08	5.10±0.13	Strongly dev. cluster
			2	196	11	1.37			
			3	85	63	9.57			
	Anti-thetic	1	1	91	26	0.00	N.A.	N.A.	N.A.
			2	346	26	0.00			
			3	219	51	1.00			
Plaza Colorado	Main	26	1	20	12	0.33	4.95±1.01	4.32±0.03	Strongly dev. cluster
			2	285	24	0.68			
			3	134	63	24.98			
Madera Cañon	Main	105	1	4	15	1.56	1.91±0.03	4.13±0.01	Strongly dev. clstr. w/ girdle
			2	266	28	6.44			
			3	118	58	97.00			
	Anti-thetic	14	1	134	16	0.04	0.54±0.04	5.85±0.09	Str. dev. girdle w/ cluster
			2	37	23	1.58			
			3	256	61	12.38			
Embudo	Cross	28	1	295	7	1.54	0.81±0.08	2.57±0.07	Mod. dev. girdle and cluster
			2	196	52	6.37			
			3						

NOTES: Vectors: 1 = minimum; 2 = intermediate; 3 = maximum.

$$K \text{ ratio} = [\ln (E_3/E_2)/\ln (E_2/E_1)]$$

$$C \text{ ratio} = \ln (E_3/E_1)$$

Pattern Determinations: If K ratio is: <0.05 uniaxial girdle; 0.05 - 0.5 girdle; 0.5 - 0.8 girdle with cluster; 0.8 - 1.25 girdle and cluster; 1.25 - 2 cluster with girdle; 2-20 cluster; >20 uniaxial cluster. If C ratio is: <0.5 randomly distributed; 0.5-1.5 weakly developed pattern; 1.5-4 moderately developed pattern; and >4 strongly developed pattern.

trend NNE (N 15-27° E) with normal faults dipping 6470° to the ENE. Antithetic faults, located tens to hundreds of meters east and parallel to the main fault, form graben structures along the faults. In addition, the two fault zones are connected by Cerrito de la Ventana, a basaltic dike and fault zone which trends approximately N 35-45° E. The orientation of this dike and fault may have kinematic significance. The Garcia fault offsets upper Abiquiu Formation south of the Rio Chama and juxtaposes lower Abiquiu Formation (on the west side of the fault) against upper Abiquiu Formation (on the east side). The Cerrito Blanco fault juxtaposes upper Abiquiu Formation (west side) against the Ojo Caliente Member of the Tesuque Formation (east side) along Cerrito Blanco. North of Cerrito Blanco, near the intersection of Cerrito Blanco fault zone with Cerrito de la Ventana, lower Abiquiu Formation and El Rito Formation (on the west side) are juxtaposed against the Ojo Caliente and ChamaEl Rito Members of the Tesuque Formation and the upper Abiquiu Formation. In general, the farther north along this fault and along Cerrito de la Ventana, the older are the strata offset by the faults.

Lineations on the fault planes of the Garcia fault zone indicate that dip-slip movement is dominant, but with a minor component of right-lateral slip (average rake of lineations on fault plane is 84° SSW). Lineations on fault planes of the Cerrito Blanco fault zone also indicate dominant dip-slip movement, but with a minor left-lateral slip (average rake of lineations is 83° SSE). Normal faulting on these two fault zones appears to have thrown the T4 surface (preserved on Cañones Mesa and Mesa de Abiquiu by burial with 3.2-2.8 Ma El Alto basalt flows) 560 ft (170 m) relative to the present-day Rio Chama surface. Combined the longterm vertical slip rate for the Garcia and Cerrito Blanco fault zones is 0.006 cm/yr (170 m/3 my). Individually, the Garcia fault zone appears to have displaced a Lobato basalt flow [3 mi (5 km) southwest of Abiquiu] by approximately 250 ft (80 m), suggesting that the average vertical slip rate for the Garcia and Cerrito Blanco fault zones individually is about 0.003 cm/yr (80-90 m/3 my). As these faults do not appear to displace Quaternary terraces in the Rio Chama valley, these long-term slip rates are minimum values.

Plaza Colorado fault zone

The Plaza Colorado fault zone strikes N 75° E and dips 68° SSE, juxtaposing upper Abiquiu Formation on both sides of the fault zone. Lineations on the fault-plane surface have an average rake of 77° ENE, again suggesting that movement on the fault is primarily dip-slip, with a minor component of left-lateral slip. We have been unable to calculate a slip rate for the Plaza Colorado fault zone because we have not located a piercing point nor observed a displacement of well-developed, dated surface.

Madera Cañon fault zone

The Madera Cañon fault zone strikes NE. The main fault plane dips an average of 62° SE. An antithetic fault plane strikes nearly parallel to the main fault trace and dips NW. The result is the formation of a distinct graben within the fault zone (Stop 8). The fault zone juxtaposes upper Abiquiu Formation on the northwest side of the fault zone against the Chama—El Rito Member of Tesuque Formation on the southeast side. The average rake of fault-plane lineations is 86° NE, indicating that the graben formed from nearly pure extension with only a minor amount of left-lateral slip.

The Madera Cañon fault zone exhibits late Pleistocene movement with disruption of the unit Q4 (Pinedale-equivalent surface?) but not the immediately younger unit Q5 (Fig. 10; Stop 8). The Q4 pediment surface on the west side of Madera Cañon has been offset about 30 ft (10 m), while the longitudinal profile of unit Q5 is undeformed, indicating that the last detectable movement on the Madera Cañon fault zone postdates formation of unit Q4, but antedates formation of the Q5 surface. A tentative late Pleistocene slip rate on this fault is about 0.01-0.007 cm/yr (10 m/ approximately 80-150 ka; see Table 2 for age estimates of Quaternary surfaces).

Embudo fault zone

The Embudo fault zone generally trends ENE and dips an average of 75° SSE. In the vicinity of Arroyo de la Presa (Stop 2), a series of NNE-trending cross-fault segments connects left-stepping, en-echelon, ENE-trending main-fault segments. Miocene sedimentary rocks and basalt flows and Pliocene(?) rocks south of the zone dip steeply to the south and are overturned locally. The Ojo Caliente Member of Tesuque Formation and the lower Chamita Formation crop out north of the fault (Dethier and Manley, 1985; Aldrich and Dethier, 1990), but are not exposed to the south.

The Embudo fault zone differs from the other faults in several important aspects. First, based on seismic images and gravity measurements, it appears to have a significant structural relief (second only perhaps to the Cañones fault zone). Second, right-lateral rather than left-lateral slip characterizes movement on main-fault segments in the Arroyo de la Presa area (Aldrich, 1986; Stop 2). However, the average rake of lineations on the short, NNE-trending cross-fault segments is 32° NNE and yields a left-lateral sense of movement. Unfortunately, we have not yet found sufficient fault-plane data to rigorously quantify movement on the ENE-trending main-fault segments of the Embudo fault zone. Finally, the Embudo fault zone appears to be an active transfer fault, accommodating differences between the faster spreading rates in the Española basin and the slower spreading rates in the Abiquiu embayment and San Luis basin (Aldrich, 1986).

Objectives of our ongoing structural analyses include enhancement of existing fault-plane data with more measurements from key fault localities which are currently under-represented in our data set (e.g. the ENE-trending main-fault segments of the Embudo fault zone). In addition, microscopic examination of oriented fault-gouge samples

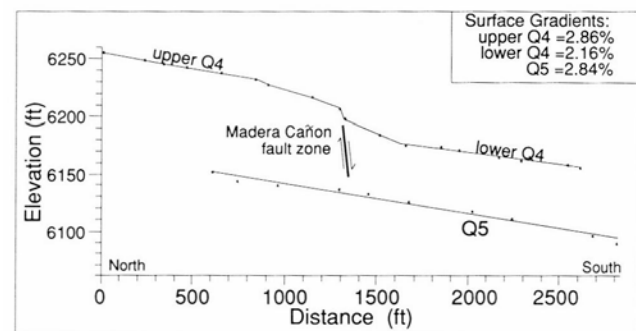


FIGURE 10—Longitudinal profile along the pediment surface of the Madera Cañon drainage. Offset of the pediment surfaces illustrates Quaternary tectonism on the Madera Cañon fault zone. The last episode of faulting offsets Q4(?) surface by 30 ft (10 m), but has not affected the Q5(?) surface.

have begun, along with observations of megascopic features, such as the attitude of dikes which presumably are oriented in a plane orthogonal to the minimum compressive stress(?).

With enhanced data sets of micro-, meso-, and megascale kinematic indicators, the regional tectonic significance of the local structures can be addressed. Important questions to address include the temporal significance of structures and the state of the regional stress field affecting the central Rio Grande rift of northern New Mexico during the Neogene and Quaternary periods. Specifically, did NNE-trending faults form coevally or successively, as suggested by the offset of progressively younger strata in an easterly direction? Are the NNE- and ENE-trending fault sets conjugate, formed in response to a single, mutually experienced stress field or, alternatively, in response to progressive change in the regional stress field (perhaps due to the 45° clockwise rotation of the Colorado Plateau reported by Zoback and Thompson, 1978; Zoback and Zoback, 1980; Zoback et al., 1981; Aldrich and Laughlin, 1984; Aldrich, 1986)? Does the fault pattern reflect transtension with formation of a pull-apart basin? Finally, is the megascale pattern congruous with an intra-rift transfer structure (i.e. Embudo fault zone) that accommodates en-echelon offset of rift grabens and differences in extension on either side of the accommodation zone (e.g. Aldrich, 1986)?

Conclusions and future work

The geomorphic history of the Abiquiu embayment and east flank of the Jemez Mountains comprises two periods of aggradation (the Puye and Bandelier aggradations); three periods of incision (the late Miocene through Pliocene, pre- and post-Bandelier periods of incision); four pre-Quaternary geomorphic surfaces (T1—T4, designated from oldest to youngest) and as many as 10 Quaternary surfaces. These geomorphic features record multiple cycles of large-scale aggradation and incision along the northern and eastern flanks of the Jemez Mountains, suggesting that the construction of the volcanic pile and the voluminous eruption of volcanic material have had an impact on the geomorphology of the area.

Structural development of a distinct morpho-tectonic rift basin began in the late Miocene (Baltz, 1978; Wood and Northrop, 1946) with the onset of Lobato volcanism and the postulated concomitant movement on the Cañones fault zone. We infer from the apparent displacement of the T4 surface that subsequent movement occurred after 3 Ma on the Garcia and Cerrito Blanco fault zones. Finally, the Embudo and Pajarito fault zones seem to have been active during the Pliocene and Quaternary (approximately 4-5 Ma; Manley, 1976a, 1978; Golombek, 1983; Gardner and Goff, 1984; Aldrich, 1986). The Embudo fault zone appears to be a transfer fault which segments the Española basin into the shallow Abiquiu embayment to the northwest and a deeper basin to the southeast. This intra-basin tectonism may have important consequences on the initial formation, subsequent preservation, and eventual correlation of geomorphic and sedimentologic features between basins as well as within a single basin.

The significance of two distinct fault sets (one oriented roughly NNE—SSW and the other ENE—WSW) is still enigmatic. Specifically, do these fault sets reflect: (1) a coeval conjugate set of related faults formed in response to one stress field; (2) a coeval set of related faults formed from

lateral-slip (or oblique-slip) motion within or adjacent to a pull-apart basin; or (3) a time-transgressive set of faults that formed as the regional stress field changed due to clockwise rotation of the Colorado Plateau.

Better temporal control on mid- to late Quaternary surfaces would assist in region-wide correlation of surfaces, better address roles of climatic—tectonic—volcanic perturbations in landscape evolution, and allow for calculation of rates of landscape evolution. Such time control is currently being pursued with attempts to use U-series disequilibria dating of carbonate rinds formed on clasts in terrace deposits.

Acknowledgments

We would like to thank S. G. Wells, C. Mawer (University of New Mexico), C. D. Harrington, W. S. Baldrige, J. N. Gardner, M. J. Aldrich, Jr., S. L. Reneau (Los Alamos National Laboratory), and J. W. Hawley (New Mexico Bureau of Mines & Mineral Resources) for advice, comments, and ideas shared with us during our years of work in the Rio Grande rift. We are grateful to S. G. Wells and C. D. Harrington for their critical reviews of an earlier draft of this paper.

Grant Meyer (University of New Mexico) provided Gonzalez with invaluable field assistance and entertained him with his humor. Anthony Garcia and Eric Montoya (Los Alamos National Laboratory) drafted figures and maps, and Barbara Hahn and Josephine Ortega (Los Alamos National Laboratory) prepared the tables. We are most grateful for their professional assistance and patience.

Financial support to Gonzalez for field work came from Sigma Xi, the Scientific Society, New Mexico Geological Society, Geological Society of America, and the Geology Department and the Student Research Allocations Fund of the University of New Mexico. The Earth and Environmental Sciences Division of the Los Alamos National Laboratory provided invaluable logistical support for field operations and equipment for laboratory analyses.

References

- Aldrich, M. J., Jr., 1986, Tectonics of the Jemez Lineament in the Jemez Mountains and Rio Grande rift: *Journal of Geophysical Research*, 91(B2): 1753-1762.
- Aldrich, M. J., Jr., and Laughlin, A. W., 1984, A model for the tectonic development of the southeastern Colorado Plateau boundary: *Journal of Geophysical Research*, 89(B 12): 10,217-10,218.
- Aldrich, M. J., Jr., and Dethier, D. P., 1990, Stratigraphic and tectonic evolution of the northern Espanola basin, Rio Grande rift, New Mexico: *Geological Society of America, Bulletin*, 102: 1695-1705.
- Aldrich, M. J., Jr., Laughlin, A. W., Meade, J. S., and Peirce, H. W., 1986, The Jemez Lineament: Structural boundaries and control on sedimentary facies, tectonism, and mineralization: *Proceedings of the 6th International Conference on Basement Tectonics*, pp. 104-113.
- Bachman, G. O., and Mehnert, H. H., 1978, New K—Ar dates and the late Pliocene to Holocene geomorphic history of the central Rio Grande region, New Mexico: *Geological Society of America, Bulletin*, 89: 283-292.
- Baldrige, W. S., Bartov, Y., and Kron, A., 1983, Geologic map of the Rio Grande rift and southeastern Colorado Plateau, New Mexico and Arizona; *supplement to Riecker, R. E., (ed.), Rio Grande rift: tectonics and magmatism: American Geophysical Union, Washington, D.C.*
- Baldrige, W. S., Olsen, K. H., and Callender, J. F., 1984, Rio Grande rift: Problems and perspectives: *New Mexico Geological Society, Guidebook* 35: 1-12.
- Baldrige, W. S., Damon, P. E., Shafiqullah, M., and Bridwell, R. J., 1980, Evolution of the central Rio Grande rift, New Mexico: New potassium—argon ages: *Earth and Planetary Science Letters*, 51: 309-321.
- Baltz, E. H., 1978, Resume of Rio Grande depression in north-central

- New Mexico: New Mexico Bureau of Mines & Mineral Resources, Circular 163: 210-228.
- Biehler, S., Ferguson, J., Baldrige, W. S., Jiracek, G. R., Aldern, J. L., Martinez, M., Fernandez, R., Romo, J., Gilpin, B., Braile, L. W., Hersey, D. R., Luyendyk, B. P., and Aiken, C. L. (in press), A geophysical model of the Espanola basin, Rio Grande rift, New Mexico: Geophysics.
- Brown, L. L., and Golombek, M. P., 1986, Block rotations in the Rio Grande rift, New Mexico: *Tectonics*, 5: 423-438.
- Bryan, K., 1938, Geology and ground-water conditions of the Rio Grande depression in Colorado and New Mexico; *in* U.S. National Resources Planning Board, The Rio Grande Joint Investigation in the Upper Rio Grande basin: U.S. Government Printing Office, 1(2): 197-225.
- Bryan, K., and McCann, F. T., 1936, Successive pediments and terraces of the upper Rio Puerco in New Mexico: *Journal of Geology*, 44: 145-172.
- Bryan, K., and McCann, F. T., 1938, The Ceja del Rio Puerco, a border feature of the Basin and Range province in New Mexico: Pt. 2, Geomorphology: *Journal of Geology*, 46(1): 1-16.
- Cabot, E. C., 1938, Fault border of the Sangre de Cristo Mountains north of Santa Fe, New Mexico: *Journal of Geology*, 46: 88-105.
- Church, R. S., and Hack, J. T., 1939, An exhumed erosion surface in the Jemez Mountains, New Mexico: *Journal of Geology*, 47: 613-629.
- Dethier, D. P. (submitted), Geologic map of the White Rock quadrangle: New Mexico Bureau of Mines & Mineral Resources, scale 1:24,000.
- Dethier, D. P., and Demsey, K. A., 1984, Erosional history and soil development on Quaternary surfaces, northwest Espanola basin, New Mexico: *New Mexico Geological Society, Guidebook 35*: 227-233.
- Dethier, D. P., and Harrington, C. D., 1987, Geologic dating of late Cenozoic erosion surfaces near Espanola, New Mexico; *in* Menges, C. M. (ed.), Quaternary tectonics, landform evolution, soil chronologies and glacial deposits—northern Rio Grande rift of New Mexico: *Friends of the Pleistocene Field-trip Guidebook*, pp. 111-131.
- Dethier, D. P., and Manley, K., 1985, Geologic map of the Chili quadrangle, Rio Arriba County, New Mexico: U.S. Geological Survey, Miscellaneous Field Studies Map MF-1814, scale 1:24,000.
- Dethier, D. P., and Martin, B. A., 1984, Geology and structure along part of the northeast Jemez Mountains, New Mexico: *New Mexico Geological Society, Guidebook 35*: 145-150.
- Dethier, D. P., Harrington, C. D., and Aldrich, M. J., 1988, Cenozoic erosion rates, Espanola basin, New Mexico: *Geological Society of America, Bulletin*, 100: 928-937.
- Dethier, D. P., Halverson, N., Marrack, L., Meagher, M., Oelkers, E., Harrington, C. D., Sarna-Wojcicki, A., and Meyer, C. E., 1990, Occurrence of the Lava Creek B tephra layer in the northwestern Espanola basin, New Mexico: *New Mexico Geology*, 12(4): 77-82.
- Dransfield, B. J., and Gardner, J. N., 1985, Subsurface geology of the Pajarito Plateau, Espanola basin, New Mexico: Los Alamos National Laboratory, Report LA-10455-MS.
- Galusha, T., and Blick, J. C., 1971, Stratigraphy of the Santa Fe Group, New Mexico: *American Museum of Natural History, Bulletin*, 144: 1-127.
- Gardner, J. N., and Goff, F., 1984, Potassium-argon dates from the Jemez volcanic field: Implications for tectonic activity in the north-central Rio Grande rift: *New Mexico Geological Society, Guidebook 35*: 75-82.
- Gardner, J. N., and House, L., 1987, Seismic hazards investigations at Los Alamos National Laboratory, 1984-1985: Los Alamos National Laboratory, Report LA-1 1072-MS.
- Gibbs, A. D., 1984, Structural evolution of extensional basin margins: *Geological Society of London, Journal*, 141: 609-620.
- Gile, L. H., Hawley, J. W., and Grossman, R. B., 1981, Soils and geomorphology in the Basin and Range area of southern New Mexico—*Guidebook to the Desert Project*: New Mexico Bureau of Mines & Mineral Resources, Memoir 39, 222 pp.
- Golombek, M. P., 1983, Geology, structure, and tectonics of the Pajarito fault zone in the Espanola basin of the Rio Grande rift, New Mexico: *Geological Society of America, Bulletin*, 94: 192-205.
- Golombek, M. P., McGill, G. E., and Brown, L., 1983, Tectonic and geologic evolution of the Espanola basin, Rio Grande rift: Structure, rate of extension, and relation to the state of stress in the western United States: *Tectonophysics*, 94: 483-507.
- Griggs, R. L., 1964, Geology and ground-water resources of the Los Alamos area, New Mexico: U.S. Geological Survey, Water-Supply Paper 1753, 107 pp.
- Harrington, C. D., and Aldrich, M. J., 1984, Development and deformation of Quaternary surfaces on the northeastern flank of the Jemez Mountains: *New Mexico Geological Society, Guidebook 35*: 235-239.
- Harvey, M. D., Germanoski, D., and Pitlick, J., 1988, Terrace-forming processes in modern fluvial systems: Implications for Quaternary studies (abs.): *Geological Society of America, Abstracts with Programs*, 20(7): A374.
- Hawley, J. W. (ed.), 1978, *Guidebook to Rio Grande rift in New Mexico and Colorado*: New Mexico Bureau of Mines & Mineral Resources, Circular 163: 241 pp.
- Ingersoll, R. V., Cavazza, W., Baldrige, W. S., Shafiqullah, M., 1990, Cenozoic sedimentation and paleotectonics of north-central New Mexico: Implications for initiation and evolution of the Rio Grande rift: *Geological Society of America, Bulletin*, 102: 1280-1296.
- Kelley, V. C., 1979, Geomorphology of Espanola basin: *New Mexico Geological Society, Guidebook 7*: 281-288.
- Kelson, K. I., 1986a, Long-term tributary adjustments to base-level lowering northern Rio Grande rift, New Mexico: Unpublished MS thesis, University of New Mexico, Albuquerque, 210 pp.
- Kelson, K. I., 1986b, Long-term tributary adjustments to base-level lowering, northern New Mexico (abs.): *Geological Society of America, Abstracts with Programs*, 18(5): 366.
- Kelson, K. I., and Wells, S. G., 1987, Present-day fluvial hydrology and long-term tributary adjustments, northern New Mexico; *in* Menges, C. M. (ed.), Quaternary tectonics, landform evolution, soil chronologies and glacial deposits—northern Rio Grande rift of New Mexico: *Friends of the Pleistocene Field-trip Guidebook*, pp. 95-109.
- Lambert, P. W., 1968, Quaternary stratigraphy of the Albuquerque area, New Mexico: Unpublished PhD dissertation, University of New Mexico, Albuquerque, 329 pp.
- Love, D. W., Reimer, R. F., Hawley, J. W., Johnpeer, G. D., and Bobrow, D. J., 1987, Summary of geotechnical investigations near Espanola, New Mexico: *Friends of the Pleistocene-Rocky Mountain cell, Field-trip guidebook*, pp. 133-157.
- Manley, K., 1976a, The late Cenozoic history of the Espanola basin, New Mexico: Unpublished PhD dissertation, University of Colorado, Boulder, 171 pp.
- Manley, K., 1976b, K-Ar age determinations of Pliocene basalts from the Espanola basin, New Mexico: *Ischron/West*, no. 16: 29-30.
- Manley, K., 1978, Pliocene deformation along the Rio Grande rift in the Espanola basin, New Mexico (abs.): *Geological Society of America, Abstracts with Programs*, 5(10): 233.
- Manley, K., 1979a, Stratigraphy and structure of the Espanola basin, Rio Grande rift: *Tectonics and magmatism*: American Geophysical Union, Washington, D.C., pp. 71-86.
- Manley, K., 1979b, Tertiary and Quaternary stratigraphy of the northeast plateau, Espanola basin, New Mexico: *New Mexico Geological Society, Guidebook 30*: 231-236.
- Manley, K., 1982, Geologic map of the Cannes quadrangle, Rio Arriba County, New Mexico: U.S. Geological Survey, Miscellaneous Field Studies Map MF-1440, scale 1:24,000.
- Manley, K., and May, S. J., 1984, Third-day road log from Taos to Tres Piedras, Tusas, Spring Canyon, Tres Piedras, Las Tablas, Petaca, La Madera, and Ojo Caliente: *New Mexico Geological Society, Guidebook 35*: 349-376.
- Manley, K., and Mehnert, H. H., 1981, New K-Ar ages for Miocene and Pliocene volcanic rocks in the northwestern Espanola basin and their relationships to the history of the Rio Grande rift: *Ischron/West*, no. 30: 5-8.
- Menges, C. M., 1988, The tectonic geomorphology of mountain front landforms in the northern Rio Grande rift, New Mexico: Unpublished PhD dissertation, University of New Mexico, Albuquerque.
- Morgan, P., and Golombek, M. P., 1984, Factors controlling the phases and styles of extension in the northern Rio Grande rift: *New Mexico Geological Society, Guidebook 35*: 13-19.
- Muehlberger, W. R., 1979, The Embudo fault between Pilar and Arroyo Hondo, New Mexico: An active intracontinental transform fault: *New Mexico Geological Society, Guidebook 30*: 77-82.
- Ruhe, R. V., 1967, Geomorphic surfaces and surficial deposits in southern New Mexico: *New Mexico Bureau of Mines & Mineral Resources, Memoir 18*: 1-66.
- Sarna-Wojcicki, A. M., Morrison, S. D., Meyer, C. D., and Hillhouse, J. W., 1987, Correlation of upper Cenozoic tephra layers between sediments of the western United States and comparison with biostratigraphic and magnetostratigraphic data: *Geological Society of America, Bulletin*, 98: 207-223.
- Schumm, S. A., 1985, Explanation and extrapolation in geomorphology: seven reasons for geologic uncertainty: *Japanese Geomorphological Union, Transactions*, 6(1): 1-18.
- Smith, C. T., Budding, A. J., and Pitrat, C. W., 1961, Geology of the southeastern part of the Chama basin: *New Mexico Bureau of Mines & Mineral Resources, Bulletin 75*, 57 pp.

- Smith, H. T. U., 1938, Tertiary geology of the Abiquiu quadrangle, New Mexico: *Journal of Geology*, 46: 933-965.
- Smith, R. L., Bailey, R. A., and Ross, C. S., 1970, Geologic map of the Jemez Mountains, New Mexico: U.S. Geological Survey, Miscellaneous Geological Investigations Map 1-571, scale 1:25,000.
- Spell, T. L., Harrison, T. M., and Wolff, J. A., 1989, ⁴⁰Ar/³⁹Ar dating of the Bandelier Tuffs and associated ignimbrites: Constraints on evolution of the Bandelier magma system: EOS, American Geophysical Union, Transactions, 70(43): 1413.
- Vernon, J. H., and Riecker, R. E., 1989, Significant Cenozoic faulting, east margin of the Española basin, Rio Grande rift, New Mexico: *Geology*, 17: 230-233.
- Waresback, D. B., 1986, The Puye Formation, New Mexico: Analysis of a continental rift-filling volcanoclastic alluvial-fan sequence: Unpublished MS thesis, University of Texas at Arlington, 269 pp.
- Waresback, D. B., and Turbeville, B. N., 1990, Evolution of a Plio-Pleistocene volcanogenic-alluvial fan: The Puye Formation, Jemez Mountains, New Mexico: Geological Society of America, Bulletin, 102: 298-314.
- Wells, S. G., Kelson, K. I., and Menges, C. M., 1987, Quaternary evolution of fluvial systems in the northern Rio Grande rift, New Mexico and Colorado: Implications for entrenchment and integration of drainage systems; *in* Menges, C. M. (ed.), Quaternary tectonics, landform evolution, soil chronologies and glacial deposits—northern Rio Grande rift of New Mexico: Friends of the Pleistocene, Field-trip Guidebook, pp. 55-69.
- Wells, S. G., McFadden, L. D., and Schultz, J. D., 1990, Eolian landscape evolution and soil formation in the Chaco dune field, southern Colorado Plateau, New Mexico: *Geomorphology*, 3: 517-546.
- Wilson, J. E., 1977, Stratigraphy and structure of part of the Abiquiu embayment of the Rio Grande rift, New Mexico: Unpublished MS thesis, University of New Mexico, Albuquerque, 89 pp.
- Wright, H. E., Jr., 1946, Tertiary and Quaternary geology of the lower Rio Puerco area, New Mexico: Geological Society of America, Bulletin, 57: 383-456.
- Wood, G. H., Jr., and Northrop, S. A., 1946, Geology of the Nacimiento Mountains, San Pedro Mountains, and adjacent plateaus in parts of Sandoval and Rio Arriba Counties, New Mexico: U.S. Geological Survey, Oil and Gas Investigations Preliminary Map 57.
- Zoback, M. L., and Thompson, G. A., 1978, Basin and Range rifting in northern Nevada: Clues from a mid-Miocene rift and its subsequent offsets: *Geology*, 6: 111-116.
- Zoback, M. L., and Zoback, M., 1980, State of stress in the conterminous United States: *Journal of Geophysical Research*, 85: 6113-6156.
- Zoback, M. L., Anderson, R. E., and Thompson, G. A., 1981, Cainozoic evolution of the state of stress and style of tectonics of the Basin and Range province of the western United States: Royal Society of London, Philosophical Transactions (A), 300: 407-434.

Appendix: Field-trip stops and topics of discussion

A detailed road log is Open-file Report no. 374, available from New Mexico Bureau of Mines & Mineral Resources, Socorro, New Mexico 87801.

Stop 1. Espanola High School. (1) Age of deposits behind high school. (2) Methods of Quaternary dating used in the region.

Stop 2. Arroyo de la Presa. (1) Importance of the Embudo fault as an intra-basin structure. (2) Discuss the changes in basin evolution across the Embudo: relative base-level stability north of the transfer fault and substantial Pliocene aggradation south of the fault (refer to Fig. 4B and 4C).

Stop 3. Arroyos between Medanales and Abiquiu. (1) Traverse a flight of axial-stream Quaternary terraces (refer to Fig. 4E). (2) Visit a deposit of Lava Creek B ash. (3) Discuss landform evolution in rift (i.e. the proclivity for landscape inversion).

Stop 4. Abiquiu Dam. View Quaternary surfaces formed in the Colorado Plateau and contrast with the landform evolution in the rift. (2) Entertain a discussion on the problems/difficulties with using soils on older Quaternary surfaces.

Overnight at Ghost Ranch.

Stop 5. Roadcut on US-84 near Ghost Ranch turnoff. (1) Snail locality and use of amino-acid racemization dating method. (2) Overlook Colorado Plateau and margin of rift to see offset of the T1 surface (Cerro Pedernal, Mesa Escoba,

Polvadera Mesa, and Cañons Mesa). (3) Discuss Eocene to late Miocene rift history.

Stop 6. US-84, 5 mi west of Abiquiu: Cañones fault zone. (1) View the Cannes fault zone, which offsets upper Paleozoic and Mesozoic rocks (to the west) against Tertiary rift-fill sediment (to the east) at the surface. (2) Gain another perspective on the offset of the T1 surface. (3) Finally view offset on the Garcia fault zone.

Stop 7 (optional). Polvadera Mesa and overlook of Cañoncito Seco. Long drive over dirt roads culminating in a lunch spot up in the ponderosa pines. (1) Cañoncito Seco illustrates the magnitude of the pre-Bandelier incision episode and the Bandelier aggradation episode (refer to Fig. 4D) and the post-Bandelier incision episode (refer to Fig. 4E).

Stop 8. Madera Canon pediments. (1) View displacement of Quaternary surfaces by the Madera Cañon fault zone (see Fig. 6). (2) Look at soil pits across the fault zone if possible.

Stop 9. White Rock Canyon overlook. Discuss: (1) the Puye aggradation episode (refer to Fig. 4C); (2) west-tilting of Española basin against Pajarito fault; (3) the pre-Bandelier incision episode and Bandelier aggradation episode preserved in the paleocanyon across the Rio Grande; (4) the age of gravel deposit (Qoal) over the Cerros del Rio basalt; and (5) wrap up the field trip.

Correlation of Triassic strata of the Colorado Plateau and southern High Plains, New Mexico

Spencer G. Lucas

New Mexico Museum of Natural History, P.O. Box 7010, Albuquerque, New Mexico 87194

Introduction

Triassic strata on the Colorado Plateau pertain to the Moenkopi and Chinle Formations of Early—Middle and Late Triassic age, respectively. On the southern High Plains of eastern New Mexico and west Texas, Triassic strata have traditionally been assigned to the Dockum Group of Late Triassic age. However, recent studies have identified the Moenkopi Formation (Anton Chico Member) as the oldest Triassic strata in eastern New Mexico (Lucas and Morales, 1985; Lucas and Hunt, 1987, 1989b).

Moenkopi, Chinle, and Dockum strata are nonmarine redbeds deposited in fluvial and lacustrine environments. Their chronology largely rests on vertebrate fossils and palynology (Lucas and Hunt, 1989a). Correlation of these Triassic strata from the Colorado Plateau to the southern High Plains has long been uncertain, partly because of a perceived absence of Triassic strata across the Rio Grande rift of central New Mexico (e.g. McKee et al., 1959; Finch and Wright, 1983). However, significant outcrops of Triassic strata are present in the Rio Grande rift of north-central New Mexico, especially in the Hagan basin between Albuquerque and Santa Fe (Fig. 1).

Recent research on the stratigraphy and paleontology of the Triassic rocks across northern New Mexico allows relatively certain correlation of Moenkopi, Chinle, and Dockum rocks from the Colorado Plateau to the southern High Plains. This correlation suggests continuity of Triassic deposition across a broad region of the Southwest and undermines the proposed existence of a Pedernal uplift separating Chinle and Dockum depositional basins during the Late Triassic. Here, I review Triassic stratigraphy, paleontology, and correlation from the eastern edge of the Colorado Plateau to the southern High Plains and discuss briefly the revised Triassic paleogeography mandated by this review. The last section of this article presents a field guide to Triassic outcrops in central New Mexico critical to the review presented here.

Colorado Plateau edge: Lucero uplift to Chama basin

Triassic stratigraphy and paleontology from the Lucero uplift to the Chama basin, along the eastern edge of the Colorado Plateau (Fig. 1), have been recently reviewed by Kurtz (1978), Kurtz and Anderson (1980), Woodward (1987), Lucas and Hayden (1989a, b), Hunt and Lucas (1989a, b),

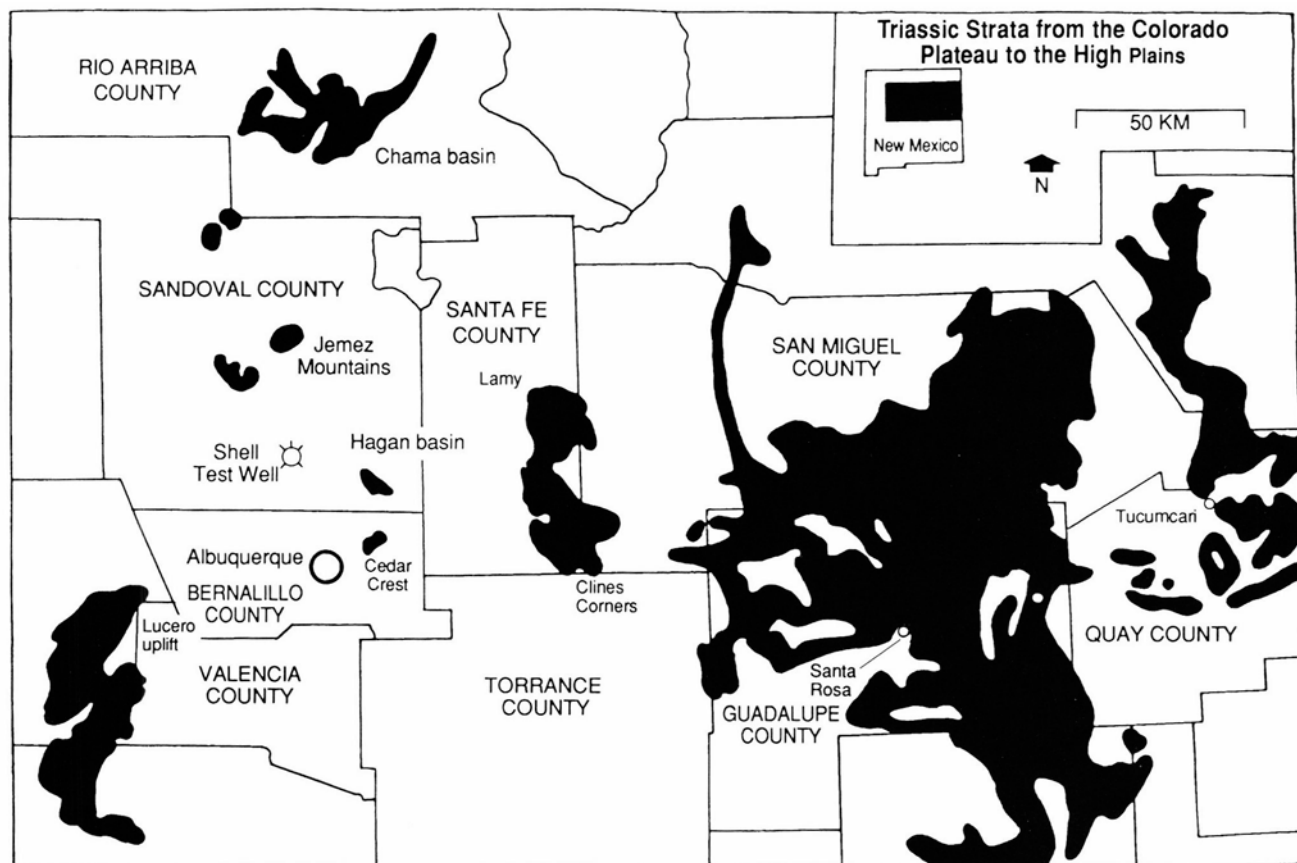


FIGURE 1—Location map of Triassic strata from the eastern edge of the Colorado Plateau to the southern High Plains of New Mexico (geology after Dane and Bachman, 1965).

1990a, b), Hunt et al. (1989a, b), and Dubiel (1989b).

The oldest Triassic strata along this transect (Figs. 1, 2) pertain to the Anton Chico Member of the Moenkopi Formation, as much as 68 m of grayish-red and reddish-brown lithic wackestones, mudstones, and siltstones that yield charophytes, ostracodes, bones of capitosauroid amphibians, and large footprints of *Chirotherium* reptiles indicative of an Early or Middle Triassic age (Kietzke, 1989a, b; Lucas and Hayden, 1989a, b). These strata, which rest disconformably on the Permian Glorieta and San Andres Formations, were earlier identified as Permian Bernal Formation in the Jemez Mountains (e.g. Wood and Northrop, 1946; Baars, 1962; Woodward, 1987).

Upper Triassic strata that rest disconformably on the Moenkopi Formation along the eastern edge of the Colorado Plateau pertain to the Chinle Formation. Two sets of member-level nomenclature are used for Chinle strata (Fig. 2). In the Lucero uplift, the Chinle consists of five members recognized across much of the southern edge of the Colorado Plateau (in ascending order): (1) Shinarump Member, as much as 24 m of silica-pebble conglomerate/sandstone and pedogenically modified siltstone, mudstone, and sandstone, the latter referred to informally as the "mottled strata"; (2) Bluewater Creek Member, 100 m or more of red sandstone and mudstone; (3) more than 1000 m of Petrified Forest Member, divided into lower and upper mudrock-dominated intervals by the Sonsela Sandstone Bed and containing the Correo Sandstone Bed at or near its top; (4) Owl Rock Member, about 36 m of grayish-red and very pale-green mudstone, grayish-red—purple bioturbated sandy siltstone and silty sandstone; and (5) Rock Point Member, about 70 m of laterally extensive beds of massive, moderately reddish-brown sandy siltstone and laminar to trough-crossbedded, moderately reddish-brown, very fine-grained, mature, quartzose sandstone. Contrary to some previous work (O'Sullivan, 1974, 1977; Dubiel, 1989), which only iden-

tified the Owl Rock and Rock Point Members as far east as Thoreau and Lupton, respectively, these units are present as far east as Petaca Pinta (T6N, R6W) in southeastern Cibola County (Maxwell, 1988a, b; Lucas and Hunt, 1991). The Middle Jurassic Entrada Sandstone overlies the Chinle Formation in the Lucero uplift.

To the north, in the Jemez and Nacimiento Mountains, the Chinle member-level terminology is different (Fig. 2), in part due to lithofacies changes and in part due to a local nomenclature developed by Huene (1911) and Wood and Northrop (1946). The oldest Chinle strata are the mottled strata and Agua Zarca Member (includes the "sandstone member" of Stewart et al., 1972; cf. Woodward, 1987), as much as 35 m of tan and gray quartzose sandstone and silica-pebble conglomerate. The Agua Zarca interfingers with the overlying Salitral Member, mostly blue, green, and gray bentonitic mudstone and siltstone as much as 30 m thick. The overlying Poleo Member is as much as 49 m of strata dominated by medium-grained sandstone and limestone-pebble conglomerate which rests unconformably on the Salitral. As much as 224 m of dominantly red and purple mudstone, sandstone, conglomerate, and pedogenic calcrete, the petrified Forest Member, overlie the Poleo. Locally, the Rock Point Member (siltstone member of Stewart et al., 1972, and Dubiel, 1989b) disconformably overlies the Petrified Forest Member. It consists of as much as 70 m of laterally extensive beds of moderately reddish-brown siltstone and sandstone. The Middle Jurassic Entrada Sandstone overlies Triassic strata in the Jemez Mountains—Chama basin area.

Correlation of the Triassic section in the Chama basin-Jemez Mountains with the Triassic section in the Lucero uplift is readily made on the basis of lithology, paleontology, and stratigraphic sequence. Thus, the Anton Chico Member of the Moenkopi Formation is present in both areas, and correlation of the Shinarump and the Agua Zarca has long

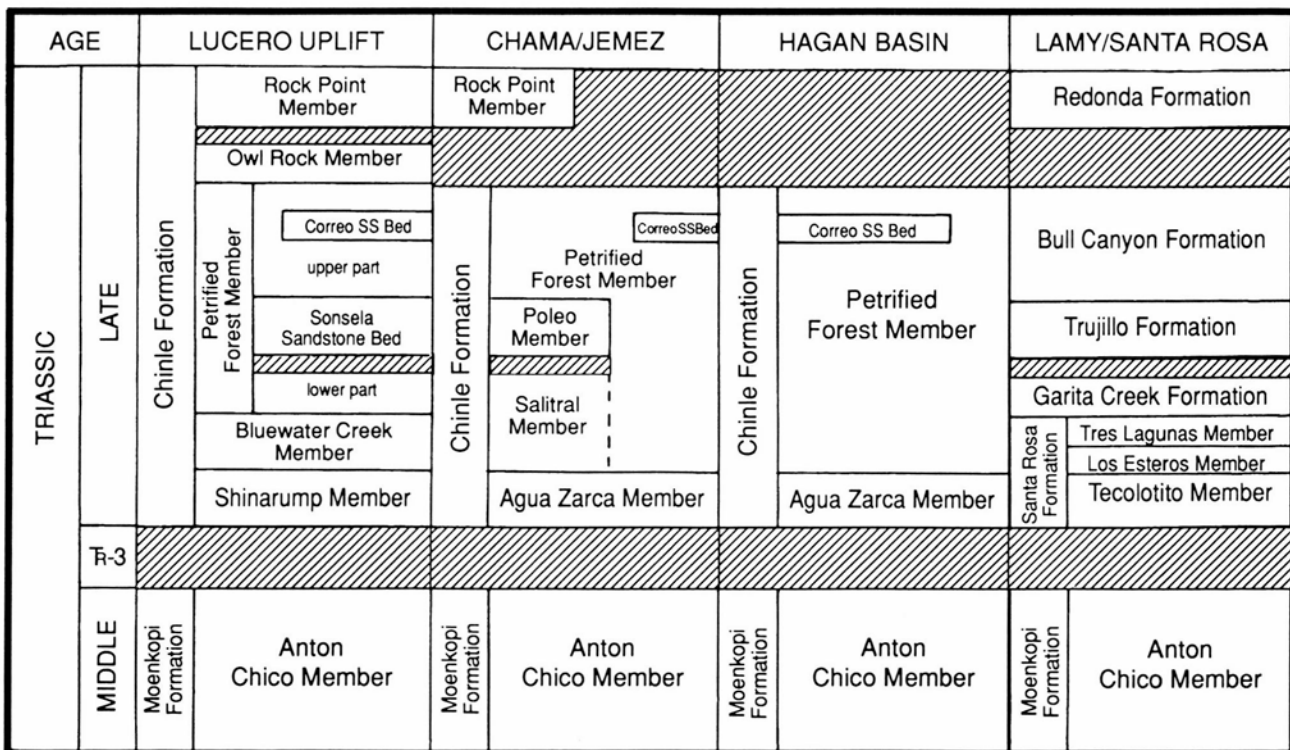


FIGURE 2—Triassic stratigraphic nomenclature and correlation for strata shown in Fig. 1.

been accepted (e.g. Wengerd, 1950). The small vertebrate fauna of the Salitral Member includes large metoposaurs, phytosaurs, the aetosaur *Longosuchus*, and a ?dinosaur (Hunt and Lucas, 1989b, 1990b). This late Carnian fauna is approximately of the same age as the fauna of the Bluewater Creek Member in west-central New Mexico, which includes the phytosaur *Angistorhinus*. Both faunas are of *Paleorhinus*-biochron age or early-late Carnian (Hunt and Lucas, in press).

In the Lucero uplift, the lower part of the Petrified Forest Member has produced large and small metoposaurs, phytosaurs, and the aetosaur *Stagonolepis* (Hunt et al., 1989a). This fauna indicates a late Carnian age slightly younger than the *Paleorhinus* biochron (Lucas, 1990; Hunt and Lucas, 1990b, in press). The Petrified Forest Member has two distinct faunas in the Jemez Mountains: an older fauna correlative with that of the lower Petrified Forest Member in the Lucero uplift and a younger fauna equivalent to that of the upper Petrified Forest Member on the southern Colorado Plateau (Hunt and Lucas, 1990a). The Rock Point Member in the Chama basin contains the mass-death assemblage of the Late Triassic dinosaur "*Coelophysis*" at Ghost Ranch (Colbert, 1989; Hunt and Lucas, 1989a, b), but at present no biochronologically useful fossils are known from the Rock Point elsewhere on the Colorado Plateau.

Rio Grande rift: Hagan basin

The Triassic section exposed in the Hagan basin (Fig. 1) is, with minor differences, very similar to that exposed in the Jemez Mountains (Fig. 2). An essentially identical Triassic section, much complicated by local structure, is exposed in the Placitas area (Fig. 1), 5-10 km southwest of the Hagan basin Triassic outcrops (Menne, 1989a, b).

The gap in Triassic exposure between the Jemez Mountains and Hagan basin is approximately 45 km. However, logs of two wildcat oil wells in this gap—Shell Oil Company Santa Fe Pacific No. 1 (Figs. 1, 3) and Avila Oil Company Odium Federal No. 1—provide stratigraphic data that indicate continuity of the Triassic section from the Jemez Mountains to the Hagan basin (Black and Hiss, 1974; though my picks of the unit contacts on these logs differ slightly from theirs). Thus, the Triassic section in the Shell well begins with 4.3 m (14 ft: 8870-8884 ft) of Anton Chico Member of the Moenkopi Formation resting on the Permian Glorieta Sandstone. The overlying 43 m (140 ft: 8730-8870 ft) of sandstone of the Chinle Agua Zarca Member are followed by 348 m (1142 ft: 7728-8870 ft) of mudstone and very minor sandstone of the Petrified Forest Member of the Chinle Formation overlain by the Entrada Sandstone. The uppermost Petrified Forest Member contains a 4.3 m (14 ft: 7736-7750 ft) thick sandstone that I identify as the Correo Sandstone Bed. A similar sandstone interval occupies the same stratigraphic position near the top of the exposed Chinle Formation along the escarpment southwest of NM-44 on the Zia Indian Reservation (T16N, R1W/R1E) in Sandoval County.

The Avila well reveals a similar stratigraphic section: 36 m (120 ft: 2495-2615 ft) of Moenkopi, 59 m (195 ft: 2300-2495 ft) of Agua Zarca, and 411 m (1350 ft: 950-2300 ft) of Petrified Forest Member. However, the Correo Sandstone Bed cannot be identified in the log, so it apparently is absent. Furthermore, the difference in the thicknesses (4.3 m vs. 36 m) of the Moenkopi Formation penetrated by the two wells reflects the unconformity at the base of the overlying

Chinle Formation. Lucas and Hayden (1989a) demonstrated a similar unconformity in outcrop between Red Mesa and Guadalupita Mesa in the Jemez Mountains.

Previous workers (Harrison, 1949; Reynolds, 1954; Kelley and Northrop, 1975; Picha, 1982; Woodward and Picha, 1989) divided the Triassic strata in the Hagan basin into basal Santa Rosa Sandstone and overlying Chinle Formation, except Smith (1961) who used Dockum Group divided into Santa Rosa Sandstone and "upper member." Strata of the Permian Bernal Formation were identified between the Santa Rosa and the Permian San Andres Formation.

The Triassic section in the Hagan basin begins with the Anton Chico Member of the Moenkopi Formation, as much as 20 m of grayish-red lithic wackestones and siltstones that rest disconformably on the San Andres Formation (Fig. 4A; Lucas and Hayden, in press). Kelley and Northrop (1975, p. 52) first identified these strata as Bernal Formation and stated that "locally the limestone of the Bernal contains small brachiopods." I have not been able to verify this claim and suspect that the brachiopods are from San Andres Limestone and were located as float on Moenkopi strata in this topographically rugged and structurally complex area.

The overlying lowermost part of the Chinle Formation is as much as 90 m of mostly laminar, grayish-white, quartzose sandstone and silica-pebble conglomerate with fossil logs (Fig. 4B, C) that have long been termed Santa Rosa Sandstone. However, I assign these strata to the Agua Zarca Member of the Chinle Formation because they closely resemble the Agua Zarca Member in lithology, occupy an identical stratigraphic position, and lack the medial mudstone interval (Los Esteros Member) characteristic of the Santa Rosa Formation near Lamy, the closest outcrops assigned with certainty to the Santa Rosa. The well-log data summarized above also support continuity of the Agua Zarca Member of the Chinle Formation between the Jemez Mountains and the Hagan basin.

Indeed, in the Hagan basin the mudstone-dominated strata immediately above the sandstones identified as Agua Zarca are mostly blue, green, and gray bentonitic mudstone similar to the Salitral Member to the west. Large metoposaur fossils from limestone-pebble conglomerates in this interval (Fig. 4D) also lend some support to this correlation. However, since the Poleo Sandstone Member is absent in the Hagan basin, I do not apply the name Salitral here. Instead, I refer the entire mudstone-dominated section above the Agua Zarca Member in the Hagan basin, the remainder of the Chinle Formation, to the Petrified Forest Member.

This unit is as much as 410 m of reddish-brown bentonitic mudstone intercalated with thin beds of laminar sandstone and limestone-cobble conglomerate (Fig. 4E). The upper part of the Petrified Forest Member is a prominent, cliff-forming bed, 5.5-24 m thick, of crossbedded quartzose sandstone and lithic- and limestone-pebble conglomerate (Figs. 4E-F, 5). These strata contain fragmentary remains of phytosaurs and metoposaurs indicative of a Late Triassic age (Fig. 6). Their stratigraphic position, lithology, and paleontology resemble closely the Correo Sandstone Bed of the Petrified Forest Member of the Chinle Formation at its type locality on Mesa Gigante in the Lucero uplift, 80 km to the southwest (Lucas et al., 1987). For this reason, I assign the Hagan basin strata to the Correo (Lucas et al., 1988). In the Hagan basin, the medial siltstone member of the Middle Jurassic Entrada Sandstone rests directly on the Correo (Figs. 4F, 5) or on a thin interval of upper Petrified

Correlation of Triassic Strata from the Colorado Plateau to the High Plains, New Mexico

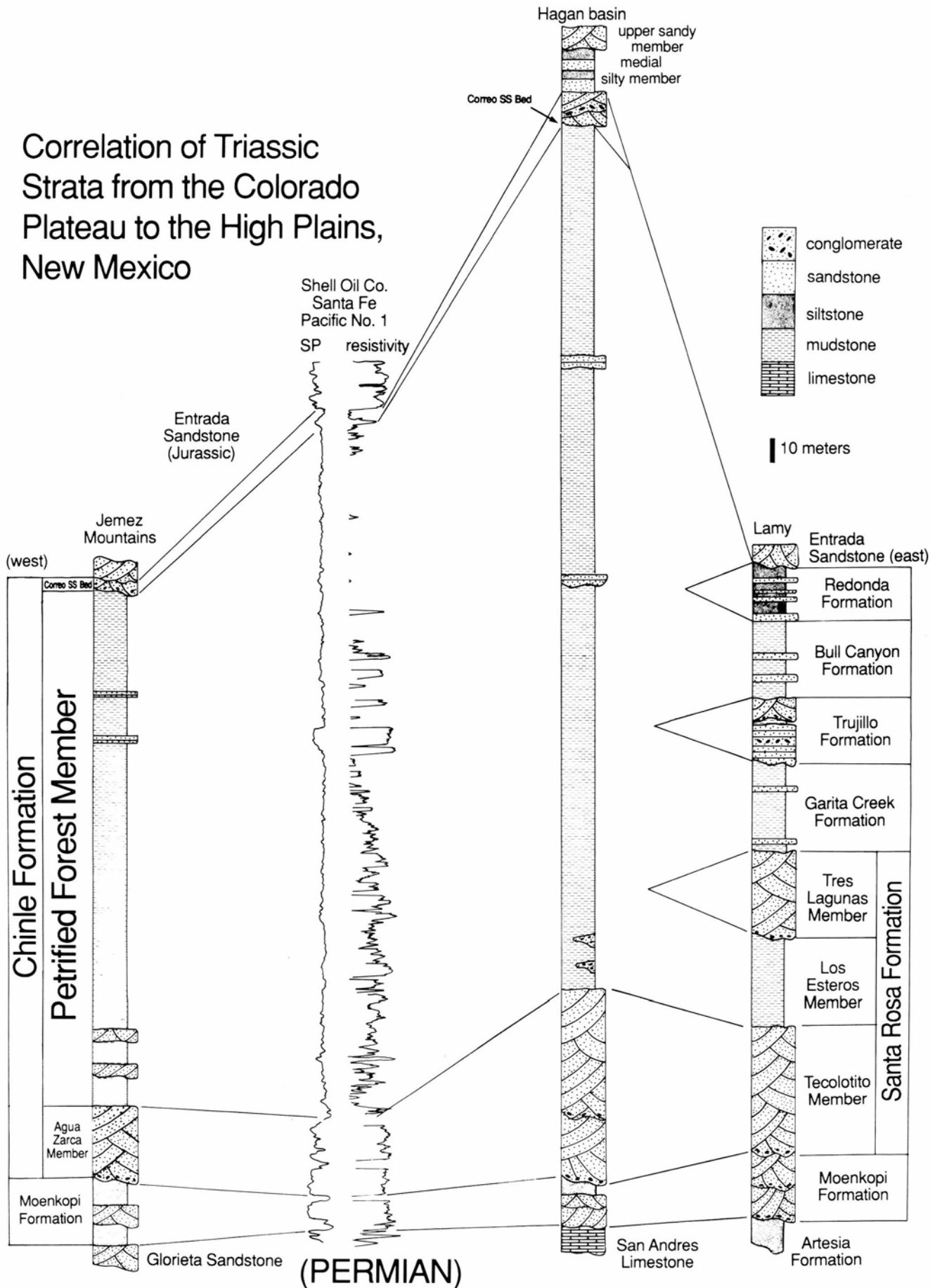


FIGURE 3—Representative Triassic stratigraphic columns for the Jemez Mountains, Shell Oil Company Santa Fe Pacific No. 1 (well log), Hagan basin, and Lamy area.

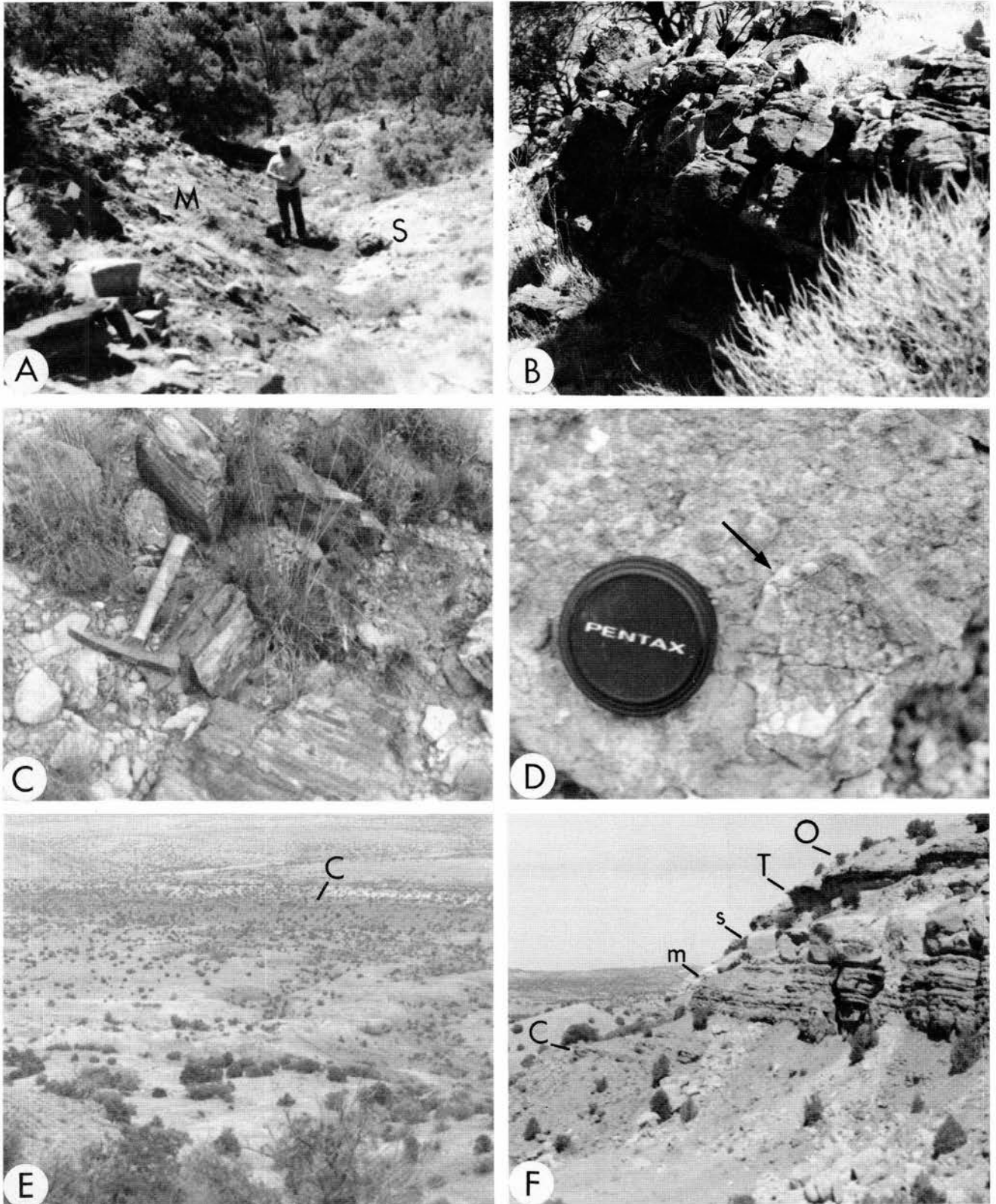


FIGURE 4—Photographs of selected outcrops of Triassic strata in the Hagan basin, New Mexico. **A**, Anton Chico Member of Moenkopi Formation (M) resting on Permian San Andres Formation (S) near the ghost town of Tejon, NE $\frac{1}{4}$, SW $\frac{1}{4}$ sec. 36, T13N, R5E. **B**, Typical crossbedded and laminar sandstone of the Agua Zarca Member of the Chinle Formation (same location as A). **C**, Silicified fossil logs in the Agua Zarca Member (same location as A). **D**, *Metoposaurus* bone in limestone-pebble conglomerate of lower part of Petrified Forest Member of Chinle Formation, SW $\frac{1}{4}$ NE $\frac{1}{4}$ sec. 1, T12N, R5E. **E**, Overview of section of Petrified Forest Member of Chinle Formation in sec. 36, T13N, R5E and sec. 1, T12N, R5E; note ridge formed by Correo Sandstone Bed (C) under lighter-colored Jurassic Entrada Sandstone. **F**, Correo Sandstone Bed (C) at its pinchout near Puertecito (SW $\frac{1}{4}$ sec. 10, T12N, R6E); note medial silty member (m) and upper sandy member (s) of Entrada Sandstone, Todilto Formation (T), and Tertiary Ortiz Gravel (O).

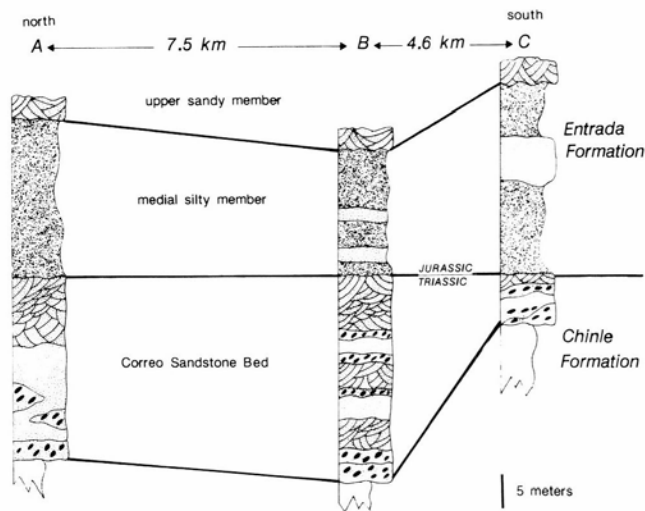


FIGURE 5—Stratigraphic sections of Correo Sandstone Bed in the Hagan basin. Lithologic symbols the same as in Fig. 3. Locations of sections are: A—west of Tonque Pueblo (NE $\frac{1}{4}$ SW $\frac{1}{4}$ sec. 13, T13N, R5E); B—southwest of Diamond Tail Ranch (NW $\frac{1}{4}$ SE $\frac{1}{4}$ sec. 6, T12N, R6E); C—west of Puertecito (SE $\frac{1}{4}$ SE $\frac{1}{4}$ sec. 9, T12N, R6E).

Forest Member mudstone above the Correo (Lucas et al., 1988; Pigman and Lucas, 1989).

Just east of the Hagan basin, small, structurally complex outcrops in the San Pedro Mountains—Cerrillos area of western Santa Fe County (e.g. Read and Andrews, 1944; Disbrow and Stoll, 1957; Bachman, 1976), poorly exposed Triassic strata in the Cedar Crest—Sandia Park area of northeastern Bernalillo County (Kelley and Northrop, 1975), and the log of a wildcat oil well north of Cerrillos (sec. 22, T15N, R8E) provide the only data on the Triassic strata west of a 20-25 km wide gap of Triassic outcrop. Published work just cited and unpublished data I have gathered indicate that these Triassic strata are essentially the same as those exposed in the Hagan basin to the west, with one significant difference: the Correo Sandstone Bed is not present. Absence of the Correo is readily verified in roadcuts along NM-14 north of Cedar Crest (sec. 2, T10N, R5E) and where Arroyo del Tuerito crosses the highway just north of Golden. At both locales, the Entrada Sandstone rests on a thick, reddish-brown mudstone section of the Petrified Forest Member of the Chinle Formation. Indeed, the apparent eastward pinch-out of the Correo Sandstone Bed occurs in the Hagan basin just north of Puertecito (SW $\frac{1}{4}$ sec. 10, T12N, R6E) where sandstone and conglomerate of the Correo thin dramatically and pinch out into mudstone of the upper part of the Petrified Forest Member (Fig. 4F).

Eastern edge of Basin and Range: Lamy area

Triassic strata in the Lamy area of Santa Fe County have long been assigned to the Dockum Group (Read et al., 1944; Stearns, 1953; Dane and Bachman, 1965). Johnson (1973), however, assigned these rocks to the Santa Rosa and Chinle Formations, producing a stratigraphic nomenclature identical to that long used in the Hagan basin.

Recent work by B. Allen, P. Birchhoff, A. Hunt, and myself, however, indicates that the Triassic section exposed in the Lamy area is very similar to that exposed in the Santa Rosa—Tucumcari region of east-central New Mexico (Allen and Lucas, 1988). Thus, the base of the Triassic section near Lamy is the Anton Chico Member of the Moenkopi

Formation, as much as 37 m thick and composed of grayish-red, trough-crossbedded litharenite and conglomerate. It contains bones of capitosauroid amphibians indicative of a Middle Triassic age. South of Lamy, the Moenkopi rests disconformably on moderately reddish-brown sandy siltstone of the Permian Bernal Formation (T 1 2-14N, R10-11E). In northern Torrance County, west of Clines Corners along 1-40 (secs. 13, 14, T9N, R11E), the Anton Chico Member of the Moenkopi also is present between the Bernal and Santa Rosa Formations.

The Santa Rosa Formation rests disconformably on the Anton Chico Member in the Lamy area. It is as much as 140 m thick, and the three members recognized by Lucas and Hunt (1987; also see Gorman and Robeck, 1946) in Guadalupe County can also be identified in the Lamy area: basal, sandstone-dominated Tecolotito Member (as much as 61 m thick), medial, mudstone-dominated Los Esteros Member (as much as 47 m thick), and upper, sandstone-dominated Tres Lagunas Member (as much as 62 m thick) (Hock, 1970; Johnson, 1973; Allen and Lucas, 1988; Hunt and Lucas, 1988).

Overlying mudstones pertain to the Garita Creek Formation. The variegated blue, gray, green, and red bentonitic mudstones and minor sandstones and limestone-pebble conglomerates are at least 40 m thick. The mass-death assemblage of *Metoposaurus fraasi* (Lamy amphibian quarry) from the Lamy area (Romer, 1939; Colbert and Imbrie, 1956; Hunt and Lucas, 1989b) is from the Garita Creek Formation south of Lamy (SW $\frac{1}{4}$ SW $\frac{1}{4}$ NE $\frac{1}{4}$ NE $\frac{1}{4}$ sec. 29, T12N, R11E).

The Trujillo Formation rests disconformably on the Garita Creek and consists of laminar and crossbedded sandstone and limestone-pebble conglomerate 30-40 m thick. It is well exposed along NM-41 south of the amphibian quarry where it caps escarpments. To the west, near White Bluffs, about 40 m of the Bull Canyon Formation, dominantly reddish-brown bentonitic mudstone, overlie the Trujillo. The Triassic section south of Lamy is culminated by 20-25 m of laterally persistent beds of moderately reddish-brown, fine-grained sandstone, siltstone, and non-bentonitic mudstone under the Entrada Sandstone at White Bluffs. The stratigraphic position and lithology of these strata are identical to the Redonda Formation of east-central New Mexico, to which they are assigned.

Southern High Plains: Santa Rosa to Tucumcari

Triassic stratigraphy and paleontology in the Santa Rosa-Tucumcari region of east-central New Mexico have been revised recently by Lucas et al. (1985), Lucas and Hayden (1987, 1989b, c), Lucas and Morales (1985), Finch (1988), Ash (1988), and Hunt et al. (1988). The Triassic section consists of the same stratigraphic units present in the Lamy area, but here they are generally thicker.

Paleogeographic significance

The stratigraphic correlations proposed here necessitate a change in current concepts of the paleogeography of central New Mexico during the Triassic. These concepts (Fig. 7) identify a positive area in central New Mexico, the Pederal uplift, that separated Triassic deposition in the Chinle basin to the west from deposition in the Dockum basin to the east (McKee et al., 1959; McGowen et al., 1983; Dubiel, 1989a). Indeed, Chinle paleocurrents on the Colorado Plateau are directed to the north, northwest, and west (e.g.

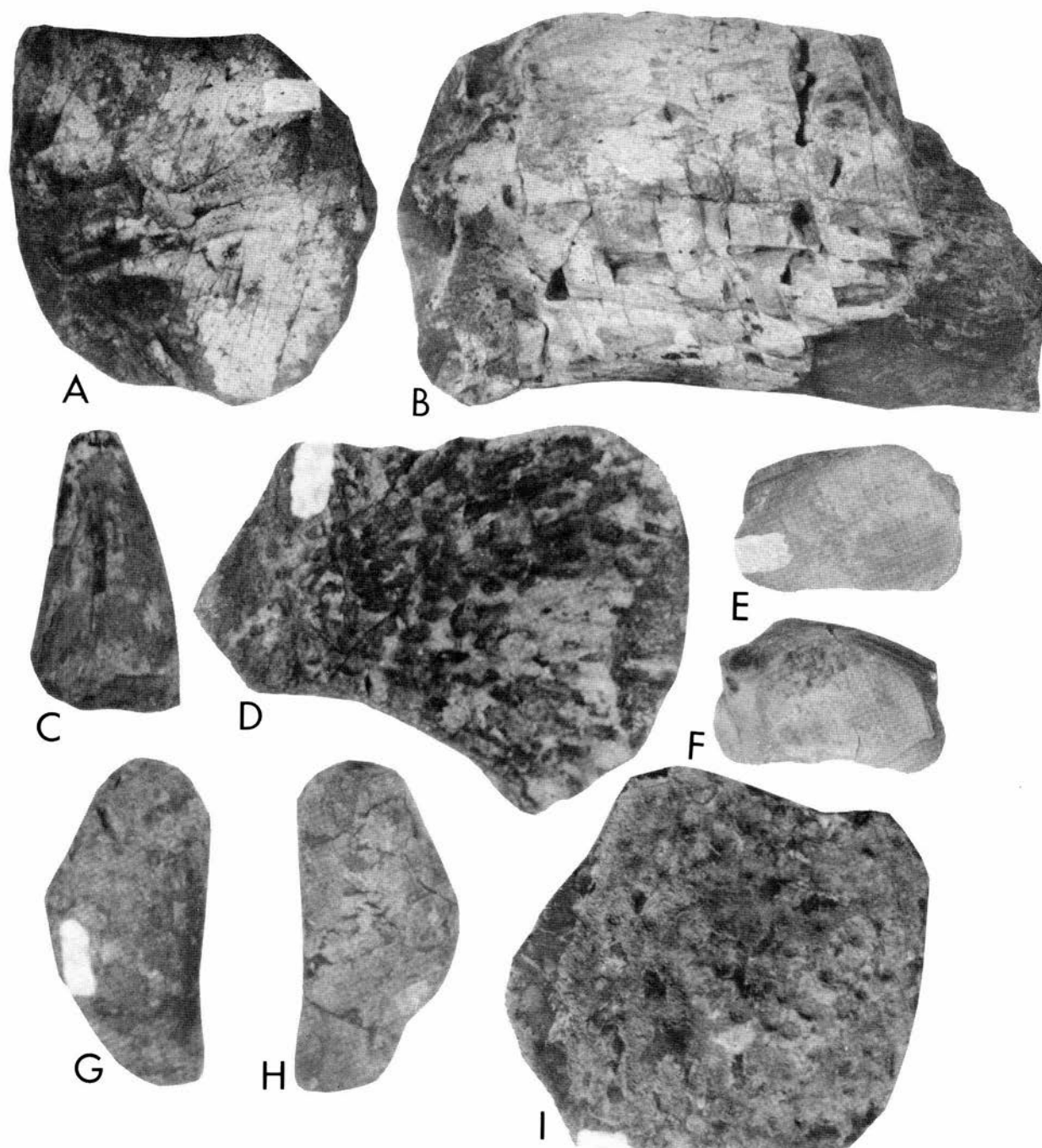


FIGURE 6—Fragmentary but biochronologically significant fossils from the Correo Sandstone Bed in the Hagan basin. All fossils are in the collection of the New Mexico Museum of Natural History (NMMNH). **A**, Dorsal view of an incomplete phytosaur scute, NMMNH P-17668, NMMNH locality 251, $\times 1$. **B**, Dorsal view of an incomplete phytosaur snout, NMMNH 17653, NMMNH locality 878, $\times 0.8$. **C**, Lateral view of a phytosaur tooth, NMMNH 17761, NMMNH locality 876, $\times 2$. **D**, Ventral view of an *Anaschisma* interclavicle, NMMNH 17646, NMMNH locality 251, $\times 1.5$. **E**, **F**, Incomplete valve of *Unio* sp., external (E) and internal (F) views, NMMNH P-14380, $\times 1.3$. **G**, **H**, Vertebrate coprolite, NMMNH P-17667, NMMNH locality 252, $\times 1.3$. **I**, Dorsal view of an incomplete paramedian scute of *?Typothorax*, NMMNH P-17647, NMMNH locality 250, $\times 0.8$.

Stewart et al., 1972; Dubiel, 1989a), consistent with the presence of an uplift to the east.

However, paleocurrents measured in Triassic strata on the High Plains of eastern New Mexico and west Texas are also generally directed to the north, northwest, and west (e.g. Caveau, 1960; Kiatta, 1960; Lupe, 1988; May, 1988; Hayden and Lucas, 1988; DeLuca and Eriksson, 1989; May and Lehman, 1989). Only a small number of paleocurrents in the Santa Rosa Formation indicates flow to the east (McGowen et al., 1979; Granata, 1981). Yet, these few paleocurrents have been combined with the generally northwest—southeast

orientation of Triassic sand bodies in the subsurface to reconstruct a regional Late Triassic paleoslope down to the east (McGowen et al., 1983, figs. 25-26). However, the orientations of the sand bodies are bidirectional indicators of flow and more likely suggest paleoflow to the northwest.

The close similarity of the Triassic section south of Lamy and in the Santa Rosa—Tucumcari area also argues against a Pedernal uplift at the location of the late Paleozoic uplift in what is now northeastern Tarrant County and southwestern San Miguel County. Indeed, Triassic strata of the Moenkopi and Santa Rosa Formations still preserved at this

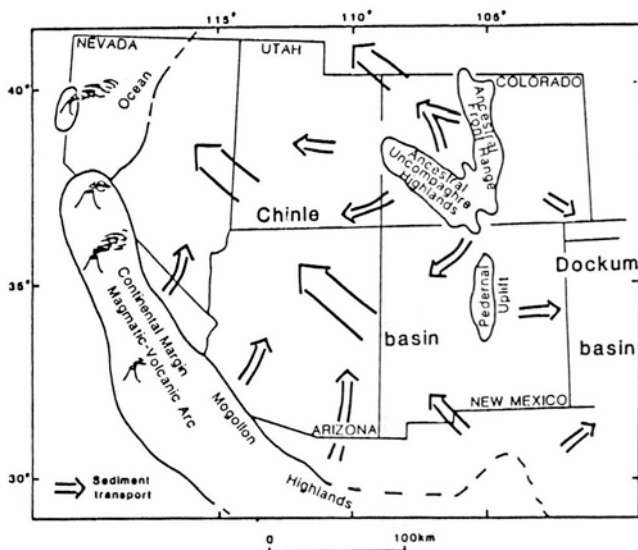


FIGURE 7—Traditional reconstruction of Late Triassic paleogeography in the American Southwest (from Dubiel, 1989a, fig. 2). Data presented in this article suggest absence of a Pedernal uplift during the Triassic.

location do not show thinning, paleocurrents, or facies changes that would suggest that an uplift was located there during the Triassic (Hock, 1970).

Some stratigraphic changes do occur in the 20-25 km gap in Triassic exposure between the outcrops south of Lamy and those just west of the Hagan basin (Fig. 1). These changes are:

1. The Los Esteros and Tres Lagunas Members of the Santa Rosa Formation, present south of Lamy, disappear to the west where the Agua Zarca Member probably is equivalent to the Tecolotito Member of the Santa Rosa Formation. A similar pinchout of the Los Esteros and Tres Lagunas Members also occurs in the Sangre de Cristo Mountains of northeastern New Mexico (Lucas et al., 1990).

2. The Trujillo Formation, present south of Lamy, is absent to the west. I suggest it pinches out westward into mudstones of the Petrified Forest Member of the Chinle Formation. This indicates the Petrified Forest Member is mostly equivalent to the Garita Creek and Bull Canyon Formations, a conclusion well supported paleontologically (Lucas and Hunt, 1989b).

3. The Redondo Formation, present south of Lamy, is absent to the west. Erosion at the base of the Entrada Sandstone almost certainly accounts for this. Thus, the Entrada rests on the much older Correo Sandstone Bed in the Hagan basin, but locally rests on the Redonda-correlative Rock Point Member of the Chinle Formation in the Lucero uplift.

These changes in the Triassic stratigraphic section between Lamy and the Hagan basin are few and do not suggest separate Triassic deposition in the two areas. Both Moenkopi and Chinle depositional systems thus were continuous from the Colorado Plateau through the southern High Plains.

Field-trip stops

Stop 1: Base of Triassic section, Hagan basin

Beginning at the intersection of I-25 and I-40 in Albuquerque, proceed north on I-25 towards Santa Fe. Leave I-25 at Exit 257 (San Felipe Pueblo) and turn right at the stop sign. The unpaved road heading east leads into the Hagan

basin. Continue 11.4 mi on this road to a locked gate on a road that enters from the right. This land is property of the Diamond Tail Ranch, and permission to enter and a key to the gate must be obtained from the ranch headquarters. Unlock gate and proceed about 2.5 mi to a left fork in the road (after the water gap, before the ghost town of Tejon). Turn left and continue 0.5 mi. Stop and climb the ridge to the southwest. Here, on the east flank of Montezuma Ridge, the Permo-Triassic boundary in the Hagan basin is well exposed. San Andres, Moenkopi, and Agua Zarca strata (Fig. 4A-C) can be examined here.

Stop 2: Top of Triassic section, Hagan basin

Return to main unpaved road through Hagan basin. Continue east on this road for 4.3 mi. Stop at the virtual ghost town of Puertecito. The bluff to the east of Puertecito well exposes the upper part of the Triassic section in the Hagan basin—Petrified Forest Member of Chinle Formation—overlain by the Jurassic Entrada Sandstone (Fig. 4F). Also note the eastward pinchout of the Correo Sandstone Bed displayed here (cf. Fig. 5).

Stop 3: Triassic strata, Lamy area

Continue east 5.7 mi on unpaved road through Hagan basin until junction with paved NM-344. Turn left on NM-344 and proceed north a total of 20.1 mi through Golden and Madrid and past Cerrillos to intersection (on right) with unpaved Santa Fe County Road 42 which leads to Galisteo. Turn right and follow the county road 9.5 mi to Galistec (intersection with paved NM-41). Turn left on NM-41 and continue 5.9 mi to junction with NM-285 just south of Lamy. Turn right and proceed south on NM-285 for 14.7 mi to pull-off at crest of hill. Here, extensive, structurally complex outcrops on the Bernal, Moenkopi, Santa Rosa, Garita Creek, and Trujillo Formations can be examined in the vicinity of the famous Lamy amphibian quarry.

Stop 4: Base of Triassic section, Clines Corners

Continue south on NM-285 for 20.0 mi to Clines Corners. Turn right and proceed west 3.4 mi on I-40. Stop on right of interstate to examine San Andres, Bernal, Moenkopi, and Santa Rosa Formations well exposed here on the axis of the Paleozoic Pedernal uplift. After stop, continue west on I40 to Albuquerque (47.5 mi).

Acknowledgments

I thank B. Allen, P. Birchhoff, S. Hayden, A. Hunt, K. Martini, P. Sealey, and M. Space for assistance in the field and the laboratory. A. Hunt, B. Kues, and J. Lorenz provided helpful reviews of the manuscript.

References

- Allen, B. D., and Lucas, S. G., 1988, Triassic stratigraphy near Lamy, Santa Fe County, New Mexico: *New Mexico Geology*, v. 10, p. 64. Ash, S. R., 1988, Fossil plants from the mudstone member of the Santa Rosa Formation at the principal reference section: *U.S. Geological Survey, Bulletin 1804*, pp. 19-27.
- Baars, D. L., 1962, Permian System of Colorado Plateau: *American Association of Petroleum Geologists, Bulletin*, v. 46, pp. 149-218. Bachman, G. O., 1976, *Geologic map of the Madrid quadrangle, Santa Fe and Sandoval Counties, New Mexico*: U.S. Geological Survey, Map GQ-1268, scale 1:62,500.
- Black, B. A., and Hiss, W. L., 1974, Structure and stratigraphy in the vicinity of the Shell Oil Company Santa Fe Pacific No. 1 test well, southern Sandoval County, New Mexico: *New Mexico Geological Society, Guidebook 25*, pp. 365-370.

- Cazeau, C. J., 1960, Cross-bedding directions in Upper Triassic sandstones of West Texas: *Journal of Sedimentary Petrology*, v. 30, pp. 459-465.
- Colbert, E. H., 1989, The Triassic dinosaur *Coelophysis*: Museum of Northern Arizona, Bulletin 57, 160 pp.
- Colbert, E. H., and Imbrie, J., 1956, Triassic metoposaurid amphibians: *American Museum of Natural History, Bulletin*, v. 110, pp. 399-462.
- Dane, C. H., and Bachman, G. O., 1965, Geologic map of New Mexico: U.S. Geological Survey, Denver, scale 1:500,000.
- DeLuca, J. L., and Eriksson, K. A., 1989, Controls on synchronous ephemeral- and perennial-river sedimentation in the middle sandstone member of the Triassic Chinle Formation, northeastern New Mexico, U.S.A.: *Sedimentary Geology*, v. 61, pp. 155-175.
- Disbrow, A. E., and Stoll, W. C., 1957, Geology of the Cerrillos area, Santa Fe County, New Mexico: *New Mexico Bureau of Mines & Mineral Resources, Bulletin* 48, 73 pp.
- Dubiel, R. F., 1989a, Depositional and climatic setting of the Upper Triassic Chinle Formation, Colorado Plateau; *in* Lucas, S. G., and Hunt, A. P. (eds.), *Dawn of the age of dinosaurs in the American Southwest*: New Mexico Museum of Natural History, Albuquerque, pp. 171-187.
- Dubiel, R. F., 1989b, Depositional environments of the Upper Triassic Chinle Formation in the eastern San Juan Basin and vicinity, New Mexico: U.S. Geological Survey, Bulletin 1808, pp. 1-22.
- Finch, W. I., 1988, Description of the principal reference section for the Santa Rosa Formation: U.S. Geological Survey, Bulletin 1804, pp. 110.
- Finch, W. I., and Wright, J. C., 1983, Measured stratigraphic sections of uranium-bearing Upper Triassic rocks of the Dockum basin, eastern New Mexico, West Texas, and the Oklahoma Panhandle with brief discussion of stratigraphic problems: U.S. Geological Survey, Open-file Report 83701, 118 pp.
- Gorman, J. M., and Robeck, R. C., 1946, Geology and asphalt deposits of north-central Guadalupe County, New Mexico: U.S. Geological Survey, Oil and Gas Investigations Preliminary Map 44.
- Granata, G. E., 1981, Regional sedimentation of the Late Triassic Dockum Group, West Texas and eastern New Mexico: Unpublished MA thesis, University of Texas at Austin, 199 pp.
- Harrison, E. P., 1949, Geology of the Hagan coal basin: Unpublished MS thesis, University of New Mexico, Albuquerque, 82 pp.
- Hayden, S. N., and Lucas, S. G., 1988, Stratigraphy of the Permo-Triassic boundary in northern New Mexico: Abstracts of the 41st Symposium on Southwest Geology and Paleontology [Museum of Northern Arizona, Flagstaff], p. 5.
- Hock, P. F., Jr., 1970, Effect of the Pedernal axis on Permian and Triassic sedimentation: Unpublished MS thesis, University of New Mexico, Albuquerque, 51 pp.
- Huene, F., von, 1911, Kurze Mitteilung Ober Perm, Trias und Jura in New Mexico: *Neues Jahrbuch für Mineralogie, Geologie und Paläontologie, Beilage-Band* 32, pp. 730-739.
- Hunt, A. P., and Lucas, S. G., 1988, Late Triassic fauna from the Los Esteros Member of the Santa Rosa Formation, Santa Fe County, New Mexico and its biochronological implications: *New Mexico Journal of Science*, v. 28, pp. 107-116.
- Hunt, A. P., and Lucas, S. G., 1989a, Stratigraphy and vertebrate biochronology of Upper Triassic strata in the Chama basin, north-central New Mexico: Abstracts of the Symposium on Southwestern Geology and Paleontology [Museum of Northern Arizona, Flagstaff] 1989, p. 15.
- Hunt, A. P., and Lucas, S. G., 1989b, Late Triassic vertebrate localities in New Mexico; *in* Lucas, S. G., and Hunt, A. P. (eds.), *Dawn of the age of dinosaurs in the American Southwest*: New Mexico Museum of Natural History, Albuquerque, pp. 72-101.
- Hunt, A. P., and Lucas, S. G., 1990a, Paleontology and biochronology of the Petrified Forest Member of the Upper Triassic Chinle Formation near San Ysidro, Sandoval County, New Mexico: *New Mexico Journal of Science*, v. 30, pp. 17-26.
- Hunt, A. P., and Lucas, S. G., 1990b, Re-evaluation of "*Typhothorax meadei*, a Late Triassic aetosaur from the United States: *Paläontologische Zeitschrift*, v. 64, pp. 317-328.
- Hunt, A. P., and Lucas, S. G. (in press), The *Paleorhinus* biochron and the correlation of the nonmarine Upper Triassic of Pangaea: *Palaeontology*.
- Hunt, A. P., Lucas, S. G., Martini, K., and Martini, T., 1989[a], Triassic stratigraphy and paleontology, Mesa del Oro, Valencia County, New Mexico: *New Mexico Geological Society, Guidebook* 40, pp. 8-9.
- Hunt, A. P., Lucas, S. G., and Sealey, P. L., 1989[b], Paleontology and vertebrate biochronology of the Upper Triassic Garita Creek Formation, east-central New Mexico: *New Mexico Journal of Science*, v. 29, pp. 61-68.
- Johnson, R. B., 1973, Geologic map of the Bull Canyon quadrangle, Santa Fe County, New Mexico: U.S. Geological Survey, Map GQ-1077, scale 1:24,000.
- Kelley, V. C., and Northrop, S. A., 1975, Geology of the Sandia Mountains and vicinity, New Mexico: *New Mexico Bureau of Mines & Mineral Resources, Memoir* 29, 135 pp.
- Kiatta, H. W., 1960, A provenance study of the Triassic deposits of northwestern Texas: Unpublished MS thesis, Texas Tech University, Lubbock, 63 pp.
- Kietzke, K. K., 1989a, Calcareous microfossils from the Triassic of the southwestern United States; *in* Lucas, S. G., and Hunt, A. P. (eds.), *Dawn of the age of dinosaurs in the American Southwest*: New Mexico Museum of Natural History, Albuquerque, pp. 223-232.
- Kietzke, K. K., 1989b, Calcareous microfossils from the Moenkopi Formation (Triassic, Scythian or Anisian) of central New Mexico: *New Mexico Geological Society, Guidebook* 40, pp. 181-190.
- Kurtz, D. D., 1978, Sedimentology and stratigraphy of the Triassic Chinle Formation, eastern San Juan Basin, New Mexico: Unpublished MS thesis, Rice University, Houston, 177 pp.
- Kurtz, D. D., and Anderson, J. B., 1980, Depositional environments and paleocurrents of Chinle Formation (Triassic), eastern San Juan Basin, New Mexico: *New Mexico Geology*, v. 2, pp. 22-27.
- Lucas, S. G., 1990, The rise of the dinosaur dynasty: *New Scientist*, no. 1737, pp. 44-46.
- Lucas, S. G., and Hayden, S. N., 1989a, Triassic stratigraphy of west-central New Mexico: *New Mexico Geological Society, Guidebook* 40, pp. 191-211.
- Lucas, S. G., and Hayden, S. N., 1989b, Middle Triassic Moenkopi Formation, Nacimiento Mountains, north-central New Mexico; *in* Lorenz, J. C., and Lucas, S. G. (eds.), *Energy frontiers in the Rockies*: *Albuquerque Geological Society, Albuquerque*, pp. 16-17.
- Lucas, S. G., and Hayden, S. N. (in press), Type section of the Permian Bernal Formation and the Permo-Triassic boundary in north-central New Mexico: *New Mexico Geology*.
- Lucas, S. G., and Hunt, A. P., 1987, Stratigraphy of the Anton Chico and Santa Rosa Formations, Triassic of east-central New Mexico: *Journal of the Arizona-Nevada Academy of Science*, v. 22, pp. 21-33.
- Lucas, S. G., and Hunt, A. P. (eds.), 1989a, Dawn of the age of dinosaurs in the American Southwest: *New Mexico Museum of Natural History, Albuquerque*, 414 pp.
- Lucas, S. G., and Hunt, A. P., 1989b, Revised Triassic stratigraphy in the Tucumcari basin, east-central New Mexico; *in* Lucas, S. G., and Hunt, A. P. (eds.), *Dawn of the age of dinosaurs in the American Southwest*: *New Mexico Museum of Natural History, Albuquerque*, pp. 150-170.
- Lucas, S. G., and Hunt, A. P. (in press), Upper Triassic Owl Rock and Rock Point Members, Chinle Formation, Petaca Pinta, Cibola County, New Mexico: *New Mexico Geology*.
- Lucas, S. G., and Morales, M., 1985, Middle Triassic amphibian from the basal Santa Rosa Formation, east-central New Mexico: *New Mexico Geological Society, Guidebook* 36, pp. 56-58.
- Lucas, S. G., Allen, B. D., and Hayden, S. N., 1987, Type section of the Triassic Correo Sandstone Bed, Chinle Formation, Cibola County, New Mexico: *New Mexico Journal of Science*, v. 27, pp. 87-93.
- Lucas, S. G., Hunt, A. P., and Huber, P., 1990, Triassic stratigraphy in the Sangre de Cristo Mountains, New Mexico: *New Mexico Geological Society, Guidebook* 41, pp. 305-318.
- Lucas, S. G., Hunt, A. P., and Morales, M., 1985, Stratigraphic nomenclature and correlation of Triassic rocks of east-central New Mexico: a preliminary report: *New Mexico Geological Society, Guidebook* 36, pp. 171-184.
- Lucas, S. G., Martini, K., and Martini, T., 1988, Upper Triassic Correo Sandstone Bed, Petrified Forest Member, Chinle Formation, Hagan basin, Sandoval County, New Mexico: *New Mexico Geology*, v. 10, p. 65.
- Lupe, R., 1988, Interpretive depositional history of the Santa Rosa Formation at the principal reference section: U.S. Geological Survey, Bulletin 1804, pp. 11-18.
- Maxwell, C. H., 1988a, Geologic map of the Cerro del Oro quadrangle, Cibola County, New Mexico: U.S. Geological Survey, Miscellaneous Field Studies Map MF-2033, scale 1:24,000.
- Maxwell, C. H., 1988b, Geologic map of the Marmon Ranch quadrangle, Cibola County, New Mexico: U.S. Geological Survey, Miscellaneous Field Studies, Map MF-2049, scale 1:24,000.
- May, B. A., 1988, Depositional environments, sedimentology, and stratigraphy of the Dockum Group (Triassic) in the Texas Panhandle: Unpublished MS thesis, Texas Tech University, Lubbock, 180 pp.
- May, B. A., and Lehman, T. M., 1989, Sedimentology of the Dockum Group (Triassic), Texas Panhandle (abs.): *Geological Society of America, Abstracts with Programs*, v. 21, p. 34.

- McGowen, J. H., Granata, G. E., and Seni, S. J., 1979, Depositional framework of the lower Dockum Group (Triassic) Texas Panhandle: Bureau of Economic Geology, University of Texas, Report of Investigations 97-1979, 60 pp.
- McGowen, J. H., Granata, G. E., and Seni, S. J., 1983, Depositional setting of the Triassic Dockum Group, Texas Panhandle and eastern New Mexico; *in* Reynolds, M. W., and Dolly, E. D. (eds.), Mesozoic paleogeography of the west-central United States: Rocky Mountain Section SEPM, Denver, pp. 13-38.
- McKee, E. D., Oriol, S. S., Ketner, K. B., MacLachlan, M. E. H., Goldsmith, J. W., MacLachlan, J. C., and Mudge, M. R., 1959, Paleotectonic maps of the Triassic System: U.S. Geological Survey, Miscellaneous Geological Investigations Map 1-300, 33 pp.
- Menne, B., 1989a, Stratigraphy and structure of the northern end of the Sandia uplift; *in* Lorenz, J. C., and Lucas, S. G. (eds.), Energy frontiers in the Rockies: Albuquerque Geological Society, Albuquerque, pp. 23.
- Menne, B., 1989b, Structure of the Placitas area, northern Sandia uplift, Sandoval County, New Mexico: Unpublished MS thesis, University of New Mexico, Albuquerque, 163 pp.
- O'Sullivan, R. B., 1974, The Upper Triassic Chinle Formation in north-central New Mexico: New Mexico Geological Society, Guidebook 25, pp. 171-174.
- O'Sullivan, R. B., 1977, Triassic rocks in the San Juan Basin of New Mexico and adjacent areas: New Mexico Geological Society, Guidebook 28, pp. 139-146.
- Picha, M. G., 1982, Structure and stratigraphy of the Montezuma salient, Hagan basin area, Sandoval County, New Mexico: Unpublished MS thesis, University of New Mexico, Albuquerque, 248 pp.
- Pigman, C., and Lucas, S. G., 1989, The Jurassic section in the Hagan basin, Sandoval County, New Mexico; *in* Lorenz, J. C., and Lucas, S. G. (eds.), Energy frontiers in the Rockies: Albuquerque Geological Society, Albuquerque, pp. 3-5.
- Read, C. B., and Andrews, D. A., 1944, Geology of a part of the upper Pecos River and Rio Galisteo region, N. Mex.: U.S. Geological Survey, Oil and Gas Investigations Preliminary Map 8.
- Read, C. B., Wilpolt, R. H., Andrews, D. A., Summerson, C. H., and Wood, G. H., 1944, Geologic map and stratigraphic sections of Permian and Pennsylvanian rocks of parts of San Miguel, Santa Fe, Sandoval, Bernalillo, Tarrant and Valencia Counties, north-central New Mexico: U.S. Geological Survey, Oil and Gas Investigations Preliminary Map 21.
- Reynolds, C. B., 1954, Geology of the Hagan-La Madera area, Sandoval County, New Mexico: Unpublished MS thesis, University of New Mexico, Albuquerque, 82 pp.
- Romer, A. S., 1939, An amphibian graveyard: Scientific Monthly, v. 49, pp. 337-339.
- Smith, C. T., 1961, Triassic and Jurassic rocks of the Albuquerque area: New Mexico Geological Society, Guidebook 12, pp. 121-128.
- Stearns, C. E., 1953, Tertiary geology of the Galisteo-Tonque area, New Mexico: Geological Society of America, Bulletin, v. 64, pp. 459-508.
- Stewart, J. H., Poole, F. G., and Wilson, R. F., 1972, Stratigraphy and origin of the Chinle Formation and related Upper Triassic strata in the Colorado Plateau region: U.S. Geological Survey, Professional Paper 690, 336 pp.
- Wengerd, S. A., 1950, Triassic rocks of northwestern New Mexico and southwestern Colorado: New Mexico Geological Society, Guidebook 1, pp. 67-75.
- Wood, G. H., and Northrop, S. A., 1946, Geology of the Nacimiento Mountains, San Pedro Mountain, and adjacent plateaus in parts of Sandoval and Rio Arriba Counties, New Mexico: U.S. Geological Survey, Oil and Gas Investigations Map OM-57, scale 1:95,000.
- Woodward, L. A., 1987, Geology and mineral resources of Sierra Nacimiento and vicinity, New Mexico: New Mexico Bureau of Mines & Mineral Resources, Memoir 42, 84 pp.
- Woodward, L. A., and Picha, M. G., 1989, Tectonic setting and structure of the Hagan basin, north-central New Mexico; *in* Lorenz, J. C., and Lucas, S. G., Energy frontiers in the Rockies: Albuquerque Geological Society, Albuquerque, pp. 167-169.

Tectonics, intrusive rocks, and mineralization of the San Pedro—Ortiz porphyry belt, north-central New Mexico

Stephen R. Maynard¹, Lee A. Woodward¹, and David L. Giles³

¹LAC Minerals, USA, Inc., P.O. Box 21390, Reno, Nevada 89515; ²Department of Geology, University of New Mexico, Albuquerque, New Mexico 87131;

Introduction

The purpose of this field trip is to examine two major tectonic and igneous features of north-central New Mexico, the Tijeras—Canoncito fault system (TCFS) and the San Pedro—Ortiz porphyry belt and their relationship to Tertiary base-and precious-metal mineralization.

Day 1 will be spent viewing the southern end of the Tijeras—Canoncito fault system, the San Pedro Mountains, and the Cerrillos Hills. The group will return to Albuquerque for the evening. On Day 2 the trip will visit the Ortiz Mountains, stopping at gold deposits or occurrences localized along the Tijeras—Canoncito fault system.

Acknowledgments

The permission of Pegasus Gold, LAC Minerals, USA, Inc., Placer Dome Mining, and Cerrillos Gravel Products to enter their properties and publish information regarding geology and mineralization is gratefully acknowledged. Many geologists, too numerous to name individually, have contributed to our understanding of the geology of the San Pedro—Ortiz porphyry belt. Alice Mueller drafted the figures. Felix Mutschler and Tommy Thompson reviewed the manuscript, made corrections, and offered useful suggestions.

Tectonic setting of the San Pedro—Ortiz porphyry belt

Lee A. Woodward

The San Pedro—Ortiz porphyry belt trends north-north-easterly, lying east of the Rio Grande rift and obliquely straddling the northeast-trending Tijeras—Canoncito fault system (Fig. 1). This belt of mid-Tertiary intrusions is in the north-trending New Mexico alkalic gold belt which includes the Nogal—Bonito, Schelerville (West Bonito), White Oaks, Jicarilla, Tecolote, and Gallinas mining districts. The New Mexico alkalic gold belt is part of a larger belt of mid-Tertiary gold-bearing alkalic intrusive centers that extends from Montana to west Texas. Major tectonic elements near the San Pedro—Ortiz porphyry belt include the Hagan and Española basins of the Rio Grande rift, the Sandia—Manzano uplift, the Estancia basin, and the Tijeras—Canoncito fault system.

The late Cenozoic Rio Grande rift is composed of several north-trending grabens (commonly called basins) arranged en-echelon north-northeasterly for a distance of about 725 km in New Mexico and Colorado (Kelley, 1952, 1977, 1978). The Española basin, north of the Ortiz porphyry belt, is 65 to 80 km long, 30 to 65 km wide, and is tilted mainly to the west where it is bounded by high-angle faults. Within this basin are antithetic and synthetic faults, forming second-order horsts and grabens. The southeast margin of the basin is marked by the Tijeras—Canoncito fault system and the San Pedro—Ortiz porphyry belt.

The Hagan basin is an east-tilted half-graben that forms an embayment or bench (Kelley, 1977) on the northeast corner of the larger Albuquerque basin (Fig. 1). On the east, the Hagan basin is bounded by the La Bajada normal fault which is downthrown on the west side. The western boundary of the basin is marked by the San Francisco normal fault which is also downthrown on the west side. A broad dip-

slope on the east side of the Sandia—Manzano uplift merges through moderately dipping beds with the southern and southwestern parts of the Hagan basin. Maximum structural relief between the deepest part of the Hagan basin and the top of the Sandia uplift is about 6000 m. A structure section that was based on seismic data (Black and Hiss, 1974) across the northern part of the basin shows about 4000 m of strati-graphic separation across the San Francisco fault and 3300 m across the La Bajada fault. Displacement along the latter dies out southward. La Bajada and San Francisco are major faults that controlled late Cenozoic sedimentation in this part of the Rio Grande rift. Structures within the Hagan basin include low- and high-angle normal faults, high-angle reverse faults, Hagan syncline, Espinaso monocline, and a few minor folds. Arcuate outcrop patterns strike northerly on the west side of the basin and swing eastward on the south margin, thus defining the gently northeast-plunging Hagan syncline. The Espinaso monocline trends north-northwesterly, faces east, and can be traced for about 10 km along strike.

The Sandia and Manzano Mountains form a north-trending, east-tilted fault block that is approximately 120 km long and up to 15 km wide. Precambrian rocks are exposed on the western fault scarp and the dip-slope to the east is developed mainly on Pennsylvanian strata dipping about 15° (Kelley and Northrop, 1975). Maximum structural relief between the Sandia uplift and the northern part of the Estancia basin is around 3000 m. Phanerozoic rocks in the Ortiz porphyry belt also generally dip 15-25° east.

The western margin of the Estancia basin is transitional with the eastern dip-slope of the Manzano uplift. On the north, this basin is bounded by the Tijeras—Canoncito fault

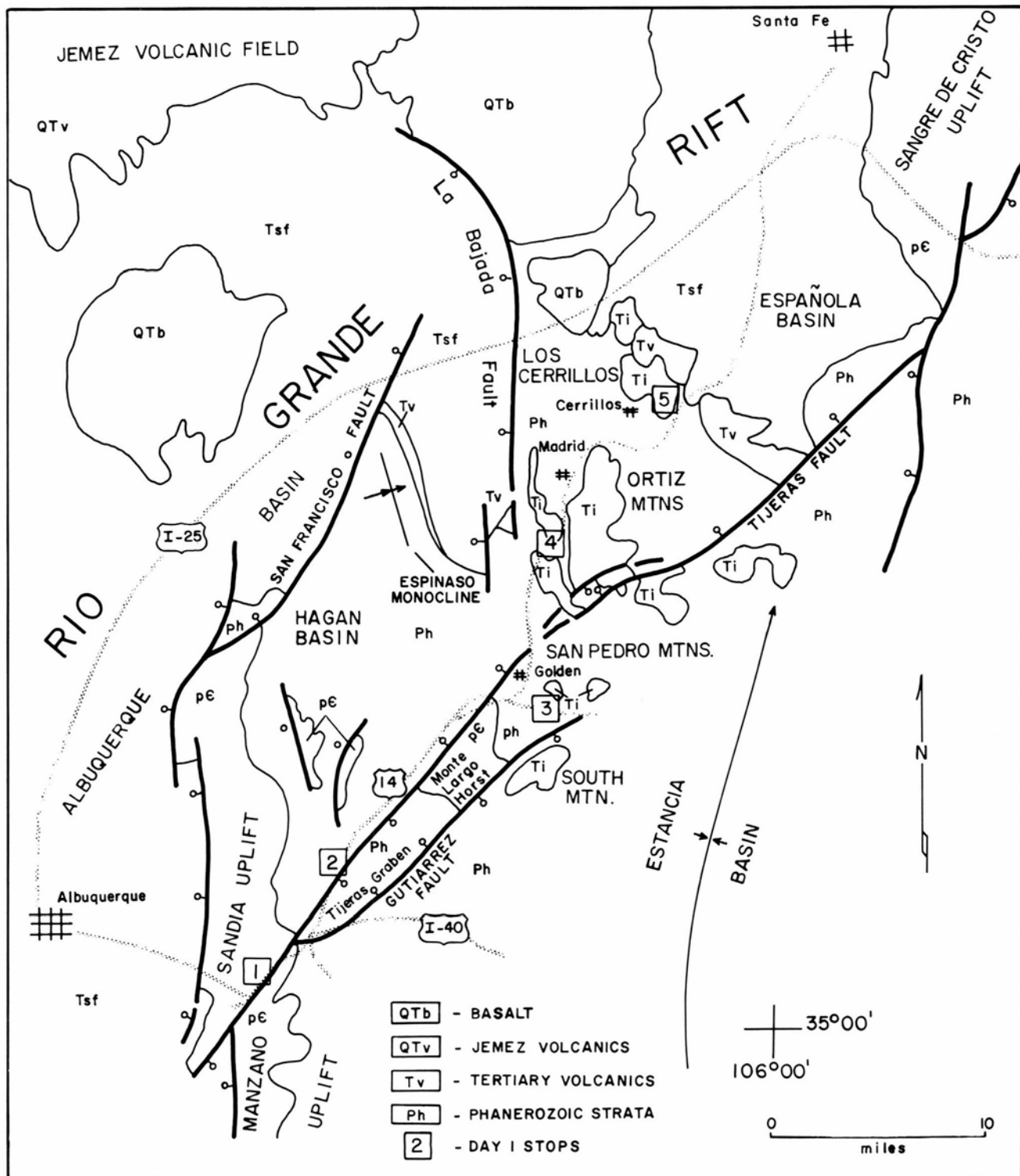


FIGURE 1—Location map and tectonic setting of the San Pedro-Ortiz porphyry belt showing locations of Day 1 stops.

system. There appears to be no major crustal extension involved in the evolution of this basin. Rather it seems to have formed in two stages, by Laramide and older rise of the Pederal uplift on the east and late Cenozoic eastward tilting of the Sandia-Manzano uplift.

The Tijeras-Canoncito fault system consists of high-angle faults that split and join along strike and form sigmoidal patterns in map view, with horsts and grabens occurring locally between major faults (Fig. 1). On its southwestern end, the Tijeras fault has Precambrian metamorphic rocks

juxtaposed with Pennsylvanian strata; Quaternary alluvium overlaps the bedrock outcrops to the southwest in the Albuquerque basin of the Rio Grande rift. To the northeast, the Tijeras fault juxtaposes Precambrian rocks of contrasting lithologies (Fig. 2) (Connolly, 1982) for nearly 10 km, with greenstone and associated rocks on the southeast (Bruns, 1959) and quartzofeldspathic gneiss on the northwest (Lodewick, 1960). In the Tijeras mining district, the greenstone hosts ore deposits that are interpreted as Precambrian syngenetic mineralization remobilized during later episodes of

ERATHM	SYSTEM	SERIES	ESPAÑOLA-HAGAN REGION	STRATIGRAPHIC POSITION OF MINERALIZATION	TECTONIC AND MINERALIZING EVENTS	
CENOZOIC	QUATERNARY	RECENT			CONTINUED T.C.F.S. ACTIVITY	
		PLEISTOCENE	Bandelier Tuff			
	TERTIARY	PLIOCENE		Cerrros del Rio Volcanics		-ORTIZ, GOLDEN PLACERS-
			Puye Fm	Ancha Fm	Sardileta Fm	
		MIOCENE	Santa Fe Group	Chamita Fm	Los Piños Fm	
		OLIGOCENE	Abiquiu Fm	Pigujua Fm		
	EOCENE		Espinosa Fm	El Rito Fm		
	PALEOCENE		Galisteo Fm			
MESOZOIC	CRETACEOUS	UPPER	Mesoverde Group	Menefee Fm Point Lookout Ss Dalton-Hosta Ss Galup Ss		-CUNNINGHAM HILL - -CARACHE CANYON-
				Mancos Fm		
		LOWER		Dakota Fm		- LUKAS CANYON -
	JURAS- SIC	UPPER		Morrison Fm		- IRON VEIN -
				Todiito Fm		
		MIDDLE		Entrada Ss		
		LOWER				
	TRIAS- SIC	UPPER		Chinle Fm		
		MIDDLE		Santa Rosa Fm		
		LOWER				
PALEOZOIC	PERMIAN	UPPER				
		LOWER		San Andres Fm		
				Yeso Fm		
				Abo Fm		
	PENN- SILVIAN	UPPER		Magdalena Group	Madera Fm	- SAN PEDRO MINE -
		MIDDLE			Sandia Fm	
		LOWER				
MISSIS- SIPPIAN	UPPER		Log Springs Fm			
	LOWER		Arroyo Peñasco Group	Espiritu Santo Fm		
PRECAMBRIAN			Sandia Granite	Tijeras Greenstone- Cibola Gneiss		TIJERAS-CANONCITO MOVEMENT EXHALATIVE (?) MINERALIZATION

FIGURE 2—Generalized stratigraphic column of San Pedro-Ortiz porphyry belt (modified after Woodward and Ingersoll, 1979).

metamorphism and deformation (Fulp et al., 1982).

The next segment of the fault extends from the eastern base of the Sandia uplift to the northeast end of the Tijeras graben. Rocks ranging in age from Pennsylvanian to Cretaceous are offset, and vertical separation along this segment ranges from 0 to at least 1000 m (Kelley and Northrop, 1975), with the southeast side down. Kelley and Northrop (1975, pp. 87-88) noted 500-600 m of left-lateral separation of fold axes and strata. The Gutierrez fault connects with the Tijeras fault and extends about 24 km to the northeast, bounding the southeastern margins of the Tijeras graben and Monte Largo horst. Limited exposures indicate that the fault is nearly vertical and has a maximum vertical separation of about 1100 m where it juxtaposes Paleozoic and Mesozoic rocks. To the northeast the fault splays toward the east and apparently dies out beneath alluvium. The northwestern boundary of Monte Largo horst is the continuation of the Tijeras fault and has Pennsylvanian strata against Precambrian metamorphic rocks, with about 1000 m of vertical separation (Kelley and Northrop, 1975). The Tijeras fault continues to the northeast and curves eastward, forming a sigmoidal bend north of the San Pedro Mountains. The San Pedro Mountains have many small faults that are parallel to the Tijeras system.

In the Ortiz Mountains a graben, confined to the northeast-trending part of a sigmoidal bend, is present where bounding faults displace Tertiary sedimentary strata and Tertiary intrusive rocks. There is about 1300 m of structural relief between the Ortiz graben and the adjacent area to the south

east (Maynard et al., 1990). Northeast of the Ortiz Mountains the fault is covered by upper Tertiary—Quaternary gravel (Bachman, 1975) but reappears at the surface where lower to middle Tertiary strata are offset by the fault.

Lisenbee et al. (1979) have shown that the complex geometry along the fault system is the result of at least four episodes of deformation, ranging from Precambrian to late Cenozoic. Direction of slip along any given segment may have varied from one deformational episode to another; also, different segments may have undergone different slip during the same episode of deformation. Precambrian movement may have been largely strike-slip (Lisenbee et al., 1979), establishing a major zone of anisotropy that probably extends through the crust and has had recurrent movement. Late Cenozoic displacement was complex and had a large component of dip-slip movement and subordinate strike-slip. The composite strike component of movement along the system from the Ortiz Mountains to the southwest appears to have been left-slip and may be responsible for dilation where faults change strike from northeast to east-northeast. This could be the origin of the Ortiz and Galisteo grabens. Thus, these features appear to be of transtensional origin.

Movement during the late Cenozoic on the Tijeras—Canoncito system is interpreted to be that of a continental transform, with extensional terrane to the northwest (Española and Hagan basins) and nonextended crust to the southeast (Estancia basin and Manzano dip-slope). North-trending extensional faults related to rifting are present

north of the Tijeras—Canoncito system in the Hagan and Espanola basins. These extensional and transform faults may have controlled the trend and location of the Ortiz porphyry belt. In a more detailed sense, faults and related fractures have exerted structural control for mineral deposits by providing shear zones in Precambrian basement rocks, open fractures for fissure filling, open-space breccias, and, of most importance, a zone of crustal weakness for magma emplacement and conduits for hydrothermal fluids. The magmas in turn appear to be genetically related to many of the mineral deposits, having been the source of mineralizing solutions or having provided heat for hydrothermal systems.

A full discussion of the stratigraphy of the San Pedro—Ortiz porphyry belt is beyond the scope of this paper. Stratigraphic relations within the belt have been extrapolated principally from exposures in the Hagan Basin (Black, 1979; Picha, 1982) and are summarized in Fig. 3.

In general, the oldest supracrustal rocks in the San Pedro—Ortiz porphyry belt are exposed at the southern end, in the San Pedro Mountains and at South Mountain. The youngest supracrustal rocks crop out at the northern end, in the Cerrillos Hills.

Certain ore deposits and mineral occurrences in the San Pedro—Ortiz porphyry belt are found in specific stratigraphic contexts. At the San Pedro mine, copper-skarn mineralization is localized in favorable beds of the Pennsylvanian Madera Formation. In the Ortiz Mountains, the Greenhorn Limestone Member of the Upper Cretaceous Mancos Shale hosts copper—gold skarn at Lukas Canyon. Sills of latite porphyry, whose emplacement was localized by Mancos and Menefee Shales, host gold mineralization at the Carache Canyon breccia pipe. And brecciated sandstone (quartzite) of the Eocene Galisteo Formation contains gold and tungsten mineralization at Cunningham Hill.

Road log: Day 1, Stop 1

Drive east on 1-40 from Albuquerque. About 3 mi after entering Tijeras Canyon, round Deadman's Curve. East of Deadman's Curve 1-40 is in the strike valley of the Tijeras fault.

Tijeras Canyon, Sandia Mountains, and Tijeras graben

Lee A. Woodward

Tijeras Canyon is underlain by the Tijeras fault which strikes northeast and separates two Proterozoic metamorphic terranes of contrasting rock types and structural styles (Connolly, 1981, 1982). The Tijeras fault has undergone at least four episodes of movement, during the Precambrian, Pennsylvanian, Tertiary, and Quaternary (Lisenbee et al., 1979). Although the fault may have had different directions of slip during the various episodes of movement, it seems likely that the cumulative sense of motion in Tijeras Canyon consists of several kilometers of left-slip as judged from contrasts in lithology, structural geometry, and metamorphic history (Connolly, 1982).

Northwest of the Tijeras fault is the Cibola gneiss, a unit derived mainly from arkose, with subordinate sandstone and shale protoliths. The gneiss is intruded by the Precambrian Sandia granite and is characterized by augen gneiss near the

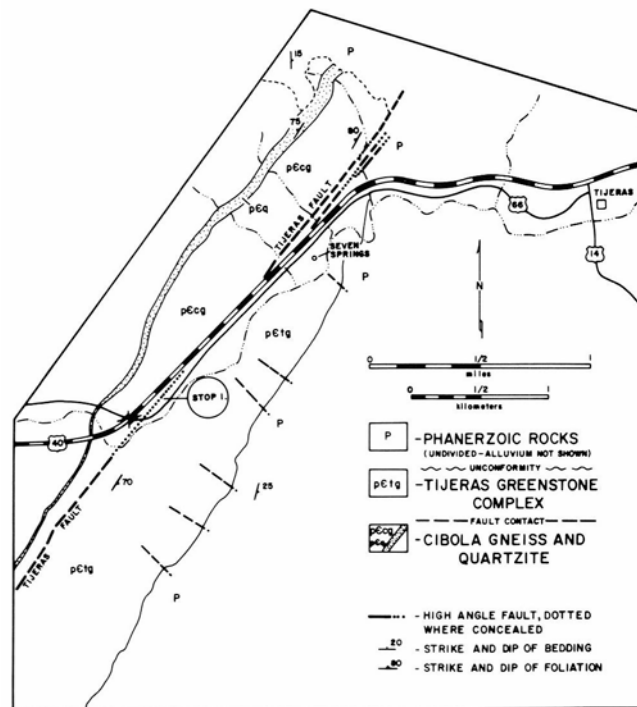


FIGURE 3—Generalized geologic map of the Tijeras Canyon area (after Lisenbee et al., 1979).

Stop 1. About 200 m east of Deadman's Curve on 1-40 in Tijeras Canyon. Be sure to park well away from the traffic lanes and stay on the shoulder.

Across the highway note the exposure of the Tijeras fault where Quaternary colluvium is in fault contact with Proterozoic Tijeras greenstone (Fig. 2). Quartzite within the Cibola gneiss makes up the bold outcrops on top of the near ridge to the north. To the south, Pennsylvanian Madera Formation limestone holds up the prominent ridge. The lower slopes of the ridge are underlain by Proterozoic Tijeras greenstone.

contact. Southeast of the fault the Tijeras greenstone consists mostly of metabasalt with subordinate metasedimentary rocks, including chlorite and biotite phyllite as well as metaquartzite. Minor felsic metavolcanic rocks are also present. Both the Cibola gneiss and Tijeras greenstone were isoclinally folded during amphibolite-facies metamorphism, but the greenstone was tightly refolded about axes nearly parallel to the older fold axes, whereas the gneiss was refolded about axes at a high angle to the earlier fold axes (Connolly, 1982).

Ore deposits hosted by the Tijeras greenstone are interpreted as syngenetic, exhalative gold—copper mineralization remobilized during metamorphism and deformation (Fulp et al., 1982). At the Great Combination and Mary M mines, gold-bearing veinlets are associated with pyrite and malachite, and at the York mine, banded, semi-massive pyrite-chalcocopyrite is present. Production from this district is small;

Elston (1967) estimated \$10,000 of production from 1828 to 1959 for the Tijeras and several nearby districts.

North of Tijeras Canyon, the dip-slope formed on Pennsylvanian strata on the east side of the Sandia Mountains is broken by a mosaic of high-angle faults mostly having small displacements and trending westerly, northwesterly, northerly, and northeasterly (Kelley and Northrop, 1975). High-angle reverse faults in the southeastern part of the Sandia Mountains were suggested to be of Laramide age (Late Cretaceous—early Tertiary) by Kelley and Northrop (1975). In the absence of stratigraphic evidence to pin down such an age, it seems more likely that these reverse faults formed in response to a local compressional stress field in the hinge or synclinal bend of the eastward-tilted Sandia fault block in the late Cenozoic.

The Tijeras graben is the southwestern part of a northeast-trending block bounded on the northwest by the Tijeras fault and on the southeast by the Gutierrez fault. This block, about 25 km long and up to 5 km wide, is tilted to the southwest, with the Tijeras graben grading northeastward into the Monte Largo horst. The boundary between the graben and the horst is placed at the change from downthrown to upthrown stratigraphic separation across the block. Precambrian rocks are exposed in the horst, and Cretaceous Mesaverde strata form the surface in the central part of the graben. These latter rocks are coal-bearing and were mined underground around 1900. Three coal seams ranging from 0.3 to 0.7 m in thickness are present (Kelley and Northrop, 1975).

Maximum structural relief from the Tijeras graben across the bounding fault on the southeast is approximately 1500 m. Within the graben are three major folds: a central, north-trending anticline; a shallow syncline on the west; and a deep syncline on the east. The origin of these folds is not clear, but they may be due to compression in the hinge of the east-tilted Sandia fault block during the late Cenozoic. Alternatively, the folds may be the result of the convergence of the Tijeras and Gutierrez faults at the southern end of the Tijeras graben.

Road log: Day 1, Stops 2-5

Return to the vans and proceed east on 1-40 to the Cedar Crest exit. Meshed and shot-creted outcrops on the left are Pennsylvanian Madera Formation limestone and Permian Abo Formation sandstone and shale that have been faulted and folded along the Tijeras fault. The Ideal Cement Co. plant and quarry on the dip-slope to the south exploit Madera Formation limestone.

Proceed north on NM-14. At 1.7 mi from 1-40 on either side of the road are hogbacks of Mesa Verde Group sandstone on the northwestern limb of the Tijeras syncline. Continue through Cedar Crest to the parking lot of the Mountain Christian Church, on the east side of NM-14, 4.7 mi from 1-40.

Stop 2. Mountain Christian Church exposure of Jurassic Todilto Formation gypsum. Gypsum was mined here by Ideal Cement Co. and has been recently used by sculptors, among whom it is known as Cedar Crest alabaster. The Todilto Formation consists of about 3 m of thinly bedded, fetid, lacustrine limestone overlain by 0 to 30 m of gypsum. The gypsum contains carbonaceous matter which gives it a marbled appearance. On Day 2, the field trip will visit the Iron Vein prospect in the Ortiz Mountains, where faulting

and hydrothermal activity have considerably altered the appearance of the Todilto gypsum.

Leave Mountain Christian Church, heading north on NM-14. Immediately after leaving, note the Entrada Sandstone (Jurassic) and Chinle Formation maroon mudstones (Triassic) in the right roadcut. Continue 12.7 mi to Rt. 344. At about 6 mi, note the Monte Largo Hills, a horst-block of Precambrian gneiss and granitic rocks on the right. Low hills to the left at about 12 mi are composed of Precambrian quartzite and schist. San Pedro Mountains are directly in front. Continue on NM-14 about 1 mi to Rt. 344, turn right, go 1.9 mi and turn left on the dirt road leading to the San Pedro mine and mill.

Stop 3. San Pedro mine and mill. Leached outcrops of copper-skarn ore may have been worked here in Spanish colonial times. Intermittent activity occurred during the 19th and the first half of the 20th centuries (Atkinson, 1961; Elston, 1967). Goldfield Mining operated the San Pedro mine in the 1960's and 1970's.

The skarn at San Pedro is developed in limestone of the Madera Formation. The intrusive body responsible for metasomatism was believed to be a monzonite-porphyry dike about 300 m north of the mine (Lindgren et al., 1910; Atkinson, 1961). The MoS₂-bearing San Lazarus stock is the more likely source of the mineralization at the San Pedro mine and at the pipe-shaped Carnahan silver—lead—zinc replacement deposit 1000 m south of the San Pedro mine (T. Thompson, pers. comm. 1990).

Return to vans and drive back to NM-14. Head north on NM-14. Mountain group to the north is the Ortiz Mountains. One mile from the Rt. 344 junction enter the hamlet of Golden, scene of a considerable gold rush in the 1830's, the first such boom west of the Mississippi. Gold was produced from dry placers, largely through "coyoteing" or sinking a shaft through the poorly consolidated gravels and following channels on the bedrock surface.

Continue north out of Golden on NM-14 about 7 mi to Stagecoach Pass. The road in Stagecoach Canyon, on the south side of the pass, is cut into Upper Cretaceous Mancos Shale which has been invaded by mainly concordant masses of Oligocene latite—andesite porphyry (Fig. 4).

Stop 4. Stagecoach Pass. Sills of Oligocene latiteandesite porphyry intruding Upper Cretaceous Mancos Shale. Concordant bodies of latite—andesite porphyry (dated at 34.0 ± 2.2 Ma by Bachman and Mehner (1978)) represent the first phase of intrusion during the Oligocene. Johnson



FIGURE 4—Oligocene latite—andesite porphyry sill intruding upper Cretaceous Mancos Shale at Stagecoach Pass.

(1904), Lindgren et al. (1910), and Stearns (1953) interpreted the San Pedro—Ortiz porphyry belt as being dominated by laccoliths. While this conclusion seems correct in the Cerrillos Hills (Disbrow and Stoll, 1957) recent investigations (Maynard et al., 1990) in the Ortiz Mountains have failed to identify a laccolithic source of the sills found in the range. The sills are thicker on the western side of the Ortiz Mountains, suggesting that the source laccolith was west of the present Ortiz Mountains and has been eroded.

Return to vans and go north on NM-14. At 1.8 mi from Stagecoach Pass come to commanding view of Cerrillos Hills, Santa Fe, and the Sangre de Cristo Range. Descend into Madrid. Just before entering Madrid, note exposures of unmetamorphosed Menefee shales. The Menefee Formation, composed of continental shale and fluvial sandstone, is host to the coal that was mined by the Albuquerque and Cerrillos Coal Co. from about 1900 until 1958 (Beau-

mont, 1979). On Day 2 the field trip will visit outcrops of metamorphosed Menefee shales in the Ortiz Mountains.

Continue north through the ramshackle of Madrid about 5 mi to the turnoff to the bucolic village of Cerrillos. Cerrillos has served as a set for motion pictures in recent years, among them the western *Young Guns*. Drive into Cerrillos, turn right at the first cross street, cross the railroad tracks, go straight, bear left at the cattle guard, cross San Marcos Arroyo, then bear right, continuing 1.3 mi up a narrow arroyo to rip-rap quarry on left. This is private land, belonging to Cerrillos Gravel Products. Be careful of large gravel trucks. Mineral rights are presently leased by Placer Dome Mining.

Stop 5. Cerrillos Sand and Gravel Co. rip-rap quarry. The walking tour across the Cerrillos porphyry copper deposit to the Mt. Chalchihuitl turquoise mines starts here.

Geologic outline of the Cerrillos mining district, Cerrillos porphyry copper deposit, and associated mineralization

David L. Giles

The 80 km² Cerrillos mining district is north of the community of Cerrillos and about 25 km southwest of Santa Fe in Santa Fe County, New Mexico. The area has a rich history of turquoise, silver, and lead mining dating back over 1000 years. Turquoise deposits at Mt. Chalchihuitl (Figs. 5, 6) are said to be "the most extensive prehistoric mining operations in North America" (Pogue, 1915) and date to 9501150 A.D. (Warren and Mathien, 1985). Artifacts from the Mina del Tiro and nearby Bethsheba lead—zinc—silver mines indicate that Indians were also mining copper oxides for pigment and lead for pottery glaze at about the same time. Under Spanish Colonial rule in the 16th and 17th centuries, it is rumored that Indians were conscripted to work the mines, and that a disastrous cave-in in one of them was the immediate cause of the Pueblo Revolt of 1680 (Schroeder, 1979). There is, however, no substantive historical evidence of this (Goodman and Levine, 1990).

Some metal mines were worked intermittently by the Spanish for lead, copper, and silver when they returned after the revolt, and again under Mexican rule from 1821 until 1845. During the Territorial period, discovery of new lead-zinc—silver lodes in the district in 1879 led to a boom that lasted several years before subsiding to sporadic production from a handful of mines. Operations had effectively ceased by the mid-1950's. Elston (1967) reports production from 1909 until 1957 as: 26,816 tons of ore; 734+ oz Au; 29,864 oz Ag; 181,224 lb Cu; 1,578,340 lb Pb; and 1,935,727 lb Zn. Most of this recorded production came from the Tom Payne and Cash Entry mines (Fig. 5).

Total production of turquoise from the known mines and many small workings and pits throughout the district is unknown. Early Indians of the region placed great value on turquoise as a trade, ornamental, and ceremonial item. They mined the Cerrillos Hills deposits, specifically Mt. Chalchihuitl, continuously for nearly 700 years to around 1700, and thereafter intermittently to the present (Warren and Mathien, 1985). The Spanish, on the other hand, had no use for the mineral.

Northrop (1959) reports that at least \$2,000,000 worth

of high-grade gem material was extracted from Turquoise Hill (also known as the Tiffany mine) in the 1890's (Fig. 5). In 1959, Bear Creek Mining Company, a subsidiary of Kennecott Copper, discovered and explored a small, low-grade porphyry copper deposit in the southern part of the district (Wargo, 1964). This deposit was then extensively studied by Occidental Minerals Corporation in the mid-1970's for possible in-situ leaching of the copper-oxide portion of the deposit (Akrigh, 1979).

The Cerrillos Hills are at the northern end of the San Pedro—Ortiz porphyry belt, a north-trending group of monzonitic stocks, laccoliths, sills, and dikes of Oligocene age (Woodward and Ingersoll, 1979; Maynard, this volume). The Cerrillos intrusive/extrusive complex lies in a tilted structural block bounded on the west by the east margin of Rio Grande rift (Rosario and La Bajada faults), and on the south and east by the northeast-trending Tijeras—Canoncito fault system (Lisenbee et al., 1979; Woodward, this volume). The Paleozoic to Tertiary strata of the block dip regionally eastward at 10-15° into the Santa Fe embayment at the southern end of the Espanola basin (Kelley, 1978). The Cerrillos block comprises the "La Bajada constriction" (Kelley, 1952), a positive salient separating the rift graben of Espanola basin from that of the Albuquerque basin to the south. No major mineral-controlling fault system similar to the Tijeras—Canoncito has been recognized in the Cerrillos district. Veins occupy northeast-trending fracture swarms in the southern and the northern parts of the area (Figs. 5, 6).

At least four major periods of Oligocene igneous activity, at a variety of separate or overlapping intrusive centers, have been recognized in the Cerrillos Hills (Disbrow and Stoll, 1957; Bachman and Mehnert, 1978). The rocks are universally quartz-poor and range from syenite to diorite, with monzonite predominating. The intrusive complex consists of stocks, plugs, sills, laccoliths, and dikes containing a wide variety of mineral compositions and textures. Exposed strata invaded by the complex include the Morrison Formation (Jurassic); Dakota Sandstone, Mancos Shale, and Mesaverde Group (Upper Cretaceous); Galisteo Formation

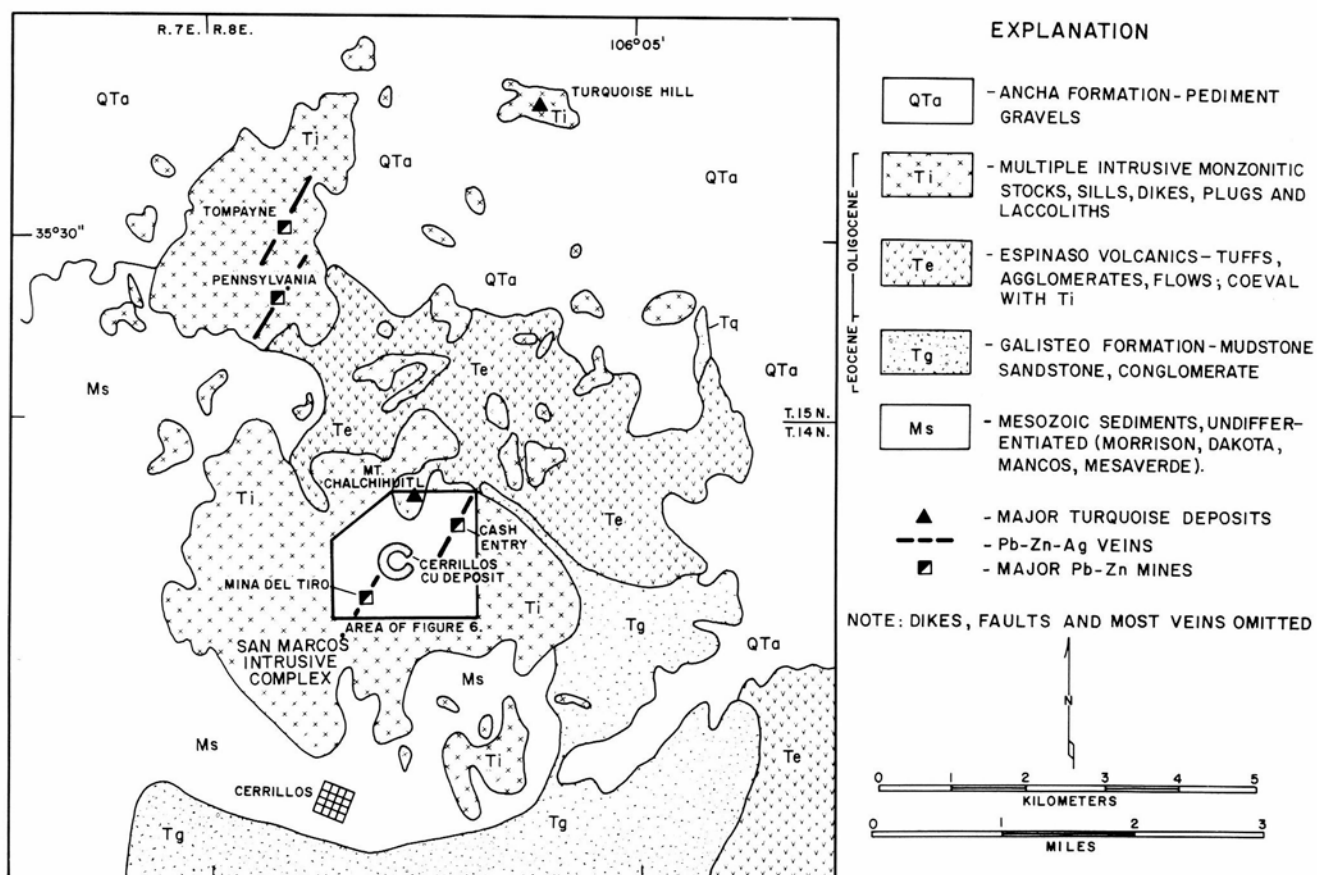


FIGURE 5—Simplified geologic map of the Cerrillos Hills (modified from Disbrow and Stoll, 1957).

(Eocene); and Espinaso Volcanics (Oligocene) (Fig. 5). The latter consists of a series of tuffs, agglomerates, and latite flows that erupted contemporaneously with various intrusive episodes throughout the Cerrillos Hills and the Ortiz Mountains (Kautz et al., 1981; Smith et al., this volume). These stratigraphic units have been upturned along the margins of the intrusive complex and occur as scattered inliers within.

The porphyry copper deposit and associated mineralization in the southern Cerrillos district is centered on a sub-circular multiple intrusive complex about 4 km in diameter (Fig. 6), herein termed the San Marcos intrusive complex (SMIC). The SMIC lies directly north of Cerrillos village and is isolated from other intrusive centers in the district by a skirt of invaded wallrock, mainly Mancos Shale (Niobrara Member) and Espinaso Volcanics (Fig. 5) (Bachman, 1975). The nature and sequence of igneous events in the SMIC are unclear due to variable lithologies and hydro-thermal overprint on the rocks. For simplicity, the sequence is grouped here as follows: monzonite porphyry (oldest) forming the core of SMIC; syenomonzonite as a small ameboid stock (about 1 km²) in the center of SMIC; and an equigranular monzonite as a small, circular plug about 360 m in diameter, emplaced into a lobe of the syenomonzonite mass (Fig. 6). Porphyry copper mineralization is spatially, and in part genetically, related to the young monzonite plug.

The monzonite porphyry is dark to medium gray and characterized by hornblende and plagioclase phenocrysts ranging in size and abundance. Most of the monzonite-porphyry sills and laccoliths were emplaced into the relatively incompetent Mancos Shale. About 1.5 km up the access road to the copper deposit from San Marcos Wash, "fingers" of monzonite appear to be gently probing into the

shales; possibly they are the leading edge of the sill-like mass on the opposite side of the arroyo. Contact effects in the shale are limited to thin baked selvages and deformation is minimal.

The syenomonzonite is pinkish gray, equigranular to coarsely porphyritic with augite (or biotite) and K-feldspar phenocrysts, and is cut by numerous pink aplite dikes. The late monzonite plug is light gray, coarse-grained equigranular, and forms a barren core around which a stockwork fracture zone has localized a ring of copper mineralization (Fig. 6). Scattered lesser rocks in the area include pre- and post-mineral monzonite dikes, late basalt(?) dikes, and flows probably belonging to the Espinaso Volcanics.

The Cerrillos copper deposit displays most of the alteration and mineral zoning features typical of hydrothermal porphyry copper systems. It is a low-grade (about 0.3% Cu), MoS₂-poor, low total-sulfide system with a high chalcopyrite/pyrite ratio in a zone coincident with strong stockwork fracturing, local vein and replacement silicification, and potassic alteration (secondary biotite and K-feldspar). There is no supergene chalcocite enrichment blanket at depth (Wargo, 1964; Akright, 1979), although secondary chalcocite did form at the present exposure level from earlier oxidation and leaching. The deposit has a well-developed pyritic halo characterized by widespread propylitization (chlorite and epidote), local clay-sericite alteration, and near-background copper values.

The copper ring, as defined by the >2000 ppm Cu-in-rock surface contour (Fig. 6), ranges from 30 to 180 m wide and encircles two-thirds of the monzonite plug. Drilling indicates that the deposit is a near-vertical cylinder adjacent to the walls of the barren monzonite plug. From the sharp

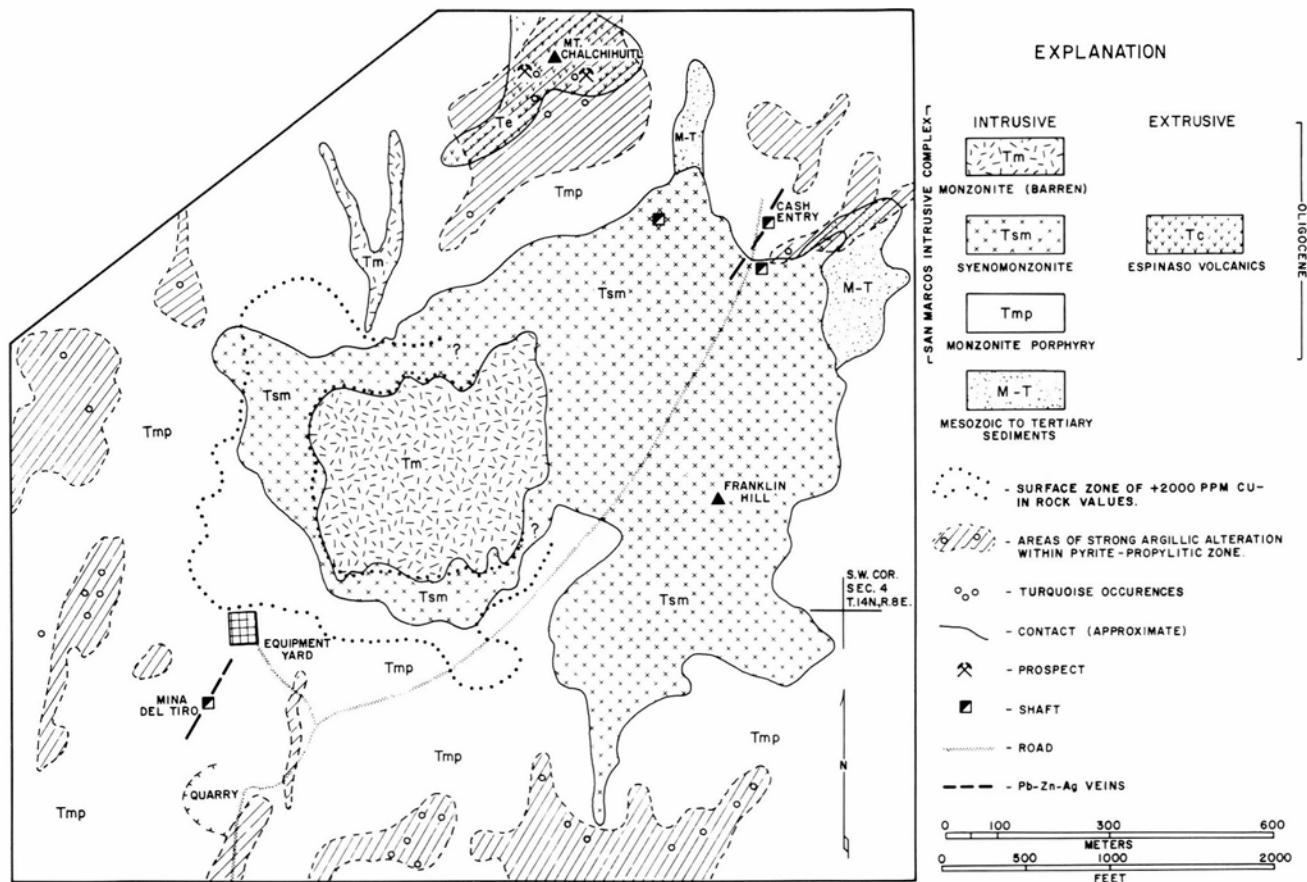


FIGURE 6—Generalized geologic map of the Cerrillos porphyry copper deposit and surrounding area (adapted from Wargo, 1964, and unpublished data).

inner boundary (an assay wall), copper grades decline gradually outward to an economic cutoff in the pyrite zone. The bulk of the copper deposit overlaps, for the most part, the porphyritic syenomonzonite lobe and its contact with the older monzonite porphyry (Fig. 6). The above relationships suggest that intrusion of the late monzonite plug was instrumental in ground preparation (stockwork fracturing) around its border, thus creating a zone of permeability for later copper-bearing hydrothermal solutions. This is the primary control of mineral deposition.

The primary sulfides in the Cerrillos deposit are chalcopyrite and pyrite, with trace amounts of bornite, marcasite, enargite, and molybdenite. Minor amounts of secondary chalcocite and covellite occur as relicts in the oxide zone and as supergene minerals in the mixed oxide—sulfide zone at depth. Significant magnetite occurs as veinlets both preceding and crosscutting primary copper mineralization, and as breccia cement. Small amounts of gold (in electrum) are present. The gold seems to correlate with zones of stronger silicification, potassic alteration, higher copper values, and magnetite veining. This genetic association has been discussed by Sillitoe (1979) and Cox and Singer (1988). All mineralization in the deposit is strongly fracture-controlled; disseminated oxides and sulfides are rare.

Late lead—zinc veins and veinlets crosscut copper mineralization and occur in all rock types in the deposit areas, including the barren monzonite core. Extensive surface rock-chip sampling shows no halo-type distribution for lead and zinc peripheral to copper; in fact, many lead—zinc highs coincide with copper highs. It would seem that lead and zinc did not participate in true spatial zoning, as in many

other porphyry systems, but were superimposed on the copper deposit along a swarm of northeast-trending veins from Mina del Tiro to Cash Entry. Similarly, the surface distribution of molybdenum does not mimic that of copper, as might be expected, but is erratic and equally prominent in both the copper zone and pyrite halo.

The principal secondary copper minerals in the oxide cap are neotocite and brochantite, with lesser chrysocolla and pitch limonite, and small amounts of malachite, azurite, cuprite, antlerite, melaconite (black earthy tenorite, CuO), hematite, residual chalcocite, and native copper. These minerals formed in a supergene environment where the copper/sulfur ratio was very high, and where the copper-sulfide suite prior to most recent oxidation was a mix of primary chalcopyrite and local secondary chalcocite. Two areas of better grade and potentially minable oxide copper have been delineated by detailed drilling in the southwest and southeast quadrants of the deposits. The goethitic-oxide cap ranges from 30 to 120 m thick, with a mixed sulfide—oxide zone at the interface and primary sulfides at depth. The variation is attributed by Akright (1979) to post-oxidation faulting.

The makeup of the limonite and copper-oxide minerals in the outcropping cap allows certain observations about the nature of the eroded higher levels of the deposits as well as the remaining deposit at depth:

- 1) upper parts of the deposit (now removed) had a high pyrite and high total-sulfide content, resulting in leaching of copper and precipitation of secondary chalcocite at about the present exposure level;
- 2) the precursor sulfide deposit at the present level was low in total sulfides (about 1-2%) and this sulfide suite had

more than 50% chalcopyrite and, locally, more than one-third chalcocite;

- 3) very little copper has been leached from the cap at the present exposure level;
- 4) the probability of a significant second-generation chalcocite blanket at depth is nil;
- 5) surface copper grades can be predicted to be essentially the same as in the sulfide zone at depth, as confirmed by drilling (Wargo, 1964; Akright, 1979; unpublished data).

The pyrite halo surrounding the copper deposit is subcircular and about 1.7 km in diameter. The halo averages about 2% pyrite, but contains scattered patches of bleached and argillized rock that initially contained about 8 to 10% pyrite. These bleached zones are characterized by jarositic limonite and numerous small occurrences of turquoise (Fig. 6) with sporadic variscite ($\text{AlPO}_4 \cdot 2\text{H}_2\text{O}$).

The turquoise shows have been prospected off and on by locals for many years, with occasional discovery of gem-quality material. An important prehistoric turquoise deposit occurs at Mt. Chalchihuitl about 1.2 km north of the equipment yard (Fig. 6). The name of the mine is a derivative of the word for turquoise in Nahuatl, the Aztec dialect, thus imparting a sense of its age. This mine is in clay-altered and weakly tourmalinized volcanics, probably in inlier of Espinaso Volcanics. A nearby drill hole collared in the unit penetrated monzonite porphyry at about 30 m. The turquoise

occurs as nodules in open spaces and as irregular veinlets with little continuity. Turquoise and variscite are secondary oxide minerals that require the presence of free phosphorus in the supergene environment in order to form. The logical source of phosphorus is apatite, which is reported as a relatively abundant accessory mineral in the monzonites. Presumably, supergene acid conditions in the high pyrite zones were strong enough to break down apatite and release phosphorus to ground waters.

Several lead—zinc—silver vein deposits in the southern Cerrillos district have had significant production. Most notable are the Cash Entry mine and Mina del Tiro (Fig. 6). According to Spanish Archives (Goodman and Levine, 1990), the latter was mined by the Spanish to obtain lead for musket balls. In general, the vein ores consist of galena and sphalerite, with lesser chalcopyrite and pyrite, in a gangue of ankerite and quartz. A little barite, stibnite, bournonite, wulfenite, rhodochrosite, amethyst, and chalcedony are reported (Disbrow and Stoll, 1957). Vein material occurs as lenses, streaks, crustifications, and disseminations in shoots that partially fill northerly trending shear zones; wallrock is mostly sericitized monzonite. Silver is associated with galena, and gold probably with chalcopyrite. Historically, average ore from the district yielded only 1.1 oz Ag and 0.03 oz Au per ton, but some small high-grade shipments contained over 600 oz/ton Ag and up to 5 oz/ton Au.

Geology and gold mineralization of the Ortiz Mountains

Stephen R. Maynard

Introduction

Approximately 350,000 oz (11,000 kg) of gold have been produced from the Ortiz Mountains since the 1820's. The 260 km² Ortiz Mine Grant was secured from the Mexican government in 1833 by Jose Francisco Ortiz for the purpose of mining gold. Surface rights were separated from mineral rights in the 1940's and are divided among several owners. The mineral rights on the Grant have remained more or less intact to the present. Mineral rights are currently owned by Ortiz Mines, Inc. of Joplin, Missouri, and are leased to Pegasus Gold, which is operator of an exploration, development, and production joint venture with LAC Minerals, USA, Inc.

Igneous rocks

Igneous rocks in the Ortiz Mountains (Fig. 7) can be divided into an earlier calc-alkaline group and a later alkaline group. Isotopic-age determinations on these groups constrain mid-Tertiary movement on the Tijeras—Canoncito fault system (TCFS) to the period 34 to 30 Ma. Most gold mineralization is spatially and temporally related to the alkaline igneous rocks.

Latite—andesite porphyry sills, laccoliths, and dikes and a granodiorite stock comprise the calc-alkaline group. The K—Ar age determination that best fits with geologic relations on the latite—andesite porphyry is 34.0 ± 2.2 Ma (Bachman and Mehnert, 1978). This date was determined from hornblende in unaltered rocks on the west side of the Ortiz

Mountains. Older age determinations of 43.2 ± 2.3 Ma (Kay, 1986) and 47.1 ± 3.2 Ma (Bachman and Mehnert, 1978) appear to contradict geologic relations and may represent contamination by upper crustal material. Latite—andesite sills appear to have propagated from laccolithic masses on the west side of the Ortiz Mountains and are cut by the TCFS. The sills generally intrude less competent lithologies, particularly shales and mudstones of the Menefee, Mancos, Morrison, and Chinle Formations, and show little evidence of thermal metamorphism at the contacts. Latite—andesite sills are important brecciated hosts for gold mineralization in the Carache Canyon breccia-pipe area.

The Candelaria granodiorite stock is probably the youngest phase of calc-alkaline magmatism, although direct cross-cutting evidence with the latite—andesite sills is not available. A large hornfels aureole is present around the stock. The garnet—pyroxene skarn-altered Greenhorn Limestone at Lukas Canyon is within this contact aureole and the Candelaria granodiorite is presumed to be the thermal source for both the hornfels aureole and the skarn.

Alkaline rocks are represented by a large nepheline-bearing augite-monzonite stock, a latite-porphyry hypabyssal plug, the Ortiz diatreme (vent breccia), and radial trachytic-latite dikes. K—Ar age determinations range from 30 to 26 Ma for the alkaline rocks (Kay, 1986). The 29.6 ± 1.5 Ma augite-monzonite stock intruded the Eocene Galisteo Formation to within 1000 m of its projected surface, cut across the Ortiz graben (the principal structure of the TCFS in the

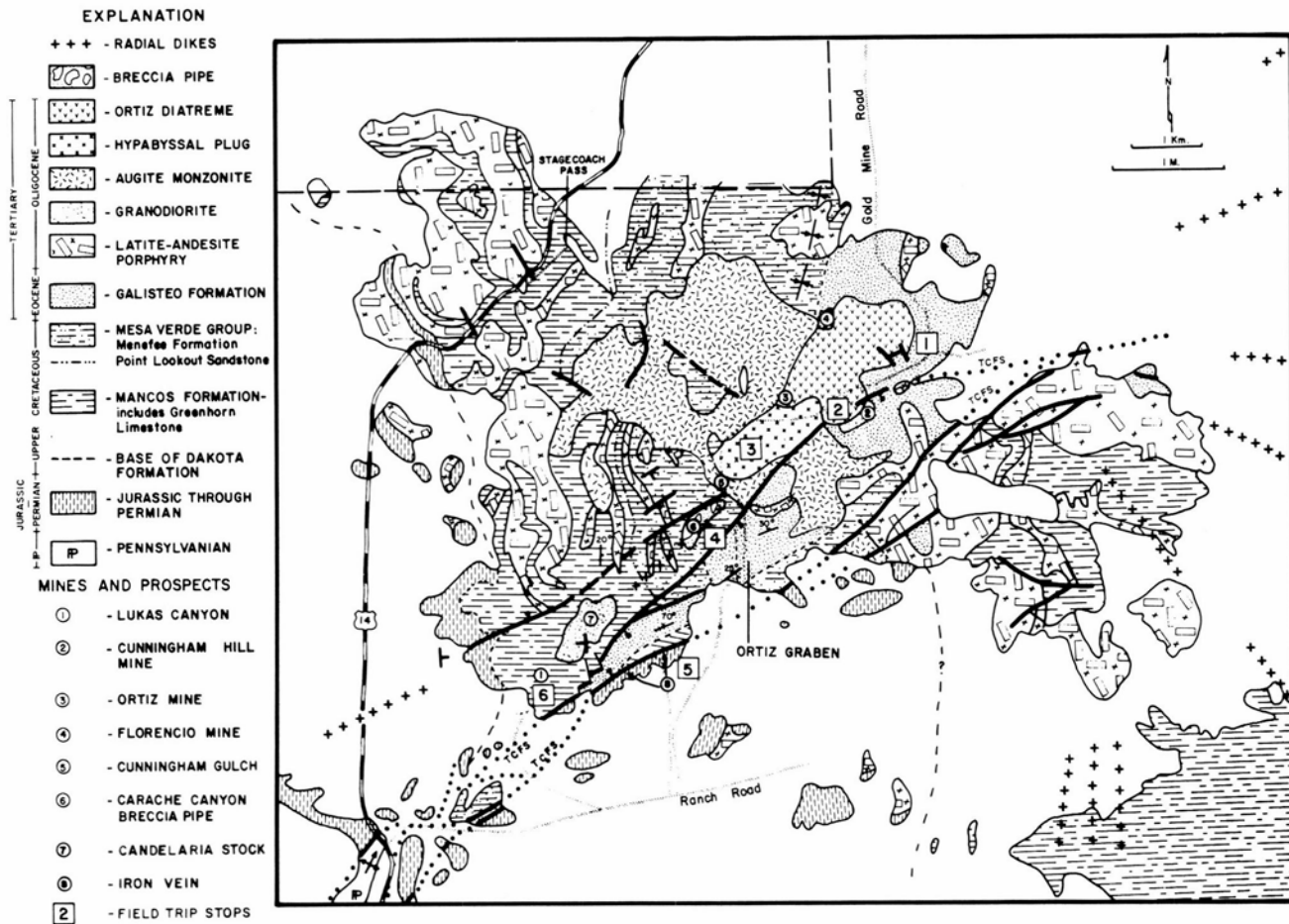


FIGURE 7—Generalized geologic map of the Ortiz Mountains showing Day 2 stops.

Ortiz Mountains), and produced a wide contact-metamorphic aureole in the surrounding sedimentary rocks. This aureole is defined by intense hornfels development and is easily mapped by topographic highs underlain by what would otherwise be recessive sedimentary rocks. The Ortiz diatreme and its related hypabyssal latite-porphphyry plug cut the augite-monzonite stock. Dikes radial to the diatreme crop out in the distance of approximately 3.5 km.

Structural geology

The Tijeras—Canoncito fault system dominates the structural geology of the Ortiz Mountains (Figs. 7, 8). The Ortiz graben, the Ortiz diatreme, and the Carache Canyon breccia pipe appear to be structurally controlled by the TCFS.

The Ortiz graben contains several tilted blocks of Galisteo and Menefee Formations. Vertical stratigraphic separations of 600-1000 m are estimated on the graben's bounding faults. Left-lateral stratigraphic separation of the Dakota Formation measures approximately 5 km across the TCFS. The northern side of the TCFS is downthrown with respect to the southern side. The true amount and direction of displacement are unknown.

The Ortiz diatreme, or vent breccia, erupted on the northwestern side of the northwestern graben-bounding fault and partly occupies it. The diatreme forms a crude ellipse approximately 2100 by 1200 m in plan. The diatreme has been drilled to a depth of 500 m (Fig. 9). It is composed principally of tuff, lithic tuff, and volcanic breccia. Lithic clasts in the tuff are composed of augite monzonite, latite—andesite

porphyry, and Cretaceous and Eocene sedimentary rocks. Breccia pipes occur in two principal zones on the southeastern and northwestern margins of the diatreme. The northwestern margin is a fault contact of vent breccia with augite monzonite. Substantial throw is suspected on this fault, bringing the vent breccia down with respect to the augite monzonite. The southeastern margin is an intrusive contact characterized by intense brecciation of the wall rocks as at the Cunningham Hill and Benton mines (Lindqvist, 1980; Wright, 1983; Kay, 1986).

The southeastern margin of the Carache Canyon collapse-breccia pipe lies about 120 m to the northwest of the north-

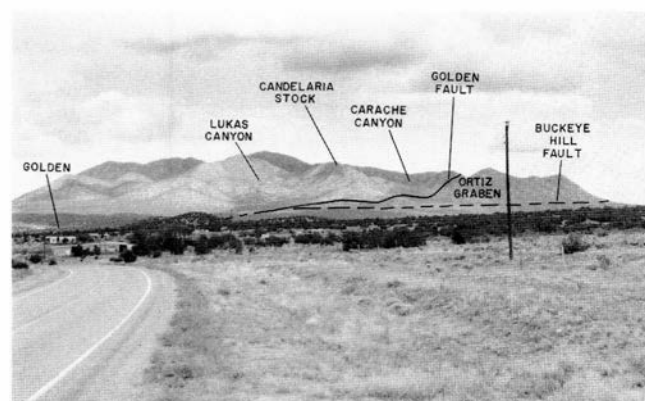


FIGURE 8—View of the Ortiz Mountains from about 1 km south of Golden.

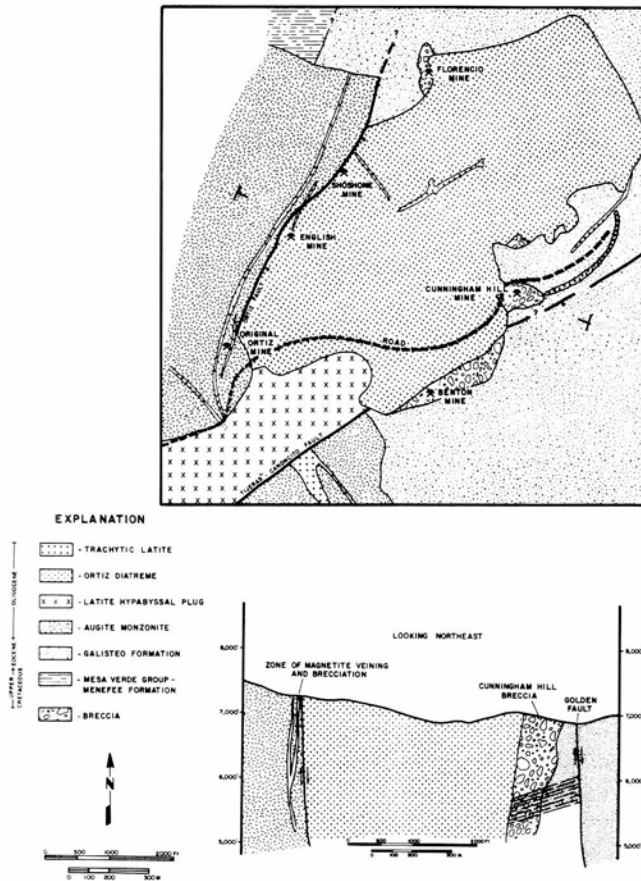


FIGURE 9—Geologic map of the Ortiz diatreme (modified after Lindqvist, 1980, and Kay, 1986) and its cross-section.

western margin of the Ortiz graben (Fig. 10). The pipe is approximately 625 by 312 m, elongate in a northeast—southwest direction, and plunges at 75° toward the southwest.

It is hypothesized that deep-seated fractures parallel to the TCFS served as a conduit for vapor release and as a zone of weakness for brecciation and subsequent collapse, forming the Carache Canyon breccia pipe. The Ortiz diatreme formed 2000 m to the northeast, parallel to the strike of the Golden fault. Magmatic withdrawal during eruption of the Ortiz diatreme may have allowed room for the collapse of the Carache breccia pipe.

Gold mineralization

Lode-gold deposits in the Ortiz Mountains generally occur along or near strands of the TCFS. Lodes are of various types including breccias, veins, skarns, and porphyry-type occurrences. A variety of breccias host gold mineralization in the Ortiz Mountains. Placer-gold deposits in Plio-Pleistocene gravels lie on the eastern and southern flanks of the mountains.

Road log: Day 2

Retrace Day 1 route north on NM-14 to Gold Mine Road, 2.8 mi north of Madrid. Note outcrops of Eocene Galisteo Formation sandstone in gulch north of Madrid. Turn south on Gold Mine Road, bear right at 2.3 mi and continue 4.3 mi to the gate and office of the Cunningham Hill mine. Go through gate and drive about 0.2 mi to vista to northeast.

Stop 1. Overview and discussion of Tijeras—Canoncito fault system northeast of the Ortiz Mountains.

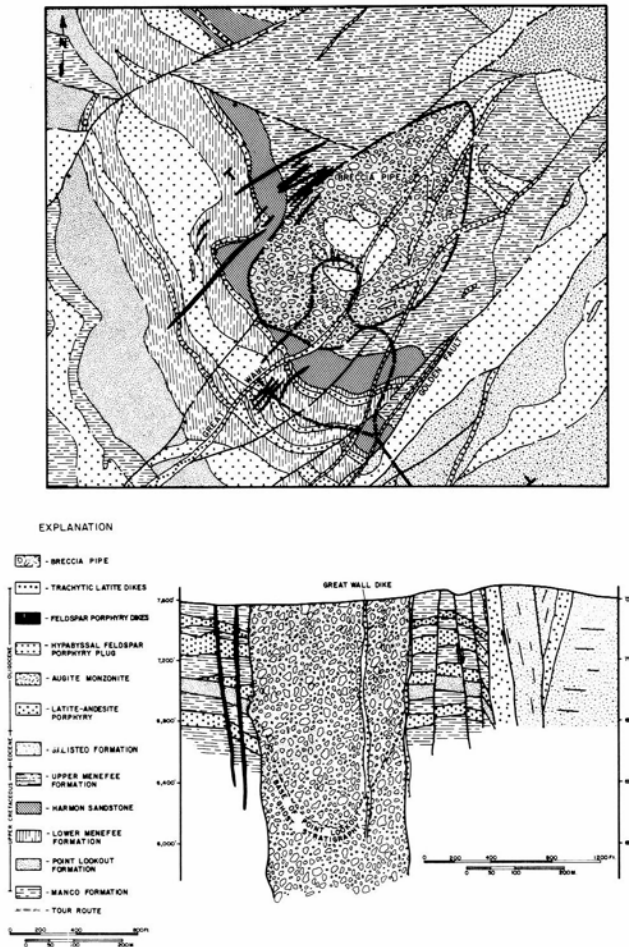


FIGURE 10—Geologic map and cross-section of Carache Canyon.

Return to the vans and head west on the road past the maintenance building and tailings piles on the left and the leach pad, mill site, and primary and secondary crusher locations on the right. Park at the east end of the Cunningham Hill open pit.

Stop 2. Cunningham Hill mine. Micron-size gold is commonly associated with crystals of pyrite, magnetite, calcite, siderite, quartz, chalcopryrite, or scheelite in open spaces between clasts of brecciated Galisteo Formation at Cunningham Hill. Kay (1986) stated that the Cunningham Hill breccia is least permeable and lowest grade on the southern and eastern borders, and most permeable and highest grade on the northern and western sides bordering the vent breccia (Figs. 8, 9, 11). Kay (1986) postulated that the ore-hosting breccia formed later than the diatreme due to explosive vapor release and he attributed the downward tapering of the breccia body to a primary stratigraphic control. That is, incompetent shales below the ore-hosting sandstone body could not maintain the open spaces.

Consolidated Gold Fields extracted approximately 250,000 oz (7800 kg) of gold from the Cunningham Hill open-pit mine in the period 1979-1987. Mined ore averaged 0.055 opt in 6 million tons (1.9 gmt in 5.4 million metric tons).

Board the vans on the western side of the pit at the scheelite stockpile and head west 0.9 mi past the old Ortiz mine. The Ortiz mine is the site of the original lode discovery in the Ortiz Mountains in 1932 and is the geographic center of the 260 km² Ortiz Mine Grant. The Ortiz, English,

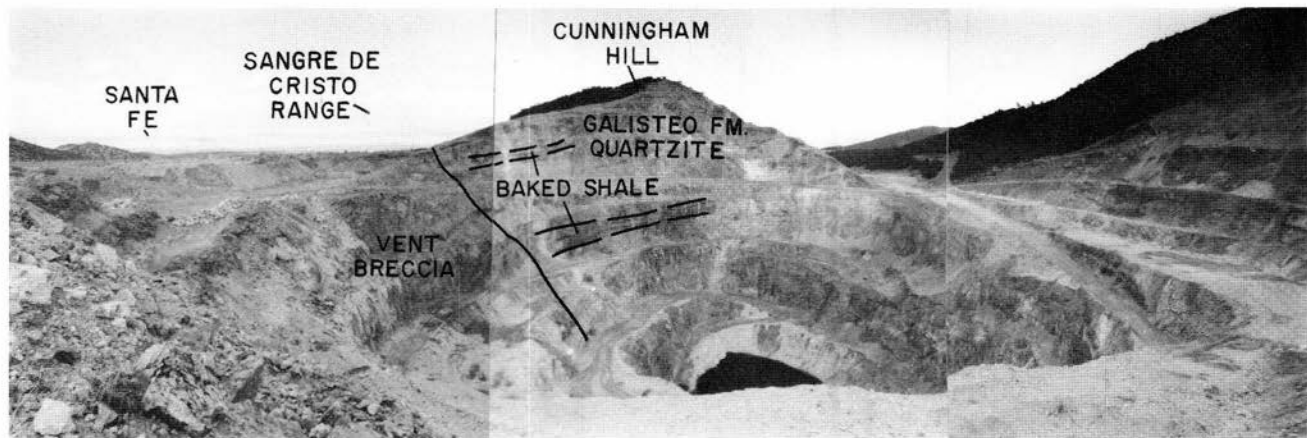


FIGURE 11—Cunningham Hill open-pit mine, looking northeast.

Shoshone, and Florencio mines lie on, or near, a N20E-trending fault contact between the augite-monzonite stock and the Ortiz diatreme (Fig. 9). Gold appears to be associated with magnetite fillings in a wide brecciated zone in the augite monzonite at the Ortiz and English mines. At the Florencio mine, the brecciated host is quartzite developed in Mesa Verde or Galisteo sandstone.

Continue in vans up the Cunningham Gulch road as far as the vans can go, then walk through the Cunningham Gulch porphyry copper—gold prospect.

Stop 4. Cunningham Gulch porphyry copper—gold prospect. The hypabyssal latite plug in Cunningham Gulch appears to be the barren core of a low-grade gold-bearing copper porphyry system (Fig. 8). Crackle breccia and stockwork veinlets filled with tenorite + magnetite ± fluorite

molybdenite are associated with gold mineralization. Included in this stop are outcrops of the barren porphyry core and roadcuts showing the copper—gold mineralization.

Continue on foot along the Cunningham Gulch road over a pass, then down to the Carache Canyon decline portal where the field trip will meet the vans for lunch. Just before arriving at the pass, the road crosses the Golden fault, the northwest-bounding fault of the Ortiz graben. Rocks along the road down to the decline portal are quartzite derived from the Galisteo Formation. After lunch, vans will take the group up Carache Canyon for a walking tour of the Carache Canyon breccia pipe.

Stop 5. Carache Canyon. The Carache Canyon deposit is associated with a collapse-breccia pipe measuring 550 by 300 m on the surface, plunging 70° S40W, and having a known down-plunge extent of over 1000 m (Fig. 10). The pipe is characterized by collapsed beds of shale and sandstone and latite—andesite porphyry sills. A relict stratigraphy, largely defined by the distinctive Point Lookout Sandstone, shows as much as 250-300 m of collapse. The breccia typically is clast-supported and locally contains as much as 10% dark-colored rock-flour matrix.

Secondary fracturing of the Carache Canyon pipe resulted in randomly oriented, open-space fractures that are concentrated in an annular zone around the southwestern margin of the pipe. The secondary fracture zones occur inside and outside the pipe margins. The open-space fracture zones developed best in the latite—andesite sills and in the Point Lookout Sandstone. In contrast, the shales of the Mancos and Menefee Formations contain few open-space fractures. Thus, outside the pipe, mineralization is concentrated in a

series of stacked, tabular bodies separated by intervals of relatively barren shale.

Unoxidized mineralization at Carache Canyon is in the form of coarse gold in open-space fractures with pyrite, pyrrhotite, chalcopyrite, sphalerite, galena, arsenopyrite, calcite, and adularia. Gold appears to have been deposited late in the paragenetic sequence (Coles, 1990). Gold mineralization at Carache Canyon appears to be closely related temporally to the intrusion of trachytic-latite dikes. Some dikes are fractured and mineralized. Others cut mineralization and are unfractured.

In May 1988, LAC Minerals announced the discovery of a geologic resource of 5 million tons grading 0.094 opt (4.5 million metric tons of 2.9 gmt) gold at Carache Canyon.

Return to the vans and drive out of Carache Canyon about 2 mi to the Lone Mountain Ranch road. The Ortiz surface, the regular plain sloping away from the Ortiz Mountains, is underlain by the late Tertiary Tuerto Gravel, host of the numerous placer deposits in the area. Turn right, cross the cattle guard, take the next right and proceed approximately 2 mi to the Iron Vein prospect.

Stop 6. Iron Vein prospect. A tectonized solution-collapse breccia is developed in the gypsum member of the Jurassic Todilto Formation along the southeastern margin of the Ortiz graben. The solution-collapse breccia is apparently a regional feature of probable Tertiary age. At the Iron Vein, the breccia consists of clasts of Jurassic Morrison Formation sandstone and shale supported by a yellowish-orange matrix of sand, calcite, clay, and gypsum. In addition, magnetite + hematite ± garnet skarn is locally developed in the Todilto limestone. Controls on gold mineralization in the Iron Vein area appear to be related to faulting and to an underlying granodiorite stock.

Return to vans, drive back to Lone Mountain Ranch road, turn right and continue 0.9 mi to power-line access road. Follow power-line road 0.9 mi, turn right. Follow road back to north, pass windmill at 0.6 mi, go 0.1 mi, turn right, and go 0.6 mi to entrance to Lukas Canyon.

Stop 7. Lukas Canyon. The Lukas Canyon deposit, a copper—gold, garnet—pyroxene skarn developed in the Greenhorn Limestone Member of the Mancos Formation, contains an announced resource of 0.03 opt gold and 0.25% copper in 6 million tons (1.02 gmt gold in 5.4 million metric tons). Gold and copper mineralization postdates the primary skarn and is believed to be related to a late retrograde alteration event when the garnet—pyroxene skarn was altered

to chlorite-actinolite-epidote. Sulfides are locally present as pyrite-chalcopyrite but the deposit has been intensely oxidized, resulting in a complex assemblage of copper- and

iron-oxides. The skarn crops out on a dip-slope, making it amenable to surface mining.

End of excursion.

Combined references

- Akright, R. L., 1979, Geology and mineralogy of the Cerrillos copper deposit, Santa Fe County, New Mexico: New Mexico Geological Society, Guidebook 30, pp. 257-260.
- Atkinson, W. W., 1961, Geology of the San Pedro Mountains, Santa Fe and Sandoval Counties, New Mexico: New Mexico Bureau of Mines & Mineral Resources, Bulletin 77, 49 pp.
- Bachman, G. O., 1975, Geologic map of the Madrid 15' quadrangle, Santa Fe and Sandoval Counties, New Mexico: U.S. Geological Survey, Geologic Quadrangle Map GQ-1268.
- Bachman, G. O., and Mehnert, H. H., 1978, New K-Ar dates and the late Pliocene to Holocene geomorphic history of the central Rio Grande region, New Mexico: Geological Society of America, Bulletin, v. 89, pp. 283-292.
- Beaumont, E. C., 1979, Geology of the Cerrillos coal field, Santa Fe County, New Mexico: New Mexico Geological Society, Guidebook 30, pp. 269-275.
- Black, B. A., 1979, Structure and stratigraphy of the Hagan embayment: a new look: New Mexico Geological Society, Guidebook 30, pp. 101-105.
- Black, B. A., and Hiss, W. L., 1974, Structure and stratigraphy in the vicinity of the Shell Oil Co. Santa Fe Pacific no. 1 test well, southern Sandoval County, New Mexico: New Mexico Geological Society, Guidebook 25, pp. 365-370.
- Bruns, J. J., 1959, Petrology of the Tijeras Greenstone, Bernalillo County, New Mexico: Unpublished MS thesis, University of New Mexico, Albuquerque, 119 pp.
- Coles, D., 1990, Alteration and mineralization of the Carache Canyon breccia pipe, Santa Fe County, New Mexico: Unpublished MS thesis, Colorado State University, Fort Collins.
- Connolly, J. R., 1981, Geology of the Precambrian rocks of Tijeras Canyon, Bernalillo County, New Mexico: Unpublished MS thesis, University of New Mexico, Albuquerque, 147 pp.
- Connolly, J. R., 1982, Structure and metamorphism in the Precambrian Cibola gneiss and Tijeras greenstone, Bernalillo County, New Mexico: New Mexico Geological Society, Guidebook 33, pp. 197-202.
- Cox, D. P., and Singer, D. A., 1988, Distribution of gold in porphyry copper deposits: U.S. Geological Survey, Open-file Report 88-46, 23 pp.
- Disbrow, A. E., and Stoll, W. C., 1957, Geology of the Cerrillos area, Santa Fe County, New Mexico: New Mexico Bureau of Mines & Mineral Resources, Bulletin 48, 73 pp.
- Elston, W. E., 1967, Summary of the mineral resources of Bernalillo, Sandoval, and Santa Fe Counties, New Mexico: New Mexico Bureau of Mines & Mineral Resources, Bulletin 81, 81 pp.
- Fulp, M. S., Cavin, W. J., Connolly, J. R., and Woodward, L. A., 1982, Mineralization in Precambrian rocks in the Manzanita-north Manzano Mountains, central New Mexico: New Mexico Geological Society, Guidebook 33, pp. 303-304.
- Goodman, L. J., and Levine, D. F., 1990, The mines of the Cerrillos District, New Mexico; myths and realities: El Palacio (Museum of New Mexico, Santa Fe), v. 96, no. 1, pp. 20-39.
- Kautz, P. F., Ingersoll, R. V., Baldrige, W. S., Damon, P. E., and Shafiqullah, M., 1981, Geology of the Espinazo Formation (Oligocene), north-central New Mexico, part 2: Geological Society of America, Bulletin, v. 92, pp. 2318-2400.
- Johnson, D. W., 1904, Geology of the Cerrillos Hills, New Mexico: New Era Printing Co., Lancaster, Pennsylvania.
- Kay, B. D., 1986, Vein and breccia gold mineralization and associated igneous rocks at the Ortiz mine, New Mexico, USA: Unpublished MS thesis, Colorado School of Mines, Golden, 179 pp.
- Kelley, V. C., 1952, Tectonics of the Rio Grande depression of central New Mexico: New Mexico Geological Society, Guidebook 3, pp. 93-105.
- Kelley, V. C., 1977, Geology of Albuquerque basin, New Mexico: New Mexico Bureau of Mines & Mineral Resources, Memoir 33, 60 pp.
- Kelley, V. C., 1978, Geology of Espanola basin, New Mexico: New Mexico Bureau of Mines & Mineral Resources, Geologic Map 48.
- Kelley, V. C., and Northrop, S. A., 1975, Geology of Sandia Mountains and vicinity, New Mexico: New Mexico Bureau of Mines & Mineral Resources, Memoir 29, 136 pp.
- Lindgren, W., Graton, L. C., Gordon, C. H., 1910, The ore deposits of New Mexico: U.S. Geological Survey, Professional Paper 68, 361 pp.
- Lindqvist, W. F., 1980, The exploration of the Ortiz gold deposit, New Mexico-geology and exploration: Colorado Mining Association, 1980 Yearbook, pp. 106-112.
- Lisenbee, A. L., 1975, Shale diapirism and the development of the Galisteo syncline; in Woodward, L. A., and Northrop, S. A. (eds.), Tectonics and mineral resources of southwestern North America: New Mexico Geological Society, Special Publication 6, pp. 88-94.
- Lisenbee, A. L., Woodward, L. A., and Connolly, J. R., 1979, Tijeras-Canoncito fault system-a major zone of recurrent movement in north-central New Mexico: New Mexico Geological Society, Guidebook 30, pp. 89-99.
- Lodewick, R. B., 1960, Geology and petrography of the Tijeras gneiss, Bernalillo County, New Mexico: Unpublished MS thesis, University of New Mexico, Albuquerque, 63 pp.
- Maynard, S. R., Nelsen, C. J., Martin, K. W., and Schutz, J. L., 1990, Geology and gold mineralization of the Ortiz Mountains, Santa Fe County, New Mexico: Mining Engineering, v. 42, pp. 1007-1011.
- Northrop, S. A., 1944, Minerals of New Mexico: University of New Mexico Press, Albuquerque, 665 pp.
- Picha, M. G., 1982, Structure and stratigraphy of the Montezuma Salient-Hagan Basin area, Sandoval County, New Mexico: Unpublished MS thesis, University of New Mexico, Albuquerque, 248 pp.
- Pogue, J. E., 1915, The turquoise; a study of its history, mineralogy, geology, archaeology, mythology, folklore and technology: National Academy of Sciences, Memoir 3, v. 12, pt. 2.
- Schroeder, A. H., 1979, The Cerrillos mining area; in Ingersoll, R. V. (ed.), Archaeology and history of Santa Fe country: New Mexico Geological Society, Special Publication 8, pp. 13-16.
- Sillitoe, R. H., 1979, Some thoughts on gold-rich porphyry copper deposits: Mineralium Deposita, v. 14, pp. 161-174.
- Stearns, C. E., 1953, Early Tertiary volcanism in the Galisteo-Tonque area, north-central New Mexico: American Journal of Science, v. 251, pp. 415-452.
- Wargo, J. G., 1964, Geology of a primary disseminated copper deposit near Cerrillos, New Mexico: Economic Geology, v. 59, pp. 1525-1538.
- Warren, A. H., and Mathieu, F. J., 1985, Prehistoric and historic turquoise mining in the Cerrillos district: time and place: Papers of the Archaeological Society of New Mexico, #10, 110 pp.
- Woodward, L. A., and Ingersoll, R. V., 1979, Phanerozoic tectonic setting of Santa Fe country: New Mexico Geological Society, Guidebook 30, pp. 51-58.
- Wright, A., 1983, The Ortiz gold deposit (Cunningham Hill)-geology and exploration: Nevada Bureau of Mines and Geology, Report 36, pp. 42-51.

Proterozoic tectonic history of the Manzano Mountains, central New Mexico

Amy G. Thompson¹, Jeffrey A. Grambling¹, and R. David Dallmeyer²

¹Department of Geology, University of New Mexico, Albuquerque, New Mexico 87131; ²Department of Geology, University of Georgia, Athens, Georgia 30602

Introduction

Proterozoic rocks of central New Mexico crop out in a north-trending, linear mountain chain along the eastern margin of the Cenozoic Rio Grande rift. The chain includes the Sandia, Manzano, and Los Pinos Mountains. A major unconformity located near the top of each range separates the basement rocks from overlying Paleozoic sedimentary rocks. The unconformity varies from flat-lying to shallowly east-dipping.

Proterozoic rocks below the unconformity record at least two superimposed tectonometamorphic events. This study describes these events within the central and southern Manzano Mountains. The study area consists of supracrustal rocks metamorphosed to the amphibolite to greenschist grade, together with two granitic plutons (Fig. 1). The supracrustal rocks are divided into two distinct tectonometamorphic sequences, juxtaposed along a northeast-trending ductile shear zone that is best exposed in Monte Largo Canyon, in the central Manzano Mountains. Kinematic indicators in both tectonic sequences indicate that the southern, amphibolite-grade sequence was thrust to the northwest over the northern, greenschist-grade sequence. A greenschist-grade metamorphic event overprinted both sequences during and after thrusting; it resulted in prograde metamorphism of the greenschist-grade crustal sequence and retrograde metamorphism of the amphibolite-grade sequence. Thrusting has been dated at about 1350 Ma by ⁴⁰Ar/³⁹Ar thermochronology (Thompson et al., 1989).

The purpose of this field trip is to examine Proterozoic structures and metamorphism within the Manzano Mountains. The focus will be on the style and timing of juxtaposition of the two tectonic sequences. The first day will concentrate on the ductile shear zone, exposed in Monte Largo Canyon, that separates the greenschist- and amphibolite-grade sequences. Metamorphic-grade and shear-sense indicators in both tectonic sequences will be examined. The second day will focus on rocks farther south in the southern tectonic sequence. The Priest pluton and the retrograded portion of the amphibolite-grade sequence in the area near Abo Pass will be examined.

Highlights en-route to Stop 1

The field-trip route is shown in Fig. 2. From Albuquerque, the trip travels south on I-25. After I-25 crosses the Rio Grande, the highway turns south through roadcuts that expose late Pleistocene basalts overlying unconsolidated sediments of the Santa Fe Group. The Manzano Mountains are visible along the eastern horizon, where the unconformity separating flat-lying Paleozoic sedimentary units from underlying Precambrian igneous and metamorphic rocks can be seen.

On the right, west of the highway immediately past the Los Lunas exit, is the Los Lunas volcano, one of many volcanic cones that dot the Rio Grande rift. Its andesitic lavas are dated at 1.3-1.1 Ma (Kudo, 1982 and references therein). Directly to the east, across the Rio Grande valley, the isolated, rounded knob is Tome Hill, another intrarift, andesitic volcano; this one, however, is dated at 3.5 Ma (Kudo, 1982 and references therein).

The view east beyond Tome Hill to the piedmont near the Manzano Mountain front shows, in the far distance, the Hubbell Springs fault scarp. Based on a study of soils and fault-scarp degradation models, Machette (1982) reported a late Pleistocene to early Holocene age for the most recent

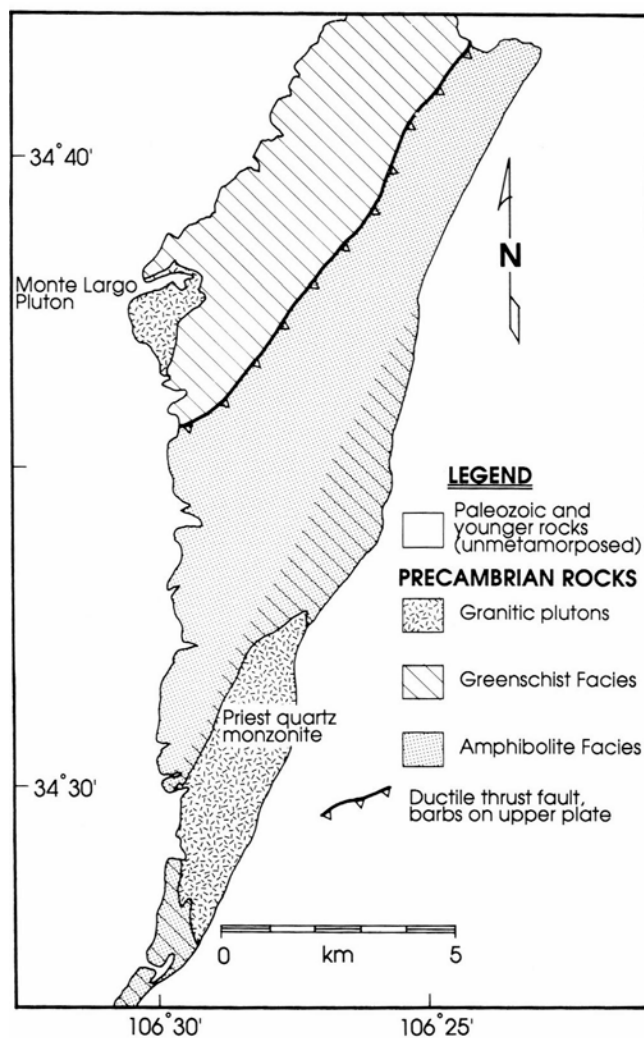


FIGURE 1—General geology of Precambrian rocks in the central and southern Manzano Mountains.

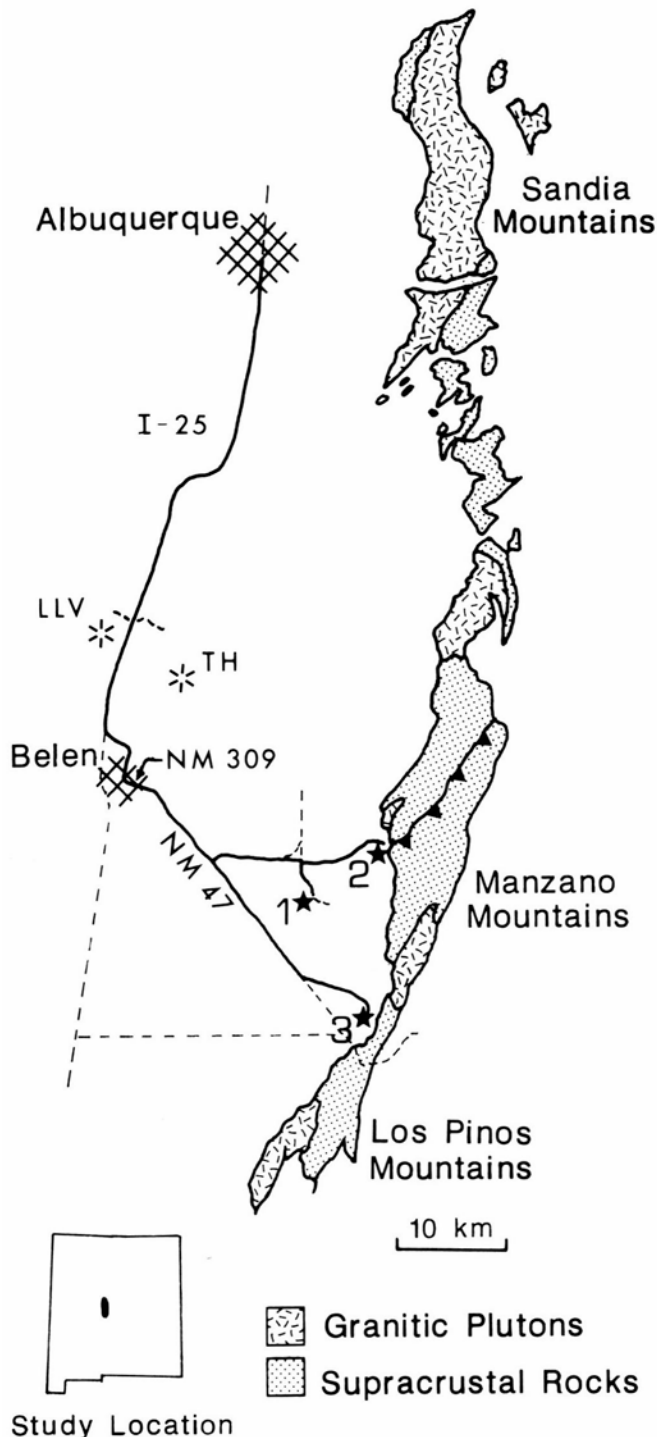


FIGURE 2—Field-trip route: LLV = Los Lunas Volcano; TH = Tome Hill. Stars with numbers indicate field-trip stops discussed in text.

rupture on this fault. The scarp height ranges from 4 to 30 m. The Hubbell Springs fault is part of the Hubbell bench, an 88 km long fault zone considered to be the major fault bounding the western edge of the Manzano Mountains (Kelley, 1982).

Continuing south on I-25, use the first Belen exit (Business I-25) to the second traffic light. Turn left (east) onto NM-309 (Reinken Avenue), continue for 2.4 mi; pass over the Rio Grande and approach a 4-way-stop intersection. At that intersection, turn south (merge right) onto NM-47 (the first sign identifying NM-47 is about 0.25 mi south of the

intersection). Continue south for 5.5 mi and look for a brown sign on the right pointing to John F. Kennedy (JFK) Campground. Turn left onto the dirt road at that sign. Continue east on the dirt road. Approximately 5.6 mi east of NM-47, a sign indicating a turn to the left toward JFK Campground is posted at a Y-intersection. Pass the sign and continue east for an additional 0.2 mi to a barbed-wire fence. Here, the east-bound road intersects a north—south road. Turn right onto the north—south road and travel south 2.2 mi to the first stop. The first stop is a view to the northeast along strike of the Monte Largo shear zone. Also, note the horizontal Paleozoic sediments capping the Manzano Mountains to the north.

Stop 1: Overview of Monte Largo shear zone

The shear zone is a northeast-trending, southeast-dipping ductile fault that emplaced amphibolite-grade rocks northwestward, on top of greenschist-grade rocks. The amphibolite-grade rocks southeast of the shear zone dip at a steeper angle than the greenschist-grade rocks to the northwest. This relation can be seen clearly in the distant mountain front (Fig. 3).

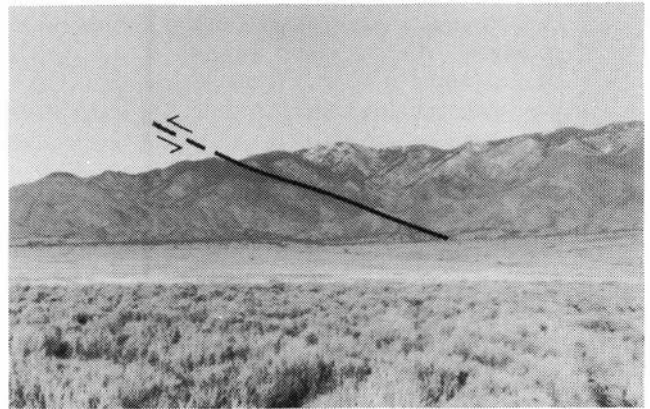


FIGURE 3—View to the northeast, along strike of the shear zone in Monte Largo Canyon that separates greenschist-grade rocks (left) from amphibolite-grade rocks (right).

Next, proceed to Stop 2 in Monte Largo Canyon where the greenschist- and amphibolite-grade rocks and the tectonic contact that separates them will be examined. Retrack 2.2 mi north to the jog in the east-bound road, then turn east. Pass a house with a large, white railroad-tank car in its front yard. Monte Largo Canyon is directly to the east. Continue on the same road through the curve to the north and across the major arroyo that drains Monte Largo Canyon, then turn right (east) on the first intersecting dirt road. Continue on that road toward the mountain front, back across the arroyo; after crossing the arroyo, turn left on the third dirt road. This road crosses the main arroyo again. About 30 ft past the north side of the arroyo, another dirt road forks to the right and leads directly east into Monte Largo Canyon. This road is fairly rough and requires a vehicle with high road clearance.

Stop 2: Monte Largo Canyon shear zone

The objectives of the second stop are to examine the metamorphic grade of each tectonic sequence and to look in detail at structures along the contact between the two tectonic sequences. The field-trip route into Monte Largo Canyon is shown in Fig. 4. The hike will start on the road

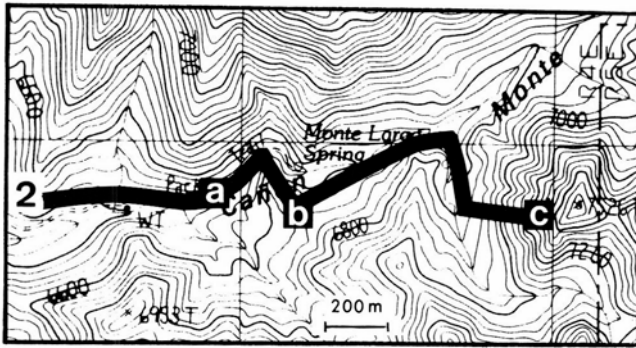


FIGURE 4—Field-trip route into Monte Largo Canyon; lower-case letters indicate stops mentioned in text.

into the canyon and proceed approximately 800 m to greenschist-grade phyllites exposed north of the main creek (stop a). The hike will then continue 200 m up the creek bed, then up a ridge to the south where its path will cross the shear zone in order to examine mylonitic fabrics in detail (stop b). Finally, the hike will proceed about 800 m farther up-canyon where the route proceeds up a knob (to the east) into hornblende—plagioclase mafic rocks of the amphibolite-grade sequence (stop c). After returning from the hike, retrace the route back to Belen. The trip will continue on a second day beginning with Stop 3.

Highlights en-route to Stop 3

The main features viewed on the second day are the contacts of the Priest pluton and the overprinting relationship between greenschist-grade and amphibolite-grade metamorphism, both best seen in the southernmost Manzano Mountains. The trip starts in Belen. Follow the route for the first day, again turning right (south) onto highway NM-47. Drive for about 14 mi to a railroad crossing. Cross the tracks and then turn left immediately onto the railroad access road south of the tracks. Drive for 4.7 mi, paralleling the railroad tracks. On the drive toward the mountain range, the Priest pluton can be distinguished from supracrustal rocks because of differences in weathering, exfoliation, and its soil that supports growth of abundant low bushes. The road trends south for the last 0.3 mi to the railroad cut just north of Abo Canyon, where the hike begins for Stop 3.

The view to the south is of the Los Pinos Mountains, the southern extension of the Manzano Mountains. The Los Pinos granitic pluton, which intruded metamorphic rocks similar to those in the southern tectonic sequence of the Manzano Mountains, forms the prominent cliffs to the south.

Stop 3: Southern margin of the Priest pluton

The purpose of this stop is to examine evidence for a greenschist-grade, retrograde metamorphic event that overprints amphibolite-grade rocks, and to examine the contact of the Priest pluton. The field-trip route into the Abo Pass area is shown in Fig. 5. The hike starts at the railroad cut and proceeds upslope to the east and north through meta-sedimentary units for about 400 m (stop a). The first stop is at a megascopic fold defined by quartzite and phyllite, the latter containing polymetamorphic garnet. The hike then continues east for about 600 m through a side arroyo and into Sand Canyon where the southern contact of the Priest pluton is exposed. Stops in Sand Canyon will be made to examine sericitized porphyroblasts of relict staurolite (stop

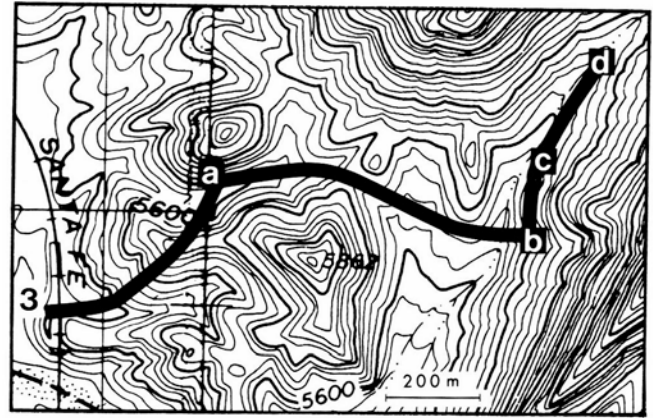


FIGURE 5—Field-trip route into Abo Pass area; lower-case letters indicate stops mentioned in text.

b), granitic dikes crosscutting the pluton and its host rocks (stop c), and the Priest pluton itself (stop d).

General geology of the central and southern Manzano Mountains

The central and southern Manzano Mountains consist of two tectonometamorphic sequences separated by a ductile shear zone. Greenschist-grade rocks are found to the northwest of the shear zone, and amphibolite-grade rocks are found to its southeast (Fig. 1). Thrusting along the shear zone emplaced a southern sequence (the amphibolite-grade rocks) to the northwest over a northern sequence (the greenschist-grade rocks) when P—T conditions were in the greenschist facies. The southern sequence has been retrograded to the greenschist grade in the area around and south of the Priest pluton, probably synchronous with the thrusting. The following text summarizes the general geology of the northern, greenschist-grade sequence, the southern, amphibolite-grade sequence, and the portion of the southern sequence that has been retrograded to the greenschist-grade. It also discusses the Priest pluton and the ages of the amphibolite-grade and greenschist-grade metamorphic events.

Greenschist-grade sequence

Mineral assemblages in the northern tectonic sequence confirm its assignment to the greenschist grade (Table 1). The most common assemblage is quartz—muscovite—chlorite ± biotite ± tourmaline ± carbonate found in pelitic phyl-

TABLE 1—Mineral assemblages for representative samples (abbreviations from Kretz, 1983), *not in textural equilibrium.

Northern Tectonic Sequence	
Mafic rock:	chl-ab-ep-qtz-act
Aluminous quartzite:	qtz-ms-chl-ky-cld
Pelitic phyllite:	qtz-ms-chl-bt-tur-grt
Southern Tectonic Sequence	
Prograde	
Mafic rock:	hbl-pl-chl-qtz-ep-FeTi oxide
Pelitic schist:	grt-bt-chl-ms-pl-qtz-ilm
Pelitic schist:	grt-bt-chl-ms-pl-qtz-ilm-st-sil
Aluminous quartzite:	qtz-ms-ky-and-sil-cld
Retrograde	
Pelitic phyllite:	grt-bt-chl-ms-pl-qtz
Pelitic phyllite:	qtz-pl-ms-chl-st*

lite. Aluminous phyllites contain quartz—muscovite—chlorite \pm kyanite \pm chloritoid. A distinctive feldspathic phyllite has alternating pink and green layers defined by varying proportions of quartz, biotite, albite, muscovite, K-feldspar, and chlorite. Rare mafic rocks contain chlorite—albite—epidote—quartz \pm actinolite. Quartzite contains minor muscovite and hematite. Rare samples found near the contact between the northern and southern sequences also contain tiny (10-50 μ m), nearly unzoned crystals of spessartitic garnet.

Metamorphic P—T conditions for the northern tectonic sequence were determined from mineral assemblages and garnet—biotite geothermometry using the calibration of Williams and Grambling (1990). Mineral compositions were obtained using the JOEL 733 electron microprobe in the Department of Geology, University of New Mexico. Assemblages in mafic rocks require temperatures below about 500°C (cf. Apter and Liou, 1983; Moody et al., 1983). The assemblage chloritoid \pm kyanite indicates temperatures of roughly 350-500°C, and the presence of kyanite indicates pressures above 2-3 kb. These constraints are consistent with garnet—biotite geothermometry which indicates temperatures of 475-485°C.

Aluminous quartzite and phyllite collected near the contact between the northern and southern sequences contain mylonitic foliation. Textures of kyanite, chloritoid, and garnet help constrain the timing of deformation and metamorphism. Kyanite grains are folded and kinked. Chloritoid porphyroblasts are folded and/or aligned in the lineation direction. Some large, randomly oriented, chloritoid porphyroblasts have grown across the mylonitic foliation. Individual mica grains in phyllite are terminated against euhedral garnet grains. These mineral textures suggest that thrusting was broadly synchronous with greenschist-grade metamorphism.

All rock types in the greenschist-grade, northern tectonic sequence (previously mapped as Blue Springs Schist and White Ridge Quartzite; cf. Stark, 1956; Bauer, 1982) are intensely foliated and lineated. Most pelitic phyllites exhibit two or three foliations (for example, compositional layering and two crosscutting grain-shape foliations). Other phyllites contain boudinaged and folded quartz veins and quartz rods (quartz veins stretched along foliation planes). Extension lineations, which commonly appear on foliation surfaces, are defined by aligned quartz or micas; crenulation lineations also can be seen in most outcrops. Feldspathic quartzite has alternating, centimeter-scale pink and green layers defined by varying amounts of biotite. Locally, these layers have been deformed into sheath folds or have been isoclinally folded, transposed, and refolded. Quartzite crops out as a 20-40 m thick, massive white or pink layer with a foliation defined by differently colored beds or by thin layers of opaque minerals. Some isoclinal fold hinges can be seen within foliation layers. Most quartzite is fine-grained, although some contains porphyroblasts of quartz deformed into tectonic "fish," which generally indicate a top-to-the-north sense of shear, in a finer-grained matrix. The quartzite seems to have behaved more coherently than the phyllites.

Rocks are more intensely deformed closer to the contact with the southern tectonic sequence. A distinctive feldspathic mylonite crops out near the contact. Its strong, typically south-dipping, mylonitic foliation is defined by alternating black and pink, tan, or orange layers (<1 cm thick). This foliation is folded in centimeter-scale folds, and a strong

extension lineation defined by aligned minerals can be seen on most foliation surfaces. On joint surfaces parallel to the lineation and perpendicular to the foliation, quartz and plagioclase porphyroclasts have asymmetric "tails." The asymmetric structures in the mylonite generally indicate a top-to-the-north sense of shear.

Amphibolite-grade sequence

Mineral assemblages observed in rocks in the southern tectonic sequence are listed in Table 1. Metarhyolite contains thin, semipelitic beds with garnet—biotite—quartz—plagioclase—K-feldspar. Mafic rocks typically have the assemblage blue-green hornblende—plagioclase—chlorite—quartz \pm epidote \pm FeTi oxides. Pelitic schist contains garnet—biotite—chlorite—muscovite—plagioclase—quartz \pm ilmenite. Aluminous schists that crop out as thin layers within quartzite have the assemblage quartz—muscovite—chloritoid—staurolite—Al₂SiO₅. The common form of the Al₂SiO₅ in these schists is kyanite, but two specimens contain kyanite—andalusite sillimanite. In these two rocks, kyanite forms bent, corroded relicts inside andalusite and muscovite. Sillimanite occurs as fibrolitic mats, with fibers aligned in the dominant foliation or bent and folded, locally defining two foliations. Andalusite forms large, undeformed porphyroblasts that have overgrown the foliations defined by kyanite and sillimanite. Textures indicate that andalusite was the last Al₂SiO₅ poly-morph to form, but do not constrain the relative timing of kyanite and sillimanite growth.

Aluminum silicate triple-point assemblages suggest that peak P—T conditions of the southern sequence approached 4 kb, 500°C (cf. Grambling et al., 1989). Garnet—biotite geothermometry (Williams and Grambling, 1990) and garnet—biotite—plagioclase geobarometry (Ghent and Stout, 1981) are consistent with this P—T estimate. They indicate that peak metamorphic conditions for the southern tectonic sequence were near 540°C, 4 kb.

Deformation is pronounced in rocks of the amphibolite-grade tectonic sequence. Foliations generally trend northeast and dip south, with extension lineations aligned down-dip on foliation planes. Metarhyolite near the tectonic contact with the greenschist-grade sequence is finer-grained and has a stronger foliation than elsewhere, suggesting that it is mylonitized. Foliation in metarhyolite is crosscut by shear bands oriented about 20° from the dominant foliation. Tectonic "fish" of plagioclase and "snails" of plagioclase and quartz occur along foliation planes. Asymmetric porphyroclasts and shear bands in metarhyolite indicate a top-to-the-north sense of shear, the same as that observed in adjacent greenschist-grade rocks.

Farther south, the metarhyolite becomes coarser-grained so that individual quartz and feldspar grains are visible in hand specimen. The metarhyolite is schistose in places and coarser-grained micas can be seen on foliation planes. Locally, it contains rare rounded cobbles of granitic rock (also with asymmetric tails) from approximately 2 x 2 cm up to 6 x 9 cm in size.

Interspersed within the metarhyolite are amphibolite pods or layers from less than 1 m to 60 m thick. Generally, the mafic layers become thicker and more abundant farther south of the shear zone. Most thin amphibolite lenses can be traced for no more than a few meters, whereas larger outcrops can be traced visually across valleys and up adjacent ridges. In larger outcrops, the amphibolite consists of very fine- and coarse-grained layers separated by sharp contacts. Amphibolite

bolite is foliated and, in some coarse-grained, foliated outcrops, clasts of finer-grained epidote, amphibole, plagioclase, and quartz have asymmetric tails of similar material drawn out along foliation planes. Once again, the asymmetric tails indicate a top-to-the-north sense of shear. Intergrowths of acicular hornblende and biotite (0.5 x 2 cm) appear randomly oriented within the foliation planes of some amphibolites.

Pelitic schists have alternating quartz-rich and mica-rich layers, with the dominant foliation defined by aligned mica grains. Quartz-rich layers contain micas that preserve an earlier foliation approximately perpendicular to the dominant foliation. Abundant inclusions of quartz in garnet are parallel to the dominant foliation or have slightly sigmoidal traces. This may indicate that the garnets are slightly rotated or that they grew over a slightly folded foliation. Micaceous layers are crenulated and crosscut by shear bands. The shear bands indicate a top-to-the-north sense of shear.

Retrograded greenschist-grade sequence

Retrograded greenschist-grade rocks are exposed in the southernmost Manzano Mountains in the Abo Pass area and include quartzite, pelitic phyllite, and quartzofeldspathic rock. Mineral assemblages are reported in Table 1. Phyllites contain the assemblage quartz—muscovite—plagioclase—chlorite ± biotite ± garnet. Quartzofeldspathic rocks contain quartz—plagioclase—K-feldspar—muscovite—biotite—garnet.

Garnet crystals in pelitic phyllites and quartzofeldspathic rocks are very small (<1 mm) and have cloudy, irregular cores surrounded by clear rims 10-50 μm thick. Chlorite in chlorite phyllite occurs as large, polycrystalline "porphyroblasts" that contain numerous FeTi-oxide inclusions. Because biotite accepts considerable titanium in its structure and chlorite does not, the chlorite—FeTi oxide "porphyroblasts" are interpreted to be pseudomorphs after biotite. Elsewhere, the phyllite contains large, relict porphyroblasts that have been partly to completely replaced by sericite. Microscopic observations show that locally sericite has replaced staurolite. This is shown by various amounts of replacement. One staurolite porphyroblast (2 x 1 mm) is surrounded by a halo of sericite about 0.2 mm thick. More commonly, relict staurolite occurs as tiny remnants (0.2x 0.2 mm) inside a mat of sericite 0.5 x 1 cm. The mineral reaction textures described here are suggestive of retrograde metamorphism accompanied by an influx of hydrous fluid.

Minerals from a pelitic phyllite with unaltered garnet—biotite—chlorite—muscovite—plagioclase—quartz were used to determine metamorphic conditions during retrogression in this area. Garnets have cloudy cores, with Xgrs of 0.150.16, surrounded by clear rims. An abrupt change in Xgrs to 0.04-0.05 marks the transition to the clear rims. Garnet cores are interpreted to represent growth during the earlier, amphibolite-grade metamorphism and rims are interpreted to represent growth during the later, retrograde, greenschist-grade thermal overprint. Biotite grains are small and unaltered in this sample, as are plagioclase and muscovite; both apparently grew or re-equilibrated during the retrograde greenschist-grade overprint. P—T conditions during the second metamorphic event, determined from garnet(rim)—biotite—plagioclase—muscovite thermobarometry (Williams and Grambling, 1990; Ghent and Stout, 1981) were 485°C, 2.75 kb.

Within the retrograded southern sequence, outcrop patterns trend north-northwest to south-southeast, parallel to

the western margin of the Priest pluton. All lithologies are fine-grained. Supracrustal rocks are crosscut by at least two foliations, one that is defined by aligned micas subparallel to compositional layering, and a second that is typically a crenulation cleavage. Phyllites generally have both an extension and crenulation lineation on foliation planes, the former defined by aligned grains of muscovite and chlorite. The chlorite phyllite exposed at the southern contact with the Priest pluton consists of alternating phyllitic and quartz-rich layers. The quartz-rich layers are discontinuous and range from less than one centimeter to several centimeters in thickness. The compositional layers are disharmonically folded. West of the southern margin of the pluton, supracrustal rocks are folded into a megascopic, upright, north-plunging antiform. Most rocks exposed in this area form the eastern limb of this fold; much of the western limb has been removed by rift-related normal faults or covered by rift-related sediments.

The Priest pluton

The Priest pluton is composed of a main body of quartz monzonite and lesser amounts of other granitic intrusive rocks and dikes. The pluton typically contains coarse-grained quartz, plagioclase, muscovite, biotite, and epidote, together with K-feldspar megacrysts and trace amounts of titanite, apatite, and zircon. Near its southern margin, the pluton appears to be composed of several different granitic rock types which vary in feldspar content and grain size. A white, medium- to coarse-grained dike contains plagioclase and no K-feldspar; it appears to crosscut the main body of the pluton. An equigranular, coarse-grained granitic portion of the pluton contains both plagioclase and K-feldspar. There appears to be a compositional and textural gradation between this portion of the pluton and the main body that contains K-feldspar megacrysts. Also near the southern margin, pink aplitic dikes crosscut the pluton and country rocks. These dikes may represent late, separate intrusions or the last stages of melt injected prior to complete crystallization of the pluton.

The contact between the Priest pluton and the country rock is intrusive, in places modified slightly by tectonism. The interior of the pluton appears to be undeformed. The southwestern and northernmost margins appear to be simple intrusive contacts; the pluton contains xenoliths of country rock, dikes of aplitic granite intrude the country rock, and the igneous rocks are not foliated. The northwestern margin appears to be tectonized. The pluton near this margin is weakly foliated with a subhorizontal north-trending extension lineation. Granitic dikes and sills in the country rock are strongly foliated. However, the appearance of xenoliths of adjacent country rock in this area, and of dikes and sills of plutonic rock in nearby country rock, suggests that motion along this contact was minimal. The eastern margin of the Priest pluton is faulted against Paleozoic sediments.

Geochronology

Muscovite and hornblende concentrates from samples collected within the amphibolite-grade sequence have been dated by ⁴⁰Ar/³⁹Ar methods to constrain the timing of deformation and metamorphism. Techniques follow those described by Dallmeyer and Keppie (1987) and Dallmeyer and Gil-Ibarguchi (1990). Results are presented in more detail elsewhere (Thompson et al., in preparation). Blocking temperatures for argon diffusion are taken to be about 500 ± 25°C

for hornblende (Harrison, 1981) and about 400°C for muscovite, the latter based upon preliminary experimental data of Robbins (1972) in diffusive equations of Dodson (1973, 1979). Hornblende and muscovite argon ages are particularly useful in this study because their blocking temperatures bracket temperatures maintained during thrusting within the shear zone in Monte Largo Canyon. Consequently, hornblende ages likely record the age of the amphibolite-grade thermal event that preceded thrusting, whereas muscovite ages likely record cooling following thrusting.

Hornblende from sample 6 displays an internally discordant release spectrum (Fig. 6a) which defines a total-gas age of 1448.8 ± 3.0 Ma. The apparent K/Ca ratio is constant over 94% of the argon release spectrum (Fig. 6b), indicating that the bulk of the experimentally derived gas evolved from a compositionally uniform population of intracrystalline

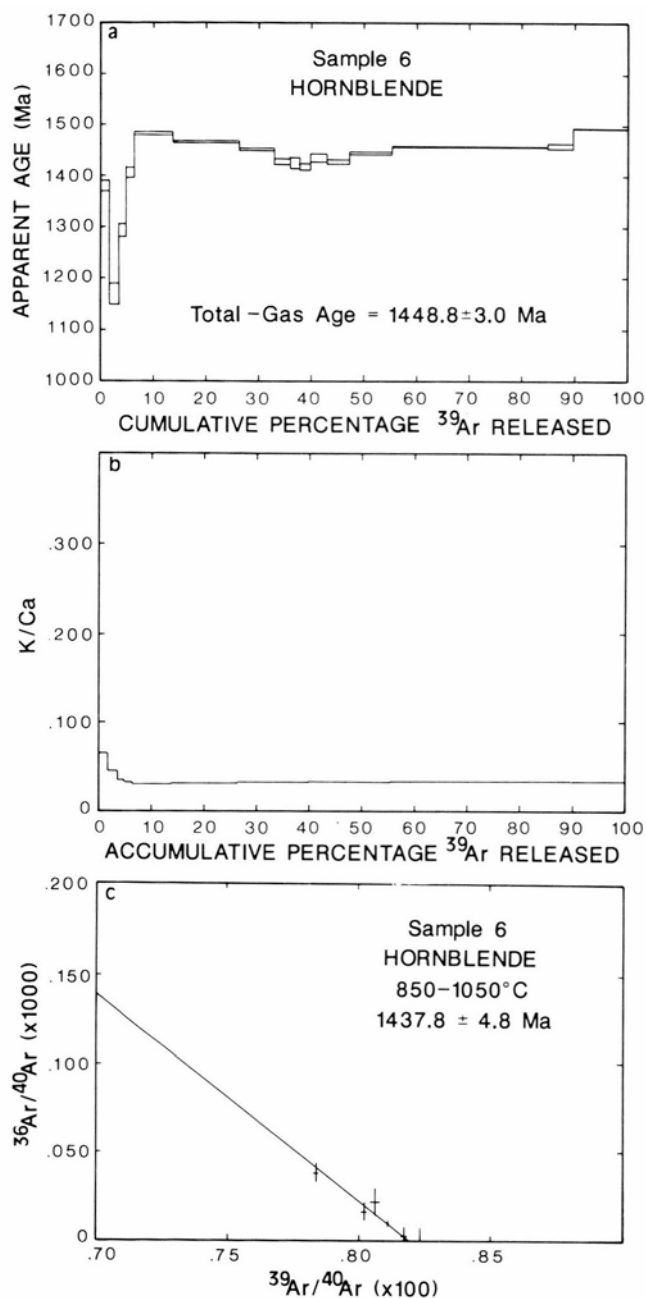


FIGURE 6— $^{40}\text{Ar}/^{39}\text{Ar}$ data for amphibolite concentrate from sample 6. **a**, $^{40}\text{Ar}/^{39}\text{Ar}$ release spectrum; **b**, apparent K/Ca ratio; **c**, isotope-correlation diagram.

"sites." Isotope data from the part of the release spectrum that corresponds to a constant apparent K/Ca ratio (experimental temperatures between 850 and 1050°C), define an isotope correlation (Fig. 6c) corresponding to an age of 1438 ± 5 Ma. This is interpreted to date cooling of the amphibolite-grade sequence through about 500°C.

Muscovite release spectra are internally discordant (Fig. 7). Sample 7 is the least discordant with low-temperature ages that systematically increase to define an intermediate-to high-temperature plateau of 1361 ± 3 Ma (Fig. 7a). The muscovite concentrate from sample 4, slightly more discordant, gives a high-temperature plateau age of 1338 ± 3 Ma (Fig. 7b). The discordant muscovite spectra are interpreted to result from a variable thermal overprint at about 1000-1100 Ma on intracrystalline systems that had initially cooled through argon retention temperatures at around 1340-1360 Ma. Because geothermometry and phase relations suggest that the temperature of thrusting was 480°C (above the closure temperature for argon diffusion in muscovite), we interpret the 1340-1360 Ma plateau ages to record the timing of thrusting.

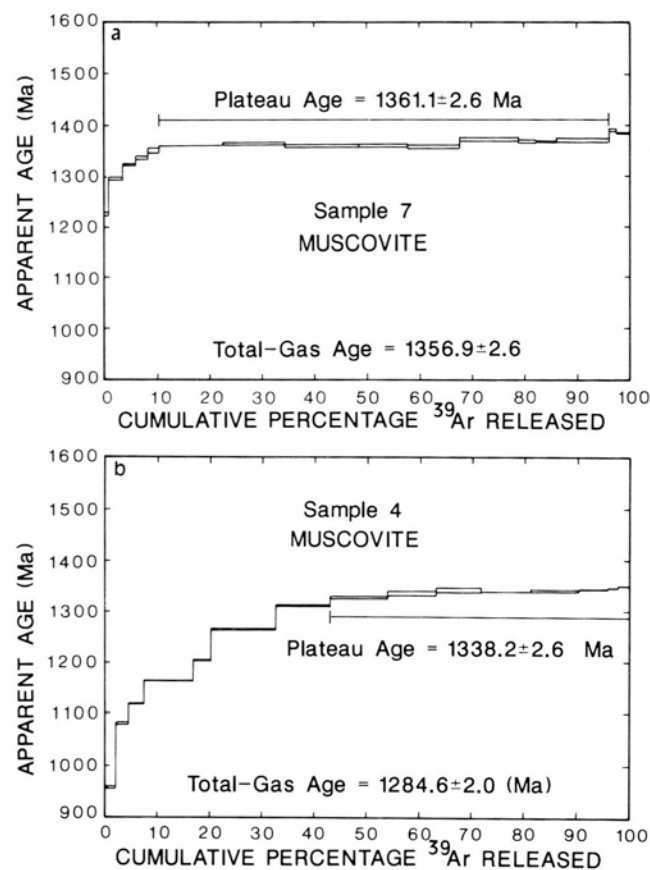


FIGURE 7— $^{40}\text{Ar}/^{39}\text{Ar}$ data for muscovite concentrates. $^{40}\text{Ar}/^{39}\text{Ar}$ release spectrum for sample 7 (**a**) and sample 4 (**b**).

Conclusions

Proterozoic rocks in the central and southern Manzano Mountains record two tectonometamorphic events recognized on the basis of metamorphic grade, structural relationships, and $^{40}\text{Ar}/^{39}\text{Ar}$ geochronology. $^{40}\text{Ar}/^{39}\text{Ar}$ ages recorded by hornblende in the southern tectonic sequence suggest that amphibolite-grade metamorphism occurred around 1440 Ma. This is interpreted to represent the age of the first tectonometamorphic event, M_1 . Aluminum-silicate triple-point assemblages and garnet—biotite—plagioclase-

muscovite thermobarometry indicate temperature and pressure conditions of 540°C, 4 kb for the peak of M, amphibolite-grade metamorphism.

⁴⁰Ar/³⁹Ar muscovite ages from the same tectonic sequence were reset during a second tectonometamorphic event, M₂. The second event was synchronous with thrusting along the Monte Largo shear zone that separates greenschist-grade rocks from amphibolite-grade rocks; argon isotopic data from muscovite suggest that thrusting occurred around 1350 Ma. Mineral assemblages and garnet—biotite geothermometry of the northern sequence indicate temperatures of 475–485°C and pressures of 2–3 kb for the upper greenschist-grade metamorphic event, M₂. Thermobarometry of rocks from the retrograded portion of the amphibolite-grade sequence suggests that P–T conditions during retrograde metamorphism were 480°C, 2.75 kb. The temperature for retrograde metamorphism is the same as the temperature associated with M₂ in Monte Largo Canyon. The similarities in temperature between these two areas suggest that M₂ resulted in retrograde metamorphism of the amphibolite-grade rocks and prograde metamorphism of the greenschist-grade rocks. The retrogression is shown clearly in the Abo Pass area, whereas the prograde metamorphism is best seen north of Monte Largo Canyon.

Dallmeyer et al. (1990) summarized four tectonometamorphic events in Proterozoic rocks of New Mexico. Their M₁ and M₂ events are recorded over a large area in central and northern New Mexico and correspond to M₁ and M₂ in the central Manzano Mountains. Dallmeyer et al. (1990) reported that M₁ involved regional ductile extension accompanied by amphibolite-grade metamorphism. Their primary evidence for M₂ comes from the ductile thrust fault discussed in this study. The age and character of M₁ and M₂ are summarized in Table 2. M₃ and M₄ (Dallmeyer et al., 1990) are later thermal events dated at about 1300 Ma and 950–1100 Ma, respectively, most evident in parts of northern New Mexico. They are represented in the present study area by a partial thermal overprint on muscovite age spectra.

TABLE 2—Summary of tectonometamorphic events.

	Age	Deformation Style	P–T
M ₁ /D ₁	1440 Ma	Regional ductile extension	4 kb, 540°C
M ₂ /D ₂	1360–1340 Ma	Ductile thrusting	2.75 kb, 480°C

References

- Apted, M. J., and Liou, J. G., 1983, Phase relations among greenschist, epidote amphibolite, and amphibolite in a basaltic system: *American Journal of Science*, v. 283-A, pp. 328–354.
- Bauer, P. W., 1982, Precambrian geology and tectonics of the southern Manzano Mountains; in Grambling, J. A., and Wells, S. G. (eds.), Albuquerque Country II: New Mexico Geological Society, Guidebook 33, pp. 211–216.
- Dallmeyer, R. D., and Gil-Ibarguchi, J. I., 1990, Age of amphibolite metamorphism in the ophiolitic unit of the Morias allochthon (Portugal): implications for Early Hercynian orogenesis in the Iberian Massif: *Journal of the Geological Society of London*, v. 147, pp. 873–878.
- Dallmeyer, R. D., and Keppie, J. D., 1987, Polyphase late Paleozoic tectonothermal evolution of the southwestern Meguma Terrane, Nova Scotia: evidence from ⁴⁰Ar/³⁹Ar mineral ages: *Canadian Journal of Earth Sciences*, v. 24, pp. 1242–1254.
- Dallmeyer, R. D., Grambling, J. A., and Thompson, A. G., 1990, Age and character of Proterozoic polymetamorphism in New Mexico (abs.): *Geological Society of America, Abstracts with Programs*, v. 22, no. 7, p. 113.
- Dodson, M. H., 1973, Closure temperature in cooling geochronological and petrological systems: *Contributions to Mineralogy and Petrology*, v. 40, pp. 259–274.
- Dodson, M. H., 1979, Theory of cooling ages; in Jager, E., and Hunziker, J. C. (eds.), *Lectures in Isotope Geology*: Springer-Verlag, Berlin, pp. 194–202.
- Ghent, E. D., and Stout, M. V., 1981, Geobarometry and geothermometry of plagioclase—biotite—garnet—muscovite assemblages: *Contributions to Mineralogy and Petrology*, v. 76, pp. 92–97.
- Grambling, J. A., Williams, M. L., Smith, R. F., and Mawer, C. K., 1989, The role of crustal extension in the metamorphism of Proterozoic rocks in New Mexico: *Geological Society of America, Special Paper 235*, pp. 87–110.
- Harrison, T. M., 1981, Diffusion of ⁴⁰Ar in hornblende: *Contributions to Mineralogy and Petrology*, v. 78, pp. 324–331.
- Kelley, V. C., 1982, Diverse geology of the Hubbell bench, Albuquerque basin; in Grambling, J. A., and Wells, S. G. (eds.), *Albuquerque Country II: New Mexico Geological Society, Guidebook 33*, pp. 159–160.
- Kretz, R., 1983, Symbols for rock forming minerals: *American Mineralogist*, v. 68, pp. 277–279.
- Kudo, A. M., 1982, Rift volcanics of the Albuquerque basin: overview with some new data; in Grambling, J. A., and Wells, S. G. (eds.), *Albuquerque Country II: New Mexico Geological Society, Guidebook 33*, pp. 285–290.
- Machette, M. N., 1982, Quaternary and Pliocene faults in the La Jencia and southern part of the Albuquerque and Belen basins, New Mexico: evidence of fault history from fault-scarp morphology and Quaternary geology; in Grambling, J. A., and Wells, S. G. (eds.), *Albuquerque Country II: New Mexico Geological Society, Guidebook 33*, pp. 161–170.
- Moody, J. B., Meyer, D., and Jenkins, J. E., 1983, Experimental characterization of the greenschist/amphibolite boundary in mafic systems: *American Journal of Science*, v. 283, pp. 48–96.
- Stark, J. T., 1956, Geology of the southern Manzano Mountains, New Mexico: *New Mexico Bureau of Mines & Mineral Resources, Bulletin 34*, 46 pp.
- Thompson, A., Grambling, J. A., and Mawer, C. K., 1989, Proterozoic tectonic assembly of southwestern North America: evidence from ductile shear zones in the Manzano Mountains, New Mexico (abs.): *Geological Society of America, Abstracts with Programs*, v. 21, no. 6, p. 215.
- Thompson, A., Grambling, J. A., Mawer, C. K., Dallmeyer, R. D., and Daniel, C. G. (in preparation), Multiple tectonothermal events in Proterozoic rocks of central New Mexico.
- Vernon, R. H., Mawer, C. K., and Grambling, J. A. (in preparation), The 1.45 Ga Sandia Granite, New Mexico: a syntectonic, high-level, Proterozoic batholith.
- Williams, M. L., and Grambling, J. A., 1990, Manganese, ferric iron, and the equilibrium between garnet and biotite: *American Mineralogist*, v. 75, pp. 886–908.

Late Pennsylvanian stratigraphy and paleontology of the Kinney Brick Quarry, Manzanita Mountains, New Mexico

Spencer G. Lucas and Phillip Huber

New Mexico Museum of Natural History, P.O. Box 7010, Albuquerque, New Mexico 87194

Introduction

Pennsylvanian—Permian strata are widely exposed in the Manzanita and Manzano Mountains of central New Mexico (Fig. 1). These rocks pertain to the Sandia Formation, Madera Group, and Abo Formation and range in age from Atokan to Wolfcampian (Fig. 2). The Kinney Brick Quarry is a clay pit developed in the lower Virgilian Pine Shadow Member of the Wild Cow Formation of the Madera Group, about 8 mi south of Tijeras (Fig. 1). Strata exposed here provide a unique glimpse of a diverse and well-preserved Late Pennsylvanian lagoonal biota. Here, we summarize previous research on this biota, describe its stratigraphic context, delineate fossil assemblages, and present a preliminary interpretation of the depositional environments of the strata exposed at the quarry.

Previous research

Students at the University of New Mexico discovered the rich fossil biota of the Kinney Quarry in 1961 (B. S. Kues, written comm. 1990). During the 1960's, large collections were made of fishes, plants, and other fossils from the quarry, especially by D. Dunkle and S. Mamay of the National Museum of Natural History. Others who have made significant collections at the quarry include D. Berman, J. P. Bradbury, R. Burton, M. D. Gottfried, P. Huber, K. Kietzke, B. Kues, N. LaFon, T. Lehman, and F. Schram.

Extensive fossil collections from the Kinney Brick Quarry are now housed at the Carnegie Museum of Natural History, National Museum of Natural History, New Mexico Museum of Natural History (hereafter NMMNH), University of Kansas Museum of Natural History, and University of New Mexico.

Stratigraphic data on the quarry have been presented by

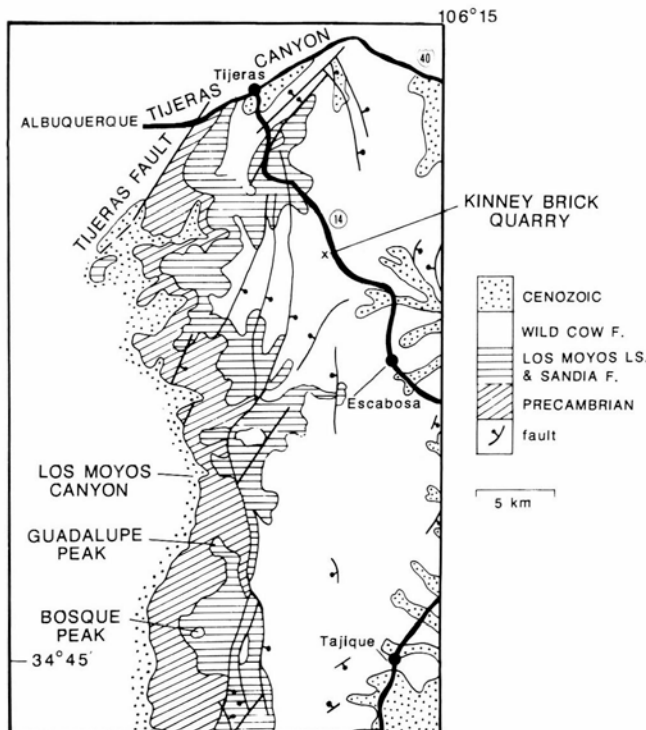


FIGURE 1—Generalized geologic map of the Manzanita and northern Manzano Mountains, New Mexico, and the location of the Kinney Brick Quarry (modified from Myers, 1982).

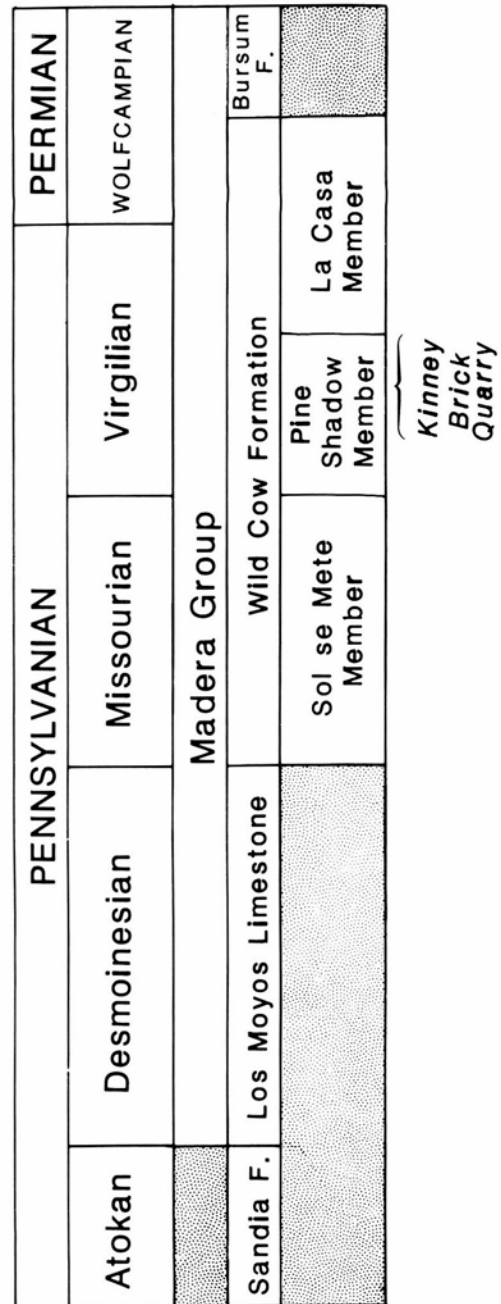


FIGURE 2—Pennsylvanian–Permian stratigraphic nomenclature and chronology in the Manzanita and Manzano Mountains, New Mexico (after Myers, 1988).

Stukey (1967), Gottfried (1987b), and Huber et al. (1989). Kelley and Northrop (1975) provided a list of the fossil biota of the quarry, although most of the taxa they listed have yet to be adequately documented. Published descriptions of organisms are: megafossil plants (Mamay, 1981, 1990; Ash and Tidwell, 1982), conodonts (Kelley and Northrop, 1975), insects (Carpenter, 1970), malacostracans (Schram and Schram, 1979; Schram, 1981), the pectinacean bivalve *Dunbarella* (Clark, 1978), eurypterids (Kues, 1985), fishes (Zidek, 1975; Gottfried, 1987a, b), and amphibians

(Berman, 1973; Hunt et al., 1989). A variety of other fossils known from the quarry that have not been described are also listed here (Table 1), but no comprehensive review of the Kinney fossil biota has yet been published.

Stratigraphy and age

The quarrying operation has exposed about 28 m of the upper part of the Pine Shadow Member of the Wild Cow Formation (Fig. 3). In the Manzanita and Manzano Mountains, the Pine Shadow Member consists of 30-50 m of

TABLE 1—Flora and fauna from the Kinney Brick Quarry. Sources: (1) Kelley and Northrop (1975); (2) Mamay (1990); (3) Mamay (1981); (4) this paper, specimens in NMMNH collection; (5) Clark (1978); (6) Schram and Schram (1979); (7) Kues (1985); (8) Carpenter (1970); (9) Zidek (1975); (10) Gottfried (1987a); (11) Gottfried (1987b); (12) Berman (1975); (13) Hunt et al. (1989); (14) Kues (1990).

FLORA:

Asterophyllites equisetiformis (1)
Calamites aff. *C. suckowi* (1)
Calamites sp. (1)
Charliea manzanitana (2)
Cordaites sp. (1)
Dicranophyllum readii (3)
Lebachia sp. (1)
Lepidodendron sp. (4)
Neuropteris cf. *N. clarksoni* (1)
Neuropteris ovata (1)
Pecopteris pseudovestita (1)
Plagiozamites sp. (1)
Walchia gracillima (1)
Walchia piniformis (1)

FAUNA:

Annelida:

Spirorbidae (4)

Conodonta:

Hibbardella cf. *H. acuta* (1)
Hindeodella delicatula (1)
Hindeodella megadenticulata (1)
Idiognathodus acutus (1)
Idiognathodus delicatus (1)
Idiognathodus humerus (1)
Idiognathodus meekerensis (1)
Ligonodina sp. (1)
Ozarkodina cf. *O. curvata* (1)
Ozarkodina delicatula (1)
Spathognathodus minutus (1)
Streptognathodus cancellosus (1)
Streptognathodus elegantulus (1)
Streptognathodus simulator (1)
Streptognathodus tenuis (1)
Synprioniodina microdenta (1)

Brachiopoda:

Antiquatonia sp. (14)
Chonetinella flemingi (14)
Composita sp. (14)
Lingula cf. *L. carbonaria* (14)

Mollusca:

Bivalvia:

Aviculopecten sp. (4)
Dunbarella striata (5) (14)
Myalina aff. *M. wyomingensis* (14)
Solemya radiata (14)
Solemya trapezoides (14)

Gastropoda:

unidentified (4)

Nautiloidea:

unidentified (4)

Ammonoidea:

unidentified (4) (14)

Bryozoa:

unidentified (4)

Arthropoda:

Ostracoda:

unidentified (4)

Branchiopoda:

unidentified (4)

Malacostraca:

Aenigmacaris minima (6)

Uronectes kinniensis (6)

Eurypterida:

Adelophthalmus luceroensis (7)

Myriapoda:

unidentified (4)

Insecta:

Madera mamayi (8)

Pseudobiella fasciata (8)

Blattaria, unidentified (8)

Vertebrata:

Elasmobranchii:

Cladodus sp. (9)

Ctenoptychius sp. (9)

Listracanthus sp. (9)

xenacanthid (4)

?*Cobelodus* sp. (4)

Dipnoi:

Proceratodus hlavini (9)

Crossopterygii:

unidentified coelacanth (9)

Actinopterygii:

Amphicentrum sp.

Elonichthys sp. (4)

new genus (4)

cf. *Bourbonella* sp. (10)

Pyritocephalus new sp. (4)

Platysomus sp. (4)

Chirodus sp. (4)

Tanyrhinichthys mcallisteri (11)

Acanthodii:

Acanthodes sp. (9)

Amphibia:

Lafonius lehmani (12)

new taxon (13)

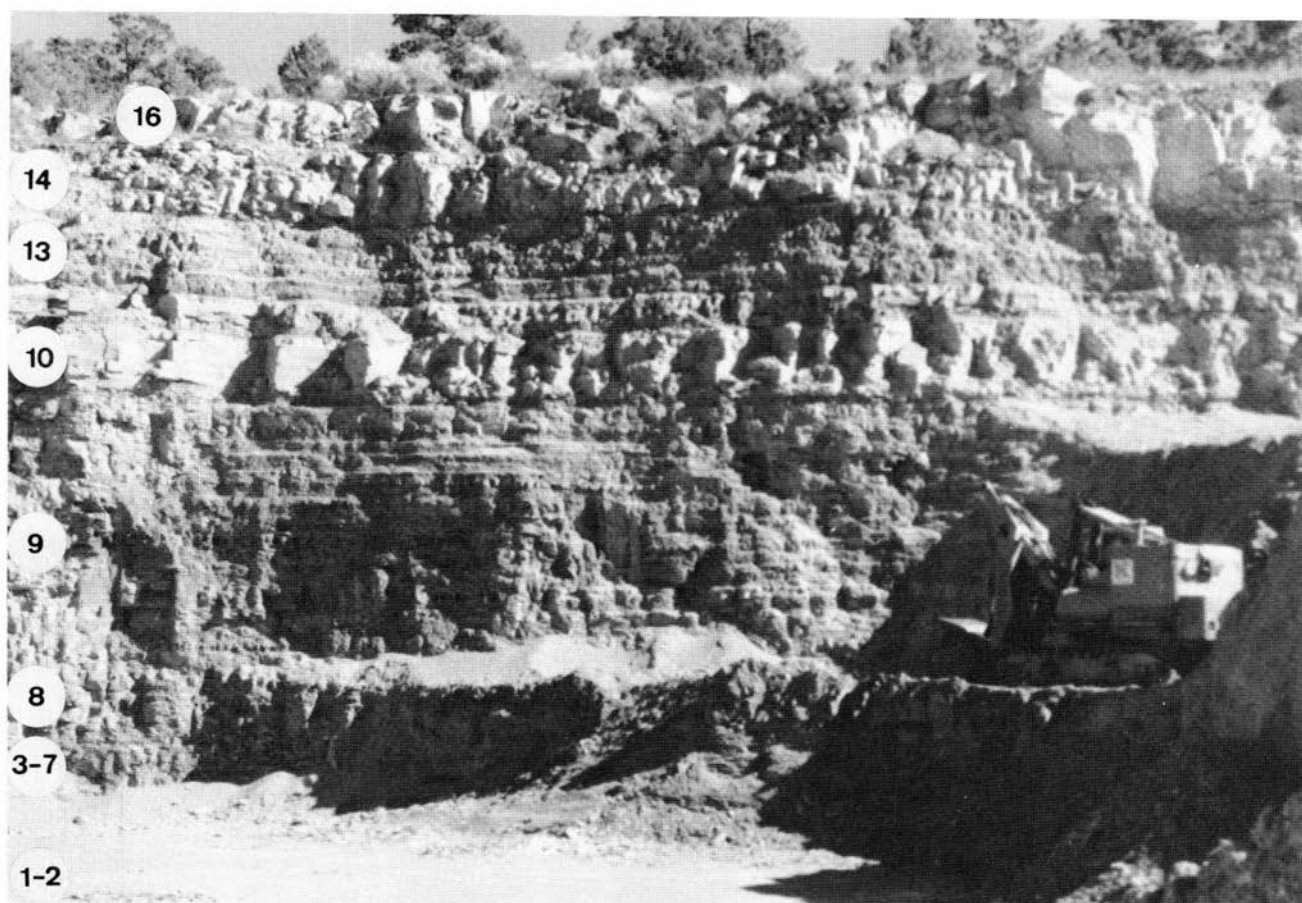


FIGURE 3—Overview of the active pit at the Kinney Brick Quarry, October 1990. Numbered units are those in the measured section of Fig. 4.

intercalated limestone, calcareous shale, and sandstone (Myers, 1973, 1982). Stukey (1967) estimated that the base of the Wolfcampian Abo Formation is stratigraphically about 100 m above the Kinney Quarry exposures.

The active quarry floor typically is developed on black, platy and laminar micrite with a high content of black clay (Fig. 4, unit 1). The upper 10 cm of this limestone are finely laminated and grade into the overlying shale (Fig. 4, unit 2).

The basal shale exposed at the quarry is 0.4 m thick, olive gray to olive black, well indurated, calcareous and highly fossiliferous (Fig. 4, units 3-4). Part of this interval is highly fissile and not calcareous. Above it is 2.0 m of olive-gray, calcareous shale that contains thin bands of plastic clay (Fig. 4, units 5-7). Individual laminae in these shales are continuous on strike for at least 10 m.

Above, and in gradational contact with the underlying shale, are 10.7 m of olive-gray and greenish-gray, laminar calcareous silty shale that are moderately bioturbated (Fig. 4, units 8-9). These strata coarsen upward slightly and are marked by a rapid decrease in floral and faunal diversity near their base. Above them are 12.7 m of olive-gray, silty shale and claystone interbedded with lenticular, yellowish-orange and grayish-brown, subarkosic/sublitharenitic, laminar and ripple-laminar sandstone ledges (Fig. 4, units 10-16). The section is completed by 1.0+ m of limestone-cobble conglomerate with clasts as much as 8 cm in diameter and grayish-yellow, trough-crossbedded subarkosic—sublitharenite (Fig. 4, unit 17).

Some early workers (e.g. Stukey, 1967; Berman, 1973)

assigned a Permian age to the Kinney fossils, based primarily on an unsubstantiated report of the Permian index-fossil *Callipteris* (cf. Read and Mamay, 1964) from the quarry (Kelley and Northrop, 1975). However, fusulinids of the Pine Shadow Member, from more open-marine facies than are those exposed at the quarry, include *Triticites* species indicative of the early Virgilian (Myers, 1982, 1988). Therefore, the Late Pennsylvanian age of the Kinney fossils seems to be well established.

Fossil assemblages

Almost all published fossils from the Kinney Quarry were collected from units 2-4 of our measured section (Fig. 4). We have sampled these units extensively and have obtained much smaller collections from other units at the quarry. All fossils we collected are housed at the NMMNH. In addition, B. S. Kues has extensively sampled units 1, 5, and 15 of our measured section; his collections are housed at the University of New Mexico. Based on Kues' and our collections, we recognize two floral and four faunal assemblages at the Kinney Quarry (Fig. 4).

1. Pteridosperm floral assemblage: The flora from units 1-4 consists of calamitaleans, pteridosperms, cordaitaleans, and *Walchia*. *Calamites* occurs in the basal micrite (unit 1) with *Asterophyllites* and *Annularia*, followed in abundance by pteridosperms and cordaitalean leaves. Pteridosperms are very common in the overlying shale (units 3-4) and are typified by *Neuropteris* (Fig. 5A). Calamitaleans still are present, as are leaves of *Cordaites*. One or more species of *Walchia* are present, though not abundant.

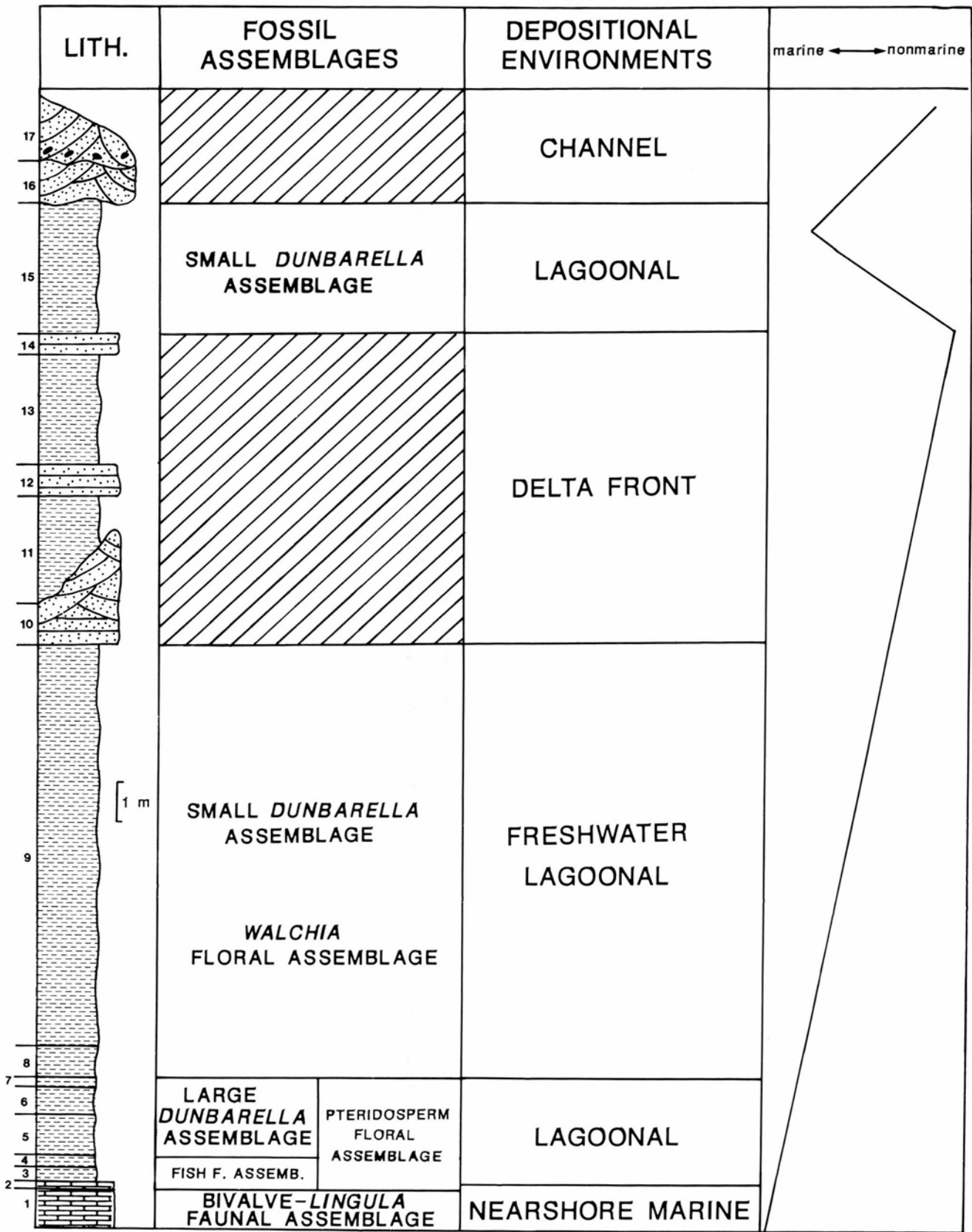


FIGURE 4—Measured stratigraphic section at the Kinney Brick Quarry, stratigraphic distribution of fossil assemblages, and inferred depositional environments. For descriptions of the lithology of numbered units see Appendix.

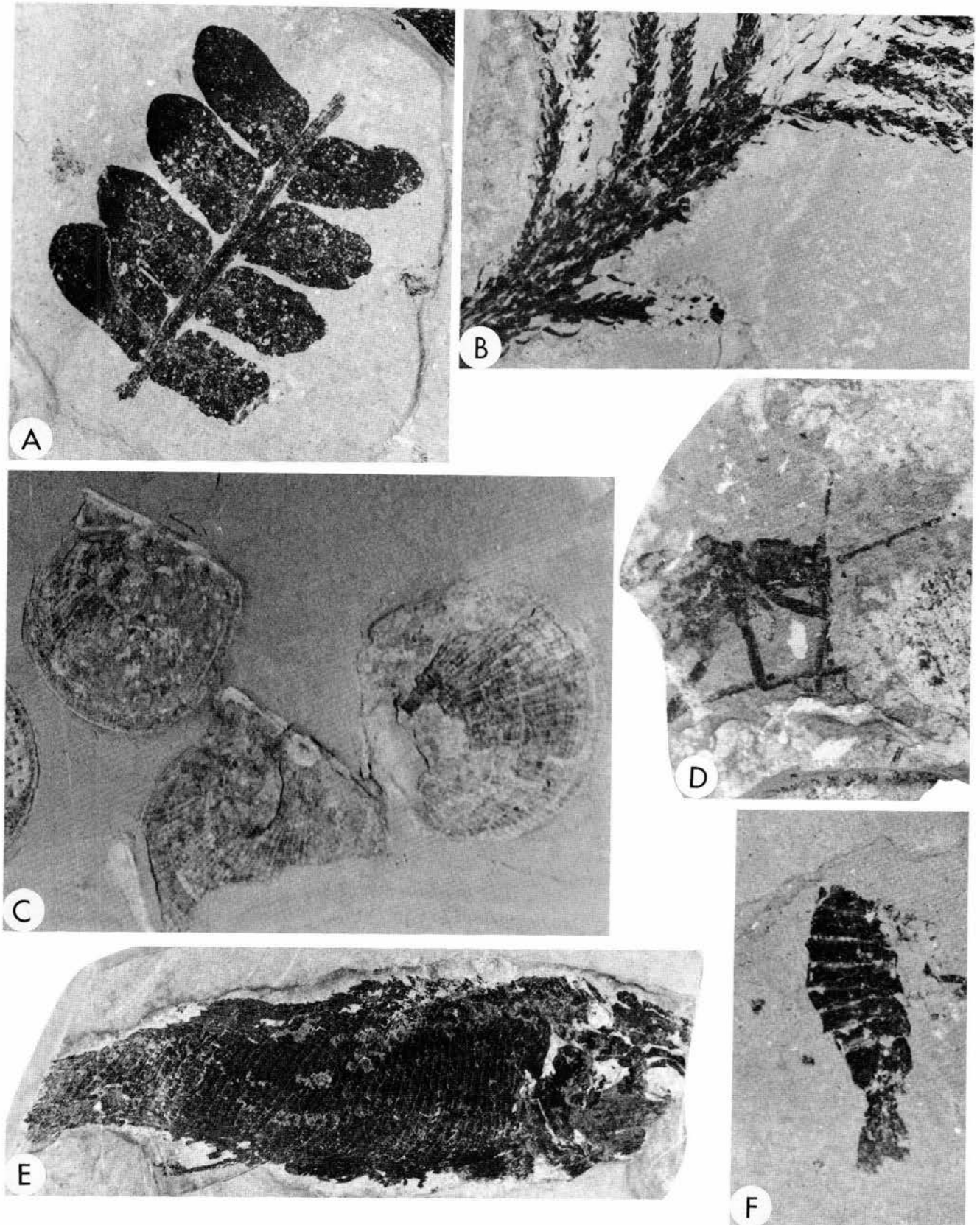


FIGURE 5—Some characteristic fossils from the Kinney Brick Quarry. **A**, The seed fern *Neuropteris*, NMMNH P-12980, $\times 2$; **B**, the conifer *Walchia*, NMMNH P-12983, $\times 1.5$; **C**, the pectinid clam *Dunbarella*, $\times 1.5$; **D**, a cockroach, $\times 2$; **E**, the actinopterygian fish *Elonichthys*, NMMNH P-12989, $\times 2$; **F**, a malacostracan, *Uronectes*, NMMNH P-12978, $\times 5$.

See comment on p. 86 concerning Fig. 5D.

2. *Walchia* floral assemblage: This assemblage consists almost entirely of walchian conifers (Fig. 5B), whose leafy shoots are abundant throughout units 8 and 9. The only other plant we recovered from unit 9 is a single, large branch of *Pecopteris*.

3. *Bivalve—Lingula* faunal assemblage: This assemblage is confined to the basal micrite (unit 1) and is dominated by the bivalves *Solemya* and *Myalina*, and by the inarticulate brachiopod *Lingula*. Subsidiary members of this assemblage include unornamented ostracodes, conchostracans, the articulate brachiopod *Chonetinella*, *Dunbarella*, and small ammonoids. Other bivalves, brachiopods, gastropods, and orthocerid nautiloids are uncommon, and bryozoan and crinoid fragments are rare. Conodonts, insect body parts, and disarticulated fish remains also are rare (Kues, 1991, in press).

4. Fish faunal assemblage: The uppermost micrite and overlying 0.4 m of shale (units 2-4) contain a fish-dominated assemblage which includes elasmobranchs, dipnoans, coelacanths, acanthodians, and actinopterygians (Fig. 5E). In terms of diversity and number of specimens, actinopterygians dominate the fish assemblage. This is the main collecting level at the quarry from which almost all of the previously reported fauna has been collected. The diverse fauna also includes spirorbid and other worms, arthropods (conchostracans, ostracodes, malacostracans [Fig. 5F], myriapods, insects [Fig. 5D]), small *Dunbarella*, gastropods and allochthonous nautiloids, brachiopods and fenestrate bryozoans, as well as rare trimerorhachid amphibians.

Spirorbid worms, ostracodes, insects, small *Dunbarella*, gastropods, and fishes occur throughout units 3 and 4. Spirorbid worms are represented by spiral tubes often attached to floral elements of the pteridosperm assemblage. The ostracodes and gastropods are generally poorly preserved, crushed, and lacking significant morphological detail. Small *Dunbarella* are common, preserved as compressed internal molds or recrystallized, disarticulated valves. The clearly allochthonous elements of this assemblage are crushed, disarticulated valves of articulate brachiopods, incomplete orthocerid shells, and small fragments of fenestrate bryozoans. Worms, millipedes, insects, and fish usually occur as carbon films. Articulated acanthodians and actinopterygians are common, whereas the dipnoans and coelacanths are mostly represented by isolated scales and dermal bones. Complete skeletons of xenacanthid elasmobranchs are rare and restricted to the lower part of unit 3, within 5 cm of the contact with the underlying shaly limestone (unit 2). Conchostracans are very abundant in the lower 8-10 cm of unit 3 and occur as isolated individuals or clusters of 10 or more carapaces. Shrimp are restricted to a narrow, 4 cm thick zone just above the conchostracan-bearing horizon.

5. Large *Dunbarella*-dominated assemblage: The transition to this assemblage, which is present in units 5-7, occurs over a vertical distance of 8 cm. Unusually large specimens of *Dunbarella* (Fig. 5C) dominate this assemblage, which also includes a few fishes. Rare eurypterids occur only here. Articulated and disarticulated, recrystallized valves of *Dunbarella* in all stages of growth abound, and individuals are restricted to specific laminae, possibly due to seasonal fluctuations (Clark, 1978).

6. Small *Dunbarella* assemblage: This consists of small valves of *Dunbarella* and, in unit 15, less common *Lingula* and *Myalina*. It is associated with the *Walchia* floral assemblage sporadically in the silty shales of units 8-9. Above

unit 9, shale units generally are unfossiliferous except for large pieces of carbonized wood and badly macerated conifer debris. However, unit 15 contains the small *Dunbarella* assemblage and moderate amounts of plant material.

Depositional environments

Several authors have suggested depositional environments for the highly fossiliferous, fine-grained rocks low in the quarry section (Fig. 4, units 1-7), including nearshore marine (Gottfried, 1987a, b), brackish marine—lagoonal (Berman, 1973; Zidek, 1975; Schram, 1981), and brackish-lagoonal with a significant fresh-water influence (Clark, 1978; Kues, 1985). All of these interpretations are reasonable, depending on which floral/faunal assemblages (and, consequently, which aspect of the Kinney strata) are studied. Combining our physical stratigraphy with the fossil assemblages, we recognize several distinct depositional environments at the Kinney Quarry (Fig. 4). These make up a regressive sequence of the "R2" type described by Smith (1989), in which limestone grades up through prodelta/delta-front clastics with a capping delta-plain facies.

The basal micrite (units 1-2) represents deposition in a nearshore marine environment that received some fresh-water/clastic sediment input. We point to its lithology (note especially the high black-clay content of this micrite) and fauna (note articulate brachiopods such as *Chonetinella*, characteristic of more open-marine-shelf facies of the Pine Shadow Member) to support this conclusion. The black-clay content, terrestrial plant debris, and euryhaline elements of the fauna (especially abundant *Lingula*) are consistent with deposition near the shoreline with a significant fresh-water input.

The overlying highly fossiliferous shales (units 3-4) were deposited in a calm lagoonal or estuarine environment with a significant fresh-water input. Uniform, fine grain size, fine lamination and lack of bioturbation, dark colors, and preservation of soft-bodied forms suggest deposition in quiet, oxygen-poor waters with restricted circulation. A lowland, pteridosperm-dominated flora and fresh-water faunal elements (especially conchostracans and trimerorhachid amphibians) suggest low salinity.

Overlying shales (units 5-7) represent a similar facies, but probably with a greater fresh-water influence. Dominant elements are *Dunbarella*, which must be euryhaline (cf. Clark, 1978), and terrestrial plants.

Overlying silty shales (units 8-9) are interpreted by us as representing increased sedimentation rates in an estuarine environment, brought about by the onset of a significant fluvial discharge. The *Walchia* floral assemblage abounds here, and there are sparse, small *Dunbarella*. Most of the floral assemblage, typically interpreted as an inland, relatively xerophytic flora (Read, 1947; Ash and Tidwell, 1982), may have been floated into an environment characterized by frequent shallow ponding and deposition on a better drained surface than the underlying shales.

Overlying laminar/ripple-laminar sandstone ledges and intercalated shales/claystones (units 10-14) are interpreted by us as delta-front, distributary mouth bars, and associated deposits. Unit 15 is a shale that shows marine influence indicated by the presence of *Lingula* and *Myalina*. This unit, and the overlying fluvial sandstone/conglomerate, may be the base of another transgressive sequence.

In conclusion, we interpret the stratigraphic sequence at the Kinney Quarry as mostly reflecting a marine regression

corresponding to the progradation of a clastic delta. Shifting sediments from the delta probably isolated an embayment from normal marine conditions as a clastic wedge developed and extended seaward. Lagoonal conditions were established and clastic input was initially restricted to clay-size particles. Eventually, the embayment was filled by silty shales from an advancing delta plain that later deposited sand. The onset of a subsequent transgression is documented by the highest strata in the quarry section.

Access to the Kinney Brick Quarry

To reach the Kinney Brick Quarry from Albuquerque, proceed east 13.9 mi on I-40 from the I-40/I-25 interchange to Exit 175, Tijeras-Cedar Crest. From the exit continue south on NM-337 (formerly NM-14) 7.6 mi (from the Tijeras Post Office) to a relatively inconspicuous dirt road on the right marked by a mailbox just south of the U.S. Forest Service Deadman Picnic Ground. This dirt road is the entrance to the Kinney Brick Quarry, which is privately owned and thus should not be entered without permission. The quarry is located in the SE1/4, sec. 18, T9N, R6E, Bernalillo County. Hawley et al. (1982, pp. 8-10) provided a road log of the route from Tijeras to the quarry. The highway mostly traverses outcrops of the Los Moyos Formation of the Madera Group (Fig. 1).

Acknowledgments

We thank B. Jurgena and the Kinney Brick Company for access to the quarry, M. Gottfried, S. Hayden, B. Kues, J. Lorenz, G. Smith, K. Toolson, and J. Zidek for diverse help, and B. Kues, J. Lorenz, and J. Zidek for their reviews of this paper.

References

- Ash, S. A., and Tidwell, W. D., 1982, Notes on the upper Paleozoic plants of central New Mexico: New Mexico Geological Society, Guidebook 33, pp. 245-248.
- Berman, D. S., 1973, A trimerorhachid amphibian from the Upper Pennsylvanian of New Mexico: *Journal of Paleontology*, v. 47, pp. 932-945.
- Carpenter, F. M., 1970, Fossil insects from New Mexico: *Psyche*, v. 77, pp. 400-412.
- Clark, G. R., II, 1979, Byssate scallops in a Late Pennsylvanian lagoon (abs.): *Geological Society of America, Abstracts with Programs*, v. 10, p. 380.
- Gottfried, M. D., 1987a, A Pennsylvanian aeuelliform (Osteichthyes, Actinopterygii) from North America with comments on aeuelliform relationships: *Palaontologische Zeitschrift*, v. 61, pp. 141-148.
- Gottfried, M. D., 1987b, A new long-snouted actinopterygian fish from the Pennsylvanian of north-central New Mexico: *New Mexico Journal of Science*, v. 27, pp. 7-19.
- Hawley, J. W., Foster, R. W., Broadhead, R., and Love, D. W., 1982, Road-log segment I-B: Tijeras Canyon to Abo Canyon via Estancia and Manzano: *New Mexico Geological Society, Guidebook 33*, pp. 8-30.
- Huber, P., Lucas, S. G., and Hayden, S. N., 1989, Stratigraphy, depositional environments and fossil assemblages of an Upper Pennsylvanian lagoonal deposit, central New Mexico: *New Mexico Journal of Science*, v. 29, p. 117.
- Hunt, A. P., Lucas, S. G., and Huber, P., 1989, Trimerorhachid amphibian from the Late Pennsylvanian of central New Mexico (abs.): *Journal of Vertebrate Paleontology*, v. 9, supplement, p. 26A.
- Kelley, V. C., and Northrop, S. A., 1975, *Geology of Sandia Mountains and vicinity*, New Mexico: New Mexico Bureau of Mines & Mineral Resources, Memoir 29, 136 pp.
- Kues, B. S., 1985, Eurypterids from the Wild Cow Formation (Upper Pennsylvanian), Manzano Mountains, New Mexico: *New Mexico Journal of Science*, v. 25, pp. 23-31.
- Kues, B. S., 1991, A Late Pennsylvanian *Lingula-Solemya-Myalina* community, Kinney quarry, Manzanita Mountains, New Mexico (abs.): *New Mexico Geology*, v. 13, no. 1.
- Kues, B. S. (in press), A Late Pennsylvanian (Virgilian) restricted marine fauna from the Kinney Quarry, Manzanita Mountains, New Mexico: *New Mexico Bureau of Mines & Mineral Resources, Bulletin 138*.
- Mamay, S. H., 1981, An unusual new species of *Dicranophyllum* Grand'eury from the Virgilian (Upper Pennsylvanian) of New Mexico, U.S.A.: *The Palaeobotanist*, v. 28-29, pp. 86-92.
- Mamay, S. H., 1990, *Charliea manzanitana*, n. gen., n. sp., and other enigmatic parallel-veined foliar forms from the Upper Pennsylvanian of New Mexico and Texas: *American Journal of Botany*, v. 77, pp. 858-866.
- Myers, D. A., 1973, The upper Paleozoic Madera Group in the Manzano Mountains, New Mexico: U.S. Geological Survey, Bulletin 1372-F, 13 pp.
- Myers, D. A., 1982, Stratigraphic summary of Pennsylvanian and Lower Permian rocks, Manzano Mountains, New Mexico: *New Mexico Geological Society, Guidebook 33*, pp. 233-237.
- Myers, D. A., 1988, Stratigraphic distribution of some fusulinids from the Wild Cow and Bursum Formations, Manzano Mountains, New Mexico: U.S. Geological Survey, Professional Paper 1446-B, 39 pp.
- Read, C. B., 1947, Pennsylvanian floral zones and floral provinces: *Journal of Geology*, v. 55, pp. 271-279.
- Read, C. B., and Mamay, S. H., 1964, Upper Paleozoic floral zones and floral provinces of the United States: U.S. Geological Survey, Professional Paper 454-K, 35 pp.
- Schram, F. R., 1981, Late Paleozoic crustacean communities: *Journal of Paleontology*, v. 55, pp. 126-137.
- Schram, F. R., and Schram, J. M., 1979, Some shrimp of the Madera Formation (Pennsylvanian), Manzanita Mountains, New Mexico: *Journal of Paleontology*, v. 53, pp. 169-174.
- Smith, G. A., 1989, Eustatic signals in cyclic deltaic to shallow-marine clastics and carbonates, Sandia Mountains, New Mexico (abs.): *Geological Society of America, Abstracts with Programs*, v. 21, p. 145.
- Stukey, A. H., Jr., 1967, Stratigraphic relations of the Pennsylvanian-Permian strata, Manzanita Mountains, New Mexico: Unpublished MS thesis, University of New Mexico, Albuquerque, 64 pp.
- Zidek, J., 1975, Some fishes of the Wild Cow Formation (Pennsylvanian) Manzanita Mountains, New Mexico: *New Mexico Bureau of Mines & Mineral Resources, Circular 135*, 22 pp.

See next page for Appendix

Appendix: Measured stratigraphic section

Measured September 1990 in the lower pit of the Kinney Brick Quarry, NW¹/₄ SW¹/₄ SE¹/₄ sec. 18, T9N, R6E, Bernalillo County; strata are horizontal.

Unit	Lithology	Thickness (m)
Wild Cow Formation		
Pine Shadow Member:		
17	Sandstone and limestone-pebble conglomerate; sandstone is moderate yellowish brown (10 YR 5/4), very fine- to fine-grained, moderately sorted, subangular, calcareous and micaceous; conglomerate has brownish-gray (5 YR 4/1) matrix and clasts are medium gray (N5) to medium dark gray (N4) limestone pebbles 1–5 cm in diameter; trough-crossbedded.	1.0+
16	Sandstone; dark yellowish orange (10 YR 6/6); very fine- to fine-grained; moderately sorted; subangular; calcareous; micaceous; trough-crossbedded and laminar-ripple laminar; forms a ledge.	1.0
15	Shale; olive gray (5 Y 4/1); slightly calcareous; finely laminar to platy; fossiliferous with abundant small, dark yellowish-orange (10 YR 6/6) <i>Dunbarella</i> .	3.2
14	Sandstone; dark yellowish-orange (10 YR 6/6) and grayish brown (5 YR 3/2); very fine- to fine-grained; moderately sorted; subrounded-subangular; calcareous; feldspathic; laminar-ripple laminar; forms a ledge.	0.5
13	Silty claystone; moderate yellowish brown (10 YR 5/4); plastic; very calcareous; laminar.	3.3
12	Sandstone; same color and lithology as unit 10.	0.8
11	Silty shale; olive gray (5 Y 4/1) and light olive gray (5 Y 5/2); calcareous; contains moderate yellowish-brown (10 YR 5/4) micritic limestone nodules 2–8 cm in diameter.	1.1
10	Sandstone; dark yellowish orange (10 YR 6/6); very fine- to fine-grained; subrounded-subangular; moderately sorted; calcareous; laminar-ripple laminar and trough-crossbedded; unit pinches out over 10 m on strike.	2.8
9	Silty shale; olive gray (5 Y 4/1); calcareous; parts weather blocky; moderately fossiliferous.	9.9
8	Silty shale; greenish gray (5 GY 6/1); slightly calcareous; blocky; forms a ledge.	0.8
7	Shale; dark greenish gray (5 GY 4/1) with moderate yellowish-brown (10 YR 5/4) mottles; plastic; calcareous; highly fossiliferous.	0.2
6	Shale and claystone; shale is olive gray (5 Y 3/2); claystone is dark greenish gray (5 GY 4/1); very calcareous; highly fossiliferous, especially with moderate yellowish-brown (10 YR 5/4) <i>Dunbarella</i> .	0.8
5	Shale; olive gray (5 Y 3/2); very calcareous; highly fossiliferous.	1.0
4	Shale; olive gray (5 Y 4/1); weathers dark yellowish brown (10 YR 4/2); plastic; very calcareous; highly fossiliferous.	0.2
3	Shale; olive black (5 Y 2/1); weathers dark yellowish orange (10 YR 6/6); calcareous; highly fossiliferous.	0.2
2	Shaly limestone; olive black (5 Y 2/1); mottled and streaked grayish orange (10 YR 7/4); well indurated; highly fossiliferous.	0.1
1	Micritic limestone; dark gray (N3); clayey; laminar to massive; highly fossiliferous; top of unit approximates active quarry floor.	1.0+

Comment

Although cockroaches do occur in the Kinney deposits, the insect illustrated in Fig. 5D (p. 83) is not one of them. According to J. Kukalova-Peck, Carleton University, Ottawa (written comm. March 1991), the specimen most likely is a megasecopteran showing the thorax and head with a sucking rostrum. (*Eds.*)

A tale of two volcanoclastic aprons: Field guide to the sedimentology and physical volcanology of the Oligocene Espinaso Formation and Miocene Peralta Tuff, north-central New Mexico

Gary A. Smith', Daniel Larsen', Steve S. Harlan', William C. McIntosh', Daniel W. Erskine', and Steve Taylor'

'Department of Geology, University of New Mexico, Albuquerque, New Mexico 87131; 'New Mexico Bureau of Mines & Mineral Resources, Socorro, New Mexico 87801

Geologic background to excursions to the Espinaso Formation and Peralta Tuff

Gary A. Smith

Introduction

Volcanism has played an important role in the Cenozoic history of New Mexico. Volcanic fields of variable size, eruptive character, and magma composition developed over large areas of the state. Volcanoclastic aprons, composed of primary, volcanic fragmental deposits as well as secondary, reworked sedimentary facies accumulated adjacent to vent areas and peripheral to the volcanic fields. The purpose of this excursion (Fig. 1) is to compare and contrast the primary and secondary volcanoclastic strata associated with volcanic centers of different compositions, tectonic settings, and ages. Emphasis is placed on relatively proximal aprons, which include alluvial and pyroclastic-flow fans. In addition to descriptions of the field-trip stops, three short papers illustrate the utility of integrating paleomagnetic, petrologic, and geochronologic methods with more obvious sedimentologic and volcanologic studies in the investigation of volcanoclastic sequences.

Espinaso Formation

The Oligocene Espinaso Formation comprises the erosional remnants of widespread aprons of coarse-grained volcanoclastic debris that accumulated adjacent to a long-active chain of volcanic-vent complexes stretching 40 km southward from near the southwestern edge of Santa Fe (Fig. 1). The vents are marked by stocks, laccoliths, sills, and dikes of the Ortiz porphyry belt (OPB; Fig. 1). Level of structural exposure rises northward so that preservation of volcanic rocks and volcanoclastic debris, assigned to the Espinaso Formation, is restricted to the northern end of the belt. Two principal areas of Espinaso Formation exposure occur, the type section at Espinaso Ridge and a larger area near the towns of Cerrillos and La Cienega (Fig. 2A). Espinaso Ridge detritus was derived from the Ortiz Mountain eruptive center, whereas the section east of Cerrillos is related to volcanism in the Cerrillos Hills.

Two petrographic suites are associated with OPB magmatism (Maynard et al., 1990). Early calc-alkaline latites and quartz latites were erupted between about 36 Ma and 34 Ma and were followed by alkaline latites, and consanguineous gold-mineralized monzonites, between about 30 and 28 Ma (Baldrige et al., 1980; Kautz et al., 1981; Maynard et al., 1990). Although few lava flows or primary pyroclastic deposits remain, the composition of Espinaso Formation conglomerate clasts and sandstones faithfully

records the two episodes of volcanism (see Smith and Erskine, this volume). The products of the two eruptive suites are easily distinguished in the field by the dominance of hornblende or hornblende + clinopyroxene as the ferromagnesian silicates in the calc-alkaline lithologies; whereas

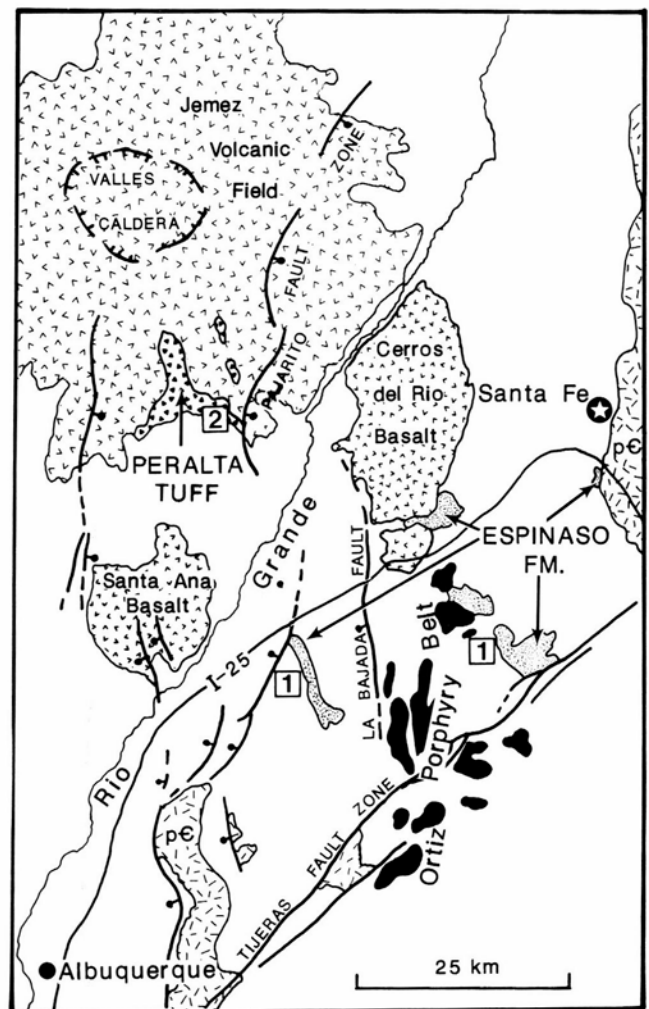


FIGURE 1—Index map of north-central New Mexico showing major structural and volcanic features. Numbers in boxes show locations of field-trip stops on day 1 (Stops 1–3) and day 2 (Stops 4–6), emphasizing the Oligocene Espinaso Formation and Miocene Peralta Tuff Member of the Bearhead Rhyolite, respectively.

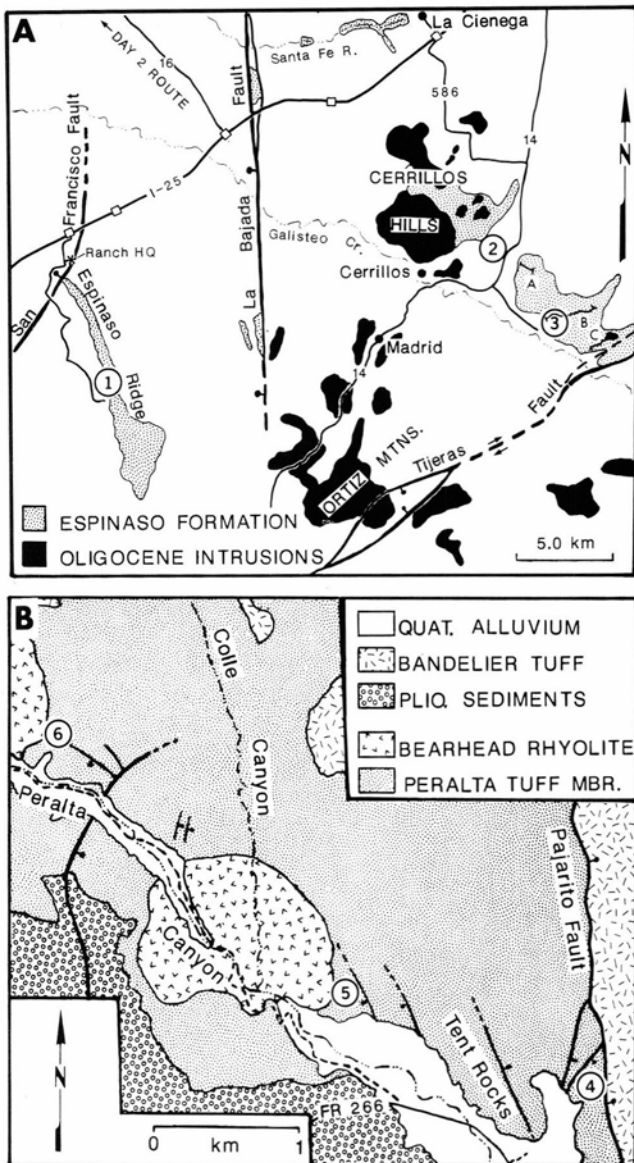


FIGURE 2—A, Distribution of the Espinaso Formation and correlative intrusions of the Ortiz porphyry belt; additional dikes coincident with the Tjeras fault zone and extending radially from the Cerrillos Hills are not shown. The locations of Stops 1, 2, and 3 are indicated; sections A, B, and C east of Cerrillos are shown schematically in Fig. 4. B, Generalized geology of lower Peralta Canyon, Jemez Mountains, showing location of Stops 4, 5, and 6.

hornblende is nearly absent in the alkaline rocks, where augite occurs alone or with biotite.

OPB magmatism occurred during the tectonic transition between the Laramide orogeny and mid-Tertiary extension. In most locations, the Espinaso Formation rests conformably upon, and grades into, the Galisteo Formation, a largely Eocene clastic unit derived from Laramide orogenic highlands. This relationship indicates continuity of deposition in Laramide basins into the initial stages of mid-Tertiary volcanism. At Arroyo Hondo, south of Santa Fe, alkaline Espinaso Formation debris, capped by a 29 Ma latite flow (Baldrige et al., 1980), records east-flowing streams that crossed an erosion surface cut on Precambrian rocks of the Laramide Sangre de Cristo uplift (Fig. 1). The Espinaso Formation at Cerrillos is overlain, along a marked angular unconformity, by Pliocene(?) Santa Fe Group sediments

(Bachman, 1975). At Espinaso Ridge, a calcic paleosol caps the Espinaso Formation and is disconformably overlain by early Miocene Santa Fe Group. There is no conclusive evidence for continued subsidence of Laramide basins or initiation of extensional rift basins during Espinaso deposition. The volcanoclastics accumulated as aprons of debris surrounding the volcanic centers that choked adjacent drainages with detritus during a period of relative structural stability, during the transition from compressional to extensional deformation.

The Espinaso Formation consists of proximal, debris-flow dominated alluvial-fan deposits, best seen east of Cerrillos, that grade distally into braidplain facies, which are well exposed on Espinaso Ridge. Lava flows are rare, but do occur at both localities. Pyroclastic-fall deposits also occur sparsely in both sections and three ignimbrites are exposed at Espinaso Ridge. Espinaso Formation latite clasts are remarkably porphyritic (45-50% phenocrysts), suggesting viscous extrusions in the form of domes, which were then the sources for numerous block-and-ash flows and avalanches of carapace debris that supplied abundant lithic pyroclastic and autoclastic fragments to adjacent alluvial fans and braidplains.

The Peralta Tuff Member of the Bearhead Rhyolite

Although best known for great episodes of Quaternary rhyolitic-ignimbrite volcanism and caldera formation, the Jemez Mountains contain a large volume of Miocene and Pliocene volcanic rocks, of diverse composition, and locally well preserved volcanoclastic aprons (Gardner et al., 1986; Waresback and Turbeville, 1990). During a 1.0 to 1.5 m.y. period in the late Miocene, high-silica rhyolite was erupted from at least a score of vents dispersed over the southern and, to a lesser extent, northern parts of the Jemez Mountains. The resulting plugs, domes, and lava flows mark the vents for the Bearhead Rhyolite. Eruptions of flows and domes were commonly preceded by phreatomagmatic explosions that constructed tuff rings and adjacent fan-shaped accumulations of pyroclastic-flow and fall deposits. Along the southeastern margin of the volcanic field, these primary pyroclastic deposits are intercalated with sheetflood and braided-stream-dominated alluvial-fan facies. The volcanoclastic deposits, which are at least 275 m thick, are collectively known as the Peralta Tuff Member of the Bearhead Rhyolite (Fig. 2B). Subsidence of the Rio Grande rift, the western bounding structures of which were active in the Jemez Mountains during Peralta Tuff deposition, partly accommodated the volcanoclastic fans along the southeastern margin of the volcanic field (Fig. 1).

Compared to the Espinaso Formation, the Peralta Tuff contains a much greater volume of primary pyroclastic deposits, whereas debris-flow facies are much less common. The more sandy nature of Peralta Tuff sediments may, in part, reflect the greater availability of relatively fine-grained pyroclastic debris. The Peralta Tuff also contains eolian tuffs resulting from wind reworking of ash-fall deposits (Smith and Katzman, in press).

Access

Many of the stops described in this guide are on private land or public land with restricted access. Stop 1 is located in a restricted Bureau of Land Management (BLM) habitat management area reached by crossing private property. Permission for access must be obtained from the ranch head-

quarters mentioned in the directions to Stop 1 (Fig. 2A). Stop 3 is partly located on private property, although representative exposures can be seen by walking through the section in Canada de la Cueva (Fig. 5), on BLM land. Stop 5 is located on private land, currently owned by Mr. Fred

Rivera of Pena Blanca, New Mexico. Stop 6 is located on land owned by the University of New Mexico. Inquiry for access should be directed to the author or to Mr. Fred Dixon, caretaker, at Rancho Canada, north of Cochiti Lake, New Mexico.

Stratigraphy and sedimentology of Espinaso Ridge (Stop 1)

Gary A. Smith

Directions to Arroyo del Tuerito (Stop 1)

From either Albuquerque or Santa Fe, travel 1-25 to the Budaghers Exit (exit 257) and turn east. A frontage road heads southward along the east side of the freeway, becoming a dirt road in 0.5 mi as it enters private property. Continue 0.9 mi to a ranch headquarters where it is necessary to obtain permission to proceed. Cross the wash, turn west, and follow the main track south along the west side of Espinaso Ridge. The route from here is on unimproved dirt roads, requiring modest vehicle clearance and four-wheel drive when wet. At 3.0 mi from the ranch headquarters the road enters BLM land near a windmill. Proceed another 2.0 mi to another gate, taking the right fork just past the gate. Continue 0.7 mi to the ford across Arroyo del Tuerito. At this point, four-wheel-drive vehicles may proceed approx

imately 0.8 mi up the wash to Stop 1. An alternative route crosses the wash and continues over rough road for an additional 0.9 mi where a short hike to the northeast leads to the Arroyo del Tuerito section (Fig. 3).

Stratigraphy of Espinaso Ridge

The exposures in Arroyo del Tuerito were designated the type section of the Espinaso Formation (then Espinaso Volcanics) by Stearns (1953). The northwest-striking ridge is held up by resistant, mostly gray volcanoclastic strata that overlie yellow and red lithic-arkosic clastics of the Eocene Galisteo Formation and are overlain to the northeast by Santa Fe Group sediments. The abrupt termination of the ridge near 1-25 marks the trace of the San Francisco fault zone, a Rio Grande rift structure (Fig. 2A). The Espinaso For-

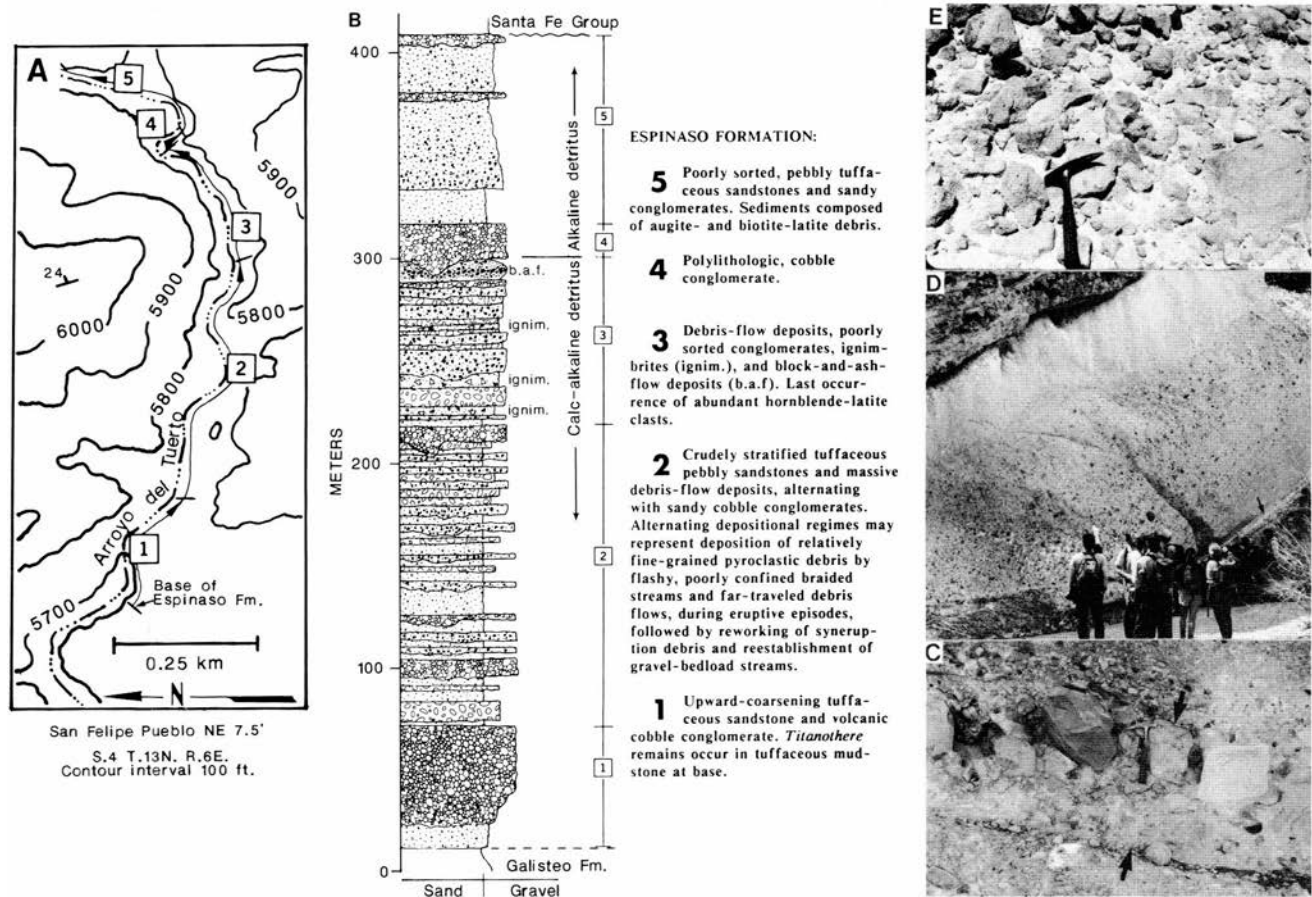


FIGURE 3—Stop 1, Arroyo del Tuerito, Espinaso Ridge. **A**, Map showing traverse. **B**, Graphic stratigraphic section and description of principal features to be seen along the traverse. **C**, Comparative textures of debris-flow deposits (between arrows) and streamflow conglomerates. Note inverse grading of large clasts in the debris-flow deposit. **D**, Ignimbrite and pumice-fall deposits (at arrow) at 236 m; note coarse-tail, inverse-to-normal grading of dark lithic fragments and concentration of large white pumice lapilli and bombs at the top (photo G. Meyer). **E**, Nearly monolithic block-and-ash flow breccia (295 m) composed of hornblende-latitude clasts with dark lamprophyre inclusions.

mation is approximately 400 m thick and includes a biotite-latitude lava flow that forms the high points along the northwest end of the ridge.

Kautz et al. (1981) interpreted the Espinaso Ridge exposures as coalesced alluvial-fan deposits extending from the Ortiz Mountains and Cerrillos Hills eruptive centers. Several observations argue against this interpretation. Facies distribution and grain size are very continuous and consistent along the entire 13 km length of the ridge (Kautz et al., 1981), which would not be expected if the outcrops included deposits derived from two different sources, and are not compatible with abrupt facies and grain-size variations typical of alluvial-fan strata. The distance between the source regions and Espinaso Ridge, approximately 20 km, would also require an unusually large fan. Facies types and distribution are more characteristic of a braidplain (Smith, 1987). Mineralogy and geochemistry of clasts collected from Espinaso Ridge are different from those found east of Cerrillos, suggesting that nearly all, if not all, the detritus at Espinaso Ridge originated at the Ortiz Mountains eruptive center (Smith and Erskine, this volume).

Stratigraphy and sedimentology of the Arroyo del Tuerto section

Fig. 3 illustrates and describes the highlights of the Espinaso Formation to be viewed by a traverse through the type section in Arroyo del Tuerto. A prominent yellow, pebbly sandstone containing petrified wood occurs high in the Galisteo Formation and is a useful regional marker, which will be seen again near Cerrillos. Volcanic grains first appear above the yellow sandstone recording the initiation of OPB volcanism while this area was still largely a braid-plain draining south from Laramide highlands. Because of the gradation between Galisteo and Espinaso lithologies, there is little agreement on where the contact should be placed (Stearns, 1953; Lucas, 1982); I define it at the base of a distinctive light-green, highly tuffaceous mudstone that contains abundant titanotheropod bone fragments. Above this level the section is dominantly volcanoclastic, although a

crystalline provenance is recorded by trace constituents through another 50 m.

The section is described in five intervals in Fig. 3. Alternating depositional regimes in interval 2 (Fig. 3C) may record episodic syneruption and inter-eruption sedimentation as described by Smith (1987; in press). Ignimbrites (Fig. 3B) and coarse-grained debris-flow deposits dominate the culminating deposition of calc-alkaline detritus in interval 3. This interval is capped by a monolithologic hornblende-latitude breccia with an ash matrix (Fig. 3E) that probably represents a block- and ash-flow deposit; this interpretation is supported by rock-magnetism studies (see Harlan, this volume). Clasts in this breccia are petrologically notable for recording the commingling of characteristic latitude magma with a calc-alkaline lamprophyre (spessartite) melt. The lamprophyre occurs as individual black clasts and as black inclusions within gray latitude blocks. The inclusions typically exhibit irregular cusped, fine-grained chill margins indicating incomplete mixing of partly crystallized melts rather than incorporation of accessory xenoliths within the latitude. An irregular erosion surface, with as much as 15 m of relief, forms a disconformity above the block- and ash-flow deposit. Above this surface is 15-20 m of relatively well sorted, well rounded conglomerate (interval 4) similar to that seen near the base of the Espinaso Formation (interval 1). Clast compositions are markedly polyolithologic compared to those in the underlying 100 m of section (interval 3) and include the first augite latites and biotite latites of the alkaline suite. The erosion surface and conglomerate probably represent initial degradation followed by the reestablishment of a gravelly braided stream during the hiatus between eruption of the compositionally distinctive magmas (a poorly constrained period, perhaps as great as 6 m.y. in duration) and during the initial rejuvenation of eruptive activity. Interval 5 consists of finer-grained, poorly sorted, scour- and fill-bedded pebbly sandstones indicating deposition by flashy discharge, poorly confined, shallow braided streams choked with sandy, lithic-pyroclastic debris generated by continued eruption of alkaline magmas.

Stratigraphy and sedimentology of the Espinaso Formation in the Cerrillos area (Stops 2 and 3)

Daniel Larsen and Steve Taylor

Directions to Garden of the Gods (Stop 2)

From Albuquerque or Santa Fe travel 1-25 to the La Cienega exit (exit 271). Take the 1-25 east-side frontage road south for 0.7 mi and turn left on NM-586. This road winds for 6.5 mi southeastward among low hills comprised of intrusive rocks that represent the late-stage alkaline phase of Ortiz porphyry belt magmatism in the Cerrillos Hills area. At the junction with NM-14, turn right and travel south for 3.8 mi. Pull off the road to the right at the "Garden of the Gods" Point of Interest sign.

Geologic setting and stratigraphy of the Espinaso Formation in the Cerrillos area

The Cerrillos Hills eruptive center lies about 3 to 4 km to the west-northwest and is composed of intrusions that deform sedimentary strata of the Cretaceous Mancos Shale

and Mesaverde Group and Eocene Galisteo Formation (Fig. 2A). Beds of the Galisteo Formation, seen here at Garden of the Gods, are inclined nearly vertically directly east of the eruptive center, but dip to progressively more shallow angles eastward. The contact between the Galisteo and Espinaso Formations is unconformable adjacent to the Cerrillos Hills (Disbrow and Stoll, 1957), but is transitional to the east. The Cretaceous and lower Tertiary units in the area are planed to a gentle slope and unconformably overlain by late Tertiary sediments, seen immediately north of Garden of the Gods.

Strata of the Galisteo Formation represent deposition in a sandy, braided alluvial system, with most of the detritus being derived from the ancestral Nacimiento and Brazos—Sangre de Cristo uplifts to the north (Ingersoll et al., 1990). The transition to volcanoclastic sedimentation of the Espi-

naso Formation is indicated by an increase in the number of latitic clasts, the occurrence of ash-fall tuff, and changes in grain size and sedimentary structures in the strata.

The Espinaso Formation is composed of up to 500 m of latitic volcanoclastic strata dominated by pebble to boulder conglomerate and breccia with common coarse-grained sandstone units and rare primary pyroclastic horizons. A lava flow with limited lateral extent occurs at the base of the section and can be seen on the low ridge 1 km to the east. The abrupt decrease in grain size and stratigraphic thickness of correlative intervals over a distance of 5 km (Figs. 4, 8), the types of facies present (see descriptions for Canada de la Cueva, Stop 3), and paleocurrent directions indicate that these volcanoclastic strata were deposited in an alluvial-fan setting, with the Cerrillos Hills eruptive center as the major source of detritus.

The change in grain size and thickness of correlative intervals with distance from the Cerrillos Hills is best exemplified by the interval with glomeroporphyritic hornblende—pyroxene-latite clasts in the lowest part of the formation. In western outcrops (section A, Fig. 4), this interval is 91 m thick and dominated by pebble- to boulder-bearing (clasts up to 2 m across) debris-flow and sheet-flood conglomerates and breccias. In contrast, 5 km to the south-

east (section C, Fig. 4) the interval is 25 m thick and dominated by scour-and-fill and horizontally bedded pebbly sandstone (rare boulders up to 40 cm across).

The predominance of sheet-like debris-flow and sheet-flood conglomerates and breccias suggests high-gradient, high-discharge, unconfined-flow conditions of deposition. Bi-directional paleocurrent data from 19 scour-and-fill structures show a strong northwest—southeast trend and a subordinate southwest—northeast trend. The paleocurrent data combined with the facies patterns indicate generally eastward sediment dispersal. The facies characteristics and relationships will be discussed further at Canada de la Cueva (Stop 3).

Directions to Canada de la Cueva (Stop 3)

From Garden of the Gods continue south on NM-14 for 0.9 mi to Santa Fe County Road 55A, turn left, and continue 2.1 mi. The log building in the side of the hill on the left at 1.5 mi is constructed of petrified wood taken from the yellow pebbly sandstone in the upper part of the Galisteo Formation, a unit also found at Espinaso Ridge (Stop 1). Before the road descends into the Canada de la Cueva Arroyo, turn right and park in the cleared area adjacent to the railroad tracks.

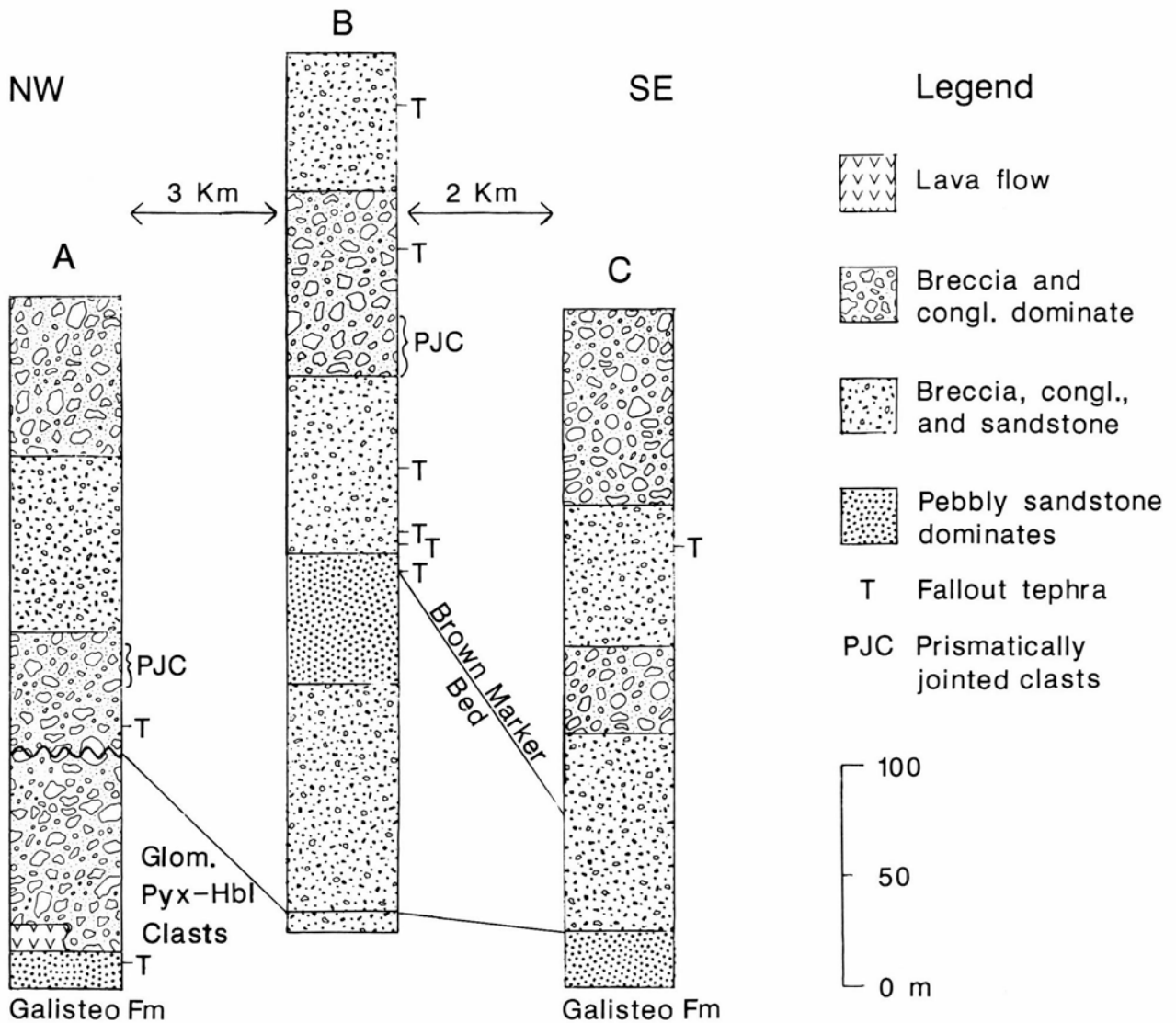


FIGURE 4—Generalized columnar sections of the Espinaso Formation from northwest (A) to southeast (C). See Fig. 2A for the location of sections.

Sedimentology of the Espinaso Formation in the Canada de la Cueva area

The small-scale map of the Canada de la Cueva area in Fig. 5A shows the traverse that will be taken at this stop. The well-exposed railroad bluff section (Fig. 5B) is stratigraphically above the transition zone between the Galisteo and Espinaso, but includes the upper 14 m of the interval with glomeroporphyritic hornblende—pyroxene-latitude clasts. Above this interval, coarse-grained units in the section contain porphyritic hornblende-latitude clasts.

The section is dominated by thin (<1 m thick), discontinuous to sheet-like, pebble- to boulder-bearing, massive, matrix-supported debris-flow breccias and vaguely stratified sheet-flood conglomerates and breccias (Fig. 5C). The debris-flow breccias include beds with inversely graded bases, ungraded beds, and inversely graded beds (see Walton and Palmer, 1988, for comparison). Scour-and-fill and horizontally bedded pebbly coarse-grained sandstone units are interbedded with the conglomerates and breccias. Interspersed throughout the section are a number of thick (>1 m), laterally continuous, pebble- to boulder-bearing debris-flow breccias. In general, these beds show well-developed inversely graded bases, sometimes extending well into the body of the unit, and normally graded tops. Although evident in some of the thinner debris-flow breccias as well, the thicker breccias commonly show signs of amalgamation of multiple-flow units (see flows at 22 and 55 m of the section).

In some cases, pebbly coarse-grained sandstones dominate over the conglomerate units. These intervals contain abundant scour-and-fill structures and small channels, some of which are filled by debris-flow breccia. Paleocurrent directions obtained from a number of scours yield northwest—southeast trend. A larger, broader channel structure with an east—west trend is observed at 32 m of the section; it is filled with vaguely stratified pebble to boulder conglomerate and scour-and fill-bedded pebbly sandstone.

These units are interpreted as having been deposited on an alluvial fan. The sheet-like debris-flow and sheet-flood breccias and conglomerates represent deposition by high-discharge, unconfined flow on the fan surface. Discontinuous conglomerate and scour-and-fill sandstones represent deposition by more confined flow in broad, shallow channels, as exemplified by the channel at 32 m of the section.

Primary pyroclastic deposits are rare in the Espinaso Formation and in the Cerrillos area are confined to pyroclastic fallout. The tuff observed in Canada de la Cueva (Fig. 5A) is only 15 cm thick and is one of the thickest observed in our study area, attesting to the dearth of these types of deposits. The tuff is comprised of mantling accretionary lapilli and lapilli-fallout tephra. Coarse-grained pyroclastic deposits and other indications of pyroclastic and autoclastic deposition, such as prismatically jointed clasts that are found throughout the Espinaso Formation (Fig. 5D) (Harlan, this volume), are important because they indicate that sedimentation was concurrent with volcanism.

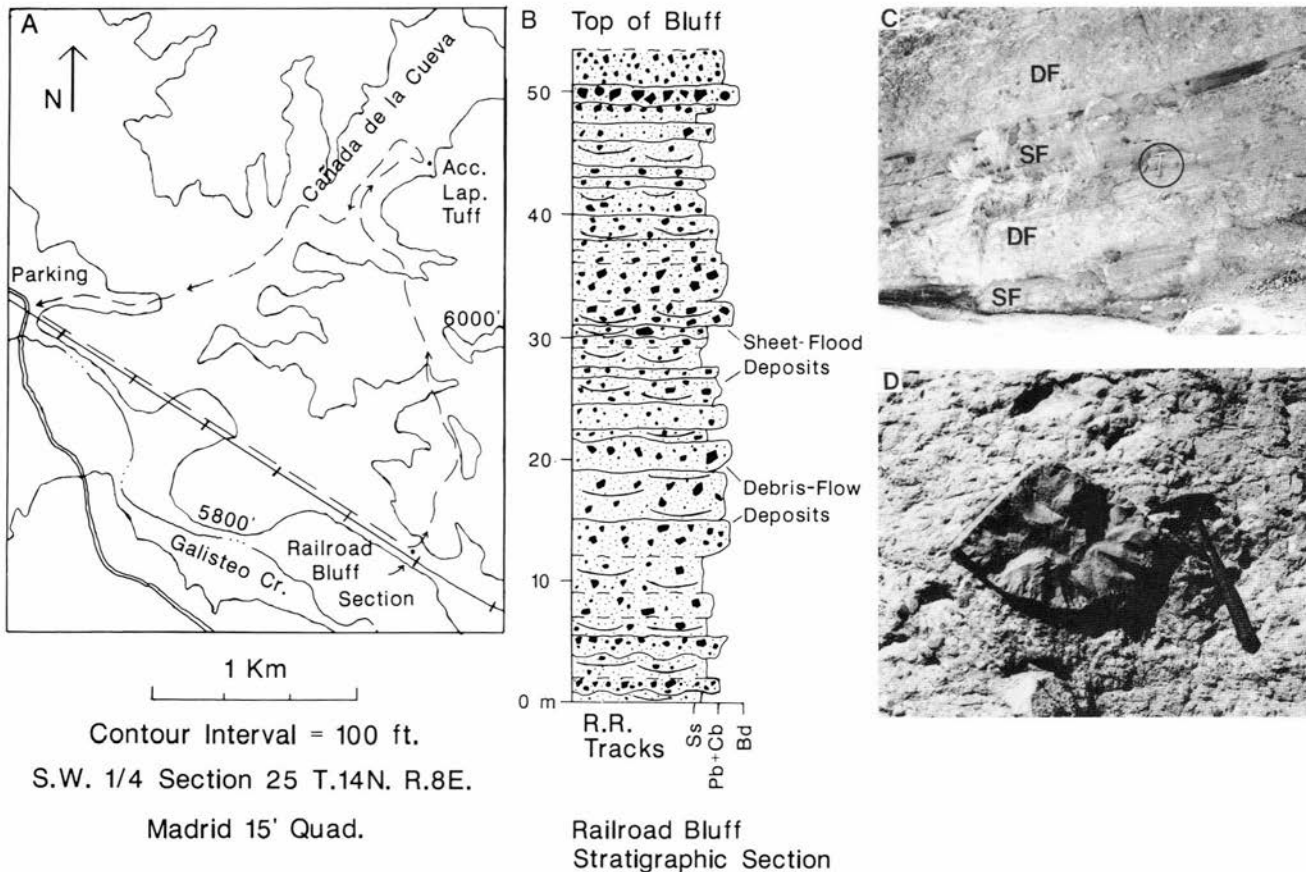


FIGURE 5—Geologic highlights of Stop 3, Cañada de la Cueva. **A**, Location of traverse. **B**, Stratigraphic column of part of the Espinaso Formation at the railroad siding section. **C**, Interbedded sheetflood conglomerates (SF) and debris-flow breccias (DF) at Cañada de la Cueva. **D**, Prismatically jointed clast in debris-flow deposit at Cañada de la Cueva.

Paleomagnetic constraints on the temperature of emplacement of two volcanic breccias in the Oligocene Espinaso Formation, New Mexico: A progress report

Steve S. Harlan

Introduction

Paleomagnetic analysis of the thermoremanent magnetization (TRM) of clastic deposits associated with volcanic centers can be used to determine whether they were emplaced at elevated or "hot" temperatures (e.g. pyroclastic flows, debris flows containing hot clasts, etc.) or at "cold" or ambient temperatures (e.g. most debris flows, glacial deposits, etc.). Thus, paleomagnetism can be used to distinguish between various types of unsorted and unstratified deposits commonly found in close proximity to many volcanoes (Aramaki and Akimoto, 1957; Hoblitt and Kellogg, 1979). More importantly, through the use of detailed thermal demagnetization of TRM, quantitative assessments of emplacement or "setting" temperatures can sometimes be determined (Hoblitt and Kellogg, 1979; McClelland and Druitt, 1989). In this study, the paleomagnetic properties of two breccias within the Oligocene Espinaso Formation have been examined to provide, if possible, an estimate of the emplacement temperatures of individual clasts or of the entire deposit. Preliminary paleomagnetic results are presented from two breccias; detailed paleomagnetic and rock-magnetic studies of these and other units are currently in progress.

Field and laboratory procedures

Sixteen samples from 13 individual blocks were collected from a heterolithic breccia, of probable debris-flow origin, exposed in Canada de la Cueva near Cerrillos, New Mexico (Fig. 5). Both prismatically jointed latite blocks (Fig. 5C), presumably emplaced at elevated temperatures (Smith, this volume), and rounded clasts were collected. At Espinaso Ridge, in Arroyo del Tuerto, both clasts and matrix were sampled from a nearly monolithic breccia with an ash matrix, which, on the basis of field relations, was probably emplaced by a block-and-ash flow (Smith, this volume; Fig. 3). Unlike the Canada de la Cueva flow, field evidence supporting emplacement at high temperature (such as the presence of prismatically jointed blocks or obvious thermal-contraction joints) is largely absent in this deposit. In addition to the latite clasts that are characteristic of this deposit, samples from mafic inclusions and silicified or glassy accidental or accessory clasts were collected.

All samples were collected as oriented cores, using a portable drill equipped with a nonmagnetic drill bit. Sample NRM directions were measured using a cryogenic magnetometer at the University of New Mexico; in order to fully characterize the rock-magnetic and directional properties of the samples, all samples were demagnetized by alternating field (AF) and/or thermal methods. For statistical purposes, only one specimen per sample has been used to calculate the site mean directions reported below; where two or more individually oriented samples were collected from the same block, their directional average was used to calculate the mean direction. Characteristic directions were identified using orthogonal vector diagrams and stereographic projections. Directions from linear segments were calculated using a least-squares technique. In general, the procedures used in this study follow those described in detail by Kent et al. (1981) and McClelland and Druitt (1989).

Results and discussion

Canada de la Cueva: In-situ NRM directions from Canada de la Cueva, prior to demagnetization treatment, are shown in Fig. 6a. Directions are scattered and are evenly distributed between normal- and reverse-polarity inclinations. Of 16 samples from 13 individual blocks, 10 samples from eight blocks (nine from prismatically jointed blocks and one from a rounded, non-jointed clast), are characterized by a common, univectoral decay to the origin of a reverse-polarity remanence during either AF or thermal demagnetization (Fig. 7a, b). The structurally corrected sample and site mean directions ($D = 170^\circ$, $I = -35^\circ$, $\kappa = 45$, $\alpha_{95} = 8.4^\circ$, $n = 8$ blocks) are shown in Fig. 6b. The mean direction is within 20° of the Oligocene (30 Ma) reference direction for this locality (Irving and Irving, 1982). Because this area appears to have experienced a counterclockwise rotation about a vertical axis and down-to-the-south tilting (Brown and Golombek, 1984), direct comparison with the time-averaged Oligocene reference direction may not be strictly appropriate. Accordingly, I have also plotted the mean direction reported by Brown and Golombek (1984) for the Espinaso Formation in Fig. 7b; the Canada de la Cueva result is in excellent agreement with their observed direction.

Four other Canada de la Cueva samples that are rounded or lack obvious thermal-contraction joints contain either single- or dual-component magnetizations that, although well-defined during demagnetization (Fig. 7c, d), have directions that diverge markedly from the mean direction (Fig. 6b). Presumably, these samples contain magnetizations acquired prior to transport and were not heated above their blocking temperatures subsequent to deposition. A remaining sample from a jointed block proved to be directionally unstable during demagnetization.

The well-grouped, univectoral reverse-polarity magnetization derived primarily from the prismatically jointed clasts and their high range of unblocking temperatures ($>500^\circ\text{C}$) suggest that the remanence is a TRM acquired during post-emplacement cooling of the Canada de la Cueva deposit. The lack of a partial TRM within the non-jointed blocks that is similar to the mean direction derived from the jointed blocks indicates that they were probably emplaced at temperatures less than $300\text{-}400^\circ\text{C}$. The mixture of both hot and relatively cold material indicates that this deposit was probably emplaced as a debris flow that included hot blocks derived from a nearby dome.

Arroyo del Tuerto, Espinaso Ridge: In-situ NRM directions from the Espinaso Ridge monolithic breccia samples are shown in Fig. 6c. Both AF and thermal demagnetization of most samples from the latite clasts and ash matrix typically remove a low coercivity or low unblocking temperature ($<250\text{-}350^\circ\text{C}$) remanence of due northerly declination and moderate positive inclination (Fig. 7e, f, g); this is probably a viscous remanent magnetization acquired in the present Earth magnetic field. At higher demagnetizations, a well-defined reverse-polarity magnetization is isolated by either thermal or AF demagnetization in most samples (Fig. 7e, f). This magnetization is unblocked over a wide range of temperatures ($375\text{-}620^\circ\text{C}$) in individual samples,

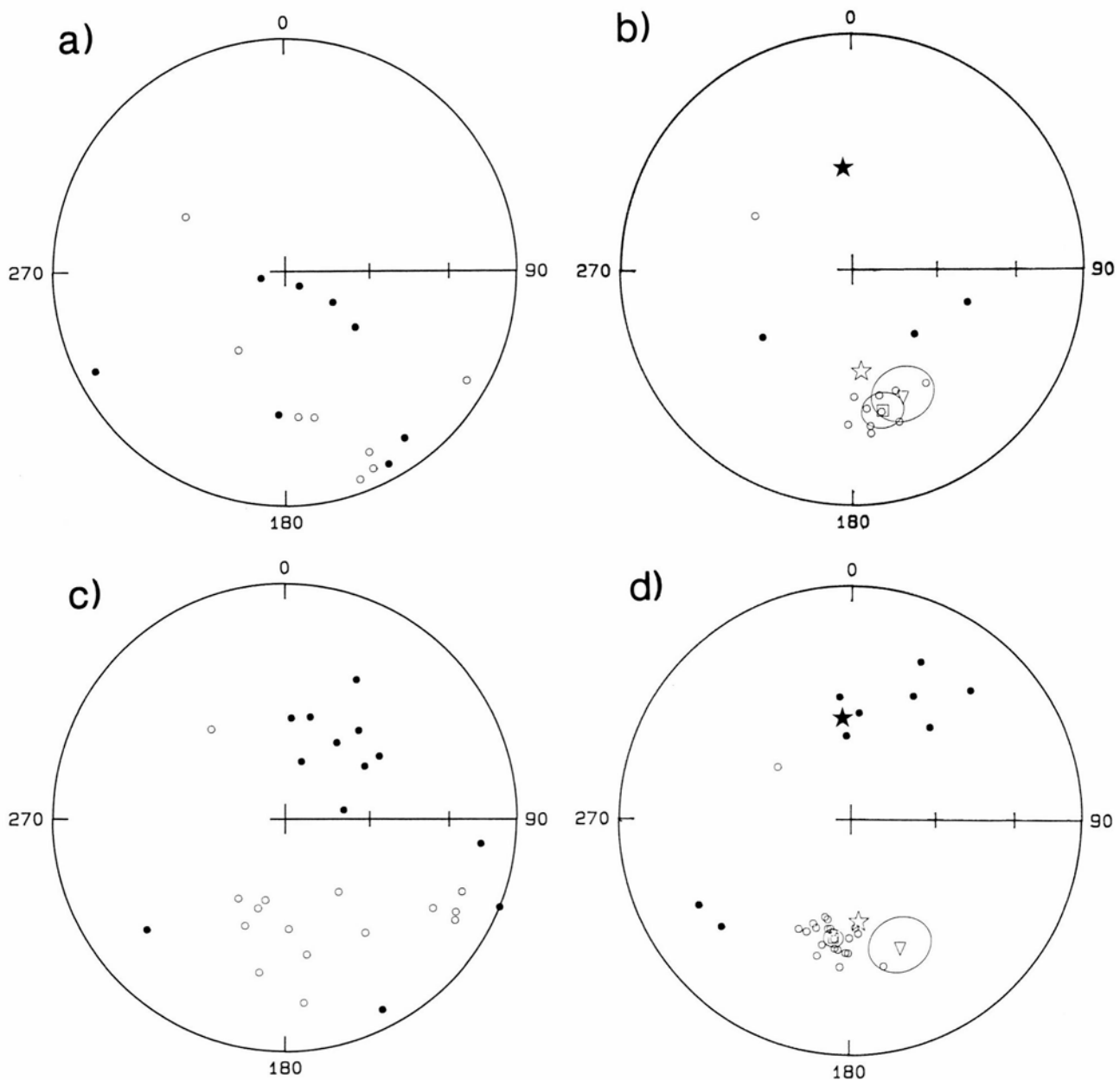


FIGURE 6—Stereographic equal-area projections of paleomagnetic sample directions from Espinaso Formation breccias. **a**, In-situ NRM directions from Cañada de la Cueva deposit. **b**, Structurally corrected characteristic sample and site mean directions from Cañada de la Cueva following AF or thermal demagnetization. **c**, In-situ NRM direction from Arroyo del Tuerto deposit. **d**, Structurally corrected characteristic sample and site mean directions from Arroyo del Tuerto following AF or thermal demagnetization. In all figures, circles = sample directions; squares = site mean directions and associated α_{95} cones of confidence; inverted triangles are the Espinaso Formation mean direction and α_{95} reported by Brown and Golombek (1984) after inverting their normal-polarity direction to reverse polarity; star = normal- and reverse-polarity Oligocene (30 Ma) reference direction for this locality. Open circles are projections on the upper hemisphere (reverse-polarity directions), closed circles are lower hemisphere projections (normal-polarity directions).

suggesting that a combination of titanomagnetite, low-Ti magnetite, and/or hematite contribute to the remanence in individual samples. This is confirmed by Curie temperature determinations from representative samples that show complex, irreversible behavior with inflections at 390-400°C and 520-560°C; all curves are characterized by oxidation of magnetite to hematite during cooling. Such complexities probably explain the erratic behavior observed in some samples after demagnetization to high temperatures.

A small number of samples exhibits similar, but directionally distinct, moderate- and high-temperature directions; an example of such behavior is illustrated in Fig. 7g. In this sample, an initial VRM aligned close to the present Earth

magnetic field (e.g. $D = 346^\circ$, $I = 65^\circ$) is removed at temperatures less than 350°C. Above this temperature two distinct linear segments, recognized by a slight inflection at 440°C, are isolated. Both the moderate-temperature (350-440°C) component ($D = 143^\circ$, $I = -52^\circ$) and the high-temperature (440-630°C) component ($D = 120^\circ$, $I = -43^\circ$) are directionally very similar; such behavior probably reflects a slight rotation of the clasts while they were still hot, but subsequent to deposition. This may be due to post-emplacement compaction or deflation of the deposit.

Seven samples from three latite blocks and a mafic inclusion yield normal-polarity directions approximately anti-parallel to the reverse-polarity directions observed in most

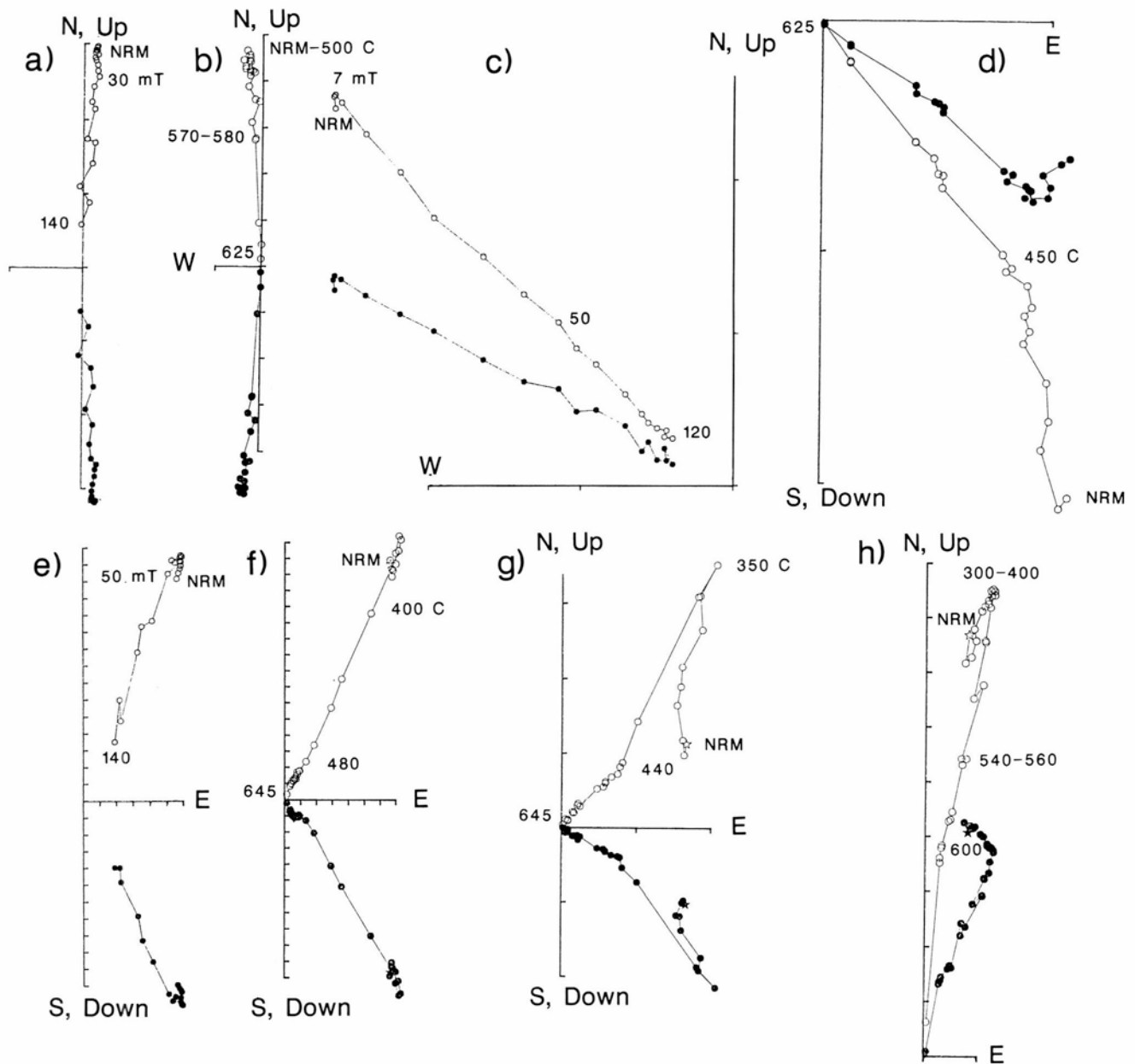


FIGURE 7—Representative orthogonal vector diagrams (in-situ) of Cañada de la Cueva (a–d) and Arroyo del Tuerto samples (e–h) illustrating demagnetization behavior during either AF (a, c, e) or thermal demagnetization (b, d, f–h). Each division = 1×10^{-1} emu/cc, except for h, where each division = 1×10^{-2} emu/cc. In all diagrams the endpoint of the demagnetization vector has been simultaneously projected onto the horizontal (closed circles) and vertical (open circles) planes. Selected demagnetization steps for AF demagnetization given in millitesla (mT); thermal demagnetization steps in °C.

clasts (Fig. 6d). It is unlikely that this small deposit cooled through a complete polarity transition; hence these directions are most readily explained as a VRM that completely dominates the remanence in these samples. Accessory or accidental latite clasts yield either single- or dual-polarity magnetizations that are randomly oriented (Figs. 7h, 6d). Apparently, like many of the Canada de la Cueva clasts, these clasts were never heated sufficiently by the Arroyo del Tuerto flow to even partially reset their magnetizations.

Structurally corrected sample directions are shown in Fig. 6d. The mean direction, calculated from samples with well-grouped reverse-polarity magnetizations ($D = 188^\circ$, $I = -48^\circ$, $\kappa = 99.6$, $\alpha_{95} = 3.3^\circ$, $n = 20$ samples), is similar to the Oligocene reference direction (Fig. 6d), but is somewhat displaced from both the Espinazo Formation mean direction of

Golombek and Brown (1984) and the Canada de la Cueva deposit. This difference is probably not significant given the expected range of secular variation expected at this latitude. As at Canada de la Cueva, this magnetization is probably a TRM imparted during cooling of the deposit.

Maximum unblocking temperatures of 375–425°C for ash-matrix samples that contain low-Ti magnetite (Curie temperatures of 540–560°C) and the absence of a similar partial TRM superimposed upon the accidental clasts suggest that this deposit was emplaced at temperatures no greater than about 400°C. Such an emplacement temperature is consistent with an origin as a small-volume pyroclastic flow, probably associated with the eruption or collapse of a nearby dome (Smith, this volume).

The composition of Ortiz porphyry belt extrusives as recorded in the Espinaso Formation

Gary A. Smith and Daniel W. Erskine

The magmatic centers of the Ortiz porphyry belt (Fig. 1) are each composed of multiple intrusions that can, in a general way, be divided into calc-alkaline and alkaline suites (Disbrow and Stoll, 1957; Sun and Baldwin, 1958; Atkinson, 1961; Maynard et al., 1990 and this volume; Coles, unpubl.). Although there are some ambiguities in field relationship and geochronologic data, Maynard et al. (1990) believe that calc-alkaline magmatism preceded alkaline magmatism, and that a hiatus and change in tectonic stresses intervened between intrusion and extrusion of the two suites. Preserved volcanic rocks are very rare, but the composition of extruded lavas and pyroclastics can be documented indirectly from study of the sediments of the Espinaso Formation. This report presents the results of a preliminary study of Espinaso Formation conglomerate clasts.

The temporal variation in composition of erupted magmas can be approximated by careful consideration of clasts from synvolcanic conglomerates. Although any sediment sample will include mixtures of recently erupted lithologies and older material, a sampling strategy was designed to emphasize the former. Samples were collected in the following order of preference:

- Clasts containing thermal-contraction joints suggesting in-situ cooling from relatively high temperature (Fig. 5d; Harlan, this volume)
- Clasts from monolithologic debris-flow breccias.
- Lowest occurrence of distinctive clast lithology regardless of depositional facies.

Using these criteria, a total of 144 clasts were sampled, 72 of which were point-counted and described petrographically, and 34 of which were analyzed for major-element composition. Selection of samples for modal and geochemical analyses was based on the degree of alteration and the order of preference given above for similar-appearing clasts.

Modal compositions are presented in Fig. 8, showing stratigraphic variation in the proportion of hornblende among the total ferromagnesian silicates (hornblende index). Only calc-alkaline lithologies are recorded by clasts in the sections east of Cerrillos. Stratigraphic variations occur in modal mineralogy that corroborate correlations based on lithologic markers (Fig. 4). Three intervals are recognized. Early deposited clasts of interval I contain a mixture of hornblende-rich (index >0.7) and augite-rich (index <0.4) latites, the latter being distinctly glomeroporphyritic. The alluvial-fan sequence containing these clasts thins dramatically to the east (Fig. 8). Interval II contains only hornblende-rich clasts and also thins rapidly eastward. Interval III is characterized by a wide range in hornblende and augite content, with repeated trends from hornblende-rich to augite-rich compositions.

At the Arroyo del Tuerto type section on Espinaso Ridge, the abrupt decrease in hornblende index above 300 m records the transition from calc-alkaline hornblende—augite latite clasts below, to alkaline augite—biotite latite clasts in the upper part of the section (Fig. 8). The discrete stratigraphic intervals over which detritus of the two magmatic suites are

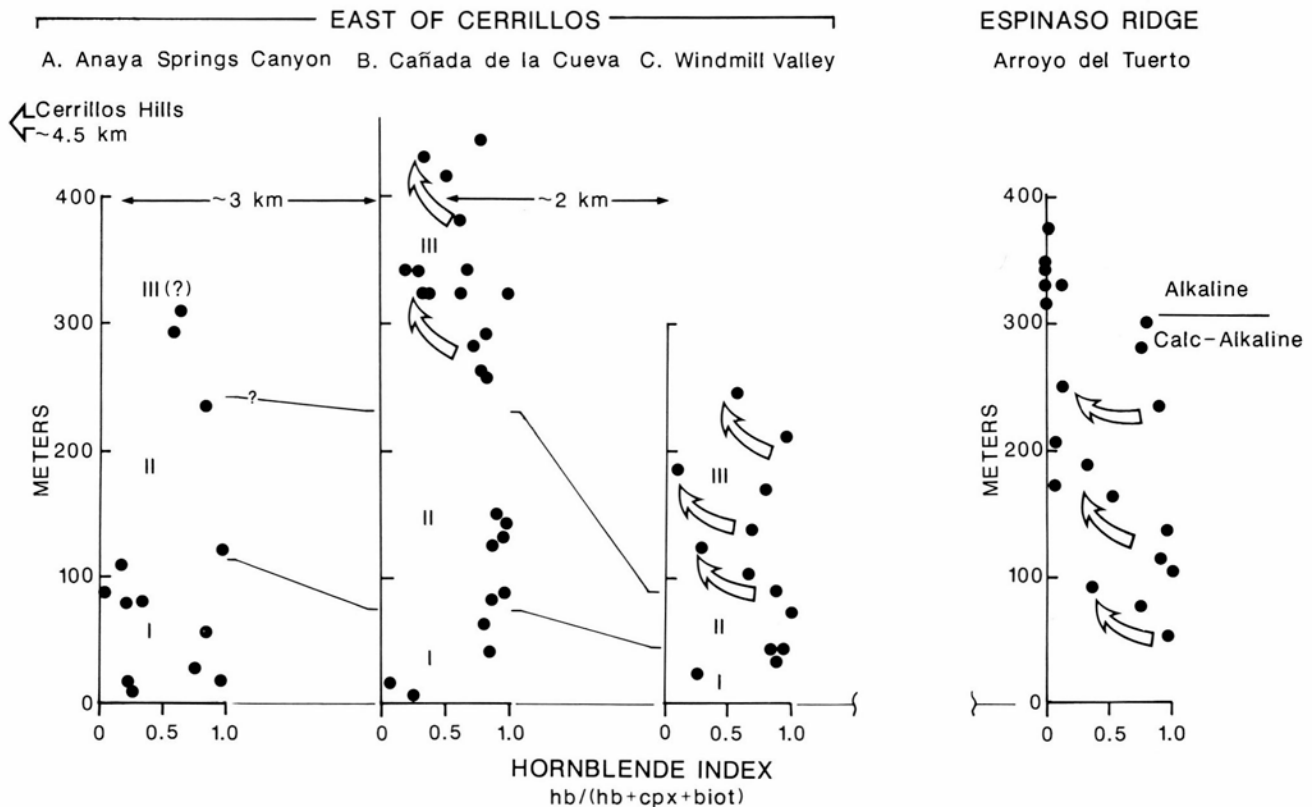


FIGURE 8—Stratigraphic variation of hornblende index in the Espinaso Formation. Datum for correlation of base of sections is the top of a prominent yellow sandstone in the uppermost Galisteo Formation. Correlations between sections near Cerrillos are based on lithology in addition to clast composition. Intervals I, II, and III near Cerrillos are discussed in the section. Open arrows show repetitive trends of upward decrease in hornblende in interval III near Cerrillos and on Espinaso Ridge. Calc-alkaline and alkaline clasts occur in the Espinaso Ridge section, but only calc-alkaline detritus occurs in the Cerrillos section. Locations of sections east of Cerrillos are shown in Fig. 2A.

found corroborates the temporal separation of calc-alkaline and alkaline magmatism. Hornblende index varies greatly within the calc-alkaline clasts. There are no obvious compositional correlations between the Arroyo del Tuerto section and those near Cerrillos. Based on thinning trends in intervals I and II at Cerrillos, distinctive clasts associated with the early phases of volcanism may not be represented at Arroyo del Tuerto, 15-20 km from vent areas, or are mixed in the conglomerates low in the section (Fig. 3, interval I) which, because of their poly lithologic clast compositions, were not extensively sampled. Trends from hornblende-rich to augite-rich clast compositions are apparent in the lower 200 m of the Arroyo del Tuerto section (Fig. 8) and resemble trends in interval III near Cerrillos. The Cerrillos clasts, however, are compositionally distinct from those at Arroyo del Tuerto (Fig. 9).

Major-element geochemical data for Espinaso Formation clasts from near Cerrillos and Arroyo del Tuerto are illustrated in Fig. 9, along with additional new data for clasts from other localities, three lava flows, and three intrusions in the Cerrillos Hills. The compositional range for Espinaso Formation data appears representative of the magmas also recorded in the Ortiz Mountains intrusions, based on unpublished data of David Coles (Colorado State University). Arroyo del Tuerto subalkaline clasts are, for the most part, more siliceous than those sampled near Cerrillos. This may account, in part, for the greater abundance of pyroclastic debris in the Espinaso Ridge section and, along with the dissimilarity in stratigraphic variations in hornblende index between the two localities (Fig. 8), it suggests that Espinaso Formation detritus on Espinaso Ridge and east of Cerrillos was derived from different sources, probably the Ortiz Mountains and Cerrillos Hills, respectively.

More detailed consideration of clast petrology and min-

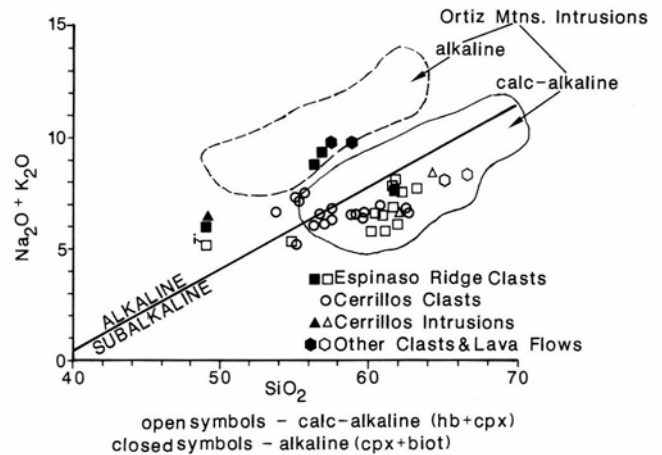


FIGURE 9—Total alkali versus silica variation for Espinaso Formation conglomerate clasts and lava flows, and Cerrillos Hills intrusive rocks compared to intrusive rocks of the Ortiz Mountains (Coles, unpublished report). Calc-alkaline lithologies have a plagioclase + hornblende ± clinopyroxene phenocryst assemblage. Alkaline lithologies have a plagioclase + clinopyroxene ± biotite ± K-feldspar ± hornblende phenocryst assemblage. The square labeled "i" represents the composition of a calc-alkaline lamprophyre inclusion. Alkaline and subalkaline fields are modified from MacDonald and Katsura (1964). Note the generally more silica-rich nature of Espinaso Ridge calc-alkaline clasts than those from Cerrillos, and the overlap in calc-alkaline compositions of Espinaso Ridge clasts and Ortiz Mountains intrusions.

eralogy, in addition to sandstone compositions, will be presented in a later paper. This study does show that valuable information about the composition of erupted materials can be derived from careful study of preserved volcanoclastic sedimentary sequences in cases where the volcanic edifices have been removed by erosion.

Stratigraphy, sedimentology, and volcanology of the Peralta Tuff Member of the Bearhead Rhyolite (Stops 4, 5, and 6)

Gary A. Smith

Directions to Stops 4, 5, and 6

Stops 4 through 6 are close to one another at, and near, a prominent feature known as the Tent Rocks (Fig. 2B). From Albuquerque or Santa Fe, take 1-25 to exit 264 and then head west on NM-16 for 8.3 mi. Turn right at the junction with NM-22 and continue for 4.5 mi on NM-22 to Cochiti Pueblo, being certain to make the marked left turn opposite the center of Cochiti Dam. At Cochiti Pueblo, turn right onto USFS road 266 and continue 4.9 mi to Tent Rocks. The traverse for Stop 4 follows a narrow canyon at the northeast edge of the Tent Rocks outcrops (Fig. 2B). To reach Stops 5 and 6, continue westward on USFS road 266 for 0.5 mi and turn right onto a narrow gravel track (Fig. 2B). To proceed farther, you will need to obtain permission and gate keys from private-property owners.

Tent Rocks (Stop 4)

The Peralta Tuff at Tent Rocks consists mainly of conglomeratic volcanic sandstones and sandy volcanic conglomerates with intercalated primary pyroclastic deposits

(Fig. 10). Nearly all of the sedimentary facies consist of poorly sorted scour- and fill-bedded units that are typical of deposition by flashy, poorly confined to unconfined shallow braided streams and sheetfloods (e.g. Smith, 1987). Massive, generally matrix-supported debris-flow deposits are rare but do occur. Conspicuous orange layers mark highly burrowed and oxidized, but otherwise poorly developed paleosols, which are typically associated with bioturbated pumice-fall layers. Most of the sediments are derived from the large, polygenetic rhyolite-dome complex at Bearhead Peak (8.5 km to the northwest) and its peripheral pyroclastic flow fans. Rapid downslope decrease of maximum grain size (Fig. 10) and downslope decrease in channel depth (510 m to 2-3 m over 5 km) are characteristic of alluvial fans.

The alluvial-fan strata are intercalated with a variety of primary pyroclastic facies. Most of the rhyolitic pyroclastic debris consists of angular, slightly vesicular to dense fragments whose angular morphology and limited vesiculation are typical of phreatomagmatic eruptions (Heiken and Wohletz, 1987). These fragments were initially deposited by

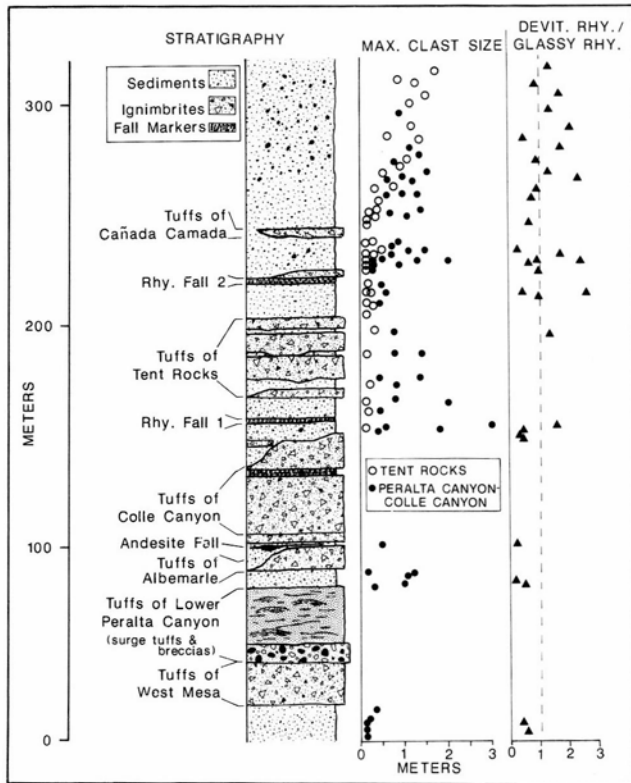
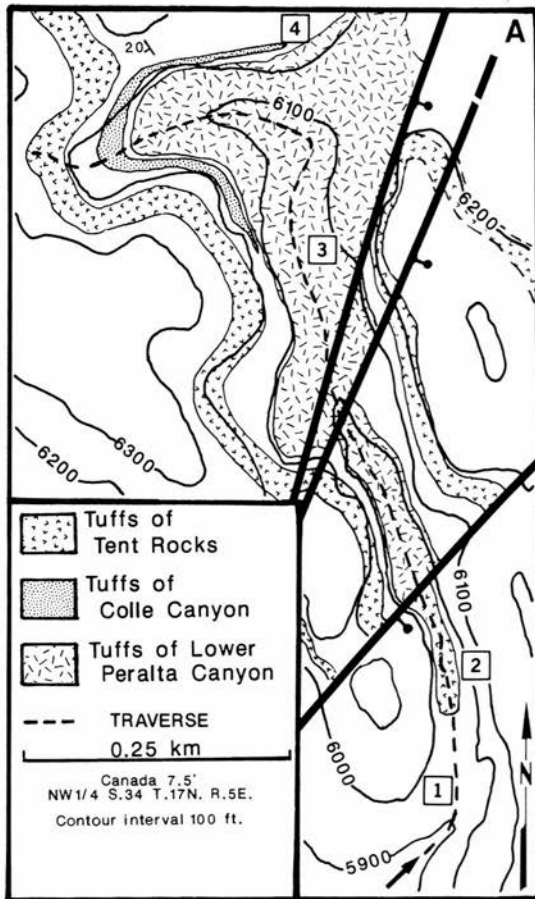


FIGURE 10—Generalized stratigraphy of the Peralta Tuff Member of the Bearhead Rhyolite in the Peralta Canyon – Tent Rocks area. Names of primary pyroclastic units are informal. Two Bearhead Rhyolite flows/domes in the field area are not shown in this diagram. The rhyolite of Bear Jump was extruded following eruption of either the tuffs of West Mesa or the tuffs of Albemarle. The rhyolite of lower Peralta Canyon was emplaced following eruption of the tuffs of lower Peralta Canyon. Columns at right show variation in maximum clast size and clast compositions in sedimentary units. Note the marked downslope decrease in maximum clast size between Peralta Canyon – Colle Canyon and Tent Rocks composite sections, which are located only 4–5 km apart. See text for discussion of vertical variation in clast size and composition.

pyroclastic falls, flows, and surges. The fall deposits are typically plane-bedded, with separate beds marked by differences in grain size or proportions of juvenile glassy pyroclasts and accidental lithic fragments; the bedded character reflects variations in eruption processes at the vent. At least 20 falls occur in the section at Tent Rocks. Most are associated with paleosols and are variably bioturbated (Fig. 11B); preservation was generally limited to inactive depositional tracts on the alluvial-fan surface. Several of the finer-grained ash-fall units are overlain by low- to high-angle crossbedded ash representing eolian reworking of the fall (Smith and Katzman, in press; see also Stop 5). The massive, poorly sorted, white pyroclastic-flow deposits contain varying proportions of ash, pumice, dense perlitic rhyolite glass, and darker accessory and accidental clasts of



4 Swale fill sequence: A swale was eroded on the flank of the lower Peralta Canyon tuff cone and subsequently filled by primary and reworked tephra, separated by paleosols, and the tuffs of Colle Canyon. The most conspicuous of the reworked fallout layers is a lenticular, black andesitic tephra.

3 Tuffs of lower Peralta Canyon: Matrix-supported breccias and cross-bedded, surge-deposited tuffs represent the outer flanks of a tuff ring centered 2.5 km to the northwest. Details of the stratigraphy are shown in Figure 12. The lower unit consists of debris-flow deposits intercalated with coarse-grained surge deposits. The upper unit is composed of sand-wave cross-bedded surge deposits.

2 Tuffs of Tent Rocks: Three of four sequences of ignimbrites comprising this map unit are exposed here, each recording a separate episode of activity at unidentified Bearhead Rhyolite vents. Each multiple-flow-unit sequence is separated by thin alluvial and eolian sediments and paleosols.

1 Upper Peralta Tuff: Well-exposed fall deposits and oxidized paleosols near the mouth of the canyon are overlain by the upper coarse-grained, sediment-dominated part of the section.

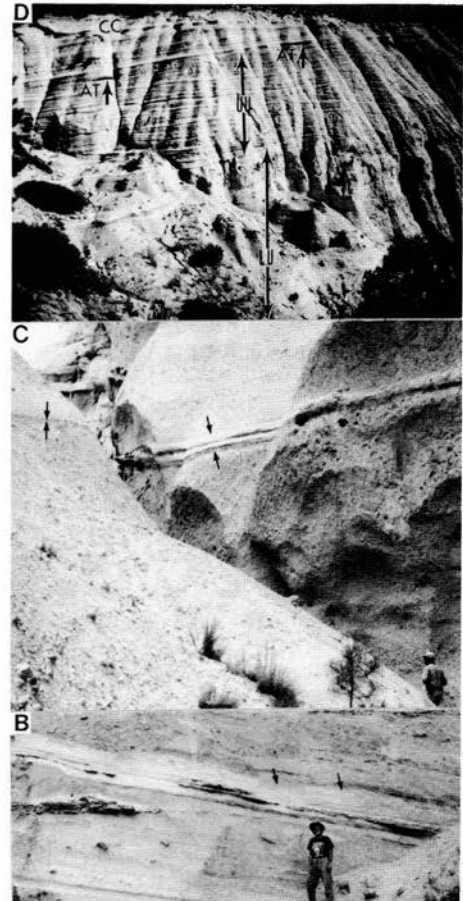


FIGURE 11—Stop 4, Tent Rocks. A, Geologic map and description of traverse. B, Poorly sorted sediments and bioturbated, slightly cemented pumice-fall deposits (arrows) in interval I. C, Ignimbrites of the tuffs of Tent Rocks. Arrows indicate contact between ignimbrite packages marked by weathered surface on left, and intervening fall-out and wind-reworked ashes on right. D, Tuffs of lower Peralta Canyon showing lower debris-flow-dominated unit (LU) and upper surge-dominated unit (UU). Overlying units, including the tuffs of Colle Canyon (CC) and lenticular reworked, black andesitic tephra (AT) form part of swale-fill sequence.

various compositions. None of the Peralta Tuff pyroclastic-flow deposits are welded because of the relatively small volumes and thicknesses (0.5 to 3.0 m) of the deposits and the cooling effects of the water—magma interaction during phreatomagmatic eruptions. Some thermal oxidation did occur, resulting in orange to pink colors in some units. Pyroclastic-surge deposits are moderately sorted, crossbedded tuffs and lapilli tuffs associated with fall beds and volcanic bombs up to 0.5 m across.

Nearly all of the primary pyroclastic deposits occur in the lower two-thirds of Tent Rocks section (Fig. 10). The sedimentary facies are notably coarser and darker-colored in the upper half of the section. The grain-size change roughly coincides with a decrease in the abundance of light-colored vesicular and dense glassy rhyolite clasts typical of the bombs and lapilli in the primary pyroclastic units, and an upward increase in partly to fully devitrified rhyolite clasts derived from the interiors of rhyolite domes (Fig. 10). The compositional and grain-size changes are interpreted as reflecting a change in sediment supply from an abundance of relatively fine-grained ash and lapilli, during the peak of pyroclastic activity, to a greater contribution of coarse epiclasts generated by weathering and dissection of the dome complexes following cessation of eruptions.

A traverse up the narrow slot canyon at the northeast corner of the Tent Rocks crosses much of the local section in a number of fault blocks (Fig. 11). Geologic features along the traverse are illustrated and described in Figs. 11 and 12. The highlight of this traverse is the observation of the tuffs of lower Peralta Canyon (Figs. 10, 11, 12), which represent the outer flanks of an annular phreatomagmatic tuff ring that was centered 2.5 km northwest of here (Fig. 2B). The initial phreatomagmatic explosions ejected slurries of juvenile pyroclastics and basin-fill sediments. The resulting debris-flow deposits are interbedded with coarse pyroclastic-surge deposits and accretionary-lapilli and ash-fall layers (lower unit of Fig. 12). The eruption culminated in the accumulation of 30 m of sand-wave crossbedded surge deposits that are notable for the preservation of steep stoss sides, rounded to sharp crests, and gentle lee sides of the migrating bedforms. At least 1.5 m of pumice fall accumulated on top of the surge subunit but was largely removed by erosion of gullies and swales on the flanks of the tuff ring. Outcrops 4 km to the north show that this eruption followed the climax of, but temporally overlapped with, a similar eruption at Bearhead Peak that produced the tuffs of West Mesa (Fig. 10).

Eolian tuff, lower Peralta Canyon (Stop 5)

Stop 5 is adjacent to a rhyolite dome (Fig. 2B) that marks the vent for the tuff ring comprising the tuffs of lower Peralta Canyon at Tent Rocks. The margin of the dome is composed of glassy, brecciated rhyolite forming a carapace around flow-banded devitrified rhyolite of the dome interior that will be seen along the road between Stops 5 and 6. This dome was completely buried by the alluvial fan that extended southeastward from Bearhead Peak. Sediments exposed along the southeast margin of the dome are stratigraphically equivalent to those seen at the mouth of the canyon at Stop 4. The most remarkable feature at this locality is the occurrence of the eroded remnant of an eolian dune that formed from wind reworking of an ash-fall deposit upon which the eolian tuff rests (Fig. 13). This crossbedded unit is much

better sorted than the surge deposits seen at Stop 4, exhibits wind-ripple and grain-flow strata, and bedsets typical of eolian sands (Smith and Katzman, in press).

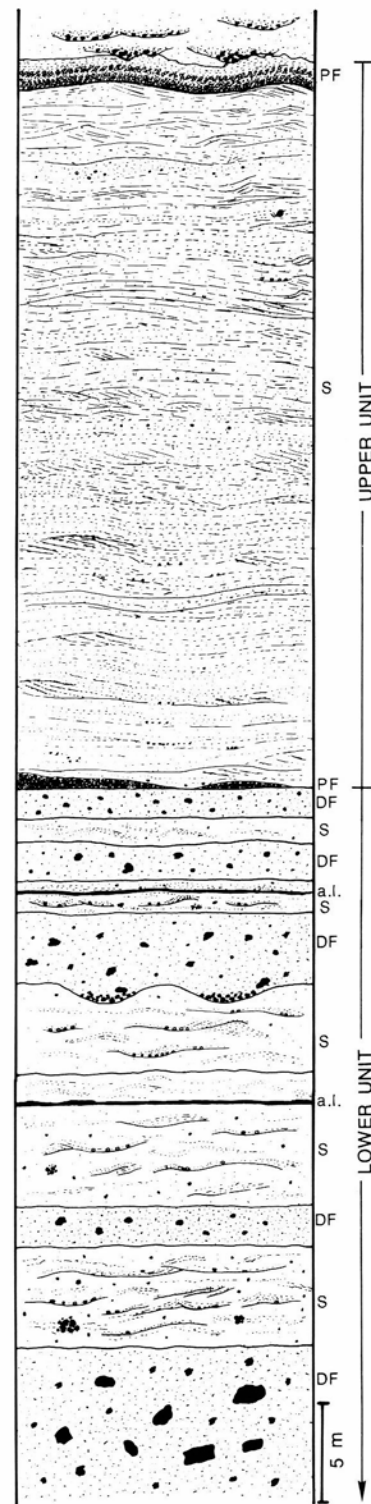


FIGURE 12—Stratigraphy of the tuffs of lower Peralta Canyon at Tent Rocks. The lower unit consists of massive debris-flow deposits (DF) composed of ashy matrix surrounding volcanic clasts up to 2 m across and clasts of underlying rift-fill sediments ranging from abundant fist-sized, pink siltstone fragments to highly deformed sandstone and conglomerate blocks up to 3 m across. These deposits are intercalated with coarse-grained, crossbedded surge deposits (S) and accretionary-lapilli fall beds (a.l.). The upper unit consists of a thick sequence of sand-wave crossbedded surge deposits (S) underlain and overlain by discontinuously preserved pumice-fall lapillistones (PF).



FIGURE 13—Plane-bedded pumice-fall deposit overlain by crossbedded eolian tuff at Stop 5. Height of crossbed sets is about 3 m. Structural dip is 12° to the left (southwest).

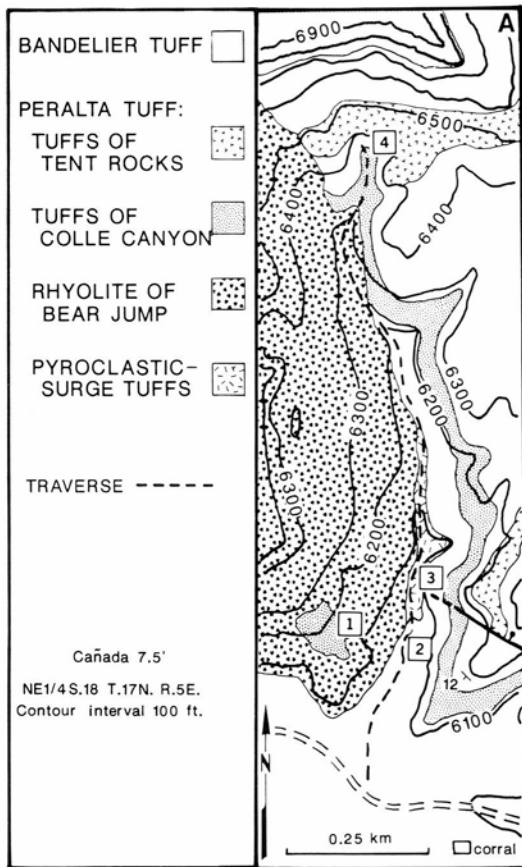
The influence of lava-flow morphology on subsequent deposition of alluvium and pyroclastic flows (Stop 6)

Stop 6 consists of a traverse up a narrow tributary canyon to Peralta Canyon that leads toward Oak Mesa and skirts the edge of a 200 m thick rhyolite flow (rhyolite of Bear

Jump) that extended 5 km southward from Bearhead Peak (Fig. 14). The presence of this thick lava flow on the alluvial/pyroclastic-flow fans profoundly influenced subsequent sedimentation, pyroclastic-flow transport and deposition, and geometry of younger deposits. Highlights of this traverse are illustrated and described in Fig. 14.

Autoclastic breccias are well exposed along the margin of the rhyolite of Bear Jump (Fig. 14B). These were the source for steep debris-flow-dominated fans whose deposits are restricted to this area (Fig. 14C) marginal to the flow, and extend less than 300 m to the east. While making this traverse, note that structural dip is southwestward and that depositional dips are steeply inclined (25-35°) to the east.

The most noteworthy volcanological features seen along this traverse are associated with the tuffs of Colle Canyon. The tuffs of Colle Canyon include as many as 25 pyroclastic-flow units and less voluminous fall deposits erupted during one eruptive episode at Bearhead Peak. The tuffs thicken eastward where the convex-up, lobate morphology of a pyroclastic-flow fan is preserved. In the area of this traverse, some pyroclastic flows moved southward adjacent to the rhyolite of Bear Jump, whereas others, having been erupted onto the top of the lava flow close to the vent, spilled off the steep front of the lava (Fig. 14). Several of these latter flow units contain planebedded and crossbedded intervals that can be traced southeastward, away from the flow front, into the typical, massive ignimbrite. Texturally, the cross-bedded intervals retain the poorly sorted and fine-ash-rich



4 Pyroclastic stratigraphy.
Tuffs of Colle Canyon: 12 lower flow units, 3.2 m of middle perlite fall, several thin upper Colle Canyon flow units, intercalated with fall beds. Rhyolite marker tephra 1: distinctive white base, pink middle, and gray top. Tuffs of Tent Rocks: four ignimbrite sequences. All units lap against or are erosionally truncated adjacent to the rhyolite of Bear Jump.

3 Pyroclastic-surge deposits.
Rhyolite breccia rests on >10 m of cross-bedded surge deposits capped by a 1.5 m-thick fall bed. Crossbed asymmetry indicates source to NW. Tuffs and the rhyolite of Bear Jump were probably erupted during the same episode.

2 Volcaniclastic breccias.
Carapace breccias (W. side of wash): Tightly packed, perlite-clast breccias, massive to inverse-graded beds. Part of the chilled, autoclastic carapace of the rhyolite of Bear Jump; scree generated during flow movement and as subsequent talus slides. Debris-flow breccias (E. side of wash): Better rounded perlite clasts largely supported in ash matrix, intercalated with primary and reworked fall deposits. Facies records small fans at mouths of gullies cut into the carapace breccia.

1 Cross-bedded ignimbrites.
Tuffs of Colle Canyon. These deposits resulted from turbulence generated as pyroclastic flows descended the steep flow front of the rhyolite of Bear Jump. Cross-bedded flow units retain the textural attributes of ignimbrites, but have bedding characteristics of surge deposits. Cross-bedded units can be traced southeastward, away from the flow front, into typical massive ignimbrite.

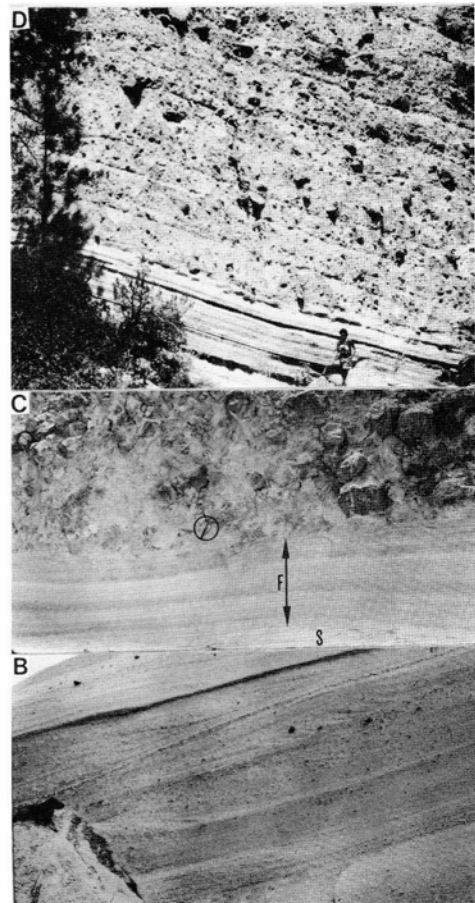


FIGURE 14—Stop 6, Peralta Canyon. A, Geologic map and description of highlights of the traverse. B, Bedded ignimbrites in the tuff of Colle Canyon produced by pyroclastic flows spilling down the steep front of the rhyolite of Bear Jump. Flow was from right to left. Note the steep, sigmoidal cross-strata on stoss side and more gentle, tabular cross-strata on lee side of crossbed set near center of view. C, Carapace breccia resting on bedded pumice-fall deposits (F) draped over surge deposits (S). D, Debris-flow deposits resting on bedded pumice-fall deposit (behind figure). Apparent structural dip is 10° to the left; note relatively steep depositional dip of these debris-flow-dominated fan deposits.

character of pyroclastic-flow deposits despite illustrating bedding that is more typical of pyroclastic-surge deposits. The stoss-side cross-strata exhibit steep, sigmoidal forms in contrast to more gentle, tabular, lee-side strata (Fig. 14B). Turbulence apparently resulted from acceleration of the flows as they descended the steep flow front and decayed as the flows subsequently decelerated upon crossing lower-gra-

dient slopes at the foot of the flow; there is no indication of entrainment of air and dilution of the flows to surges as they crossed this topographic irregularity. Other flow units exhibit marginal onlap of the lava flow along a steep contact near the north end of the traverse and are typical, massive ignimbrite; this argues against generation of turbulence as a marginal boundary eddy.

Preliminary $^{40}\text{Ar}/^{39}\text{Ar}$ age determinations and paleomagnetic results from the Peralta Tuff Member, Bearhead Rhyolite, Tent Rocks area, Jemez Mountains, New Mexico

William C. McIntosh and Steve S. Harlan

Introduction

Paleomagnetic and geochronologic studies of the Peralta Tuff Member of the Bearhead Rhyolite and associated lavas exposed in the Tent Rocks area of the Jemez Mountains (Fig. 10) were initiated for two purposes: (1) to use high-precision $^{40}\text{Ar}/^{39}\text{Ar}$ dating and paleomagnetic analysis to constrain the timing and duration of the rhyolitic activity that produced the Peralta tuff; and (2) to use paleomagnetic analysis of thermoremanent magnetization to evaluate the emplacement temperatures of primary pyroclastic units in the Peralta Tuff. Analysis of samples is not yet complete; this report summarizes some preliminary findings.

$^{40}\text{Ar}/^{39}\text{Ar}$ dating

Five samples were collected for $^{40}\text{Ar}/^{39}\text{Ar}$ analysis, four from pumice-fall deposits distributed throughout the Peralta Tuff sequence, and a fifth from the rhyolite of lower Peralta Canyon (Fig. 10). The fallout-deposit samples were split into pumice and loose crystal fractions, and sanidine separates (>99.5% purity) were prepared from these splits and from the rhyolite lava. To date five samples have been analyzed at the U.S. Geological Survey isotopic dating facility in Reston, Virginia, using analytical procedures similar to those described in McIntosh et al. (in press).

Results from samples of the stratigraphically lower pumice-fall deposit, the tuff of West Mesa, and the rhyolite lava show generally flat $^{40}\text{Ar}/^{39}\text{Ar}$ age spectra (Fig. 15), yielding statistically indistinguishable plateau ages ranging from 6.81 ± 0.2 to $6.87 \pm .02$ Ma (Table 1). The remaining two samples, from pumice falls immediately below the tuffs of Canada Camada (Fig. 10), failed to yield age plateaus (Fig. 15), probably due to the presence of abundant large glass

inclusions. Their total gas ages (6.71 and 7.08 Ma, Table 1) bracket the plateau ages from the samples lower in the sequence. Although total gas ages are considered to be less reliable than the plateau ages, these preliminary data are consistent with eruption of the entire Peralta sequence within a brief interval of time.

TABLE 1— $^{40}\text{Ar}/^{39}\text{Ar}$ results from the Peralta Tuff sequence.

sample	deposit	unit (Fig. 10)	fraction	result	age	error
GSPT1	pumice fall	tuffs of West Mesa	pumice	plateau	6.87	± 0.02
GSPT1	pumice fall	tuffs of West Mesa	crystals	plateau	6.85	± 0.02
GSPT5	lava	rhyolite of lower Peralta Canyon		plateau	6.81	± 0.02
GSPT3	pumice fall	tuffs of Cañada Camada	pumice	total gas	7.08	-----
GSPT3	pumice fall	tuffs of Cañada Camada	crystals	total gas	6.71	-----

All ages calculated relative to Fish Canyon Tuff (28.83 Ma) flux monitor. "Total gas" indicates analyses that failed to produce a plateau. No errors were calculated for these age determinations; they are considered to be less reliable than the plateau ages.

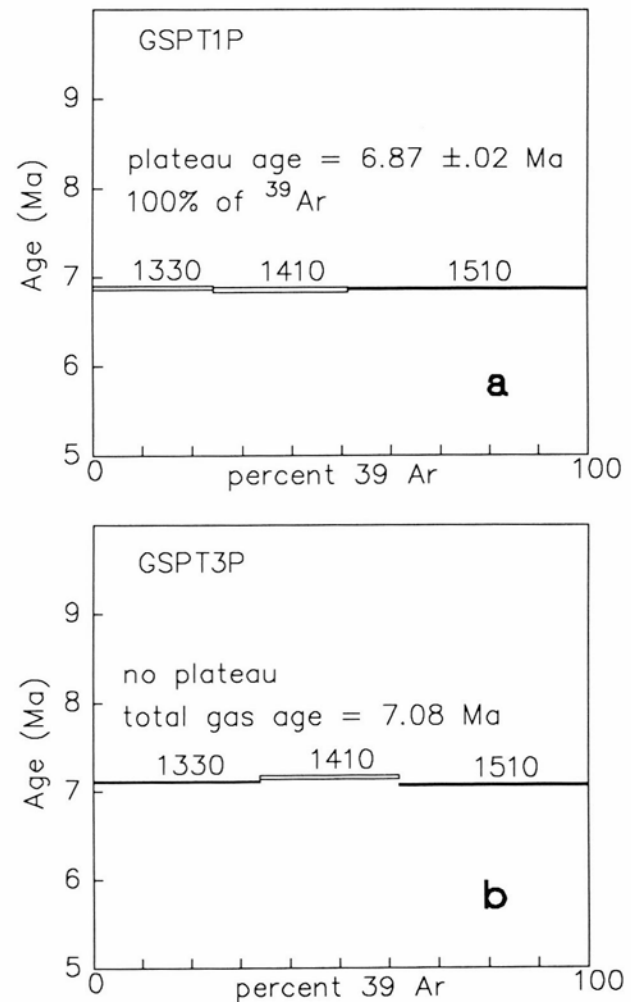


FIGURE 15—Representative $^{40}\text{Ar}/^{39}\text{Ar}$ age spectra from Peralta Tuff sanidine separates. **a**, Completely concordant age spectrum for sample GSPT1, yielding a plateau age of 6.87 ± 0.02 Ma. **b**, Slightly disturbed spectrum that failed to meet plateau criteria; this sample, GSPT3, contains abundant large melt inclusions that probably adversely affect the data.

Paleomagnetism

Oriented samples for paleomagnetic analysis were collected from 25 sites throughout the Peralta Tuff section shown in Fig. 10. At three sites in lavas, 8 to 12 cores were collected using a portable drill; individual cores were oriented using both sun and magnetic compasses. At 22 sites in tuffs, 8 to 12 pumice or lithic clasts were collected using either the drill or taking oriented block samples. Samples from selected sites have been analyzed using a cryogenic magnetometer at the University of New Mexico. Initially, pilot samples from each site were subjected to stepwise alternating field (AF) demagnetization to peak fields of 140 mT. For three sites, thermal demagnetization behavior has also been investigated using stepwise heating to temperatures of 600°C.

Samples from the three sites in the Bearhead Rhyolite lavas are characterized by nearly univectoral behavior during AF demagnetization, indicating the presence of a single well-defined magnetization component throughout the demagnetization interval (Fig. 16a). Sample remanence directions are well-grouped at the site level; all three sites yield reverse-polarity site mean directions with southerly declinations ($D = 130^\circ$ to 180°) and moderate negative inclinations ($I = -45^\circ$ to -60°).

Demagnetization behavior of samples from sites in the tuffs is usually more complex and typically varies with lithology. White, highly inflated pumice clasts typically yield low-intensity, randomly oriented remanence directions and unstable AF demagnetization behavior, probably reflecting Fe—Ti oxides in the superparamagnetic size range. Denser vesiculated rhyolite and accidental or accessory lithic clasts show natural remanent magnetizations that tend to be poorly grouped at the site level, although reverse-polarity directions are most common. Most of the samples show approximately univectoral decay of the magnetization vector during AF demagnetization (Fig. 16b), but more complex AF demagnetization behavior was observed in some samples (Fig. 16c).

Preliminary results from the three sites that were thermally demagnetized indicate that samples from these ignimbrites carry a paleomagnetic record of their emplacement or "setting" temperatures. Magnetizations unblocked at low temperatures (250–440°C) are generally well-grouped and display reverse-polarity directions, whereas magnetizations unblocked at higher temperatures tend to be randomly directed (Fig. 16d). The lower-temperature magnetizations are interpreted to have been acquired by cooling subsequent to deposition of the clasts, thus recording emplacement at temperatures between 250 and 400°C. This method of paleomagnetically estimating emplacement temperature has been successfully applied elsewhere (e.g. Hoblitt and Kellogg, 1979).

Although the paleomagnetic study is still in its initial stages, the poorly grouped but generally reversely polarized directions shown by well-behaved samples from all sites in the Peralta Tuff are interpreted as resulting from emplacement below their maximum blocking temperatures (e.g. 580°C, the Curie temperature of pure magnetite) during a period of reversed geomagnetic polarity.

Discussion

Preliminary data from the Peralta Tuff and Bearhead Rhyolite in the Bearhead Peak—Tent Rocks area indicate that

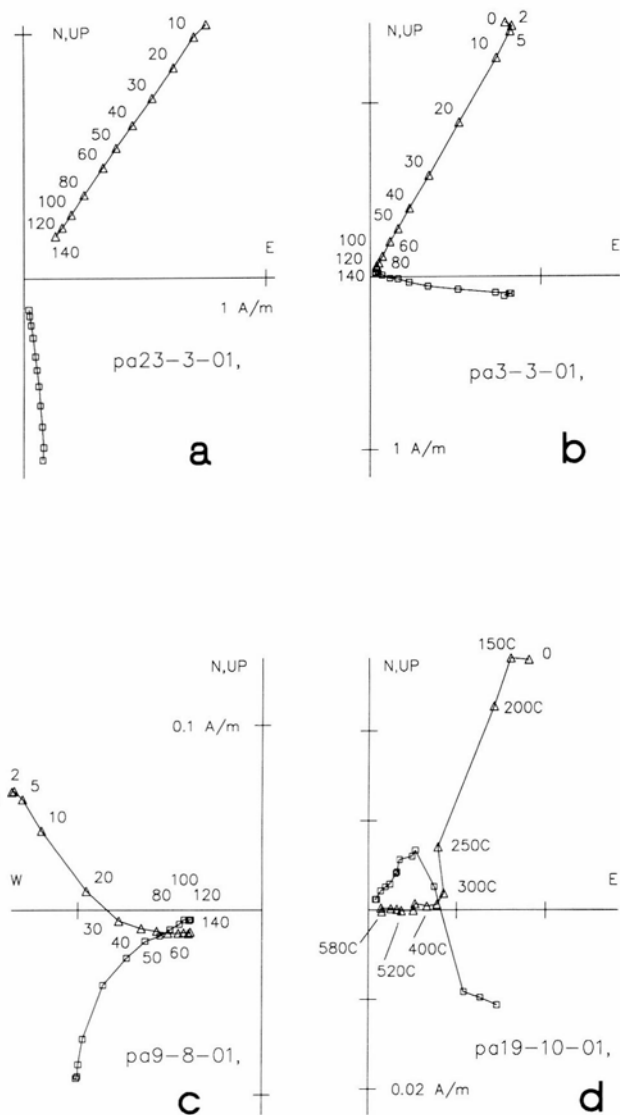


FIGURE 16—Representative orthogonal demagnetization diagrams (in-situ) of Bearhead Rhyolite and Peralta Tuff samples illustrating typical behavior during AF or thermal demagnetization. **a**, AF demagnetization of Bearhead Rhyolite lavas typically produces univectoral decay of the magnetization vector to the origin of the diagram, indicating the presence of a single, well-defined magnetization component. **b**, An example of an ignimbrite clast that also shows the isolation of a single component of magnetization during AF demagnetization. **c**, An example of multi-component behavior of an ignimbrite clast observed during AF demagnetization. **d**, Thermal demagnetization of an ignimbrite clast with a low-unblocking temperature, reverse-polarity magnetization that is isolated between temperatures of 150 and 400°C; such behavior is interpreted as evidence for emplacement at temperatures between ~250 and ~400°C. In all diagrams the endpoint of the demagnetization vector is simultaneously projected on the horizontal (squares) and vertical (triangles) planes. AF demagnetization steps in **a**, **b**, and **c** given in millitesla; thermal demagnetization steps in **d** given in °C.

they were emplaced during a single geomagnetic reversed-polarity interval near 6.85 Ma. The geomagnetic polarity time scale of Berggren et al. (1985) shows three potentially correlative reverse-polarity intervals at 6.50 to 6.70 Ma, 6.78 to 6.85 Ma, and 7.28 to 7.35 Ma. The maximum eruptive interval for the Peralta Tuff is therefore estimated at 70 to 200 Ka. Additional $^{40}\text{Ar}/^{39}\text{Ar}$ work now in progress will further constrain this eruptive interval.

Combined references

- Aramaki, S., and Akimoto, S., 1957, Temperature estimation of pyroclastic deposits by natural remanent magnetism: *American Journal of Science*, v. 255, pp. 617-627.
- Atkinson, W. W., Jr., 1961, Geology of the San Pedro Mountains, Santa Fe County, New Mexico: New Mexico Bureau of Mines & Mineral Resources, Bulletin 77, 50 pp.
- Bachman, G. O., 1975, Geologic map of the Madrid quadrangle, Santa Fe and Sandoval Counties, New Mexico: U.S. Geological Survey, Geologic Quadrangle Map GQ-1268, scale 1:62,500.
- Baldrige, W. S., Damon, P. E., Shafiqullah, M., and Bridwell, R. J., 1980, Evolution of the central Rio Grande rift, New Mexico: New potassium-argon ages: *Earth and Planetary Science Letters*, v. 51, pp. 309-321.
- Berggren, W. A., Kent, D. V., and Flynn, J. J., 1985, Jurassic to Paleogene: Part 2, Paleogene geochronology and chronostratigraphy; *in* Snelling, N. J. (ed.), *The chronology of the geological record*: Geological Society of London, Memoirs, v. 10, pp. 141-195.
- Brown, L. L., and Golombek, M. P., 1984, Block rotations in the Rio Grande rift, New Mexico: *Tectonics*, v. 5, pp. 423-438.
- Disbrow, A. E., and Stoll, W. C., 1957, Geology of the Cerrillos area, Santa Fe County, New Mexico: New Mexico Bureau of Mines & Mineral Resources, Bulletin 48, 73 pp.
- Gardner, J. N., Goff, F., Garcia, S., and Hagan, R. C., 1986, Stratigraphic relations and lithologic variations in the Jemez Volcanic Field, New Mexico: *Journal of Geophysical Research*, v. 91, no. B2, pp. 17631778.
- Heiken, G., and Wohletz, K., 1987, Tephra deposits associated with silicic domes and lava flows; *in* Fink, J. H. (ed.), *The emplacement of silicic domes and lava flows*: Geological Society of America, Special Paper 212, pp. 55-76.
- Hoblitt, R. P., and Kellogg, K. S., 1979, Emplacement temperature of unsorted and unstratified deposits of volcanic rock debris as determined by paleomagnetic techniques: *Geological Society of America, Bulletin*, v. 90, pp. 633-642.
- Ingersoll, R. V., Cavazza, W., Baldrige, W. S., and Shafiqullah, M., 1990, Cenozoic sedimentation and paleotectonics of north-central New Mexico: Implications for initiation and evolution of the Rio Grande rift: *Geological Society of America, Bulletin*, v. 102, pp. 1280-1296.
- Irving, E., and Irving, G. A., 1982, Apparent polar wander paths, Carboniferous through Cenozoic and the assembly of Gondwana: *Geophysical Surveys*, v. 5, pp. 141-188.
- Kautz, P. F., Ingersoll, R. V., Baldrige, W. S., Damon, P. E., and Shafiqullah, M., 1981, Geology of the Espinazo Formation (Oligocene), north-central New Mexico: *Geological Society of America, Bulletin*, v. 92, pt. I, pp. 980-983, pt. II, pp. 2318-2400.
- Kent, D. V., Dragoslav, N., Pescatore, T., and Sparks, R. S. J., 1981, Paleomagnetic determination of emplacement temperature of Vesuvius AD 79 pyroclastic deposits: *Nature*, v. 290, pp. 393-396.
- Lucas, S. G., 1982, Vertebrate paleontology, stratigraphy, and biostratigraphy of Eocene Galisteo Formation, north-central New Mexico: New Mexico Bureau of Mines & Mineral Resources, Circular 186, 34 pp.
- Maynard, S. R., Martin, K. W., Nelsen, C. J., and Schutz, J. L., 1990, Geology and gold mineralization of the Ortiz Mountains, Santa Fe County, New Mexico: *Mining Engineering*, v. 42, pp. 1007-1011.
- MacDonald, G. A., and Katsura, T., 1964, Chemical composition of Hawaiian lavas: *Journal of Petrology*, v. 5, pp. 82-133.
- McClelland, E. A., and Druiitt, T. H., 1989, Paleomagnetic estimates of emplacement temperatures of pyroclastic deposits on Santorini, Greece: *Bulletin of Volcanology*, v. 51, pp. 16-27.
- McIntosh, W. C., Sutter, J. F., Chapin, C. E., and Kedzie, L. L. (in press), High-precision $^{40}\text{Ar}/^{39}\text{Ar}$ sanidine geochronology of ignimbrites in the Mogollon-Datil volcanic field, southwestern New Mexico: *Bulletin of Volcanology*.
- Smith, G. A., 1987, Sedimentology of volcanism-induced aggradation in fluvial basins: Examples from the Pacific Northwest, U.S.A.; *in* Ethridge, F. G., Flores, R. M., and Harvey, M. D. (eds.), *Recent developments in fluvial sedimentology*: Society of Economic Paleontologists and Mineralogists, Special Publication 39, pp. 217-229.
- Smith, G. A. (in press), Facies sequences and geometries in continental volcanoclastic sediments; *in* Fisher, R. V., and Smith, G. A. (eds.), *Sedimentation in volcanic settings*: SEPM, The Society for Sedimentary Geology, Special Publication.
- Smith, G. A., and Katzman, D. (in press), Discrimination of eolian and pyroclastic surge processes in the generation of cross-bedded tuffs, Jemez Mountains volcanic field, New Mexico: *Geology*.
- Steams, C. E., 1953, Early Tertiary volcanism in the Galisteo-Tongue area, north-central New Mexico: *American Journal of Science*, v. 251, pp. 415-452.
- Sun, M.-S., and Baldwin, B., 1958, Volcanic rocks of the Cienega area, Santa Fe County, New Mexico: New Mexico Bureau of Mines & Mineral Resources, Bulletin 54, 80 pp.
- Walton, A. W., and Palmer, B. A., 1988, Lahar facies of the Mount Dutton Formation (Oligocene-Miocene) in the Marysvale Volcanic Field, southwestern Utah: *Geological Society of America, Bulletin*, v. 100, pp. 1078-1091.
- Waresback, D. B., and Turbeville, B. N., 1990, Evolution of a Plio-Pleistocene volcanogenic-alluvial fan: The Puye Formation, Jemez Mountains, New Mexico: *Geological Society of America, Bulletin*, v. 102, pp. 298-314.

Quaternary and Neogene landscape evolution: A transect across the Colorado Plateau and Basin and Range provinces in west-central and central New Mexico

John W. Hawley and David W. Love

New Mexico Bureau of Mines & Mineral Resources, Socorro, New Mexico 87801

with supplemental articles by

J. L. Betancourt, R. M. Turner, and S. Tharnstrom / L. Thompson, E. Mosley-Thompson, J. L. Betancourt, D. W. Love, A. Wilson, G. Leonard, and R. S. Anderson / P. G. Drake, C. D. Harrington, S. G. Wells, F. V. Perry, and A. W. Laughlin / R. P. Lozinsky, J. W. Hawley, and D. W. Love / W. C. Haneberg / R. C. Lohmann, J. M. Davis, D. W. Love, and F. Phillips / B. D. Allen / and P. J. Slavin

Introduction

Emphasis of this transect across west-central and central New Mexico is on the Quaternary to late Miocene evolution of the great variety of landforms and associated surficial deposits that, in aggregate, make up the landscape in parts of two contrasting physiographic provinces: the Colorado Plateau (Acoma—Zuni and Navajo sections), and the Basin and Range (Mexican Highland and Sacramento sections). Grants, at the base of the Pliocene Mount Taylor volcanic center, is the starting point for Day 1 and Day 2 tours of the upper Rio San Jose, and Puerco and Zuni River basins (Fig. 1). The latter two drainage systems are west of the Continental Divide in the Gallup and Zuni Pueblo area; and all three head in the Zuni uplift.

The second-day tour between Grants and Mountainair crosses the Albuquerque basin of the Rio Grande rift, as well as the flanking Lucero and Manzano—Los Pinos uplifts at the margins of the Colorado Plateau and Great Plains *structural* provinces (Fig. 2). Highlights of the first two days include Quaternary alluvial chronologies and changing environments, both in the Puerco and Zuni basins of the Colorado River system and in the Rio San Jose and Rio Puerco basins of the upper Rio Grande. Pliocene and Quaternary volcanic and neotectonic features of Zuni—Bandera, Mount Taylor, and Lucero fields are also covered.

Part two of the second-day tour includes an introduction to ongoing studies of late Quaternary lacustrine, playa, eolian, and paleohydrologic features of the closed-drainage Estancia basin east of Mountainair (Fig. 2) and in the transition zone (Sacramento section) between the Basin and Range and Great Plains physiographic provinces. The highest shoreline deposits of late Wisconsin Lake Estancia are visited on the morning of Day 3; and after traversing the Rio Grande rift-bounding Sandia—Manzano uplifts, via Tijeras Canyon, the field trip concludes with a tour of the Albuquerque—Rio Rancho urban area. In addition to urban environmental geology, tour stops emphasize Miocene to Pleistocene basin-fill stratigraphy, Quaternary evolution of the Rio Grande valley, and Plio-Pleistocene basaltic volcanism and neotectonism.

The New Mexico Highway Geology Map (1982) published by the New Mexico Geological Society, Inc. (Campus Station, Socorro, New Mexico 87801) is recommended as a supplement to this field guide. Stratigraphic nomenclature for the region (Anderson, Lucas, and Love, 1989) is summarized in Fig. 3.

Acknowledgments

The compilers of this field guide thank the many persons and organizations who have assisted in this undertaking. First and foremost are all the contributors. Particular thanks goes to Steve Wells, who organized the field trip, developed the outline, and solicited most of the contributed articles. This field guide could not have been compiled without the strong support of Frank E. Kottowski, Director and State Geologist, and Jiri Zidek, Chief Editor—Geologist, New Mexico Bureau of Mines & Mineral Resources, and other members of the Bureau scientific and technical staff. The New Mexico Geological Society, Inc. graciously allowed citation and use of illustrations from their Guidebook and Special Publication series.

Persons and organizations who for this field trip, or in the past, have granted us access to lands that they own or administrate are also gratefully acknowledged. They include the Laguna and Zuni Tribal Governments, the Navajo Nation, the U.S. Forest Service, the U.S. Bureau of Land Management, the U.S. Fish and Wildlife Service, the New Mexico State Land Office, and the Huning Land Trust. Individual articles by field-guide contributors also contain acknowledgment sections.

Directions and comments en-route from Albuquerque to Grants

Take 1-40 west from its interchange with 1-25 (just east of MP 159). Proceed 73 mi to Grants. **MP 86.** *Prepare to take Exit 85 in 0.5 mi to motel area*, and access to Business-40 through Grants and Mount Taylor area. The following synopsis of geologic features along the way is taken from the New Mexico Geological Society 40th Field Conference road log by Maxwell et al. (1989).

This segment of the tour takes us west 75 mi from Albuquerque to Grants, New Mexico. The route crosses the Rio Grande valley (to just west of MP 156) and ascends across two major Pleistocene river terraces to an early middle Pleistocene geomorphic surface, the Llano de Albuquerque (MP 150-145), that marks the culmination of basin filling in the Albuquerque basin. The Llano surface has been faulted and southward-trending valleys have been cut as much as 300 m into the basin fill (Santa Fe Group) by both the Rio Grande and Rio Puerco. The 150 ka Albuquerque

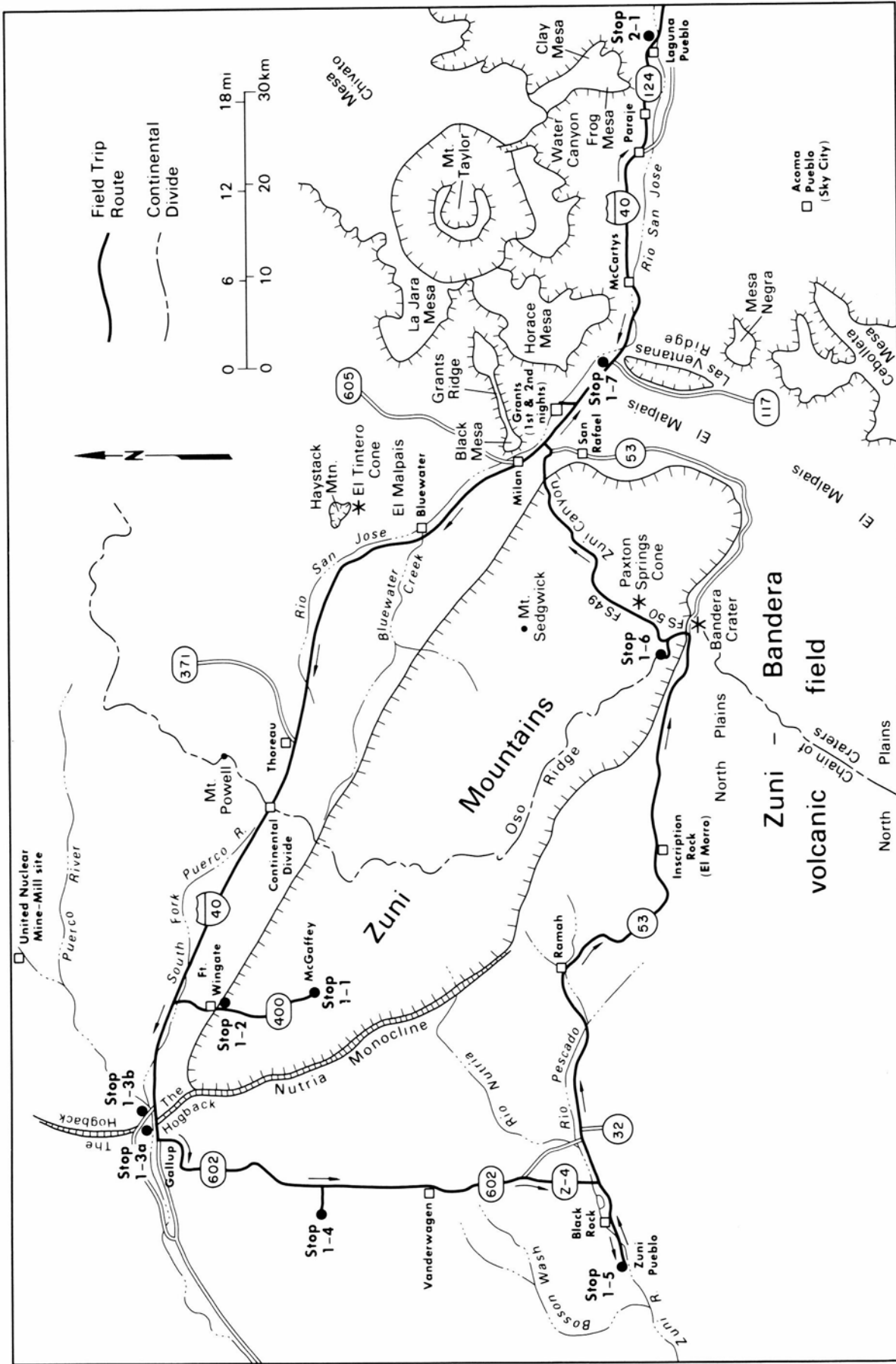


FIGURE 1—Route of field trip (Days 1 and 2) through the southeastern Colorado Plateau region of west-central New Mexico, including Stops 1-1 to 1-7 (Grants–Gallup–Zuni Mountain loop) and Stop 2-1 (Rio San Jose–Laguna area).

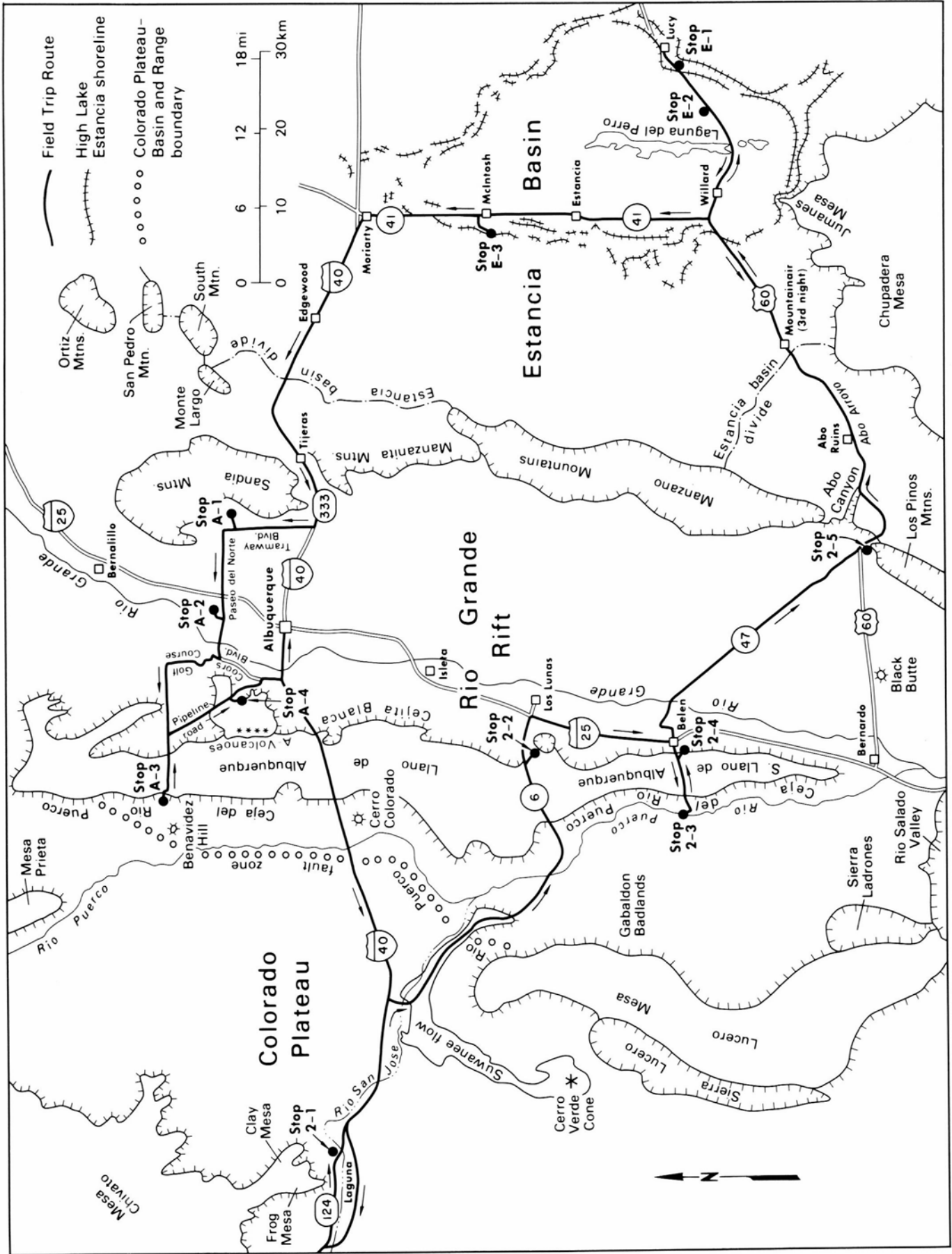
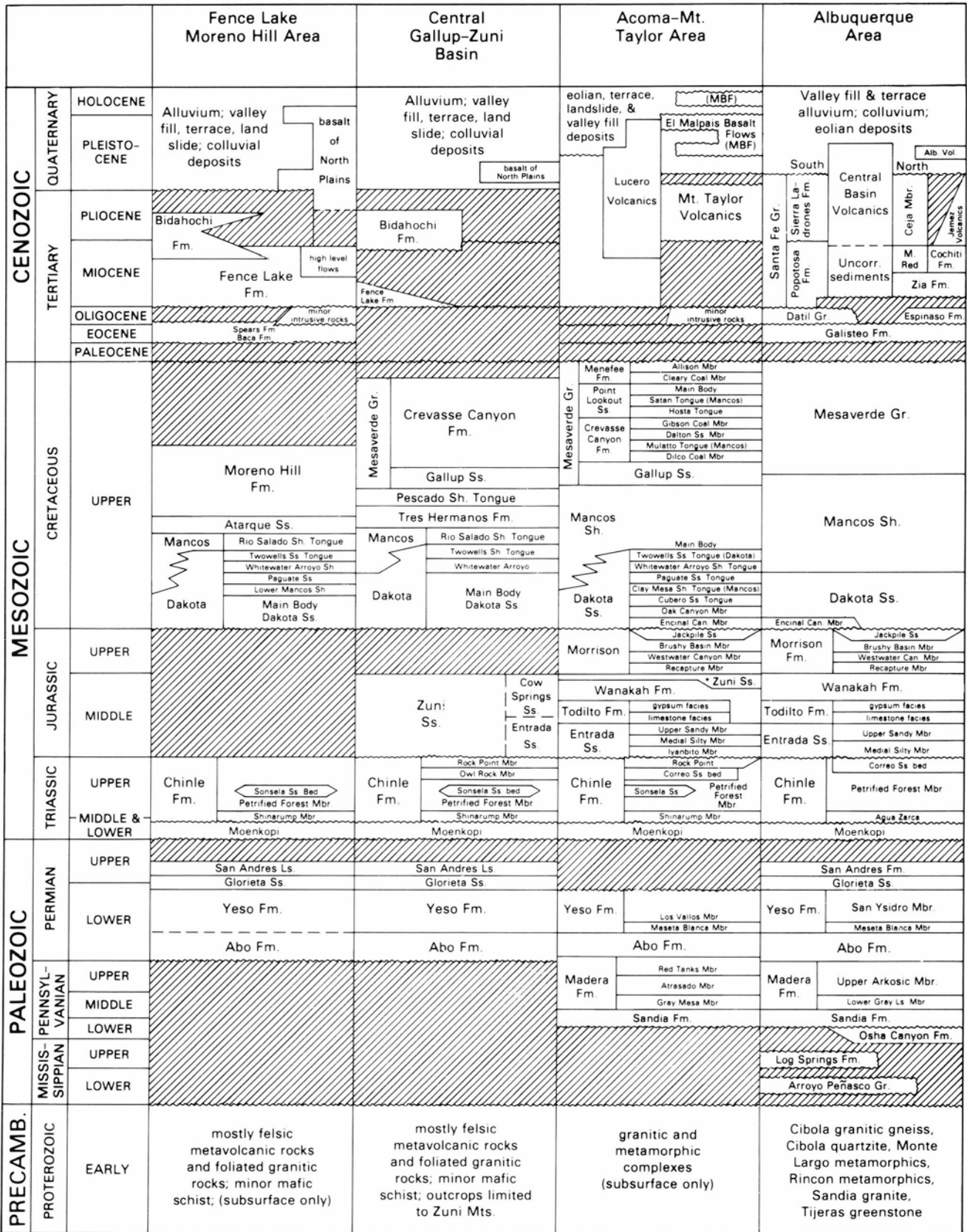


FIGURE 2—Route of field trip (Days 2 and 3) across the Basin and Range province in central New Mexico, including Stops 2-2 to 2-5 and A-1 to A-4 in Albuquerque basin (Rio Grande rift), and Stops E-1 to E-3 in the Lake Estancia basin (Basin and Range, Sacramento section).



*Zuni Ss. of Maxwell (1976)

FIGURE 3—Stratigraphic-nomenclature chart (Anderson, Lucas, and Love, 1989) for the field-trip region.

Volcanoes erupted on the eastern margin of the Llano and flowed to terraces along the Rio Grande (Stop A-4).

West of the Rio Puerco (near MP 140) the route crosses the Rio Puerco fault zone, which forms the structural boundary between the Colorado Plateau and the Basin and Range province (Rio Grande rift). Adjacent to 1-40, the 620,000 yrs old Lava Creek B ash is preserved in sediments filling the Apache graben, a relatively small structure within the fault zone. On the Colorado Plateau, the route passes nearly flat-lying multicolored Triassic, Jurassic, and Cretaceous

continental and marine strata and Plio-Pleistocene volcanoes and flows. West of Exit 126 and the junction with NM-6, the route follows the Rio San Jose, a major tributary of the Rio Puerco. Its valley has been affected repeatedly during Pliocene-Quaternary time by large-scale erosion and back-fill processes, as well as by episodic emplacement of basalt flows (discussed at Stops 1-7 and 2-1). This segment of the trip to Grants follows the eastbound route covered in Part 1 of the Day 2 section of the tour guide.

Day 1: Grants-Gallup-Zuni Mountain loop

Summary

This segment of the tour traverses parts of the Acoma-Zuni and Navajo sections of the Colorado Plateau province between Grants, Gallup, and Zuni Pueblo (Fig. 1). Emphasis is on (1) the Quaternary and late Neogene geomorphic evolution of the upper Little Colorado (Puerco-Zuni) River basin of west-central New Mexico; and (2) Quaternary environments of the Zuni-Bandera volcanic field which straddles the Continental Divide to the upper valley of the Rio San Jose near Grants. Tour highlights include discussions of Quaternary history and late Holocene ecological changes on the summit and flanks of the Zuni Mountains (Stops 11, 1-2, 1-5, and 1-6); mid-to-late Quaternary alluvial chronologies in the upper Puerco and Zuni River valleys west of the Continental Divide (Stops 1-2, 1-3, and 1-5); Pleistocene basaltic volcanism of the Zuni-Grants area (Stops 1-5, 1-6, and 1-7); and Mio-Pliocene erosion surfaces and associated alluvial deposits (Bidahochi Formation) on the western flank of the Zuni uplift (Stop 1-4).

Most of the comments en-route to the tour stops are adapted from road logs by Anderson et al. (1989); Anderson, Love, and Lucas (1989); Chamberlin et al. (1989); Colpitts et al. (1989); Maxwell et al. (1989); Hawley, Crumpler, and Wells (1982); and Wells et al. (1983). Supplemental geologic maps recommended for this tour are by Dillinger (1990), Goddard (1966), Hackman and Olson (1977), and Maxwell (1986).

Directions and comments en-route to Stop 1-1

From the parking lot of the Inn at Grants go south 0.5 mi to 1-40 Interchange (85) and take westbound onramp to 1-40. Milepost (MP) 85 is the 0.0 mi point. Proceed 51 mi northwest on 1-40 to Exit 33 (McGaffey, Fort Wingate), and 10 mi south on NM-400 to McGaffey and Stop 1-1 (optional excursion). Optional Stop 1-2 is 7 mi north of McGaffey and overlooks Fort Wingate east of MP 7 on NM-400. The tour route from Grants to Fort Wingate is along the northern edge of the Acoma-Zuni section of the Colorado Plateau physiographic province (Hawley, 1986a).

0.0 mi, MP 85, crossing basalt flow from El Calderon center for next 1 mi. The vent is located about 16 mi (26 km) to the southwest in the Bandera-Oso Ridge area viewed at Stop 1-6. Note nearly continuous eolian veneer and locally well-developed calcic soils in cuts. Preliminary attempts at K-Ar and magnetostratigraphic dating of this flow have yielded ages ranging from early to late Pleistocene. **MP 84**,

route for next 3 mi on upper Pleistocene aa-lava flow from the Paxton Springs center. The final part of today's tour (Stops 1-6, 1-7) follows this flow from its source area in the southeastern Zuni Mountains through Zuni Canyon.

MP 83, at 9:30 in foreground spring-travertine mound on Chinle Formation is surrounded by Paxton Springs flow. Beyond the mound at the foot of Zuni Mountains near San Rafael are active springs described by White (1989). The dip-slope flanking the northeastern Zuni uplift from 9:00 to 12:00 is capped by limestones of the Permian San Andres Formation. The Precambrian-cored Zuni uplift forms the southern edge of the San Juan basin and has been a positive area during most of Phanerozoic time. Chamberlin and Anderson (1989a) describe a model for the complex, horizontally directed, compressive forces that may have produced the major structural components of the Zuni uplift during the late Laramide (Eocene).

2.9 mi, Exit 81 to right; access to West Grants and Zuni Canyon Rd. (0.2 mi south of interchange); and (via NM-53) to San Rafael, Bandera, and Oso Ridge craters, El Morro National Monument, and Zuni Pueblo. At 1:00 to 3:00, upper Pliocene basalt of Black Mesa (southwest end of West Grants Ridge) is flanked by landslide deposits on Triassic Chinle Formation mudstones and sandstones. **4.0 mi**, mouth of Zuni Canyon at 10:30; crossing Rio San Jose at north edge of Paxton Springs flow and south edge of Milan. Ditch ahead on right (4.3 mi) exposes older (unidentified) flow with calcic soils partly formed in capping deposits.

5.6 mi, Exit 79 to right; access via NM-605 to Milan, San Mateo, and Ambrosia Lake areas of the Grants uranium region (Kelley, 1963; Rautman, 1980; Brod and Stone, 1981) and Lee Ranch coal mine. **6.8 mi**, "Thoreau 25, Gallup 56" mi; at 2:30, about 4 mi to the northeast, the large white tailings pile of United-Nuclear-Homestake Partners mill is visible on the broad floor of San Mateo Creek valley. See Reith and Thomson (1991) for discussion of UMTRA program to stabilize large uranium-mill tailings in the San Juan basin region.

6.0 mi, MP 76, at 10:00 to 12:00 limestones and sandstones of the San Andres and underlying Glorieta Formations form cuesta dip-slope on the northeastern flank of the Zuni Mountains. Underlying gypsum, sandstone, and limestone of the Lower Permian Yeso Formation and basal Abo Formation redbeds overlap an undulating erosion surface on Precambrian metamorphics (see Colpitts et al., 1989, and

road log between Stops 1-6 and 1-7). **MP 77**, crossing cuesta dip-slope for next 2 mi, with excellent roadcut exposures of San Andres limestones.

10.0 mi, MP 75, Haystack Mountain at 2:00 is the site of the initial (1950) Grants region uranium discovery in the Jurassic Todilto Formation (Kelley, 1963). This butte is capped by Upper Cretaceous Dakota Sandstone. Jurassic rocks exposed in the south face are, in ascending order, the Entrada Sandstone (massive red), Todilto Formation (gray limestone and gypsum), Wanakah Formation (reddish-brown sandstone and mudstone), and members of the Morrison Formation (variegated shales, siltstones, and sandstones). Triassic Chinle and Moenkopi Formations (mudstones and sandstones) underlie the broad strike valley between Haystack Mountain and this point. El Tintero cone on the valley floor just south of the mountain is the source of "the Malpais" basalt flow (middle? Pleistocene) that covers much of the floor of this part of the upper Rio San Jose (and Blue-water Creek) valley. Fine- to medium-grained alluvial valley fill (mid-to-late Quaternary) is locally thick (as much as 3040 m, 100-130 ft; Gordon, 1961) and commonly has expansive (vertic) surface soils.

11.5 mi, Anaconda (uranium) mill site to right in middle distance. **12.5 mi**, Exit 72 to Bluewater. Small outcrops and roadcut exposures of El Tintero flow for next 4.0 mi. **14.5 mi**, mouth of Bluewater Canyon at 10:00 is cut in San Andres limestones and sandstones. Lower Chinle/Moenkopi redbeds crop out to right of canyon and are capped by Sonsela Sandstone Bed of the Petrified Forest Member of Chinle Formation. Roadcuts for the next 46 mi (to McGaffey-Ft. Wingate area between Stops 1-1 and 1-2) are primarily in the Petrified Forest Member; and the Sonsela Sandstone Bed is the main cuesta dip-slope caprock (Hackman and Olson, 1977).

15.5 mi, Sonsela Sandstone caps dip-slope remnant to left. For next 20 mi the route follows strike valley of upper Rio San Jose developed in middle and upper part of the Chinle Formation. **16.0 mi**, Cibola-McKinley County line. El Tintero cone at 2:00 and roadcuts ahead in El Tintero flow. Haystack Mountain (7833 ft, 2387 m) at 2:30.

19.0 mi, rising on Sonsela Sandstone dip-slope; roadcuts for the next 34 mi primarily in Sonsela Sandstone Bed and contiguous mudstones and sandstones of the Petrified Forest Member. **20.4 mi**, at 3:00, across valley, Morrison Formation (variegated to grayish-brown slopes) is downthrown to the east against Entrada Sandstone (red cliffs) by north-trending Bluewater fault. **21.5 mi**, Exit 63 to Prewitt.

24.0 mi, MP 61, Escalante Generating Station of Plains Electric Power Coop at 3:00, at base of Entrada Sandstone cliffs, has an initial capacity of 233 megawatts, which is furnished to 16 rural cooperatives. Coal used in the operation comes by unit trains from Lee Ranch mine north of Ambrosia Lake.

29.0 mi, MP 56, from 2:00 to 3:00 a Jurassic-Cretaceous stratigraphic sequence (Entrada, Todilto-Wanakah, Morrison, capping Dakota Formation) is exposed in prominent cuesta scarp north of (strike) valley of upper Rio San Jose. The sequence is capped by a mid-Tertiary diabase sill at Mount Powell (2:00) on Continental Divide. **31.2 mi**, Exit 53 at Thoreau. Access, via NM-371, to Crownpoint and Chaco Canyon area of the San Juan basin and the site of the 1983 American Geomorphological Field Group Conference (Wells et al., 1983). **33.0 mi, MP 52**, at 3:00, relay

towers on Mount Powell (8748 ft, 2666 m) are on Continental Divide. Route on "spectacular" ascent to Continental Divide for next 3.8 mi.

36.8 mi, Exit 47. Continental Divide (about 7270 ft, 2216 m). Access to "Top of The World" service center. Route crosses from upper basin of the Rio San Jose-Rio Puerco system (tributary to the Rio Grande) to the Colorado River watershed and the upper end of the Puerco River (Little Colorado) drainage basin. **37.0 mi, MP 48**, strike valley on Chinle Formation dip-slope continues to the west another 20 mi almost to The Hogback (Nutria monocline) belt at the east edge of Gallup.

40.1 mi, Exit 44 to Coolidge. **44.9 mi**, Exit 39 to Rest Area and refinery. **46.7 mi**, valley-border surfaces to right have thin cap of gravelly alluvium (mid? to late Pleistocene). **48.0 mi**, Exit to Iyanbito. **49.0 mi, MP 36**, shallow channel to right is South Fork of the Puerco River (Rio Puerco of the West in older literature). **50.0 mi, MP 35**, thin Pleistocene terrace gravels cap Sonsela Sandstone outliers ahead on right.

51.0 mi, MP 34, *prepare to exit 1-40 in 0.5 mi*. **51.5 mi**, *take Exit 33* to McGaffey, Fort Wingate, and optional excursion to Stops 1-1 and 1-2 (via NM-400). **51.2 mi**, *turn left* (west) on frontage road. **51.5 mi**, *turn left* (south) on NM-400; cross 1-40 and shallow channel of South Fork of the Puerco River (51.8 mi).

52.0 mi, MP 10 on NM-400, route ahead crosses low strath terrace on Petrified Forest Member of Chinle Formation capped by thin gravelly fill and then ascends to summit of cuesta dip-slope on Sonsela Sandstone Bed. **53.0 mi, MP 9**, descending cuesta-scarp slope cut in sandy mudstones of the Petrified Forest Member. **53.9 mi**, Fort Wingate High School to right. **54.3 mi**, historical marker to left at entrance to 19th-century military post of Fort Wingate (see Stop 1-2 discussion). **54.8 mi**, Saint Elenors Church to right. *Winding road and steep grade ahead*, with roadcuts in mudstones and limestone-pebble conglomerate bed in Chinle to left.

55.0 mi, MP 7, parking area on left for Fort Wingate overlook and Stop 1-2 (optional); proceed through cattle guard (mi 55.1) on NM-400. Note typical development of piñon-juniper forest (*Pinus edulis* and *Juniperus monosperma*) ahead. *Winding road and steep grade* (55.4 mi) with roadcuts in lower Chinle mudstones and sandstones. Landslides are common.

56.0 mi, MP 6, note scattered ponderosa pine (*Pinus ponderosa*) in piñon-juniper forest. Varicolored Petrified Forest Member crops out on both sides of road. **56.3 mi**, crest of grade; extensive ponderosa stands in forest ahead (56.7 mi); mottled strata are characteristic of the basal Chinle Formation.

57.0 mi, MP 5, cattle guard; entering Cibola National Forest. **57.4 mi**, San Andres Formation thins in this area and may be locally absent, with the base of the Triassic redbed sequence resting directly on Glorieta Sandstone. **57.6 mi**, Glorieta Sandstone crops out in canyon wall to right, and roadcut ahead on left (57.9 mi) exposes San Andres/ Glorieta (limestone/sandstone) contact.

58.0 mi, MP 4, approaching head of Milk Ranch Canyon cut in San Andres Formation limestones, here as much as 50 ft (16 m) thick. **59.0 mi, MP 3**, on summit of northwestern Zuni Mountains, with high ridges capped with thick fluvial sandstones of the Chinle Formation (probably Sonsela Sandstone Bed). **59.4 mi**, cattle guard. Quaking Aspen

Campground ahead on right. **61.5 mi**, drainage divide at about 7805 ft (2379 m). Forest Service road to right crosses steep western slope of Zuni Mountains and continues to NM-602 (Stop 1-4 area) via "west wall" of the Nutria mono-cline and Bread Springs (see Anderson, Love, and Lucas, 1989).

62.0 mi, MP 0, at McGaffey (elevation 7780 ft, 2371 m). Area of Stop 1-1.

Stop 1-1 (optional): Forest ecosystems of Zuni Mountain area: Impact of timber management practices. Optional discussion of late Holocene—historical changes in forest ecosystem by Loren Potter and S. G. Wells.

Retrace route on NM-400 to overlook at Fort Wingate Centennial Monument (MP 7) and Stop 1-2.

Stop 1-2 (optional): Western Puerco River basin from Fort Wingate Centennial Monument (J. W. Hawley and D. W. Love). This stop (elevation about 7140 ft, 2176 m) provides an excellent view of the upper Puerco River basin and the southern border of the Navajo section of the Colorado Plateau (Fig. 1-1). The Acoma—Zuni section to the south (Hawley, 1986a) was originally included in the northern Datil section (Fenneman, 1931; Hunt, 1974) which comprised a poorly defined, transitional physiographic subdivision between the southeast Colorado Plateau and Basin and Range provinces.

Fort Wingate was originally established as Fort Fauntleroy in 1860, but the post's garrison withdrew in 1861 because of the Confederate invasion of New Mexico's Rio Grande valley. Only a mail station was maintained here during the Civil War. In 1868 the post was re-established as Fort Wingate (for Capt. Benjamin Wingate, who died of wounds received in the Battle of Valverde south of Socorro in 1862).

The prominent cliffs north of 1-40, on the opposite side of South Fork of Puerco River valley, expose the following

Mesozoic sequence (ascending): Chinle (Triassic), red Entrada Sandstone (basal Jurassic unit), thin white band of Todilto limestone and gypsum, Beclabito and Horse Mesa Members of Wanakah Formation, light-colored Cow Springs Sandstone and variegated Morrison Formation (uppermost Jurassic unit), and thin, generally cliff-forming Dakota Formation capping the section. The Navajo Church (Church Rock) and Pyramid Rock pinnacles and "White Cliffs" west of the mainstem Puerco River valley (Fig. 1), are developed in Westwater Canyon Member of Morrison Formation.

Retrace route to 1-40 Interchange 33. Turn left on north frontage road and proceed 0.1 mi to 1-40 West access road.

Directions and comments en-route to Stop 1-3

0.0 mi, turn left onto 1-40 west. **0.5 mi, MP 33**, proceed 5.5 mi west down the valley of Puerco River's South Fork to Exit 26 and Stop 1-3a at The Hogback in eastern Gallup. **1.5 mi, MP 32**, note large dunes at base of Entrada Sandstone and underlying Owl Rock Member of Chinle Formation. **3.0 mi**, at bridge over railroad spur, bunkers of Fort Wingate U.S. Army Ordnance Depot to left; Pyramid Rock and Navajo Church (Church Rock) on skyline at 2:00 and 3:00. **3.5 mi, MP 30**, crossing South Fork of the Puerco River; roadcuts in Chinle Formation mudstone and sandstone. **4.1 mi**, Entrada Sandstone cliffs at Redrock State Park to right. Site of Navajo—Intertribal Ceremonial event every August. Note large dunes at cliff base. **5.5 mi, MP 28**, at 1:00 to 2:00 Dakota-capped light-colored Morrison Formation/Cow Springs Sandstone escarpment forms the "White Cliffs." Dakota Sandstone and Mesaverde Group-capped cuestas of the northwestern Zuni uplift are on the skyline.

6.5 mi, MP 27, prepare to take next exit (Gallup East). Confluence of mainstem and South Fork of the Puerco River on valley floor to right. **7.1 mi**, take Exit 26 to right. **7.5 mi**, turn left on US-66 (Business 1-40) and proceed west through underpass into Gallup. **8.0 mi**, watergap through double hogback belt of the west-dipping Nutria monocline ahead (Dakota Sandstone to the east, strike valley in Mancos Shale and Gallup Sandstone to the west). This steep monoclinical structure, "The Hogback," marks the western edge of the Zuni uplift and eastern border of the Gallup sag. Prepare for right turn on a narrow road in 0.5 mi.

8.5 mi, turn right on graded road to Superman Canyon. Continue under ATSF Railroad and across bridge over Puerco River. **8.55 mi**, park off road at eastern base of Dakota Sandstone hogback; walk to tip of hogback for Stop 1-3 orientation and then continue down Puerco valley floor about 200 m to Stop 1-3a.

Stop 1-3a: Alluvial fills of the Puerco River valley—Gallup Hogback area, and impacts of the 1979 uranium tailings spill north of Church Rock (D. W. Love and J. W. Hawley). The Puerco River of the West (as opposed to the Rio Puerco of the East and Rio Puerco of the North, both east of the Continental Divide) drains about 558 me (1445 km²) east of Gallup. Its drainage area expands to several thousand square miles before it joins the Little Colorado River near Holbrook, Arizona, 90 mi (145 km) to the west. The maximum historic flood was 12,000 ft³/s (340 m³/s) on July 17, 1972. Stage was 15.3 ft (4.66 m). Over a million dollars of damage was done in Gallup. Floods in Gallup have repeated since then, but the Army Corps of Engineers is planning a flood-control channel north of the natural channel.

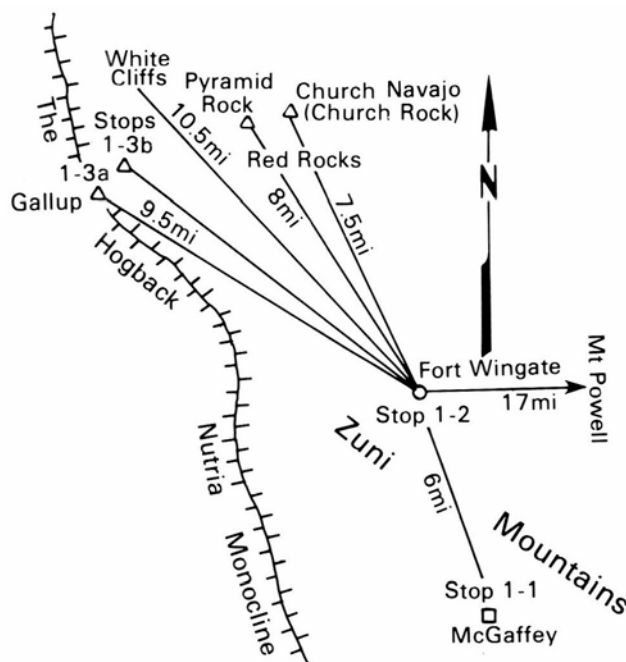


FIGURE 1-1—Panoramic location diagram for major landmarks seen from Stop 1-2 at Fort Wingate Centennial Monument overlooking the valley of the Puerco River South Fork.

In 1979 a uranium-mill tailings dam about 14 mi (23 km) upstream from this stop breached and 1.1 ton (1×10^3 kg) of radioactive and acidic sediment and 124×10^6 ft³ (3.5×10^6 m³) of liquid wastes swept down the Puerco River (Gallaher and Goad, 1981; Miller and Wells, 1986). Miller studied the downstream variation in conditions for sediment storage along the Puerco River and looked for contaminated sediments five years after the spill. He was unable to locate consistent storage areas of contaminated sediments. He attributed the lack of contaminated sediments to dilution and possible eolian transport out of the arroyo system. Gray et al. (in progress) have found ample evidence of ground-water contamination beneath the Puerco River channel in Arizona; however, much of this appears to be due to long-term impacts of discharge from uranium-mine dewatering operations.

The elevation of the valley floor between the two spurs of The Hogback is about 6560 ft (2000 m). The 20 ft (6 m) section of younger valley fill exposed in walls of the Puerco River "arroyo" from the area of this stop (Fig. 1-2) to central Gallup (2 mi downstream) comprises three major units: (1) light brown to light yellowish-brown (mostly 10YR hues) silty clay with thin, fine-sand interbeds and local gravelly lenses; this unit makes up most of the exposed valley fill; (2) reddish-brown clay and sand that backfill broad channels cut into and locally bury unit 1; and (3) light brown sandy alluvium forming the fill of low inset terraces along the present Puerco channel.

Leopold and Snyder (1951) briefly studied the stratigraphy of valley-floor alluvium in downtown Gallup and divided the fill into two units. The lower, older alluvium of late? Pleistocene age is called the Gamerco formation and consists of reddish and reddish-brown sand with hard calcareous concretions and tubes overlying partially cemented gravelly sand. A reddish calcareous soil is locally preserved at the top. The upper, younger alluvium is called the Nakaibito formation and consists of sand, sandy silt, and clay with minor pebbly lenses typical of Holocene alluvium. Since the local valley fill was first described (in 1946) by Leopold and Snyder (1951), urban expansion, railroad-maintenance activities, and various river-channel changes have resulted in obliteration of many features observed in 1946. However, the 20 ft (6 m) "arroyo channel" with dimensions similar to the present one was already present in 1946, in marked contrast to the 6 ft (2 m) deep channel observed here by N. H. Darton in 1901 (see photographs in fig. 2 of Leopold and Snyder, 1951).

The fine-grained valley fill (unit 1) exposed in the 20 ft (6 m) arroyo walls between the two spurs of "The Hogback" at this stop (Fig. 1-3) is part of the Nakaibito "formation" of Leopold and Snyder. These sediments contain a very sparse fossil snail fauna that has not been studied. Extensive systems of "pipes" and related surface-collapse depressions are present back from the arroyo walls. Underlying older alluvium (Gamerco formation) is not presently exposed in the tour-stop area. Overlying channel fills (unit 2) are also



FIGURE 1-2—Aerial photograph of The Hogback area at the eastern edge of Gallup. Stop 1-3a (left center) starts at the tip of the eastern (Dakota Sandstone) ridge north of the Puerco River. Stop 1-3b (upper right) is in the gravel pit east of Superman Canyon Rd. and northwest of the I-40 overpass.

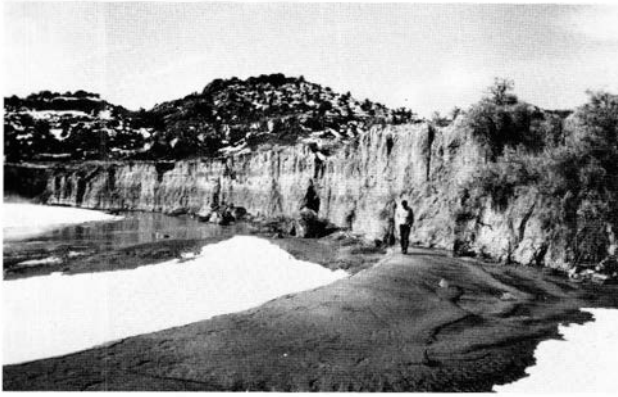


FIGURE 1-3—Looking west from Stop 1-3a down Puerco River at valley-wall exposure of Holocene Nakaibito formation of Leopold and Snyder (1951). Western ridge (Gallup Sandstone) of The Hogback in background.

poorly exposed in this reach of the Puerco. The very young (modern) inset terrace fill (unit 3) is very well expressed here, however.

Leopold and Snyder (1951) note that the inner valley fill is at least 95 ft (29 m) thick downstream from Gallup, but they infer that the fill is only about 20 ft (6 m) thick in this area. However, no systematic study of valley-fill thickness or facies distribution has been done in the upper Puerco River basin (e.g. drilling and geophysical studies), and maximum thickness of valley fill in and upstream from The Hogback narrows may be much greater than 20 ft (6 m).

In some drainages, Leopold and Snyder (1951) recognized two depositional episodes in the Nakaibito formation. Pueblo I and II (A.D. 700-1150) potsherds were found buried 14 ft (4.3 m) below the surface in the type section (in the Chaco drainage basin to the north!). Few, if any, radiocarbon dates have been obtained in the Puerco River basin. This stratigraphy is typical in many drainages in the region, but the names of the formations have not been applied elsewhere even in this drainage basin. Roughly equivalent stratigraphic units (Jeddito = Gamercio, Tsegi = Nakaibito) introduced by Hack (1942) in the Black Mesa area of Arizona have been mapped in parts of the San Juan basin (e.g. Blagbrough, 1965; Weide et al., 1979).

Later workers have divided Quaternary alluvium in the Puerco, Rio San Jose, and Chaco drainages into four mappable units (e.g. Robertson, 1974). The oldest unit, Qoa, consists of "grayish orange to yellowish gray, poorly to partly consolidated silt, sand, and gravel . . . generally more than 20 ft (6.1 m) above the level of modern valley flood plains." On maps within the drainage basin, Qoa occurs at as many as seven discrete levels ranging up to 1224 ft (373 m) above the valley floors (Love and Gillam, in press). The next oldest unit, Qa3, consists of "grayish orange to pink semiconsolidated silt, sand, and gravel in terraces 5 to 20 ft (1.5-6.1 m) above graded valley flood plains and underlies . . . surfaces and upper reaches of stream valleys. Generally underlain by older alluvium." Qa2 is Holocene sand, gravel, silt, and clay of graded valley bottoms and floodplains prior to latest cycle of entrenchment. It grades laterally to colluvium. Qa1 consists of sand and gravel in arroyos, fans, and valley floors that have been deposited since the latest cycle of erosion (presumably post-1850). In the area of this stop, Green and Jackson (1976) simply divide the valley-fill alluvium into two broad units, Qal (Holocene)

and Qoa (Pleistocene). Thick deposits of their older alluvium (Qoa) are seen at Stop 1-3b.

After Stop 1-3a continue northeast 0.45 mi on graded road through 1-40 underpass. **9.0 mi**, cross North Frontage Rd. and proceed northeast 0.2 mi on Superman Canyon Rd. to entrance of a large borrow pit at north edge of Puerco River valley. *Turn right* into western part of pit (watch for muddy conditions) and park near base of bluff for Stop 1-3b.

Stop 1-3b: Older alluvial deposits near South Fork and mainstem Puerco River confluence (J. W. Hawley and D. W. Love). This stop (elevation range 6580-6660 ft, 2005-2030 m) is located on a large remnant of older valley-fill alluvium (Qoa map unit of Green and Jackson, 1976) overlooking the valley floor at the confluence of the main-stem and South Fork of the Puerco River (0.5 mi, 0.8 km to the east-southeast; elevation about 6560 ft, 2000 m). Major landmarks of the area are shown in Fig. 1-4. These include the White Cliffs (2 mi, 3.2 km, to the north), the Gallup watergap through The Hogback (1 mi, 1.6 km, to the southwest), the valley of the South Fork and Fort Wingate Army Depot to the east-southeast, the Red Rocks cliffs and Red Rock State Park (3.5 mi, 5.6 km, to the east), Pyramid Rock (3.5 mi, 5.6 km, to the east-northeast; elevation 7487 ft, 2289 m), and the Church Rock uranium mine and mill site (12 mi, 19.3 km, to the northeast) up the Puerco River valley. The Entrada Sandstone is probably the main bedrock substrate at this site (Green and Jackson, 1976; Hackman and Olson, 1977).

As much as 80 ft (24.4 m) of older valley-fill deposits are exposed in borrow pits at this stop (Fig. 1-2). 5YR hues are dominant in these deposits in contrast to the 10YR hues in the younger valley fill seen at Stop 1-3a. An axial-fluvial (ancestral Puerco River) facies is exposed in most of the pits between elevations of about 6580 and 6650 ft (2005-2027 m). This unit is primarily clean pink to pinkish-white

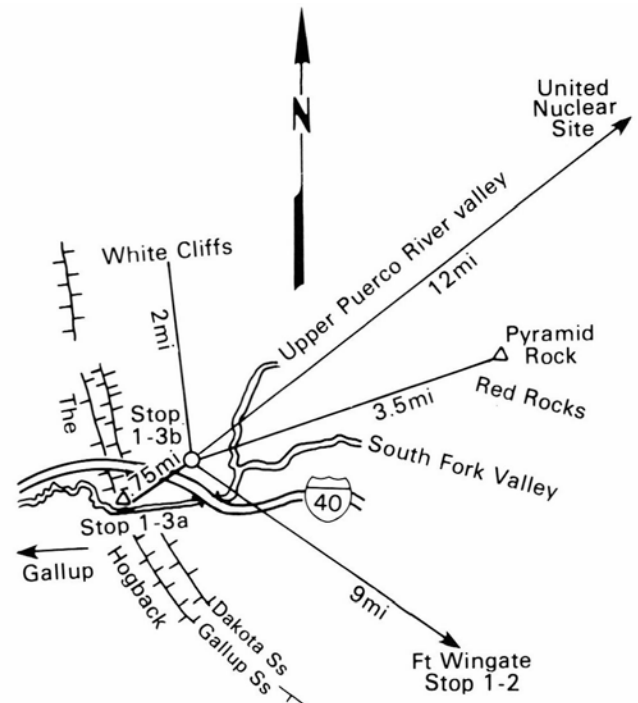


FIGURE 1-4—Panoramic location diagram for major landmarks seen from Stop 1-3b overlooking the confluence of the mainstem and South Fork of the Puerco River.

sand with thin interbedded layers of light reddish-brown silt-clay and lenses of sandy gravel. In the highest and northernmost pits at this stop (elevations up to 6660 ft, 2030 m) the fluvial facies is overlain by channel gravel (pebbles, small cobbles, and a few boulder-size mud clasts) representing ancient tributary (arroyo) deposits derived from uplands in the White Cliffs-Hogback area to the northwest. One large fragment of a proboscidean tusk was noted in the uppermost part of the fluvial facies.

Original constructional surfaces of the "older" axial-fluvial or tributary alluvial deposits are not preserved here and the upland erosion surfaces on these units are mantled with a complex of light reddish-brown to brown local alluvial, colluvial, and eolian deposits. Strongest soils (surficial and shallowly buried) developed in this veneer and immediately underlying beds of the "older alluvium" have weakly to moderately developed argillic horizons and weak stage-III carbonate horizons (as defined by Gile et al., 1966, 1981).

Middle to late Quaternary alluvial chronologies worked out in adjacent part of the Chaco River basin to the north (see Wells et al., 1983) and Rio Grande basin to the east (see Days 2 and 3, and supplemental articles, this volume) support the inference that the thick valley-fill remnant preserved at this stop represents a major, climatically controlled episode of valley entrenchment followed by an interval of equally widespread aggradation of at least the inner valley areas. The youngest possible age for these deposits would be from early to middle Wisconsin, and could range back to late middle Pleistocene (including the last pre-Wisconsin full-glacial interval; marine 0-isotope stage 6).

The final major period of widespread valley entrenchment presumably occurred in the late Wisconsin prior to emplacement of the younger valley-fill units observed at Stop 1-3a. The time(s) of maximum incision of the deepest parts of the "thalweg" below the Gamerco (Jeddito)-type units in this area has (have) still not been determined. It is possible that the deepest entrenchment occurred prior to the deposition of the "older" axial Puerco deposits seen at this stop.

Retrace route to US-66 through ATSF Railroad underpass south of Stop 1-3a.

Directions and comments en-route to Stop 1-4

0.0 mi, stop sign at US-66. *Turn right* and continue west on Business 1-40. **0.6 mi**, traffic light at Patton Rd. *Prepare for left turn at next light* (0.7 mi) at Boardman Rd. **1.3 mi**, *turn left and proceed south on Boardman Rd.* (NM-564) across Aztec Ave. (traffic light at 1.4 mi). Boardman Rd. curves to right past Gallup High School (2.2 mi), and continues west past Gallup Branch of the University of New Mexico (to left of four-way stop at 3.9 mi) to junction with NM-602 at south edge of Gallup. **4.6 mi**, traffic light at intersection of Boardman Rd. and S. 2nd St. *Turn left and proceed south* 10 mi on NM-602 to Skeets Rd. **14.6 mi**, *turn right on graded Skeets Rd. and proceed 2.3 mi west to Stop 1-4.*

The US-66 route through eastern Gallup is on the floor of the Puerco River valley and passes the two ridges of The Hogback through a 0.15 mi (0.25 km) wide watergap. The route from here to Zuni Pueblo is in the Gallup sag, the narrow structural depression between the western Zuni and southern Defiance uplifts that connects the San Juan and Zuni basins.

The US-66-Boardman Rd. intersection (1.3 mi) is just

upstream from the confluence of the Catalpa Canyon and Puerco River arroyos and the area north of El Rancho Hotel described by Leopold and Snyder (1951) in their discussion of the "type" Gamerco and Nakaibito formations (see Stop 1-3a). South of US-66 Boardman Rd. follows Catalpa Canyon, climbing out of the Puerco River valley across outcrops of the Crevasse Canyon Formation (Dilco Coal Member, Mesa Verde Group). Reclamation work at former Carbon Coal No. 2 strip mine is visible about 1.5 mi up Catalpa Canyon south of Boardman Rd. at 3.2 mi.

4.6 mi, traffic light at Boardman Rd.-NM-602 intersection. *Turn left and proceed south* toward Zuni Pueblo on NM-602. **5.3 mi, MP 28**, roadcuts for next 7 mi in sandstones, shales, and thin coals in Crevasse Canyon Formation. Route crosses irregular, hilly, erosional topography developed on nonmarine Upper Cretaceous rocks, which contrasts markedly with the even-crested mesa and cuesta surfaces formed on extensive marine sandstone units such as the Gallup and Dakota.

8.3 mi, MP 25, highway skirts arroyo of Bread Springs Wash to right. Incision of the present 20-25 ft (6-8 m) deep channel probably occurred during the past two centuries.

9.1 mi, bridge over Bread Springs Wash.

13.3 mi, MP 20, for next 11.5 mi NM-602 crosses a broad upland erosion surface on Upper Cretaceous rocks; the surface slopes gently to the west and is cut by shallow valleys of Puerco and Zuni River tributaries that head on the western slope of the Zuni Mountains. Locally thick alluvial and eolian deposits of the upper Miocene-lower Pliocene Bidahochi Formation cap this "Zuni" erosion surface (see Stop 1-4). The unit is mainly poorly cemented sandstone and mudstone, with local lenses of volcanic ash and thin, well-indurated beds of siliceous sandstone. **14.3 mi, MP 19**, *prepare for right turn on Skeets Rd. in 0.3 mi.*

14.6 mi, *turn right on Skeets Rd.*, cross cattle guard and proceed west for 2.3 mi to Stop 1-4. Note typical development of piñon-juniper forest. **16.9 mi**, *park on right side of Skeets Rd.* on crest of interfluvium and carefully walk across road to left to examine Bidahochi exposures in valley to south.

Stop 1-4: Bidahochi Formation (D. W. Love and O. J. Anderson; modified from Love, 1989b, and Anderson et al., 1989). At this stop about 100 ft (30 m) of Bidahochi Formation rest unconformably on the Crevasse Canyon Formation. To the west, the Bidahochi Formation is up to 787 ft (240 m) thick and covers over 6178 mi² (16,000 km²) in western New Mexico and eastern Arizona. The depositional "basin" consisted of paleovalleys and interfluvies sloping southwest and west from Black Mesa, Defiance and Zuni uplifts, and north from the White Mountains toward the ancestral Little Colorado River. After initial erosion of valleys through tilted older rocks, deposition occurred in many facies, such as alluvial, lacustrine, eolian, monchiquitic eruptive, travertine and other spring deposits, and silicic ash. Here on the flanks of the Zuni uplift, only the alluvial, eolian, and silicic ash facies are apparent (see 19 in. thick ash just below road level at this stop). Age relationships with older and younger Tertiary units are not well constrained. Parts of the mid-Miocene Fence Lake Formation (McLellan et al., 1982) may be lateral equivalents or precursors of the Bidahochi Formation. Deposition near Sanders, Arizona, started by 9 Ma and perhaps as early as 12 Ma based on fossil evidence (Love, 1989b). Aggradation

of Bidahochi Formation ceased by about 4 Ma in most areas. Pliocene and Pleistocene terraces are inset into the Bidahochi Formation. In general, depositional setting, facies, and age of the Bidahochi are similar to the Ogallala Formation in eastern New Mexico and northwestern Texas, implying similar tectonic, geographic, and climatic reasons for both accumulations.

In this area, McCann (1938) called the erosion surface at the base of the Bidahochi the "Zuni" surface. To the north and west, other erosion surfaces beneath other units or within the Bidahochi Formation have been correlated with the "Zuni" surface (cf. Akers, 1964; Cooley and Akers, 1961). Much of the correlation of erosion surfaces was done before the advent of radiometric ages. Much work remains to be done to revise the nomenclature of unconformable and disconformable Tertiary surfaces in the Little Colorado drainage basin.

Retrace route to NM-602.

Directions and comments en-route to Stop 1-5

0.0 mi, stop sign on Skeets Rd. at NM-602. *Turn right* and proceed south for 14.2 mi on NM-602 toward Zuni Pueblo through Vanderwagen (Vander Wagen of Pearce, 1965; 6.3 mi). Bear right on Zuni Hwy 4 half a mile south of MP 5 and continue south for 4.7 mi to NM-53. Turn right on NM-53 and continue west for 6 mi through Black Rock (20.7 mi) to central Zuni Pueblo (25 mi) and access to Stop 1.5.

0.0 mi, for the next 10 mi the route continues south on NM-602 across broad upland surfaces capped with Bidahochi Formation. Cretaceous bedrock is only exposed in a few valleys of major streams. **0.5 mi**, Bread Springs-Pine Haven Rd. to left is route of New Mexico Geological Society Field Conference tour (Anderson, Love, and Lucas, 1989) to McGaffey-Fort Wingate area (Stops 1-1 and 1-2). Crossing shallow upper valley of Manuelito Wash (Puerco tributary). **0.7 mi, MP 18**, Joe Milo's Trading Post to right. Elvis reportedly appeared here in September 1986 (Anderson et al., 1989). **1.7 mi, MP 17**, white silicic ash bed in Bidahochi exposed in roadcut ahead to right. **3.7 mi, MP 15**, road to right leads to BIA elementary schools at Chichiltah and Jones Ranch. Route ahead crosses shallow upper valley of Whitewater Arroyo (5.1 mi, Puerco tributary), with local outcrops of Crevasse Canyon Formation/Gallup Sandstone "basement complex." **6.3 mi**, Vanderwagen and Whitewater Trading Post to right. Valley of Nelson Wash ahead with exposures of Gallup Sandstone.

6.7 mi, MP 12, drainage divide between Puerco and Zuni river basins capped with Bidahochi Formation. **8.0 mi**, McKinley County Rd. 6 to right to Kiwanis Park and Cousins Brothers Trading Post. **9.9 mi**, McKinley County Rd. 8 to right. *Entering Zuni Indian Reservation.*

10.2 mi, leaving upland surface capped with Bidahochi Formation. View to south down valley of tributary to Rio Nutria, which joins Rio Pescado to form Zuni River about 8 mi (13 km) downstream. As highway drops into the valley, note dip-slope to right formed on Dakota Formation. Strike valley ahead is eroded into Rio Salado (Shale) Tongue of Mancos Formation; and escarpment to left capped by Atarque (Sandstone) Member of Tres Hermanos Formation. Dips here are 3-5° to the east-northeast.

11.7 mi, MP 7, watershed management practices implemented by local U.S. Soil Conservation Service staff have

led to successful reclamation of arroyos in this segment of the Rio Nutria drainage system. Prominent cliffs forming eastern valley wall are Atarque (Sandstone) Member overlain by carbonaceous Carthage Member of Tres Hermanos Formation. Twowells (Sandstone) Tongue of the Dakota overlies Whitewater Arroyo (Shale) Tongue of the Mancos in a small hill at left edge of highway. **13.7 mi, MP 5**, *keep right for Zuni Hwy 4 in 0.5 mi.*

14.2 mi, *bear right on Zuni Hwy 4* and proceed south to valley of Zuni River across cuesta dip-slope capped with sandstones of the Dakota Formation. Roadcut exposures ahead in carbonaceous shales near base of Dakota. **15.7 mi**, crossing west-facing cuesta rim. **15.9 mi**, contact of Dakota on Jurassic Zuni Sandstone (Cow Springs/Entrada Sandstone equivalent with Todilto interval missing). **17.2 mi**, crossing thick Quaternary eolian sand sheet at base of escarpment. Broad alluvial toeslope ahead, with eolian veneer, is graded to floor of Zuni River valley, which here coincides with surface of Pleistocene basalt flow east of Black Rock (about 3 mi, 5 km, to the southwest). **18.6 mi**, bridge over Zuni River, which is shallowly entrenched into basalt flow of Rio Pescado lobe (North Plains section of the ZuniBandera field). The tip of this flow forms Black Rock promontory 2 mi to the west. A K-Ar age determined here by Laughlin et al. (1982) is 0.7 ± 0.55 Ma (olivine tholeiite sampled about 0.7 mi upstream). *Prepare for right turn ahead.*

18.9 mi, *stop sign at NM-53. Turn right on NM-53* and proceed west toward Black Rock and Zuni Pueblo. **19.7 mi, MP 17**, prominent mesa from 11:00 to 12:00 is Dowa Yalanne (Corn Mountain) capped by Dakota Sandstone which overlies about 500 ft (150 m) of Zuni Sandstone. Bosque to right is on delta of Zuni River at upper end of Black Rock Reservoir. The dam is about 1 mi to the west-northwest. Kirk Bryan examined one of its failures in 1928 and made recommendations on dam reinforcement. He summarized the Quaternary history of the area in his unpublished report. **20.7 mi, MP 16**, Black Rock community to right on basalt flow. Chinle redbed exposures ahead on right and left.

21.9 mi, basalt of Black Rock caps Chinle Formation and/or Chinle-derived alluvium to right at end of Rio Pescado lobe of North Plains flow. Continue west on NM-53 across low scarp to floor of broad alluvial valley underlain by Chinle Formation. Orr (1982) recorded as much as 236 ft (72 m) of alluvial fill in the valley to the west. **22.7 mi, MP 14**, Zuni Pueblo Historical Marker on right. Corn Mountain road to left (22.8 mi). See Chamberlin et al. (1989) and Lucas and Anderson (1989) for overview of Zuni area geology and history.

23.2 mi, NM-53 bridge over Zuni River. **24.0 mi**, *caution! School Crossing*; Zuni High School to left. **24.6 mi**, *congested area*; Tribal Headquarters and shopping center to right; older part of Pueblo to left. **25.0 mi**, four-way stop. Access to west and north to gullied valleys of the Zuni area, including Bosson Wash (Optional Stop 1-5). Please note that all visits to Zuni tribal lands outside the central Pueblo area must be done with permission from the Tribal Governor's Office and other appropriate officials.

Stop 1-5 (optional): Arroyo processes and valley-fill sequences: The impacts of Holocene climatic changes, and land and water management practices. Comments and discussion by S. G. Wells. Retrace route on NM-53 to junction with Zuni Hwy 4 (0.8 mi east of MP 17).

Directions and comments en-route to Stop 1-6

Route is eastbound on NM-53 from junction with Zuni Hwy 4. Continue 41.2 mi east on NM-53, via Ramah and El Morro National Monument to junction with U.S. Forest Service Road 50 (FS-50; 0.1 mi west of MP 59). Turn left and proceed 1.5 mi north on FS-50 to junction with FS-187. Turn left on FS-187 and continue about 1.4 mi northwest to Stop **1-6** at Oso Ridge Lookout Tower on summit of Oso Crater. Four-wheel drive is usually needed to reach the summit, so park other vehicles on straight section of FS-187 below switchback about 0.5 mi from lookout tower and walk to Stop 1-6.

0.0 mi, Zuni Route 4 to left; *continue east on NM-53* up valley of Zuni River through watergap in east-dipping cuesta developed on Dakota/Zuni sandstones. **0.3 mi, MP 18**, radio towers on skyline at 10:00 are in area of cuesta summit where patches of siliceous gravels on the Dakota Sandstone caprock have been noted. Age and origin of these and similar very high-level deposits elsewhere in the Zuni Mountain region have not yet been determined. However, they could be as old as Eocene and as young as Pliocene. **1.3 mi, MP 19**, Rio Pescado tongue of North Plains basalt flow to left along river. Spectacularly banded exposures of Zuni Sandstone in cliff faces noted by Dutton (1885).

2.3 mi, MP 20, head of Zuni River to left at confluence of Rio Nutria (from the north) and Rio Pescado. Continue east up valley of Rio Pescado. **3.3, MP 21**, major junctions ahead: NM-602 to left (3.4 mi) and NM-36 to right (3.9 mi); *continue east on NM-53* toward Ramah and El Morro National Monument.

4.3 mi, MP 22, cliff face from 9:00 to 11:00, capped by Gallup Sandstone, is reference section for Tres Hermanos Formation. Lower part of valley cut in Mancos Shale tongues. This northeast-dipping marine (intertonguing sandstone and shale) section disappears below road level over the next 3.3 mi. **7.6 mi**, nonmarine (upper) Gallup Formation exposed in valley walls and tableland escarpments ahead for next 5 mi. This coal-bearing part of the section is characterized by reddish, coarse, feldspathic sandstones.

9.9 mi, cross bridge over Rio Pescado. Village of Pescado ahead. **10.8 mi**, at 10:00 to 11:00 Rio Pescado lobe of North Plains basalt flow in stream bottom. **13.0 mi**, leave Zuni Reservation.

14.3 mi, MP 32, descend into Ramah Valley of Rio Pescado. **14.8 mi**, Ramah watergap at 10:30 exposes light-color-banded cliffs of Zuni Sandstone with darker Dakota Sandstone capping dip-slope of cuesta-forming southwestern flank of Zuni Mountains. **15.4 mi**, enter Ramah, settled by LDS pioneers in 1874 and named after a figure in the *Book of Mormon*. **16.3 mi, MP 34**, leave Ramah.

16.9 mi, low sandstone bench on valley floor to left is Dakota Sandstone. **18.0 mi**, McKinley-Cibola County line. Road follows the southwestern edge of the Zuni uplift in a broad synclinal valley cut in Mancos Shale. Forested mesa from 1:00 to 4:00 capped by sandstones of Tres Hermanos Formation.

18.6 mi, tree-covered dip-slope on Dakota Sandstone to left. **20.3 mi, MP 38**, Lewis Trading Post to left. **21.0 mi**, crossing lobe of basalt from Rio Pescado tongue for about next 2 mi. **22.3 mi, MP 40**, pinnacles of Zuni Sandstone in watergap at 9:00 are "Los Gigantes"; note crest of Zuni Mountains (Oso Ridge) in distance beyond cuesta capped with Dakota/Zuni Sandstones.

23.2 mi, roadcuts in Two Wells Sandstone Tongue of

Dakota. At 11:00, Inscription Rock (El Morro National Monument) is in Zuni Sandstone cliff at east end of mesa capped by Dakota Sandstone. Basalt cinder cone of North Plains section of Zuni-Bandera field in distance at 12:00. **23.9 mi**, Navajo Hwy 125 to right leads to Ramah Agency headquarters. **24.5 mi**, for next 8 mi basalt flows of the western Zuni-Bandera (North Plains) field cover most of the valley floor. These flows may be as young as late middle Pleistocene (Laughlin et al., 1982). **25.7 mi**, enter El Morro National Monument. **26.3 mi, MP 44**, Zuni Sandstone cliff to right. Inscription Rock at base of cliff (26.5 mi) has the oldest known Spanish inscription in New Mexico: Don Juan Oñate, 16 April 1605. **27.2 mi**, road to El Morro National Monument Visitor Center to right. The tour route is back in the Acoma-Zuni (physiographic) section from here to the Laguna Pueblo area east of Grants (Day 2, Stop 2-1).

27.8 mi, roadcut exposures of North Plains basalt flow. **28.2 mi**, Inscription Rock RV Park to right. Crest of Zuni Mountains (Oso Ridge) forms northern skyline. **29.2 mi**, more roadcuts in North Plains flow. **30.6 mi**, cinder cones in El Malpais and Chain of Craters (North Plains) areas of the Zuni-Bandera field at 12:30 to 3:00. **31.3 mi, MP 49**, Oso Ridge, on northern skyline, is composed of Glorieta Sandstone and overlying limestones and minor sandstones of the San Andres Formation. The Continental Divide follows this segment of Oso Ridge and the chain of cinder cones to the east and south.

31.8 mi, Tinaja Bar and Trading Post on right. **33.3 mi, MP 51**, for the next 6 mi the route skirts the northern edge of the North Plains section of Zuni-Bandera field. The alkali-basalt flow here is locally buried by upper Quaternary sediments (alluvial, eolian, lacustrine), which also lap onto the southward-dipping Permian and Triassic rocks that flank the southern Zuni uplift. Features of the broad strike valley (mainly cut in Chinle Formation) that parallels the tour route are completely masked by a cap of Pliocene-Quaternary basalts. **33.8 mi**, road to left to limestone quarry in San Andres Formation.

36.3 mi, MP 54, red-maroon beds exposed at 10:00 are sandstones of Moenkopi and basal Chinle Formations.

37.3 mi, MP 55, lava cone to right. Bandera Crater (left) and Cerro Bandera (right) cinder cones at 12:00 about 5 mi (8 km) to east-southeast. **38.8 mi**, Oso Ridge cinder cone (Stop 1-6), on skyline at 10:00, is on the southeast end of Oso Ridge. **40.3 mi, MP 58**, Oso Ridge cone (9:00), Bandera Crater (1:00), and Cerro Bandera (1:30) are all on the Continental Divide. K-Ar age of alkali-basalt flow sampled along NM-53 about 1 mi northwest of Bandera Crater (near MP 59) is 0.199 ± 0.042 Ma (Laughlin et al., 1982). *Prepare for left turn in 0.9 mi.*

41.2 mi, *turn left on Forest Service Road 50*; proceed north on FS-50 up cuesta dip-slope on San Andres Limestone and Glorieta Sandstone. **42.4 mi**, crossing Continental Divide (elevation 8190 ft, 2496 m). **42.7 mi**, *turn left on FS-287* to Oso Ridge Lookout Tower on Oso Ridge cinder cone (8713 ft, 2656 m). Walk to Oso Ridge lookout tower and Stop 1.6.

Stop 1-6: Southern El Malpais area of Zuni-Bandera volcanic field area from Oso Ridge cinder cone (A. W. Laughlin, J. W. Hawley, and D. W. Love). The summit of the Oso Ridge cinder cone offers a broad vista of the region south of the broad Zuni Mountain summit area. Mt. Sedgwick (9256 ft, 2818 m) 10 mi (16 km) to the north, and

the crest of Oso Ridge (>9000 ft, 2743 m) to the northwest are high points of the uplift (Fig. 1-5). The route to Stop 1-7 crosses the Precambrian core of the Zuni uplift and descends to the Rio San Jose valley at Grants through Zuni Canyon, which heads about 8 mi (13 km) to the northeast at the prominent gap northwest of San Rafael Mesa (Fig. 1-5). Basalt from the Paxton Springs cone, 3.5 mi (5.6 km) to the east-northeast, flowed through this canyon onto the plain southwest of Grants in latest? Pleistocene time.

This tour stop provides an overview of the local volcanic terrane (western El Malpais and North Plains of the Zuni-Bandera field; Laughlin et al., 1982) and ongoing work in local ice caves on their potential as sites for paleoclimatological research. The Pliocene-Quaternary geology of the northern and eastern part of the plains area (El Malpais lava field of Maxwell, 1982, 1986) and emplacement of the late Holocene McCartys flow are discussed in more detail at Stop 1-7.

An ancient upland erosion surface, which probably started to form as early as in the Eocene, is preserved beneath the extensive flows that mantle the plains to the south and east of this stop. Significant Oligocene to Pliocene extensional tectonic and erosional features may underlie the North Plains area, particularly east of the Continental Divide (Fig. 1; Chain of Craters belt, Fig. 1-5). Post-Laramide evolution of the southeastern margin of the Colorado Plateau is discussed by Cather (1989) and Chamberlin and Anderson (1989b).

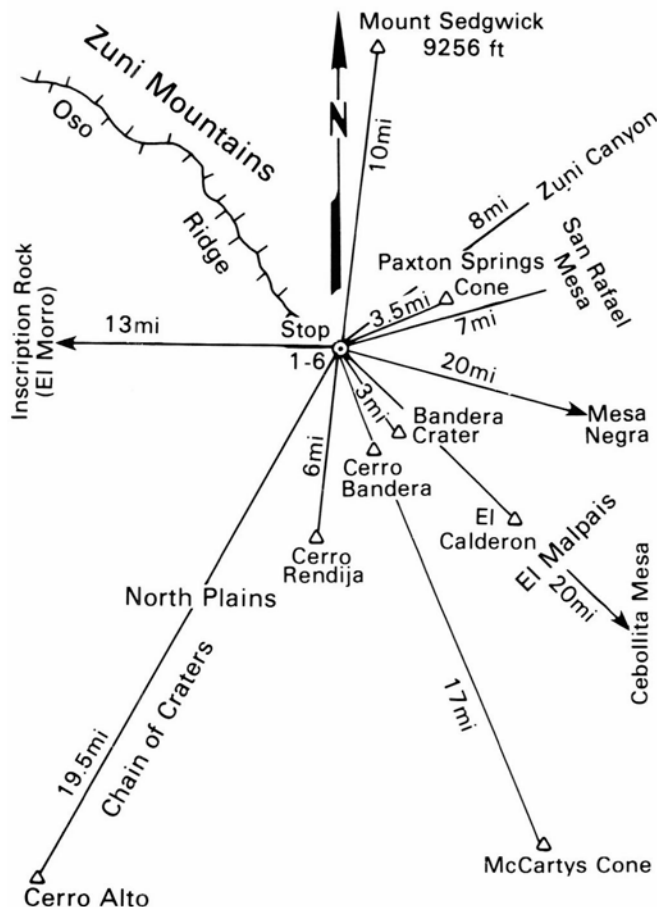


FIGURE 1-5—Panoramic location diagram for major landmarks seen from Stop 1-6 at Forest Service Lookout on Oso Ridge cinder cone; southeastern Zuni Mountains overlooking Zuni-Bandera (El Malpais and North Plains) volcanic field.

According to Baldrige, Perry, Vaniman, et al. (1986, p. 196):

The oldest basalt recognized in the Zuni-Bandera field is 3.8 Ma [sampled at southern base of Cerro Rendija, Fig. 1-5] (. . . Laughlin et al., 1982). Most of the basalts presently exposed in the . . . field are Quaternary in age. Older Quaternary rocks were erupted mainly from a group of 30 cones called the Chain of Craters . . . Younger Quaternary basalts were erupted mainly northeast of the chain, forming an area referred to [by Maxwell, 1982, 1986] as El Malpais . . . On geomorphic evidence, Gawell (1975) and Gawell and Laughlin (1975) recognized a gradual decrease in age from southwest to northeast along the northern portion of the Chain of Craters. A progressive change from alkalic basalts to tholeiites . . . accompanied this change. Elsewhere in the Zuni-Bandera field, compositions range from basanites to tholeiites.

The following comments on the Bandera Crater area by Baldrige, Perry, Nealy, et al. (1989, pp. 217-218) introduce a discussion of laminated ice bodies in collapsed lava tubes (ice caves) at El Malpais National Monument by Thompson et al. (this volume):

Bandera Crater is a breached symmetrical cinder cone about 1 km [0.6+ mi] in diameter and 150 m [500 ft] high. The central depression is about 180 m [600 ft] deep, extending 80 m [260 ft] below the level of the breach. A large lava tube, which extends at least 20 km [12.4 mi] to the south, is exposed in the breach. Although collapsed for the first 800 m [2625 ft], most of the remainder of the tube is intact. After the McCartys flow [Stop 1-7], the flows from Bandera Crater are the youngest in the Zuni-Bandera [El Malpais] lava field. The [alkalic basalt] lavas flowed south and east around the Zuni Mountains to a point of 12 km [7.5 mi] south of Grants. The Bandera flows overlie 0.199 Ma basalt [near MP-59, NM-56; Laughlin et al., 1982] but are themselves too young to date by the K-Ar method . . . The Ice Caves are located in the main lava tube from Bandera Crater. Here, because of the overhang of the collapsed lava tube and the insulating properties of basalt, ice that forms in the winter is preserved throughout the year. The green color of the ice is due to presence of algae. In frontier days, ice from the caves was transported to nearby Fort Wingate [original site near San Rafael]. Other ice caves occur in lava tubes of this area, but are not open to the public.

Return to junction of Forest Service Roads 50 and 187.

Directions and comments en-route to Stop 1-7

This log is adapted primarily from Colpitts et al. (1989). **0.0 mi**, proceed north on FS-50 from its junction with FS-187. **2.9 mi**, FS-50 turns left towards McGaffey (Stop 11) at junction with FS-49. *Continue straight ahead on FS-49* across summit of Zuni Mountains and through Zuni Canyon to southwest edge of Grants. **14.9 mi**, cattle guard; leaving Cibola National Forest. *Continue down paved Zuni Canyon Rd.* **18.4 mi**, Grants city limits. **19.2 mi**, sharp right turn followed by sharp left turn, passing Zuni Canyon Trading Post on left. **19.3 mi**, stop sign at end of Zuni Canyon Rd.; rejoin NM-53, turning left towards Grants. *Prepare for right turn ahead onto 1-40.* **19.5 mi**. *Take eastbound onramp to 1-40.* **20.6 mi**, MP 83, proceed 6.2 mi east on 1-40 to Exit 89. **26.8 mi**, take Exit 89. **26.9 mi**, stop sign at NM-117; turn left, cross over 1-40, and park at west edge of Stuckeys Service area for Stop 1-7.

0.0 mi, proceed northwest on FS-50, descending cuesta escarpment cut on Glorieta Sandstone. Cross concealed Glorieta-Yeso contact beneath hillslope deposits at switchback (0.2 mi). At 12:00 cinders from Oso Ridge cone rest on

upper Yeso beds. **0.5 mi**, base of basalt flow from Oso Ridge vent rests on cinder deposit to left. Flow continues down valley ahead (11:30 to 12:00).

1.0 mi, "No Easy Life Ranch" entrance on left. Low ridge to right (2:00 at 1.1 mi) is formed by Meseta Blanca Sandstone Member of Yeso Formation, which also underlies the Oso Ridge flow to left for the next mile. Road is primarily on thin cover of upper Quaternary valley fill with a few exposures of Meseta Blanca Sandstone. Entering area of detailed mapping by Goddard (1966).

2.0 mi, on Oso Ridge flow with discontinuous sedimentary cover for next 0.3 mi. Quaternary units conceal Yeso/Abo rebedded contact. Paxton Springs road to right (2.1 mi). Cattle guard and Cibola National Forest boundary (2.2 mi). **2.3 mi**, Abo Formation exposed in roadcuts at north edge of Oso Ridge flow; route on Abo rebeds for next 0.7 mi.

2.7 mi, cattle guard. At 2:30, Paxton Springs cinder cone and associated basalt flows (latest? Pleistocene). This is the source of the flow in Zuni Canyon and southwestern Grants area (9.2-21.6 mi). **2.8 mi**, crossing old railroad grade, part of an old logging route extending through Zuni Canyon. **2.9 mi**, junction; *continue straight ahead on FS-49*. Arkosic sandstones and pebble conglomerates near base of Abo Formation are exposed in roadcut ahead. **3.0 mi**, bridge over Agua Fria Creek. Contact of Abo Formation on deeply weathered and fractured granitic gneiss (Precambrian) along creek bed about 200 yards upstream (Stop 1 of Colpitts et al., 1989). Cinder cones marking Paxton Springs vent 1 mi to the east-northeast (2:30). On upper Quaternary valley fill for next 0.2 mi.

3.2 mi, cross exhumed erosion surface cut on granitic gneiss forming core of Zuni uplift for next 3 mi. Basalt from the Paxton Springs vents caps this surface to the east of FS-49. **5.0 mi**, road ascends to surface of small western lobe of Paxton Springs flow. Note pressure ridge to right. For the next mile, route is mainly on valley fill and parallels old logging railroad grade to right.

6.4 mi, back on granitic gneiss; approaching Abo/Precambrian contact in road ahead. **6.5 mi**, possible marine limestone of Pennsylvanian age (pre-Abo?) is exposed in ridge to left (Colpitts et al., 1989, Stop 2). **6.7 mi** cattle guard. Basal Abo sandstone and conglomerate to left. **7.0 mi**, at 11:00 fault contact between Abo and Precambrian, with head of Limekiln Canyon forming break in escarpment on skyline.

7.2 mi, cross bridge in lower La Jara Canyon; on valley fill for next 1.8 mi. Abo rebeds form low ridge in middle distance. High ridge on skyline is escarpment of cuesta capped by northeast-dipping San Andres Formation (limestone, sandstone, and dolomite). The San Andres is underlain by light-colored, quartzose sandstones of the Glorieta Formation, which in turn overlies pale reddish-brown to reddish-gray sandstones and dark-gray limestones of the Yeso Formation. **7.8 mi**, Paxton Springs flows on valley floor at head of Zuni Canyon from 2:00 to 3:00. Cuesta summit to east of canyon is called San Rafael Mesa.

8.3 mi, junction with Forest Service Road 480 (to left). *Continue straight ahead on FS-49*. Basalt flow ahead and to left is a "pre-Paxton Springs" unit derived from a vent on the west side of Cerro Colorado (peak of Precambrian gneissic aplite 2 mi to the northwest). Lobes of this flow ("Zuni flow" of Maxwell, 1986) also extend down canyons in the cuesta escarpment north and east of Cerro Colorado (e.g. Limekiln Canyon). **8.5 mi**, steeply dipping Abo strata

occur adjacent to fault separating Abo and Yeso Formations. **8.7 mi**, end of "Zuni flow" to left. **8.8 mi**, Stop 3 (upper Yeso Formation stratigraphy) of Colpitts et al. (1989).

9.2 mi, junction with Forest Service Road 447 (to right) at head of Zuni Canyon. *Proceed down canyon on FS-49*, with remnant of Paxton Spring flow to left. Permian units exposed in 600 ft (190 m) canyon walls ahead are (ascending) Yeso, Glorieta, and San Andres Formations. **9.8 mi**, old logging slide at 3:00. Logs cut on San Rafael Mesa were run down the slide by cable and used as railroad ties. **10.4 mi**, at top of cliff at 9:00 note exhumed pre-Triassic karst features in upper part of San Andres. **10.6 mi**, remnants of Paxton Springs basalt flow on both sides of road. **12.4 mi**, canyon crosses broad anticlinal flexure. **12.7 mi**, cattle guard. **13.0 mi**, basalt crops out in canyon bottom to left. Yeso rebeds at 3:00 in canyon wall. At 10:00, three-quarters of the way upslope, is the San Andres/Glorieta contact. Basalt flow crops out in canyon bottom at 9:00. **13.7 mi**, basalt in roadcut to left.

14.9 mi, cattle guard; leaving Cibola National Forest; continue on paved Zuni Canyon Rd. Note basalt rims along base of canyon walls ahead. **15.2 mi**, canyon now only in San Andres/Glorieta Formations. **15.7 mi**, last canyon exposures of Paxton Springs flow ahead. Flow is buried by late Quaternary (Holocene?) valley-fill deposits down canyon. **16.7 mi**, San Andres-Glorieta contact in lower canyon walls. **16.9 mi**, Mount Taylor on skyline at 12:00 is flanked to the north by La Jara Mesa and to the south by Horace Mesa. **17.4 mi**, cattle guard. Limestone quarry in San Andres Formation ahead on left; approaching mouth of Zuni Canyon.

17.9 mi, on alluvial plain at canyon mouth; valley fill thins to east and large areas of aa-lava surface on Paxton Springs flow are exposed. **18.4 mi**, Grants city limits. **19.2 mi**, *sharp right followed by sharp left turn*. **19.3 mi**, stop sign at NM-53. *Turn left (north) on NM-53; keep to right and take onramp to I-40 East* (19.5 mi).

20.0 mi, *eastbound on I-40*. Spring mound at 2:00, surrounded by distal part of Paxton Springs flow. **21.6 mi**, **MP 84**, back on older Pleistocene flow from El Calderon center. **22.4 mi**, Exit 85 to motel area in east Grants. Continue southeast on I-40 across northern edge of El Calderon flow and adjacent alluvial flats of the Rio San Jose. **23.4 mi**, Rancho del Padre Spring is in small draw to right, and other springs and seeps are in the marsh area to the left (White, 1989). Spring discharge between here and the Acoma Reservation boundary (about 5 mi, 8 km, downstream) contributes much of the base flow and good-quality water to the Rio San Jose.

23.6 mi, **MP 86**, a faulted Pliocene basalt flow caps Horace Mesa at 9:00 to 11:00 (see Drake et al., this volume). Mesa escarpments are nearly continuously mantled with landslides and colluvium. East-dipping Upper Cretaceous rocks of the Dakota-Mancos-Gallup-Crevasse Canyon sequence are poorly exposed in most areas. **26.6 mi**, **MP 89**, highway cuts across a narrow "neck" of upper Holocene McCartys flow. *Keep right for next exit*. **26.8 mi**, *take Exit 89*. Note basal Dakota Sandstone and small thrust fault in roadcut to right. **26.9 mi**, stop sign. *Turn left* on NM-117 for Stop 1-7 at Stuckeys Service area northwest of I-40 Interchange.

Stop 1-7: Northern El Malpais area of the Zuni-Bandera field from the McCartys flow (D. W. Love, J. W. Hawley,

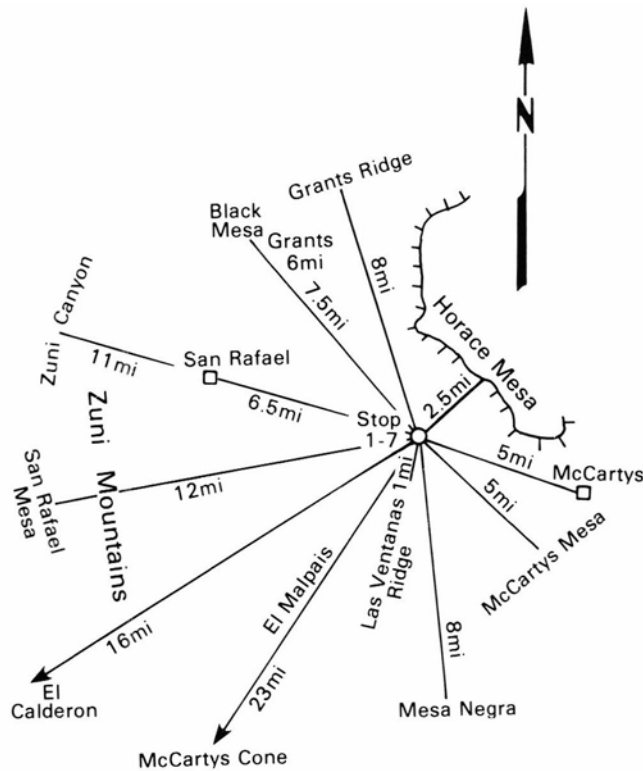


FIGURE 1-6—Panoramic location diagram for major landmarks seen from Stop 1-7, northeastern El Malpais area southeast of Grants.

and P. G. Drake). The McCartys basalt flow at this stop overlies the steep, east-dipping Grants monocline (western limb of the McCartys syncline) within the Acoma sag east of the Zuni uplift (Figs. 1-6, 1-7). Dakota Sandstone caps Las Ventanas Ridge to the south and the low ridge at El Canoncito of the Rio San Jose (0.5 mi to the northwest). The broad, lava-covered plains to the southwest between the east end of the Zuni Mountains and Las Ventanas Ridge/Cebolleta Mesa (Fig. 1), have been inundated by basalts of the El Malpais and North Plains (Zuni—Bandera field) numerous times during the Pliocene and Quaternary. The most recent event was emplacement of the Upper Holocene McCartys flow. The flow, originally described by Nichols (1946), is about 30 mi (48 km) long and originated at a small cinder cone about 23 mi (37 km) south-southwest of this stop (Fig. 1-6; Maxwell, 1986). The flow is about 5 mi (8 km) wide at its source, but is confined in a narrow (as little as 60 m) valley immediately southwest of this stop. Geomorphic expression and stratigraphic relationships with respect to adjacent valley-fill deposits (alluvial, lacustrine, and eolian) indicate that the flow is about 1000 years old. Thus the after A.D. 700 age estimate of Nichols (1946), based on Indian legends and indirect archaeological evidence, is quite reasonable.

There is now no integrated surface runoff, and no name has been given to the former major tributary of the Rio San Jose that cut this valley buried by the El Malpais flows. One rancher at the southern (upper) end of the plains re-



FIGURE 1-7—Aerial view, toward the south of McCartys flow (late Holocene) at I-40–NM-117 interchange southeast of Grants. Stop 1-7 is at Stuckeys service area northwest of interchange in center foreground. Las Ventanas Ridge cuesta is beyond interchange with Cebolleta Mesa on the far upper left. The El Malpais area of the Zuni–Bandera field is to the right of the McCartys flow. Note smooth surface of El Calderon flow (lower right) with thin mantle of eolian and colluvial deposits (photo A. W. Laughlin).

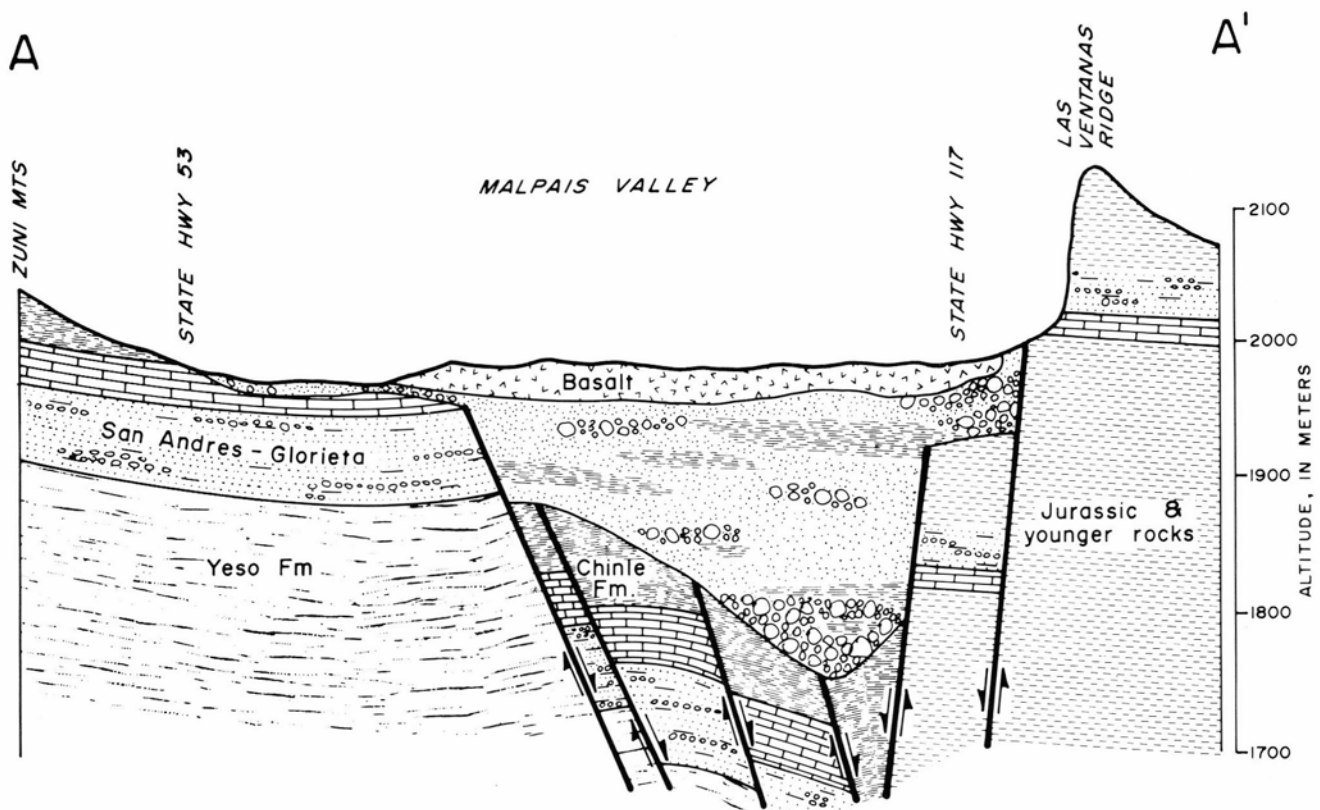


FIGURE 1-8—Geologic cross-section of "Malpais Valley." Interpretations based on shallow seismic-refraction survey (from Kelley and Reynolds, 1989, fig. 2; with New Mexico Geological Society permission).

ported drilling through about 900 ft (275 m) of basalt flows before reaching gravel overlying bedrock (Triassic?; C. Maxwell, pers. comm. 1988). Kelly and Reynolds (1989) show about 600 ft (183 m) of fill at the lower end of the valley about 4 mi southwest of this stop. Their seismic-profile interpretation (Fig. 1-8) indicates that the basalts, ancestral Rio San Jose fluvial deposits, and other valley-fill facies (eolian, lacustrine) occupy a moderately deep structural basin (graben) of late Cenozoic age.

Flows exposed on the valley floor have K—Ar ages ranging back to 3.8 Ma (Laughlin et al., 1982; Stop 1-6). The older reported ages are questionable at least for flows in the northeastern part of the field, because flows could not have been emplaced near the present valley-surface level before extrusion of the high-level Horace Mesa flows 2.5 to 2.9 Ma (Lipman and Mehnert, 1980) and possibly correlative basalts capping Mesa Negra (Fig. 1-6) and Cebolleta Mesa south of this stop (Maxwell, 1986). Two younger flows with

K—Ar ages of about 1.5 Ma (Laughlin et al., 1982) may indicate that maximum valley entrenchment occurred prior to that time. Maxwell (1986) and Kelly and Reynolds (1989) show a young fault along the southeastern margin of the valley (Fig. 1-8); but even if subsidence has occurred during relatively recent tectonic movement, it is unlikely that basalts as old as 3.8 Ma could have been displaced more than 1000 ft (300 m) to form the present valley.

Valley margins along the El Malpais—North Plain flows have not eroded back appreciably since the flows' emplacement. Numerous landslides, talus cones, and alluvial—colluvial aprons grade to the present valley base level. The lack of extensive hillslope retreat suggests that mass-wasting processes also take place episodically and, on the average, rather slowly, over long intervals. See Drake et al. (this volume) for additional information on the area of this stop.

Return to Grants via 1-40; take Exit 85 to motel area. End of Day 1.

Day 2: Grants to Estancia basin

Summary

Part 1 of today's tour traverses the southeastern Colorado Plateau (Acoma—Zuni section, Fig. 1) and the central Rio Grande rift area of the Basin and Range province (Mexican Highland section, Fig. 2). Emphasis is on the Pliocene—Quaternary geomorphic evolution of the lower Rio San Jose and Rio Puerco valleys, and the southern Albuquerque basin. Volcano-tectonic and geomorphic evolution of San Jose

drainage system in the Colorado Plateau—Basin and Range transition zone is discussed at Stop 2-1 near Laguna Pueblo (Fig. 1). Stop 2-2 introduces the structural framework of the Albuquerque basin (central Rio Grande rift), and volcanic units and basin-fill (Santa Fe Group) stratigraphy in the south-central part of the basin west of Los Lunas. Emphasis at Stop 2-3 is on late Quaternary geomorphic processes and valley-fill stratigraphy in the Rio Puerco valley

west of Belen. Optional Stop 2-4 on the Rio Grande valley rim overlooking Belen focuses on the hydrogeologic framework of the upper Santa Fe Group (Plio-Pleistocene) aquifer system. Discussion at Stop 2-5 at the Sevilleta National Wildlife Refuge in southeastern Albuquerque basin emphasizes late Holocene ecologic changes at the northern end of the Chihuahuan Desert. This locality is also near the boundary between the Basin and Range (Rio Grande rift) and southern Great Plains structural provinces.

Part 2 of today's tour (as well as the first stop of Day 3) is in the closed Estancia basin east of Mountainair (Fig. 2),

which is the site of late Pleistocene Lake Estancia (Meinzer, 1911). Tour stops (E-1, E-2, E-3) emphasize lake and playa features of late Wisconsin and Holocene age. Estancia basin and highlands to the south and east also mark a physiographic transition from the Basin and Range province (Sacramento section) to the southern Great Plains (Pecos valley section).

Road log entries between Grants and Mountainair are primarily compiled from Hawley, Crumpler, and Wells (1982); Hawley, Love, and Wells (1982); and Maxwell et al. (1989).

Day 2, Part 1: Grants to Mountainair

Directions and comments en-route to Stop 2-1

From the parking lot of the Inn at Grants go south (0.5 mi) to 1-40 Interchange (85) and east on 1-40. **1.7 mi, MP 86**, crossing the El Calderon flow. **4.9 mi**, Exit 89 to right (Day 1, Stop 2-7), crossing narrow neck of McCartys flow confined in a former arroyo by Las Ventanas Ridge (east, Morrison and Dakota Formations) and Pleistocene El Calderon flow (west). Route crosses El Calderon and McCartys flows for next 4.8 mi. **6.7 mi, MP 91**, crossing Rio San Jose; for next 2 mi route crosses distal segment of McCartys flow. Note pressure ridges and water-filled depressions of collapsed lava tubes. **8.7 mi, MP 93**, rest area ahead (0.2 mi) on McCartys flow. **9.7 mi, MP 94**, end of McCartys flow; route ahead on upper Holocene fill of Rio San Jose valley. Bridge over Rio San Jose; exposures before railroad underpass are Whitewater Arroyo Tongue of Mancos Shale overlain by Twowells Tongue of Dakota Formation.

12.7 mi, MP 96, a small, steep dome is visible in middle distance in front of Mt. Taylor at 10:00-10:30 where beds of Crevasse Canyon Formation dip steeply away on all sides. A drill hole in the center of the dome encountered a mafic intrusive just below the surface. Broad cuestas to right are capped by Cubero Sandstone Tongue of the Dakota over the Oak Canyon Member; a veneer of high-level terrace gravel is commonly present. **15.7 mi, MP 100**, Acoma Dam and reservoir to right; at 1:00 is Flower Mountain volcanic center. **17.0 mi**, broad, flat area adjacent to 1-40 on right is interpreted to be the site of a small Pleistocene lake in an erosional depression in the Mancos Shale. **18.7 mi, MP 103**, ahead, route descends through Cubero and Oak Canyon Members of Dakota Formation.

20.2 mi, take Exit 104 to Cubero, Budville, and Paraje. Turn left across 1-40, then turn right (east) toward Paraje on NM-124 (mi 20.6). Dakota/Morrison contact exposed near top of mesas on both sides of valley. Numerous landslides covering Morrison Formation below. **23.3 mi**, downtown Paraje, road to right leads to Casa Blanca and Acoma Pueblo. **24.9 mi**, turn off to Laguna—Acoma High School on left. A well near here penetrated 160 ft of alluvium. Stratigraphy of Frog Mesa (9:30-11:00) from top down: basalt flows from Wheat Mountain cone overlying Clay Mesa Tongue of Mancos Shale, light-colored Cubero Tongue of Dakota Sandstone, paludal shale of Oak Canyon Member of Dakota, and dark-gray sandstone ledge of Encinal Canyon Member of Dakota. Landslide debris covers the Brushy Basin Member of the Morrison Formation. The surface be

low the basalt flows is called the Wheat Mountain surface by Moench and Schlee (1967) and represents an early stage of valley entrenchment by the Rio San Jose. The youngest flow on Frog Mesa has a K—Ar age of 2.42 Ma (Lipman and Mehnert, 1980). **25.1 mi**, buried well-developed soil in arroyo cuts on both sides of bridge. **26.2 mi, MP 22** and New Laguna Post Office. Landslides over eolian sandstone of Morrison ahead. **27.9 mi**, NM-279 to left goes to Jackpile uranium mine and villages of Paguete, Bibo, and Seboyeta. **28.1 mi**, cross AT&SF Railroad. *Prepare to turn left for Stop 1.* **28.3 mi**, *turn left toward old baseball field, park, and walk to railroad cut.*

Stop 2-1: Geomorphic and tectonic evolution of the lower Rio San Jose drainage basin. See Drake et al. (this volume) for tour-stop discussion.

Directions and comments en-route to Stop 2-2

Entries for this part of the trip are modified from Maxwell et al. (1989), Hawley, Love, and Wells (1982), Hawley, Crumpler, and Wells (1982), Wells et al. (1983), and Love and Hadley (1986). Late Neogene and Quaternary geology of the area between here and Stop 3 was first studied in detail by Wright (1946). For the next 25 mi the route continues to closely follow the Rio San Jose valley (via 1-40 and NM-6) through the easternmost Acoma—Zuni section of the Colorado Plateau to the western border of the Basin and Range province (Mexican Highlands section). See Love and Young (1983) for a review of the geomorphic history of this part of the Rio Grande—Rio Puerco drainage basin. Volcanic and extensional tectonic features along the route to Stop 2 (Los Lunas volcano) are reviewed by Baldrige et al. (1987, 1989).

From Stop 1 continue southeast on NM-279. **0.3 mi**, roadcut in crest of hill through eolian facies of Morrison Formation. Descend hill into valley past turnoff to Laguna on right. **0.7 mi**, cross Rio San Jose. Note younger valley fill inset against Laguna basalt and dissection of alluvium by present stream. **1.0 mi**, *get into left lane to return to 140 East* at Interchange 114. **1.9 mi**, entering 1-40, dikes cutting Morrison Formation exposed in roadcuts on both sides of road; descend hill through roadcuts of eolian facies of Morrison Formation and Horse Mesa and Beclabito Members of Wanakah Formation cut by diabase dikes. At 4:00 dunes cascade down from mesa rim. **2.7 mi**, wavy bedding in Wanakah Formation to right is due to collapse below. **3.1**

mi, clastic dikes in Horse Mesa Member of Wanakah on both sides of 1-40. **3.4 mi**, large collapse feature at 3:00-4:00 in Horse Mesa Member of Wanakah Formation; to east across valley is section of Entrada Sandstone, Todilto limestone and gypsum, Beclabito, and Horse Mesa Members of Wanakah, and lower eolian facies of Morrison Formation. Laguna flow is dissected in valley.

4.2 mi, MP 117, Mesita exit ahead; route is in Quaternary alluvium and Triassic Chinle Formation. **7.2 mi, MP 120**, bridge across Rio San Jose ahead. Valley at 4:00 is Arroyo Colorado, location of several Pliocene and Pleistocene volcanic centers (Baldrige et al., 1987). **9.0 mi**, railroad overpass; lowest cuesta on left for next several miles is Correo Sandstone bed in Petrified Forest Member of Chinle Formation. Note toeva blocks partially buried by alluvium near base of slope to left. **10.2 mi, MP 123**, section above Chinle Formation exposed on Mesa Gigante to north consists of Entrada, Wanakah, Morrison, and Dakota Formations, with the latter forming top of mesa. **13.7 mi**, take exit 1-40 to NM-6. Turn south toward Los Lunas (mi 14.0).

14.7 mi, MP 1 on NM-6, descend alluvial apron to Rio San Jose. Mesa Redonda is at 10:00, Sierra Lucero at 12:00; Cerro Verde, volcanic source of the 0.32 Ma (K-Ar) Suwanee basalt flow is at 1:00 (Bachman and Mehnert, 1978; Baldrige et al., 1987; Leavy and Shafiqullah, 1987). The Suwanee basalt flow is 44 mi (70 km) long, flowing north to the Rio San Jose, east, and then south. The flow is partially covered with alluvium and eolian deposits and controls the amount of incision upstream from the flow. **15.0 mi**, cross Rio San Jose. According to U.S. Geological Survey records, present average discharge is 11.6 cfs (0.33 m³/s). The largest estimated historic flood here was 11,000 cfs (312 m³/s) on August 21, 1935. **15.8 mi**, route crosses old US-66. Wild Horse Mesa Bar to left, Correo townsite to west across railroad overpass.

17.9 mi, head of Rio San Jose Canyon in Suwanee basalt to left; Suwanee Peak at 9:30; Mesa Redonda at 1:00-2:00 is composed of the same units exposed in Mesa Gigante, from the Todilto gypsum up to the Dakota Formation. The units have been folded and faulted and are capped with a basalt flow about 3 Ma old. Beyond Mesa Redonda is the northern edge of the Lucero uplift. The northern end is capped with a basalt flow 3.4 Ma (K-Ar; Bachman and Mehnert, 1978; Baldrige et al., 1987). Numerous landslides have developed in the mudstones of the Chinle Formation around the margin of the mesa. **18.7 mi, MP 5**, site of Suwanee Station on AT&SF Railroad to right. **20.7 mi**, roadcuts in Todilto Gypsum. To east are squeeze-ups of Suwanee basalt. Mesa beyond San Jose Canyon at 11:00 consists of Jurassic and Cretaceous sandstones. There is no sharp topographic break between the Colorado Plateau and Basin and Range physiographic provinces at this point (Hawley, 1986a), but we are close to the boundary shown on most physiographic maps (e.g. Fenneman, 1931; Hunt, 1974).

22.5 mi, view at 9:30 down Rio San Jose toward Rio Puerco. This area provides spectacular views of the northern Lucero uplift and lower Rio San Jose. The Rio San Jose joins the Rio Puerco about 3 mi (5 km) downstream. Note the reddish color of the San Jose alluvium, derived from Permian and Triassic redbeds. **23.2 mi**, the structural boundary between the Colorado Plateau and the Rio Grande rift is beneath the basalt flow in this area. The rift-bounding Santa Fe fault along the front of the Lucero uplift has been

projected northward to 1-40 and farther north toward the Nacimiento Mountains. Note Manzano (12:00) and Sandia (10:00) uplifts on the far eastern skyline beyond the Llano de Albuquerque. See Lozinsky et al. (this volume) for geological overview of the Albuquerque (rift) basin and Santa Fe Group basin-fill stratigraphy.

25.7 mi, MP 12, Ladron Mountains are at 12:00, faulted edge of Lucero uplift at 12:30-1:00; fill of Albuquerque basin is exposed in hills east of the mountain front. Travertine from springs along the faulted edge of the Lucero uplift makes up the white deposits at 3:00. Hidden Mountain at 10:30. **27.3 mi**, road descends off tip of Suwanee (Cerro Verde) basalt flow toward Arroyo Garcia. This is a site of experimental work on surface-exposure dating of basalt flows using the CL-36 method (Phillips et al., 1986; Leavy et al., 1987). Note ancestral Rio San Jose gravel beneath the flow. An outlier of Santa Fe Group basin fill (late Miocene to early Pleistocene) at 10:00 lies between the valley of the ancestral Rio San Jose and Rio Puerco. **31.7 mi, MP 18**, valley of Rio Puerco at 10:00-1:00; Hidden Mountain at 2:30 is a subvolcanic igneous intrusion cutting basin-fill sediments. The plug is dated at about 8 Ma.

32.1 mi, bridge over Rio Puerco. Gaging station at AT&SF Railroad bridge to right. According to Hawley, Love, and Wells (1983), the average discharge is 57 ft³/sec (1.6 m³/sec). Water flows here about 55% of the year (200 days). Bankfull discharge for the present inner channel is approximately 3250 ft³/sec (92 m³/sec). Extreme floods occurred on August 12 and September 23 of 1929. The flood of September 23 had a flood stage of 18 ft (5.5 m), destroyed the railroad bridge, and had an estimated discharge of 37,700 ft³/sec (1,070 m³/sec). The highest recorded sediment concentration for the Rio Puerco was 680,000 ppm, 75% of which was sand (Nordin, 1963).

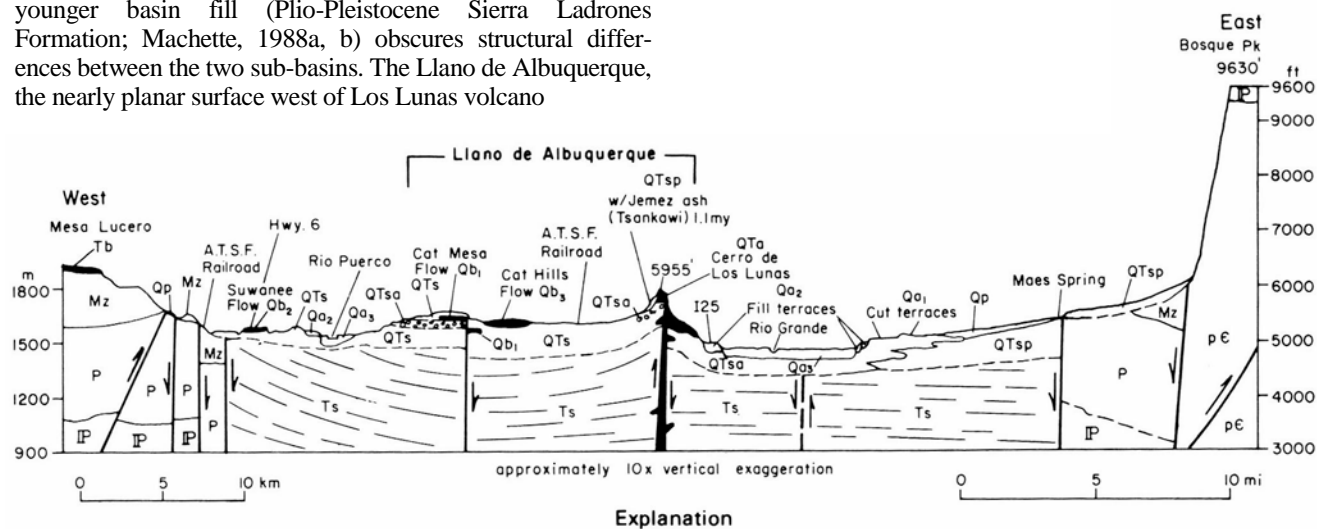
The Rio Puerco in this reach has developed an active inner channel and inner floodplain within Rio Puerco arroyo since the floods of 1929. Common geomorphic and sedimentologic features within the channel include thalweg, sand bars, several levels of battures, and berms with ripples and dunes. Features developed along the inner floodplain include natural levees, chute channels across point bars, oxbows, splays, and accumulations of eolian sand. Tamarix (*Tamarix* sp.), willows (*Salix* sp.), and rabbit brush (*Crysothamnus nauseosus*) dominate the vegetation within the arroyo. Also see discussion in Hawley, Love, and Wells (1982) and Wells et al. (1982, 1983). Stop 2-3 is about 13 mi (21 km) down valley from this point.

32.3 mi, ascending alluvial apron derived from basin fill. The basin fill (upper Santa Fe Group) in this area was deposited by southeastward-flowing ancestral Rio Puerco-Rio San Jose systems. Fossils within the fill near here are between 1.4 and 4 Ma (Blancan age). **32.7 mi, MP 19**, Mohinas Mountain south of Hidden Mountain at 2:30 is another igneous intrusion cutting basin fill. For the next few miles, tributary washes crossed by the road were quite active on July 1, 1986, resulting in road damage and temporary closure. **34.3 mi**, lower Rio Puerco valley at 2:00-3:30. Pottery Mound Pueblo site and University of New Mexico research area on valley floor adjacent to Rio Puerco arroyo at 3:30. The ruined 500-room pueblo was occupied between A.D. 1325 and 1475 and may have housed 1000 people (Cordell, 1982a). Occupants brought pottery from all over the Southwest to the site. Potsherds were thrown into a channel of the Rio Puerco about 20 ft (6 m) deep. The

channel filled during the occupation and the modern channels are north of the pueblo.

37.2 mi, ascending eroded edge of Llano de Albuquerque; then crossing old valley graded toward Rio Puerco. Cat Hills basalt flow from cinder cones at 10:30 has been dated at approximately 140,000 yrs. **41.5 mi**, bridge over AT&SF Railroad. **41.6 mi**, prepare to turn right. **42.4 mi**, turn right on gravel road toward Cerro de Los Lunas (Los Lunas volcano). **42.7 mi**, turn left onto dirt track that heads southeast toward volcano along edge of Llano. Route ascends alluvial apron from Los Lunas volcano. **44.1 mi**, turn left before juniper tree. **44.3 mi**, park vehicles in wide spot for Stop 2-2.

Stop 2-2: Los Lunas volcano (David W. Love, Richard P. Lozinsky, and Bruce Hallett). This stop (elevation about 5500 ft, 1675 m) is on the northwest flank of Los Lunas volcano along a 260 ft (80 m) escarpment exposing 660 ft (200 m) of upwarped basin fill and a section of post-volcano alluvial apron. The volcano and exposed basin fill lie along a southwest—northeast-trending accommodation zone that divides the Albuquerque basin into two half-grabens (Lozinsky et al., this volume). The northern Albuquerque basin is deeper on the east side and steps up to the west; the southern Albuquerque basin is deeper on the west side and steps up to the east (see Lozinsky et al., this volume). Fifteen kilometers to the north-northeast from this stop, a Shell Oil well penetrated 4407 m (14,458 ft) of upper Oligocene to lower Pleistocene basin fill (Santa Fe Group) and did not reach pre-Tertiary rocks at a total depth of 6482 m (21,266 ft). The younger basin fill (Plio-Pleistocene Sierra Ladrones Formation; Machette, 1988a, b) obscures structural differences between the two sub-basins. The Llano de Albuquerque, the nearly planar surface west of Los Lunas volcano



Post-Santa Fe Group		Santa Fe Group	Pre-Santa Fe Group	Volcanic Units
Qa ₃ —Younger valley fill; axial deposits of Rio Puerco and Rio Grande	QTs— Sierra Ladrones Fm. undivided	Mz—Mesozoic rocks	Qb— Quaternary basalt	Qb ₃ — Cat Hills flow (late Pleistocene)
Qa ₂ —Older-fill terrace deposits of Rio Puerco and Rio Grande	QTsa— Sierra Ladrones Fm. axial-river facies	P— Permian rocks	Qb ₂ — Suwanee flow (middle to late Pleistocene)	Qb ₁ — Cat Mesa flow (early Pleistocene)
Qa ₁ —Axial Rio Grande cut terraces (thin fill on QTsa)	QTsp— Sierra Ladrones Fm. piedmont facies	IP— Pennsylvanian rocks		
Qp— Piedmont deposits; interfinger with and/or overlie Qa units	Ts— Lower Santa Fe Gr. (Popotosa Fm. equivalent)	pE—Precambrian rocks		QTa—Plio-Pleistocene andesite of Cerro de Los Lunas (>1.1 my)
				Tb— Tertiary basalt

FIGURE 2-1—Diagrammatic cross-section of central Albuquerque basin near Los Lunas showing stratigraphic relationships of basin fill and later Quaternary deposits and volcanics (from Hawley, Love, and Wells, 1983).

that slopes gently to the south, is a remnant of a broad fluvial plain that predated initial river-valley entrenchment in early to middle(?) Pleistocene time. To the northwest, the Cat Hills are a line of cinder cones capping the Llano de Albuquerque. A related basalt flow that descends to a terrace (probably Segundo Alto Surface of Bryan, 1938) has a K—Ar date of $140,000 \pm 38,000$ yrs (Kudo et al., 1977). To the north is Wind Mesa, an undated shield volcano of basaltic andesite with a post-eruptive graben trending north—south through the center. Farther north-northeast are the Albuquerque Volcanoes, Sierra Nacimiento, and Jemez Mountains. To the northeast is Isleta volcano, a tuff-ring, cinder cone, and flow complex of alkali-olivine basalt dated at 2.78 ± 0.12 Ma (Kelley and Kudo, 1978), which is interbedded with ancestral Rio Grande deposits.

Los Lunas volcano consists of five flows, two vents, and some intrusive centers (Kelley and Kudo, 1978). A separate older, faulted sequence of flows occurs to the south and west (see below). Conventional K—Ar dates on several of the flows on the main volcano range from 1.31 ± 0.05 to 1.01 ± 0.10 Ma (Bachman et al., 1975). The oldest flows of Los Lunas volcano lie on an angular unconformity on previously folded and possibly faulted Santa Fe beds (Fig. 2-1).

The series of flows seen on the north side of Los Lunas volcano are light-brown to gray in color, medium- to fine-grained, and finely vesiculated. Quartz-rich blebs and granitic and mafic granulite xenoliths occur in some flows. A 1-6 m (3-20 ft) reddish-orange spatter-fed flow is seen

bedded between two darker flows. With the exception of this flow, others seen here in outcrop can be traced to the east, descending into the Rio Grande valley. There is no evidence that these flows have been buried by Rio Grande gravels. The intrusive andesites, observed mainly to the southwest of the central peak, are typically a darker gray to black, finer-grained, and also finely vesiculated.

The volcanic rocks at Los Lunas define two chemically distinct trachyandesite groups. The intrusive rocks are slightly subalkalic, while the flows tend to be more alkalic in composition. These intrusives, although more "mafic" looking, have higher SiO_2 and lower TiO_2 , MgO , CaO , Na_2O , Sr , Zr , and Nb (Hallett, unpubl. data) compared to the flows. High K/P and Ba/Nb , low Y/Nb and Zr/Nb , positively correlated "SeSr and SiO_2 values, in conjunction with crustal xenoliths all suggest that the Los Lunas trachyandesites have undergone crustal contamination.

Escarpsments northwest and southwest of Los Lunas volcano expose similar basin-fill stratigraphy. The base of the section directly below Stop 2-2 is a local angular unconformity between a deformed pumice-bearing fluvial unit dipping from 12 to 85° to the northwest, and a nearly horizontal overlying alluvial channel and eolian complex. To the north, this complex dips 8-15° northwest and accounts for the bulk of the exposures seen at this stop. Lozinsky (1988) measured about 145 m (476 ft) of basin fill between the angular unconformity and the base of tephra from Los Lunas volcano. The lower part of the section is dominated by pedogenically modified eolian sand with rare crossbedding. The upper part of the section is fluvial sandy gravels from the northwest (Rio Puerco drainage). Within the section are several pumice- and obsidian-bearing gravels derived from the Jemez Mountains. One distinctive unit is a stack of pumice debris flows within a thicker section of overbank silts and clays (a date is pending). Blancan fossils are reported from this section (Galusha, unpubl. data; Tedford, 1981), but none were found during the current study.

The lowest fallout tephra from Los Lunas volcano is about 1 m thick where it is preserved in a syncline closest to the volcano (1 km north of Stop 2-2) and is deformed (see Haneberg, this volume). This tephra is reworked to fill the syncline with horizontal debris flows. Within a smaller graben farther north, three or more fallout tephra beds drape across eolian sand and clay dunes (Fig. 2-2). Farther north along NM-6 the single tephra layer thins to 20 cm.



FIGURE 2-2—Tephra beds interfingering with fine-grained eolian dunes north of Los Lunas volcano. Each ledge is a different tephra bed. Middle and upper beds are draped over dunes. View to northeast across Rio Grande valley, toward Sandia Mountains.

Overlying the tephra with a local unconformity at the base is the undeformed alluvial apron shed from Los Lunas volcano and uplifted basin fill. The alluvial apron ranges up to about 50 m (165 ft) thick. At Stop 2-2, a gravelly channel truncates the older basin fill. Ash from the 1.1 Ma old upper Bandelier eruption (Tsankawi tephra at base of Tshirege Member, communication of Manley, 1976; referenced by Bachman and Mehnert, 1978) is well preserved in this channel fill along with boulders of Los Lunas andesite. The upper part of the alluvial apron contains a stack of two or more soils with stage II to III pedogenic carbonate horizons.

The southwest escarpment (over the hill from Stop 2-2) exposes similar units, but the lowest part of the section consists of andesitic lava domes and flows buried by eolian units. The emplacement of these eruptives may account for the earlier deformation seen near the base of both exposed sections.

Controversies regarding the stratigraphy and geomorphology around Los Lunas volcano may be settled by analysis of the stratigraphy and geochemistry of the flows. As summarized by Hawley (1978; Hawley, Love, and Wells, 1982), Bachman (Bachman et al., 1975; Bachman and Mehnert, 1978) interpreted the upper paleosol-soil sequence as the culmination of aggradation of the Llano de Albuquerque surface. He also correlated the dated Los Lunas andesite with the outlying, largely buried andesite flows low in the section. Thus Bachman interpreted the Los Lunas volcano as a partially exhumed volcanic center and the Llano de Albuquerque surface as being post-Los Lunas volcano. He also demonstrated that the Llano de Albuquerque surface is not the same surface as the Ortiz erosion surface described by Bryan (1938).

In contrast, Kelley (Kelley et al., 1976; Kelley, 1977; Kelley and Kudo, 1978) interpreted the eruption of Los Lunas volcano as post-dating formation of the Llano de Albuquerque surface with flows descending to a lower surface within the Rio Grande valley. Kelley correlated the surface along truncated basin fill at Stop 2-2 with the Ortiz erosion surface of Bryan (1938) and Bryan and McCann (1938). Kelley also interpreted the andesites within the section south of Los Lunas volcano as being intrusives.

The controversy may be resolved by taking interpretations from both groups. The southwestern andesites are demonstrably flows interbedded with Santa Fe Group eolian sediments, are chemically distinct (Kasten, 1977), and are older than Los Lunas volcano. The volcano erupted from the uplifted edge of the Llano de Albuquerque and lavas flowed to a lower level to the east and were not buried by basin fill. The amount of tectonism involved in the differential elevation of the volcano and the flows remains to be determined. The Llano de Albuquerque surface west of Los Lunas stabilized by 1.1 Ma and was buried by the alluvial apron shed from Los Lunas volcano and underlying deformed sediments. Soils associated with the alluvial apron are products of pedogenesis that started 1.1-0.5 Ma ago. The Llano de Albuquerque and the alluvial apron are both much younger than the mid-Pliocene Ortiz surface.

Directions and comments en-route to Stop 2-3

Stop 2-3 is in the Rio Puerco valley west of Belen. From Stop 2-2 return 1.9 mi to NM-6 and turn right (east) 4.0 mi to 1-25. Route descends to Segundo Alto geomorphic surface, here a terrace about 40 m (130 ft) above the Rio

Grande floodplain, formed on mid-Pleistocene fluvial deposits of the Los Duranes alluvium (Lambert, 1968). *Turn right (south) on I-25.* To west are flows of Los Lunas volcano. Continue south 11.2 mi to Exit 191 (Sosimo Padilla Blvd.). *Turn right (west) on Sosimo Padilla Blvd.;* ascend hill past exposures of Sierra Ladrones Formation (upper Santa Fe Group) to Llano de Albuquerque. Study of the spatial variability of facies and permeability of these deposits is summarized by Lohmann et al. (this volume). Route crosses the Llano rim 0.9 mi west of I-25 Interchange 191. *This is the site of Optional Stop 2-4.* Continue past New Mexico Travertine processing plant to end of pavement at Belen International Airport (2 mi). Continue 0.6 mi and turn right (west) on county road (slightly improved). Road west crosses several subdued fault scarps before reaching the escarpment "Ceja del Rio Puerco" 2.6 mi from turn. Descend Ceja toward Rio Puerco and *turn right 0.9 mi below the escarpment rim toward abandoned windmill.* Drive 0.4 mi off county road past windmill and park. Walk to arroyo edge at meander bend.

Stop 2-3: Rio Puerco (David W. Love and John W. Hawley). At this stop (elevation 4900 ft, 1495 m) we examine depositional environments of the modern Rio Puerco and an exposure of facies in a buried arroyo of late Holocene age, to determine the way it filled. Topics covered besides specific features within the arroyo and their paleohydrologic implications are (1) the thickness and age of basin and valley fills of the southern Albuquerque basin, (2) spatial variability of permeability within depositional units (Stop 2-4), (3) terraces along the Rio Puerco, and (4) regional and perched ground water in relation to recharge and evapotranspiration along the modern Rio Puerco. This part of the lower Rio Puerco valley is the site of several recent geoarchaeological and environmental geochemical studies relating to proposed dam construction and downstream effects of uranium mine—mill operations (Love et al., 1982; Love and Young, 1983; Popp et al., 1984, 1988).

Exposures along the lower Rio Puerco (Shepherd, 1976, 1987; Young, 1982; Love et al. 1982; Love and Young, 1983; Robinson and Love, 1986) show at least two episodes of arroyo cuts-and-fills similar in size and shape to the modern arroyo and other buried channels with different facies (Fig. 2-3). At Stop 2-3 we can compare similar facies of the modern Rio Puerco and a buried channel to speculate about similar processes and conditions in the past and what to expect in the future.

The lower Rio Puerco is a losing stream, that is, it loses water to its bed. A flow of as much as $0.14 \text{ m}^3/\text{s}$ (5 cfs) at the stream gage along NM-6 west of Los Lunas is lost to seepage and evaporation before it reaches the stream gage at Bernardo (Heath, 1983; Heath and Love, 1986). In this reach west of Belen, the permanent water table is 10-13 m

(30-40 ft) below the base of the modern channel, but there are seasonally fluctuating perched water tables on clay layers within the alluvium above the permanent water table (Figs. 2-4, 2-5). These perched water lenses tend to be recharged from the Rio Puerco when it is flowing on loose sand, and to be depleted by seepage to lower levels and by transpiration by tamarisks and willows.

The channel shape of the lower Rio Puerco reflects repeated attempts at adjustment to extremely variable flows and an extremely high sediment load. Flows much larger than bankfull tend to scour the base of the channel and even scour the floodplain locally. Smaller flows tend to build sand bars attached to both sides of the channel and to aggrade the floor of the channel.

Within the buried arroyo exposed in the modern arroyo wall, extensive floodplain deposits are scoured by both large and small channels (Fig. 2-6). The large channel shows multiple episodes of scour and fill before the whole arroyo was filled in. The "last gasp" channel of the fill is redder, more poorly sorted, and is interpreted to be due to local runoff from the surrounding valley sides (local sources for red clay and well rounded gravel). Apparently less and less runoff and sediment from upstream reached the lower Rio Puerco as its arroyo filled up. Does this imply (1) a drying climate, (2) increased retention of water upstream due to better vegetation cover, or (3) some other complex response (Schumm, 1977) mechanism upstream in the basin resulting in decreased sediment and/or water delivery? Can we draw any conclusions regarding how the present arroyo will fill in? Can we draw any conclusions about climatic cyclicity with conditions even more arid than now?

Valley fill and terraces along the Rio Puerco reflect longer-term cyclic adjustments in sediment storage and delivery (Love, 1986). The valley fill in this reach of the Rio Puerco is at least 135 ft (41 m) thick. Drill holes have not encountered extensive coarse facies at the base or within the fill. The most obvious terrace along the Rio Puerco is the Montano Flats surface 100-140 ft (30-42 m) above the Rio Puerco west of Stop 3-3; other possible terrace remnants are at 10 ft (3 m), 20-25 ft (6-8 m), 80-100 ft (24-30 m), and 180-200 ft (55-61 m) (Fig. 2-7; Love and Young, 1983).

Directions and comments en-route to Optional Stop 2-4

From Stop 2-3 return to the county road and back (4.1 mi) across the Llano de Albuquerque to the rim of the escarpment forming the western wall of the Albuquerque-Belen Valley (elevation about 5175 ft, 1575 m). Turn right on dirt road and continue 0.5 mi east-southeast to tip of a small mesa promontory (Stop 2-4). Note strong calcic soil capping the Llano surface. The eastern rim of the Llano de Albuquerque was designated Cejita Blanca (little white eye-

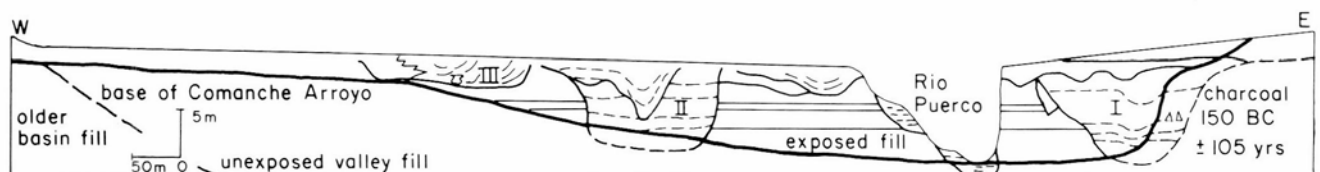


FIGURE 2-3—Schematic cross-section of Rio Puerco valley fill near the mouth of Comanche Arroyo showing buried channels. Channels I and II are similar in magnitude to the modern Rio Puerco and are filled in a similar manner. Channel III, containing pueblo II pottery, is smaller, more clay-dominated, and cut laterally in sinuous meanders (from Love and Young, 1983; with New Mexico Geological Society permission).

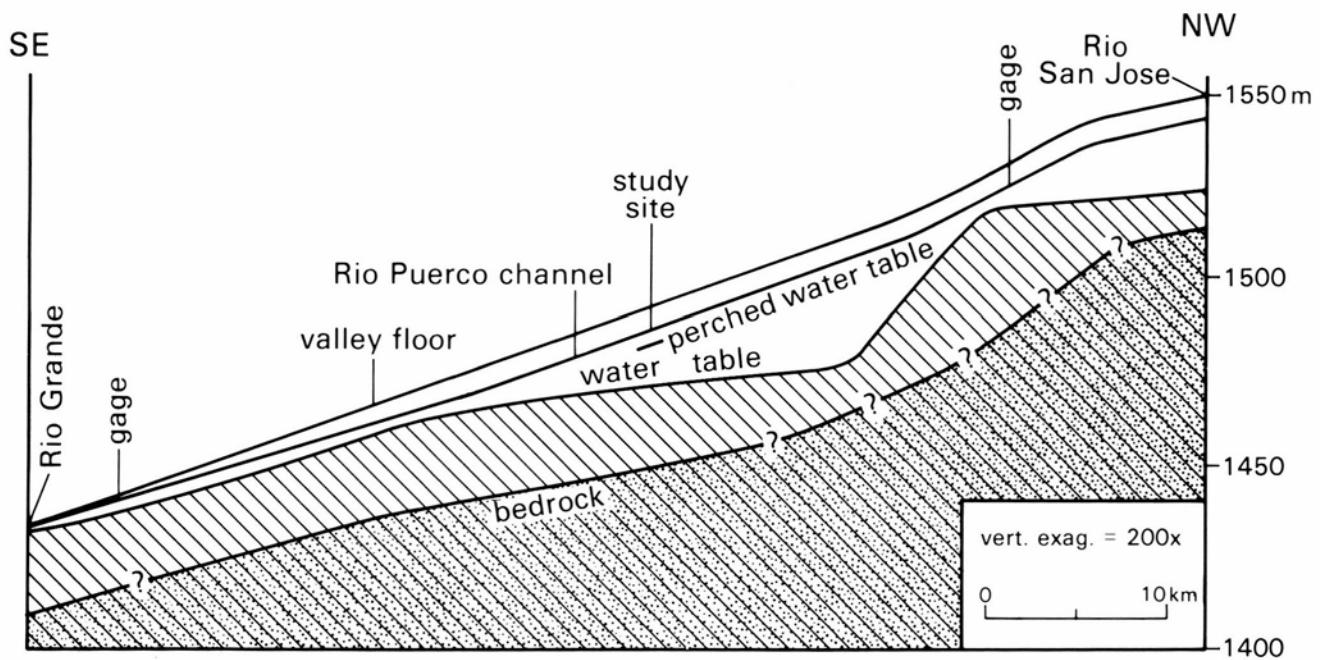


FIGURE 2-4—Diagrammatic cross-section along Rio Puerco valley from confluence of Rio San Jose to confluence of Rio Grande, showing thickness of valley fill, water table, local perched lenses, gradient of modern arroyo channel, and gradient of valley floor.

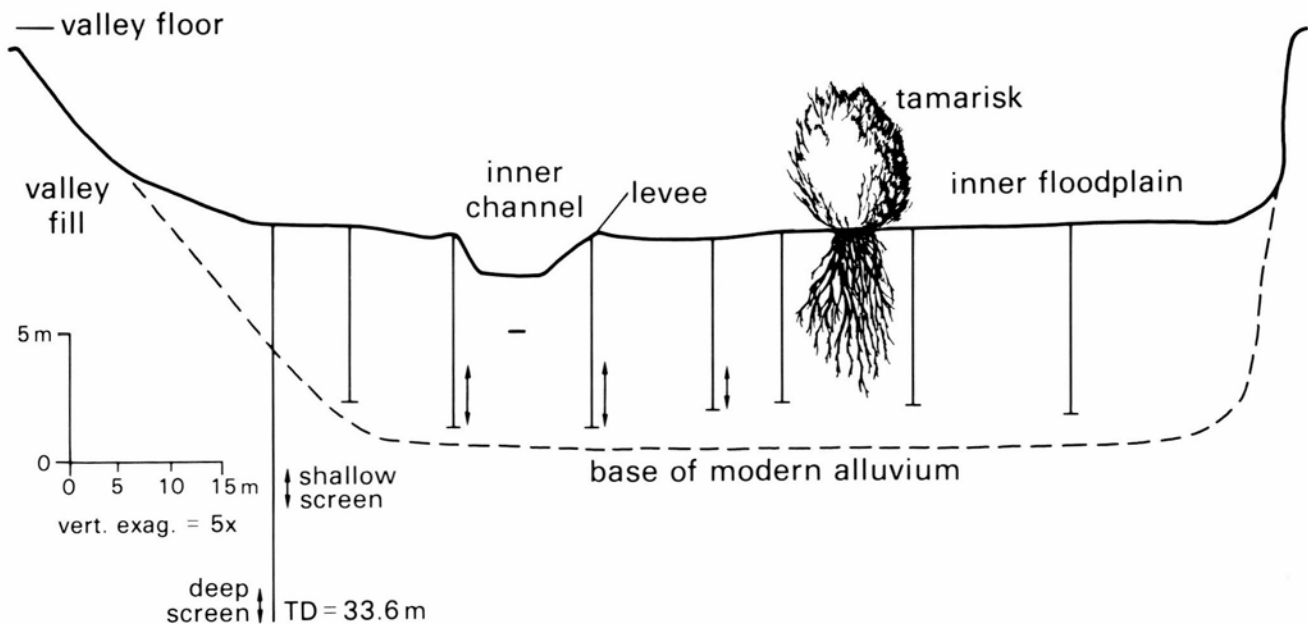


FIGURE 2-5—Diagrammatic cross-section across Rio Puerco showing profile of arroyo walls, floodplain, and active inner channel in relation to fluctuating depth to upper perched water table and to root zone of tamarisks and willows.

brow) by Bryan and McCann (1938) because of the prominent light-colored soil-carbonate horizon at the upper edge of the escarpment.

Stop 2-4 (optional): Hydrogeologic investigations of Sierra Ladrones Formation. See Lohmann et al. (this volume) for tour-stop discussion.

Directions and comments en-route to Stop 2-5

From Stop 2-4 retrace route on county road down the escarpment to the 1-25 Interchange (0.9 mi). Entering Belen; continue east on Sosimo Padilla Blvd. under the 1-25 overpass to Main St. (1.0 mi). Turn left (north) on Main St. and

go 0.6 mi before turning right on Reinken St. (NM-309). Continue 2.3 mi east on NM-309. After crossing a railroad overpass (0.5 mi) and the Rio Grande (2.2 mi), turn right on NM-47 at Rio Communities. The route continues southeast 19.4 mi on NM-47 to its junction with US-60 (Stop 2-5). A New Mexico Geological Society Field Conference road log by Hawley, Love, and Lambert (1982) covers the trip route from Belen to US-60 (reverse orientation).

The Rio Grande floodplain at Belen is underlain by a fining-upward valley-fill sequence of late Quaternary age that is as much as 120 ft (36 m) thick (Titus, 1963). Most large-capacity irrigation wells obtain water from a basal fluvial gravel zone below 80 ft (24 m). Underlying sandy

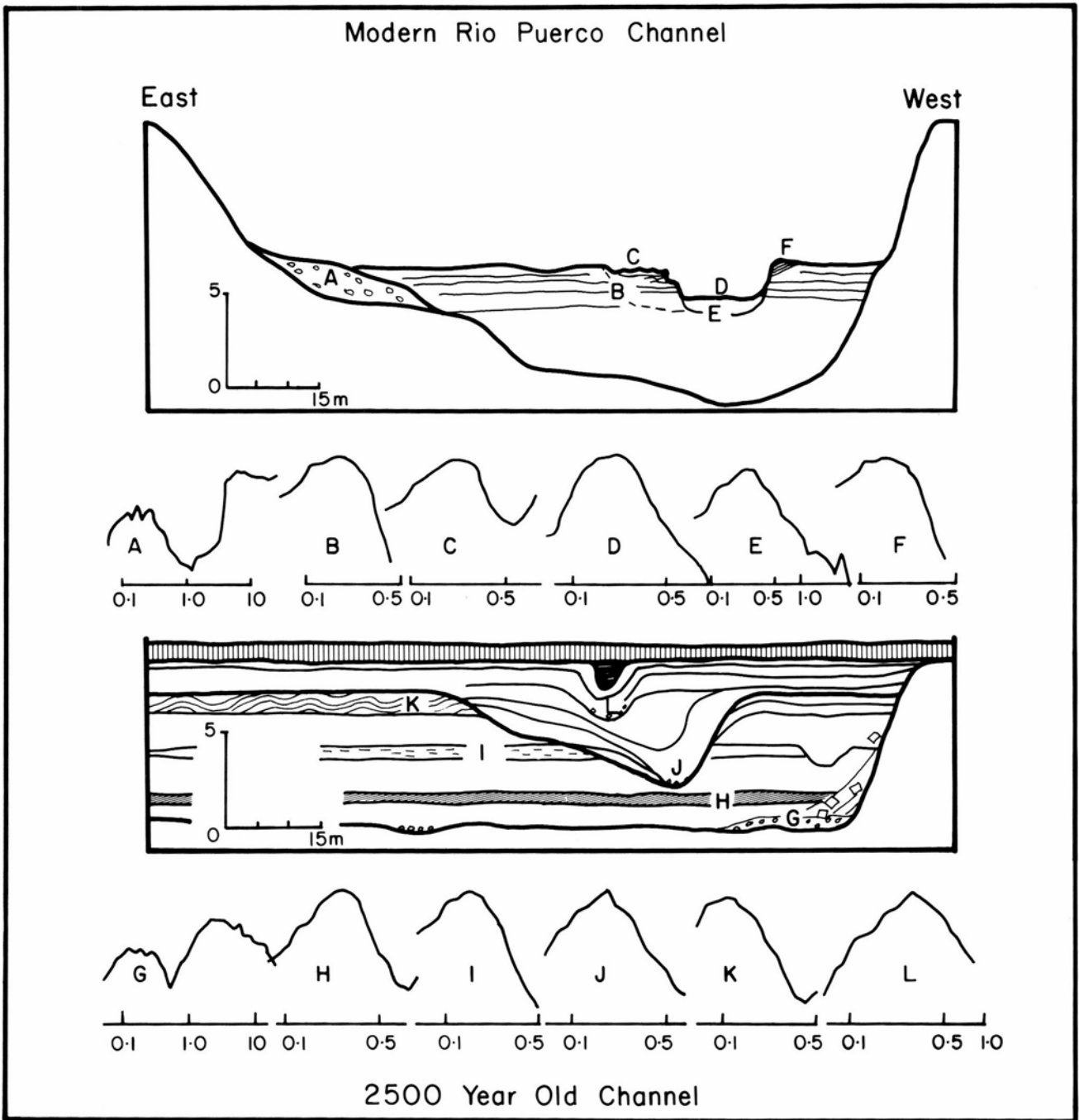


FIGURE 2-6—Comparison of facies and grain-size distribution of modern arroyo with buried arroyo.

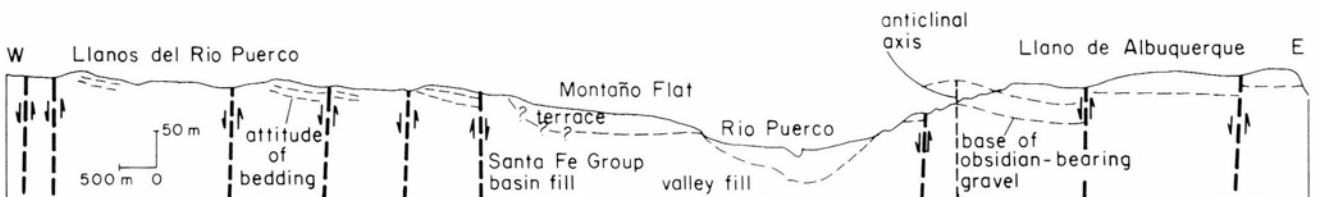


FIGURE 2-7—Schematic cross-section across Rio Puerco valley illustrating valley fill, terraces, faults, and basin fill (from Love and Young, 1983; with New Mexico Geological Society permission).

fluvial deposits of an ancestral Rio Grande system (upper Santa Fe Group, Pliocene) are the main producers for municipal and domestic water supplies.

For the first 6 mi on NM-47 (Rio Communities to turnout to John F. Kennedy Campground) the route ascends a sequence of fluvial terraces formed during middle to late Pleistocene episodes of valley cutting and partial backfilling (Titus, 1963). The highest surfaces (170-280 ft, 55-85 m) are offset by north-trending faults (Machette, 1982; Machette and McGimsey, 1983). Thin terrace fills, with calcic soils, are inset into intertonguing fluvial and distal-piedmont facies of the upper member of the Sierra Ladrones Formation (upper Santa Fe Group). Southeast of MP 11 the route ascends to the broad piedmont alluvial plain (bajada) formed by coalescence of fans at the western base of the Manzano Mountains (maximum elevation 10,098 ft, 3079 m). The major piedmont geomorphic surface dates from late middle Pleistocene and has been designated the Llano de Manzano by Machette (1978c, 1985). This surface is cut by the broad valley of Abo Arroyo (MP 2). Between MP 9 and Stop 25 the route crosses shallowly buried segments of the two major rift-boundary fault zones in the southeastern Albuquerque basin, the Hubbell Springs and Manzano—Los Pinos faults (Kelley, 1977; Machette and McGimsey, 1983). Park at US-60—NM-47 junction opposite MP 183.

Stop 2-5: Overview of southeastern Albuquerque basin and Sevilleta National Wildlife Refuge area. The low bedrock knob of Precambrian metasediments and metavolcanics (elevation 5700 ft, 1800 m) 250 m south of the US-60—NM-47 junction offers a good view of the southeastern Albuquerque basin and the Abo Pass area between the southern Manzano and northern Los Pinos Mountains (Fig. 2-8). The complex Precambrian metamorphic terrane of the Los Pinos block (Myers et al., 1981; Reiche, 1949; Stark and Dapples, 1946; Stark, 1956) is thrust against upper Paleozoic marine rocks along a high-to-low-angle reverse fault zone, the early Tertiary "Montosa thrust" (Fig. 2-9). The late Cenozoic Los Pinos fault zone is buried by upper Qua-

ternary fan alluvium about 0.35 mi (560 m) west-northwest of this stop (Machette and McGimsey, 1983). The Consortium for Continental Reflection Profiling (COCORP) has done deep seismic-reflection profiling across the Rio Grande rift in this area (Brown et al., 1980; de Voogd et al., 1986).

Stop 2-5 is near the northeast corner of the Sevilleta National Wildlife Refuge administered by the U.S. Fish and Wildlife Service. The refuge (area about 400 me, 1036 km²) is the center for a number of research projects involving both biological and earth sciences, including a National Science Foundation-funded Long-Term Ecological Research Project (LTER). Paleocological aspects of ongoing project research are discussed below.

Vegetation history of the Sevilleta LTER

Julio L. Betancourt¹, Raymond M. Turner²,
and Steve Tharnstrom²

¹U.S. Geological Survey, Tucson, Arizona 84701-1393;
²Sandia National Laboratories, Albuquerque, New Mexico 87115

From south to north in New Mexico, creosote bush (*Larrea tridentata*) gradually gives way to one-seed juniper (*Juniperus monosperma*) as the dominant shrub in the lowlands. This transition is most evident in and near the Sevilleta Long-Term Ecological Research (LTER) site, along the western piedmont of the Los Pinos Mountains, where minimum elevations rise above 5000 ft (1525 m). Here aggregates of creosote bush surround numerous snags of junipers that died during the prolonged drought of 1946-1950, a graphic example of the dynamic interactions across this ecotone. Knowledge about the past distribution of creosote bush, about the rates of its migration and subsequent expansion, may be critical for anticipating its penetration to Albuquerque and points beyond. Toward this goal, we have initiated a study of the vegetation history of the Sevilleta LTER, based primarily on packrat midden analysis and repeat photography. Plant debris accumulated by packrats from close range (mostly <30 m away) commonly becomes encased in crystallized urine to form middens. These deposits can persevere for tens of millennia in caves and rock crevices and are now the primary source of vegetation reconstructions in the arid interior of North America (Betancourt et al., 1990). Repeat photography involves comparison of vegetation in photographs taken at various times from the same camera station (Hastings and Turner, 1965). The initial phase of the study involves analyses of 50 middens from the Los Pinos Mountains and numerous paired photographs from the area in and around the Sevilleta LTER.

During the latest Wisconsin, woodlands of Colorado piñon (*Pinus edulis*) and Rocky Mountain juniper (*Juniperus scopulorum*) dominated limestone cliffs below 1830 m elevation. A midden in Palo Duro Canyon (23 km south-southwest of Stop 2-4) represents the northernmost glacial occurrence of piñon in New Mexico and Rocky Mountain juniper no longer grows in the Los Pinos Mountains. Piñon needles in this 12,000 years old deposit contain high-molecularweight DNA; application of new molecular techniques, specifically polymerase chain reaction (PCR), will help document changes in genotype frequencies associated with piñon's migration upward and northward during the Holocene. Piñon is now missing from sites it occupied during the late Holocene between 1770 and 1860 m. Piñon's lower limit retreated upward about 100 m sometime during the last 300 years. Packrat middens from Mesa del Yeso, at the southern

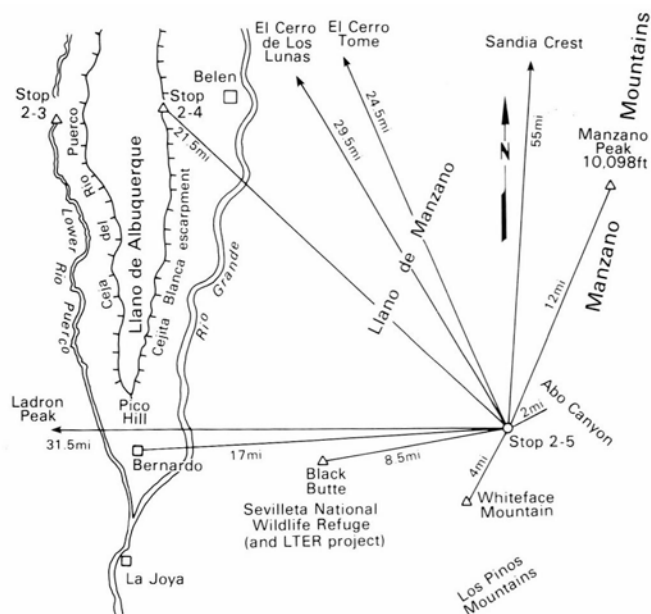
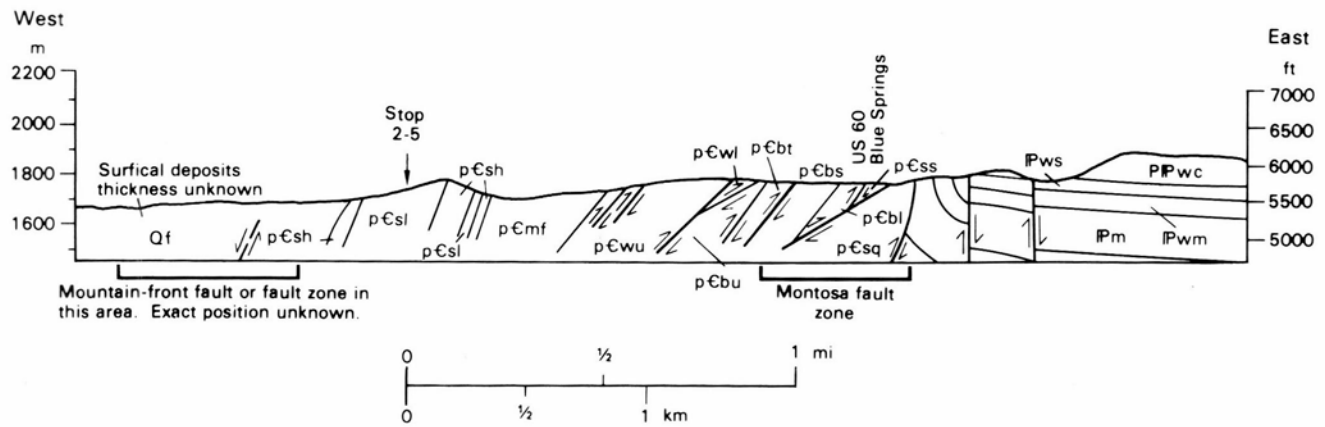


FIGURE 2-8—Panoramic location diagram for major landmarks seen from Stop 2-5, southeastern Albuquerque basin at north end of Los Pinos Mountains.



Explanation

Quaternary unit: **Qf**—alluvial-fan deposits

Upper Paleozoic units (Madera Gr.): **Wild Cow Fm.**—sandstone and conglomerate, siltstone and shale, and limestone; **PIPwc**—La Casa Member (Lower Permian and Upper Pennsylvanian); **IPws**—Pine Shadow Member, and **IPwm**—Sol se Mete Member (Upper Pennsylvanian). **Los Moyos Limestone** (Middle Pennsylvanian)—**IPm**—gray calcarenite cherty, cliff- to ledge-forming, contains minor amounts of dark-gray shale; about 92 m exposed in hogback near Blue Springs, lower beds removed by faulting.

Precambrian units: **Sevilleta rhyolite** of Stark and Dapples (1946); thickness as much as 1,525 m; **sm**—middle metarhyolite member; **sl**—lower metarhyolite member; **sh**—hornblende schist. **Mixed flow unit** of Myers and others (1981); **mf**—greenstone, schist, quartzite, and metarhyolite; thickness ranges from 275 to 793 m; lower part of unit interfingers to south with White Ridge quartzite. **White Ridge quartzite** of Stark and Dapples (1946); **wu**—upper quartzite member, thickness ranges from 305 to 488 m; **wl**—lower schist member, thickness ranges from 107 to 305 m, upper contact in most places is bedding plane fault (Paloma fault zone). **Blue Springs schist** of Stark and Dapples (1946); thickness up to 854 m; **bu**—upper metarhyolite member, **bs**—middle schist, **bl**—lower metarhyolite member. **Sais quartzite** of Stark and Dapples (1946); thickness about 728 m; **ss**—upper schist member, and **sq**—lower quartzite member.

FIGURE 2-9—West-to-east structure section of northern end of Los Pinos Mountains, through Stop 2-5 area south of Abo Canyon (adapted from Myers et al., 1981, Section A-A').

end of the Sevilleta LTER, document more widespread ocotillo (*Fouquieria splendens*) during the late Holocene, including north-facing limestone slopes. Today stands of ocotillo are restricted to south-facing slopes at its northernmost limits in the Sevilleta LTER.

Accelerated expansion of creosote bush in central New Mexico, poorly dated and sparsely documented, has been blamed on overgrazing and droughts of the past two centuries (Gardner, 1951). In the long term, this expansion represents the northern terminus of a migration that began at the end of the last ice age. For reference, not until 4000 years ago did creosote bush colonize sites in far west Texas and southern New Mexico (Van Devender, 1990). The arrival of creosote bush on limestone slopes in the Sevilleta LTER by 2500 years B.P. predates overstocking of ranges, but colonization of fine-grained soils and other substrates (sandstone, granite, and basalt) happened only within the last 200 years.

Directions and comments en-route to Mountainair

From Stop 2-5 (MP 183) continue 48 mi east on US-60 through Abo (15 mi), Mountainair (22 mi), and Willard (33 mi) to Lake Estancia Stop E-1 near Lucy Siding (ATSF Railroad). See Hawley, Foster et al. (1982) for more detailed information on the tour route to Mountainair (reverse direction). Geologic maps by Myers (1977) and Myers et al. (1981) also cover the first 11 mi (to MP 194).

Near MP 185, US-60 crosses the Montosa fault zone and the edge of the major structural uplift (Manzano—Los Pinos)

that forms the eastern boundary of the Rio Grande rift (Fig. 2-9). To the east is the transition zone between the Basin and Range and Great Plains structural provinces, which is characterized by gently east-tilted sedimentary rocks of late Paleozoic age. Pennsylvanian and Permian marine carbonates and Permian continental to marine clastic and gypsiferous evaporites dominate the section (Madera Group and Bursum, Abo, Yeso, Glorieta, and San Andres Formations, in ascending order). The route follows the broad upper valley of Abo Arroyo. Extensive upper Quaternary valley-fill deposits have been deeply incised by modern arroyo channels. This is another area of New Mexico where work needs to be done on valley cut-and-fill history. The Abo Ruins Unit of Salinas National Monument (pre-1680 pueblo and mission) is located about 0.5 mi north of US-60 at MP 195.

MP 204. At the western edge of Mountainair, the route crosses the divide (elevation about 6550 ft, 2000 m) between the Rio Grande (Abo Arroyo) watershed and the closed Estancia drainage basin (Fig. 2). This point is also near the boundary between the Mexican Highland (Rio Grande subsection) and Sacramento sections of the Basin and Range physiographic province (Fenneman, 1931; Hunt, 1974; Hawley, 1986a). The Sacramento section comprises a physiographic transition zone, here about 50 mi (80 km) wide and characterized by high tablelands and shallow structural basins, that lies between the Pecos valley section of the Great Plains and the high fault-block ranges forming the eastern edge of the southern Rio Grande rift. Solution-subsidence landforms are locally a major feature of the Sacramento section.

Day 2, Part 2: Lake Estancia basin tour
(Leaders: Bruce D. Allen and John W. Hawley)

Introduction

For about 10 mi east of Mountainair (from MP 205) the route descends across a broad, moderately dissected piedmont slope which grades to a base level slightly above the highest shorelines of Pleistocene Lake Estancia (about 6210 ft, 1893 m; Fig. 2). Soils on the broad interfluvies (Bourlier et al., 1970) have well-developed calcic horizons that are locally strongly indurated (morphogenetic stages III to V of Gile et al., 1966; and Machette, 1985). Basin-fill thickness increases eastward from about 100 ft (30 m) near Mountainair to about 250 ft (75 m) along the basin axis near Willard (Fig. E-1; Smith, 1957). The basin fill includes alluvial, eolian, and lacustrine facies of Plio-Pleistocene age, and the oldest deposits may correlate with the upper Miocene Ogallala Formation of the southern Great Plains region (Titus, 1973; Frye et al., 1982; Hawley, 1984). Lower Permian Abo Formation redbeds (mainly sandstone and mudstone) are the dominant substrate west of the high Estancia shoreline, while interbedded sandstone, siltstone, gypsite, and limestone of the Yeso Formation immediately underlie basin fill in much of the area inundated by Lake Estancia (Smith, 1957; Titus, 1969, 1973). Upper Permian limestone, gypsite, and sandstone of the San Andres and Glorieta Formations cap the high plateau (Chupadera and Jumanes Mesas) that forms the south rim of Estancia Valley (Bates et al., 1947; Hawley, 1986b). The following comments cover the tour route to Stops E-1 and E-2 in the southern Lake Estancia basin. Stop E-3 is discussed in Part 1 of Day 3.

Directions and comments en-route to Stops E-1 and E-2

MP 215 (10 mi east of Mountainair). Scarp ahead (elevation 6200-6220 ft, 1890-1896 m) is a complex erosional feature initially cut during highest stands of middle(?) to late Pleistocene Lake Estancia (Meinzer, 1911). No clear-cut evidence has yet been found for shoreline features higher than about 6210 ft (1893 m). Allen (this volume) describes

ongoing University of New Mexico studies of Late Quaternary features of the ancient lake-plain area (lake, playa, and dune deposits and associated wave-cut and deflational landforms).

One mile east of wave-cut scarp is the junction with NM-41 (start of Day 3 route to Stop E-3). Continue east on US-60 through Willard (MP 218; elevation 6100 ft, 1860 m) on nearly level basin floor, here a relict Wisconsin lake bed that has been modified by late Quaternary eolian processes. About 0.7 mi east of the NM-42 junction in Willard (rounding southeast bend in highway) clay dunes (lunettes) from 9:00 to 2:00 are associated with lake-plain deflation.

East of MP 222 (rounding northeast bend in highway) the route crosses southern end of Laguna del Perro, a north-trending playa-lake depression that is about 12 mi (20 km) long and about 1 mi (1.6 km) wide (Fig. 2). This deflation basin is the largest of nearly 100 such features that occur on the valley floor. Several deflation basins with playa lakes will be crossed in the next 4 mi. Accumulation of deflated material along downward margin of the basins has resulted in large clay dunes (lunettes). **Near MP 224** note small mounds to the left (north) forming hummocky topography. These gypsum-rich dunes (Titus, 1969, 1973) predate the major deflational basins, such as Laguna del Perro, and date from the initial desiccation of Wisconsin Lake Estancia 12,000 to 11,000 yrs ago. **MP 225**. Large deflation basins with playa lakes to left and right. *Stop E-2 will be at rest area ahead on left.* **MP 226**. Crossing another area dotted with low, gypsum-rich dune mounds. **0.8 mi east of MP 227** cross north-trending gypsum beach ridge (elevation about 6100 ft, 1860 m) described by Allen (this volume, fig. 1) and discussed at Stop E-1. **MP 231**, on highest late Wisconsin shoreline of Lake Estancia opposite railroad cut in Permian Glorieta Sandstone at Lucy Siding (AT&T Railroad; elevation 6190 ft, 1887 m). *Turn around, retrace route to MP 230, and park near windmill on north side of US-60.*

Stop E-1: Lake Estancia shoreline. This stop (elevation

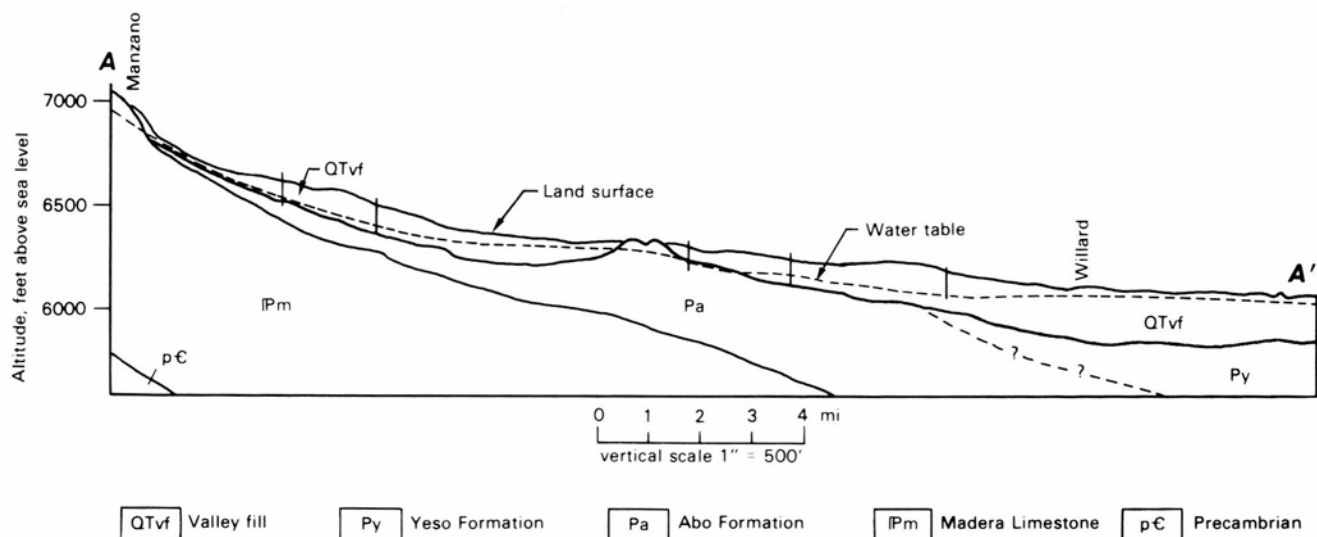


FIGURE E-1—Hydrogeologic section from southern Manzano Mountains, north of Mountainair, to Estancia Valley near Willard (from Smith, 1957, pl. 2).

about 6145 ft, 1873 m) at the southwest end of Lucy Siding is on one of the most prominent shoreline features of Meinzer's (1911) Lake Estancia (Fig. 2). Landforms include beaches, wave-cut benches, spits, and bay-mouth bars between 6090 and 6210 ft (1856 to 1893 m). The shorelines here are in Harbour's (1958) "Group C" and appear as undulations in the highway to the northeast and southwest of this stop. Lacustrine features at and below an elevation of about 6200 ft (1890 m) are associated with latest Pleistocene (late Wisconsin), glacial-maxima highstands. At the 6200 ft (1890 m) level, Lake Estancia would have inundated an area of about 430 mi² (1114 km²) and was over 140 ft (43 m) deep. This highstand occurred between about 15,500 and 19,500 yrs B.P. (Allen, this volume). The linear feature about 1 mi (1.6 km) to the west-northwest, just above the basin floor, is the gypsum beach ridge noted east of MP 227. The reworked gypsum in the beach ridge was derived from the small gypsum dune mounds that dot the relict lake-plain surface to the west at elevations below 6100 ft (1860 m). The gypsum beach ridge corresponds to a 25 ft (8 m) deep lake that postdates initial (pre-Holocene) desiccation of Lake Estancia after a major highstand about 13,000 yrs B.P. (Allen, this volume, fig. 4).

The lowest point on the Estancia drainage-basin divide (elevation 6340-6345 ft, 1932-1933 m) is located near Cedarvale, about 19 mi (30 km) south-southeast of this stop. The surficial deposits in the divide are conglomeratic sandstones of Pliocene to latest Miocene(?) age, correlated by Frye et al. (1982) with the Ogallala Formation. Surficial beds are cemented into a pedogenic calcrete (caprock caliche) layer with dense pisolitic morphology (morphogenetic stage VI of Machette, 1985; McGrath and Hawley, 1987). There is no evidence of Quaternary lake or fluvial discharge over this "sill" into the chain of large structural and/or solution-subsidence basins (Pinos Wells, Encino, Vaughn) located to the northeast.

Evidence for and against Pleistocene surface drainage from the Estancia basin, across the east-bounding and basement-cored Pedernal uplift, and onto the Pecos slope has been presented by a number of workers (notably Lyons, 1969; Titus, 1969, 1973; Bachhuber, 1971, 1982, 1989; and Kelley, 1972). The presence of abundant trout fossils in late Pleistocene lake sediments (Bachhuber, 1989) indicates that a past surface drainage connection has existed, but not necessarily via the Encino—Pintado Canyon spillway route suggested by Bachhuber (1971, 1982) or the Encino—Vaughn route discussed by Kelley (1972). Trout could have been introduced through ancestral stream systems (present Rio Grande or upper Pecos tributaries) that headed in the southern Sangre de Cristo Range and originally discharged into the Estancia basin in Pliocene or early Pleistocene time. Perennial streams and springs in the higher parts of the Manzano Mountains could have provided refugia for fish populations during dry intervals after diversion of Sangre de Cristo tributaries to external drainage systems. The important role that subsurface-flow systems may play in Lake Estancia paleohydrology is discussed at Stop E-2.

Return on US-60 to rest area 0.4 mi southwest of MP 226 and Stop E-2; cross gypsum beach ridge 0.2 mi southwest of MP 228.

Stop E-2: Lake Estancia stratigraphic record. Details of the lacustrine stratigraphic record exposed in deflation basins near this stop are presented by Allen (this volume).

Note the tan and gray lake beds exposed in the northern escarpment of the playa-lake basin opposite the rest area. These sediments of latest Pleistocene age (<20,000 yrs) are overlain by a white horizon marking the top of the lacustrine sequence and the position of the ancient valley floor (con-structural lake-plain surface). Overlying sediments are eolian deposits associated with deflation of the large playa-lake depressions of Holocene age.

The section exposed here is only the upper part of a sequence of lake, playa, eolian, and minor alluvial beds described in detail by Titus (1969, 1973) and Bachhuber (1971, 1989) at a number of surface and borehole sites in the lake-plain and deflation-basin area north of this stop. Sediments associated with middle to late Pleistocene episodes of lake expansion (Dog Lake Formation of Titus, 1973), including an early late Pleistocene interlacustrine interval, have a maximum thickness of about 100 ft (30 m). Underlying sand, clay, and pebble-gravel deposits with gypsum- and carbonate-impregnated zones are part of an extensive pre-late Pleistocene deposit (Estancia Formation of Titus, 1973) that rarely exceeds thicknesses of 300 ft (90 m; Smith, 1957). Titus (1973) suggested that much of this older fill was deposited by an ancestral through-going drainage system which was disrupted by structural downdropping of the present valley area relative to the bounding Manzano, Sandia, and Pedernal uplifts. The possible significant role of solution subsidence resulting from partial dissolution of gypsum beds in the underlying Yeso Formation and basin fill has been recognized, but is not well documented.

Regional and local ground-water flow systems in the Estancia basin have been studied by Meinzer (1911), Smith (1957), Titus (1969, 1973, 1980), DeBrine (1971), and Jenkins (1982). Most of these workers have assumed that the basin had been closed in terms of both surface and shallow subsurface flow during much of middle to late Quaternary time (Brady et al., 1984). However, some (starting with Meinzer) have inferred that a deep interbasin-flow regime may exist, at least with respect to the major carbonate aquifer in the region, the Pennsylvanian Madera Group (Jenkins, 1982, pp. 383-384).

Recent work by Hawley (1986b) on a hazardous-material disposal site on Chupadera Mesa shows that contrary to other published information, there is no major ground-water divide on Chupadera and Jumanes Mesas that would limit subsurface discharge from Estancia basin during the documented lake maxima (as high as 6210 ft, 1893 m) since late middle Pleistocene time (last 150,000 yrs). This study also suggests that a broad, south-trending fault zone (complex extensional, compressional, and strike-slip components with pre-Permian initial deformation), extending the length of Chupadera Mesa, provides a connection between the regional carbonate aquifer and the shallow Estancia basin fill and Yeso Formation ground-water system. Thus, there may have been times of significant discharge from the Estancia hydrologic basin southward into the Tularosa basin, the site of late Pleistocene Lake Otero of Herrick (1904) and Meinzer and Hare (1915).

Recent studies on a candidate site for the Superconducting Super Collider (SSC) project in northern Estancia basin (Johnpeer et al., 1987) also support the hypothesis (first proposed by Bates et al., 1947) that the north—south zone of structural deformation on Chupadera Mesa extends northward through the present Estancia basin into north-central New Mexico (see Woodward et al., 1978). Laguna del Perro

is aligned along this trend, as is a Laramide fault zone that affects the Glorieta—Yeso aquifer system in the northeastern Estancia Valley. In addition, detailed stratigraphic and geotechnical studies during the two-year SSC project revealed no lacustrine deposits or landforms at elevations above 6220 ft (1896 m) in the Lake Estancia basin.

A question that needs to be asked at this tour stop concerns the entire problem of lake-basin paleohydrology, including the role that the playa-lake basins have played throughout middle to late Quaternary time, both in terms of groundwater outflow as well as inflow, and in the context of both regional and local aquifer systems. Paleohydrologic models

(Meinzer, 1922; Leopold, 1951; Antevs, 1954; Galloway, 1970; Brakenridge, 1978; Smith and Anderson, 1982) that neglect ground-water—surface-water linkages cannot explain many of the lacustrine and playa-basin features observed in the Estancia basin. This is a very exciting area with great potential for research in the Quaternary sciences (see Wood and Sanford, 1990; Kreider et al., 1990). The excellent field studies by workers such as Meinzer, Smith, Harbour, Lyons, Titus, and Bachhuber provide a solid basis for all current and future investigations.

Return to Mountainair and historic Shaffer Hotel via US-60; end of Day 2.

Day 3, Part 1: Continuation of Lake Estancia basin tour

(Leaders: Bruce D. Allen and John W. Hawley)

Directions and comments en-route to Stop E-3

Return on US-60 to junction with NM-41. Continue 18.6 mi north on NM-41 through Estancia (10.6 mi) and McIntosh (18.2 mi) to junction with Torrance County Road A72 (0.6 mi north of MP 18 and 0.4 mi north of McIntosh Post Office). Turn left on CR-A72, and continue west 1.5 mi to crossroad. Turn left (south) and follow section-line road 0.9 mi to junction with unimproved road to gravel pit in lower Cienega Draw. Turn right (west) and continue about 0.7 mi up the draw to floor of gravel pit and Stop E-3 (Fig. 2).

Refer to Day 2 comments on the Lake Estancia basin tour from Mountainair to the NM-41 junction west of Willard. The route north on NM-41 through Estancia and McIntosh is almost entirely on a relict-lake-floor surface (elevation range 6100-6140 ft, 1859-1871 m), which dates from the last major highstand of Lake Estancia (about 13,000 yrs B.P.). Fig. E-2 is an oblique aerial photo of shorelines between 6150 and 6180 ft (1875-1884 m), about 1 mi southwest of Estancia. About 0.8 mi west of NM-41 (elevation 6170 ft, 1881 m) County Road A72 crosses ridges and swales of the Wisconsin glacial-maximum shoreline. The elevation range of nearshore gravel deposits at Stop E-3 is about 6185 to 6200 ft (1885-1890 m).



FIGURE E-2—Oblique aerial view, to south, of faint shoreline ridges of late Wisconsin Lake Estancia about 1 mi southwest of Estancia. Note gravel pit in lower center (from Hawley, Foster, et al., 1982; with New Mexico Geological Society permission).

Stop E-3: Lake Estancia glacial-maximum shoreline deposits. Nearshore deposits associated with the glacial-maximum highstand of Lake Estancia are exposed in the walls of numerous gravel pits along the western margin of the ancient lake basin. Gravel-size clasts consist primarily of Madera Limestone, which forms the eastern slope of the Manzano Mountains to the west. At this locality, the upper part of the shoreline sequence exhibits several decimeter-scale cycles which consist of a basal, planar erosion surface overlain by fine-grained sediments which coarsen upward into landward-dipping, parallel-bedded gravels. The bedded gravels at the top of each cycle are abruptly overlain by fine-grained sediments of the next cycle. One interpretation for this succession of asymmetric, coarsening-upward cycles is that they represent transgressive—regressive cycles of the ancient lake, with an erosional transgressive surface occurring between the gravel beds and the overlying fine-grained sediments of the next cycle.

The late Pleistocene nearshore deposits are overlain by an eolian "cap" of fine-grained material with an associated weakly developed, cummulic soil that extends into the beach gravels. The soil has developed since Lake Estancia fell below this elevation, or subsequent to the last glacial maximum. Subsurface soil horizons are light in color due to illuvial carbonate, and exhibit stage II carbonate morphology (after Gile et al., 1966).

Directions and comments en-route to 1-40 at Moriarty

Retrace route to NM-41. Turn left and continue 9.2 mi north on NM-41 to Moriarty and the junction with the business route of 1-40 (historic Highway 66).

For 5.5 mi north of the Stop E-1 turnoff (County Road A72) NM-41 rises gradually (from 6150 to 6200 ft, 1875 to 1890 m) across the gently undulating topography constructed during the Wisconsin glacial-maximum stage of Lake Estancia. A large gravel-bar complex deposited at the mouth of Buffalo Draw is located about 500 yds east of NM-41 at the 5.5 mi point. About 0.5 mi farther north, one of the highest remnants of beach deposits preserved in the basin is exposed in an old railroad cut 200 ft east of the highway (elevation about 6210 ft, 1893 m). This outcrop of partly cemented pebble gravel and coarse sand may be

a shoreline deposit associated with a glacial maximum predating the last interglacial (>130,000 yrs). Exposures of such possible late middle Pleistocene lake deposits are very rare in the Estancia Valley because deep dissection of the basin fill occurs mainly in the deflation basins of Laguna del Perro area (Stops E-1 and E-2). Prime lake-front property ahead in Moriarty during the next glacial maximum.

End of Lake Estancia basin tour.

Directions and comments en-route from Moriarty to Albuquerque

From Moriarty continue west on 1-40 about 22 mi to the Tijeras exit and then take old Hwy 66 (NM-333) through Tijeras Canyon (6.8 mi) to the eastern edge of Albuquerque at Central Ave. and Tramway Blvd. The zero mileage point for this trip segment is the NM-41 and Business 1-40 junction near the north edge of Moriarty (Fig. 2).

Go west on Business 1-40 to overpass and westbound onramp of 1-40 (1.7 mi). Route ascends on lower and middle Pleistocene piedmont deposits derived from Pennsylvanian and Permian rocks of the Manzano and Manzanita Mountains (Reiche, 1949; Titus, 1980). Engineering geology in this area was investigated by Johnpeer et al. (1987) as part of the Superconducting Super Collider project (SSC). Depth to bedrock (Permian Abo and Yeso Formations) near Moriarty is about 150-250 ft (46-76 m). Depth to water is currently about 50-100 ft (15-30 m). **MP 193. 3.2 mi**, ascend from Quaternary alluvium onto older basin fill (QTA) of late(?) Miocene to early(?) Pleistocene age that may be partly correlative with the Ogallala Formation. **5.9 mi**, the New Mexico version of the SSC was to pass beneath 1-40 in this area in a tunnel 130 ft (40 m) below the surface. **7.5 mi**, outcrops of Upper Pennsylvanian Madera Group seen in arroyo and in hills to southwest. For next 3 mi, the area north of the highway is underlain by caves and karst.

8.5 mi, Edgewood exit; young alluvium in valley; older

basin fill exposed in low ridges to north; Madera Group to south and west. Fig. 3-1 is a hydrogeologic section (Titus, 1980) covering the tour-route area between here and the Sandia Mountain crest on the horizon. At 1:30-2:30 is South Mountain, a mid-Tertiary monzonite laccolith with Permian Glorieta Sandstone and San Andres Limestone on top. Beyond South Mountain at 2:30 are the San Pedro Mountains, another mid-Tertiary intrusive with abundant gold and copper mineralization. **9.1 mi**, Madera Group outcrops before crossing young alluvium in Juan Tomas Canyon; entering area of Pennsylvanian—Permian rocks mapped by Myers and McKay (1976). **13.7 mi**, Sedillo exit; drainage divide of Estancia basin at crest of hill. Descend into Tijeras Canyon cut in Wild Cow Formation (upper unit of Madera Group). **16.4 mi**, fault in Wild Cow Formation down to northwest. Northwest-dipping section on right for next 0.3 mi (presently covered with wire mesh and concrete) originally showed cyclic deposition (clastic to carbonate) in members of Wild Cow Formation below the Permian Abo Formation. **16.6 mi**, road curves southwest into strike valley of Permian Abo Formation. Permian Yeso Formation forms ridge to northwest of 1-40 for next mile.

17.4 mi, Zuzax exit. **18.3 mi**, road passes northwest-dipping Permian Yeso, San Andres, sliver of Triassic Chinle, and Tertiary lamprophic dikes before crossing the Gutierrez fault, a major branch of the Tijeras fault that forms the southeast side of a graben holding the Tijeras syncline and anticline seen topographically expressed in resistant Cretaceous Mesa Verde Sandstone to the north on ridge. **18.7 mi**, road crosses alluvium burying Gutierrez fault and returns to Yeso and Abo Formations. Road continues southwest in strike valley of Abo Formation on local reddish-brown alluvium.

20.0 mi, take exit to NM-14. At stop sign turn left (south). **20.3 mi**, underpass (below 1-40) and 90° bend to right in road. **20.8 mi**, stop sign. Village of Tijeras. Continue straight

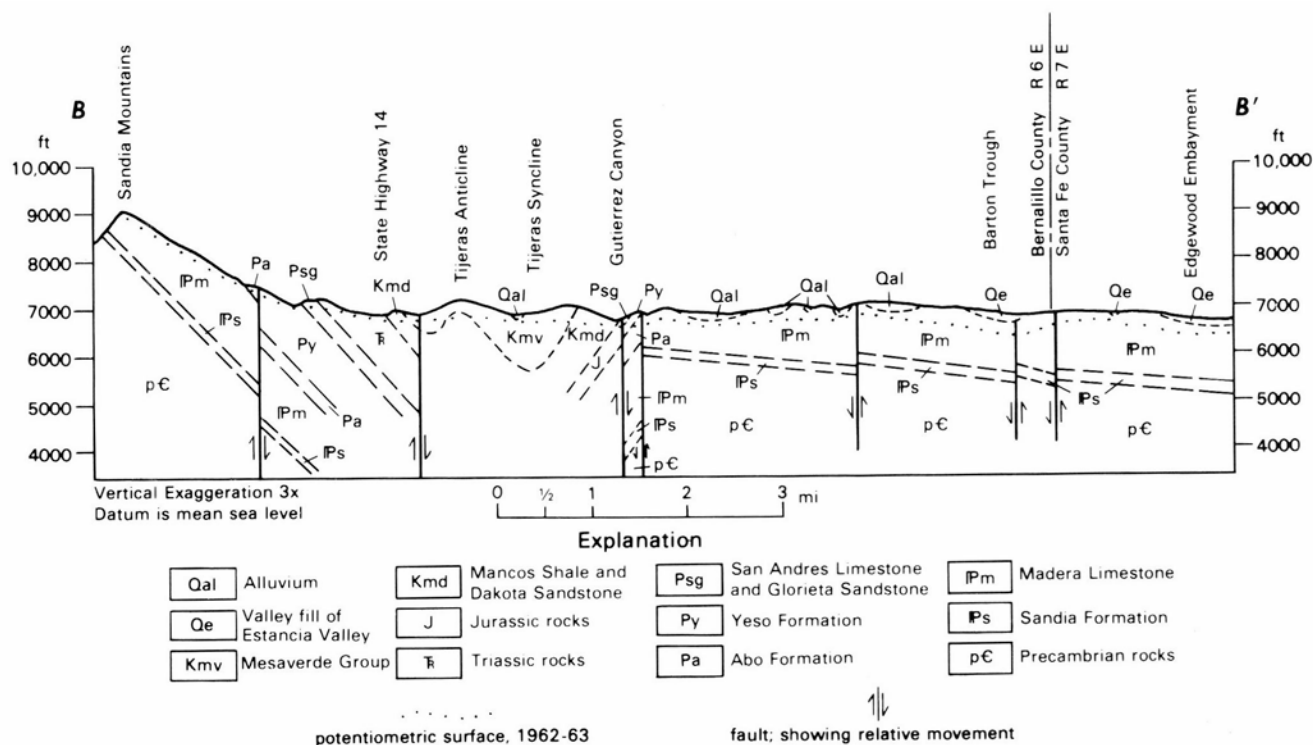


FIGURE 3-1—Hydrogeologic section from crest of the Sandia Mountains to Edgewood "embayment," showing depth to potentiometric surface (from Titus, 1980, fig. 15).

through intersection on US-66. Village of Tijeras was founded in 1856 near site of a prehistoric Indian Pueblo (Cordell, 1982b). See Connolly et al. (1982) for more detailed information on the tour route from Tijeras to Albuquerque (reverse direction). The complex of canyons crossing the mountains resembles open scissors, the translation of "tijeras." **21.0 mi**, roadcuts are Lower Permian Abo Formation. **21.8 mi**, good exposures of highly deformed Precambrian metavolcanics of Tijeras greenstone in roadcut to left under boulder gravels.

22.1 mi, Seven Springs to left. Both alluvium and fractured Precambrian rocks serve as aquifers (Titus, 1980). Alluvium in the inner valley locally is more than 100 ft thick. South of Tijeras is faulted section of Sandia Formation and lower Madera Group overlying Tijeras greenstone; north of highway is a sliver of greenstone on south side of Tijeras fault, a major fault showing both strike-slip and later vertical motion. The highway crosses the fault at an oblique angle between here and Deadman's curve. North of the Tijeras fault is meta-arkosic Cibola gneiss, isoclinally folded quartzite, and Sandia granite. Radiometric ages for the Sandia granite are about 1445 ± 40 Ma and for the Cibola gneiss about 1576 ± 73 Ma. Tertiary lamprophyre dikes cut the gneiss and granite down canyon. Smith et al. (1982) discuss the stepped and stacked sequences of Quaternary alluvium and colluvium and associated paleosols that cap canyon and piedmont erosion surfaces from here to the mouth of Tijeras

Canyon. **22.4 mi**, terrace gravel and fan deposits to left cap metamorphic rocks in cut above Tijeras Creek.

22.9 mi, Deadman's curve cut through Cibola gneiss and quartzite. **23.4 mi**, gradational contact between Cibola gneiss and less and less foliated Sandia granite in slopes to right. Note spheroidal weathering of granite. The "granite" in this area is generally quartz monzonite to granodiorite with large pinkish porphyroblasts of microcline of metasomatic origin. Differential weathering makes mafic inclusions stick out on the granite corestones like raisins out of cookie dough. **24.1 mi**, Village of Carnuel and Tijeras Creek to left. This old Spanish village was established in the 18th century, but was repeatedly destroyed by Apache raids. To the south, gold, barite, and fluorite mines were developed in Precambrian greenstone terrane. Route ahead on pediment cut on Sandia granite with discontinuous veneer of Quaternary alluvium and colluvium deposited in apex area of Tijeras Creek fan. **25.2 mi**, onramp to 1-40 to right. *Bear left* and cross overpass. **26.4 mi**, break in slope (piedmont angle at 3:00 to 4:00) between mountain front and piedmont erosion surfaces on Sandia granite at western end of Tijeras Canyon. **27.0 mi**, sharp curve to left. Crossing shallowly buried segment of Sandia fault zone (Kelley and Northrop, 1975; Machette, 1982). **27.1 mi**, stop sign. *Bear right*. **27.3 mi**, intersection of Tramway Blvd. and Central Ave. and start of Albuquerque—Rio Rancho urban-area tour.

Day 3, Part 2: Albuquerque—Rio Rancho urban-area tour

(Leaders: John W. Hawley and Stephen G. Wells)

Summary

This tour of the Albuquerque area (Fig. 2) emphasizes environmental and engineering geology, geomorphology, and Quaternary stratigraphy of valley- and basin-fill deposits. The route starts at the Central Ave. (Hwy 66)—Tramway Blvd. intersection and traverses the urban area in a loop about 58 mi long. Local points of interest are discussed at four stops. Much of the following discussion has been adapted from road logs by Hawley, Lambert et al., Kelley et al., and Lambert et al. (1982). Fig. A-1 is a diagrammatic cross-section of the northern Albuquerque basin that emphasizes late Cenozoic features (landforms, basin and valley fills, ground water, and major structural components) in the area between Stops A-1, A-3, and A-4.

The first segment of the tour route, via Tramway Blvd., crosses the upper piedmont alluvial plain (Llano de Sandia) at the foot of the Sandia Mountains. Stop A-1 is at Elena Gallegos Municipal Park on upper Arroyo del Pino. This stop provides an overview of the northeast Albuquerque area and western front of the Sandia Mountains. Discussions center on environmental concerns related to surficial deposits and hydrology of the Llano de Sandia.

The route between Stops A-1 and A-2 traverses the Llano de Sandia between the mountain front and the Rio Grande floodplain, via Tramway and Paseo del Norte Blvds. Stop A-2 is at an exposure of ancient river deposits along Edith Blvd. at the eastern edge of the floodplain. Discussion cen-

ters on fluvial deposits of Pleistocene age that have been dated by volcanic-ash correlation and vertebrate faunas.

We then cross the Los Ranchos de Albuquerque section of the floodplain on the new Paseo del Norte Freeway, exiting on north Coors Blvd. for a tour of the western valley border and Llano de Albuquerque area. This route follows Irving Blvd. and Golf Course Rd. northward through Paradise Hills and Rio Rancho. We then turn west on Southern Blvd. and traverse the dissected Llano de Albuquerque tableland west of Rio Rancho and northwest of the Albuquerque Volcanoes. Stop A-3 on the rim of the Ceja del Rio escarpment overlooks the Rio Puerco valley and fault zone, which forms the western Rio Grande rift boundary. This is an excellent vantage point for viewing the eastern Colorado Plateau, which extends from Mount Taylor to the Nacimiento Mountains, as well as the northern Albuquerque basin and southern Jemez Mountains. Concepts of Santa Fe Group stratigraphy and late Cenozoic landscape evolution, originally developed in the northern Albuquerque basin by Kirk Bryan (1909, 1938) and his students, are emphasized.

Following Stop A-3 we retrace our route east across the Llano de Albuquerque on Southern Blvd. to the New Mexico Gas Company pipeline road (northwestern extension of Atrisco Dr.). The tour continues southeast on this road to Stop A4 at the (Albuquerque) Volcano Cliffs overlooking Petroglyph Park (new National Monument area) and the inner Rio Grande valley. Pleistocene activity of the Albuquerque

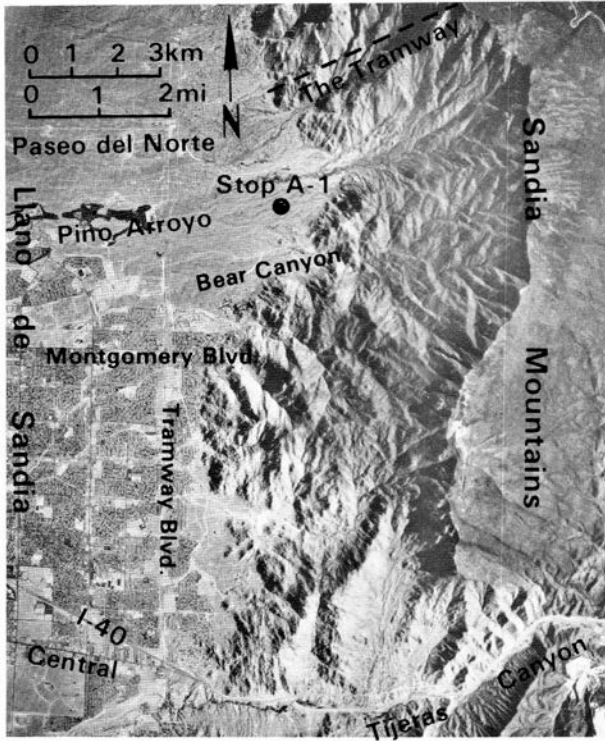


FIGURE A-2—Aerial photograph of Sandia Mountains and Llano de Sandia piedmont surface between Tijeras Canyon and the Tramway. Elena Gallegos Park and area of Stop A-1 in upper center (from Kelley et al., 1982; with New Mexico Geological Society permission).

crosses main distributary channel from Embudo and Embudito fans. Small fan spreads out from mouth of Piedra Lisa (smooth rock) canyon at 2:30. **4.0 mi**, traffic light, crossing Comanche Rd.; ascend south slope of Embudito Canyon fan.

4.5 mi, traffic light at Montgomery Blvd. Road narrows; continue north on Tramway Blvd. Ponderosa Reservoir and Well are 1.25 mi downslope at an elevation of about 5675 ft (1730 m). The 1242 ft (378 m) well is developed in Santa Fe Group basin fill, and it is only 1.75 mi (2.8 km) from the Sandia frontal fault mapped by Kelley and Northrop (1975). Static-water-level elevation is about 4950 ft (1510 m), approximately the same elevation as the water table

beneath the river floodplain 6 mi (10 km) to the west (Kelley, 1982, pp. 41-43). The essentially flat water table from here to the Rio Grande is indicative of very permeable and thick basin fill (Kaehler, 1990; Kernodle and Scott, 1986). Fig. A-3 shows the profiles of the land surface and water table across this part of the Albuquerque basin.

4.7 mi, crossing Embudito Arroyo; note large granite boulders. **5.1 mi**, crossing main Bear Canyon Arroyo; flood-control structure downstream at 8:30. Granite boulders are common in coalescent-fan deposits here, but these boulders decrease in size and abundance northward due to increasing distance from the mountain front and flattening of the piedmont-slope profile. **5.5 mi**, traffic light, crossing Spain Rd. and northern distributary channel from Bear Canyon. **6.0 mi**, traffic light, crossing Academy Blvd.; prepare for right turn. **6.3 mi**, turn right (east) on road to Elena Gallegos Municipal Park, continue up valley of Arroyo del Pino. **7.8 mi**, Elena Gallegos Park entrance booth. Stop A-1 parking area is 0.4 mi to the east.

Stop A-1: Elena Gallegos Park and Sandia Mountain piedmont. This stop (elevation 6500 ft, 1980 m) is in a large embayment in the Sandia Mountain front known as the Bear/Pino reentrant (Fig. A-2). Kelley (1982, p. 72; Kelley and Northrop, 1975) suggested that the embayment is caused by the eastward deflection of the Sandia fault opposite the middle part of the mountains. He also considered that this part of the Sandias was uplifted first and subjected to erosion longer than adjacent areas. Drainage from three large canyons enters the embayment: Bear (south), Pino (central), and Domingo Baca (north). The most prominent alluvial fan is at the mouth of Cañon Domingo Baca. The material making up this fan is typical of the older-piedmont sediment near the mountain front. It consists of arkosic sandy gravel containing numerous granite boulders 2.5 m in diameter, with some as large as 3.5 x 11 m. On the main part of the Llano de Sandia (a coalescent-fan piedmont or bajada extending about 8 mi, 13 km, to the west) arkosic sandy pebble gravel to pebbly sand is the dominant lithology.

Presumably an extensive buried pediment, or suballuvial bench, cut on Sandia granite occurs at shallow depths east of the buried trace of the Sandia fault (about 0.5 mi, 0.8 km, east of Tramway Blvd.; Kelley and Northrop, 1975, p.

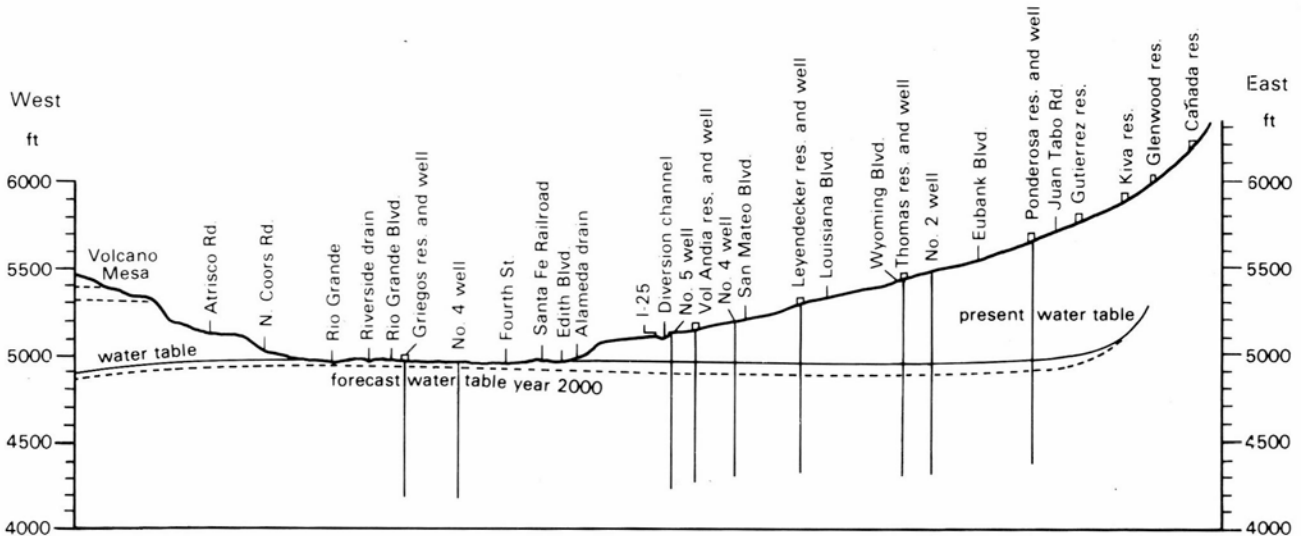


FIGURE A-3—Land-surface and water-table profile across eastern Albuquerque basin and Montgomery Blvd. and Griegos Rd. (from Kelley, 1982).

78). Within the Bear/Pino reentrant, granite is exposed in some of the deeper arroyo bottoms for distances as much as 1 mi (1.6 km) out from the mountain front (Lambert, 1968). Pediments with well-developed rock-fan morphology (Johnson, 1932) and discontinuous alluvial cover are present on the uppermost piedmont slope between the alluvial fan of Cation Domingo Baca and Rincon Ridge (northwestern ridge of the Sandias). Gravity studies by the U.S. Geological Survey (Cordell, 1978a, b) indicate that a buried, major boundary fault of Sandia uplift may be present about 3 km (2 mi) west of this stop.

The undulating, upper-piedmont terrain at the southern base of the Sandias is characterized by alternating alluvial fans and interfan areas (Kelley, 1982, pp. 27, 28). Fans at the mouths of larger canyons form major topographic highs and extend about 3 mi (5 km) from the mountain front. Broad topographic lows between the proximal parts of large fans commonly receive drainage from fan distributaries as well as from adjacent mountain fronts and flanking alluvial aprons. The latter include small fans and cones derived from small, steep canyons. The large Bear (Oso), Embudo, and Embudito fans to the south coalesce downslope to form a relatively smooth landscape that grades to valley-border surfaces along the inner Rio Grande valley.

Whereas much of the Pleistocene runoff spread out on the piedmont slope in fan distributaries, more recent concentration of flow in arroyos has resulted in landscape dissection. With gradients ranging from 3 to 6%, the present arroyo system (and late Quaternary precursors) has produced high-energy flows of water and sediment with competence to move clasts up to large-boulder size. The detention dam, located just west of Tramway Blvd. on Arroyo del Pino, as well as the numerous other flood-control structures observed on this tour are operated by the Albuquerque Metropolitan Arroyo Flood Control Authority (AMAFCA). AMAFCA is a local-government subdivision which was created in 1963 and has a district covering the City of Albuquerque and portions of the surrounding Bernalillo County. AMAFCA derives revenues through property taxes to construct and maintain flood-control structures. In the first 10 years of AMAFCA's history, efforts were devoted to the construction of the North and South diversion channels that cost \$28,619,000, of which the taxpayers contributed a total of \$11,410,000. Since 1973, several additional flood-control structures have been completed in the Northeast Heights of Albuquerque and on the West Mesa; these include Embudo Arroyo Canal and Calabacillas Arroyo structures.

The Juan Tabo Dam, located about 3 mi (5 km) to the southwest on Bear Canyon Arroyo, is designed for the following conditions: (1) flow from the probable maximum precipitation (PMP; 6-hour PMP effective rainfall = 39.9 cm) will not overtop the structure; (2) the crest of the emergency spillway is at an elevation that will not be overtopped by the 100-year frequency flood; (3) a continuously open culvert, primary spillway 2.4 m in diameter, provides a maximum discharge of 54.6 m³/s (1930 ft³/s) during the 100-year frequency flood; and (4) the outlier culvert will drain the dam following a flood that uses all available storage within eight hours from beginning of storm event. The dam is constructed from piedmont deposits excavated within the reservoir area. The structure has a maximum height of 60 ft (18.1 m), maximum length of 1820 ft (554.7 m), and a maximum width at base of 280 ft (85.3 m). The slope of the upstream face and downstream face are 3:1 and 2:1

(horizontal to vertical), respectively. The elevation at the crest of the dam is 5779.5 ft (1761.6 m), and the detention capability at the crest of the emergency spillway is 564,717 m³ (458 acre-ft). The drainage area above the Juan Tabo dam is 26.33 km² (10.17 mi²). The basin heads at the crest of the Sandia Mountains (elevation —9400-9600 ft, 2865-2926 m) and includes both Bear Canyon and Embudito Arroyos. The total relief between the crest of the mountains and the primary spillway of the dam is 1235 m (4053 ft).

In contrast to areas to the south near Tijeras Canyon, piedmont aggradation over most of the Llano de Sandia continued through late Pleistocene time, and erosion surfaces on upper Santa Fe Group deposits have been buried by younger alluvium. The latter materials are predominantly arkosic sandy gravel to gravelly sand with loamy to silty zones. As noted by Kelley (1982, pp. 70-73), these deposits are commonly bouldery in a zone extending several miles out from the mountain front. Surface sediments in most topographically high areas on the piedmont slopes comprise a complex of stream, hyperconcentrated floodflow, and debris-flow deposits emplaced before entrenchment of the latest Pleistocene and Holocene arroyo-valley systems. Distal piedmont facies interfinger with, and partly overlap, the river-terrace deposits adjacent to the inner valley of the Rio Grande.

Stable surfaces on piedmont deposits are characterized by well-developed soil profiles with pedogenic horizons of clay accumulation over weak secondary carbonate zones. Such features typify the most extensive soils on the Llano de Sandia (Hacker, 1977). The amount and depth of pedogenic clay and carbonate translocation in these soils (as well as other weathering features) are indicative of wetter soil-moisture regimes that have not occurred in this region since Wisconsin glacial-pluvial times (>10,000 years B.P.). The late Pleistocene fan surfaces are cut by numerous small draws and several broad arroyo valleys with Holocene fills. Soil development is weak or essentially absent in these materials except for increasing amounts of organic matter in surficial horizons as one approaches the mountain front. Holocene valley fills on upper-piedmont slopes also comprise bouldery stream to debris-flow deposits and locally contain artifacts and charcoal.

In the areas southwest and northwest of this stop, Holocene arroyos have locally built low fans and alluvial aprons on the upper piedmont slope (e.g. Chelwood Park area between Lomas Blvd. and Indian School Rd., east of Juan Tabo Blvd.). Engineering interpretations by the Soil Conservation Service of soils developed in Holocene and upper Pleistocene alluvium indicate that many surficial deposits have limitations due to compressibility, susceptibility to piping, and consolidation under load, and pose significant geotechnical problems to engineering geologists and civil engineers. Underconsolidated piedmont deposits with high void ratios are subject to hydrocompaction when wetted and are thus particularly troublesome materials in terms of current and potential construction hazards (Clary et al., 1984).

Directions and comments en-route to Stop A-2

Return to Tramway Blvd. (0.0 mi) and continue north across Arroyo del Pino. AMAFCA flood-control structure to left. **0.5 mi**, traffic light, crossing San Rafael Ave. Base of Sandia Peak Tramway at **1:00** is between La Cueva rock-fan area (12:30) and bouldery alluvial fan of Cation Domingo Baca (2:00). Juan Tabo reentrant in the Sandia front

at 12:00 separates the main part of the uplift from Rincon Ridge on the west. The ridge is composed of Precambrian metamorphic rocks intruded by pegmatite dikes. **1.0 mi**, crossing paved flood-runoff channel at San Bernardino Dr.; *prepare for left turn*. **1.2 mi**, *turn left on Paseo del Norte Dr.*

For the next 6 mi, route descends the Llano de Sandia piedmont plain, dropping from an elevation of 6000 ft to 5000 ft (1830-1525 m) at Stop A-2 on the edge of the floodplain. The piedmont slope in this area is a coalescent-fan surface dissected by subparallel, west-flowing streams into a subdued ridge and swale topography. Arroyo gradients are about 4%. Upper Pleistocene alluvium underlies the low ridges and Holocene alluvium underlies the grass- and shrub-covered surfaces in the arroyo bottoms. The alluvium is predominantly arkosic sandy gravel and gravelly sand with loamy (sand-silt-clay) interbeds. **2.6 mi**, flood-water and sediment-control structure to right.

3.8 mi, traffic light, crossing Ventura St. An east-west gravity profile (Cordell, 1978a, b) made along Tramway Rd. about 2 mi (3.2 km) north of Paseo del Norte shows a steep westward gradient with a north-south linear trend. The belt of steep gravity gradient crosses the tour route in this area and indicates the presence of a large buried fault (downthrown to the west). **4.8 mi**, traffic light, crossing Wyoming Blvd. In 1940, the 5025 ft (1531 m) Norrins Realty Co. exploratory well no. 2 was drilled about 0.3 mi (0.5 km) southwest of this intersection (surface elevation about 5350 ft, 1630 m). According to the driller's log, the upper 2150 ft (655 m) is dominated by coarse, granite-derived basin fill interpreted by Stearns (1953, pp. 475-476) as "Santa Fe Formation." It should be noted that the upper 150 ft (46 m) of fill is uncemented and bouldery, and may represent post-Santa Fe, middle to upper Pleistocene alluvium. The lower 2874 ft (876 m) penetrated by the Norrins well includes mainly "gray sand" and "gray shale" that possibly correlate with the lower part of the Santa Fe Group (Zia Formation) and/or the Espinazo Formation (Oligocene).

5.2 mi, Federal Aviation Administration facility to left, crossing Louisiana Blvd. ahead at light. **6.1 mi**, traffic light, crossing I-25 and frontage roads. **6.4 mi**, *continue west on Paseo del Norte*. Journal Center to left. **6.7 mi**, traffic light, crossing Jefferson St. Route ahead is on distal part of Llano de Sandia. Alluvium is late Quaternary and is part of a local fan apron that spreads out from the mouths of arroyo valleys heading in the Bear/Pino reentrant area. **7.1 mi**, railroad crossing; Reeves Power Plant to left. This is the zone of emergence of the Llano de Sandia piedmont slope with terrace surfaces bordering the inner valley of the Rio Grande. Active and abandoned gravel pits to the right and left are developed in Edith alluvium, which is the major source of gravel and sand in the metropolitan area. **7.4 mi**, cross North Drainage Canal, one of two major outlet channels for flood runoff in Albuquerque. This canal system intercepts runoff from the entire Llano de Sandia area between I-25 and the Tramway. For the period of record (1968-1979), the maximum discharge measured at the gaging station 1.7 mi north of this point was 142 m³/s (5000 cfs) on July 26, 1971 (U.S. Army Corps of Engineers, 1979). **7.7 mi**, gravelly Edith alluvium exposed under power poles to left.

7.9 mi, Edith Blvd. overpass (Stop A-2) 0.3 mi to north. **8.1 mi**, crossing mainline Santa Fe Railroad. *Prepare for right turn at next traffic light*. **8.4 mi**, turn right (north) on

2nd St.; continue 0.2 mi to Ortega Rd. and then turn right (east) 0.5 mi on Ortega to Edith Blvd. **9.1 mi**, turn left, go north 0.1 mi, and park at east edge of Edith at roadcut exposure of basin-fill and terrace deposits (elevation 5000 ft, 1525 m).

Stop A-2: North Edith section of Lambert (1968) and environmental geology of the eastern valley-border area.

An axial-river facies of the upper Santa Fe Group (Upper Buff[?]) sand of Lambert, 1968) is exposed in cut to right. In the Albuquerque area, similar ancestral-river deposits of early Pleistocene age are discontinuously exposed in the lower part of the eastern valley-border scarp. In this area, this fluvial unit has a maximum exposed thickness of 3343 ft (1013 m) and is overlain with erosional unconformity by gravelly Edith alluvium. However, because of inadequate exposures, the unit cannot be physically traced to well-dated Sierra Ladrones Formation (Ceja Member) deposits that crop out along Tijeras Arroyo and the Llano de Albuquerque escarpments to the south and west (Stops A-3 and A-4).

The axial-river facies is here composed mainly of water-deposited rhyolitic pumice in the sand- and pebble-size range. About 2 mi (3.2 km) north of this stop the water-deposited pumice is conformably underlain by an air-fall ash layer resting on clay to clayey sand (Lambert, 1976). The air-fall ash and, presumably, the overlying water-deposited pumice have long been regarded as derived from one or more caldera-forming eruptions in the Jemez Mountains (Lambert, 1968, Appendix A; Smith et al., 1970). These eruptions produced the two members of the Bandelier Tuff and the intra-Bandelier Cerro Toledo Rhyolite; all units are between 1 and 1.5 m.y. old (Bailey and Smith, 1978; Goff et al., 1989). A sample of the air-fall ash collected by Ray Wilcox (U.S. Geological Survey) and Lambert has been correlated by Izett et al. (1981) with the Guaje Pumice Bed, the basal unit of the Bandelier Tuff. The K-Ar age of the Guaje Pumice is about 1.5 m.y., thus placing this part of the upper Santa Fe Group in the early Pleistocene. This age fits well with other deposits of the ancestral Rio Grande (Sierra Ladrones, Palomas, and Camp Rice Formations) dated both by K-Ar and zircon fission-track methods and by vertebrate faunas (Hawley, 1978, chart 1; Gile et al., 1981; Tedford, 1981; Lozinsky and Hawley, 1986).

The overlying Edith alluvium is middle to upper Pleistocene Rio Grande terrace deposit with an approximate thickness of 40-50 ft (12-15 m); however, at this stop the upper part has been removed by erosion and excavation. It is composed of gray sandy gravel and light-colored overbank mud and sand. The gravel is characterized by abundant, well-rounded pebbles and cobbles of metaquartzite. The Edith is exposed along the east side of the Rio Grande between Albuquerque and Bernalillo and occurs on both sides of the river in Albuquerque. It is locally inset against older valley fill and contains middle to late Pleistocene (Rancholabrean) fauna (Lambert, 1968, pp. 174-178; O'Neill and Rigby, 1982).

It has long been common practice to "reclaim" gravel pits in the Edith and other fluvial units with various types of municipal and industrial wastes. Land-fill operations using abandoned gravel pits extend from here to the valley of Tijeras Arroyo. The danger of this practice, particularly in terms of potential for ground-water pollution, is readily apparent at this stop. The water table here is within 15 to 30 ft (5 to 10 m) of the surface, and the permeable Edith

deposits are in direct contact with the equally permeable upper Santa Fe Group beds of unknown but significant thickness and wide subsurface extent. It is quite probable that the older fluvial beds seen here continue southeastward under the Llano de Sandia, as well as other areas where the upper Santa Fe Group is a major component of the basin-fill aquifer system.

Most cases of ground-water pollution are located near the inner Rio Grande valley where depth to ground water is shallow (Wilson, 1981; Stone, 1984; Anderholm, 1987). Regional, low-level pollution of the Rio Grande valley-fill aquifer with fecal coliform appears to be related to local unsanitary conditions of on-site waste disposal systems rather than to regional microbial pollution. The majority of these systems are septic tanks. In addition to pollution by nitrates, which has a 20-year record for portions of the Rio Grande valley, pollution by organic compounds has been detected by the Environmental Improvement Division (EID) of New Mexico. The primary pollutant is hydrocarbon-fuel oils such as gasoline and diesel fuel. These pollutants have been found in a variety of locations in the Rio Grande valley of the Albuquerque area. Federally funded grants to the State EID are supporting studies of pollution by nitrates, hydrocarbons, and other toxic organics in the Rio Grande valley (McQuillan, 1982; Thomson and McQuillan, 1984).

Return to Paseo del Norte Blvd. via Ortega Rd. and 2nd St.

Directions and comments en-route to Stop A-3

This road-log segment starts at the 2nd St. entrance to the Paseo del Norte Freeway (westbound lanes-0.0 mi). For the next 2.4 mi, the freeway is on the Rio Grande floodplain, crossing several irrigation canals, drains, and abandoned channel segments, as well as the modern river channel and floodway (1.5 mi). Floodplain gradient is 5 ft/mi (<1 m/km), which contrasts markedly with the greater than 50 ft/mi (>10 m/km) slopes of valley-border and piedmont terrains. At Albuquerque, upper Quaternary river deposits, dating from the past 20,000 years, are about 75 ft (23 m) thick according to Kelley (1982, pp. 13, 90-93). They include a basal gravel and sand zone that grades upward to sand with gravel lenses and thin surficial layers of clay and silt. This fluvial-facies assemblage, locally as much as 130 ft (40 m) thick, characterizes Rio Grande valley-floor deposits from the Albuquerque basin to Hueco bolson below El Paso, Texas (Hawley et al., 1976; Gile et al., 1981). Basal coarse-grained deposits relate to episodes of valley cutting during late Wisconsin glacial maxima. The upper sand-to-clay zone represents Holocene and latest Pleistocene aggradation, a process characteristic of stream valleys throughout the region.

This part of the city is susceptible to flooding caused by rainstorm-runoff events in local valley-border (Fig. A-4) and piedmont watersheds rather than by overbank flood discharges of the river. Large river floods are now controlled by upstream structures such as Cochiti Dam (Lagasse, 1981). Historical peak flows of the middle Rio Grande (1866-1967; as much as 100,000 cfs, 2850 m³/s) are shown in Fig. A5 (Kelley, 1982, p. 19). Stay in right lane for Coors Blvd. exit at west end of Paseo del Norte Freeway.

2.3 mi, take Coors Blvd. exit; keep to right. **2.5 mi**, take North Coors Blvd. exit. Continue 0.5 mi north on Coors to Irving Blvd.; *quickly move to far left lane for left turn*. **3.0 mi**, traffic light. *Turn left (west) on Irving Blvd.* Route rises



FIGURE A-4—Oblique aerial photo (to the west) near Corrales, showing extent of flooding and sedimentation on fan at mouth of Arroyo de los Montoyos and adjacent parts of Rio Grande floodplain after August 1975 rainstorm. This is the first large arroyo system north of Arroyo de las Calabacillas (photo Dick Kent).

across dissected valley-border surfaces (fans and terraces) of middle to late Quaternary age.

3.8 mi, crossing terrace overlooking Arroyo de las Calabacillas (to right). This arroyo system drains much of the northern Llano de Albuquerque (basin area of about 220 km²). Leopold (1946) described the effects of a severe thunderstorm that moved northeastward across the Llano de Albuquerque northwest of Albuquerque on the afternoon of September 20, 1941. Rainfall amounts of as much as 3864 mm may have been produced by the storm. Peak flow at the mouth of Arroyo de las Calabacillas was estimated to have been 285 m³/s (10,000 ft³/s). Arroyos north of Arroyo de las Calabacillas had estimated peak flows of 60-115 m³/s (2000 to 4000 ft³/s). According to local testimony, a similar flash flood occurred in Arroyo de las Calabacillas in 1904. The fan deposited at the mouth of Arroyo de las Calabacillas by the 1941 flood was described by Leopold (1946, p. 539) as follows:

At the mouth of Calabacillas Arroyo, an estimated 250 acre-ft of sediment, primarily sand, were deposited as a fan which forced the flow of the Rio Grande into a narrow channel against the east bank of the main floodplain. The total contribution of sediment must have been even larger because much was carried downstream by the combined flow of the arroyo and the Rio Grande. The depth of deposition was nine feet in places. Some large boulders were deposited in the fan. One, estimated weight 1,400 pounds, was deposited 700

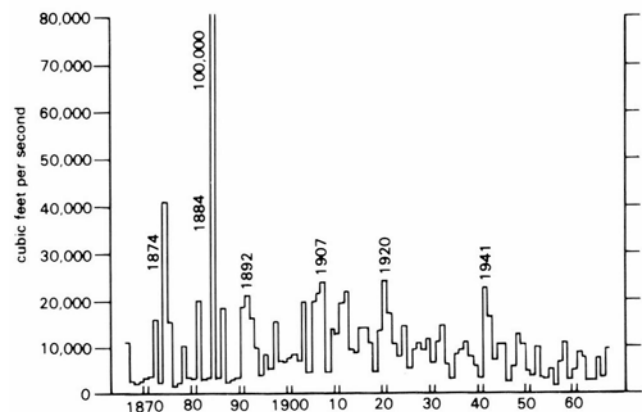


FIGURE A-5—Peak discharges of the Rio Grande (from Kelley, 1982).

feet from the mouth of the arroyo and five feet above the normal streambed.

In 1941, the Arroyo de las Calabacillas area was largely undeveloped. The only damage reported by Leopold was the washing out of a primary gas main feeding the City of Albuquerque. If a similar flood occurred today, damage could be much more severe (Fig. A-4).

4.6 mi, traffic light. Turn right (north) on Golf Course Rd. across channel of Arroyo de las Calabacillas. Construction of flood-water-retention structures in this area has been plagued by problems because of susceptibility of sandy-substrate units to piping and seepage, and lack of nearby sources for suitable clayey fill materials. **5.0 mi**, traffic light at Ellison. **5.7 mi**, crossing Black Arroyo. **5.9 mi**, Bernalillo—Sandoval County line; entering the City of Rio Rancho (New Mexico's fastest growing urban area). Continue north on Golf Course Rd. across dissected, older valley-border surface (about 246-263 ft, 75-80 m, above the valley floor) that is part of the mid-Pleistocene Tercero Alto geomorphic-surface complex of Machette (1985). The surface is locally covered by basalts of the Albuquerque Volcanoes field (Stop 4) dated at <200,000 yrs by Geissman et al. (1990). Middle to late Quaternary alluvial, colluvial, and eolian deposits mantle Plio-Pleistocene basin fill of the upper Santa Fe Group—Sierra Ladrones Formation (Ceja Mem-

ber?). **7.3 mi**, traffic light ahead, prepare for left turn. **7.5 mi**, turn left (west) on Southern Blvd. **7.7 mi**, Albuquerque Volcanoes at 9:30. Continue west about 10 mi on Southern

Blvd. Route ahead crosses broad undulating surface on upper Santa Fe Group veneered with Quaternary alluvium and eolian deposits. **8.7 mi**, traffic light, crossing 20th St. **9.4 mi**, route ascends slope cut in Ceja Member of Sierra Ladrones Formation gravelly sand. This is the eroded scarp of Kelley's (1977) Star Heights fault.

10.3 mi, on crest of high ridge about 650 ft (200 m) above floodplain level. Mount Taylor on skyline. For next 8.3 mi route crosses upper Arroyo de las Calabacillas watershed (Fig. A-6). An outlier of the Llano de Albuquerque north of this point is locally capped with a strong calcic soil developed on pebbly sand of the Ceja Member, Sierra Ladrones Formation. The water table here is about 700 ft (213 m) below the surface and has a trough-like configuration (Fig. A-1), sloping southward away from adjacent parts of the Rio Grande and Rio Puerco valley floors (Titus, 1961; Kernodle and Scott, 1986; Anderholm, 1987, 1988; Hawley and Longmire, in press). Wells for public water supplies in this part of the Albuquerque basin are commonly more than 1000 ft (300 m) deep and are developed in the middle to upper part of the Santa Fe Group. Near the western rim of the Llano de Albuquerque, depths to the basin-fill aquifer locally exceed 1000 ft (300 m).

11.5 mi, on graded road descending into valley of Arroyo de las Calabacillas across slopes cut in sandy basin fill (upper Santa Fe Group). **11.7 mi**, caution, dip in road ahead at Arroyo de las Calabacillas. Southern Blvd. occasionally washes out at this point during large storm-runoff events. For next 3.5 mi route is on thin veneer of upper Quaternary

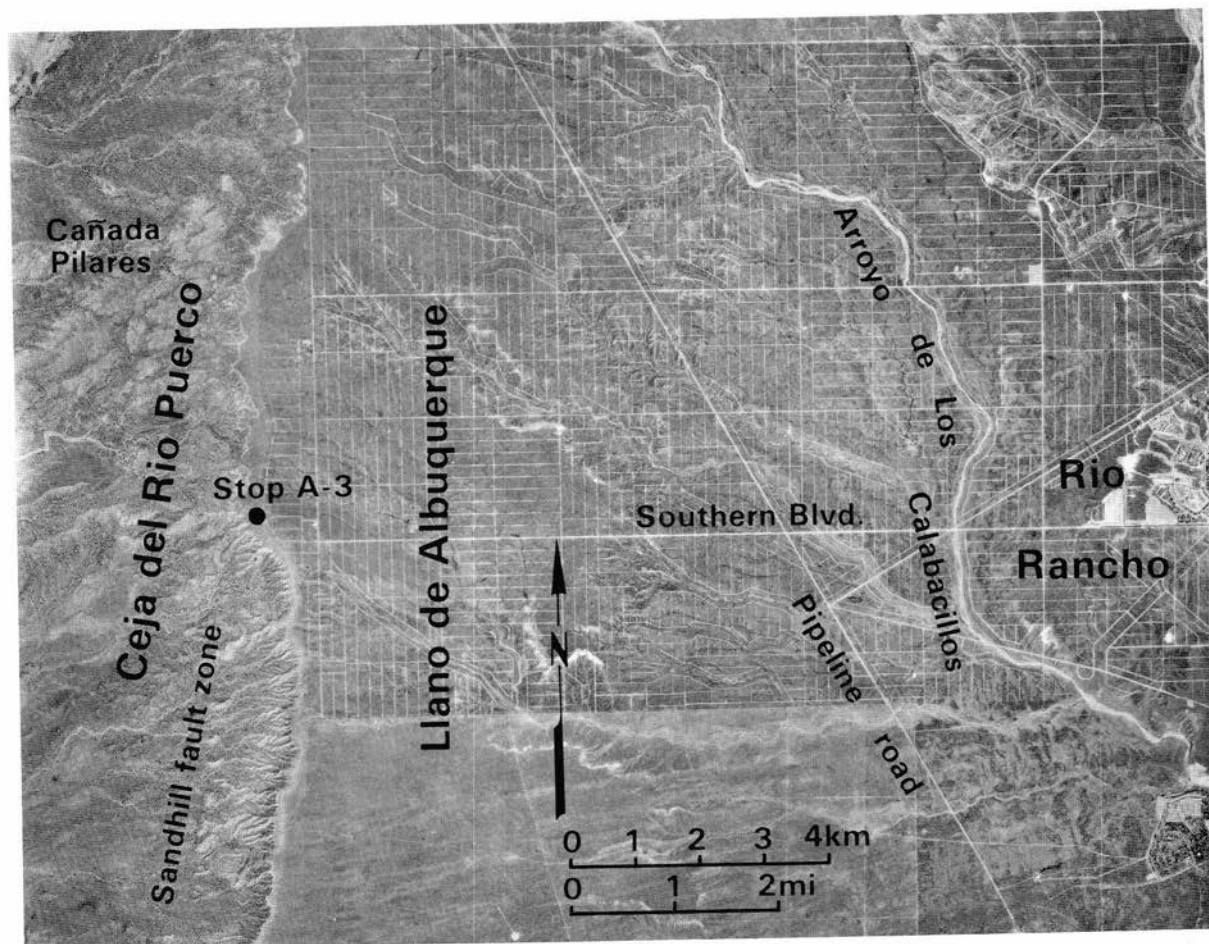


FIGURE A-6—Aerial photograph of Llano de Albuquerque area west of Rio Rancho. Ceja del Rio Puerco rim marked by prominent sand-dune south of Stop A-3 (U.S. Geological Survey photo).

valley fill underlain by upper Santa Fe Group basin fill. **12.9 mi**, on line with north—south trend of Albuquerque Volcanoes (Kelley and Kudo, 1978; Geissman et al., 1990). The northernmost cone is about 5 mi (8 km) to the south at eastern edge of the Llano de Albuquerque surface. In this area the route crosses at least two faults that are along the trend of the Albuquerque Volcanoes fissure. Displacement is down to the east. These faults line up to the south with the County Dump—Nine Mile fault trend of Machette (1978a) and Kelley (1977), and they are aligned to the north with the Duval and Zia faults of Kelley (1977). Machette's (1978c) study of the County Dump fault, near 1-40, shows that there has been recurrent movement on this feature during middle to latest Pleistocene time.

13.4 mi, intersection with Gas Company of New Mexico pipeline road. (*Route to Stop A-4.*) **15.2 mi**, near top of scarp that forms the western edge of the Arroyo de las Calabacillas valley. Coarse-grained fluvial deposits of the Ceja Member, Sierra Ladrones Formation, form the upper unit of the Santa Fe Group in this area. Clasts are in the pebble-to-small-cobble range, commonly rounded, and include quartzite, chert, basalt, and granite. Some of the chert is derived from the Pedernal Chert Member of the Abiquiu Formation (Oligocene—Miocene; see Vazzana and Ingersoll, 1981). A calcic soil is developed in the uppermost sand and gravel beds and forms the light-colored (Cejita Blanca) rim of the Llano de Albuquerque ahead. This strong horizon of soil-carbonate accumulation is probably correlative with calcic horizons in surficial soils of the eastern Llano de Albuquerque scarp seen at Stops 2-2 and 2-4 on Day 2.

15.4 mi, military training area to right; crossing remnant of Llano de Albuquerque. This early to middle Pleistocene geomorphic surface represents a relict central-basin plain that predates entrenchment of the present Rio Grande and Rio Puerco valleys (Lambert, 1968; Machette, 1985). The original basin-floor and distal-piedmont components of this constructional landscape have been faulted, partly dissected by erosion, and locally buried by later eolian and alluvial-colluvial deposits. The Llano surface to the south and west is crossed by north-trending linear depressions at the base of eroded fault scarps. Offsets are mainly down to the east (Kelley, 1977; Machette, 1982). **16.5 mi**, crossing broad, north-trending swale. **17.0 mi**, note high dunes on the skyline extending south from the AT&T Co. relay tower (10:00-1:00). These dunes partly cover the western rim of the Llano de Albuquerque and are derived from the Rio Puerco valley area to the west (Lambert, 1968, 1974).

17.8 mi, turn right (north) on 60th St. **18.0 mi**, opposite AT&T Co. relay installation. Turn left (west) on dirt road. **18.1 mi**, powerline crossing. Road ahead jogs to right and then to left. Route ascends Holocene alluvial and eolian apron at eastern base of high rim dunes. **18.4 mi**, keep left at road fork. Continue west to base of large dune and park for Stop A-3 (**18.6 mi**). Road to right is recommended only for offroad vehicles due to loose sand. It skirts the northern end of the rim dunes and leads to the Ceja del Rio Puerco ([eye]brow of the Rio Puerco [escarpment]).

Stop A-3: Ceja del Rio Puerco and Sand Hill fault zone. Walk to crest of dune for orientation and then west to Sand Hill fault zone at rim of Ceja del Rio Puerco escarpment (Figs. A-1, A-6, A-7).

The rim-dune crest (elevation 6263 ft, 1909 m) offers a broad vista of the northern Albuquerque basin and adjacent

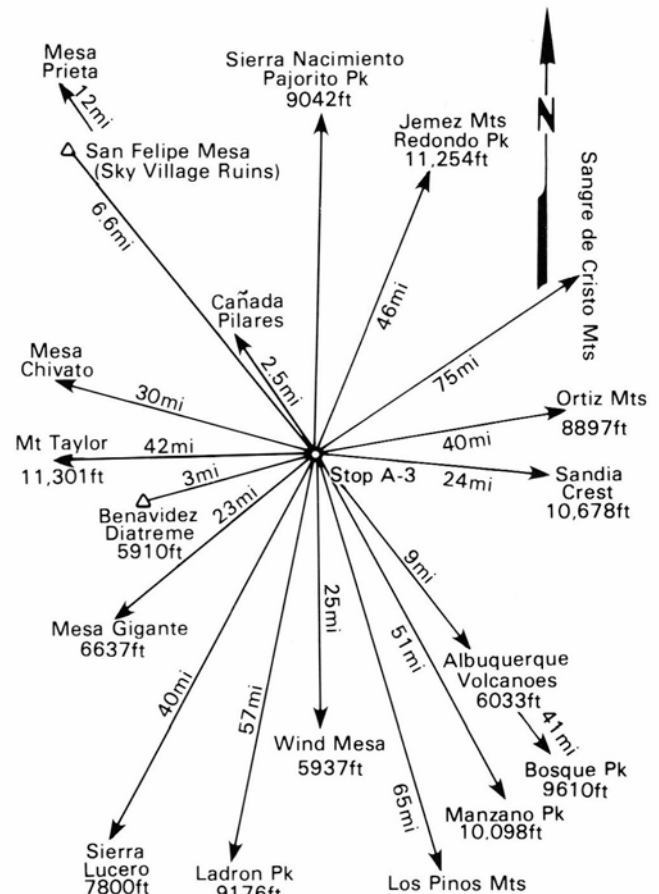


FIGURE A-7—Panoramic location diagram for major landmarks seen from Stop A-3 on west (Ceja del Rio Puerco) rim of Llano de Albuquerque.

parts of the Colorado Plateau and Southern Rocky Mountain provinces. Mount Taylor (west) and the Lucero uplift (south-southwest) flank the Acoma sag area of the Colorado Plateau visited on Day 2 (Stop 2-1). Basalt-capped Mesa Prieta, about 12 mi (20 km) to the northwest, is located east of the Rio Puerco valley (see Slavin, this volume). The Nacimiento Mountains to the north and the Sangre de Cristo Mountains on the northeastern skyline form the southernmost prongs of the Southern Rockies. The Jemez Mountain volcanic center (north-northeast) of middle Miocene to Pleistocene age is between these ranges (Bailey and Smith, 1978; Goff et al., 1989).

The base of the escarpment in the foreground is along the eastern margin of the Rio Puerco fault zone (Kelley and Wood, 1946; Wright, 1946; Slack and Campbell, 1976). About 4 mi (6.4 km) west of here the lower part of the Santa Fe Group is down-faulted against Upper Cretaceous rocks along the Moquino fault of Kelley (1977; Canada Moquino fault of Bryan and McCann, 1937). This fault and the Sand Hill fault, which crosses the Ceja rim at this stop, appear to form the two major rift-boundary faults in this area (Bryan and McCann, 1937; Wright, 1946; Kelley et al., 1976; Kelley, 1977; Machette, 1982).

This stop is near the southern end of the Ceja del Rio Puerco area where Bryan and McCann (1937) first subdivided the "Santa Fe formation" into broad mapping units (Tedford, 1982). Their threefold subdivision of the Santa Fe into "Lower Gray, Middle Red, and Upper Buff members" was based primarily on variations in color, texture,

and cementation. They characterized the Lower Gray and Middle Red members as having mainly sandy textures, with clay and gravel beds and calcareous concretionary sandstones locally present. The main distinguishing feature was color, white to gray in the Lower Gray unit and common shades of red to buff in the Middle Red unit. The presence of gravel, buff colors, and variable textures characterized their Upper Buff member. These basic Santa Fe subdivisions have been used (with some modifications) by most subsequent workers in the northern Albuquerque basin, including Wright (1946), Campbell (1967), Lambert (1968), and Kelley (1977); they are still commonly used for general descriptions of basin-fill stratigraphy. Even these broad Santa Fe mapping units have been useful in making estimates of minimum throw on major basin-margin and intrarift faults, and they allowed Bryan and McCann (1937, p. 801) "to speculate on the amount of the depression of the basin as a result of this faulting."

Galusha (1966) mapped the Lower Gray and Middle Red type area in the Rincones de Zia about 20 mi (33 km) to the north, and he made the first definitive studies of vertebrate faunas and biostratigraphy. Galusha formally named the lower to middle Miocene Zia Sand Formation (now called the Zia Formation), and showed that it was equivalent to the type Lower Gray member of Bryan and McCann (1937). Galusha and Blick (1971, pp. 39-40, 70) demonstrated that at least the lower part of the Middle Red member correlated with the upper part of the middle Miocene Tesuque Formation, the main type Santa Fe subdivision in the Española basin (Spiegel and Baldwin, 1963). Gawne (1973, 1981) refined the Zia Formation stratigraphic nomenclature in the Canada Pílares—Arroyo Benavidez area (2.5 mi, 4 km) to the north-northwest of this stop, as well as in the type Zia area along the valley of the Jemez River. Kelley (1977) described the Zia and lower Middle Red units at the Benavidez Ranch measured section about 3.5 mi (5.6 km) west-southwest of this stop.

Current work by Tedford and Barghoon of the American Museum of Natural History involves completion of biostratigraphic studies in the northern Ceja area that were initiated by the late Ted Galusha. Detailed measured sections have been made between here and Canada Pílares, and work on magnetostratigraphy as well as biostratigraphy is in progress. The exposed Santa Fe Group section is about 1000 ft (300 m) thick and thickens southeastward. The lower 415 ft (126 m) is the Zia (Sand) Formation described by Gawne (1981). This predominantly eolian sand unit is angularly unconformable on Upper Cretaceous sandstone and shale with very thin remnants of the Galisteo Formation locally present between the Cretaceous and basal Zia. The upper Zia, Canada Pílares Member of Gawne (1981), a red clay with local sandstone lenses up to 92 ft (28 m) thick, has been included with the Middle Red member by previous workers. The upper part of the Middle Red member of Kelley (1977) is here about 650 ft (200 m) thick and consists mainly of light reddish-brown sand to silty sand. The unit has thin beds of volcanic ash and one prominent zone of algal tufa heads and lacustrine clay to sand. The "Middle Red member" contains eolian-sand bodies very similar to the bulk of the underlying Zia Formation, and it is included in that formation by Tedford (pers. comm. 1990) as an unnamed upper member.

The upper Santa Fe Group at this stop includes the Ceja

Member of Kelley (1977), a sand-and-gravel to conglomeratic sandstone facies with local thick lenses of loamy to clayey sediments and buried soils in structural sags adjacent to faults. The Ceja Member as mapped by Kelley (1977) includes much of the Upper Buff member of Bryan and McCann (1937), Wright (1946), and Lambert (1968), and it is a basin-floor facies of the Sierra Ladrones Formation of Machette (1978a, b). Along the escarpment near this stop, the Ceja Member is as much as 250 ft (76 m) thick and the upper 50-100 ft (15-30 m) of the unit contain scattered angular boulders of basalt and Cretaceous sandstone, probably derived from the area to the northwest that is now part of the Rio Puerco valley. The bulk of the gravel clasts are rounded pebbles of mixed siliceous rock types derived from as far north as the northern Nacimiento uplift. The Ceja Member is capped with a strong calcic soil and thick eolian sand of the rim-dune sequence.

Tedford (1981, 1982) reviewed the mammalian biochronology of the Santa Fe Group and the development of stratigraphic terminology in the Ceja del Rio Puerco and Jemez Valley areas. The lower Zia Formation contains faunas of late Arikareean and Hemingfordian provincial age (about 21 to 16 Ma). Sites in the Middle Red member (upper Zia of Tedford) have late Barstovian and Clarendonian faunas (about 15 to 10 Ma). Faunas of the Ceja Member, Sierra Ladrones Formation, are primarily of Blancan age (less than 4.5 Ma).

Nearby volcanics within the Rio Puerco valley include the basalt flow capping Mesa Prieta about 12 mi (20 km) to the northwest, numerous basaltic necks, and the Benavidez diatreme 3 mi (5 km) west of this stop. The Mesa Prieta flow with a K—Ar age of 2.2 ± 0.3 m. y. (Armstrong et al., 1976) rests on an erosion surface correlated with the Ortiz surface by Bryan and McCann (1938). The Benavidez diatreme, first described by Kelley and Kudo (1978), is associated with a partly exhumed maar center emplaced in the lower and middle parts of the Santa Fe Group section. Volcanic necks and geomorphic evolution of the region to the northwest are discussed by Slavin (this volume).

The Sand Hill fault zone of Bryan and McCann (1937) is well exposed at this stop (Fig. A-6). It was first described in detail by Wright (1946). He noted the episodic movement and growth of the main fault segment exposed at this stop, which involves offset (down to east) of both Middle Red and Upper Buff members. As at the County Dump fault (Machette, 1978c), episodic fault displacement alternating with intervals of erosion of the upthrown block has resulted in episodic sediment accumulation and soil development on the downthrown block.

The lower Rio Puerco valley area, including summits of flanking tablelands (e.g. Llano de Albuquerque), contains several proposed sites for large solid-waste management facilities (Hawley and Longmire, in press). A regional landfill for Bernalillo County (Cerro Colorado facility) has already been developed on the Ceja del Rio Puerco about 15 mi (24 km) south of this stop. Proposed sites are characterized by thick vadose zones (500 to 1000 ft, 150-300 m) in fine- to medium-grained Neogene basin fill or Cretaceous rocks and absence of large fresh-water aquifers. Siting problems include (1) avoiding geomorphically unstable areas with potential for rapid erosion—sedimentation rates or intense seismic activity, and (2) protecting ecologically and culturally sensitive areas.

Directions and comments en-route to Stop A-4

Retrace route 5.2 mi via Southern Blvd. (4.4 mi) to junction with Gas Company of New Mexico pipeline road (Figs. 2 and A-6). 0.0 mi, turn right (southeast) on pipeline road (graded extension of Atrisco Dr.—Unser Blvd.). Route descends erosion surface cut on upper Santa Fe Group—Sierra Ladrones Formation (Ceja Member?). **4.0 mi**, crossing basalt flows of Albuquerque Volcanoes field from here to Stop A-4; note extensive eolian cover. **6.1 mi**, start of pavement at Unser Blvd.; approaching Volcano Cliffs. Turn right (southwest) on paved road to Maloof Memorial Airpark and La Boca Negra Park for 0.15 mi; turn left (southeast) at power poles on gravel (pipeline) road and continue 0.45 mi past pipeline enclosure; turn left and continue east to edge of basalt flow and Stop A-4 (**6.8 mi**). Pipeline crosses rim of Volcano Cliffs escarpment at this point (elevation 5300 ft, 1615 m).

Stop A-4: Albuquerque Volcanoes and Volcano Cliffs. Kelley and Kudo (1977) mapped ten basalt flows in the Albuquerque volcanic field, including an extensive basal (Qbl) flow of olivine basalt capping cliffs at this top (Fig.

A-8). This flow has been K—Ar dated at $190,000 \pm 40,000$ years by Bachman et al. (1975). According to Machette (1978c, pp. 374-375), the most extensive flows spread easterly over the two highest Rio Grande terraces (Tercero and Segundo Alto) between about 200,000 and 100,000 years ago. Geissman et al. (1990) show that all flows of the Albuquerque Volcanoes record a short-excision, magnetic-polarity episode. K—Ar age determinations (weighted average: 155 ± 47 ka) and morphology of calcic soils developed in flow veneers enriched in eolian materials suggest that the short extrusion episode occurred sometime between 250 and 80 ka.

A series of at least ten small volcanoes and spatter cones are aligned along the trend of the County Dump fault—Albuquerque Volcanoes fissure (Lambert, 1968). The Vulcan "J" Cone center is the most prominent topographic feature. The cone is about 200 ft (60 m) high and 2100 ft (640 m) in diameter. It is a steep-sided cinder and lava cone flanked on the north by a questionable collapse structure and on the south by two small adventive cones.

Poorly consolidated sediments, locally exposed beneath the flows, include pink and green clay and silt as well as clean, light-colored sand. These beds were originally mapped

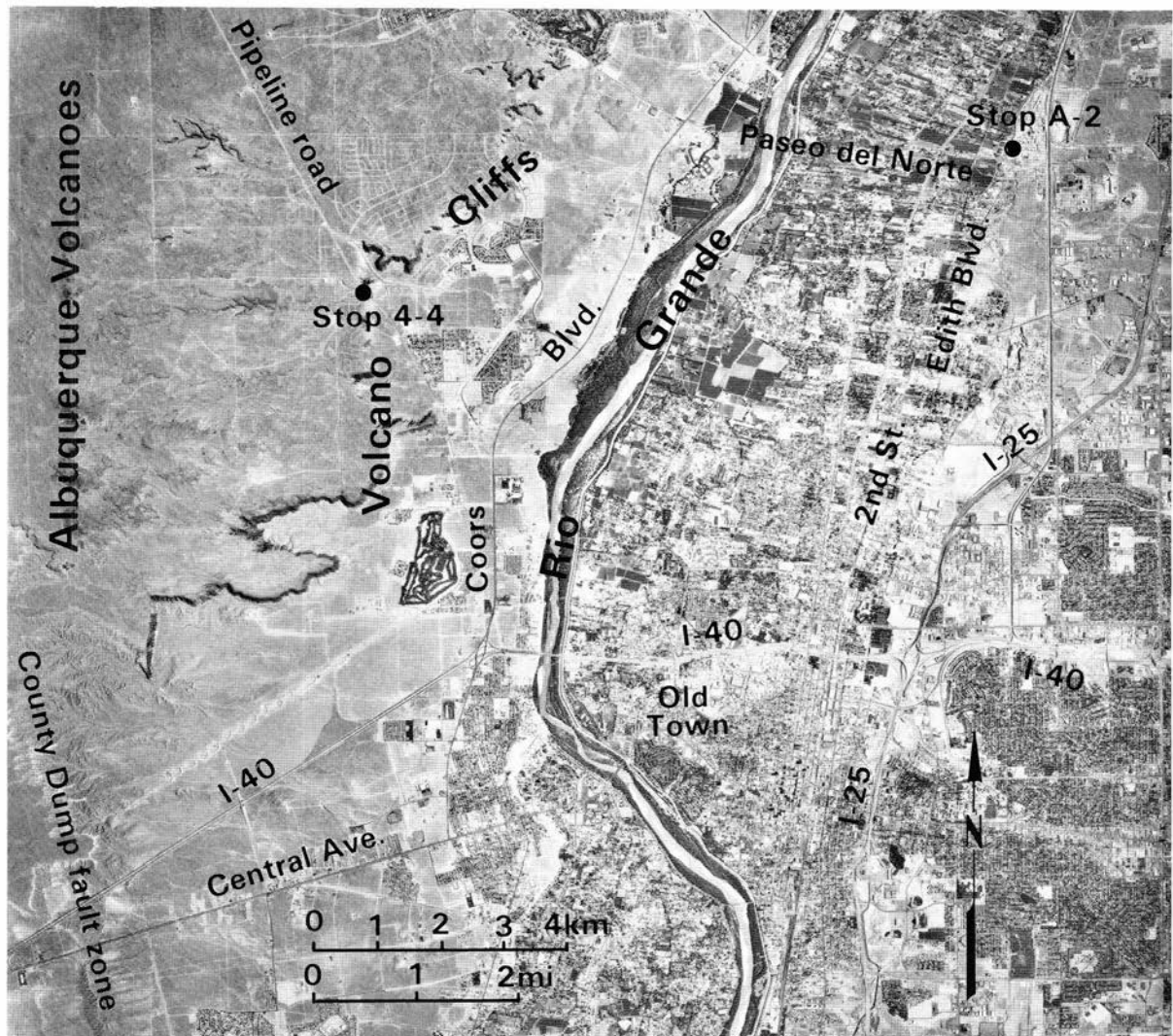


FIGURE A-8—Aerial photograph of western part of Albuquerque, including inner valley and floodplain of the Rio Grande and the Albuquerque volcanic field at the east edge of the Llano de Albuquerque. Stop A-4 is on the Volcano Cliffs escarpment near Indian Petroglyph State Park (U.S. Geological Survey photo).

by Lambert (1968, pp. 73, 103) as Upper Buff member (Ceja Member equivalent) of the Santa Fe Formation. They may instead correlate with older valley fill beneath the "Tercero Alto" surface of Machette (1985), which includes terrace alluvium in the Volcano Cliffs area that is associated with surfaces about 240 ft (73 m) above the valley floor. An older, axial-river gravel that is poorly exposed in low hills at the base of the Volcano Cliffs escarpment north and south of this stop was mapped by Lambert (1968, p. 94) as Upper Buff(?) gravel. This cobbly, erosion-resistant unit, which is up to 50 ft (15 m) thick, is probably an exhumed channel zone within the upper (Pliocene—early Pleistocene) part of the Sierra Ladrones Formation. The channel gravel crops out discontinuously along the west border of the river valley from near Bemalillo to Isleta Pueblo, where it is offset by at least one major fault and may be partly buried by a basalt flow of the Isleta volcanic center, with a K—Ar age of 2.78 Ma (Kelley and Kudo, 1978; Kudo et al., 1977).

Directions and comments en-route from Stop A-4 to I-40-1-25 Interchange

Retrace route to Unser Blvd. (0.0 mi). Continue southeast on Unser, descending Volcano Cliffs escarpment. **0.5 mi**, entrance to Indian Petroglyph State Park on left. **1.0 mi**, intersection with Montaña Blvd. San Antonio Arroyo flood-water channel on right cut in exhumed cobbly river-channel deposit in the Sierra Ladrones Formation, possibly as old as late Pliocene. This is the Upper Buff(?) gravel of Lambert (1968). **1.8 mi**, drainage channel and powerline crossing at foot of basalt-capped spur of basin- and/or valley-fill alluvium, with mantle of basalt-block colluvium. Route ahead on Atrisco Dr. descends to Segundo Alto constructional terrace, here about 140 ft (43 m) above the Rio Grande floodplain. The terrace fill comprises the Los Duranes alluvium (alloformation) of Lambert (1968) and locally exceeds 140 ft (43 m) in thickness. Deposits are primarily sand, silt, and clay, with a basal gravel zone. One flow tongue of the Albuquerque Volcanoes is exposed in a valley cut below the Segundo Alto surface; it may have been buried during deposition of the underlying Los Duranes alluvium and subsequently exhumed.

2.9 mi, intersection of Atrisco Dr. and Ladera Dr.; *turn left (east) on Ladera and prepare for right turn*. **3.2 mi**, intersection with Coors Blvd. Turn right on Coors and continue 1.5 mi south across Segundo Alto terrace. *Stay in center lane; prepare to take second exit to right (I-40 East)*.

4.7 mi, *take I-40 East (Santa Rosa) exit to right*. **4.9 mi**, merge with I-40 and continue east across inner Rio Grande valley to interchange with I-25. Route descends from Segundo Alto surface to river-valley floor. Roadcuts ahead in Los Duranes alluvium. **5.6 mi**, crossing Rio Grande channel and floodway. Route on Rio Grande floodplain for next 3 mi. Historic Old Town Plaza ahead on right at Rio Grande Blvd. exit. **6.7 mi**, Rio Grande Blvd. exit to right; Old Town Plaza, Albuquerque Museum, and New Mexico Museum of Natural History. **7.4 mi**, 12th St. exit to right. Pueblo Museum three blocks north of freeway on 12th. I40 and I-25 ("Big I") Interchange ahead. Prepare to take I-25 South. **8.9 mi**, *take I-25 South exit to University of New Mexico (Lomas and Grand exits), and to Airport (Girard exit)*. End of Albuquerque urban-area tour and Day 3 of field trip.

References

- Akers, J. P., 1964, Geology and ground water in the central part of Apache County, Arizona: U.S. Geological Survey, Water-Supply Paper 1771, 107 pp.
- Anderholm, S. K., 1987, Reconnaissance of hydrology, land use, ground-water chemistry, and effects of land use on ground-water chemistry in the Albuquerque—Belen basin, New Mexico: U.S. Geological Survey, Water-Resources Investigations Report 86-4174, 37 pp.
- Anderholm, S. K., 1988, Ground-water geochemistry of the Albuquerque—Belen basin, central New Mexico: U.S. Geological Survey, Water-Resources Investigation Report 86-4094, 110 pp.
- Anderson, O. J., Love, D., and Lucas, S. G., 1989, Supplemental road log 3, from intersection of NM-602 and Bread Springs Road to Fort Wingate, via Stinking Springs and McGaffey: New Mexico Geological Society, Guidebook 40, pp. 71-73.
- Anderson, O. J., Lucas, S. G., and Love, D. W., 1989, Stratigraphic nomenclature chart: New Mexico Geological Society, Guidebook 40, p. xiv.
- Anderson, O. J., Lucas, S. G., Love, D. W., Maxwell, C. H., and Chamberlin, R. M., 1989, Third-day road log, from Gallup to Upper Nutria, Ramah, El Morro and Grants: New Mexico Geological Society, Guidebook 40, pp. 49-66.
- Antevs, E., 1954, Climate of New Mexico during the last glacial—pluvial: *Journal of Geology*, v. 62, pp. 182-191.
- Armstrong, R. L., Speed, R. C., Graustein, W. C., and Young, A. Y., 1976, K—Ar dates from Arizona, Montana, Nevada, [New Mexico], Utah, and Wyoming: *Isochron/West*, no. 16, pp. 1-6.
- Bachhuber, F. W., 1971, Paleolimnology of Lake Estancia and the Quaternary history of the Estancia Valley, central New Mexico: Unpublished PhD dissertation, University of New Mexico, Albuquerque, 238 pp.
- Bachhuber, F. W., 1982, Quaternary history of the Estancia Valley, central New Mexico: New Mexico Geological Society, Guidebook 33, pp. 343-346.
- Bachhuber, F. W., 1989, The occurrence and paleolimnologic significance of cutthroat trout (*Oncorhynchus clarki*) in pluvial lakes of the Estancia Valley, central New Mexico: *Geological Society of America, Bulletin*, v. 101, pp. 1543-1551.
- Bachman, G. O., and Mehnert, H. H., 1978, New K—Ar dates and the late Pliocene to Holocene geomorphic history of the central Rio Grande region, New Mexico: *Geological Society of America, Bulletin*, v. 89, pp. 283-292.
- Bachman, G. O., Marvin, R. F., Mehnert, H. H., and Merritt, V., 1975, K—Ar dates of Los Lunas and Albuquerque basalts: *Isochron/West*, no. 13, pp. 3-4.
- Bailey, R. A., and Smith, R. L., 1978, Volcanic geology of the Jemez Mountains, New Mexico; in Hawley, J. W. (compiler), *Guidebook to Rio Grande rift in New Mexico and Colorado*: New Mexico Bureau of Mines & Mineral Resources, Circular 163, pp. 184-196.
- Baldrige, W. S., Perry, F. V., and Shafiqullah, M., 1987, Late Cenozoic volcanism of the southeastern Colorado Plateau, I. Volcanic geology of the Lucero area, New Mexico: *Geological Society of America, Bulletin*, v. 99, pp. 463-470.
- Baldrige, W. S., Perry, F. V., Vaniman, D. T., Nealey, L. D., Leavy, D. B., Laughlin, A. W., Kyle, P., Bartov, Y., Steinitz, G., and Gladney, E. S., 1989, Excursion 8A: Magmatism associated with lithospheric extension: Middle to late Cenozoic magmatism of the southeastern Colorado Plateau and central Rio Grande rift, New Mexico and Arizona; in Chapin, C. E., and Zidek, J. (eds.), *Field excursions to volcanic terranes in the western United States, Volume I: Southern Rocky Mountain region*: New Mexico Bureau of Mines & Mineral Resources, Memoir 46, pp. 187-202.
- Baldrige, W. S., Perry, F. V., Nealey, L. D., Laughlin, A. W., and Wohletz, K. H., 1989, Field guide to Excursion 8A: Oligocene to Holocene magmatism and extensional tectonics, central Rio Grande rift and southeastern Colorado Plateau, New Mexico and Arizona; in Chapin, C. E., and Zidek, J. (eds.), *Field excursions to volcanic terranes in the western United States, Volume I: Southern Rocky Mountain region*: New Mexico Bureau of Mines & Mineral Resources, Memoir 46, pp. 202-230.
- Bates, R. L., Wilpolt, R. H., MacAlpin, A. J., and Vorbe, G., 1947, Geology of the Gran Quivira quadrangle: New Mexico Bureau of Mines & Mineral Resources, Bulletin 26, 52 pp.
- Betancourt, J. L., VanDevender, T. R., and Martin, P. S. (eds.) 1990, Fossil packrat middens: The last 40,000 years of biotic change: University of Arizona Press, Tucson, 469 pp.
- Blagbrough, J. W., 1865, Quaternary geology of the northern Chuska

- Mountains and Red Rock Valley, northeastern Arizona and northwestern New Mexico: Unpublished PhD dissertation, University of New Mexico, Albuquerque, 138 pp.
- Bourlier, B. G., Neher, R. E., Crezee, D. B., Bowman, K. J., and Meister, D. W., 1970, Soil survey of Torrance area, New Mexico: U.S. Soil Conservation Service, U.S. Government Printing Office, Washington, D.C., 149 pp.
- Brackenridge, G. R., 1978, Evidence for a cold, dry full-glacial climate in the American Southwest: Quaternary Research, v. 9, pp. 22-40.
- Brady, B. T., Mulvihill, D. H., Hart, D. L., Jr., and Langer, W. H., 1984, Maps showing ground-water levels, springs, and depth to ground water, Basin and Range province, New Mexico: U.S. Geological Survey, Water-Resources Investigation Report 83-4118-B.
- Brod, R. C., and Stone, W. J., 1981, Hydrogeology of Ambrosia Lake-San Mateo area, McKinley and Cibola Counties, New Mexico: New Mexico Bureau of Mines & Mineral Resources, Hydrogeologic Sheet 2, scale 1:62,500.
- Brown, L. D., Chapin, C. E., Sanford, A. R., Kaufman, S., and Oliver, J., 1980, Deep structure of the Rio Grande rift from seismic reflection profiling: Journal of Geophysical Research, v. 85, pp. 4773-4800.
- Bryan, K., 1909, Geology of the vicinity of Albuquerque: University of New Mexico, Bulletin 51, Geological Series, v. 3, 24 pp.
- Bryan, K., 1938, Geology and groundwater conditions of the Rio Grande depression in Colorado and New Mexico; *in* U.S. Natural Resources Planning Board, The Rio Grande Joint Investigations in the upper Rio Grande Basin: U.S. Government Printing Office, Washington, D.C., v. 1, pt. 2, pp. 197-225.
- Bryan, K., and McCann, F. T., 1937, The Ceja del Rio Puerco: A border feature of the Basin and Range province in New Mexico, Part I: Journal of Geology, v. 45, pp. 801-828.
- Bryan, K., and McCann, F. T., 1938, The Ceja del Rio Puerco: A border feature of the Basin and Range province in New Mexico, Part II: Journal of Geology, v. 46, pp. 1-16.
- Campbell, J. A., 1967, Geology and structure of a portion of the Rio Puerco fault belt, western Bernalillo County, New Mexico: Unpublished PhD dissertation, University of New Mexico, 89 pp.
- Cather, S. M., 1989, Post-Laramide tectonic and volcanic transition in west-central New Mexico: New Mexico Geological Society, Guidebook 40, pp. 91-97.
- Chamberlin, R. M., and Anderson, O. J., 1989a, The Laramide Zuni uplift, southeastern Colorado Plateau: a microcosm of Eurasian-style indentation-extrusion tectonics: New Mexico Geological Society, Guidebook 40, pp. 81-90.
- Chamberlin, R. M., and Anderson, O. J., 1989b, The southern margin of the Colorado Plateau: a ragged edge bounded by Neogene domains of crustal extension: New Mexico Geological Society, Guidebook 40, pp. 37-38.
- Chamberlin, R. M., Anderson, O. J., Lucas, S. G., Maxwell, C. H., and Love, D. W., 1989, Second-day road log, from Grants to El Malpais, Fence Lake, Zuni Pueblo and Gallup: New Mexico Geological Society, Guidebook 40, pp. 25-48.
- Clary, J. H., Korecki, N. T., and Mondragon, R. R., 1984, Geology of Albuquerque, New Mexico, United States of America: Bulletin of Association of Engineering Geologists, v. 21, no. 2, pp. 127-156.
- Colpitts, R. M., Jr., Bauer, P., and Smith, C. T., 1989, Supplemental road log 4, from intersection of NM-53 and Forest Road 50 (near Bandera Crater) to Grants, via Forest Roads 50 and 49: New Mexico Geological Society, Guidebook 40, pp. 73-75.
- Connolly, J. R., Woodward, L. A., and Hawley, J. W., 1982, Road-log segment I-A: Albuquerque to Tijeras Canyon: New Mexico Geological Society, Guidebook 33, pp. 2-8.
- Cooley, M. E., and Akers, J. P., 1961, Ancient erosion cycles of the Little Colorado River, Arizona and New Mexico: U.S. Geological Survey, Professional Paper 424-C, pp. 244-248.
- Cordell, Lindrith, 1978a, Gravity profile along Tramway road; *in* Hawley, J. W. (compiler), Guidebook to Rio Grande rift in New Mexico and Colorado: New Mexico Bureau of Mines & Mineral Resources, Circular 163, 156 pp.
- Cordell, Lindrith, 1978b, Regional geophysical setting of the Rio Grande rift: Geological Society of America, Bulletin, v. 89, pp. 1073-1090.
- Cordell, L. S., 1982a, Pottery Mound: New Mexico Geological Society, Guidebook 33, pp. 42-43.
- Cordell, L. S., 1982b, Prehistoric archaeology in Tijeras Canyon: New Mexico Geological Society, Guidebook 33, pp. 8-9.
- DeBrine, D. E., 1971, Quantitative hydrologic study of a closed basin with a playa, Estancia Valley, New Mexico: Unpublished PhD dissertation, New Mexico Institute of Mining & Technology, 165 pp.
- Dillinger, J. K., 1990, Geologic map of the Grants 30' X 60' quadrangle, west-central New Mexico: U.S. Geological Survey, Coal Investigations Map C-118-A, scale 1:100,000.
- de Voogd, B., Brown, L. D., and Meroy, C., 1986, Nature of the eastern boundary of the Rio Grande rift from COCORP surveys in the Albuquerque basin, New Mexico: Journal of Geophysical Research, v. 91, pp. 6305-6320.
- Dutton, C. E., 1885, Mt. Taylor and the Zuni Plateau: U.S. Geological Survey, 6th Annual Report.
- Fenneman, N. M., 1931, Physiography of western United States: McGraw-Hill Book Co., New York, 534 pp.
- Frye, J. C., Leonard, A. B., and Glass, H. D., 1982, Western extent of Ogallala Formation in New Mexico: New Mexico Bureau of Mines & Mineral Resources, Circular 175, 41 pp.
- Gallaher, B. M., and Goad, M. S., 1981, Water-quality aspects of uranium mining and milling in New Mexico: New Mexico Geological Society, Special Publication 10, pp. 85-91.
- Galloway, R. W., 1970, The full-glacial climate in the southwestern United States: Annals of the Association of American Geographers, v. 60, pp. 245-256.
- Galusha, T., 1966, The Zia Sand Formation, new early to medial Miocene beds in New Mexico: American Museum Novitates, no. 2271, 12 pp.
- Galusha, T., and Buick, J. C., 1971, Stratigraphy of the Santa Fe Group, New Mexico: American Museum of Natural History, Bulletin, v. 14, pp. 1-128.
- Gardner, J. L., 1951, Vegetation of the creosote bush area of the Rio Grande valley in New Mexico: Ecological Monographs, v. 21, pp. 379-403.
- Gawell, M. J., 1975, Chemical and petrographic variations in the Cerro Negro-Cerrito Arizona undertone chain, Valencia [now Cibola] County, New Mexico: Unpublished MS thesis, Kent State University, Kent, Ohio, 57 pp.
- Gawell, M. J., and Laughlin, A. W., 1975, Chemical and petrographic variations in the Cerro Negro-Cerrito Arizona cinder cone Lineation, Valencia [now Cibola] County, New Mexico (abs.): Geological Society of America, Abstracts with Programs, v. 7, p. 1084.
- Gawne, C. E., 1973, Faunas and sediments of the Zia Sand, middle Miocene of New Mexico: Unpublished PhD dissertation, Columbia University, New York, 352 pp.
- Gawne, C. E., 1981, Sedimentology and stratigraphy of the Miocene Zia Sand of New Mexico: Geological Society of America, Bulletin, v. 92, part I, pp. 999-1007, part II, p. 2484-2552.
- Geissman, J. W., Brown, L., Turrin, B. D., McFadden, L. D., and Harlan, S. S., 1990, Brunhes chron excursion/polarity episode recorded during the late Pleistocene, Albuquerque Volcanoes, New Mexico, USA: International Geophysical Journal, v. 102, pp. 73-88.
- Gile, L. H., Peterson, F. F., and Grossman, R. B., 1966, Morphological and genetic sequences of carbonate accumulation in desert soils: Soil Science, v. 101, pp. 347-360.
- Gile, L. H., Hawley, J. W., and Grossman, R. B., 1981, Soils and geomorphology in the Basin and Range area of southern New Mexico: Guidebook to the Desert Project: New Mexico Bureau of Mines & Mineral Resources, Memoir 39, 222 pp.
- Goddard, E. M., 1966, Geologic map and sections of the Zuni Mountains fluorspar district, Valencia [now Cibola] County, New Mexico: U.S. Geological Survey, Miscellaneous Investigations Series Map 1-454, scale 1:31,680.
- Goff, F., Gardner, J. N., Baldrige, W. S., Hulen, J. B., Nielson, D. L., Vaniman, D., Heiken, G., Dungan, M. A., and Braxton, D., 1989, Excursion 17B: Volcanic and hydrothermal evolution of Pleistocene Valles caldera and Jemez volcanic field; *in* Chapin, C. E., and Zidek, J. (eds.), Field excursions to volcanic terranes in the western United States, Volume I: Southern Rocky Mountain region: New Mexico Bureau of Mines & Mineral Resources, Memoir 46, pp. 381-434.
- Gordon, E. D., 1961, Geology and ground-water resources of the Grants-Bluewater area, Valencia [now Cibola] County, New Mexico: New Mexico State Engineer, Technical Report 20, 109 pp.
- Green, M. W., and Jackson, T. J., 1976, Geologic and structure contour maps of the Gallup East quadrangle, McKinley County, New Mexico: U.S. Geological Survey, Open-File Report 76-453, scale 1:24,000.
- Gustayson, T. C., and Winkler, D. A., 1988, Depositional facies of the Miocene-Pliocene Ogallala Formation, northwestern Texas and eastern New Mexico: Geology, v. 16, no. 3, pp. 203-206.
- Grambling, J. A., and Wells, S. G. (eds.) 1982, Albuquerque country II: New Mexico Geological Society, Guidebook 33, 370 pp.
- Hack, J. T., 1942, Sedimentation and volcanism in the Hopi Buttes, Arizona: Geological Society of America, Bulletin, v. 53, pp. 335-372.

- Hacker, L. W., 1977, Soil survey of Bernalillo County and parts of Sandoval and Valencia Counties, New Mexico: U.S. Soil Conservation Service, 101 pp.
- Hackman, R. J., and Olson, A. B., 1977, Geology, structure, and uranium deposits of the Gallup 1° x 2° quadrangle, New Mexico and Arizona: U.S. Geological Survey, Miscellaneous Investigations Series Map I981, scale 1:250,000.
- Harbour, J., 1958, Microstratigraphic and sedimentational studies of an early man site near Lucy, New Mexico: Unpublished MS thesis, University of New Mexico, Albuquerque, 111 pp.
- Harrington, E. R., 1934, The origin of ice caves: *Journal of Geology*, v. 43, pp. 433-436.
- Hastings, J. R., and Turner, R. M., 1965, *The changing mile*: University of Arizona Press, Tucson, 317 pp.
- Hawley, J. W. (compiler) 1978, Guidebook to Rio Grande rift in New Mexico and Colorado: New Mexico Bureau of Mines & Mineral Resources, Circular 163, 241 pp.
- Hawley, J. W., 1984, The Ogallala Formation in eastern New Mexico; *in* Whetstone, G. A. (ed.), *Proceedings of the Ogallala Aquifer Symposium*: Texas Tech University, Water Resources Center, pp. 157-175.
- Hawley, J. W., 1986a, Physiographic provinces of New Mexico; *in* Williams, J. L. (ed.), *New Mexico in maps*, 2nd edition: University of New Mexico, Albuquerque, pp. 23-27.
- Hawley, J. W., 1986b, Environmental geology of the Keers Environmental, Inc. Asbestos Disposal Site, Torrance County, New Mexico: New Mexico Bureau of Mines & Mineral Resources, Open-file Report 245, 12 pp., 5 figs.
- Hawley, J. W., and Longmire, P. A. (in press), Site characterization and selection (Chapter 3); *in* Reith, C. C., and Thomson, B. M. (eds.), *Deserts as dumps*: University of New Mexico Press, Albuquerque.
- Hawley, J. W., Bachman, G. O., and Manley, K., 1976, Quaternary stratigraphy in the Basin and Range and Great Plains provinces, New Mexico and Texas; *in* Mahaney, W. C. (ed.), *Quaternary stratigraphy of North America*: Dowden, Hutchinson, and Ross, Inc., Stroudsburg, Pennsylvania, pp. 235-274.
- Hawley, J. W., Crumpler, L. S., and Wells, S. G., 1982, Road-log segment II-B: I-40/NM-6 interchange to LaJara Mesa northwest of Mount Taylor: New Mexico Geological Society, Guidebook 33, pp. 49-70.
- Hawley, J. W., Love, D. W., and Lambert, P. W., 1982, Road-log segment I-C: Abo Canyon-Blue Springs area to Albuquerque via Belen and Los Lunas: New Mexico Geological Society, Guidebook 33, pp. 24-30.
- Hawley, J. W., Love, D. W., and Wells, S. G., 1982, Road-log segment II-A: Albuquerque to Correo via El Cerro de Los Lunas and Rio Puerco: New Mexico Geological Society, Guidebook 33, pp. 38-49.
- Hawley, J. W., Love, D. W., and Wells, S. G., 1983, Summary of the hydrology, sedimentology, and stratigraphy of the Rio Puerco valley; *in* Wells, S. G., Love, D. W., and Gardner, T. W. (eds.), *Chaco Canyon country*: American Geomorphological Field Group, Field Trip Guidebook, pp. 33-36.
- Hawley, J. W., Foster, R. W., Broadhead, R., and Love, D. W., 1982, Road-log segment I-B: Tijeras Canyon to Abo Canyon via Estancia and Manzano: New Mexico Geological Society, Guidebook 33, pp. 8-23.
- Hawley, J. W., Lambert, P. W., Kelley, V. C., and Woodward, L. A., 1982, Road-log segment III-B: Sandia Mountains at tramway terminal to Placitas via Alameda, Rio Rancho, Ceja del Rio Puerco, Loma Duran, and Bernalillo: New Mexico Geological Society, Guidebook 33, pp. 80-94.
- Heath, D. L., 1983, Flood and recharge relationships of the lower Rio Puerco: New Mexico Geological Society, Guidebook 34, pp. 329-337.
- Heath, D. L., and Love, D. W., 1983, Multivariate historical processes increasing thresholds for erosion within the Rio Puerco, north-central New Mexico. (abs.): *Geological Society of America, Abstracts with Programs*, v. 18, no. 5, pp. 360.
- Henderson, J., 1933, Caverns, ice caves, sinkholes, and natural bridges II: Ice caves and related phenomena: *University of Colorado Studies*, v. 20, pp. 115-158.
- Herrick, C. L., 1904, Lake Otero, an ancient salt lake in southeastern New Mexico: *American Geologist*, v. 34, pp. 174-189.
- Hunt, C. B., 1974, *Natural regions of the United States and Canada*: W. H. Freeman & Co., San Francisco, 725 pp.
- Izett, G. A., Obradovich, J. D., Naeser, C. W., and Cebula, G. T., 1981, Potassium-argon and fission-track zircon ages of Cerro Toledo Rhyolite tephra in the Jemez Mountains, New Mexico: U.S. Geological Survey, Professional Paper 1199-D, pp. 37-43.
- Jenkins, D. N., 1982, Geohydrology of the Madera Group, western Estancia Basin, New Mexico: New Mexico Geological Society, Guidebook 33, pp. 361-366.
- Johnpeer, G., Robinson-Cook, S., Bobrow, D., Barrie, D., Kelliher, J., and McNeil, R., 1987, Geology and tunnelling, v. 3; *in* Lattman, L. H., and Roser, H. E. (authorized representatives), *Estancia Basin, New Mexico Superconducting Super Collider*: New Mexico Bureau of Mines & Mineral Resources, Open-file Report 258, 224 pp.
- Johnson, D. W., 1932, Rock fans of and regions: *American Journal of Science* (5), v. 23, pp. 389-420.
- Kaehler, C. A., 1990, Lithology of basin-fill deposits in the Albuquerque-Belen basin, New Mexico: U.S. Geological Survey, Water-Resources Investigations Report 89-4162, 14 pp.
- Kasten, J. A., 1977, Petrology and geochemistry of calc-alkaline andesites within the Albuquerque basin, Valencia County, New Mexico: Unpublished MS thesis, University of New Mexico, Albuquerque, 78 pp.
- Kelley, V. C. (compiler) 1963, Geology and technology of the Grants uranium region: New Mexico Bureau of Mines & Mineral Resources, Memoir 15, 277 pp.
- Kelley, V. C., 1972, Geology of the Fort Sumner sheet, New Mexico: New Mexico Bureau of Mines & Mineral Resources, Bulletin 98, 55 pp.
- Kelley, V. C., 1977, Geology of Albuquerque Basin, New Mexico: New Mexico Bureau of Mines & Mineral Resources, Memoir 33, 59 pp.
- Kelley, V. C., 1982, Albuquerque, its mountains, valley, water, and volcanoes: New Mexico Bureau of Mines & Mineral Resources, *Scenic Trips to the Geologic Past* No. 9, 106 pp.
- Kelley, V. C., and Kudo, A. M., 1978, Volcanoes and related basalts of the Albuquerque basin, New Mexico: New Mexico Bureau of Mines & Mineral Resources, Circular 156, 30 pp.
- Kelley, V. C., and Northrop, S. A., 1975, Geology of Sandia Mountains and vicinity, New Mexico: New Mexico Bureau of Mines & Mineral Resources, Memoir 29, 136 pp.
- Kelley, V. C., and Wood, G. H., Jr., 1946, Lucero uplift, Valencia, Socorro and Bernalillo Counties, New Mexico: U.S. Geological Survey, *Oil and Gas Investigations Preliminary Map* 47.
- Kelley, V. C., Woodward, L. A., Kudo, A. M., and Callender, J. F., 1976, Guidebook to Albuquerque basin of the Rio Grande rift, New Mexico: New Mexico Bureau of Mines & Mineral Resources, Circular 153, 30 pp.
- Kelley, V. C., Hawley, J. W., and Wells, S. G., 1982, Road-log segment III-A: Albuquerque to Sandia Peak Tramway via 1-25, Montgomery Blvd., and Tramway Blvd.: New Mexico Geological Society, Guidebook 33, pp. 76-80.
- Kelly, T. E., and Reynolds, C. B., 1984, Structural geology of the Malpais Valley, San Rafael, New Mexico: New Mexico Geological Society, Guidebook 40, pp. 119-121.
- Kemodle, J. W., and Scott, W. B., 1986, Three-dimensional model simulation of steady-state ground-water flow in the Albuquerque-Belen basin, New Mexico: U.S. Geological Survey, Water-Resources Investigations Report 84-4353, 58 pp.
- Kreitler, C. W., Mullican, W. F., and Nativ, R., 1990, Hydrogeology of the Diablo Plateau, Trans-Pecos Texas; *in* Hydrogeology of Trans-Pecos Texas: The University of Texas at Austin, Bureau of Economic Geology, Guidebook 25, pp. 49-58.
- Kudo, A. M., Kelley, V. C., Damon, P. E., and Shafiqullah, M., 1977, K-Ar ages of basalt flows at Canjilon Hill, Isleta volcano, and the Cat Hills volcanic field, Albuquerque-Belen, central New Mexico: *Ischron/West*, no. 18, pp. 15-16.
- Lagasse, P. F., 1981, Geomorphic response of the Rio Grande to dam construction; *in* Wells, S. G., and Lambert, W. (eds.), *Environmental geology and hydrology in New Mexico*: New Mexico Geological Society, Special Publication 10, pp. 27-46.
- Lambert, P. W., 1968, Quaternary stratigraphy of the Albuquerque area, New Mexico: Unpublished PhD dissertation, University of New Mexico, 329 pp.
- Lambert, P. W., Hawley, J. W., and Wells, S. G., 1982, Supplemental road-log segment III-S: Urban and environmental geology of the Albuquerque area: New Mexico Geological Society, Guidebook 33, pp. 97-119.
- Laughlin, A. W., Aldrich, M. J., Jr., Ander, M. E., Heiken, G. H., and Vaniman, D. T., 1982, Tectonic setting and history of late Cenozoic volcanism in west-central New Mexico: New Mexico Geological Society, Guidebook 33, pp. 279-284.
- Leavy, B. D., and Shafiqullah, M., 1987, New K-Ar analyses of basalts from southern California and central New Mexico: *Ischron/West*, no. 48, pp. 19-20.
- Leavy, D. G., Phillips, F. M., Elmore, D., Kubick, P. W., and Gladney, E., 1987, Measurement of cosmogenic ³⁶Cl/³⁷Cl in young volcanic rocks: an application of accelerator mass spectrometry in geochronology: *Nuclear Instruments and Methods in Physics Research*, B26, pp. 246-250.

- Lee, W. T., 1926, An ice cave in New Mexico: *Geographical Review*, v. 16, pp. 55-59.
- Leopold, L. B., 1946, Two intense local floods in New Mexico: *American Geophysical Union, Transactions*, v. 27, pp. 535-539.
- Leopold, L. B., 1951, Pleistocene climate in New Mexico: *American Journal of Science*, v. 249, pp. 152-168.
- Leopold, L. B., and Snyder, C., 1951, Alluvial fills near Gallup, New Mexico: U.S. Geological Survey, Water-Supply Paper 1110-A, 19 pp.
- Lindsey, A. A., 1951, Vegetation and habits in a southwestern volcanic area: *Ecological Monographs*, v. 21, pp. 227-253.
- Lipman, P. W., and Mehnert, H. H., 1980, Potassium-argon ages from the Mount Taylor volcanic field, New Mexico: U.S. Geological Survey, Professional Paper 1124-B, 8 pp.
- Love, D. W., 1986, A geological perspective of sediment storage and delivery along the Rio Puerco, central New Mexico; in Hadley, R. F. (ed.), *Drainage basin sediment delivery: International Association of Hydrological Sciences, Publication 159*, pp. 305-322.
- Love, D. W., 1989a, Geomorphic development of the Rio San Jose valley: *New Mexico Geological Society, Guidebook 40*, pp. 11-12.
- Love, D. W., 1989b, Bidahochi Formation: An interpretive summary: *New Mexico Geological Society, Guidebook 40*, pp. 273-280.
- Love, D. W., and Gillam, M. (in press), Navajo and Acoma-Zuni sections; in Morrison, R. B. (ed.), *Quaternary non-glacial geology; conterminous U.S.: Geology of North America*, v. K-2, Geological Society of America, Boulder, Colorado.
- Love, D. W., and Hadley, R. F., 1986, Second day, road log from Albuquerque to Rio Puerco, Correo, Los Lunas, Belen, and Bernardo, and return to Albuquerque; in Hadley, R. F. (ed.), *International symposium on drainage basin sediment delivery, program of paper sessions and road logs of field trips: University of Denver, Denver, Colorado*, pp. 1-9.
- Love, D. W., and Young J. D., 1983, Progress report on the late Cenozoic evolution of the lower Rio Puerco: *New Mexico Geological Society, Guidebook 34*, pp. 277-284.
- Love, D. W., Hawley, J. W., and Young J. D., 1982, Preliminary report on the geomorphic history of the lower Rio Puerco in relation to archeological sites and cultural resources of the lower Hidden Mountain Dam Site; in Eidenbach, P. (ed.), *Inventory survey of the lower Hidden Mountain floodpool, lower Rio Puerco drainage, central New Mexico: Human Systems Research, Tularosa, New Mexico*, pp. 20-65.
- Lozinsky, R. P., 1988, Stratigraphy, sedimentology, and sand petrology of the Santa Fe Group and pre-Santa Fe Tertiary deposits in the Albuquerque basin, central New Mexico: Unpublished PhD dissertation, New Mexico Institute of Mining & Technology, 298 pp.
- Lozinsky, R. P., and Hawley, J. W., 1986, Upper Cenozoic Palomas Formation of south-central New Mexico: *New Mexico Geological Society, Guidebook 37*, pp. 239-248.
- Lucas, S. G., and Anderson, O. J., 1989, Supplemental road log 2, from Black Rock to Ojo Caliente: *New Mexico Geological Society, Guidebook 40*, pp. 69-70.
- Lyons, T. R., 1969, A study of the paleo-Indian and desert culture complexes of the Estancia Valley area, New Mexico: Unpublished PhD dissertation, University of New Mexico, Albuquerque, 355 pp.
- Machette, M. N., 1978a, Geologic map of the San Acacia quadrangle, Socorro County, New Mexico: U.S. Geological Survey, Geologic Quadrangle Map GQ-1415, scale 1:24,000.
- Machette, M. N., 1978b, Preliminary geologic map of the Socorro 1° by 2° quadrangle, central New Mexico: U.S. Geological Survey, Open-File Report 78-607.
- Machette, M. N., 1978c, Dating of Quaternary faults in the southwestern United States by using buried calcic paleosols: U.S. Geological Survey, *Journal of Research*, v. 6, pp. 369-381.
- Machette, M. N., 1982, Quaternary and Pliocene faults in the La Jencia and southern part of the Albuquerque-Belen basins, New Mexico: Evidence of fault history from fault-scarp morphology and Quaternary geology: *New Mexico Geological Society, Guidebook 33*, pp. 161-169.
- Machette, M. N., 1985, Calcic soils of the southwestern United States: *Geological Society of America, Special Paper 203*, pp. 1-21.
- Machette, M. N., and McGimsey, R. G., 1983, Map of Quaternary and Pliocene faults in the Socorro and western part of the Fort Sumner 1° x 2° quadrangles, central New Mexico: U.S. Geological Survey, *Miscellaneous Field Studies Map MF-1465-A*, scale 1:250,000, 12 pp. pamphlet.
- Maxwell, C. H., 1982, El Malpais: *New Mexico Geological Society, Guidebook 33*, pp. 299-301.
- Maxwell, C. H., 1986, Geologic map of El Malpais lava field and surrounding areas, Cibola County, New Mexico: U.S. Geological Survey, *Miscellaneous Investigations Map 1-1595*, scale 1:62,500.
- Maxwell, C. H., Anderson, O. J., Lucas, S. G., Chamberlin, R. M., and Love, D. W., 1989, First-day road log, from Albuquerque to Mesita, Laguna, Acoma, McCartys and Grants: *New Mexico Geological Society, Guidebook 40*, pp. 1-24.
- McCann, F. T., 1938, Ancient erosion surface in the Gallup-Zuni area, New Mexico: *American Journal of Science* (5), v. 36, pp. 260-279.
- McGrath, D. B., and Hawley, J. W., 1987, Geomorphic evolution and soil-geomorphic relationships in the Socorro area, central New Mexico; in McLemore, V. T., and Bowie, M. R. (compilers), *Guidebook to the Socorro area, New Mexico: New Mexico Bureau of Mines & Mineral Resources*, pp. 55-67.
- McLellan, M. W., Robinson, L. N., Haschke, L. R., Carter, M. D., and Medlin, A., 1982, Fence Lake Formation (Tertiary), west-central New Mexico: *New Mexico Geology*, v. 4, pp. 53-55.
- McQuillan, D. M., 1982, Pollution of the Rio Grande valley-fill aquifer: *New Mexico Geological Society, Guidebook 33*, pp. 357-360.
- Meinzer, O. E., 1911, Geology and water resources of Estancia Valley, New Mexico: U.S. Geological Survey, Water-Supply Paper 275, 89 pp.
- Meinzer, O. E., 1922, Map of the Pleistocene lakes of the Basin and Range province and its significance: *Geological Society of America, Bulletin*, v. 33, pp. 541-552.
- Meinzer, O. E., and Hare, R. E., 1915, Geology and water resources of the Tularosa Basin, New Mexico: U.S. Geological Survey, Water-Supply Paper 343, 317 pp.
- Miller, J. R., and Wells, S. G., 1986, Types and processes of short-term sediment and uranium-tailings storage in arroyos: an example from the Rio Puerco of the West, New Mexico; in Hadley, R. F. (ed.), *Drainage basin sediment delivery: International Association of Hydrological Sciences, Publication 159*, pp. 335-353.
- Moench, R. H., and Schlee, J. S., 1967, Geology and uranium deposits of the Laguna district, New Mexico: U.S. Geological Survey, Professional Paper 519, 117 pp.
- Myers, D. A., 1977, Geologic map of the Scholle quadrangle, Socorro, Valencia, and Torrance counties, New Mexico: U.S. Geological Survey, Geologic Quadrangle Map GQ-1412, scale 1:24,000.
- Myers, D. A., and McKay, E. J., 1976, Geologic map of the north end of the Manzano Mountains, Tijeras and Sedillo quadrangles, Bernalillo County, New Mexico: U.S. Geological Survey, *Miscellaneous Geologic Investigations Map 1-968*.
- Myers, D. A., McKay, E. J., and Sharps, J. A., 1981, Geologic map of the Becker quadrangle, Valencia and Socorro counties, New Mexico: U.S. Geological Survey, Geologic Quadrangle Map GQ-1556.
- Nichols, R. L., 1946, McCartys basalt flow, Valencia [Cibola] County, New Mexico: *Geological Society of America, Bulletin*, v. 57, pp. 10491066.
- O'Neill, F. M., and Rigby, J. K., Jr., 1982, A rare fossil skeleton of *Camelops* from Pleistocene deposits near Albuquerque: *New Mexico Geological Society, Guidebook 33*, pp. 82-84.
- Phillips, F. M., Leavy, B. D., Jannik, N. O., Elmore, D., and Kubik, P. W., 1986, The accumulation of cosmogenic chlorine-36 in rocks: a method of surface exposure dating: *Science*, v. 231, pp. 41-43.
- Popp, C. J., Love, D. W., Hawley, J. W., and Novo-Gradac, K., 1984, Radionuclide and heavy metal distribution in 20th century sediments of major streams in the eastern part of the Grants uranium region, New Mexico: *New Mexico Bureau of Mines & Mineral Resources, Hydrologic Report 7*, pp. 34-48.
- Popp, C. J., Hawley, J. W., Love, D. W., and Dehn, M., 1988, Use of radiometric (Cs-137, Pb-210), geomorphic, and stratigraphic techniques to date recent oxbow sediments in the Rio Puerco drainage, Grants uranium region, New Mexico: *Environmental Geology and Water Science*, v. 11, no. 3, pp. 253-269.
- Pearce, T. M., 1965, *New Mexico place names, a geographical dictionary: University of New Mexico, Albuquerque*, 187 pp.
- Rautman, C. A. (compiler) 1980, *Geology and mineral technology of the Grants uranium region 1979: New Mexico Bureau of Mines & Mineral Resources, Memoir 38*, 400 pp.
- Reiche, P., 1949, *Geology of the Manzanita and north Manzano Mountains, New Mexico: Geological Society of America, Bulletin*, v. 60, pp. 1183-1212.
- Robertson, J. F., 1975, Preliminary geologic map of the Pinedal, McKinley County, New Mexico: U.S. Geological Survey, Open-File Report 74244, scale 1:24,000.
- Robinson, S., and Love, D. W., 1986, Applications of detailed sedimentologic studies of modern waning-flow deposits to alluvial stratigraphy (abs.): *Geological Society of America, Abstracts with Programs*, v. 18, no. 5, p. 407.
- Schumm, S. A., 1977, *The fluvial system: John Wiley & Sons, New York*, 238 pp.
- Shepherd, R. G., 1976, Sedimentary processes and structures of ephemeral stream point bars, Rio Puerco west of Albuquerque, New Mexico (abs.):

- Geological Society of America, Abstracts with Programs, v. 8, no. 6, p. 1103.
- Shepherd, R. G., 1987, Lateral accretion surfaces in ephemeral-stream point bars, Rio Puerco, New Mexico; *in* Ethridge, F. G., Flores, R. M., and Harvey, D. D. (eds.), Recent developments in fluvial sedimentology: Society of Economic Paleontologists and Mineralogists, Special Publication 39, pp. 93-98.
- Slack, P. B., and Campbell, J. A., 1976, Structural geology of the Rio Puerco fault zone and its relationship to central New Mexico tectonics: New Mexico Geological Society, Special Publication 6, pp. 46-52.
- Smith, R. E., 1957, Geology and ground-water resources of Torrance County, New Mexico: New Mexico Bureau of Mines & Mineral Resources, Ground-Water Report 5, 186 pp.
- Smith, R. L., Bailey, R. A., and Ross, C. S., 1970, Geologic map of the Jemez Mountains, New Mexico: U.S. Geological Survey, Miscellaneous Investigations Map I-571.
- Smith, L. N., and Anderson, R. Y., 1982, Pleistocene-Holocene climate of the Estancia Basin, central New Mexico: New Mexico Geological Society, Guidebook 33, pp. 347-350.
- Smith, L. N., Bullard, T. F., and Wells, S. G., 1982, Quaternary geology and geomorphology of Tijeras Canyon, New Mexico: New Mexico Geological Society, Guidebook 33, pp. 5-7.
- Spiegel, Z., and Baldwin, B., 1963, Geology and water resources of the Santa Fe area, New Mexico: U.S. Geological Survey, Water-Supply Paper 1525, 158 pp.
- Stark, J. T., and Dapples, E. C., 1946, Geology of the Los Pinos Mountains, New Mexico: Geological Society of America, Bulletin, v. 57, pp. 1121-1172.
- Stark, J. T., 1956, Geology of the south Manzano Mountains, New Mexico: New Mexico Bureau of Mines & Mineral Resources, Bulletin 34, 49 pp.
- Stone, W. J., 1984, Localization of fresh ground-water bodies—a special consideration in siting landfills along the Rio Grande valley: New Mexico Bureau of Mines & Mineral Resources, Hydrologic Report 7, pp. 227-238.
- Stearns, C. E., 1953, Tertiary geology of the Galisteo-Tonque area, New Mexico: Geological Society of America, Bulletin, v. 64, pp. 459-508.
- Tedford, R. H., 1981, Mammalian biochronology of the later Cenozoic basins of New Mexico: Geological Society of America, Bulletin, v. 92, part I, pp. 1008-1022.
- Tedford, R. H., 1982, Neogene stratigraphy of the northwestern Albuquerque basin: New Mexico Geological Society, Guidebook 33, pp. 273-278.
- Thomson, B. M., and McQuillan, D. M., 1984, Nitrate contamination of ground water in Albuquerque: New Mexico Bureau of Mines & Mineral Resources, Hydrologic Report 7, pp. 204-216.
- Titus, F. B., Jr., 1961, Ground-water geology of the Rio Grande trough in north-central New Mexico, with sections on the Jemez caldera and the Lucero uplift: New Mexico Geological Society, Guidebook 12, pp. 186-192.
- Titus, F. B., Jr., 1963, Geology and ground-water conditions in eastern Valencia County, New Mexico: New Mexico Bureau of Mines & Mineral Resources, Ground-Water Report 7, 113 pp.
- Titus, F. B., Jr., 1969, Late Tertiary and Quaternary hydrogeology of Estancia basin, central New Mexico: Unpublished PhD dissertation, University of New Mexico, Albuquerque, 179 pp.
- Titus, F. B., Jr., 1973, Hydrogeologic evolution of Estancia Valley, a closed basin in central New Mexico: New Mexico Bureau of Mines & Mineral Resources, Open-File Report 69, 184 pp.
- Titus, F. B., Jr., 1980, Ground water in the Sandia and northern Manzano Mountains, New Mexico: New Mexico Bureau of Mines & Mineral Resources, Hydrologic Report 6, 66 pp.
- U.S. Army Corps of Engineers (compilers) 1979, Albuquerque Greater Urban Area Studies Program: U.S. Government Printing Office, Washington, D.C., 13 volumes.
- Van Devender, T. R., 1990, Late Quaternary vegetation and climate of the Chihuahuan Desert, United States and Mexico; *in* Betancourt, J. L., Van Devender, T. R., and Martin, P. S. (eds.), Fossil packrat middens: The last 40,000 years of biotic change: University of Arizona Press, Tucson, pp. 104-133.
- Vazzana, M. E., and Ingersoll, R. V., 1981, Stratigraphy, sedimentology, petrology, and basin evolution of the Abiquiu Formation (Oligo-Miocene), north-central New Mexico: Summary: Geological Society of America, Bulletin, v. 91, Part I, pp. 990-992.
- Weide, D. L., Schneider, G. B., Mytton, J. W., and Scott, G. R., 1979, Geologic map of the Pueblo Bonito quadrangle, San Juan County, New Mexico: U.S. Geological Survey, Miscellaneous Field Studies Map MF-1119, scale 1:24,000.
- Wells, S., Bullard, T. F., Condit, C. D., Jercinovic, M., Lozinsky, R. P., and Rose, D. E., 1982, Geomorphic processes on the alluvial valley floor of the Rio Puerco: New Mexico Geological Society, Guidebook 33, pp. 45-47.
- Wells, S. G., Love, D. W., and Gardner, T. W. (eds.) 1983, Chaco Canyon country, a field guide to the geomorphology, Quaternary geology, paleoecology, and environmental geology of northwestern New Mexico: American Geomorphological Field Group, Field Trip Guidebook, 253 pp.
- White, W. D., 1989, Geohydrologic and environmental indicators of a dewatered wetland: Ojo del Gallo, San Rafael, New Mexico: New Mexico Geological Society, Guidebook 40, pp. 337-345.
- Wilson, L., 1981, Potential for ground-water pollution in New Mexico; *in* Wells, S. G., and Lambert, W. (eds.), Environmental geology and hydrology in New Mexico: New Mexico Geological Society, Special Publication 10, pp. 47-54.
- Wood, W. W., and Sanford, W. E., 1990, Ground-water control of evaporite deposition: Economic Geology, v. 85, pp. 1226-1235.
- Woodward, L. A., Callender, J. F., Seager, W. R., Chapin, C. E., Gries, J. C., Shaffer, W. L., and Zilinsky, R. E., 1978, Tectonic map of the Rio Grande rift region in New Mexico, Chihuahua, and Texas, Sheet 2; *in* Hawley, J. W. (compiler), Guidebook to Rio Grande rift in New Mexico and Colorado: New Mexico Bureau of Mines & Mineral Resources, Circular 163.
- Wright, H. E., Jr., 1946, Tertiary and Quaternary geology of the lower Rio Puerco area, New Mexico: Geological Society of America, Bulletin, v. 57, pp. 383-456.
- Young, J. D., 1982, Late Cenozoic geology of the lower Rio Puerco, Valencia and Socorro Counties, New Mexico: Unpublished MS thesis, New Mexico Institute of Mining & Technology, Socorro, New Mexico, 126 pp.

Laminated ice bodies in collapsed lava tubes at El Malpais National Monument, central New Mexico

Lonnie Thompson¹, Ellen Mosley-Thompson¹, Julio L. Betancourt², David W. Love¹, Alex Wilson¹, Greg Lecnard⁴, and R. Scott Anderson¹

¹Byrd Polar Research Institute, Ohio State University, Columbus, Ohio 43210-1308; ²U.S. Geological Survey, 1675 W. Anklam Rd., Tucson, Arizona 85705; ³New Mexico Bureau of Mines & Mineral Resources, Socorro, New Mexico 87801; ⁴Department of Geosciences, University of Arizona, Tucson, Arizona 85721; ⁵Quaternary Studies Program, Northern Arizona University, Flagstaff, Arizona 86011

Ice deposits in caves have a global distribution, primarily in high-elevation or high-latitude lava tubes (Henderson, 1933). Unlike ice sheets, cave ice has been virtually ignored as a climate proxy. Laminated ice bodies from collapsed lava tubes at El Malpais National Monument, central New Mexico (Fig. 1; Lee, 1926; Harrington, 1934; Lindsey, 1951; Elston and Wohletz, 1987) are now being evaluated for paleoclimatic value. The ice-cave systems can be thought of as frozen and very local, perched water tables. In June 1990, three cores were extracted from Candelaria and La Marchanita Caves. These cores are now being dated and analyzed for pollen, microparticle concentrations, oxygen-isotope ratios, and NO⁻³, Cl⁻, SO²⁻, and PO⁴.

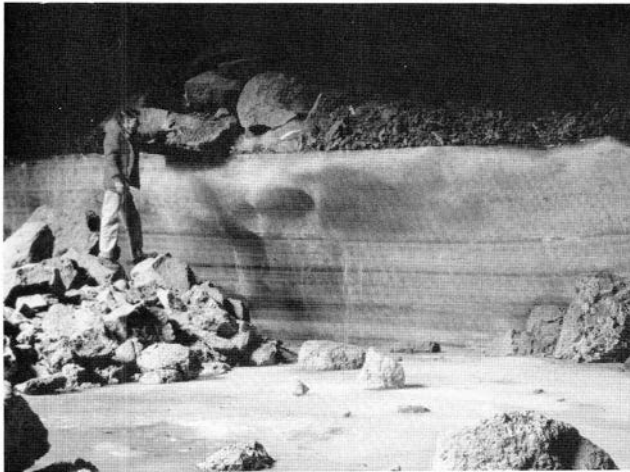


FIGURE 1—Bank of laminated ice in Candelaria Cave ca. 1950.

Our preliminary results suggest that the ice laminations (Fig. 1) are not annual, but instead represent occasional layers between periods of melt. While interpretation of these data is still evolving, measurements made at all depths within the cores vary greatly between laminations. Opportunities exist to calibrate the older parts of the ice body against ice accumulated entirely within the 20th century. This younger ice has refilled an area excavated by U.S. Army Cavalry stationed at nearby Ft. Wingate beginning ca. 1850. Radiocarbon dates of the older ice deposits were obtained using accelerator mass spectrometry. At Candelaria Cave, we dated a twig enclosed near the bottom of the 4 m bank of laminated ice to 3166 ± 77 yrs B.P. Direct dates on the CO₂ gas within the ice ranged from 1857 ± 56 yrs B.P. near the bottom to near modern at the top. More work in the more accessible deposits, such as Candelaria and La Marchanita Caves, could provide basic approaches to develop the paleoclimatic worth of these deposits and of cave ice in other parts of the world.

References

- Elston, W. E., and Wohletz, K. H., 1987, Quaternary basalt fields of west-central New Mexico: McCartys pahoehoe flow, Zuni Canyon as flow, Auni Ice Cave, Bandera Crater, and Zuni Salt Lake Maar: Rocky Mountain Section of the Geological Society of America, Centennial Field Guide, v. 2, pp. 431-436.
- Harrington, E. R., 1934, The origin of ice caves: *Journal of neology*, v. 43, pp. 433-436.
- Henderson, J., 1933, Caverns, ice caves, sinkholes, and natural bridges II: Ice caves and related phenomena: *The University of Colorado Studies*, v. 20, pp. 115-158.
- Lee, W. T., 1926, An ice cave in New Mexico: *Geographical Review*, v. 16, pp. 55-59.
- Lindsey, A. A., 1951, Vegetation and habitats in a southwestern volcanic area: *Ecological Monographs*, v. 21, pp. 227-253.

Late Cenozoic geomorphic and tectonic evolution of the Rio San Jose and tributary drainages within the Basin and Range/Colorado Plateau transition zone in west-central New Mexico

P. G. Drake¹, C. D. Harrington¹, S. G. Wells¹, F. V. Perry¹, and A. W. Laughlin¹

¹Glorieta Geoscience Inc., P.O. Box 5727, Santa Fe, New Mexico 87502;

²Earth and Space Sciences Division, Los Alamos National Laboratory, Los Alamos, New Mexico 87545;

³Department of Geology, University of New Mexico, Albuquerque, New Mexico 87131

Introduction

Purpose

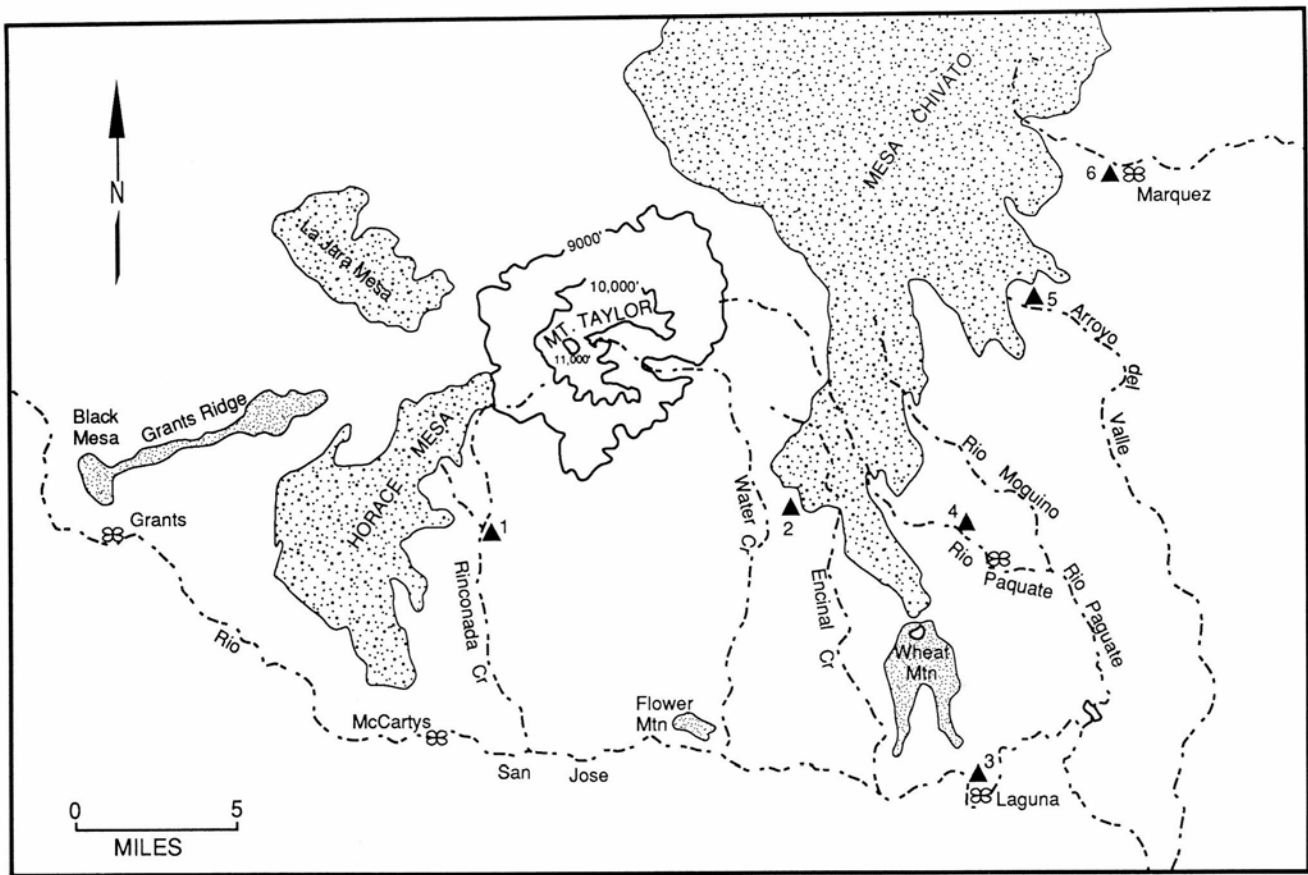
This paper examines the late Cenozoic stratigraphy and geologic history of the Rio San Jose and tributary drainages between Grants and Laguna, New Mexico. The focus of this research is to document the timing and spatial variation in tectonism/uplift across the Colorado Plateau/Basin and Range transition zone in west-central New Mexico during the late Cenozoic.

Setting

The Rio San Jose originates at the Continental Divide on the Colorado Plateau and flows eastward for a distance of

approximately 185 km before emptying into the Rio Puerco within the Rio Grande rift. The Rio San Jose drains an area of 9700 km² (Wright, 1946; Love, 1989), including parts of the Zuni Mountains, Mt. Taylor, the Zuni—Bandera volcanic field, and the Lucero uplift. The portion of the Rio San Jose examined in this study lies within the transition zone between the tectonically active Rio Grande rift and the less tectonically active Colorado Plateau (Fig. 1). The study area extends from the Zuni uplift across the Acoina sag to the edge of the Lucero uplift—Puerco fault zone (Fig. 2) and lies athwart the Jemez lineament.

The bedrock stratigraphy within the study area consists of nearly flat-lying Mesozoic sedimentary rocks overlain unconformably by Pliocene and Quaternary volcanic rocks

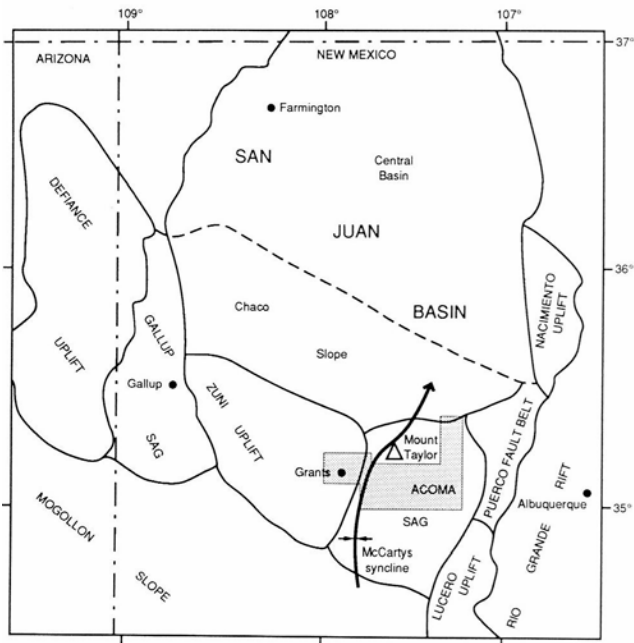


- ▲ Location of terrace cross-profiles with soil descriptions
- ▨ High Mesa Basalts (Tp1)
- ▩ Lower Basalt-Capped Mesas (Tp2)

FIGURE 1—Generalized physiographic map of the Grants-Laguna area.

which form high mesas located 200 to 300 m above local base level. These high mesa basalts and associated volcanic rocks of the Mt. Taylor area were erupted during a geologically brief period between 4 and 1.5 m.y. (Lipman and

Mehnert, 1979; Crumpler, 1982; Perry et al., 1990). Younger Pleistocene and Holocene basalt flows lie at the level of the modern valley floor along the Rio San Jose (Lipman and Mehnert, 1979; Maxwell, 1982; Perry and Laughlin, unpubl. data).



STUDY AREA (Modified From Grimm (1985))

FIGURE 2—Tectonic setting of the Grants-Laguna area.

Previous work

Early work on the geology of the Rio San Jose drainage basin, by Bryan and McCann (1938) and Wright (1946), focused on the geomorphic history of the Llano de Albuquerque and the lower Rio Puerco basin. Bryan and McCann (1938) suggested that the erosion surface underlying Mt. Taylor was correlative with the late Tertiary regionally extensive Ortiz surface of the central rift. This hypothesis was supported by Bachman and Mehnert (1978) through the use of K—Ar dates on basalt flows in the rift and in the Mt. Taylor area. Wright (1946) defined the Mush Mesa and Suwane surfaces which are inset below the Ortiz surface along the lower Rio San Jose.

Several recent studies have considered aspects of the geomorphic history of the Rio San Jose and tributary drainages. Moench and Schlee (1967) defined the Wheat Mountain surface, a Pliocene pediment surface overlain by basalt flows on Frog and Clay Mesas northwest of Laguna (Fig. 1) which is inset below, and is much less extensive than, the Ortiz surface. Love (1989) suggests that the Rio San Jose drainage basin developed in late Oligocene time and has evolved in response to subsidence of the Albuquerque basin to the east and episodic uplift of the Colorado Plateau to the west.

Maximum valley incision occurred between 1.5 and 0.38 m.y. (Love, 1989). Geomorphic surfaces in Lobo Canyon, a tributary to the Rio San Jose which drains westward from Mt. Taylor, have been described by Hunt (1938) and Grimm (1985).

Pliocene and Quaternary geology

Stratigraphy

The Plio-Quaternary stratigraphy in the Grants/Laguna area consists of two Pliocene and five Quaternary units that lie above the modern flood plain or arroyo floor (Fig. 3). Pliocene deposits (Tpal 1 and Tpal2) underlie erosion surfaces Tpl and Tp2 and are limited to pediment and axial gravel deposits (Table 1) which cap geomorphic surfaces cut on Cretaceous sedimentary rocks. Tpal 1 and Tpal2 are generally coarse-grained and contain greater proportions of granite and quartzite clasts than are observed in Quaternary deposits (Table 1). Tpal 1 includes both a granite- and quartzite-dominated axial facies and a volcanic-dominated tributary facies. Associated fine-grained deposits are reddened but do not show evidence of pedogenesis.

Quaternary sediments (Qal1—Qal5) are dominated by fan and terrace deposits, with pediment gravel limited to isolated Qal1 deposits (Table 1). Quaternary deposits contain a predominance of volcanic clasts, primarily basalt, porphyritic andesite, and latite or quartz latite. Qal4 and Qal5 deposits are generally comprised of fine-grained sand, silt, and clay which form the modern valley fill, whereas preserved remnants of older Quaternary deposits (Qal3, Qal2, and Qal1) are coarser, comprised primarily of coarse-grained gravelly sediments. Drill logs for wells in the Laguna and Grants areas indicate that 40 to 60 m of interbedded basalt and alluvium are present below the level of the modern valley floor along the Rio San Jose drainage (Gordon, 1961; Risser and Lyford, 1983), contrasting with a 20 m maximum observed (preserved) thickness of Qal1—Qal3.

Soils

Carbonate soils have developed in the semiarid climate of the Grants—Laguna area, and soil carbonate morphology and Bt horizon development are the morphologic characteristics which best distinguish these soils. Soils in the study area exhibit stage I through III carbonate morphology (Table 2) (terminology after Gile et al., 1981, and Machete, 1985). Bt horizons exhibit a maximum 5YR color, strong angular blocky or prismatic structure, and thick, continuous clay films (Table 2). Soils formed in Pliocene deposits and Qal1 are commonly stripped, lacking carbonate and B1 horizons (Table 2).

Spatial variation of surficial deposits and geomorphic surfaces

The high Pliocene pediment surface (Tp 1) occurs as extensive mesas throughout the study area, whereas Quaternary surfaces older than the valley floor are preserved only as isolated remnants, primarily in tributary drainage basins (Fig. 4). Pliocene surfaces generally slope away from Mt. Taylor or toward the Rio San Jose with gradients of 1-4°.

Quaternary surfaces located above the valley floor (Q1—Q3) are highly dissected. The Q1 surfaces include both an extensive pediment surface located along the upper Arroyo del Valle drainage and a large fan-surface remnant preserved at the mouth of Water Canyon (Fig. 4). Q2 surfaces are preserved primarily as surfaces cut on terrace deposits along tributary drainages and along the Rio San Jose near Old Laguna (Fig. 5). Q3 includes surfaces underlain by fan and terrace deposits located along tributary streams, and surfaces associated with erosional terrace deposits along the Rio San Jose (Fig. 4). Q4 surfaces consist of locally preserved proximal fans and terraces at, or less than, 10 m above the modern valley floor. Q5 terrace and fan surfaces form the valley floor along the Rio San Jose and tributary drainages.

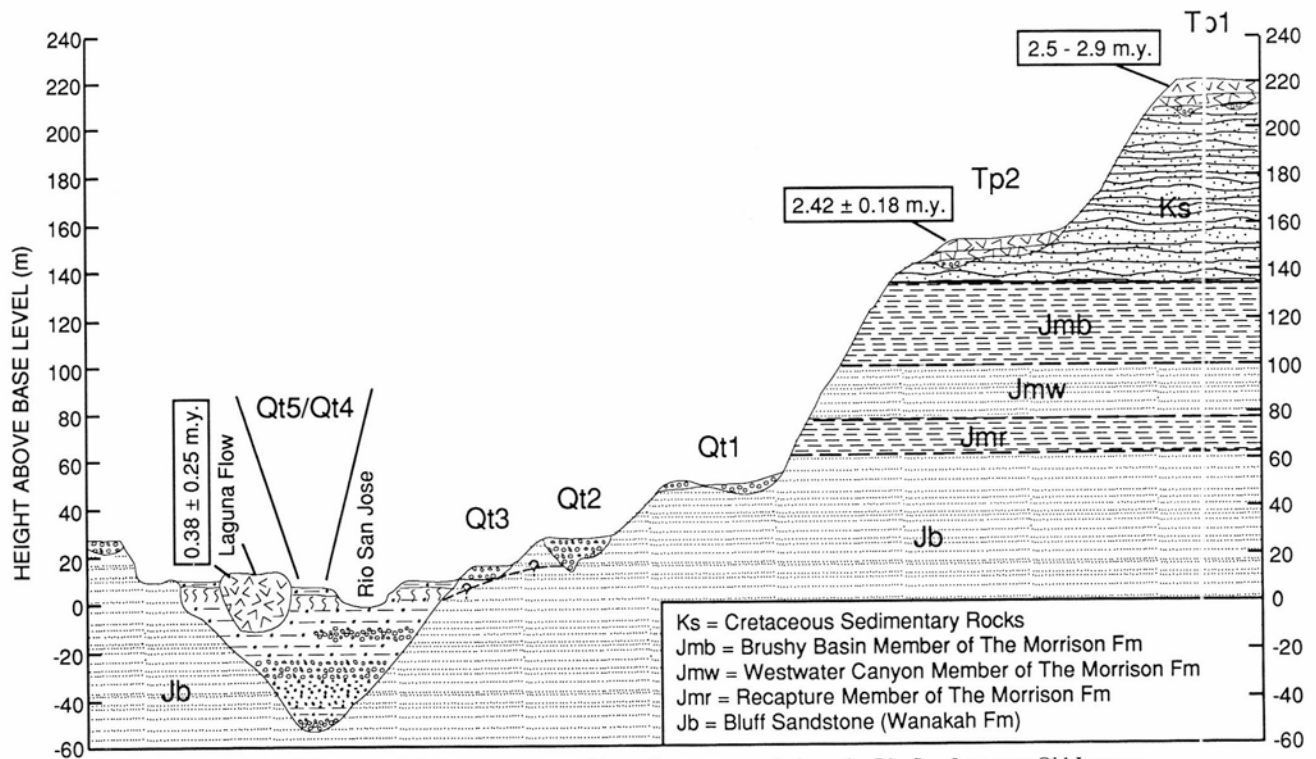


FIGURE 3—Pliocene and Quaternary geomorphic surfaces preserved along the Rio San Jose near Old Laguna.

TABLE 1—Summary of Pliocene–Pleistocene stratigraphy in the Grants–Laguna area.

DEPOSIT	THICKNESS	CLAST LITHOLOGY	SEDIMENTARY FEATURES	BURIED SOILS	TYPE OF DEPOSIT
Tpa1	1-5 m	up to 90% granite and quartzite, plus sandstone, volcanics	upward-fining gravel, trough- and cross-stratified sand	none observed	pediment and axial gravel
Tpa2	1-5 m	granite, quartzite, limestone, sandstone; minor volcanics	none observed	none observed	pediment and axial gravel
Qa1	1-20 m	predominantly volcanic, with up to 10% sandstone and 1-2 % quartzite; minor granitic clasts	upward-fining gravel; interbedded silt and clay	12 m below fan surfaces	fan, pediment and terrace deposits
Qa2	2-12 m	predominantly volcanic, with minor sandstone, quartzite, and rare granitic clasts	cross-bedded sand, upward-fining sand and gravel	none observed	terrace deposits
Qa3	2-10 m	predominantly volcanic, with minor sandstone, quartzite, and rare granitic clasts	parallel- and cross-bedded sand; upward-fining sand and gravel	2.5 m below fan surfaces	fan and terrace deposits
Qa4	greater than 4-5 m	predominantly volcanic with minor sandstone and quartzite	interbedded sand and clay; upward-fining sand and gravel	none observed	fan and terrace deposits
Qa5	0.5-4 m	predominantly volcanic with minor sandstone and quartzite	planar and trough cross-bedded sand; upward-fining sand and gravel	typically buries Q4 soil	fan and terrace deposits

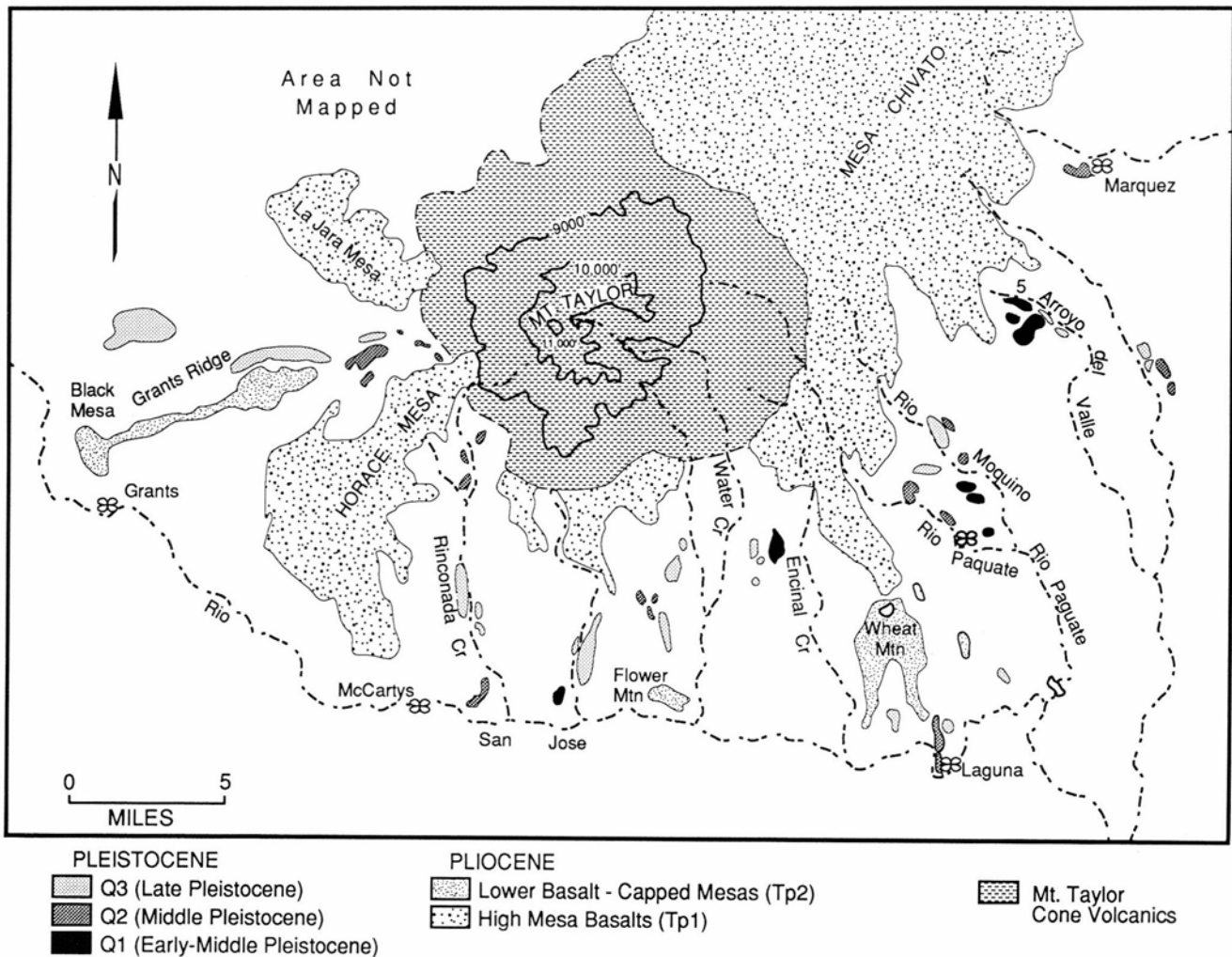


FIGURE 4—Generalized Pliocene–Pleistocene geologic map of the Grants–Laguna area.

TABLE 2—Summary of soil characteristics for Laguna area.

UNIT	SURFACE ELEV	LOCATION	CaCO3 STAGE	COLOR (DRY)	Bk HORIZON THICKNESS	STRUCTURE	CLAY FILMS	Bt or Btk THICKNESS	AGE ESTIMATE
Qt5	5760	R. San Jose	--	10YR	0	nr	n.o.	0	Holocene
Qf5	6460	Water Canyon	trace	10YR	0	m-2msbk	n.o.	0	
Qt4	5760	R. San Jose	stage I	8.75YR	0.7-0.8 m	nr	nr	0.6-0.7 m	Latest Pleistocene
Qt4	6440	A. del Valle	stage I	10YR	1-2 m	2msbk	3mk	0.3 m	
Qf4	6460	Water Canyon	stage I	7.5-10YR	0.5 m	2m-csbk	1n	0.5-0.8 m	Late Pleistocene (50-100 ka)
Qt3	5830	R. San Jose	I+ to II	7.5YR	0.8 m	2msbk	2mk	0.2 m	
Qt3	7140	Rinconada Cr.	II	7.5YR	nr	2-3fsbk/abk	3mk	> 0.65 m	Middle Pleistocene (200-600 ka)
Qf3		Mouth of Rinconada canyon	I+ to II	8.75YR	0.7 m (1.25 m m with Bck)	2msbk	2n	0.2 m	
Buried Qf3 soil	6460		no CaCO3	5YR	0	2msbk	2mk	> 0-0.1 m	
Qf3	6600	Water Canyon	II	8.75YR	1 m	2-3msbk	3-4mk	0.2 m	Middle Pleistocene (200-600 ka)
Qt2	5860	R. San Jose	II-III	8.75YR	0.5-1.0 m	2msbk	2-3mk	0.3m	
Rinconada Cr. 28 m terrace	7200	Rinconada Canyon	III	5YR	> 0.3 m	3mabk	4mk-k	0.4-0.5 m	
Qt2	6340	Rio Paguete	II	5YR	0	3mabk-pr	4mk-k	> 1.2 m	
Qt2	7100	Marquez Can.	III	6.75YR	0.3-0.4 m	3msbk/abk	4mk-k	0.6 m	Early-Middle Pleistocene
Grimm's S2a soil	7500	Lobo Canyon	III	5YR-7.5YR	> 0.9 m	3mabk	4mk	0.4 m	
Qf1		Water Canyon	III	7.5-8.75 YR	> 1.0 m	2m-csbk	2n	0.2 m	
Buried Qf1 soil	6770		no CaCO3	7.5YR	0	2-3mabk	3n-mk	> 1.1 m	Pliocene
Qt1	6000	R. San Jose	Stripped	--	--	--	--	--	
Tp2			Stripped	--	--	--	--	--	Pliocene
Tp1			Stripped	--	--	--	--	--	

EXPLANATION:

Color: obtained from Munsell Soil Color Charts

Structure: Grade: 1 = weak, 2 = moderate, 3 = strong; Size: f = fine, m = medium, c = coarse, vc = very coarse

Type: sg = single grain, pl = platy, m = massive, gr = granular, sbk = subangular blocky, abk = angular blocky, pr = prismatic; nr = not reported

Clay Films: n.o. = not observed; Frequency: v = very few, 1 = few, 2 = common, 3 = many, 4 = continuous

Thickness: n = thin, mk = moderately thick, k = thick

Morphology: pf = ped faces, po = pore linings, br = bridges, co = colloidal stains on grains; nr = not reported

Terrace heights and longitudinal profiles

The height of surfaces along the Rio San Jose and tributary streams ranges from 5 to 300 m above local base level. Pliocene surfaces lie between 200-300 m (Tp 1) and 140180 m (Tp2) above local base level. Quaternary surfaces are located within 90 m, and Holocene surfaces within 5 m, of local base level (Table 3). Notably, relative elevations of correlative surfaces increase both to the north and east (Table 3). A distinct nickpoint in the Rio San Jose long profile occurs between Encinal Creek and Old Laguna, where the river has downcut through the Laguna flow (as named by Lipman) (Fig. 5).

TABLE 3—Height of surfaces above local base level. Drainages arranged schematically on south to north axis.

S	DRAINAGE	Q1	Q2	Q3
		ELEV (M)	ELEV (M)	ELEV (M)
	Rio San Jose at Laguna..	.40-50**	.25-30..	.15...
	Water Creek.....	.70...	..70...	.18...
	Rinconada Creek.....	..70...	..28-32..	.14-15..
	Rio Paguete.....	.70-75..	.35-40..	.15-20..
	Rio Moquino.....	.70-75..	.35-50..	.15-20..
	Arroyo del Valle.....	.80-90..	.45-50..	.25-30..
	Marquez Canyon.....	..70...	.45-50..	..70...
N				

**Based on 50 m terrace near San Fidel

Pliocene and Quaternary faults

Several Pliocene and two Quaternary faults are recognized within the study area. The Pliocene faults exhibit a predominant north to northeast trend throughout the Mount Taylor volcanic field (Perry et al., in press). Structures offsetting Pliocene basalts were mapped on Grants Ridge, East Grants Ridge, and Horace Mesa by Thaden et al. (1967) and between Rinconada and San Jose Canyons by Lipman et al. (1979). A group of faults with offsets ranging from 14 to 60 m defines a series of northeast-trending horsts and grabens along the southern end of Horace Mesa (Thaden et al., 1967; Maxwell, 1977; Drake, unpubl. data). In contrast, Tp2 surfaces are offset 1.5 and 3 m on Black Mesa and Grants Ridge (Thaden et al., 1967; Drake, unpubl. data). Faults do not offset the volcanic rocks that comprise the Mt. Taylor volcanic cone (Perry et al., 1990).

Possible Quaternary faults were identified at Cañon Seama and one mile north of Old Laguna. A small graben appears to offset the buried Laguna flows by 4 to 6 m at Callon Seama just east of Flower Mountain (Fig. 5), based on drill logs from Risser and Lyford (1983). A subvertical fault which offsets Quaternary fluvial sediments a minimum of 6 m is exposed in a roadcut on Highway 279 approximately one mile north of Old Laguna.

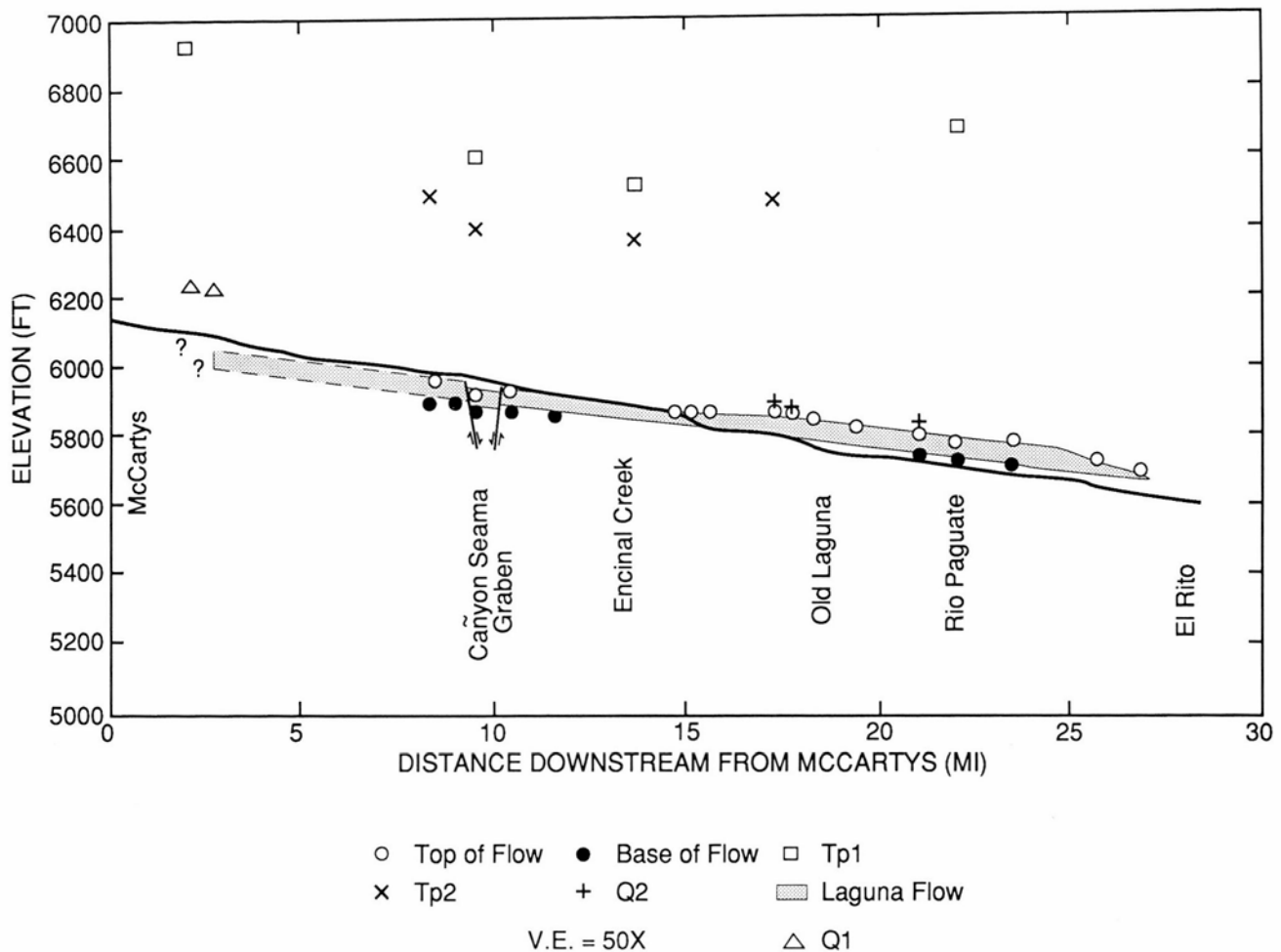


FIGURE 5—Rio San Jose and Laguna flow long profile from McCartys to Mesita.

Results

Methods for estimating deposit and surface ages

The estimated ages of surficial deposits in the Grants/Laguna area are based on stratigraphic and geomorphic position with respect to K—Ar-dated basalt flows and on comparison to radiometrically dated soil profiles developed in alluvium under similar climatic conditions. Using the state-factor approach of Jenny (1941), ages of soil profiles may be estimated by comparison with similarly developed soil profiles for which absolute-age determinations are available, if climate, topography, vegetation, and parent material are similar (Harden, 1982; Birkeland, 1984). Soils used for comparison in this study are located in the Albuquerque basin, on the Llano de Albuquerque, and in the Española basin.

Stratigraphic and geomorphic evolution of the Grants—Laguna area

The Pliocene and Quaternary deposits and associated geomorphic surfaces in the Grants—Laguna area record a history of long-term incision interrupted by relatively brief periods of base-level stability and/or aggradation. In contrast to the overall Plio-Quaternary history, the late Quaternary has been characterized by alternating periods of erosion and deposition. The 200-300 m of incision into Tp1 between 2.5 m.y. and the present time (using surface age estimated in Table 4) is probably a response to regional uplift, whereas

periods of erosion and deposition during the late Quaternary may be in response to climatic fluctuations, episodic volcanism, or differential uplift.

Tp1 was deposited as a veneer capping an extensive pediment surface formed between 4 and 2.5 m.y. (Table 4) during a period of regional base-level stability and pedimentation in west-central New Mexico. Tp1 surfaces, which are correlative with the Ortiz surface of the rift, were graded to an ancestral Rio San Jose that flowed near its present course. The eruption of Mt. Taylor volcanic rocks onto Tp1 began by 3.73 ± 0.09 m. y. (Perry et al., 1990) and continued until incision of Tp1 began at ca. 2.5 m.y.

Rapid incision of valleys followed abandonment of Tp1, with approximately 60 m of incision between ca. 2.5 and 2.4 ± 0.18 m.y. (based on ages of flows capping Tp1 and Tp2 surfaces). During Tpal2 deposition the Rio San Jose was a high-energy stream transporting coarse gravel from the Zuni Mountains and the Mt. Taylor area. Fluvial processes during Tpal2 deposition were dominated by lateral planation and pedimentation.

Regional incision resumed along the Rio San Jose at ca. 2.4 m.y. and persisted into early—middle Pleistocene time (from 2.4 to 0.7-0.8 m.y.). This was a time of relatively continuous base-level fall, evidenced by the absence of early Pleistocene surfaces, with 50-100 m of incision between the time of Tp2 and Q1. The formation of the Q1 surface marks the end of regional base-level fall during the early Pleistocene.

TABLE 4—Age estimates of surfaces in the Grants–Laguna area.

SURFACE	AGE ESTIMATE	DATING METHOD	RANGE OF AGE ESTIMATES; MISCELLANEOUS NOTES	REFERENCES
Tp1	2.5-4 m.y.	K-Ar	K-Ar dates range from 1.56 ± 0.17 to 3.73 ± 0.09 m.y. 1.56 m.y. age postdates surface	Lipman and Mehnert (1979) Perry et al. (1990)
Tp2	2.4 m.y.	K-Ar	2.42 ± 0.18	Lipman and Mehnert (1979)
Q1	0.7-0.8 m.y.	correlation with Mush Mesa; paleomag data; soil development (stage III CaCO ₃)	K-Ar dates on Mush Mesa flows range from 0.5-1.1 m.y. Qa1 deposits have reversed polarity (> 0.7 m.y.). Soils correlation suggests an age of 0.6-0.2 m.y.	Baldrige et al. (1987) Harlan, personal communication (1990) (paleomagnetic data) Machette (1985)
Q2	0.2-0.6 m.y.	Relative soil development (Stage III CaCO ₃)	Comparison with soils developed in deposits in the Albuquerque and Española basins.	Machette (1985) Dethier et al. (1988) Hawley et al. (1976)
Q3	0.01-0.1 m.y.	Relative soil development (Stage I+/Stage II CaCO ₃)	Comparison with soils developed in deposits in the Albuquerque basin.	Machette (1985)
Q4	Holocene	Relative soil development (Stage I CaCO ₃ for Q4)	Comparison with soils developed in deposits in the Albuquerque and Española basins.	Machette (1985) Dethier et al. (1988)
Q5	Late Holocene			

Deep incision into the Mt. Taylor volcanic cone by Water Creek began during Qa11 deposition, producing a large fan at the mouth of Water Canyon. During Q1 time stream systems located east of Water Creek were forming strath terrace and pediment surfaces. The concurrent formation of depositional and erosional surfaces suggests that: (1) initial breaching of the Mount Taylor amphitheater provided an excess sediment load to Water Creek and resulted in deposition of the Water Canyon fan, or (2) this may have been a period of differential uplift with the Water Canyon fan forming in a structural depression (the Acoma sag, Fig. 6).

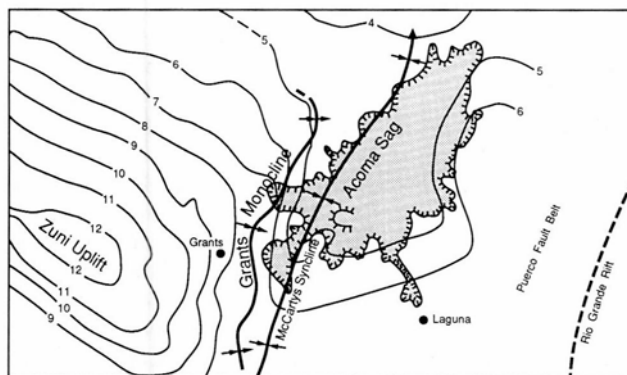
A period of regional base-level lowering characterized by a minimum of 100 m of incision along the ancestral Rio San Jose during the early–middle Pleistocene resulted in erosion of Q1 surfaces and formation of a deep valley 5060 m below the modern valley floor. This period of incision lasted until ca. 0.4–0.5 m.y., at which time the Rio San Jose valley began aggrading. A change from incision to aggradation at this time also occurred along the Rio Grande in the Albuquerque basin (Lambert, 1968), suggesting a

regional climatic control as opposed to a local tectonic influence. Episodic eruption of mid-to-late Pleistocene basalts into the Rio San Jose and some tributary valleys obstructed drainages and resulted in periodic upstream aggradation of valley floors by the streams. This damming of valleys by lava flows contributed to aggradation both along the Rio San Jose and tributary streams during the late Pleistocene.

Valley-floor aggradation culminated after eruption of the Laguna and Suwanee (or Cerro Verde) flows about 0.2 to 0.3 m.y. (Lipman and Mehnert, 1979; Baldrige et al., 1987; Perry and Laughlin, unpubl. data). The timing of maximum valley-floor aggradation within the study area appears to be time-transgressive, occurring first along downstream reaches near the terminus of the Laguna flow (in the Laguna–Mesita area) and progressively later along upstream reaches (near McCarty's and Rinconada Creek). This time-transgressive end to aggradation along the Rio San Jose is probably related to upstream migration of the nickpoint (Fig. 5) as the Rio San Jose cuts through the Laguna flow. The upper surface of the valley fill is represented by the Q2 surface near Old Laguna and by the Q3 surface between Water Creek and the community of McCarty's.

Renewed incision and subsequent lateral erosion of the Rio San Jose during the late Pleistocene partially exhumed the Laguna flow and deposited Qa13 materials as a thin deposit capping a strath terrace near Old Laguna and along tributaries entering the Rio San Jose downstream from Old Laguna (Rio Paguate, Rio Moquino, and Arroyo del Valle). Upstream from Old Laguna, the Rio San Jose continued to aggrade and tributary streams formed fan deposits graded to the valley floor. Deposition of fine-grained Qa14 terrace or fan deposits throughout the study area represents a period of aggradation during the latest Pleistocene and early Holocene.

Valley incision followed by aggradation during the middle to late Holocene is recorded by deposition of Qa15 materials and burial of Qa14 deposits along the Rio San Jose. Modern



Structural contours in thousands of feet referenced to the base of the Dakota Sandstone (after Kelley, 1955).

FIGURE 6—Location of the Acoma sag.

TABLE 5—Incision rates based on height above base level of Tp1, Tp2, and Q1 in the Grants–Laguna area.

SURFACE	AGE ESTIMATE*	HEIGHT (M) ABOVE LOCAL BASE LEVEL	INCISION RATE	INCISION RATE BASED ON: 50-M DEEP VALLEY AT 500 KA	SHORT TERM INCISION RATE
Tp1	greater than 2.5-3 m.y.	200-300	0.07-0.12 m/ka	0.10-0.17 m/ka	--
Tp2	2.4 m.y.	140-180	0.06-0.07 m/ka	0.10-0.12 m/ka	(From Tp1 to Tp2) 0.6 m/ka
Qt1	0.7-0.8 m.y.	40-90	0.05-0.13 m/ka	0.3-0.7 m/ka	(From Tp2 to Q1) 0.06 m/ka

*See Table 4.

arroyos have incised 2-12 m below valley floors during the late Holocene.

Pliocene—Quaternary deformation and uplift

Projection of surface gradients relative to present stream profiles graded to the modern Rio San Jose valley floor indicates the Tp1 and Tp2 surfaces are downwarped a minimum of 50 m into a broad syncline (Fig. 5). This deformation occurs in approximately the same location as the Acoma sag (Fig. 6), a structure active in Cretaceous time (described by Kelley, 1955). This demonstrates that the Acoma sag was active during the late Pliocene or early Pleistocene. It is unclear when this late Cenozoic period of deformation may have begun.

Correlative Quaternary surfaces exhibit increasing height above base level along a southwest to northeast axis from Laguna to Marquez and from Water Creek to Arroyo del Valle (Table 4). Assuming that incision below these surfaces is in response to uplift, then the increase in height of surfaces above local base level indicates an increase in uplift rates from southwest to northeast across the eastern half of the study area during the Quaternary. This variation in uplift rates may be related to (1) distance from the axis of the Acoma sag, or (2) proximity to the Rio Grande rift, with greater uplift along the rift margin than away from the rift.

The location of erosional landforms and deposits in the Grants–Laguna area provides evidence for active Quaternary deformation within the Acoma sag. Qal 1 and Qal3 fan deposits are limited primarily to the area between Encinal Creek and Rinconada Creek (Fig. 4), suggesting that Quaternary subsidence occurred in the central part of the Acoma sag. Erosional terrace and pediment deposits are restricted to drainages marginal to the Acoma sag (Rio Moquino, Rio Paguete, Arroyo del Valle, and Marquez Creek) (Fig. 4).

Timing and rates of incision

Average incision rates from the late Pliocene to the present based on the height of Tp1 above local base level range from 0.07 to 0.12 m/ka (Table 5). Periods of relatively rapid incision (approximately 0.3 to 0.7 m/ka) occurred between the time of abandonment of Tp1 and formation of Tp2 (between ca. 2.5 and 2.4 ± 0.18 m.y.) and between formation of Q1 and incision of the deep valley below the modern Rio San Jose (from ca. 0.8 to 0.5 m.y.) (Table 5). The initiation of rapid incision at ca. 2.5 m.y. corresponds to a period of rapid extension along the margin of the Rio Grande rift from 2.6 to 1.5 m.y., proposed by Perry et al. (1990) to account

for an abrupt change from highly evolved rhyolite and quartzlatite magmas to less evolved latite magmas in the Mount Taylor volcanic field. Similar incision rates occurring from 0.8 to 0.5 m.y. may record the initiation of a later period of extension along the rift margin.

Conclusions

Between 200 and 300 m of incision occurred in the Grants–Laguna area during the past 2.5 m.y. in response to regional uplift. Periods of rapid incision (of as much as 0.6 m/ka) occurred between ca. 2.5 and 2.4 m.y. and possibly between 0.7-0.8 and around 0.5 m.y. Episodic entrenchment and aggradation of fluvial systems during the late Quaternary may be in response to uplift, climatic fluctuations, and periodic obstruction of drainages during volcanic eruptions.

Faulting was most active during the late Pliocene to early Pleistocene. Pliocene surfaces are warped across the Acoma sag, a Cretaceous structure which exhibits evidence of activity during the Pliocene and Quaternary. Tributary drainages flowing into the Acoma sag have been aggrading during the Quaternary concurrent with formation of erosional surfaces by drainages located marginal to the sag. Correlative Quaternary surfaces located progressively farther from the axis of the Acoma sag exhibit an increasing height above base level. Finally, periods of rapid uplift and incision and more voluminous eruption of volcanic materials between 2.5-2.4 and 0.8-0.5 m.y. may both be related to periods of rapid extension in the transition zone along the rift margin.

Acknowledgments

This research was completed with funding from the 1SR (Institutional Supporting Research) program at Los Alamos National Laboratory and from the University of New Mexico. The authors would like to thank the Pueblo of Laguna for allowing access to Pueblo lands during the course of this investigation. The authors also express their appreciation to the Cebolleta Land Grant Commission and the owners of the L Bar Ranch for allowing access to land-grant and private lands. Several graduate students at the University of New Mexico, including Mark Gonzalez, Steven Harlan, and Claire Renault, volunteered help and provided valuable criticism during the completion of field work. We also wish to extend our thanks to Steve Reneau for a thorough manuscript review and to Anthony Garcia and James Archuleta for their assistance in drafting the figures.

References

- Bachman, G. O., and Mehnert, H. H., 1978, New K-Ar dates and the late Pliocene to Holocene geomorphic history of the central Rio Grande region, New Mexico: Geological Society of America, Bulletin, v. 89, pp. 283-292.
- Baldrige, W. S., Perry, F. V., and Shafiqullah, M., 1987, Late Cenozoic volcanism of the southeastern Colorado Plateau: I. Volcanic geology of the Lucero area, New Mexico: Geological Society of America, Bulletin, v. 99, pp. 463-470.
- Birkeland, P. W., 1984, Soils and geomorphology: Oxford University Press, New York, 372 pp.
- Bryan, K., and McCann, F. T., 1938, The Ceja del Rio Puerco—a border feature of the Basin and Range province in New Mexico, pt. II, geomorphology: Journal of Geology, v. 46, pp. 1-16.
- Crumpler, L. S., 1982, Volcanism in the Mount Taylor region; in Grambling, J. A., and Wells, S. G. (eds.), Albuquerque country II: New Mexico Geological Society, Guidebook 33, pp. 291-298.
- Dethier, D. P., Harrington, C. D., and Aldrich, M. J., 1988, Late Cenozoic rates of erosion in the western Espanola Basin, New Mexico: Evidence from geologic dating of erosion surfaces: Geological Society of America, Bulletin, v. 100, pp. 928-937.
- Gile, L. H., Hawley, J. W., and Grossman, R. B., 1981, Soils and geomorphology in the Basin and Range area of southern New Mexico—Guidebook to the Desert Project: New Mexico Bureau of Mines & Mineral Resources, Memoir 39, 222 pp.
- Gordon, E. D., 1961, Geology and ground-water resources of the Grants-Bluewater area, Valencia County, New Mexico: Technical Report 20, New Mexico State Engineer, Santa Fe, 109 pp.
- Grimm, J. P., 1985, The late Cenozoic geomorphic history of the Lobo Canyon area of the Mount Taylor volcanic field, Cibola County, New Mexico: Unpublished MS thesis, University of New Mexico, Albuquerque, 159 pp.
- Harden, J. W., 1982, A quantitative index of soil development from field descriptions: Examples from a chronosequence in central California: Geoderma, v. 28, pp. 1-28.
- Hawley, J. W., Bachman, G. O., and Manley, K., 1976, Quaternary stratigraphy in the Basin and Range and Great Plains provinces, New Mexico and western Texas; in Mahaney, W. C. (ed.), Quaternary stratigraphy of North America: Dowden, Hutchinson & Ross, Inc., Stroudsburg, Pennsylvania, pp. 235-274.
- Hunt, C. B., 1938, Igneous geology and structure of the Mount Taylor volcanic field, New Mexico: U.S. Geological Survey, Professional Paper 189-B, pp. 51-80.
- Jenny, H., 1941, Factors of soil formation: McGraw-Hill, New York.
- Kelley, V. C., 1955, Regional tectonics of the Colorado Plateau and relationship to the origin and distribution of uranium: University of New Mexico Publications in Geology No. 5, 120 pp.
- Lambert, P. W., 1968, Quaternary stratigraphy of the Albuquerque area, New Mexico: Unpublished PhD dissertation, University of New Mexico, Albuquerque, 300 pp.
- Lipman, P. W., and Mehnert, H. H., 1979, Potassium-argon ages from the Mount Taylor volcanic field, New Mexico: U.S. Geological Survey, Professional Paper 1124-B, 8 pp.
- Lipman, P. W., and Moench, R. H., 1972, Basalts of the Mount Taylor volcanic field, New Mexico: Geological Society of America, Bulletin, v. 83, pp. 1335-1344.
- Lipman, P. W., Pallister, J. S., and Sargent, K. A., 1979, Geologic map of the Mount Taylor quadrangle, Valencia County, New Mexico: U.S. Geological Survey, Map GA-1523.
- Love, D. W., 1989, Geomorphic development of the Rio San Jose valley; in Anderson, O. J., Lucas, S. G., Love, D. W., and Cather, S. M. (eds.), Southeastern Colorado Plateau: New Mexico Geological Society, Guidebook 40, pp. 11-12.
- Machette, M. N., 1985, Calcic soils of the southwestern United States; in Weide, D. L. (ed.), Soils and Quaternary geology of the southwestern United States: Geological Society of America, Special Paper 203, pp. 1-22.
- Maxwell, C. H., 1977, Preliminary geologic map of the McCarty's quadrangle, Valencia County, New Mexico: U.S. Geological Survey, Open-File Report 77-380.
- Maxwell, C. H., 1982, El Malpais; in Grambling, J. A., and Wells, S. G. (eds.), Albuquerque country II: New Mexico Geological Society, Guidebook 33, pp. 299-301.
- Moench, R. H., and Schlee, J. S., 1967, Geology and uranium deposits of the Laguna district, New Mexico: U.S. Geological Survey, Professional Paper 519, 117 pp.
- Perry, F. V., Baldrige, W. S., DePaolo, D. J., and Shafiqullah, M. (in press), Evolution of a magmatic system during continental extension: the Mount Taylor volcanic field, New Mexico: Journal of Geophysical Research.
- Risser, D. W., and Lyford, F. P., 1983, Water resources on the Pueblo of Laguna, west-central New Mexico: U.S. Geological Survey, Water-Resources Investigations Report 83-4038, 308 pp.
- Thaden, R. E., Santos, E. S., and Raup, O. B., 1967, Geologic map of the Grants quadrangle, Valencia County, New Mexico: U.S. Geological Survey, Geologic Quadrangle Map GQ-680.
- Wright, H. E., Jr., 1946, Tertiary and Quaternary geology of the lower Rio Puerco area, New Mexico: Geological Society of America, Bulletin, v. 57, pp. 383-456.

Geologic overview and Pliocene-Quaternary history of the Albuquerque basin, central New Mexico

Richard P. Lozinsky, John W. Hawley, and David W. Love

New Mexico Bureau of Mines & Mineral Resources, Socorro, New Mexico 87801

Introduction

The approximately 1000 km long Rio Grande rift forms one of the major structural features in the southwestern United States. The rift is composed of a series of roughly north-south-trending, en-echelon basins (Chapin, 1971, 1988) that are characterized by thin crust, elevated heat flow, young faulting, recent volcanism, and thick basin fills (Seager and Morgan, 1978; Morgan et al., 1986). One of the largest and deepest basins of the rift is the Albuquerque basin (Fig. 1). Over the past 60 years, this basin has been the focus of many studies that have examined its stratigraphy, structure, and complex depositional history (see previous-work section in Lozinsky, 1988). This paper presents a brief geologic overview and discusses the Quaternary evolution of this important basin.

Covering an area of about 7400 km², the Albuquerque basin lies within the northern portion of the Mexican High

land section (Rio Grande subsection) of the Basin and Range physiographic province (Fenneman, 1931; Hawley, 1986). Elevations of the margin uplifts are as much as 3050 m in the east and up to 2134 m in the west. Low topographic relief characterizes much of the area within the Albuquerque basin. Elevations range from about 1310 m along the Rio Grande to around 1830 m along the eastern piedmont slope. The valleys of the Rio Grande and Rio Puerco are the two major erosional landforms within the basin. A long, southward-narrowing tableland known as the Llano de Albuquerque lies between these two valleys. Other landforms within the basin include mesas and structural benches, low hills and ridges, inset stream terraces, and graded alluvial slopes.

Geologic setting

As structurally defined here, the Albuquerque basin extends from the San Felipe fault belt in the north to the Joyita

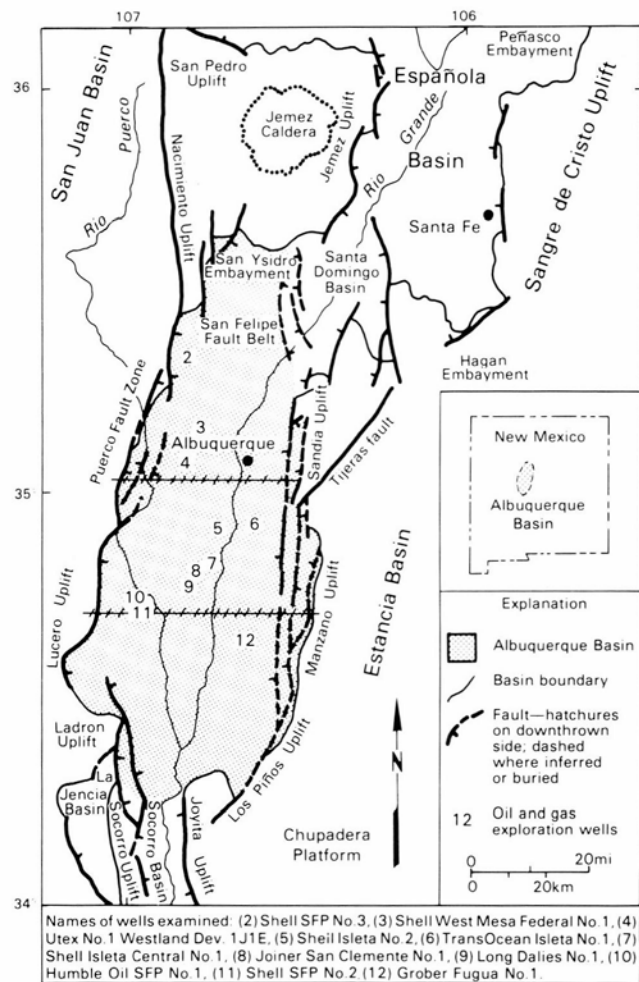


FIGURE 1—Tectonic map of Albuquerque basin as defined in this study. Hatched lines show the locations of the north and south cross-section lines. Modified from Anonymous (1961) and Woodward et al. (1978).

uplift in the south (Fig. 1). The eastern and western border features are distinctly different. The eastward-tilted Sandia-Manzano—Los Pinos uplift forms the prominent, relatively linear eastern border. These uplifts consist primarily of Precambrian plutonic and metamorphic rocks which are unconformably overlain by upper Paleozoic limestone, shale, and sandstone. The western border is more irregular, more varied in structural style, and in some places has only minor amounts of displacement along margin faults.

The Ladoron and Lucero uplifts form the southwestern basin border. The Ladoron uplift is a pyramid-shaped, structurally complex horst that consists mainly of Precambrian plutonic and metamorphic rocks with minor upper Paleozoic units. The fault zone that separates the Lucero uplift from the basin is extremely complex and shows Laramide-age reverse and possibly strike-slip motion with later late Cenozoic normal faulting (Callender and Zilinski, 1976; Hammond, 1987). The gently west-dipping Lucero uplift contains upper Paleozoic limestone, shale, and sandstone capped by late Cenozoic basalt flows.

North of the Lucero uplift, the basin boundary is marked by the topographically subdued Puerco fault zone. This region west of the fault zone is part of the southeastern Colorado Plateau and rocks exposed here include Cretaceous sandstone and shale, and, to a lesser extent, Jurassic clastic units. The Nacimiento and Jemez uplifts border the basin

to the northwest and north, respectively. Precambrian plutonic and metamorphic rocks overlain by Paleozoic and Mesozoic units crop out in the Nacimiento uplift (Woodward, 1987). The Jemez uplift is part of a large volcanic pile and caldera complex (Smith et al., 1970; Gardner et al., 1986).

Basin structure

Although the Albuquerque basin appears topographically as only one basin, seismic reflection work by the Shell Oil Company (staff comm. December 1986; Russell and Snelson, in press) indicates that the basin is actually composed of a northern eastward-tilted half-graben and southern westward-tilted half-graben (Fig. 2). An accommodation zone that appears to be an extension of the Tijeras fault separates the two half-grabens (see Fig. 1). The half-graben morphology of the Albuquerque basin is not unusual, most basins of the rift display this type of morphology.

As shown in Fig. 2, the half-grabens within the Albuquerque basin are characterized by a deep, inner graben that is flanked by a stepped sequence of shallow, faulted ramps that lead up to the margin areas. Faults with the largest displacements occur several kilometers basinward from the topographically high margins. The structural relief of the basin is well over 10,000 m, based on the vertical distance between the Precambrian strata on top of the eastern margin uplifts and within the deepest part of the basin (Lozinsky, 1988).

In the north half-graben, the largest displacement fault with as much as 2871 m of offset is located under the present position of the Rio Grande. Based on seismic and groundwater data, the largest displacement fault in the south half-graben appears to occur under the present position of the Rio Puerco. According to seismic work by Shell Oil Company (staff comm. December 1986; Russell and Snelson, in press), many of these faults are listric.

Basin-fill stratigraphy

The fill within the Albuquerque basin consists mostly of siliciclastic continental sediments with minor volcanic rocks that can be subdivided into three units: (1) pre-Santa Fe Tertiary deposits, (2) the Santa Fe Group, and (3) post-Santa Fe Quaternary deposits. Pre-Santa Fe Tertiary deposits crop out only in limited exposures within the basin and were mainly studied by examining data from deep oil test wells. In most areas of the basin, Upper Cretaceous strata underlie the basin-fill deposits; however, along the eastern margin, Paleozoic units underlie the basin fill deposits (Fig. 2).

Pre-Santa Fe Tertiary deposits

These deposits underlie the Santa Fe Group and indicate the existence of at least two depositional basins that predate the Albuquerque basin. By examining cuttings and cores from several of the deep oil test wells, Lozinsky (1988) subdivided the pre-Santa Fe Tertiary deposits into the Eocene Galisteo and Baca Formations and an overlying late Eocene to late Oligocene unit informally referred to as the "unit of Isleta #2 well." This informal unit generally correlates with the Datil Group and the Oligocene volcanic sequence that overlies the Datil Group (Osburn and Chapin, 1983). The Galisteo and Baca deposits consist of interbedded sandstone, siltstone, and shale derived mainly from nonvolcanic source areas. The Isleta #2 rocks were derived, at least partly, from intermediate volcanic source areas and include sand-

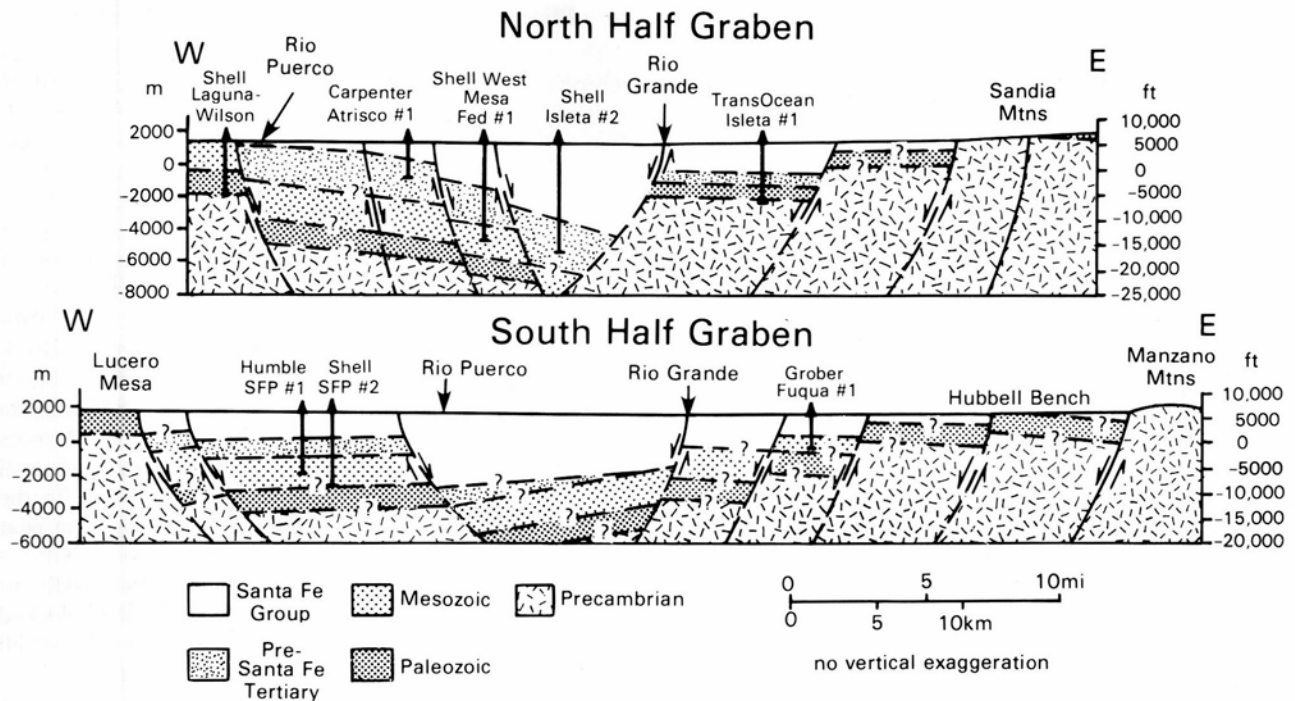


FIGURE 2—Diagrammatic cross-sections of the Albuquerque basin. Cross-section locations shown in Fig. 1.

stones with locally interbedded volcanic flows and ash of intermediate composition. Thicknesses of the Galisteo—Baca deposits are generally less than 500 m, whereas thicknesses of the unit of Isleta #2 range up to as much as 2185 m (Lozinsky, 1988).

Santa Fe Group

The major basin-fill unit of the Rio Grande rift is the uppermost Oligocene to middle Pleistocene Santa Fe Group. It is the main synrift deposit and can be subdivided into upper and lower units based on depositional environment and age.

The lower Santa Fe Group represents deposition in basins with internal drainage. In the southern part of the basin, these units are called the Popotosa Formation by Machette (1978b, c). In the northern part, the Zia Formation of Tedford (1982) generally correlates with the lower and middle Popotosa. Lower Santa Fe basin fill ranges in age from 30 to 5 Ma and is dominated by intertonguing piedmont, eolian, and fine-grained basin-floor deposits. The bulk of the lower Santa Fe Group was probably deposited between 5 and 10 Ma, when tectonism was most active in the rift.

Unlike the lower Santa Fe, the upper Santa Fe Group was deposited in an externally drained basin. This lithostratigraphic unit is referred to as the Ceja Member by Kelley (1977) and as the Sierra Ladrone Formation by Machette (1978b, c). Upper Santa Fe Group basin fill ranges in age from about 5 to 0.5 Ma and is characterized by intertonguing piedmont (alluvial-fan) and basin-floor (axial-stream) deposits. Piedmont units consist of poorly sorted, weakly stratified sand and conglomerate. The basin-floor deposits include a sand-dominated, cross-stratified axial-river facies and an interbedded sand and clayey silt overbank facies. Abundant trough crossbedding and high sand-to-clay ratios in the axial-river facies indicate that these sediments were deposited within a large braided-river system. The overbank facies represents deposition that was occurring in regions where

major braided-river systems were merging, as for example the confluence of the ancestral Rio Grande and Rio Puerco just west of Belen. Santa Fe Group deposition culminated with the construction of a broad, central-basin plain, now partly preserved between the Rio Grande and Rio Puerco valleys as the Llano de Albuquerque.

Several volcanic features were emplaced during the later stages of upper Santa Fe Group deposition. Tome Hill, located about 8 km north of Los Lunas, is a small andesitic center that stands over 100 m above the present Rio Grande floodplain. It has been dated at 3.4 ± 0.4 Ma by Bachman and Mehnert (1978) and is probably an exhumed feature. Near the western edge of the Llano de Albuquerque, the undated Wind Mesa volcano forms a subdued hill along the horizon. It is a shield volcano of probable Pliocene age that has been considerably disrupted by faulting.

Just west of where 1-25 crosses the Rio Grande south of Albuquerque is the Isleta volcano, a basal maar crater overlain by several basaltic flow units. It has been dated by Kudo et al. (1977) at 2.78 Ma. The flow units intertongue with axial-river-facies deposits.

One of the most prominent features within the southern Albuquerque basin is the Los Lunas volcano, located just west of Los Lunas. This volcano consists primarily of andesite flows that have a range of K—Ar dates from 1.31 ± 0.05 to 1.01 ± 0.10 Ma (Bachman and Mehnert, 1978). This volcano straddles deformed basin fill containing earlier local andesitic eruptives and pumiceous debris flows probably derived from the Jemez Mountains. A thick alluvial mantle was shed from this uplifted volcano, but it is not buried by basin fill and some of the flows descend to the east into the ancestral Rio Grande valley. The locally derived mantle contains the 1.1 Ma ash of the Upper Bandelier Tuff.

Thicknesses within the Santa Fe Group range from 1000 to 2000 m along the margin areas to as much as 4407 m in the deeper portions of the basin. The thickest section was penetrated in the Shell Isleta #2 test well and represents

Most of the deposition at this time was occurring along the river systems in the central portion of the basin. These river systems were bringing in detritus of mixed lithologies from considerable distances outside the Albuquerque basin. Detritus was continuing to be shed off the surrounding uplifts, but not in the great volumes seen during lower Santa Fe time.

Volcanism, primarily mafic, continued within the basin (i.e. emplacement of Isleta and Los Lunas volcanoes). Volcanic ashes, erupted from the Jemez caldera and as far away as the Yellowstone area, were also deposited within the basin (Izett, 1981).

Between about 1 and 0.5 Ma, a major change in the depositional regime occurred when the Rio Grande fluvial system underwent its first major incision episode, perhaps in response to becoming integrated with drainages to the Gulf of Mexico (Hawley et al., 1976; Seager et al., 1984) and receiving increased runoff from the southern Rocky Mountains region (Wells et al., 1987; Heffern, 1990). This depositional change is a critical event in the late Cenozoic history of the Albuquerque basin because, prior to this time, the basin had been undergoing net aggradation. Subsequently, however, the basin has been subjected to net degradation as several more cycles of river incision produced the present-day inner valley of the Rio Grande (Lambert, 1968; Hawley et al., 1976; Machette, 1985). The initial episode of valley entrenchment also marked the end of Santa Fe Group deposition and isolated basin-floor areas (such as the Llano de Albuquerque) from further major deposition and erosion.

Tectonism has been relatively less active in the past 0.5 Ma. Uplifts around the basin continue to shed detritus into the basin, but not as extensively as during Santa Fe time. There are large areas within the basin that are receiving relatively little sediment (i.e. Llano de Albuquerque). These areas preserve degraded fault scarps showing multiple but relatively inconsequential movement (Bachman and Machette, 1977). Significant aggradation in the major drainages during back-filling episodes is documented by thick, inset terrace deposits and undissected valley fill (Lambert, 1968; Hawley et al., 1976). Major fluvial systems are still delivering mixed lithologies derived in part from outside the basin. Volcanism also continued as the Albuquerque and Cat Hills volcanic fields developed on the Llano de Albuquerque. Following a major interval of fluvial incision to levels 25 to 40 m below modern valley floors, probably between 25,000 and 10,000 yrs B.P., the Rio Grande base level has been slowly rising, accompanied by deposition of latest Quaternary valley fill (Hawley et al., 1976).

Acknowledgments

The work on the Santa Fe Group was part of Lozinsky's PhD dissertation completed at the New Mexico Institute of Mining & Technology. Funding was provided by the New Mexico Bureau of Mines & Mineral Resources (Frank E. Kottowski, director) and by the New Mexico Geological Society.

References

- Anonymous, 1961, Structural problems of the Rio Grande trough in Albuquerque country: New Mexico Geological Society, Guidebook 12, pp. 144-147.
- Bachman, G. O., and Machette, M. N., 1977, Calcic soils and calcretes in the southwestern United States: U.S. Geological Survey, Open-file Report 77-794, 163 pp.
- Bachman, G. O., and Mehnert, H. H., 1978, New K-Ar dates and the late Pliocene to Holocene geomorphic history of the central Rio Grande region, New Mexico: Geological Society of America, Bulletin, v. 89, pp. 283-292.
- Bryan, K., 1909, Geology of the vicinity of Albuquerque: University of New Mexico Bulletin 51, Geological Series, v. 3, 24 pp.
- Bryan, K., 1938, Geology and groundwater conditions of the Rio Grande depression in Colorado and New Mexico; in U.S. Natural Resources Planning Board, The Rio Grande Joint Investigations in the upper Rio Grande Basin: U.S. Government Printing Office, Washington, D.C., v. 1, pt. 2, pp. 197-225.
- Bryan, K., and McCann, F. T., 1937, The Ceja del Rio Puerco: A border feature of the Basin and Range province in New Mexico, Part I: Journal of Geology, v. 45, pp. 801-828.
- Bryan, K., and McCann, F. T., 1938, The Ceja del Rio Puerco: A border feature of the Basin and Range province in New Mexico, Part II: Journal of Geology, v. 46, pp. 1-16.
- Callender, J. C., and Zilinski, R. E., 1976, Kinematics of Tertiary and Quaternary deformation along the eastern edge of the Lucero uplift, central New Mexico: New Mexico Geological Society, Special Publication no. 6, pp. 53-61.
- Chapin, C. E., 1971, The Rio Grande rift, Part I—modifications and additions: New Mexico Geological Society, Guidebook 22, pp. 191-201.
- Chapin, C. E., 1988, Axial basins of the northern and central Rio Grande rifts; in Sloss, L. L. (ed.), Sedimentary cover—North American Craton (U.S.): Geological Society of America, Geology of North America, v. D-2, pp. 165-170.
- Fenneman, M. N., 1931, Physiography of the western United States: McGraw-Hill, New York, 534 pp.
- Gardner, J. N., Goff, F., Garcia, S., and Hagan, R. C., 1986, Stratigraphic relations and lithologic variations in the Jemez volcanic field, New Mexico: Journal of Geophysical Research, v. 91, pp. 1763-1778.
- Geissman, J. W., Brown, L., Turrin, B. D., McFadden, L. D., and Harlan, S. S., 1990, Brunhes chron excursion/polarity episode recorded during the late Pleistocene, Albuquerque Volcanoes, New Mexico, U.S.A.: Geophysical Journal International, v. 102, pp. 73-88.
- Gile, L. H., Hawley, J. W., and Grossman, R. B., 1981, Soils and geomorphology in the Basin and Range area of southern New Mexico—Guidebook to the Desert Project: New Mexico Bureau of Mines & Mineral Resources, Memoir 39, 222 pp.
- Hammond, C. M., 1987, Geology of the Navajo Gap area between the Ladrón Mountains and Mesa Sarca, Socorro County, New Mexico: a structural analysis: Unpublished MS thesis, New Mexico Institute of Mining & Technology, Socorro, 212 pp.
- Hawley, J. W., 1986, Physiographic provinces; in Williams, J. L. (ed.), New Mexico in maps (2nd edition): University of New Mexico Press, Albuquerque, pp. 23-27.
- Hawley, J. W., Bachman, G. O., and Manley, K., 1976, Quaternary stratigraphy in the Basin and Range and Great Plains provinces, New Mexico and western Texas; in Mahaney, W. C. (ed.), Quaternary stratigraphy of North America: Dowden, Hutchinson, and Ross, Inc., Stroudsburg, Pennsylvania, pp. 235-274.
- Heffern, E. L., 1990, A geologic overview of the Wild Rivers Recreation Area, New Mexico: New Mexico Geological Society, Guidebook 41, pp. 229-236.
- Izett, G. A., 1981, Volcanic beds: recorders of upper Cenozoic silicic pyroclastic volcanism in the western United States: Journal of Geophysical Research, v. 86, pp. 10200-10222.
- Kelley, V. C., 1977, Geology of Albuquerque basin, New Mexico: New Mexico Bureau of Mines & Mineral Resources, Memoir 33, 59 pp.
- Kudo, A. M., Kelley, V. C., Damon, P. E., and Shafiqullah, M., 1977, K-Ar ages of basalt flows at Canjilon Hill, Isleta volcano, and the Cat Hills volcanic field, Albuquerque-Belen basin, central New Mexico: Isochron/West, no. 18, pp. 15-16.
- Lambert, P. W., 1968, Quaternary stratigraphy of the Albuquerque area, New Mexico: Unpublished PhD dissertation, University of New Mexico, Albuquerque, 257 pp.
- Lambert, P. W., Hawley, J. W., and Wells, S. G., 1982, Supplemental road-log segment III-S: Urban and environmental geology of the Albuquerque area: New Mexico Geological Society, Guidebook 33, pp. 97-119.
- Lozinsky, R. P., 1988, Stratigraphy, sedimentology, and sand petrology of the Santa Fe Group and pre-Santa Fe Tertiary deposits in the Albuquerque basin, central New Mexico: Unpublished PhD dissertation, New Mexico Institute of Mining & Technology, Socorro, 298 pp.
- Lozinsky, R. P., and Hawley, J. W., 1986, The Palomas Formation of

- south-central New Mexico—a formal definition: *New Mexico Geology*, v. 8, no. 4, pp. 73-78, 82.
- Machette, M. N., 1978a, Dating of Quaternary faults in the southwestern United States by using buried calcic paleosols: U.S. Geological Survey, *Journal of Research*, v. 6, pp. 369-381.
- Machette, M. N., 1978b, Geologic map of the San Acacia quadrangle, Socorro County, New Mexico: U.S. Geological Survey, *Geologic Quadrangle Map GQ-1415*, scale 1:24,000.
- Machette, M. N., 1978c, Preliminary geologic map of the Socorro 1° x 2° quadrangle, central New Mexico: U.S. Geological Survey, *Open-file Report 78-607*, scale 1:250,000.
- Machette, M. N., 1985, Calcic soils of the southwestern United States: Geological Society of America, *Special Paper 203*, pp. 1-21.
- Menges, C. M., 1990, Late Cenozoic rift tectonics and mountain-front landforms of the Sangre de Cristo Mountains near Taos, northern New Mexico: *New Mexico Geological Society, Guidebook 41*, pp. 113-122.
- Morgan, P., Seager, W. R., and Golombek, M. P., 1986, Cenozoic thermal, mechanical and tectonic evolution of the Rio Grande rift: *Journal of Geophysical Research*, v. 91, pp. 6263-6276.
- Pazzaglia, F. J., and Wells, S. G., 1990, Quaternary stratigraphy, soils and geomorphology of the northern Rio Grande rift: *New Mexico Geological Society, Guidebook 41*, pp. 423-430.
- Osburn, G. R., and Chapin, C. E., 1983, Nomenclature for Cenozoic rocks of northeast Mogollon-Datil volcanic field, New Mexico: *New Mexico Bureau of Mines & Mineral Resources, Stratigraphic Chart 1*.
- Russell, L. R., and Snelson, S. (in press), Structural style and tectonic evolution of the Albuquerque basin segment of the Rio Grande rift; in Pinet, B., and Bois, C. (eds.), *Potential of deep seismic profiling for hydrocarbon exploration*: French Petroleum Institute, *Research Conference Proceedings*.
- Seager, W. R., and Morgan, P., 1978, Rio Grande rift in southern New Mexico, west Texas, and northern Chihuahua; in Riecker, R. E. (ed.), *Rio Grande rift: tectonics and magmatism*: American Geophysical Union, Washington, D.C., pp. 87-106.
- Seager, W. R., Shafiqullah, M., Hawley, J. W., and Marvin, R. F., 1984, New K-Ar dates from basalts and the evolution of the southern Rio Grande rift: *Geological Society of America, Bulletin*, v. 95, pp. 87-99.
- Smith, R. L., Bailey, R. A., and Ross, C. S., 1970, Geologic map of the Jemez Mountains, New Mexico: U.S. Geological Survey, *Miscellaneous Investigations Series, Map 1-571*, scale 1:250,000.
- Tedford, R. H., 1982, Neogene stratigraphy of the northwestern Albuquerque basin: *New Mexico Geological Society, Guidebook 33*, pp. 273-278.
- Titus, F. B., 1963, Geology and ground-water conditions in eastern Valencia County, New Mexico: *New Mexico Bureau of Mines & Mineral Resources, Ground-water Report 7*, 113 pp.
- Wells, S. G., Kelson, K. I., and Menges, C. M., 1987, Quaternary evolution of fluvial systems in the northern Rio Grande rift, New Mexico and Colorado: implications for entrenchment and integration of drainage systems; in Menges, C. M. (ed.), *Quaternary tectonics, landform evolution, soil chronologies and glacial deposits—northern Rio Grande rift of New Mexico*: Friends of the Pleistocene Field Trip *Guidebook*, pp. 55-69.
- Woodward, L. A., 1987, Geology and mineral resources of Sierra Nacimiento and vicinity, New Mexico: *New Mexico Bureau of Mines & Mineral Resources, Memoir 42*, 84 pp.
- Woodward, L. A., Callender, J. F., Seager, W. R., Gries, J. C., Shaffer, W. L., and Zilinski, R. E., 1978, Tectonic map of the Rio Grande rift region in New Mexico, Chihuahua, and Texas; in Hawley, J. W. (compiler), *Guidebook to the Rio Grande in New Mexico and Colorado*: *New Mexico Bureau of Mines & Mineral Resources, Circular 163*, Sheet 2.

Cusate-lobate folds along a sedimentary contact, Los Lunas volcano, New Mexico

William C. Haneberg

New Mexico Bureau of Mines & Mineral Resources, Socorro, New Mexico 87801

Background

Cusate-lobate folds are characteristic of strongly compressed interfaces separating media of differing mechanical competence, with the lobate folds cored by the more competent material and the cusate folds cored by the less competent material (e.g. Ramsay and Huber, 1987, p. 403). Other commonly used terms for this type of feature include *mullion*, *fold mullion*, and *arc-and-cusp structure*. Although cusate-lobate folds are commonly associated with high-grade metamorphic rocks, their morphology is similar to that of alternating load casts and flame structures in sedimentary sequences. In addition to having geologic significance as indicators of both competence contrast and shortening direction, cusate-lobate folds are also amenable to theoretical and experimental analysis.

Ramsay and Huber (1987, pp. 392-393) maintain that cusate-lobate folds form only along interfaces separating media of low viscosity contrast, perhaps less than an order of magnitude. Smith (1975, 1977) and Fletcher (1982) analyzed the growth of instabilities along interfaces separating both linear and nonlinear fluids, and concluded that, although so-called mullion instabilities have small growth rates, mullion growth is enhanced in nonlinear fluids. One important conclusion of such analyses is that no first-order dynamic instability, which would maximize the growth of structures with a preferred wavelength, will develop between two semi-infinite fluids. Instead, there is only kinematic amplification of pre-existing perturbations along the

interface. Johnson and Pfaff (1989) provided a detailed geometric analysis of the waveforms necessary to produce different forms of folds, including cusate-lobate folds, and showed how cusate-lobate folds might evolve from sinusoidal folds in linear viscous multilayers subjected to shortening of 6-8%. Recent experimental work with strain-softening silicon putty models (Sokoutis, 1990) has shown that cusate-lobate structures grow rapidly along a single interface separating two semi-infinite fluids with low viscosity contrast, but again with no preferred wavelength, subjected to shortening greater than 10%.

Observations

A series of exceptionally well-developed cusate-lobate folds is exposed along a sedimentary contact at Los Lunas volcano (Fig. 1). Below the contact is a buff to orange alluvium composed of silt and fine sand, with no distinct bedding. Above the contact are a 1-2 cm thick white ash, a 10-15 cm thick gray tephra ranging in size from sand to granule, and a coarser orange tephra up to 1 m thick. Much of the less-resistant alluvium beneath the contact has been removed by erosion, showing that both cusps and lobes extend at least a meter back into the outcrop; therefore, these folds can be analyzed as two-dimensional structures. Most cusps in the sequence point downward, suggesting that the finer-grained alluvium was generally the more competent material during deformation; however, a few very low-amplitude cusps do point upward. The lobe portions of

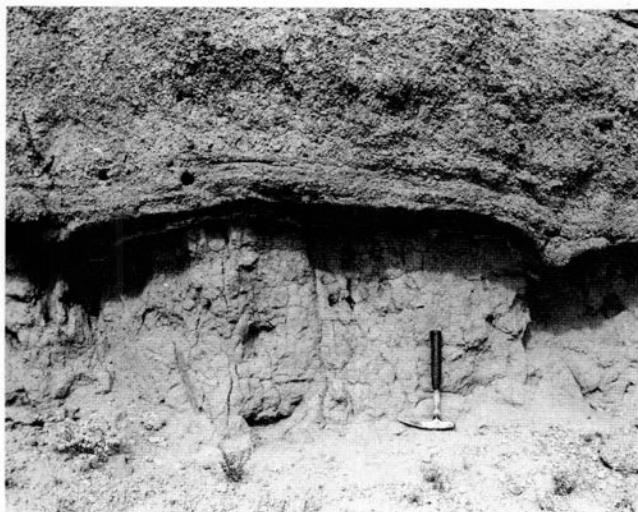


FIGURE 1—Example of cuspate-lobate folds developed along interface between fine-grained alluvium (lower) and ash/tephra sequence (upper) at Los Lunas volcano. Note changes in cusp amplitude and peakedness along bedding surfaces in volcanoclastic sediments. Hammer handle is approximately 33 cm long.

the folds are somewhat flat, similar to a theoretical pattern consisting of a positive first waveform and a negative second waveform (Johnson and Pfaff, 1989, p. 128). Cusp amplitude and peakedness both decrease along the ash and tephra contacts above the alluvium. In addition to the prominent cuspate-lobate folds, the interface is also folded into a gentle syncline with a wavelength on the order of 10^2 m, and cut by two small thrust faults with shortening of 0.19 and 0.48 m. The distribution of 54 fold wavelengths, measured by stretching a tape between adjacent cusps, has a fairly strong central tendency (Fig. 2), with an arithmetic mean of 1.78 m and a standard deviation of 0.76 m.

Conclusions

The existence of both cuspate-lobate folds and small thrust faults shows that the sedimentary contact described in this paper has been shortened significantly, and cusp orientation shows that the alluvium was from one to ten times more competent than the volcanoclastic sediments during deformation. If mass was conserved during shortening, the thickness of the stratigraphic section must also have grown proportionally. Although measurements of arc length are more appropriate for preferred wavelength studies (Sherwin and Chapple, 1968), straight-line cusp-to-cusp measurements are much easier to collect and provide a useful first approximation of wavelength distribution. Because neither theory nor experiment predict the existence of a preferred wavelength for cuspate-lobate folds along a single interface, we are faced with two alternative explanations for our observation of somewhat uniform wavelength. First, the cuspate-lobate folds could represent the amplification of pre-existing perturbations along the interface, for example ripple marks. Second, it is possible that a preferred wavelength

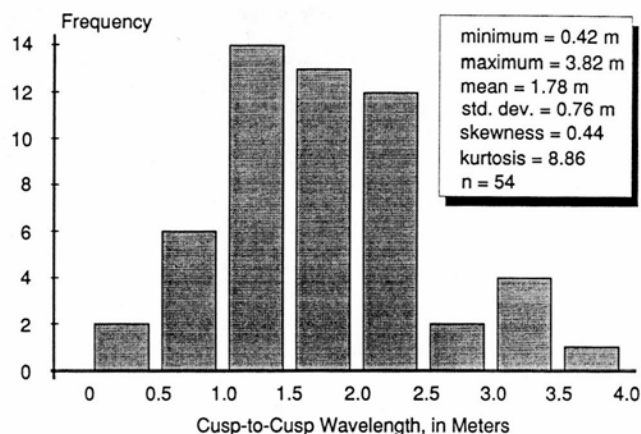


FIGURE 2—Histogram and sample statistics of cusp-to-cusp wavelengths of 54 cuspate-lobate folds measured at Los Lunas volcano.

evolved because the sediments on one or both sides of the interface behaved as finite layers, for which dynamic instabilities will arise. Smith (1975), for example, suggests that many cuspate-lobate folds along single interfaces in the field are actually the erosional remnants of a finite layer with cuspate-lobate folds along both interfaces. At present, meager knowledge of the depositional and deformational history of these sediments does not allow either of these explanations to be favored over the other. It is hoped, however, that detailed mapping and mechanical analysis will provide a better understanding of the exceptional structures at Los Lunas volcano.

Acknowledgments

This work was supported by the New Mexico Bureau of Mines & Mineral Resources. David Love introduced me to a number of structural problems along the flanks of Los Lunas volcano, assisted with wavelength measurements, and, along with John Hawley, read drafts of this contribution.

References

- Fletcher, R. C., 1982, Analysis of the flow in layered fluids at small, but finite, amplitudes with application to mullion structures: *Tectonophysics*, v. 81, pp. 51-66.
- Johnson, A. M., and Pfaff, V. J., 1989, Parallel, similar and constrained folds; in Johnson, A. M., Burnham, C. W., Allen, C. R., and Muehlberger, W. (eds.), *Richard H. Jahns Memorial Volume: Engineering Geology*, v. 27, pp. 115-180.
- Ramsay, J. G., and Huber, M. I., 1987, *The techniques of modern structural geology*, Vol. 2: *Folds and fractures*: Academic Press, London, 700 pp.
- Sherwin, J., and Chapple, W. M., 1968, Wavelengths of single layer folds: a comparison between theory and observation: *American Journal of Science*, v. 266, pp. 167-179.
- Smith, R. B., 1975, Unified theory of the onset of folding, boudinage, and mullion structure: *Geological Society of America, Bulletin*, v. 86, pp. 1601-1609.
- Smith, R. B., 1977, Formation of folds, boudinage, and mullions in non-Newtonian materials: *Geological Society of America, Bulletin*, v. 88, pp. 312-320.
- Sokoutis, D., 1990, Experimental mullions at single and double interfaces: *Journal of Structural Geology*, v. 12, pp. 365-373.

mated with the log data. As shown, an exponential model with a correlation length of approximately 40 cm was fitted to the data.

The results of the CH-I study, not shown here (see Davis, 1990), indicate that the permeability data are also log-normally distributed. In this case, a nested exponential model was fitted to the horizontal variogram. The nested structure is attributed to the two different lithologies present in the CH-I outcrop.

Our preliminary analysis suggests that the upper part of the Sierra Ladrones exposed along the Llano de Albuquerque escarpment is the product of deposition of the ancestral Rio Grande and its tributaries to the west. The patterns of permeability appear to coincide well with the mappable geologic features. Ultimately, we hope to develop a means of quantifying patterns of permeability using sedimentologically based models.

This work is being funded by the U.S. Department of Energy, Subsurface Science Program.

References

Allen, J. R. L., 1974, Studies in fluvial sedimentation: Implications for

- pedogenic carbonates units, Lower Old Red Sandstone, Anglo-Welsh outcrop: *Geological Journal*, v. 9, pp. 181-208.
- Davis, J. M., 1990, An approach for the characterization of spatial variability in the Sierra Ladrones Formation, Albuquerque Basin, central New Mexico: Unpublished MS thesis, New Mexico Institute of Mining & Technology, Socorro, 137 pp.
- Gile, L. H., Peterson, F. F., and Grossman, R. B., 1966, Morphological and genetic sequences of carbonate accumulation in desert soils: *Soil Science*, v. 101, pp. 347-360.
- Goggin, D. J., Thrasher, R., and Lake, L. W., 1988, A theoretical and experimental analysis of minipermeameter response including gas slippage and high velocity flow effects: *In Situ*, v. 12, pp. 79-116.
- Kraus, M. J., and Bown, T. M., 1986, Paleosols and time resolution in alluvial stratigraphy; Chapter 6 in Wright, V. P. (ed.), *Paleosols: Their recognition and interpretation*: Princeton University Press, Princeton, New Jersey, pp. 180-207.
- Machette, M. N., 1978a, Geologic map of the San Acacia quadrangle, Socorro County, New Mexico: U.S. Geological Survey, Geologic Quadrangle Map GQ-1415, scale 1:24,000.
- Machette, M. N., 1978b, Preliminary geologic map of the Socorro 1°x 2° quadrangle, central New Mexico: U.S. Geological Survey, Open-file Report 78-607.
- Machette, M. N., 1985, Calcic soils of the southwestern United States: *Geological Society of America, Special Paper 203*, pp. 1-21.
- Miall, A. D., 1985, Architectural-element analysis: A new method of facies analysis applied to fluvial deposits: *Earth Science Reviews*, v. 22, pp. 261-308.

Effect of climatic change on Estancia Valley, New Mexico: Sedimentation and landscape evolution in a closed-drainage basin

Bruce D. Allen

Department of Geology, University of New Mexico, Albuquerque, New Mexico 87131

Introduction: Estancia Valley as a climatic—hydrologic model

For over 80 years, Estancia Valley in central New Mexico has attracted the attention of geologists and hydrologists interested in the basin's natural history. The first comprehensive study of the basin was conducted by O. E. Meinzer during the summer of 1909. Meinzer's primary task was to report on the feasibility of ground-water irrigation in Estancia Valley. He also assisted in the classification of land under the homestead act. Meinzer (1911), in just six weeks of field work, produced a classic paper which provided a conceptual model of the interplay between geology, climate, and hydrology. Meinzer's paper also contained an extensive description of the geomorphic and stratigraphic evidence for an ancient lake in Estancia Valley.

Subsequently, Antevs (1935, 1954) and Leopold (1951) refined the evidence for past climatic changes in Estancia Valley and formulated relationships between specific climatic variables and the hydrologic balance in the topographically closed basin. Their objective was to derive estimates of glacial-age climate for this region by using semi-quantitative models that were constrained by the evaporative surface area represented by the preserved shorelines of ancient Lake Estancia. Estancia Valley was well suited for this exercise because the absence of mountain glaciers in the Estancia drainage basin during the late Pleistocene eliminated a complicating factor (the storage of precipitation as ice and its delayed release as meltwater) that was present in many of the Great Basin "pluvial" lake basins. Antevs

and Leopold concluded that climate during the last glacial maximum was both wetter and colder than today.

Since these pioneering efforts, several researchers have derived other estimates of paleoclimate for the Estancia area by using different initial assumptions (see review in Smith and Anderson, 1982). The intent of this paper is not to determine which of these climatic estimates is most correct, but to provide a brief description of the geologic evidence for hydrologic—climatic change in the area for the time interval from the last glacial maximum to the present. The discussion of the late Pleistocene lacustrine stratigraphic record is based on the author's ongoing research. Geomorphic records in the Estancia Valley provide the primary evidence for changes in the Holocene.

Hydrogeologic setting

Estancia Valley (Fig. 1) lies in the Sacramento section of the Basin and Range physiographic province, which is transitional to the Great Plains physiographic province to the east (Hawley, 1986). Playa lakes currently occupy an extensive complex of nearly 100 deflation basins that are cut into the valley floor in the southern part of the basin. Topographic closure between the valley floor (1852 m) and the sill with the Pinos Wells basin to the southeast is about 80 m. The Manzano Mountains, which form the western margin of the basin, exhibit the highest elevations, with peaks of over 3050 m. Paleozoic marine and terrestrial strata dip gently eastward into the Estancia Valley from the Manzano Mountains and occur at depth under most of the basin (Smith,

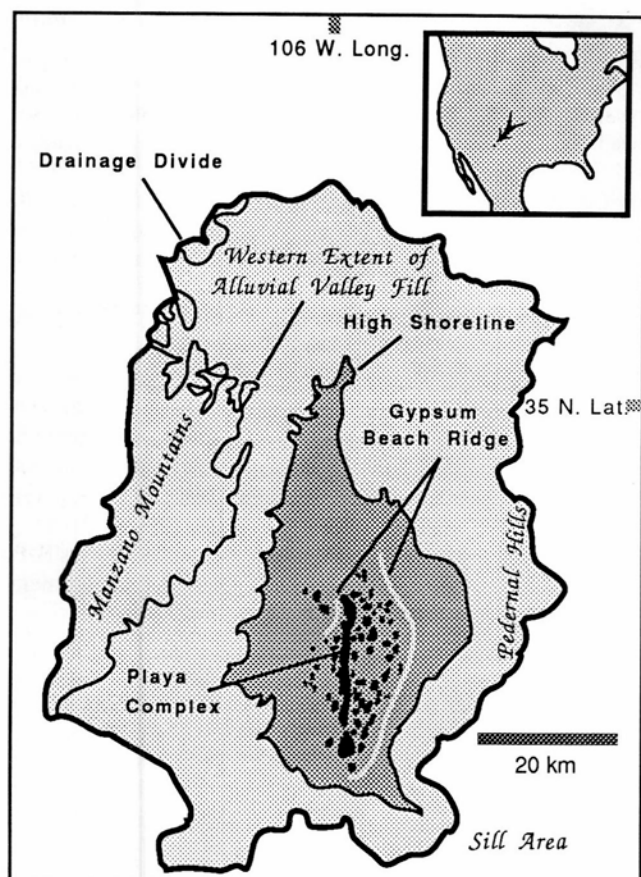


FIGURE 1—Index map of Estancia Valley in central New Mexico.

1957). Precambrian crystalline rocks of the Pederal Hills are exposed on the eastern drainage divide, where elevations are less than 2285 m.

Most geologists working in the area, beginning with Darton (1928), surmised the existence of a north—south-trending fault zone that downdrops Estancia Valley along its eastern margin. Smith (1957) and subsequent workers, citing the apparent absence of Paleogene strata in the valley fill, have suggested that formation of the modern basin was related to late stages in the development of the Rio Grande rift.

Smith (1957) divided the sequence of unconsolidated sediments in Estancia Valley into the alluvial "valley fill," which he considered to be of late Pliocene(?) and Pleistocene age, and younger "lake and dune deposits." The combined thickness of the basin-filling sediments is over 122 m in the axial portion of the basin (New Mexico State Engineer Office, 1967), becoming thinner towards the margins and overlapping Paleozoic bedrock at an elevation of approximately 2010 m along the eastern slope of the Manzano Mountains (Fig. 1).

The sediments of the alluvial valley fill form a large aquifer that is utilized for irrigation on the western side of the basin. Recharge to the aquifer is derived principally from precipitation at higher elevations, especially in the Manzano Mountains (DeBrine, 1971). A map of the total dissolved solids in the Estancia ground-water basin (New Mexico Engineer Office, 1965) reveals a pattern of concentric contour lines that converge along the axis of the basin, where several of the modern playas seasonally precipitate halite.

The pattern of increasing solute load towards the center of the basin suggests that little ground water is presently

lost from the Estancia basin through shallow subsurface flow, although it is reasonable to assume that some leakage and deep interbasin flow occurs through the Paleozoic carbonate strata underlying the basin (Jenkins, 1982). DeBrine (1971) monitored hydrologic and climatic conditions at one of the Estancia playas for two years and estimated that 33 to 45 million m³ of ground water is evaporatively discharged from the playas each year, assuming negligible subsurface leakage.

A substantial contribution to the volume of Lake Estancia in the late Pleistocene must have been provided by groundwater discharge. The area of the drainage basin, and especially the recharge area, was quite small with respect to the area of the lake (Fig. 1). The combination of continuous ground-water discharge and a large evaporative surface area produced a lake which rose and fell dramatically during the late Pleistocene, but not to the point of complete desiccation and deflation. As a result, sedimentation in the ancient lake basin was essentially uninterrupted and combined hydrologic and climatic sensitivity with a continuous stratigraphic record.

Stratigraphic and sedimentational expression of climatic change

Lacustrine sediments

Up to 10 m of the lacustrine sequence is exposed in the walls of the numerous deflation basins in the southern part of the basin (Fig. 1). Examination of water-well cuttings and well logs from the southern part of the basin by Titus (1969) suggests that the lacustrine sequence may be more than 30 m thick, with an interbedded quartz-sand interval ("medial sand") occurring at a depth of about 18 m. The discussion here is limited to the upper part of the exposed lacustrine sequence, which includes the interval deposited during the last glacial maximum. Bachhuber (1989) discusses the stratigraphy of the entire exposed sequence.

Sediments deposited in Lake Estancia consist primarily of carbonate-rich clay and gypsum silt and sand. The larger gypsum grains are morphologically similar to "type II" and "type IV" lenticular gypsum crystals grown by Cody and Cody (1988) under analog saline terrestrial conditions, and commonly show evidence of abrasion. The size, shape, and mechanical weathering of the gypsum grains suggest that they grew in muddy areas around the margin of the lake where they were exposed, sorted, and eventually carried into the lake. A marginal gypsum source area implies that stratigraphic variations in gypsum content reflect past fluctuations in: (1) the areal extent of the mudflats and their proximity to the basin center (a function of lake area), and (2) the amount of wind and wave energy available for transport from marginal areas to the basin center (a function of wind intensity). The proportion of gypsum, carbonates, and clays in the lake sediments, whose distribution was controlled by the rise and fall of the lake and fluctuations in wind intensity, underwent significant change that can be recognized at all time scales.

Evidence for millennial-scale climatic cycles

Two major sedimentary facies can be recognized in the exposed lake sequence, a laminated facies and a non-laminated (bioturbated) facies. The two facies alternate vertically on a scale of decimeters to meters. The absence of delicate sedimentary structures in the non-laminated facies

is due to burrowing activity, probably by aquatic oligochaete worms, as indicated by the size and shape of infilled burrows. Most aquatic oligochaetes are able to thrive in low concentrations of dissolved oxygen (Pennack, 1989), suggesting that changes in salinity and presumably lake level, rather than disaerobic conditions, were principally responsible for the elimination and introduction of bioturbating organisms. The presence of fossil trout (*Oncorhynchus clarki*) and freshwater mollusks and ostracodes in bioturbated intervals (Bachhuber, 1971, 1989) supports the hypothesis that the bioturbated facies developed with freshening of the lake. Decimeter- and meter-scale alternations between laminated and bioturbated sediments are therefore thought to reflect changes in the balance between inflow and evaporation, water depth, and surface area of Lake Estancia.

The upper 5 m of the lacustrine sequence consist of two such bioturbated intervals and two laminated intervals (Fig. 2), which can be correlated across the central part of the lake basin. Radiocarbon dates from the lacustrine sequence (V. Markgraf, pers. comm. 1988; Bachhuber, 1989; this study) indicate that these major facies changes reflect fluctuations in lake volume and area that occurred over 2 to 4 kyrs.

Three radiocarbon dates obtained from bulk sediment samples were not used in establishing a chronostratigraphy for the Estancia sequence. Microscopic examination of the bulk material represented by unaccepted radiocarbon dates

"A" and "C" (Fig. 2; 9830 ± 240 and $13,450 \pm 170$ yrs B.P., respectively) revealed the presence of rootlet tubes, suggesting that contamination by modern organic material may be reflected in the dates obtained from these samples. Another sample, collected from sediments deposited during a saline phase near the top of a laminated interval, yielded a radiocarbon date of $15,410 \pm 650$ yrs B.P. Thompson et al. (1990) note anomalously old radiocarbon dates from dispersed organic material deposited during saline phases of lakes in the Great Basin, and a similar association may be responsible for what appears to be an anomalously old date for the Estancia material (date "B" in Fig. 2).

The lower bioturbated interval (Fig. 2) was deposited during a highstand of the lake that was contemporaneous with the last glacial maximum. A 2 m sequence of laminated sediments above the glacial-maximum sediments indicates a substantial decrease in the size of Lake Estancia about 15,000 yrs B.P. A progressive lowering of lake level during the deposition of the laminated interval near 15,000 yrs B.P. (Fig. 2) is indicated by the upward appearance of sedimentary structures associated with wave/bottom interactions. The upper bioturbated interval represents another highstand near 13,000 yrs B.P. Bioturbated sediments deposited during the last highstand are in turn overlain by laminated sediments that signify a decline in lake area and, ultimately, desiccation of the lake. The timing of the last two major highstands in Estancia Valley is similar to the record of highstands in other dated paleolakes near this latitude in the western U.S. (Allen and Anderson, 1989), including paleo-lakes Mojave, California (Wells et al., 1989), and Cochise, Arizona (Waters, 1989).

Evidence for centennial-scale climatic changes

Centennial changes in lake area and volume are recorded in the stratigraphic section as relative changes in carbonates, clay, and gypsum silt and sand. Relationships between relative changes in carbonates and clay are not yet clear, and the discussion of centennial and decadal changes in this and the following section is limited to gypsum.

Variations in the flux of gypsum during highstands of the lake are represented in the basin center as stratigraphic changes in relative percent of gypsum (Fig. 3). Time-series based on analyses at 2.5 cm contiguous intervals, and using average accumulation rates to extrapolate between radiocarbon dates, reveals significant variability in gypsum flux during highstands of the lake. In the portion of the glacial-maximum sequence deposited between $-18,000$ and $15,800$ yrs B.P., five major episodes of gypsum transport can be recognized, with an average period of about 560 years (Fig. 3A).

Major changes in transport of gypsum to the center of the basin were probably accompanied by contraction and expansion in the area of marginal mudflats and a corresponding rise and fall of lake level. As lake levels rose, an increasing proportion of the marginal mudflats that supplied gypsum silt and sand were inundated, effectively shutting off the supply of gypsum for transport. Conversely, a moderate loss of water volume and a lowering of lake level resulted in large muddy areas exposed to deflation on the relatively flat floor of the basin, producing a source of gypsum silt and sand. Thus, variation in gypsum flux during overall highstands of the lake are believed to represent changes in lake volume and area.

Better age control is needed, but the evidence so far shows

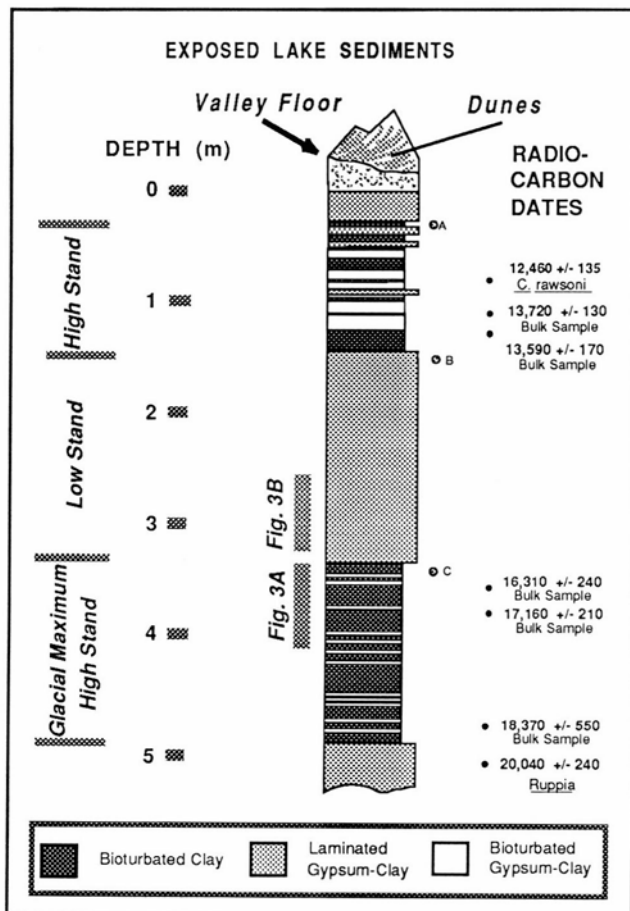


FIGURE 2—Schematic stratigraphic column of upper 5 m of Estancia lake sediments showing radiocarbon dates (V. Markgraf, pers. comm. 1988; Bachhuber, 1989; this study) and position of time-series illustrated in Fig. 4. Unaccepted bulk-sample radiocarbon dates: (A) 9830 ± 240 ; (B) $15,410 \pm 650$; (C) $13,450 \pm 170$.

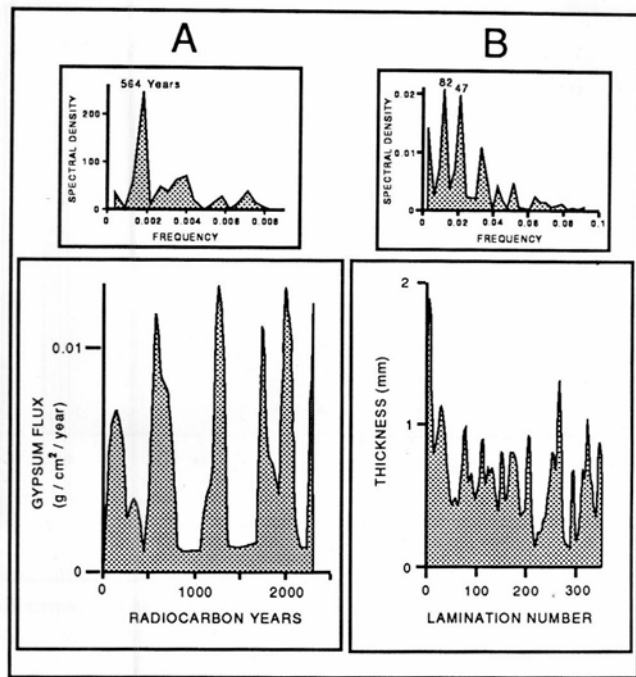


FIGURE 3—Reconstructed time-series from laminated and bioturbated intervals (below) and corresponding power spectra (above). **A**, Time-series from bioturbated interval showing centennial oscillations in gypsum flux. **B**, Time-series from laminated interval showing decadal oscillations in thickness of gypsum laminae. See Fig. 2 for position of time-series.

that cycles in gypsum flux of 100-400 years were recorded shortly after the lake rose to its maximum extent during the last glacial maximum. Later during the glacial-maximum highstand, only longer cycles of 500-600 years were recorded. Oscillations in gypsum flux of less than 200 years are preserved in the highstand sequence near 13,000 yrs B.P.

Evidence for decadal-scale climatic changes

Bioturbating organisms were eliminated from bottom muds near the center of the basin during prolonged lowstands of the lake. As a result, the processes that carried and deposited gypsum silt and sand in the lake left their signature as millimeter-scale structures in the lacustrine sequence. The laminated facies is characterized by discrete, nearly pure layers of gypsum silt and sand which are separated by laminae of carbonate-enriched clay in the upper part of the exposure. If one assumes a fairly constant sedimentation rate during accumulation of the laminated facies, the thickness of successive gypsum laminae provides an approximate measure of changes in gypsum flux at the site of deposition. A smoothed plot of consecutive gypsum laminae thicknesses (Fig. 3B) shows the variability in gypsum accumulation at a particular locality (playa in secs. 29 and 30, T5N, R10E) after the recession of the glacial-maximum lake. A power spectrum of the time-series identifies periods of 47 and 82 laminae.

Interpolation of accumulation rates between radiocarbon dates indicates that the periods of the largest spectral peaks in Fig. 3B correspond to cycles of —50 and —90 years in gypsum flux. This estimate is approximate, but serves to show that variations in the flux of gypsum occurred at all time scales, whereas only lower-frequency changes are preserved in highstand intervals due to disruption of the record by bioturbation. In contrast to highstands, during prolonged

lowstands extensive areas of mudflats were available for the production and transport of gypsum silt and sand. A reasonable interpretation for the millimeter-scale interannual to decadal changes in gypsum flux therefore is that they represent changes in gypsum transport, which ultimately reflects wind intensity, rather than changes in lake area and volume. If this hypothesis is corroborated by additional research, Estancia sediments may provide a rare record of changes in paleo-wind intensity over portions of the last deglaciation.

Geomorphic expression of climatic change

Late Pleistocene shorelines

Meinzer (1911) described the occurrence of numerous wave-cut cliffs, beaches, beach ridges, spits, and bars associated with ancient Lake Estancia. The continuous record of climatic and hydrologic changes is thus supplemented by geomorphic features which provide information about the absolute depth of the lake at various times.

All of the shoreline features described by Meinzer (1911) occur well below the level of the topographic sill (1932 m), suggesting that the lake remained closed throughout its history. Subsequent workers, including Titus (1969), have identified geomorphic features near the elevation of the sill, which are cited as evidence for a lake that overflowed the basin. If these features are lacustrine in origin, then they must be much older than the last glacial-maximum highstand of Lake Estancia (Hawley et al., 1982), as evidenced by the degree of pedogenic-carbonate development in accompanying soils. Bachhuber (1989) suggested that the shorelines in question may correspond to a lake that overflowed the sill during the Illinoian glacial episode, while Hawley (pers. comm. 1990) finds no evidence of overflow in the sill area (Fig. 1) during the Quaternary.

An absolute chronology for the definite Estancia shorelines has not as yet been established, although a reasonable correlation between shoreline groups and the late Pleistocene lacustrine sequence has been proposed by Bachhuber (1989) based upon facies relationships in exposures of littoral lake sediments. The highest shorelines correspond to the glacial-maximum highstand of Lake Estancia and consist of 12 to 14 recessional beaches and associated beach bars (Harbour, 1958). The highest definite shoreline in this group occurs at an elevation of about 1890 m, encompassing an area of 1120 km² ("high shoreline" in Fig. 1). The highest shorelines are fairly well preserved around the entire margin of the lake basin and are associated with the variety of littoral landforms, such as wave-cut cliffs and spits, described by Meinzer (1911). Good exposures of the beach sediments comprising this shoreline group can be found in numerous gravel pits on the western side of the basin.

The highstand of Lake Estancia that occurred near 13,000 yrs B.P. is thought to have reached an elevation of about 1870 m, covering an area of 610 km² (Bachhuber, 1989). Shorelines at this elevation are poorly preserved, possibly because they would have developed on fine-grained sediments deposited during the previous highstand rather than on the alluvial gravels of the higher shorelines. Linear shoreline features are visible on air photos in the southeastern part of the basin at about 1871 m, where a large gravel spit from the glacial-maximum lake extends into the basin.

The lowest distinct shoreline feature in the Estancia Valley consists of a linear beach bar occurring at about 1860 m

(Fig. 1), or 8 m above the valley floor. This feature is composed of gypsiferous material that was clearly derived from numerous small gypsum dunes that postdate the perennial lake. Thus, the gypsum beach bar indicates that a shallow lake reoccupied the basin subsequent to the initial desiccation of Lake Estancia and the formation of the gypsum-dune field.

Ground-water fluctuation and wind activity: the Holocene record

Desiccation of Lake Estancia between 12,000 to 11,000 yrs B.P. is preserved stratigraphically as ~50 cm of homogeneous gypsiferous sediment that overlies and fills in mudcracks that extend into laminated lake sediments at the top of the lacustrine sequence. This white, partially indurated stratum comprises the central floor of the Estancia Valley and marks the level of the water table upon desiccation of the lake.

Two compositionally and genetically distinct dune features rest on the Estancia Valley floor. The first set to develop consists of relatively small dunes (<4 m high) composed of gypsiferous sediment apparently derived from gypsum silt and sand accumulations associated with the desiccation of Lake Estancia. The gypsum dunes were reworked by wave and current action to form the gypsum beach bar at 1860 m. No gypsum-sand dunes occur outside the area circumscribed by the beach bar, suggesting that dune migration may have been halted by the rise in the lake and that subaqueous conditions not only modified the interior dunes into their present, hummocky form, but also stabilized them against further migration.

The second, and most spectacular, dune structures on the valley floor developed during a period of extensive wind deflation of previously deposited lake sediments. The material removed by deflation accumulated along the leeward side of the deflation basins to form a series of large dunes (lunettes) that rise up to 40 m above the valley floor. These large dunes are composed primarily of reworked late Pleistocene lake sediments and contain a much higher proportion of clay than the older gypsum dunes.

Bowler (1973) studied the processes responsible for clay pelletization, deflation, and the formation of clay dunes, and among other factors cites the necessity of strong seasonality in temperature, a saline environment, and the presence of water at or near the surface. The formation and deflation of clay pellets in the Estancia playas is no longer occurring on a large scale, although the requirements of shallow, saline water are met, suggesting that the clay dunes may represent past periods of stronger seasonality and higher summer temperatures.

Cursory examination of the blowouts and their associated clay dunes indicates that deflation may have proceeded during at least two distinct episodes, as evidenced by large-scale truncation surfaces that cut both earlier clay dune deposits and the late Pleistocene lake sediments. An additional feature of the Estancia blowouts, as noted by Meinzer (1911), is the common presence of a well-developed bench occurring a few meters above the level of the modern playa floors. This feature may represent a gradation to base level during a brief lake stand between episodes of deflation or subsequent to deflation. Since the period of wind deflation, 1 to 2 m of aggradation and accumulation of playa sediments has occurred on the floors of the blowouts, signifying a net rise in the water table in the area of the playas.

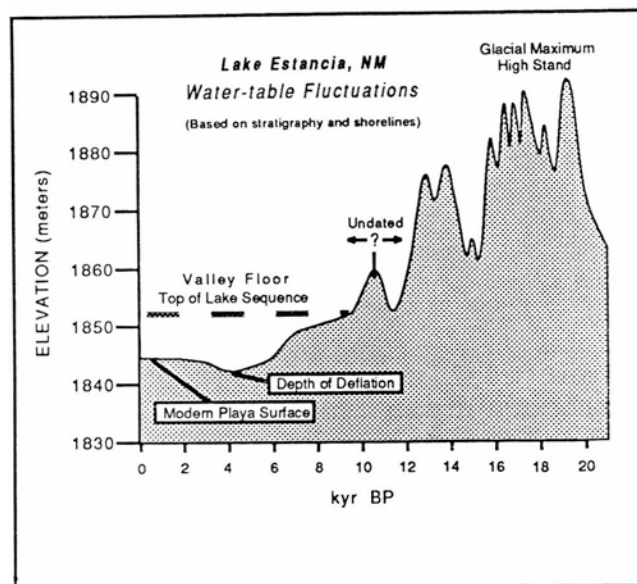


FIGURE 4—Preliminary lake-level and water-table curve for the past 20 kyrs, Estancia Valley.

Very little is known about the absolute timing of the post-glacial geomorphic evidence for climatic and hydrologic change that exists in Estancia Valley. Inferred changes in the water table for the past 20 kyrs are depicted diagrammatically in Fig. 4, which assumes that: (1) the brief lake stand represented by the gypsum beach bar occurred shortly after desiccation of Lake Estancia, and (2) deflation occurred primarily in the mid-Holocene. The timing and magnitude of the inferred ground-water fluctuations, and the shape of the curve in Fig. 4, will undoubtedly change somewhat as more dates and further geological information become available.

Acknowledgments

Support for my research in Estancia Valley has been provided by the National Science Foundation (grant EAR-8903840), the New Mexico Geological Society, and Sigma Xi. I am grateful to L. V. Benson and J. P. Bradbury for their reviews of this manuscript, and to R. Y. Anderson and J. W. Hawley for sharing their thoughts on the Estancia record.

References

- Allen, B. D., and Anderson, R. Y., 1989, Decadal to millennial climatic variability in lacustrine deposits from central New Mexico (abs.): EOS, v. 70, p. 1129.
- Antevs, E., 1935, Age of the Clovis lake clays: Philadelphia Academy of Natural Sciences, Proceedings, v. 87, pp. 304-312.
- Antevs, E., 1954, Climate of New Mexico during the last glacio-pluvial: Journal of Geology, v. 62, pp. 182-191.
- Bachhuber, F. W., 1971, Paleolimnology of Lake Estancia and the Quaternary history of the Estancia Valley, central New Mexico: Unpublished PhD dissertation, University of New Mexico, Albuquerque, 238 pp.
- Bachhuber, F. W., 1989, The occurrence and paleolimnologic significance of cutthroat trout (*Oncorhynchus clarki*) in pluvial lakes of the Estancia Valley, central New Mexico: Geological Society of America, Bulletin, v. 101, pp. 1543-1551.
- Bowler, J. M., 1973, Clay dunes: their occurrence, formation and environmental significance: Earth Science Reviews, v. 9, pp. 315-338.
- Cody, R. D., and Cody, A. M., 1988, Gypsum nucleation and crystal morphology in analog saline terrestrial environments: Journal of Sedimentary Petrology, v. 58, pp. 247-255.
- Darton, N. H., 1928, "Red beds" and associated formations in New Mexico: U.S. Geological Survey, Bulletin 794, 356 pp.

- DeBrine, B. E., 1971, Quantitative hydrologic study of a closed basin with a playa (Estancia Valley, New Mexico): Unpublished PhD dissertation, New Mexico Institute of Mining & Technology, Socorro, 165 pp.
- Harbour, J., 1958, Microstratigraphic and sedimentation studies of an Early Man site near Lucy, New Mexico: Unpublished MS thesis, University of New Mexico, Albuquerque, 111 pp.
- Hawley, J. W., 1986, Physiographic provinces; in *Williams, J. L. (ed.)*, New Mexico in maps: University of New Mexico Press, Albuquerque, pp. 23-27.
- Hawley, J. W., Foster, R. W., Broadhead, R., and Love, D. W., 1982, Road-log segment 1-B: Tijeras Canyon to Abo Canyon via Estancia and Manzano: New Mexico Geological Society, Guidebook 33, pp. 8-24.
- Jenkins, D. N., 1982, Geohydrology of the Madera Group, western Estancia basin, New Mexico: New Mexico Geological Society, Guidebook 33, pp. 361-366.
- Leopold, L. B., 1951, Pleistocene climate in New Mexico: *American Journal of Science*, v. 249, pp. 152-168.
- Meinzer, O. E., 1911, Geology and groundwater resources of Estancia Valley, New Mexico: U.S. Geological Survey, Water-Supply Paper 275, 89 pp.
- New Mexico State Engineer Office, 1965, Chemical characteristics of ground water, Estancia underground water basin: New Mexico State Engineer, Open-File Map.
- New Mexico State Engineer Office, 1967, Thickness of alluvium, valley fill and lake deposits, Estancia underground water basin: New Mexico State Engineer, Open-File Map.
- Pennak, R. W., 1989, Fresh-water invertebrates of the United States: John Wiley and Sons, Inc., New York, 628 pp.
- Smith, L. N., and Anderson, R. Y., 1982, Pleistocene—Holocene climate of the Estancia basin, central New Mexico: New Mexico Geological Society, Guidebook 33, pp. 347-350.
- Smith, R. E., 1957, Geology and ground-water resources of Torrance County, New Mexico: New Mexico Bureau of Mines & Mineral Resources, Ground-Water Report 5, 186 pp.
- Thompson, R. S., Toolin, L. J., Forester, R. M., and Spencer, R. J., 1990, Accelerator-mass spectrometer (AMS) radiocarbon dating of Pleistocene lake sediments in the Great Basin: *Palaeogeography, Palaeoclimatology, Palaeoecology*, v. 78, pp. 301-313.
- Titus, F. B., 1969, Late Tertiary and Quaternary hydrogeology of Estancia basin, central New Mexico: Unpublished PhD dissertation, University of New Mexico, Albuquerque, 179 pp.
- Waters, M. R., 1989, Late Quaternary lacustrine history and paleoclimatic significance of pluvial Lake Cochise, southeastern Arizona: *Quaternary Research*, v. 32, pp. 1-11.
- Wells, S. G., Anderson, R. Y., McFadden, L. D., Brown, W. J., Enzel, Y., and Miossec, J.-L., 1989, Late Quaternary paleohydrology of the eastern Mojave River drainage, southern California: New Mexico Water Resources Research Institute, Report 242, 253 pp.

Summary of recent work on the geomorphology of the upper Rio Puerco

Paula J. Slavin

Department of Geology, University of New Mexico, Albuquerque, New Mexico 87131

Introduction

The Rio Puerco is an entrenched meandering river of high suspended load that heads in the Nacimiento Mountains of north-central New Mexico and flows approximately 250 km to its confluence with the Rio Grande near Bernardo, New Mexico. Many investigators have concentrated on the geomorphology of the lower reaches of the Rio Puerco (Wells et al., 1982; Love and Young, 1983; Love, 1986), but little work has been done on the geomorphology of the upper reaches of the river.

The Rio Puerco, in its northern reaches, encounters the Jemez lineament near the town of San Luis, New Mexico. The Jemez lineament was first defined by the alignment of volcanic features stretching from southwestern Arizona through New Mexico to southeastern Colorado (Mayo, 1958). Subsequent investigations have demonstrated a structural basis for the lineament, suggesting that its roots extend to the mantle and that it may be a reactivated Precambrian feature (Lipman and Mehnert, 1979; Ander, 1980; Lipman, 1980; Aldrich and Laughlin, 1984). The effect of the lineament on the geomorphic development of the Rio Puerco is presently under investigation by the author in partial fulfillment of the requirements for a Master of Science degree at the University of New Mexico. A brief summary of some of this work follows.

The MS thesis study area extends from La Ventana south to Mesa Prieta. Several geomorphic surfaces have been described in the area, ranging in age from approximately 2.2 m.y. to the present. One set of these surfaces is described below.

Rio Puerco volcanic necks

The Jemez lineament in New Mexico is defined by basalt flows and volcanic necks aligned from southwestern to

northeastern New Mexico. In the vicinity of San Luis, the 20 to 30 volcanic necks are collectively termed the Rio Puerco necks. The most famous of these is Cabezon Peak, visible for nearly 100 miles in all directions because of its mammoth size, rising 538 m above the floor of the Rio Puerco.

A comparison of the heights of the Rio Puerco necks above base level (the Rio Puerco's channel) is presented in Fig. 1. It is assumed that the tops of the necks represent former positions of the Rio Puerco valley floor and that the Mesozoic bedrock (shales and sandstones) and alluvial ma-

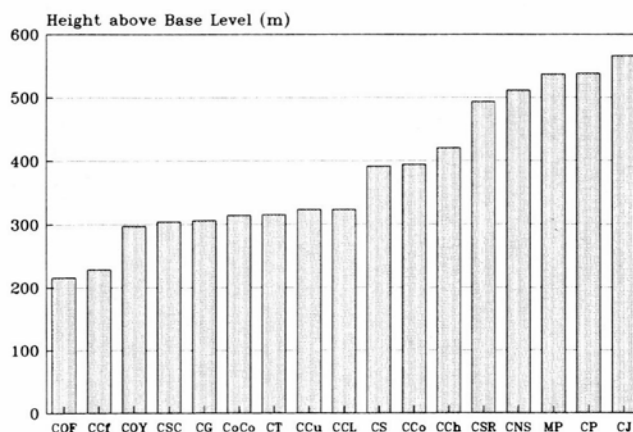


FIGURE 1—Comparison of heights of Rio Puerco volcanic necks above base level. Note four different surfaces at 200 m, 300 m, 400 m, and 500–600 m. Key to names of Rio Puerco necks: COF = Cerro del Ojo Frio, CCf = Cerro Chafó, COY = Cerro Ojo de las Yeguas, CSC = Cerro de Santa Clara, CG = Cerro de Guadalupe, CoCo = Cerrito Cochino, CT = Cerro Tinaja, CCu = Cerro Cuate, CCL = Cerro Chamisa Losa, CS = Cerro Salado, CCo = Cerro Cochino, CCh = Cerro Chato, CSR = Cerro de Santa Rosa, CNS = Cerro de Nuestra Señora, MP = Mesa Prieta, CJ = Cerro de Jacobo, CP = Cabezon Peak.

terial through which the basalt was extruded were subsequently stripped away by the river.

It appears possible that four surfaces (i.e. former valley floors) were developed over time by the Rio Puerco as cut down through its alluvium and Mesozoic bedrock. The highest surface, S_1 , ranging in height from 493 to 566 m (1618-1857 ft) above base level, and defined by Mesa Prieta, Cabezon Peak, and Cerro Jacobo, may be approximately 2.2 m.y. old (Armstrong et al., 1976). The next surface, S_2 , ranges in height from 391 to 420 m (1281-1378 ft) above base level. The most striking surface, S_3 , at approximately 300 m (985 ft) is defined by seven of the 17 Rio Puerco necks examined (e.g. Cerro de Guadalupe, Cerro Tinaja, Cerrito Cochín). It ranges in elevation from 297 to 323 m (974-1060 ft) above base level. The fourth surface, S_4 , is defined on the basis of two necks, and is approximately 200 m (655 ft) above base level. One of the S_4 necks (Cerro Chafo) has been sampled for dating by Frank Perry of the University of New Mexico (results pending). If a date for this neck is obtained, an average incision rate can be calculated for the Rio Puerco from the time of the highest surface to the lowest surface.

Implications for the geomorphology of the Rio Puerco

The Rio Puerco is presently in a phase of incising in its northern reaches. Photographic evidence from the late 1880's indicates that the river has incised up to 15 m (50 ft) in 100 years, an extremely rapid incision rate. Paleochannels within the walls of the river's channel indicate that it has undergone many cycles of cutting and filling. It is possible that the incision of the Mesozoic shales and alluvial material surrounding the Puerco necks was similarly rapid and that an extraordinarily fast base-level change is recorded in the surfaces of the Rio Puerco valley. It is conceivable that 400 m or more (>1312 ft) of bedrock and alluvial material were removed over a very short span of time (i.e. tens of thousands to only thousands of years, based on the above incision rate for the alluvial material eroded over the past 100 years). Even if the erosion of 400 to 500 m (1312-1640 ft) of material has occurred over as much as the last 2.2 m.y.,

these postulated incision rates may force a reconsideration of previously held notions that geologic processes occur slowly over long periods of time.

Acknowledgments

I would like to thank the following people for their support and interest in this project: S. G. Wells, F. V. Perry, C. D. Harrington, L. D. McFadden, L. A. Woodward, D. Love, and J. Hawley. This work has benefitted greatly by financial and material support from the Los Alamos National Laboratory, the New Mexico Geological Society, the Bureau of Land Management, and the University of New Mexico Student Research Allocations Committee.

References

- Aldrich, M. J., Jr., and Laughlin, A. W., 1984, A model for the tectonic development of the southeastern Colorado Plateau boundary: *Journal of Geophysical Research*, v. 89, no. 10, pp. 10,207-10,218.
- Ander, M. E., 1980, Geophysical study of the crust and upper mantle beneath the central Rio Grande rift and adjacent Great Plains and Colorado Plateau: Unpublished PhD dissertation, University of New Mexico, 218 pp.
- Armstrong, R. L., Speed, R. C., Graustein, W. D., and Young, R. L., 1976, K—Ar dates from Arizona, New Mexico, Montana, Nevada, Utah, and Wyoming: *Isochron/West*, no. 16, pp. 1-16.
- Lipman, P. W., 1980, Cenozoic volcanism in the western United States: Implications for continental tectonics; *in* *Continental tectonics*: National Academy of Sciences, Washington, D.C., pp. 161-174.
- Lipman, P. W., and Mehnert, H. H., 1979, Potassium—argon ages from the Mount Taylor volcanic field, New Mexico: U.S. Geological Survey, Professional Paper 1124-B, pp. 131-138.
- Love, D. W., 1986, A geological perspective on sediment storage and delivery along the Rio Puerco, central New Mexico; *in* Hadley, R. F. (ed.), *Drainage basin sediment delivery*: International Association of Hydrological Sciences, Publication 159, pp. 305-322.
- Love, D. W., and Young, J. D., 1983, Progress report on the late Cenozoic evolution of the lower Rio Puerco: New Mexico Geological Society, Guidebook 34, pp. 277-284.
- Mayo, E. B., 1958, Lineament tectonics and some ore districts of the Southwest: *American Institute of Mining Engineers, Transactions*, v. 211, pp. 1169-1175.
- Wells, S. G., Bullard, T. F., Condit, C. D., Jercinovic, J., Lozinsky, R. P., and Laughlin, D. E., 1982, Geomorphic processes on the alluvial valley floor of the Rio Puerco: New Mexico Geological Society, Guidebook 33, pp. 45-47.

Lower and Middle Pennsylvanian stratigraphic relations, type Derryan region, southern New Mexico and westernmost Texas

William W. Clopine¹, Walter L. Manger², Patrick K. Sutherland¹, and David A. Kaiser¹

¹Conoco Inc., P.O. Box 51266, Lafayette, Louisiana 70505; ²Department of Geology, University of Arkansas, Fayetteville, Arkansas 72701;

³School of Geology and Geophysics, University of Oklahoma, Norman, Oklahoma 73019; ⁴Anadarko Petroleum, 211 N. Robinson, Oklahoma City, Oklahoma 73102

Introduction

Thompson (1942) proposed the name Derry as a series to include all rocks between the basal Pennsylvanian System and the Desmoinesian Series in central and south-central New Mexico. At its type section in the Derry Hills (Stop 1), strata of the Derry Series rest unconformably on the Upper Devonian Percha Formation, and Thompson (1942) stated that nowhere in the region was the base of the series conformable. Precise biostratigraphic limits were not assigned to the series, although Thompson (1942, p. 29) stated that unspecified species of the fusulinids *Profusulinella* and *Eoschubertella* could be used to recognize and zone the Derryan below the Zone of *Fusulinella*. He reported *Millerella* and *Ozawainella*(?) from the beds below the first appearance of *Profusulinella*, but he did not discuss the relationship of the base of the Derryan Series to the Morrowan Series. That omission was addressed by assigning the Derryan a post-Morrowan and pre-Desmoinesian age, as part of the Middle Pennsylvanian (Thompson, 1948, p. 69), but the series received little attention outside of New Mexico.

Spivey and Roberts (1946, p. 186) rejected the name Derryan in favor of their new Atokan Series because the type Derryan section was much thinner than typical Atokan strata, although no type section for the Atokan Series was proposed. Moore and Thompson (1949) utilized the names Derryan and Atokan interchangeably to designate the lowest stage of their proposed Oklan Series, but the latter chronostratigraphic unit has been ignored. Subsequently, the Derryan Series has become equated with the Zones of *Profusulinella* and *Fusulinella* and as a synonym of the Atokan (Douglass, 1977). In spite of the failure of the Derryan Series to gain widespread acceptance, its type region in southern New Mexico and westernmost Texas remains a significant reference for Atokan biostratigraphy, particularly based on fusulinids.

This field trip will examine the stratigraphic relations of Morrowan and Atokan strata on the Robledo shelf and Orogrande basin in the type "Derryan" region, with an emphasis on series boundaries. Papers by Clopine, Sutherland, and Kaiser and Manger are included as a supplement to the stop descriptions, to provide additional faunal information. Detailed descriptions of the measured sections comprising the three stops visited on this field trip are available as New Mexico Bureau of Mines & Mineral Resources Open-file Report 373 (Clopine, 1991).

Acknowledgments

The field and laboratory studies upon which this field trip is based were undertaken with the support of National Science Foundation grants EAR-8520684 to Manger and EAR-85171591 to Sutherland. The support of the New Mexico Bureau of Mines & Mineral Resources and the encourage-

ment of Frank Kottowski, Director, are gratefully acknowledged. We also thank Jiri Zidek, New Mexico Bureau of Mines & Mineral Resources, for his help in editing this manuscript and, most of all, for his patience.

Geologic setting

The Early and Middle Pennsylvanian strata under consideration reflect deposition on the broad Robledo carbonate shelf bounded by the Pedernal uplift (east and northeast), Zuni—Defiance arch (northwest), Florida axis (southwest), and Orogrande basin (southeast) (Fig. 1). The axis of the Orogrande basin had a northeast—southwest orientation during Morrowan time (Fig. 2), changing through time to its present north—south orientation. The type Derryan section (Stop 1) lies well onto the Robledo shelf, while the Bishop Cap section (Stop 2) is near the shelf margin and the Vinton Canyon section (Stop 3) lies along the Orogrande basin axis.

Pennsylvanian deposition followed a regional regression and sustained period of erosion. The Helms Formation (Chesterian), dominated by terrigenous clastics, is the youngest pre-Pennsylvanian unit involved with the unconformity and its present distribution is confined to the Orogrande basin. Post-Helms carbonate deposition began with early Morrowan phylloid algal banks and associated mixed skeletal wackestones in the slowly subsiding Orogrande basin. The hiatus at the base of the Pennsylvanian System increases northward, reflecting transgression from that basin. Northward and westward transgression continued through the Morrowan, resulting in the onlap of shallow, subtidal

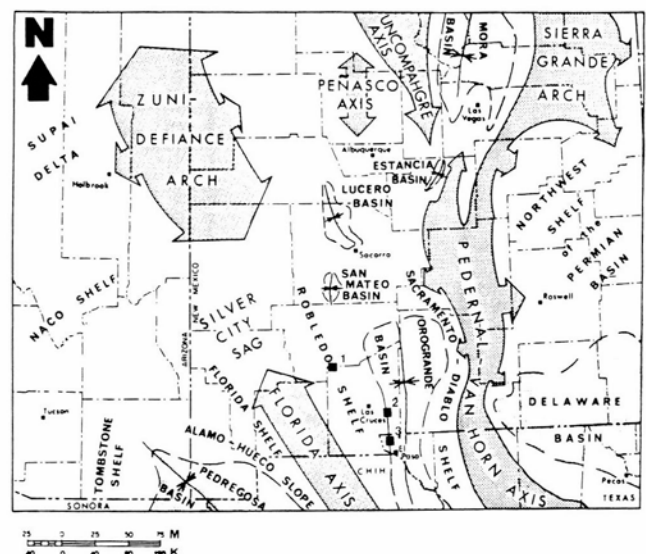


FIGURE 1—Pennsylvanian paleotectonic and geographic map of southwestern New Mexico and adjacent Texas showing location of field trip stops. North-south orientation of Orogrande basin reflects Late Pennsylvanian bias (modified from LeMone et al., 1974).

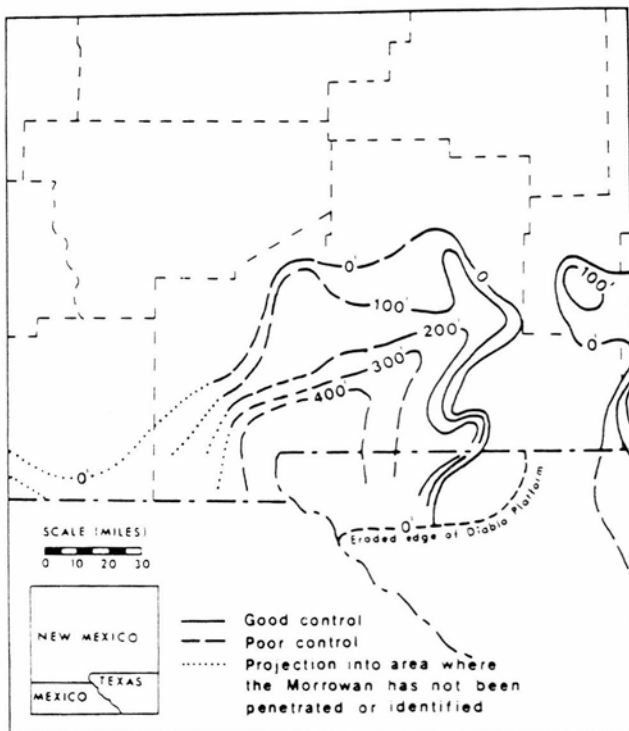


FIGURE 2—Morrowan isopach map of southwestern New Mexico and adjacent areas showing southwest orientation of Orogrande basin in early Pennsylvanian (modified from Connolly and Stanton, 1986).

carbonate-shelf deposits onto progressively older strata. By late Morrowan time, transgression reached the central Robledo shelf, producing the thin algal mudstones and shales at the type Derryan section (Stop 1). Coeval coral and/or *Chaetetes* boundstones developed in the more basinward settings seen at Bishop Cap (Stop 2) and Vinton Canyon (Stop 3). Terrigenous clastic influx was confined to thin quartz sands and silty shales derived from the Pederal uplift, scattered unpredictably through the carbonate sections.

There is no apparent depositional break at the Morrowan/Atokan boundary within the Orogrande basin, but an apparently minor unconformity occupies that position on the basin margin and Robledo shelf (type Derryan section, Stop 1; Bishop Cap section, Stop 2). Continued transgression during the lower Atokan finally covered the Robledo shelf, but relative subsidence rates remained higher in the Orogrande basin, where carbonate deposition kept pace with subsidence. Thus, the lower Atokan Series is represented by a blanket-like sequence of shallow subtidal, intertidal, and supratidal carbonates across the entire shelf. During middle Atokan time, both the Zuni—Defiance arch and Pederal uplift began to contribute terrigenous clastics that resulted in thicker and more frequent shale intervals in the Orogrande basin and central Robledo shelf. Nevertheless, shallow-shelf carbonate deposition continued into Desmoinesian time, with the same pattern of variable subsidence rates reflected by thick sequences in the Orogrande basin and its margin, and thinner sequences on the Robledo shelf.

Lithostratigraphy

Pennsylvanian lithostratigraphy has seen the proposal of a plethora of names, yet little clarification of its relationships; a situation that remains unresolved. Fig. 3 illustrates

the various lithostratigraphic classifications proposed by previous workers in the region.

Gordon (1907) proposed the name Magdalena Group for Pennsylvanian strata exposed in the Magdalena mining district of Socorro County, New Mexico. As defined, it encompassed the entire sedimentary succession in central New Mexico between the Mississippian and Permian Systems. Gordon (1907) incorporated names already used by Herrick (1900) and Keyes (1903) as subdivisions of the Magdalena Group: Sandia Formation for a basal terrigenous clastic unit, and the succeeding Madera Limestone. Needham (1937) rejected the usage of Sandia and Madera as formations on the grounds that they could not be recognized consistently, thus reducing the Magdalena to formational status. He also provided the first account of fusulinids from these rocks in New Mexico.

The terrigenous clastic lithologies developed in the type Magdalena region are absent in the more completely carbonate sequences in southern New Mexico and westernmost Texas. That relationship led Nelson (1940) to subdivide the Magdalena Formation in the northern Franklin Mountains, west Texas, informally into the La Tuna, Berino, and Bishop Cap members (Fig. 3). While no criteria for differentiating those members were provided, later workers, including Thompson (1948), Harbour (1958), Lane et al. (1972), Seager (1973), and Lane (1974), used Nelson's names as either members or formations.

Thompson (1942) rejected all previous lithostratigraphic classifications for the Pennsylvanian strata of central and southern New Mexico because they lacked adequately described boundaries. He proposed a new nomenclature involving one new series, eight new groups, fifteen new formations, and one new member, based mainly on measured sections in the Mud Springs Mountains and Derry Hills, Sierra County, New Mexico (Fig. 3). Type sections for many of Thompson's units were poorly defined and unit boundaries were not clearly differentiated. While Thompson's nomenclature received some limited acceptance (Gehrig, 1958; Kottowski, 1960; King, 1973), none of the subdivisions is currently utilized by the New Mexico Bureau of Mines & Mineral Resources.

Kelley and Silver (1952) argued that Thompson's lithostratigraphic divisions were actually faunal zones and not mappable units. They proposed three new names for Pennsylvanian rocks in the Caballo Mountains, Sierra County, New Mexico, to replace those of Thompson. These are, in ascending order: Red House, Nakaye, and Bar B (Fig. 3). No faunal evidence was used in their definition, formation contacts were poorly defined, and these units have gained little acceptance.

Biostratigraphic studies reported in this volume are based on detailed measured sections (Clopine, 1991), but they have not addressed the problems with lithostratigraphic nomenclature for the Pennsylvanian System. Consequently, formal lithostratigraphic divisions are not employed and all correlations suggested herein are based on biostratigraphic data.

Biostratigraphy

Fusulinids provide the basic biostratigraphic framework for analysis of these Morrowan—Desmoinesian sections in southern New Mexico and westernmost Texas. Clopine (this volume) describes the general biostratigraphic succession, which includes the Zones of *Millerella* (Morrowan),

PENNSYLVANIAN SYSTEM	SERIES	FUSULINID BIOZONE	Gordon 1907	Needham 1937	Nelson 1940	Thompson 1942, 1948	Kelley & Silver 1952				
	PENNSYLVANIAN SYSTEM	Virgilian	Zone of <i>Triticites</i>	Magdalena Group	Madera Limestone	Magdalena Formation	unnamed upper member	Fresnal Group	Bruton Fm.		
Missourian		Keller Group						Moya Formation	Del Cuerto Formation		
		Desmoinesian	Zone of <i>Fusulina</i>				Hansonburg Group	Story Fm.	Burrego Fm.	Bar B Formation	
Veredas Group							Council Spring Limestone	Adobe Formation	Coane Fm.		
		Atokan	Zone of <i>Fusulinella</i>				Sandia Formation	Bishop Cap Member	Bolander Group	Armendaris Group	Garcia Fm.
Morrowan									Zone of <i>Millerella</i>		La Tuna Member
		Green Canyon Group	Fra Cristobal Formation				Apodaca Formation				
										Arrey Formation	

FIGURE 3—Pennsylvanian lithostratigraphic nomenclatorial history in southwestern New Mexico and adjacent areas.

Eoschubertella, *Profusulinella*, *Fusulinella* (Atokan), and *Fusulina* (= *Beedeina*) (Desmoinesian). The Zone of *Profusulinella* may be further subdivided into a lower interval characterized by *P. copiosa*, a middle interval with *P. sp.*, and an upper interval containing *P. munda*. The Zone of *Fusulinella* may be further subdivided into a lower *F. acuminata* and upper *F. devexa* intervals. The fusulinid succession in southern New Mexico and westernmost Texas closely approximates that of the North American midcontinent.

The basal 3.7 ft of the type Derryan section is of Morrowan age based on brachiopods reported by Sutherland (this volume). That conclusion does not conflict with the associated fusulinids. Reports of *Profusulinella* near the base of the type Derryan section (Lane et al., 1972) are reinterpreted to be *Eoschubertella*. The Morrowan/Atokan boundary at type Derryan is an unconformity, which also occurs in the Bishop Cap section. In both sections, the conodont *Diplognathodus coloradoensis*, indicative of upper lower Atokan strata, either occurs with *Eoschubertella* or succeeds its appearance within a few feet.

Fusulinids from the remaining Derryan succession correlate with the midcontinent and indicate equivalence to the Atokan Series. The upper boundary of the type Derryan section falls just below the first occurrence of *Fusulina*, which corresponds to the generally accepted Atokan/Desmoinesian boundary. Conodonts from the Derryan section above the appearance of *Diplognathodus* are dominated by *Idiognathodus* and do not reflect the Atokan/Desmoinesian boundary.

Regional correlations

Figs. 4-6 illustrate correlation of fusulinid zones between the sections examined as stops on this field trip. Fig. 4

documents the northwestward transgression of Morrowan seas from the Orogrande basin and the onlap of progressively younger Morrowan beds on strata of the Robledo shelf, although some consideration must be given to Morrowan/Atokan boundary erosion to explain thinning of Morrowan strata. Figs. 5 and 6 reflect the continued transgression of Atokan and lower Desmoinesian seas that developed the blanket-like character of these strata in the region. Differential subsidence of the Orogrande basin compared to the Robledo shelf is illustrated by comparative thicknesses of the type Derryan section and those at Bishop Cap and Vinton Canyon.

Stop descriptions

Stop 1: Type Derryan section, Sierra County, New Mexico

Location: This section is a roadcut along I-25 located in the Derry Hills, just north of the Dona Ana County line, approximately 0.8 mi east of Derry, New Mexico (sec. 29, T175, R4W, Garfield 7 1/2' quadrangle). This exposure includes Thompson's (1942) section 19.

Significance: Thompson (1942) proposed the section exposed in the draw on the northwest end of this roadcut as the type section for the Derryan Series. The lithologic succession can be easily matched to his description, although the formation names Thompson proposed are not recognizable. Fig. 7 illustrates the general lithologic succession and fusulinid occurrences at this section.

Of particular interest here is the excellent exposure of the basal Pennsylvanian boundary relations. "Derryan" strata rest on sandstone and shale of the Upper Devonian Percha Formation. Basal Morrowan strata comprise approximately

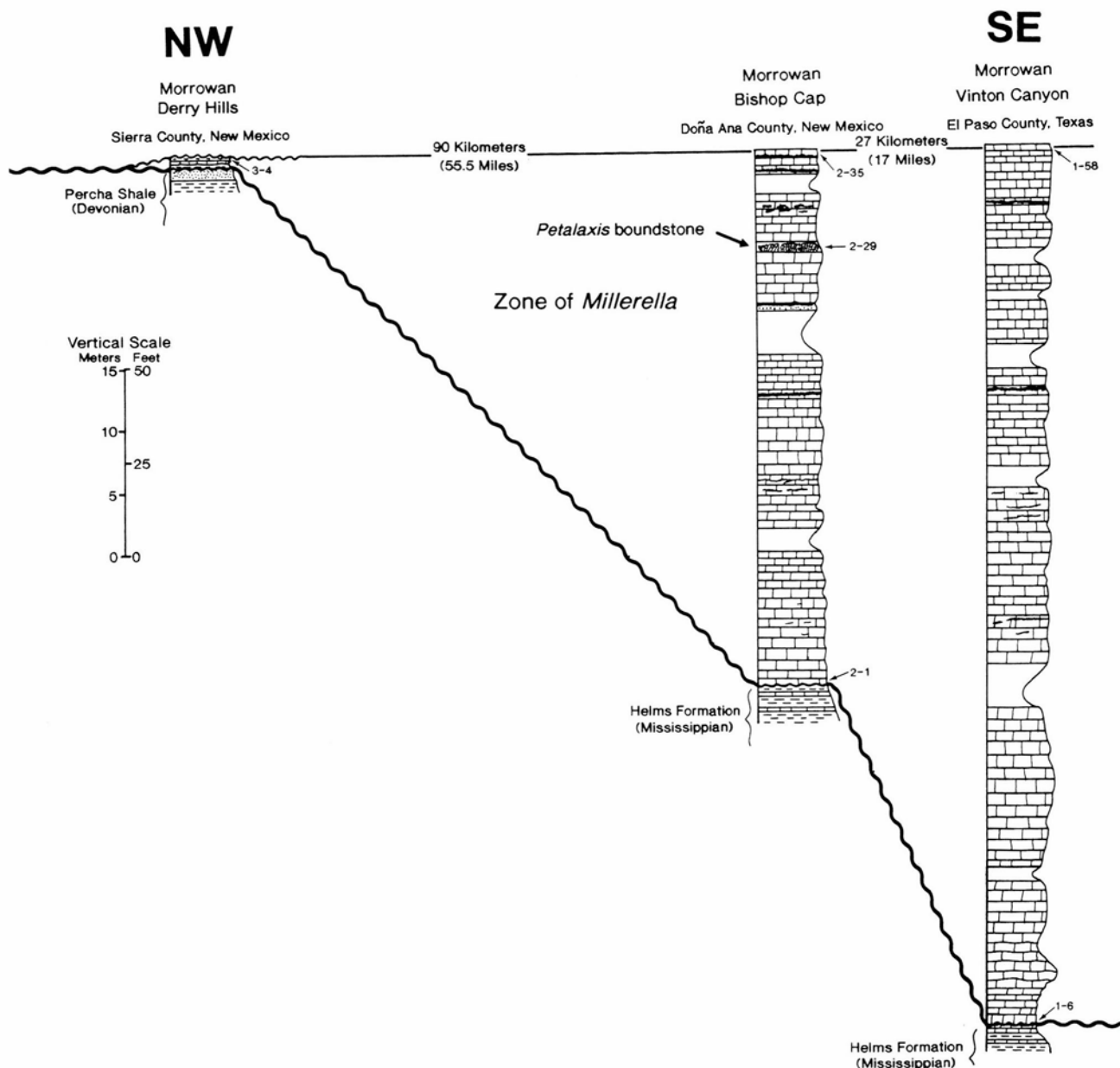


FIGURE 4—Correlation of *Millerella* Zone between type Derryan section and Vinton Canyon. Datum is appearance of *Eoschubertella*.

2 ft of shaly, nodular wackestone grading upward into 1 ft of nodular wackestone. A typical upper Morrowan brachiopod assemblage, including *Zia novamexicana*, *Spirifer goreii*, and *Neochonetes platynotus*, has been recovered from this interval together with nondiagnostic but presumably Morrowan foraminifers (see Clopine, this volume, and Sutherland, this volume).

Above the wackestone, 0.7 ft of gray to tan clay, with fine quartz silt and plant(?) fragments, may represent a paleosol developed at the Morrowan/Atokan boundary. Conodonts from this unit are obviously reworked and include *Idiognathodus* and *Adetognathus*. The light clay is overlain by 0.8 ft of fissile black shale that contains horizontal gypsum laminae and lenses. Cleavage is well developed in the lower clay, but the cleavage planes do not pass through the succeeding black shale. In contrast, the black shale is highly fractured, but the fractures do not correspond to structures continuing from the underlying shale (Fig. 8).

Carbonates succeeding the black shale contain *Diplogna*

thodus and *Eoschubertella*(?). *Profusulinella* appears at the base of unit 23, at a horizon 44 ft above the appearance of *Eoschubertella*(?) and 44.8 ft above the Morrowan/Atokan unconformity. That occurrence is the only *Profusulinella* from the type Derryan. *Fusulinella* appears in unit 25, 85 ft above the base of the section. The Atokan/Desmoinesian boundary, marked by *Fusulina*, appears in unit 60, 125 ft above the base of the section.

The entire type Derryan section is dominated by the *Idiognathodus* biofacies (see Kaiser and Manger, this volume). That taxon was the most frequently occurring element, followed by *Neognathodus*. Recoveries varied from barren, or depauperate to lag concentrations of hundreds of ramiforms, particularly from units 15, 19, 38, and 43.

Stop 2: Bishop Cap section, Dona Ana County, New Mexico

Location: This section is located on the steep north-facing slope of Pyramid Peak, 1 mi north of Bishop Cap, approx-

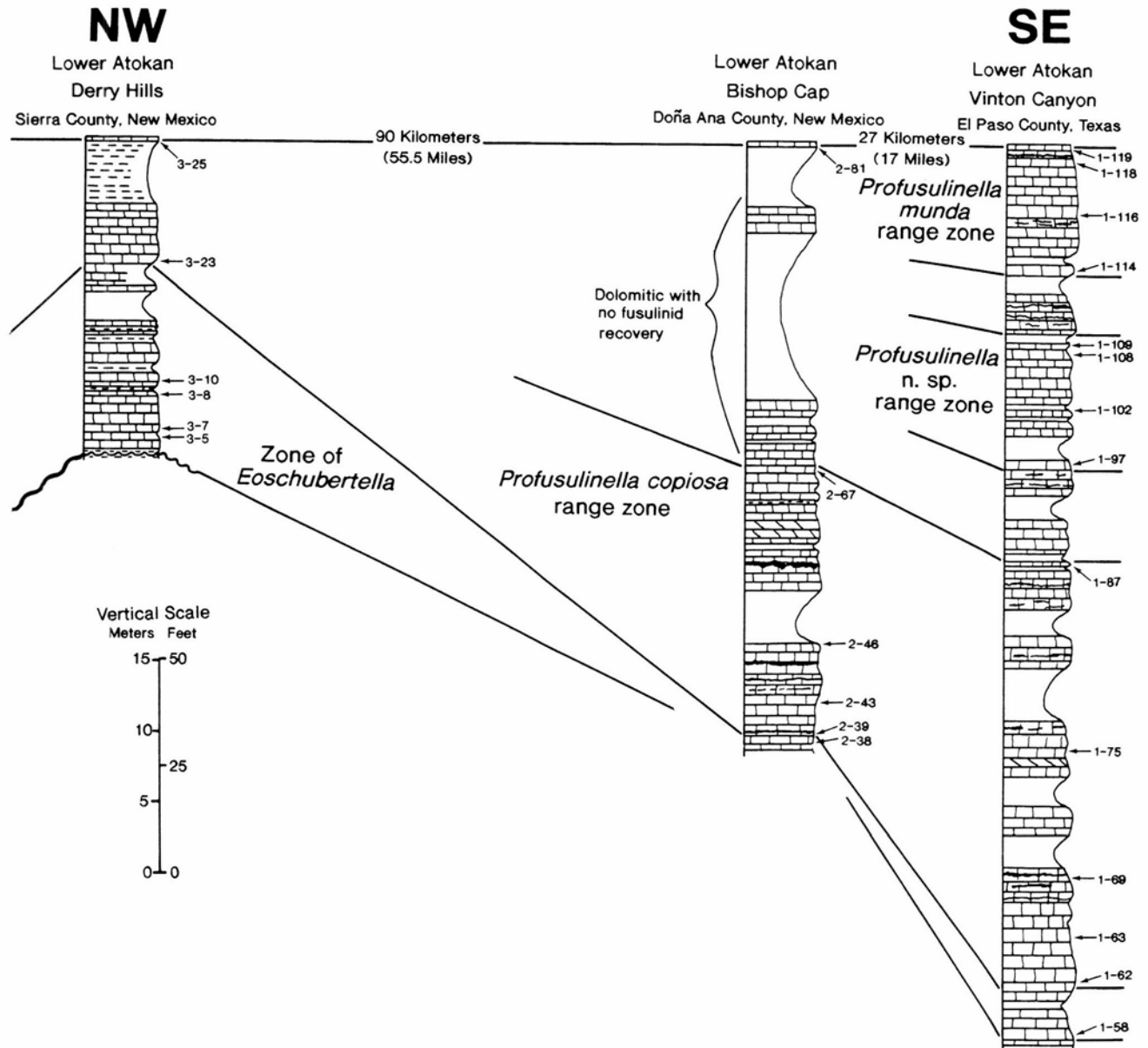


FIGURE 5—Correlation of the Zones of *Eoschubertella* and *Profusulinella* between type Derryan section and Vinton Canyon. Datum is appearance of *Fusulinella*.

imately 15 mi southeast of Las Cruces, New Mexico (sec. 23, T24S, R3E, Bishop Cap 71/2' quadrangle). New Mexico Bureau of Mines & Mineral Resources Geologic Map 29 (Seager, 1973) provides a composite stratigraphic column, geologic history, and geologic map of the area.

Significance: The Bishop Cap section occupied a shelf-margin position, and its thicker sequence of carbonate lithologies tends to be more grain-dominated and fossiliferous than those seen at the type Derryan section (Figs. 9, 10). Corals are particularly common in the lower portion of this section, and of particular interest here is a boundstone of the colonial rugose coral *Petalaxis* (unit 29). Sutherland (1985) noted three other occurrences of *Petalaxis* similar to the one at Bishop Cap: southwestern Ozark region, northeastern Oklahoma; Ardmore basin, south-central Oklahoma; and the Llano uplift, central Texas. All North American midcontinent *Petalaxis* localities seem to fall within the upper Morrowan *Idiognathodus sinuosus* conodont zone and may in fact represent precisely the same age, although the

genus ranges into strata equivalent to the Desmoinesian Series elsewhere. The *Petalaxis* boundstone succeeds an interval with a thin arkosic sandstone (unit 21).

The Mississippian—Pennsylvanian boundary is not particularly well exposed at this locality, but Morrowan conodonts occur through the basal 138 ft of the Bishop Cap section in association with nondiagnostic foraminifers, including *Millerella*. *Diplognathodus coloradoensis* was recovered from unit 35 and the first *Eoschubertella* was found in unit 38, with *Profusulinella* appearing in unit 39, only 1.2 ft higher. Thus, the interval that could possibly represent the zone of *Eoschubertella* is quite thin, and the Morrowan/Atokan boundary is probably an unconformity here as well as at the type Derryan section (Stop 1), since *Diplognathodus* is typical of an upper lower Atokan position.

Fusulinella makes its appearance in unit 81, 283 ft above the base of this section, followed by *Fusulina*, marking the Atokan/Desmoinesian boundary in unit 117, 398 ft above the base of the section. Conodont recoveries from the Mor-

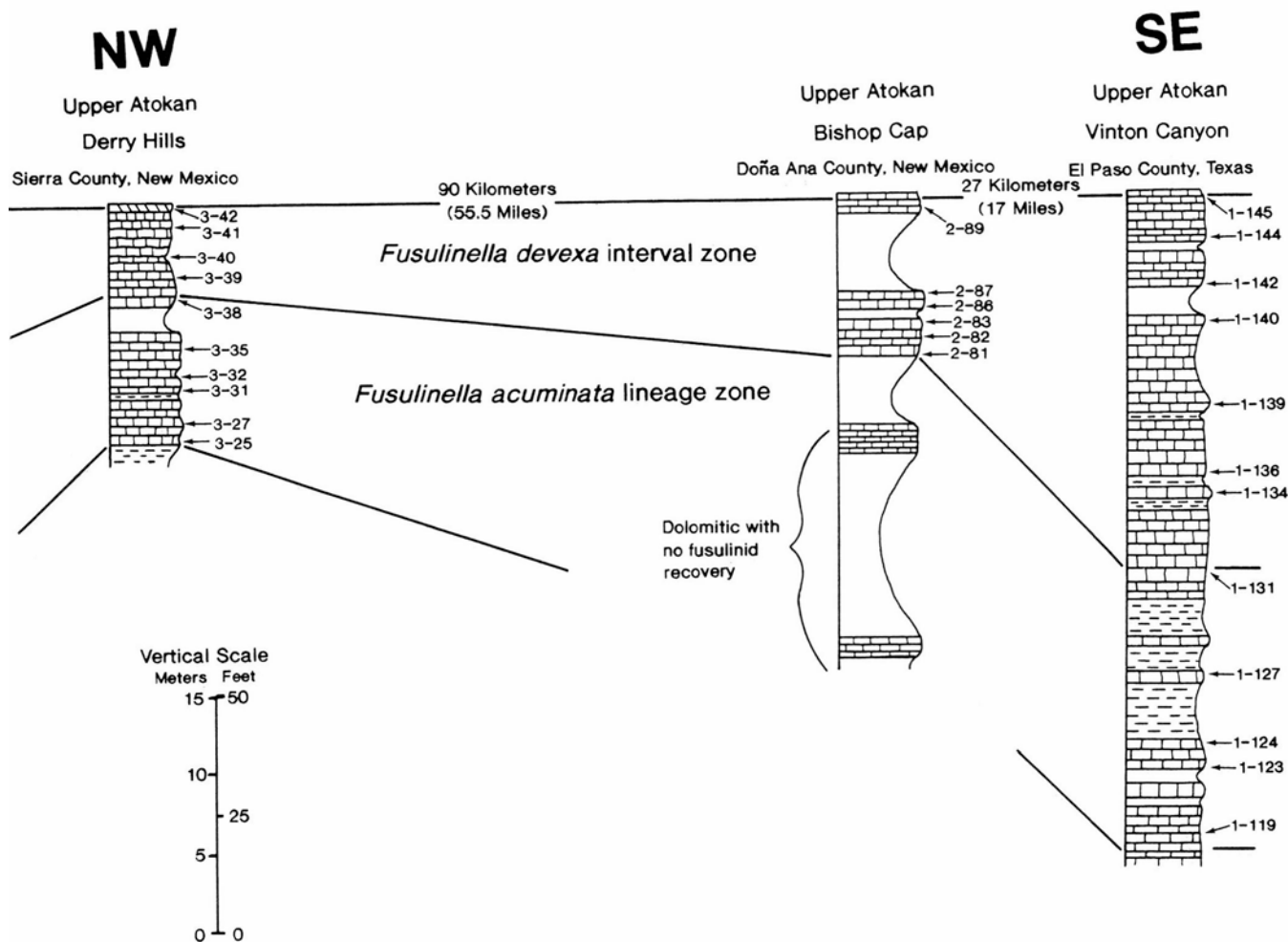


FIGURE 6—Correlation of the Zone of *Fusulinella* between type Derryan section and Vinton Canyon. Datum is appearance of *Fusulina*.

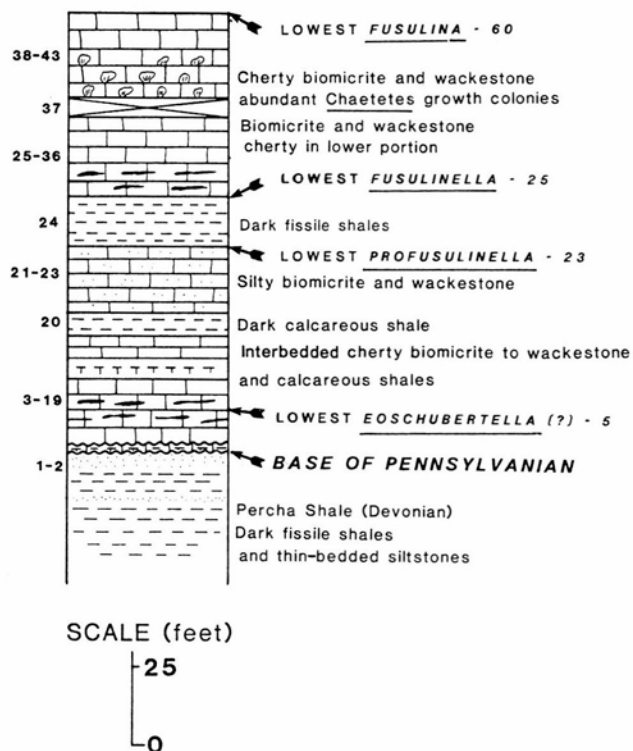


FIGURE 7—Diagrammatic illustration of type Derryan section (Stop 1).

rowan interval are poor, and the *Adetognathus* biofacies dominates that portion of the Bishop Cap section. *Idiognathodus* appears in samples from unit 17, with *Neognathodus bassleri*, but conodonts do not become common until the level of unit 70. From that horizon through the remainder of the Atokan section, lag concentrates of ramiform elements, dominated by *Idiognathodus* and *Neognathodus*, are typical, particularly in units 93, 95, 100, and 111. The *Idiognathodus* biofacies characterizes the Atokan interval at Bishop Cap.

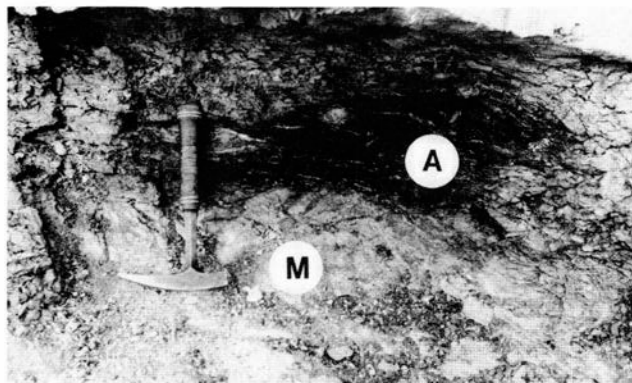


FIGURE 8—Morrowan-Atokan boundary interval at type Derryan section. Gray shale (M) may be paleosol at top of Morrowan interval. Base of Atokan is fissile black shale (A). Brachiopods occur in limestones below gray shale at bottom of photograph.

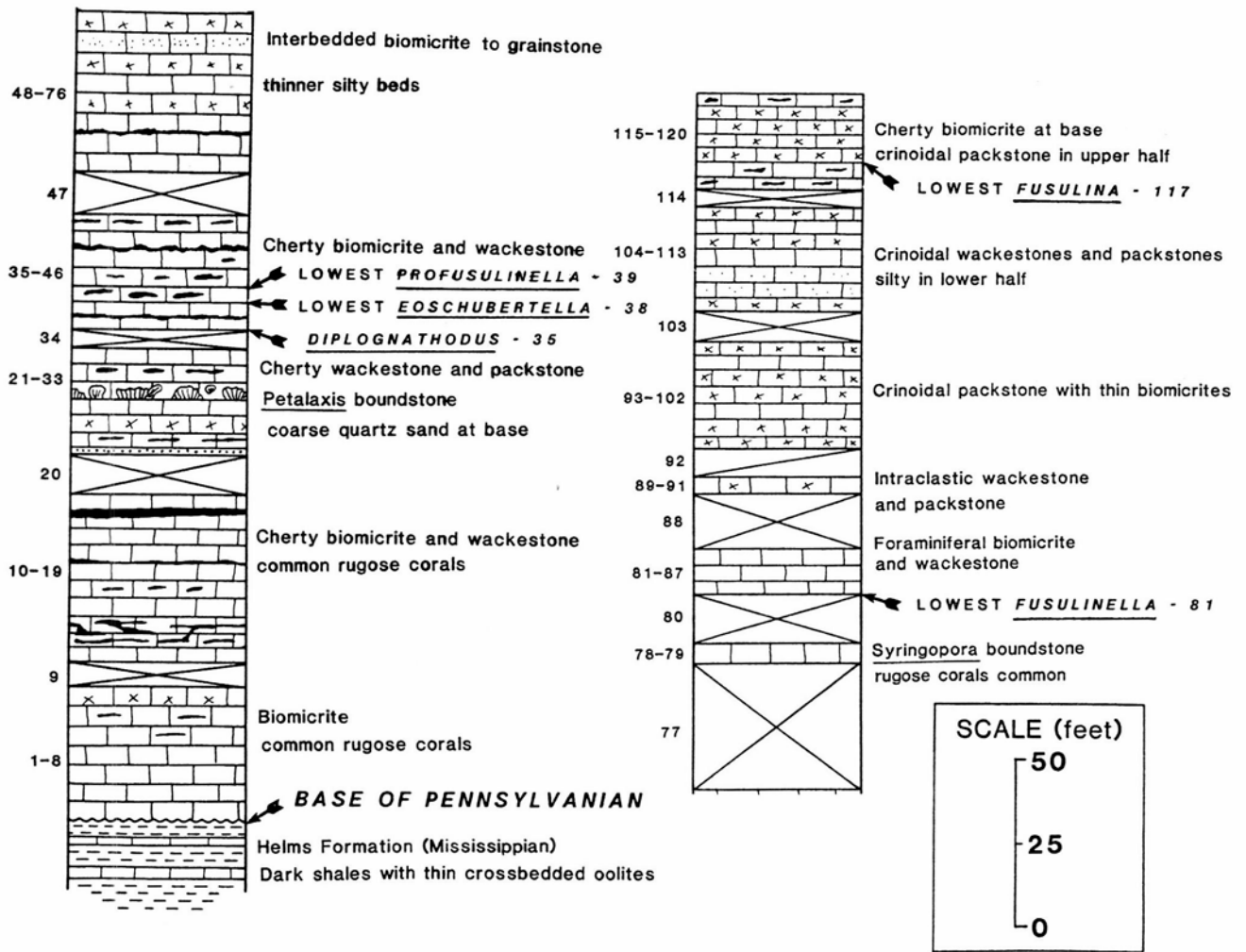


FIGURE 9—Diagrammatic illustration of the section exposed near Bishop Cap (Stop 2).



FIGURE 10—Sequence of carbonate lithologies exposed near Bishop Cap (Stop 2).

Stop 3: Vinton Canyon section, El Paso County, Texas

Location: Vinton Canyon is located on the west side of the northern Franklin Mountains, approximately 23 mi south of Las Cruces, New Mexico, and 15 mi north of El Paso, Texas (Canutillo 7 1/2' quadrangle). Nelson (1940) proposed the La Tuna, Berino, and Bishop Cap members of the Magdalena Formation from the Vinton Canyon section. Lane (1974) included conodont data from this section in his analysis of the wedge-on-wedge relationships in the Mississippian and Lower Pennsylvanian sequences of the region.

Significance: Vinton Canyon preserves the thickest and least variable succession of Pennsylvanian strata seen on the field trip (Fig. 11). The section always occupied a po

sition along the axis of the Orogrande basin. As subsidence kept pace with deposition, Pennsylvanian carbonates are dominated by algal biomicrites, with wackestones being the next best represented lithology; grainstones are thin and rarely developed.

The contact of Pennsylvanian carbonates with the Helms Formation (Chesterian) is particularly well exposed at Vinton Canyon, but its placement is somewhat problematic because of poor fossil recoveries through similar-appearing lithologies. The base of the Pennsylvanian System is placed at the base of unit 6 (Fig. 12).

Morrowan algal biomicrites and wackestones with *Milnerella* and impoverished conodont recoveries extend to the appearance of *Eoschubertella* in unit 58, 246 ft above the base of the Pennsylvanian. *Profusulinella* appears in unit 62, 11 ft higher. Neither fusulinid appearance is accompanied by diagnostic conodonts. No unconformity at the Morrowan/Atokan boundary is indicated or suspected at Vinton Canyon.

The appearance of *Fusulinella* occurs in unit 119, 446 ft above the base of the Pennsylvanian section, followed by *Fusulina* at the Atokan/Desmoinesian boundary in unit 164, 674 ft above the base of the section. Samples processed for conodonts from those levels were essentially barren but contained *Idiognathodus*, suggesting that the Atokan portion of the Vinton Canyon section also falls within the biofacies characterized by that taxon.

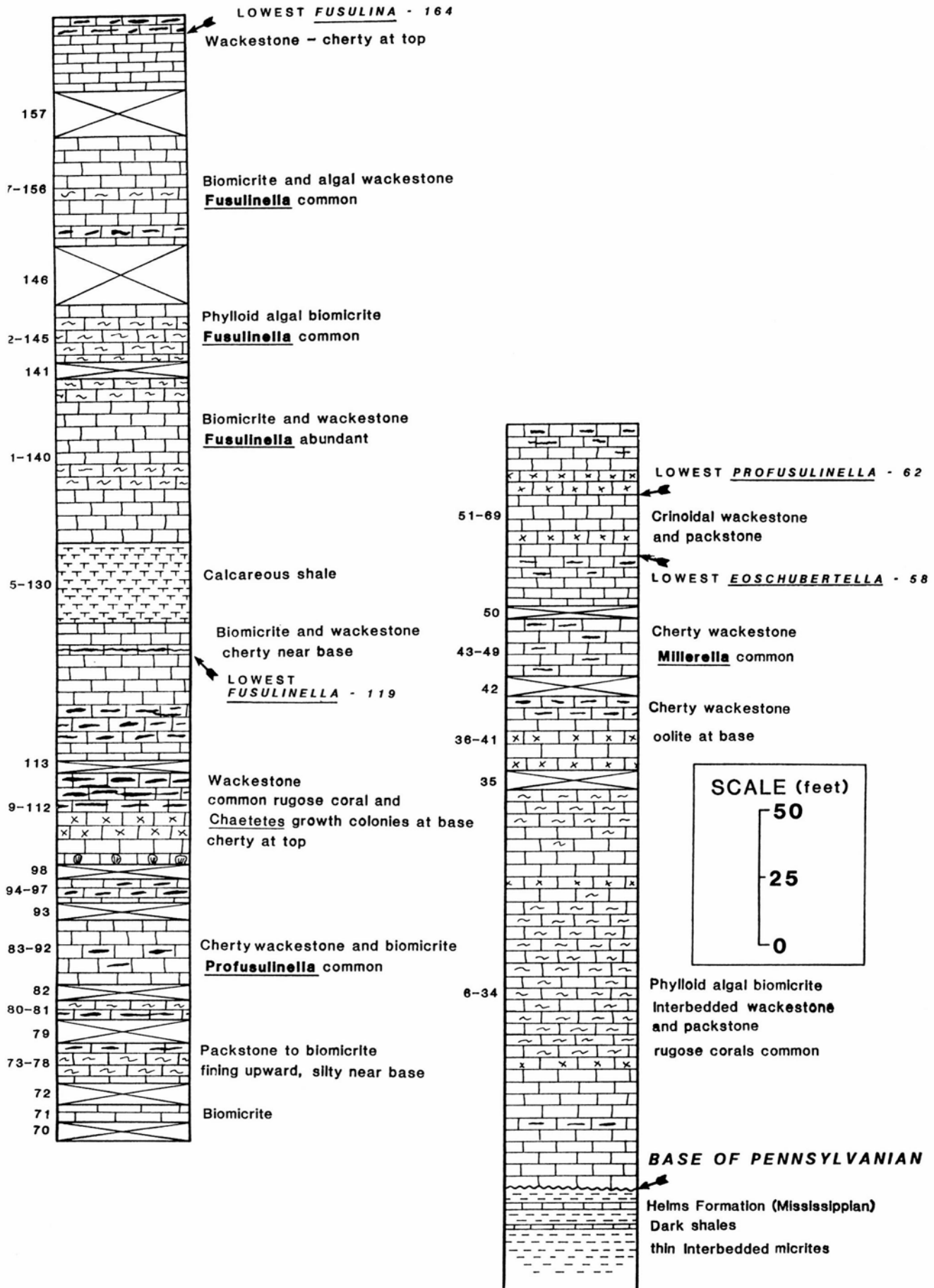


FIGURE 11—Diagrammatic illustration of the section exposed at Vinton Canyon (Stop 3).



FIGURE 12—Mississippian–Pennsylvanian boundary at Vinton Canyon. Mississippian Helms Formation is succeeded by Morrowan strata at bed 6 (arrow).

References

- Clopine, W. W., 1991, Lower and Middle Pennsylvanian measured sections, type Derryan region, southern New Mexico and westernmost Texas: New Mexico Bureau of Mines & Mineral Resources, Open-file Report 373, 121 pp.
- Connolly, W. M., and Stanton, R. J., 1986, Lower Pennsylvanian (Morrowan) sedimentation in the Orogrande Basin; *in* Southwest Section of A.A.P.G., Transactions and guidebook of 1986 Convention, Ruidoso, New Mexico: New Mexico Bureau of Mines & Mineral Resources, pp. 129-142.
- Douglass, R. C., 1977, The development of fusulinid biostratigraphy; *in* Kauffman, E. G., and Hazel, J. E. (eds.), Concepts and methods of biostratigraphy: Dowden, Hutchinson, and Ross, Stroudsburg, Pennsylvania, pp. 463-481.
- Gehrig, J. L., 1958, Middle Pennsylvanian brachiopods from the Mud Springs Mountains and Derry Hills, New Mexico: New Mexico Bureau of Mines & Mineral Resources, Memoir 3, 24 pp.
- Gordon, C. H., 1907, Mississippian (Lower Carboniferous) formations in the Rio Grande Valley: American Journal of Science (4), v. 24, no. 174, pp. 58-64.
- Herrick, C. L., 1900, The geology of the White Sands of New Mexico: Journal of Geology, v. 8, pp. 112-128.
- Harbour, R. L., 1958, Pennsylvanian and Permian rocks in the northern Franklin Mountains, Texas (abs.): Geological Society of America, Bulletin, v. 69, no. 12, pt. 2, pp. 1727-1728.
- Kelley, V. C., and Silver, C., 1952, Geology of the Caballo Mountains: University of New Mexico Publications in Geology, No. 4, 286 pp.
- Keyes, C. R., 1903, Geological sketches of New Mexico: Ores and Metals, v. 12, p. 48.
- King, W. E., 1973, Fusulinids *Millerella* and *Eostaffella* from the Pennsylvanian of New Mexico and Texas: New Mexico Bureau of Mines & Mineral Resources, Memoir 26, 34 pp.
- Kottowski, F. E., 1960, Summary of Pennsylvanian sections in southwestern New Mexico and southeastern Arizona: New Mexico Bureau of Mines & Mineral Resources, Bulletin 66, 187 pp.
- Lane, H. R., 1974, Mississippian of southeastern New Mexico and West Texas: a wedge-on-wedge relation: American Association of Petroleum Geologists, Bulletin, v. 58, pp. 269-282.
- Lane, H. R., Sanderson, G. A., and Verville, G. J., 1972, Uppermost Mississippian-basal Middle Pennsylvanian conodonts and fusulinids from several exposures in the south-central and southwestern United States: Twenty-fourth International Geological Congress, Montreal, sec. 7, pp. 549-555.
- LeMone, D. V., King, W. E., and Cunningham, J. E., 1974, Pennsylvanian System of Chloride Flat, Grant County, New Mexico: New Mexico Bureau of Mines & Mineral Resources, Circular 131, 18 pp.
- Moore, R. C., and Thompson, M. L., 1949, Main divisions of Pennsylvanian period and system: American Association of Petroleum Geologists, Bulletin, v. 33, pp. 275-301.
- Needham, C. E., 1937, Some New Mexico Fusulinidae: New Mexico Bureau of Mines & Mineral Resources, Bulletin 14, 59 pp.
- Nelson, L. A., 1940, Paleozoic stratigraphy of Franklin Mountains, west Texas: American Association of Petroleum Geologists, Bulletin, v. 24, pp. 157-172.
- Seager, W. R., 1973, Geologic map and sections of Bishop Cap-Organ Mountains area: New Mexico Bureau of Mines & Mineral Resources, Geologic Map 29, scale 1:24,000.
- Spivey, R. C., and Roberts, T. G., 1946, Lower Pennsylvanian terminology in central Texas: American Association of Petroleum Geologists, Bulletin, v. 30, pp. 181-186.
- Sutherland, P. K., 1985, The colonial rugose coral genus *Petalaxis* in the Middle Carboniferous of North America and its stratigraphic significance (abs.): Geological Society of America, Abstracts with Programs, v. 17, no. 7, p. 730.
- Thompson, M. L., 1942, Pennsylvanian System in New Mexico: New Mexico Bureau of Mines & Mineral Resources, Bulletin 17, 92 pp.
- Thompson, M. L., 1948, Studies of American fusulinids: University of Kansas Paleontological Contributions, Protozoa, Article 1, pp. 1-184.

Lower and Middle Pennsylvanian fusulinid biostratigraphy in south-central New Mexico and westernmost Texas: A brief review

William W. Clopine

Introduction

Lower and Middle Pennsylvanian strata in southern New Mexico and westernmost Texas include an abundant and, for the most part, well preserved fusulinid fauna. Previous studies of this fauna include those by Thompson (1942a, 1948), Stewart (1970), Lane et al. (1972), King (1973), and Verville and Sanderson (1986). This paper is a brief review of the fusulinid biostratigraphic succession in this region as documented by those studies and by Clopine (1990).

Location of study area

The study area is located in south-central New Mexico and westernmost Texas (Fig. 1). Four sections have been measured within the study area (Clopine, 1990, 1991) along a roughly linear northwest-southeast trend of approximately 160 km (100 mi). Pennsylvanian strata crop out along this trend in a series of discontinuous fault-block mountains.

The measured sections are located in the northern Franklin Mountains, El Paso County, Texas, on the northwest slope of Pyramid Peak at Bishop Cap in Doña Ana County, New Mexico, and on the southwest slope of the Derry Hills and in Whiskey Canyon in the northern Mud Springs Mountains, Sierra County, New Mexico (Fig. 1). See Clopine (1991) for specific directions to each of these measured sections.

Zone of *Millerella*

The Zone of *Millerella* was designated by Thompson (1945, p. 40) as the lowermost Pennsylvanian fusulinid zone. For the purpose of this paper, the Zone of *Millerella* is modified from Thompson (1945, 1948) to range from the first occurrence of *Millerella* and/or *Eostaffella* (base of the Pennsylvanian System in the study area) to the first occurrence of *Eoschubertella* and/or *Pseudostaffella* (i.e. the widely accepted Morrowan Series boundary markers). The occur-

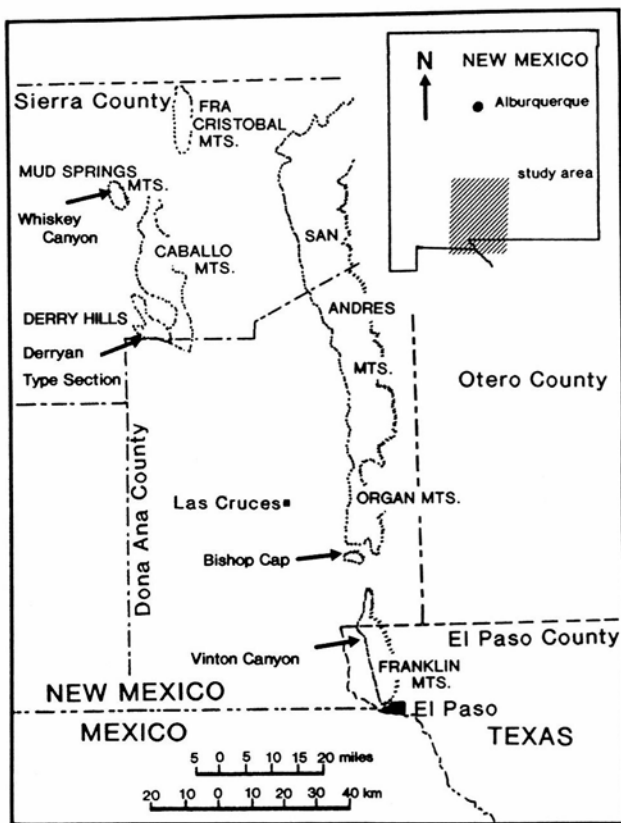


FIGURE 1—Index map of southern New Mexico and westernmost Texas (modified from Kottlowski, 1960).

rence of *Eoschubertella* and/or *Pseudostaffella* below the first occurrence of *Profusulinella* (= Mamet and Skipp, 1970, Faunal Zone 21) is informally termed the zone of *Eoschubertella*.

The Zone of *Millerella* occurs in three of the four studied measured sections. It reaches its maximum thickness at Vinton Canyon where it includes 75 m (246 ft) of Morrowan strata. Northward, at Bishop Cap, the Zone of *Millerella* is reduced to 44 m (143 ft). This is a thickness loss of over 40% in 25 km (15.5 mi). Most, if not all, of the thickness reduction in Morrowan strata from Vinton Canyon to Bishop Cap is due to loss of lower Morrowan strata at the basal Pennsylvanian unconformity.

Northwest of Bishop Cap, the Zone of *Millerella* is greatly reduced or absent. It includes less than 1 m (3.2 ft) at the type Derryan section. Here the Morrowan strata rest on the Devonian Percha Shale. *Millerella* and *Eostaffella* (Fig. 2.27—

36) occur in carbonate wackestone, in the absence of more advanced forms, 0.5 m (1.6 ft) above the base of the Pennsylvanian System. The upper limit of the Zone of *Millerella* is interpreted to fall at an unconformity marking the Morrowan/Atokan boundary.

Zone of *Eoschubertella*

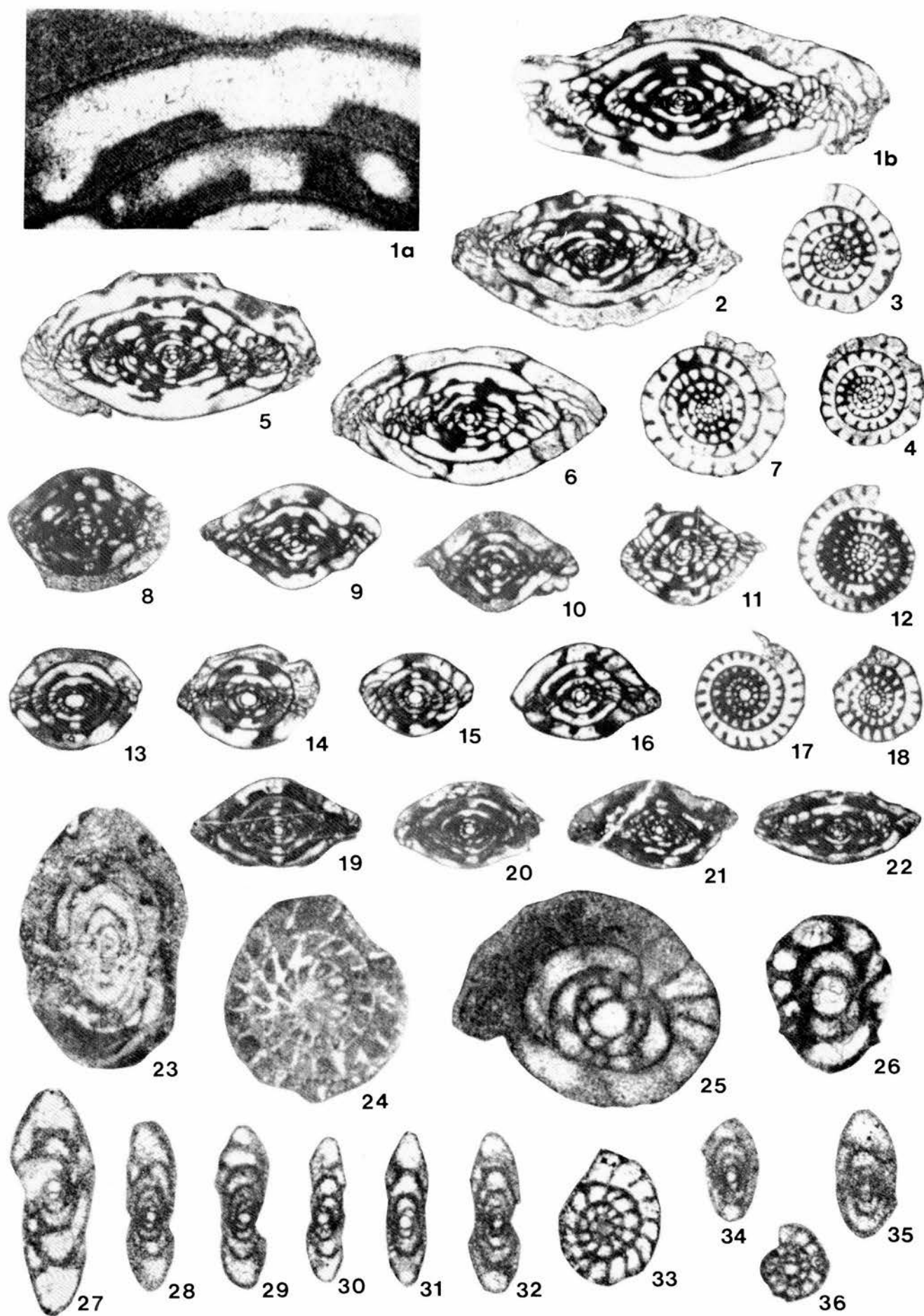
The zone of *Eoschubertella* is equivalent to Mamet and Skipp's (1970, p. 338) Faunal Zone 21 (basal Atokan) as used in the Midcontinent and western United States. The zone of *Eoschubertella* is recognized by the occurrence of *Eoschubertella* and/or *Pseudostaffella* below the first occurrence of *Profusulinella*. This zone is recognized at each of the sections. The lowest *Eoschubertella* sp. at Vinton Canyon occurs 75 m (246 ft) above the base of the Pennsylvanian. Rare *Eoschubertella* sp. occur throughout the zone which is 3.75 m (12 ft) thick at this section. *Eoschubertella*(?) first occurs 44 m (143 ft) above the base of the Pennsylvanian at Bishop Cap. *Profusulinella copiosa* occurs only 0.75 m (2.5 ft) above the first *Eoschubertella*(?). This may only reflect the rarity of the latter species at this locality.

The base of the Atokan Series at the type Derryan section falls at a minor unconformity within a poorly fossiliferous shale interval (between units 3A and 3B). *Eoschubertella*(?) first occurs 0.25 m (0.8 ft) above this unconformity and 1.2 m (3.9 ft) above the base of the Pennsylvanian (unit 3-5). Rare unequivocal *Eoschubertella* (Fig. 2.26) first occurs 1.2 m (3.9 ft) higher in the section (unit 3-7). *Eoschubertella mexicana* (Fig. 2.25) becomes somewhat more abundant and occurs with *Pseudoendothyra* sp. (Fig. 2.23-24) slightly higher in the type Derryan section (unit 3-8). The thickness of the zone of *Eoschubertella* at the type Derryan section has been a matter of some disagreement.

Thompson (1942a, p. 33) reported *Profusulinella* in the "Arrey Formation" at the type Derryan section 5 m (16.5 ft) above the base of the Pennsylvanian System (unit 3 of Thompson, 1942a; unit 3-10 of Clopine, 1990). Thompson (1948, p. 82) altered his earlier interpretation, stating that further study seemed to indicate specimens from his unit 3, formerly referred to as *Profusulinella*, may be a primitive form of *Eoschubertella*. Thompson's latter view, supported by data of Clopine (1990), has apparently not been noted by other workers.

Lane et al. (1972, p. 553) reported *Profusulinella* 4.5 m (15 ft) above the base of the type Derryan section (same as Thompson's, 1942a, lowest "*Profusulinella*" horizon). However, these specimens have been re-examined by George Verville (pers. comm. 1989), who states that they should

FIGURE 2—Oklahoma Museum of Natural History (OU) numbers in parentheses. **1a, b**, *Profusulinella apodacensis* Thompson, 1948, Whiskey Canyon, top of unit 4-5; a, ×100 enlargement of axial section showing typical profusulinellid 3-layered wall structure; b, ×20, axial section (OU10962). **2-4**, *Profusulinella decora* Thompson, 1948, ×20, Vinton Canyon, top of unit 1-116; 2, axial section (OU10949), 3, sagittal section (OU10956), 4, sagittal section (OU10954). **5-7**, *Profusulinella munda* Thompson, 1948, ×20, Vinton Canyon, unit 1-114; 5, axial section (OU10937), 6, axial section (OU10940), 7, sagittal section (OU10939). **8-12**, *Profusulinella* sp., ×20, 8, 9, and 11 from Vinton Canyon, unit 1-109, 10 and 12 from Vinton Canyon, unit 1-108; 8, axial section (OU10921), 9, axial section (OU10923), 10, axial section (OU10931), 11, axial section (OU10922), 12, sagittal section (OU10936). **13-18**, *Profusulinella copiosa* Thompson, 1948, ×20, 13, 14, and 17 from Vinton Canyon, unit 1-69; 15, 16, and 18 from Bishop Cap, top of unit 2-46; 13, axial section (OU10903), 14, axial section (OU10904), 15, axial section (OU10918), 16, axial section (OU10917), 17, sagittal section (OU10914), 18, sagittal section (OU10920). **19-22**, *Profusulinella* cf. *fitti* (Thompson, 1935), ×20; 19, axial section, Bishop Cap, unit 2-39 (OU10899); 20, axial section, Vinton Canyon, unit 1-62 (OU10900); 21, 22, type Derryan, unit 3-23; 21, axial section (OU11057), 22, axial section (OU11058). **23, 24**, *Pseudoendothyra* sp. Mikhailov, 1939, ×40; type Derryan, top of unit 3-8; 23, axial section (OU10886), 24, sagittal section (OU10887). **25, 26**, *Eoschubertella mexicana* Thompson, 1948, ×100; 25, axial section, type Derryan, top of unit 3-8 (OU10897); 26, axial section of juvenile, type Derryan, base of unit 3-7 (OU10892). **27-33**, *Millerella* spp. of Thompson, 1942b, ×100; 27-31 and 33 from type Derryan, unit 3-3; 32 from type Derryan, unit 3-7; 27, axial section (OU10866), 28, axial section (OU10867), 29, axial section (OU10868), 30, axial section (OU10869), 31, axial section (OU10870), 32, axial section (OU10875), 33, sagittal section (OU10878). **34-36**, *Eostaffella* spp. of Rauzer-Chernousova, 1948, ×100; 34 and 36 from type Derryan, unit 3-3; 35 from type Derryan, top of unit 3-8; 34, axial section (OU10879), 35, axial section (OU10880), 36, sagittal section (OU10883).



be assigned to *Eoschubertella*. King (1973, p. 2) reported *Profusulinella* in bed 2 of Thompson (1942a; unit 3-7 of this author). In addition, King (1973, p. 2) suggested from "unidentifiable fragments" that the lowest *Profusulinella* occurrence may be in Thompson's bed 1. He now believes, however, that those specimens were probably *Eoschubertella* (William King, pers. comm. 1989).

The only documented occurrence of *Profusulinella* at the type Derryan section is reported by Clopine (1990, base of unit 3-23; unit 10 of Thompson, 1942a) 13.4 m (44 ft) above the base of *Eoschubertella*(?) and 13.65 m (44.8 ft) above the lowest Atokan strata. This interval includes all of Thompson's (1942) "Arrey Formation" and the lower 2.7 m (9 ft) of his "Apodaca Formation."

Zone of *Profusulinella*

The Zone of *Profusulinella* was designated by Thompson (1945, pp. 40-41) as the lower and middle "Derryan" (Atokan) fusulinid zone. It is bounded by the first occurrences of *Profusulinella* and *Fusulinella* and falls between the zones of *Eoschubertella* and *Fusulinella*. The Zone of *Profusulinella* has gained widespread acceptance as the lower—middle Atokan fusulinid biozone.

The Zone of *Profusulinella* includes three distinct intervals in the study area, a lower interval characterized by *Profusulinella copiosa* (Fig. 2.13-18), a middle interval characterized by *Profusulinella* sp. (Fig. 2.8-12), and an upper interval characterized by *Profusulinella munda* (Fig. 2.5-7), *Profusulinella decors* (Fig. 2.2-4), and *Profusulinella apodacensis* (Fig. 2.1a, b). The Zone of *Profusulinella* is 61.5 m (202 ft) thick at Vinton Canyon. Rare *Profusulinella* cf. *fittsi* (Fig. 2.19-22) occur with *P. copiosa* at the base of the zone. The zone is reduced to 41.6 m (136.5 ft) at Bishop Cap, where *P. copiosa* is also associated with *P. cf. fittsi*. The Zone of *Profusulinella* is further reduced to approximately 8.5 m (27.9 ft) at the type Derryan section. *P. copiosa* has not been recovered here or at the Whiskey Canyon section. A single horizon yielding rare *P. cf. fittsi* (base of unit 3-23), however, occurs at the type Derryan section. This horizon is tentatively correlated with the lower portion of the *P. copiosa* range zone. No other *Profusulinella* have been recovered from the type Derryan section.

The Zone of *Profusulinella* is recognized at Whiskey Canyon, but it is restricted to a single horizon. Thompson (1948, p. 73) correlated this horizon (Thompson's unit 11-5; unit 4-5 of Clopine, 1990) with the upper "Apodaca Formation" at the type Derryan section, based on his reported occurrence of *Profusulinella apodacensis*. However, all fusulinids recovered from the upper "Apodaca Formation" at the type Derryan section by Clopine (1990) have proven to be *Fu*

sulinella, and Thompson's correlation thus does not appear justified.

Zone of *Fusulinella*

The Zone of *Fusulinella* was designated by Thompson (1945, p. 41) to include upper Derryan (Atokan) and lowermost Desmoinesian strata. Thompson (1948, p. 23) modified his earlier definition of the Zone of *Fusulinella*, lowering its upper datum to "just below the lowest occurrence of *Fusulina* (*Beedeina*)." The base of the zone remained unchanged at the first occurrence of *Fusulinella*. The zone of *Fusulinella* has gained widespread acceptance as the upper Atokan fusulinid biozone.

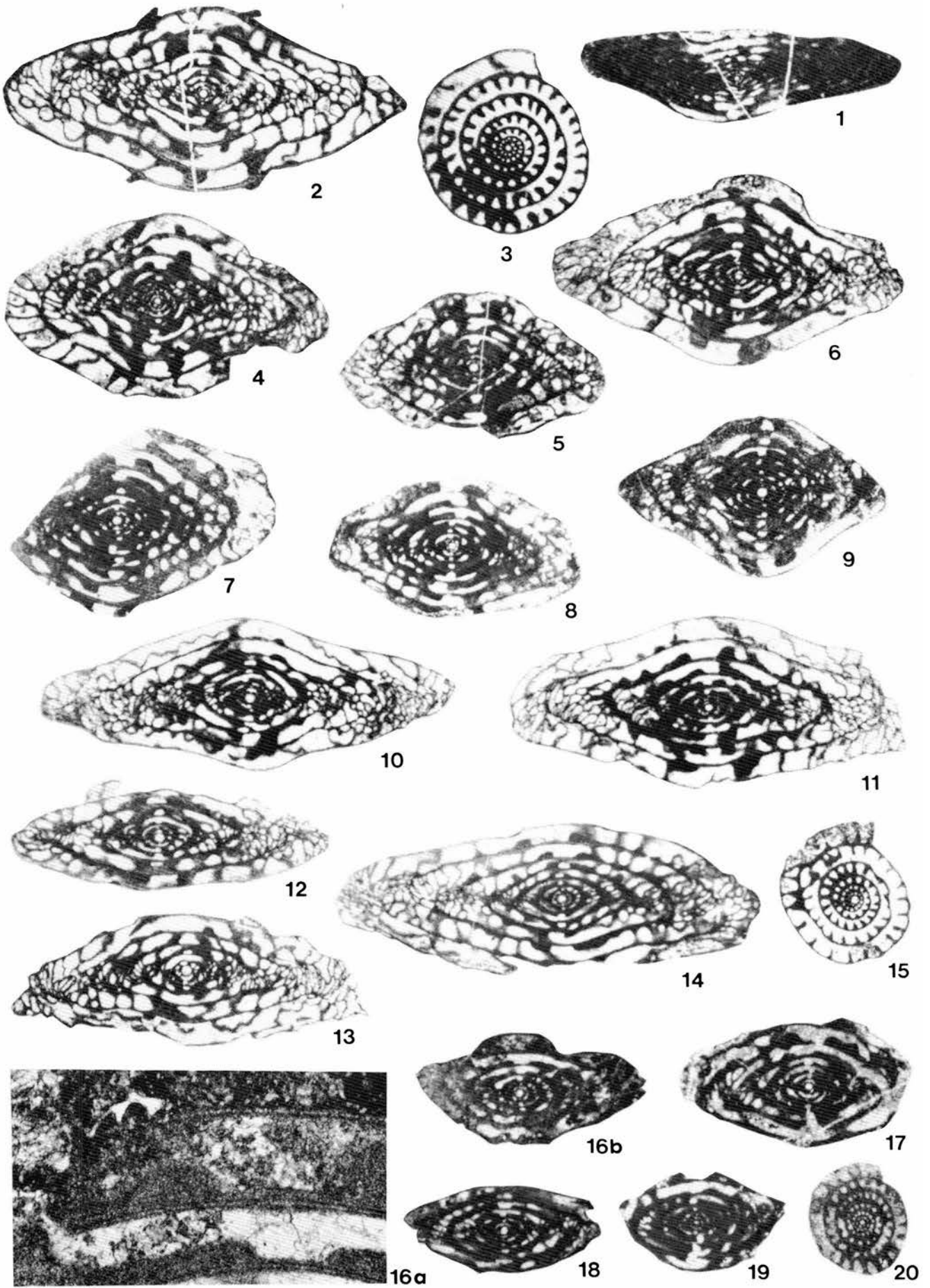
The Zone of *Fusulinella* in the study area includes a lower interval characterized by *Fusulinella acuminata* (Fig. 3.1215) and an upper interval characterized by *Fusulinella devexa* (Fig. 3.10-11). The Zone of *Fusulinella* reaches its maximum thickness within the study area at Vinton Canyon, where it is 42.18 m (138.4 ft) thick. It is reduced to 9.25 m (30.4 ft) at the Bishop Cap section locality, where *Fusulinella acuminata* interval does not occur due to the lack of fusulinids in the dolomitic lithologies below *Fusulinella devexa*.

The Zone of *Fusulinella* is 15.05 m (49.4 ft) thick at the type Derryan section. Here *Fusulinella fugax* (Fig. 3.1620) occurs with *Fusulinella acuminata* in the upper portion of Thompson's (1942a) "Apodaca Formation." Thompson (1948) indicated the occurrence of *Profusulinella apodacensis* in this horizon. However, only members of the genus *Fusulinella* were recovered from the upper "Apodaca Formation" by Clopine (1990). The upper boundary of the Zone of *Fusulinella* corresponds to the top of the type Derryan Series, which lies immediately below the first occurrence of *Beedeina insolita* (Fig. 3.4-6). Somewhat more advanced *Beedeina* (Fig. 3.2-3) and the first *Wedekindellina* (Fig. 3.1) occur slightly higher in the section.

Acknowledgments

This paper is part of a University of Oklahoma PhD dissertation supported by National Science Foundation Grant EAR-8517591 through Patrick K. Sutherland, by a grant from Amoco Research Laboratory in Tulsa, Oklahoma, by the University of Oklahoma School of Geology and Geophysics, and by the New Mexico Bureau of Mines & Mineral Resources. Interpretations benefitted from observations made in the field by Patrick K. Sutherland, Walter L. Manger, and George J. Verville. I would also like to thank and express my appreciation to Patrick K. Sutherland, George J. Verville, George A. Sanderson, Walter L. Manger, and John R. Groves for their significant contributions to this study.

FIGURE 3—Oklahoma Museum of Natural History (OU) numbers in parentheses, all figures $\times 20$ except as noted. 1, *Wedekindellina excentrica* Roth and Skinner, 1930, type Derryan, base of unit 3-60, axial section (OU11061). 2, 3, *Beedeina* aff. *hayensis* (Ross and Sabins, 1965), 2, type Derryan, unit 3-44, axial section (OU11038); 3, Whiskey Canyon, unit 4-61, sagittal section (OU11046). 4-6, *Beedeina insolita* (Thompson, 1948), axial sections; 4 and 5 from type Derryan, base of unit 3-47; 6 from type Derryan, unit 3-44; 4 (OU11028), 5 (OU11022), 6 (OU11027). 7-9, *Fusulinella famula* Thompson, 1948, axial sections; 7 and 8 from Vinton Canyon, top of unit 1-145; 9 from Vinton Canyon, top of unit 1-147; 7 (OU11011), 8 (OU11012), 9 (OU11014). 10, 11, *Fusulinella devexa* Thompson, 1948, axial sections, type Derryan, base of unit 3-39; 10 (OU11007), 11 (OU11008). 12-15, *Fusulinella acuminata* Thompson, 1936; 12 and 14 from type Derryan, unit 3-32; 13 and 15 from Vinton Canyon, unit 1-119; 12, axial section (OU10978), 13, axial section (OU10981), 14, axial section (OU10971), 15, sagittal section (OU10982). 16-20, *Fusulinella fugax* Thompson, 1948, type Derryan, unit 3-25; 16a, $\times 100$ enlargement of axial section showing thin but consistent development of diaphanotheca in fourth, fifth, and sixth volutions; 16b, axial section (OU10960), 17, axial section (OU10967), 18, axial section (OU10961), 19, axial section (OU10970), 20, sagittal section (OU10968).



References

- Clopine, W. W., 1990, Middle Pennsylvanian fusulinid biostratigraphy of the type Derryan area in southern New Mexico and westernmost Texas: Unpublished PhD dissertation, University of Oklahoma, Norman, 271 pp.
- Clopine, W. W., 1991, Lower and Middle Pennsylvanian measured sections, type Derry region, southern New Mexico and westernmost Texas: New Mexico Bureau of Mines & Mineral Resources, Open-file Report 373, 122 pp.
- Groves, J. R., 1986, Foraminiferal characterization of the Morrowan-Atokan (lower Middle Pennsylvanian) boundary: Geological Society of America, Bulletin, v. 97, pp. 346-353.
- King, W. E., 1973, Fusulinids *Millerella* and *Eostaffella* from the Pennsylvanian of New Mexico and Texas: New Mexico Bureau of Mines & Mineral Resources, Memoir 26, 34 pp.
- Kottlowski, F. E., 1960, Summary of Pennsylvanian sections in southwestern New Mexico and southeastern Arizona: New Mexico Bureau of Mines & Mineral Resources, Bulletin 66, 187 pp.
- Lane, H. R., 1974, Mississippian of southeastern New Mexico and West Texas: A wedge-on-wedge relation: American Association of Petroleum Geologists, Bulletin, v. 58, no. 2, pp. 269-282.
- Lane, H. R., Sanderson, G. A., and Verville, G. J., 1972, Uppermost Mississippian-basal Middle Pennsylvanian conodonts and fusulinids from several exposures in the south-central and southwestern United States: Twenty-fourth International Geological Congress, Montreal, Section 7, pp. 549-555.
- Mamet, B. L., 1975, Carboniferous foraminifera and algae of the Amsden Formation (Mississippian and Pennsylvanian) of Wyoming: U.S. Geological Survey, Professional Paper 848-B, 18 pp.
- Mamet, B. L., and Armstrong, A. K., 1972, Lisburne Group, Franklin and Romanzof Mountains, northeastern Alaska: U.S. Geological Survey, Professional Paper 800-C, pp. C127-C144.
- Mamet, B. L., and Skipp, B., 1970, Preliminary foraminiferal correlations of Early Carboniferous strata in the North American Cordillera: Congress et Colloques, Colloque sur la Stratigraphie du Carbonifere, Universite de Liege, v. 55, pp. 325-348.
- Manger, W. L., Sutherland, P. K., and Clopine, W. W., 1987, Morrowan-Atokan boundary relations, type "Derryan" section, New Mexico (abs.): Geological Society of America, South-Central Section Abstracts with Programs, v. 19, no. 3, p. 173.
- Mikhailov, A. V., 1939, K kharakteristike rodov nizhnnekamenougol'nykh foraminifer territorii SSSR: Sbornik Leningradskogo Geologicheskogo Upravleniya, Glavnoe Geologicheskoe Upravlenie, v. 3, pp. 47-62 (not seen).
- Rauzer-Chemousova, D. M., 1948, Some new species of Foraminifera from the Lower Carboniferous sediments of the Moscow Basin [in Russian]: Akademia Nauk SSSR, Trudy Geologicheskogo Instituta, v. 62, no. 19, pp. 227-238.
- Ross, C. A., and Sabins, F. F., 1965, Early and Middle Pennsylvanian fusulinids from southeast Arizona: Journal of Paleontology, v. 39, pp. 173-209.
- Roth, R., and Skinner, J., 1930, The fauna of the McCoy formation, Pennsylvanian of Colorado: Journal of Paleontology, v. 4, pp. 332-352.
- Stewart, W. J., 1970, Fusulinids of the Joyita Hills, Socorro County, central New Mexico: New Mexico Bureau of Mines & Mineral Resources, Memoir 23, part 2, pp. 32-82.
- Sutherland, P. K., and Manger, W. L., 1984, Morrowan brachiopods in the type "Derryan" Series (Pennsylvanian), New Mexico (abs.): Geological Society of America, Abstracts with Programs, v. 16, no. 2, p. 115.
- Thompson, M. L., 1935, Fusulinids from the Lower Pennsylvanian Atokan and Boggy formations of Oklahoma: Journal of Paleontology, v. 9, pp. 291-306.
- Thompson, M. L., 1936, Fusulinids from the Black Hills and adjacent areas in Wyoming: Journal of Paleontology, v. 10, pp. 95-113.
- Thompson, M. L., 1942a, Pennsylvanian System in New Mexico: New Mexico Bureau of Mines & Mineral Resources, Bulletin 17, 92 pp.
- Thompson, M. L., 1942b, New genera of Pennsylvanian fusulinids: American Journal of Science, v. 240, pp. 403-420.
- Thompson, M. L., 1945, Pennsylvanian rocks and fusulinids of east Utah and northwest Colorado correlated with Kansas section: State Geological Survey of Kansas, Bulletin 60, part 2, pp. 19-84.
- Thompson, M. L., 1948, Studies of American fusulinids: University of Kansas Paleontological Contributions, Protozoa, Article 1, 184 pp.
- Verville, G. J., Sanderson, G. A., and Madsen, M. E., 1986, Pennsylvanian fusulinids from the Fra Cristobal Range, Sierra County, New Mexico: New Mexico Geological Society, Guidebook 37, pp. 215-223.

Morrowan brachiopods from the type "Derryan" Series (Pennsylvanian), southern New Mexico

Patrick K. Sutherland

Introduction

The Derry Series was originally defined by Thompson (1942) as including all pre-Desmoinesian Pennsylvanian strata in southern New Mexico. Lane et al. (1972) equated the Derryan with the Atokan Series in Oklahoma, but their detailed analysis of Thompson's (1942) type section started at the lowest cliff-forming limestone (Fig. 1, unit 5). A subsequently developed prominent roadcut on 1-25 at the type Derry, east of Derry, exposes the Pennsylvanian unconformity with the Upper Devonian sandstone and shale of the Percha Formation and a 2.5 ft interval of shale and nodular limestone that is poorly exposed at the base of Thompson's (1942) type sequence.

Sutherland and Manger (1984) recovered a well-preserved late Morrowan brachiopod fauna from the nodular limestone and shale interval (Fig. 1, units 3a, 3b) found at the base of the Pennsylvanian in the 1-25 roadcut, and selections from this fauna are here illustrated for the first time (Fig. 2). Later, after further, detailed examination of this exposure, they (Manger et al., 1987) observed the presence of a post-Morrowan - pre-Atokan unconformity that falls within a thin shale interval immediately above the brachiopod-

bearing units. There, a lower 0.5-0.7 ft of brown shale, possibly a paleosol (Fig. 1, unit 4a), carries reworked conodonts with upper Morrowan affinities. This unit is overlain by 0.5-0.8 ft of barren fissile black shale (Fig. 1, unit 4b). Thick-bedded limestones (Fig. 1, unit 5) immediately overlie this black shale and contain upper lower Atokan conodonts succeeded by *Profusulinella* within 13 ft (Manger et al., 1987).

Numerous thin sections of the nodular limestone (Fig. 1, unit 3b) produced the foraminifers *Millerella extensa* and *Eostaffella* sp. to the exclusion of more advanced forms (identified by J. R. Groves, pers. comm. 1985). These species are typically found in Morrowan faunas, but they also range higher stratigraphically.

Brachiopod occurrences

The Morrowan series in the southern Midcontinent has produced a large, varied, and highly distinctive brachiopod fauna. Sutherland and Harlow (1973) recorded 41 Morrowan brachiopod species from the La Pasada Formation in the southern Sangre de Cristo Mountains in northern New Mexico. In that area, however, conodonts indicate that only

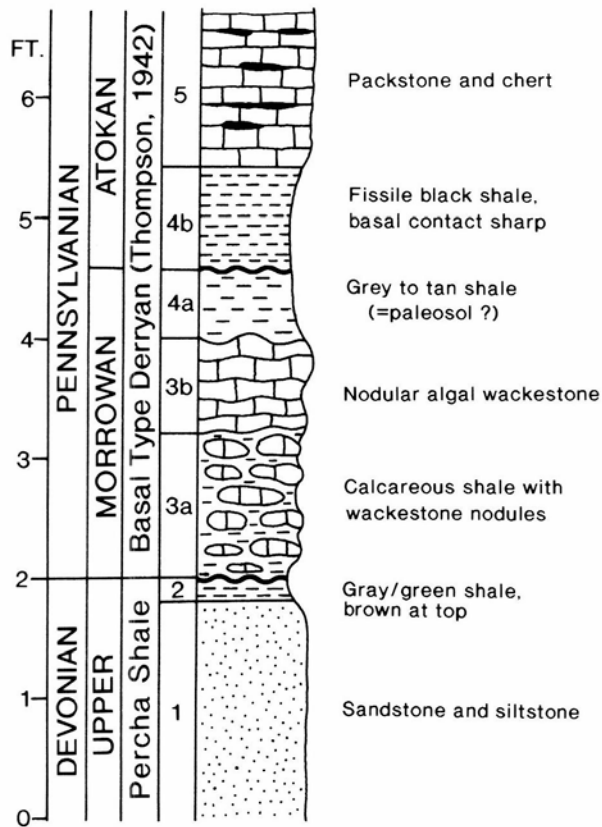


FIGURE 1—Basal beds of type "Derryan" section.

the upper part of the Morrowan Series is represented (Sutherland and Harlow, 1973). In the type Morrowan area, in northwestern Arkansas and northeastern Oklahoma, where the Morrowan series is more complete, Henry and Sutherland (1977) reported the occurrence of about 80 brachiopod species. However, detailed descriptions and illustrations of the new elements in that fauna have not yet been published. Many of the species that occur in northern New Mexico also occur in Arkansas and Oklahoma, but a few unique species are restricted to each area.

The 2.5 ft Morrowan interval at the base of the type "Derryan" section has produced a late Morrowan brachiopod fauna of 12 species that are particularly similar to the equivalent species that occur in the La Pasada Formation in northern New Mexico. Of these, the following nine are restricted to the Morrowan in all known occurrences:

1. *Zia novamexicana* Sutherland and Harlow (Fig. 2.1a, 2.1b); common
2. *Spirifer goreii* Mather (Fig. 2.3); rare
3. *Neochonetes? platynotus* (White) (Fig. 2.8); fairly common
4. *Plicochonetes? arkansanus* (Mather) (Fig. 2.9a, 2.9b); rare
5. *Linoproductus nodosus* (Newberry) (not figured); rare
6. *Sandia welleri* (Mather) (Fig. 2.4a, 2.4b); rare
7. *Punctospirifer morrowensis* Sutherland and Harlow (Fig. 2.5); fairly common
8. *Rhynchopora magnicosta* Mather (not figured); rare
9. *Composita cf. gibbosa* Mather (not figured); common

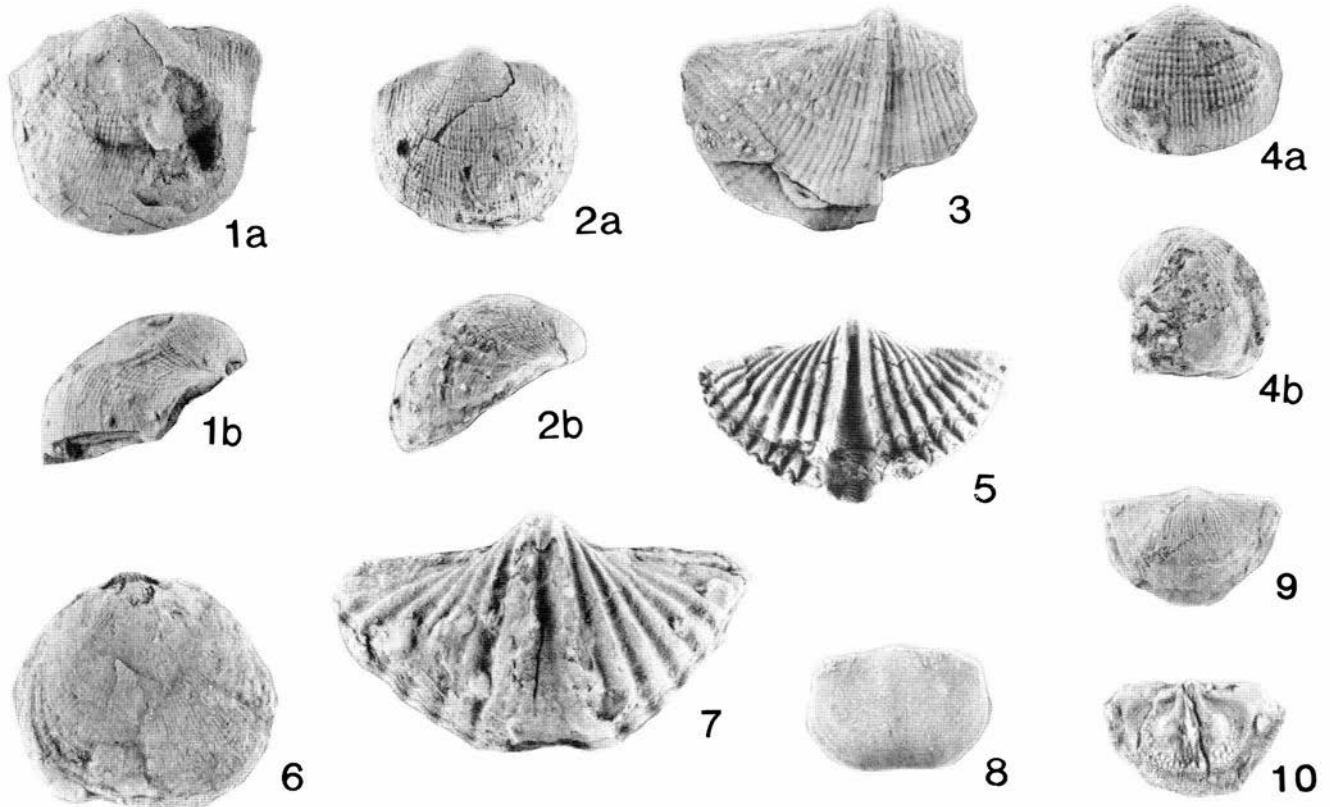


FIGURE 2—1, 2, *Zia novamexicana* Sutherland and Harlow: 1, OU 7144, $\times 1$, a = pedicle valve, b = side view. 2, OU 7146, $\times 1$, a = pedicle, b = side view. 3, *Spirifer goreii* Mather, OU 7148, $\times 1$, pedicle. 4, *Sandia welleri* (Mather), OU 9106, $\times 1$, a = pedicle, b = side view. 5, *Punctospirifer morrowensis* Sutherland and Harlow, OU 9107, $\times 2$, pedicle. 6, *Rhipidomella* sp., OU 9653, $\times 2$, pedicle. 7, *Punctospirifer?* sp., OU 9654, $\times 2$, pedicle. 8, *Neochonetes? platynotus* (White), OU 9655, $\times 2$, pedicle. 9, 10, *Plicochonetes? arkansanus* (Mather): 9, OU 9656, $\times 2$, pedicle; 10, OU 9657, $\times 2$, brachial interior. All figured specimens are from the basal Pennsylvanian beds at the type "Derryan" section (Fig. 1, units 3a, 3b). These specimens are part of the University of Oklahoma (OU) Invertebrate Paleontology Repository at the Oklahoma Museum of Natural History.

gies (Fig. 2). Other previous investigations have included the Vinton Canyon section and exposures near the Bishop Cap section and have provided similar interpretations of the microfacies (Mims, 1971; Osleger, 1981). The present study concentrated on Clopine's skeletal wackestone/packstone (Fig. 2-C/D) and crinoidal grainstone/packstone (Fig. 2-E) microfacies. Modal analyses of 300 counts on 85 thin-sections cut from those lithologies further recognized a mixed skeletal wackestone/packstone and intraclast packstone microfacies (Kaiser, 1990) (Fig. 2).

The depositional history of shallow-marine carbonates on the Robledo shelf and in the Orogrande basin can be interpreted by the standard facies scheme of Wilson (1975). Transgression began in the Morrowan from the Orogrande basin and covered the Robledo shelf by upper Atokan time. Subsidence in the basin kept pace with deposition retaining the low-energy, shallow-marine character, particularly high mud content, and blanket distribution of the Pennsylvanian carbonates throughout the region.

Conodont biofacies

Eight platform elements assignable to 24 form species are represented among the 3318 elements recovered from 76 productive samples; six samples were barren. Each sample was assigned to a carbonate microfacies and its conodont occurrence data were tabulated. Biofacies were based on (1) element abundances, (2) platform to ramiform ratios (**P/R** ratios), and (3) form-generic abundances (Fig. 3). Three conodont biofacies were identified: *Adetognathus*, *Idiognathodus*, and *Idiognathoides*.

The *Adetognathus* biofacies is recognized by the total dominance of that form taxon, which may be the only element recovered in a particular sample. The only other associated platforms are *Rhachistognathus* and *Idiognathoides*, recovered from a total of only three samples. The biofacies is developed in the shallow, near-shore lithologies of the mixed skeletal wackestone/packstone and intraclast pack-

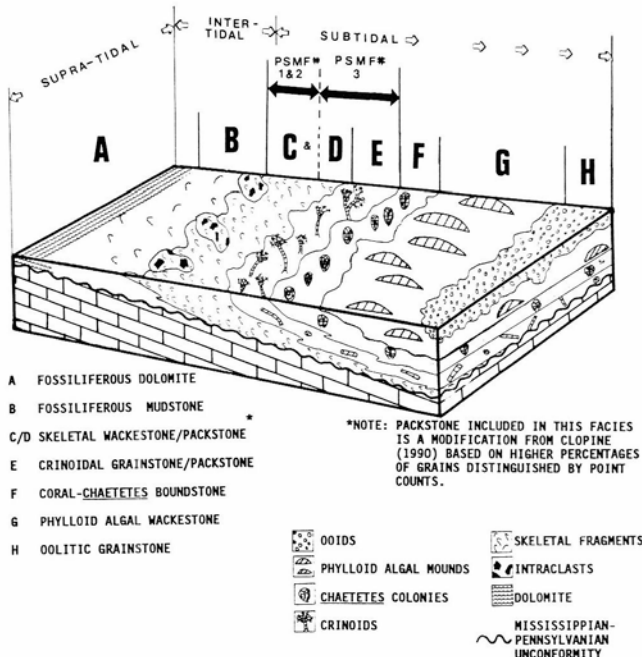


FIGURE 2—Pennsylvanian carbonate microfacies tracts, southern New Mexico and adjacent areas. PSMF #1 = mixed skeletal wackestone/packstone. PSMF #2 = intraclast packstone. PSMF #3 = crinoidal packstone/grainstone (modified from Clopine, 1990).

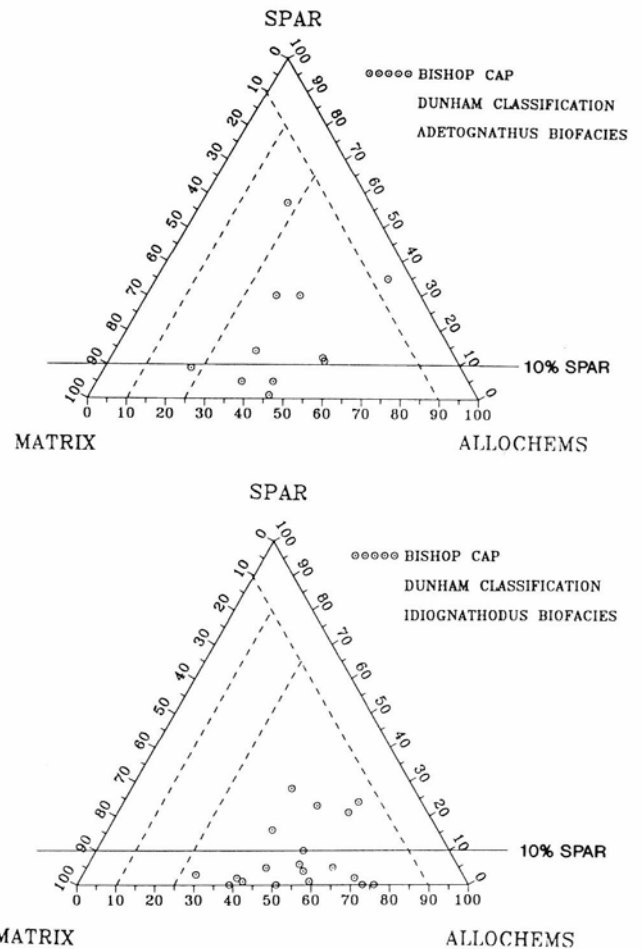


FIGURE 3—Example of relationship of biofacies and microfacies in samples from Bishop Cap. 10% spar line reflects higher energy and better sorting.

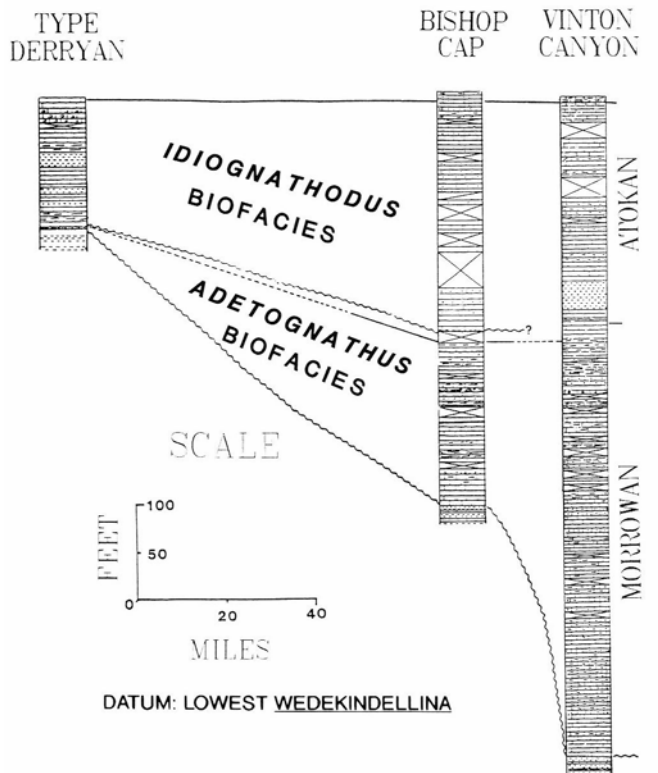


FIGURE 4—Biofacies correlation between type Derryan section and Vinton Canyon.

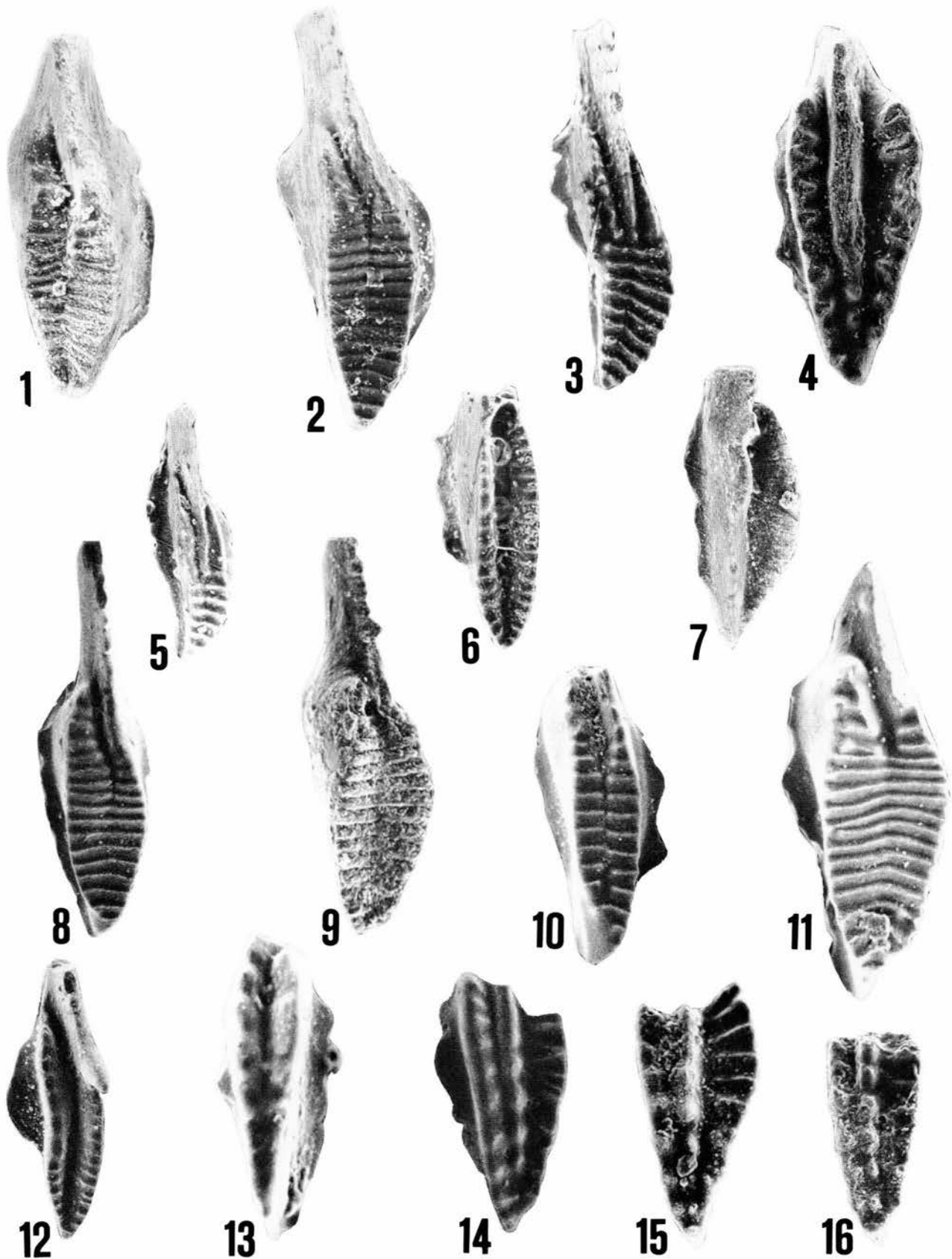


FIGURE 5—*Idiognathodus* and *Idiognathoides* biofacies.

Idiognathodus biofacies platform elements: **1**, *Idiognathoides ouachitensis*, $\times 58$, unit 2-25; **2**, *Idiognathoides sinuatus*, $\times 58$, unit 2-31B; **3**, *Idiognathodus delicatus*, $\times 58$, unit 2-31B; **4**, *Neognathodus bothrops*, $\times 58$, unit 2-25; **5**, *Streptognathodus parvus*, $\times 60$, unit 2-25; **6**, *Adetognathus lautus*, $\times 58$, unit 2-31B; **7**, *Adetognathus lautus*, $\times 60$, unit 2-25.

Idiognathoides biofacies platform elements: **8**, *Idiognathoides sinuatus*, $\times 60$, unit 2-17; **9**, *Idiognathoides expansus*, $\times 58$, unit 2-17; **10**, *Idiognathoides ouachitensis*, $\times 60$, unit 2-17; **11**, *Idiognathoides ouachitensis*, $\times 62$, unit 2-17; **12**, *Adetognathus lautus*, $\times 60$, unit 2-17; **13**, *Rhachistognathus muricatus*, $\times 93$, unit 2-17; **14**, *Neognathodus bassleri*, $\times 60$, unit 2-17; **15**, *Neognathodus bassleri*, $\times 60$, unit 2-17; **16**, *Neognathodus bassleri*, $\times 58$, unit 2-17.

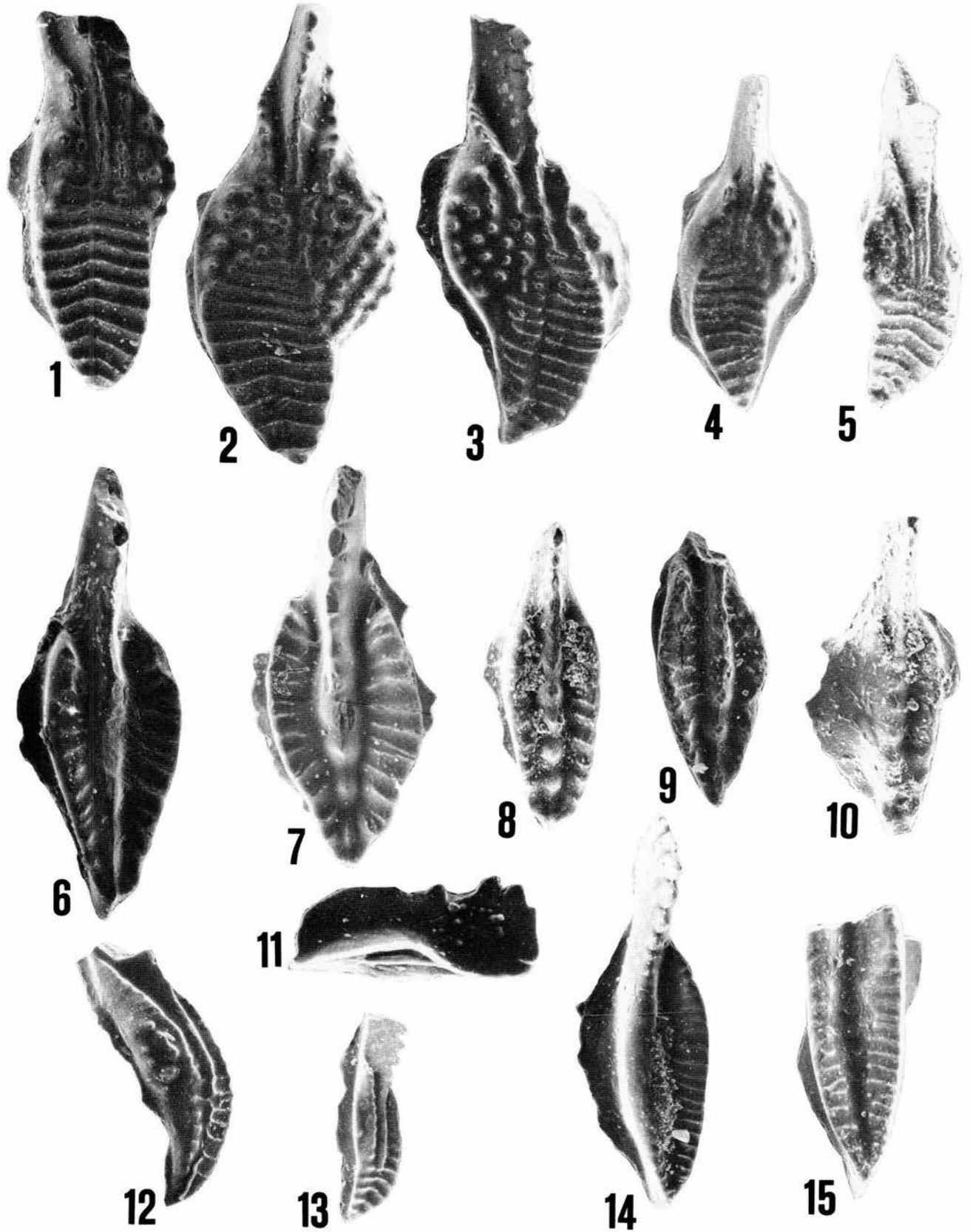


FIGURE 6—*Idiognathodus* biofacies platform elements: 1, *Idiognathodus delicatus*, $\times 60$, unit 2-95; 2, *Idiognathodus delicatus*, $\times 58$, unit 2-117; 3, *Idiognathodus delicatus*, $\times 60$, unit 2-117; 4, *Idiognathodus delicatus*, $\times 59$, unit 2-117; 5, *Idiognathodus delicatus*, $\times 61$, unit 2-71; 6, *Neognathodus bothrops*, $\times 59$, unit 2-117; 7, *Neognathodus bothrops*, $\times 58$, unit 2-117; 8, *Neognathodus symmetricus*, $\times 59$, unit 2-95; 9, *Neognathodus?*, $\times 59$, unit 2-95; 10, *Rhachistognathus muricatus*, $\times 80$, unit 2-95; 11, *Diplognathodus coloradoensis*, $\times 93$, unit 2-117; 12, *Streptognathodus* sp., $\times 63$, unit 2-71; 13, *Streptognathodus* sp., $\times 59$, unit 2-117; 14, *Adetognathus lautus*, $\times 59$, unit 2-117; 15, *Adetognathus lautus*, $\times 63$, unit 2-71.

stone microfacies. Environments associated with the *Adetognathus* biofacies had moderate energy levels and possibly fluctuating salinities. Most samples from this biofacies exhibit low abundance and low P/R ratios. High abundances and high P/R ratios in samples from this biofacies represent lag concentrates, while low abundances and high P/R ratios probably represent transportation into otherwise inhospitable environments. This biofacies is equivalent to that previously recognized by Merrill and von Bitter (1976), Driese et al. (1984), and Davis and Webster (1985). It was confined to rocks of Morrowan age, and reflects the transgressive nature of those strata across the Robledo shelf (Fig. 4). Its dominance of the Morrowan section at Vinton Canyon reflects persistent shallow environments as deposition kept pace with subsidence in the Orogrande basin.

The *Idiognathodus* biofacies (Figs. 5, 6) is recognized in samples in which that taxon comprises 50% or more of the platform elements recovered. Associated platform elements include: *Neognathodus*, *Streptognathodus*, *Idiognathoides*, *Adetognathus*, and *Diplognathodus*. Three samples at Bishop Cap fell below the abundance level for *Idiognathodus*, but were included in this biofacies because of the similar elemental association. The *Idiognathodus* biofacies is developed in the crinoidal packstone/grainstone microfacies that reflects more off-shore, deeper, marine environments of normal salinity basinward of the *Adetognathus* biofacies. Samples from this biofacies typically have high abundances but low P/R ratios, indicating optimal living conditions (natural assemblages suggest a P/R ratio of 0.2). Lag concentrates of high abundance and high P/R ratios also occur in samples from this biofacies. The *Idiognathodus* biofacies was recognized by Merrill and von Bitter (1976) and Driese et al. (1984). It is represented in the highest Morrowan section at Bishop Cap and Vinton Canyon, and comprises the entire Atokan record at all three sections studied (Fig. 4). The replacement of the *Adetognathus* biofacies by the *Idiognathodus* biofacies is consistent with the continued transgression and deepening of environments across the Robledo shelf and in the Orogrande basin during Atokan time.

An *Idiognathoides* biofacies (Fig. 5) is recognized in samples in which that taxon comprises 50% or more of the platform elements present. Associated platform elements include: *Neognathodus*, *Adetognathus*, *Streptognathodus*, *Idiognathodus*, and *Rhachistognathus*. This biofacies was found in two samples of the mixed skeletal wackestone/packstone microfacies at Bishop Cap, and reflects a transition from the *Adetognathus* to *Idiognathodus* biofacies. Too large a sampling interval may account for the absence of this biofacies at Vinton Canyon, while transitional intervals may not have been preserved at the type Derryan section. This biofacies is equivalent to that recognized by Davis and Webster (1985), but may represent the *Neognathodus* biofacies of Merrill and von Bitter (1976) and Davis and Webster (1985) as well. Abundant *Neognathodus*

may reflect stressed environments allowing success of only that platform taxon.

Biostratigraphic considerations

The biofacies domination of conodonts exhibited by the Morrowan—Atokan succession limits their biostratigraphic utility in the Orogrande basin and on the Robledo shelf. The Morrowan zonal name-bearers are present, but their occurrences are sporadic and all may appear simultaneously in a lag concentrate (e.g. Bishop Cap). Most samples contain *Adetognathus* to the exclusion of other platform taxa. Neither the Morrowan—Atokan nor Atokan—Desmoinesian boundaries are accompanied by a pronounced change in conodonts, although the abrupt appearance of *Diplognathodus coloradoensis* suggests an unconformity at the former boundary in the type Derryan and Bishop Cap sections. Atokan *Neognathodus* occurrences offer general discrimination of lower and upper portions of the series that are compatible with associated foraminifers. However, no zonation is recognizable through that interval on the basis of conodonts.

References

- Clark, D. L. (ed.), 1984, Conodont biofacies and provincialism: Geological Society of America, Special Paper 196, 340 pp.
- Clopine, W. W., 1990, Middle Pennsylvanian fusulinid biostratigraphy of the type Derryan area in southern New Mexico and westernmost Texas: Unpublished PhD dissertation, University of Oklahoma, Norman, 271 pp.
- Davis, L. E., and Webster, G. D., 1985, Late Mississippian to early Pennsylvanian conodont biofacies in central Montana: *Lethaia*, v. 18, pp. 67-72.
- Driese, S. G., Carr, T. R., and Clark, D. L., 1984, Quantitative analysis of Pennsylvanian shallow-water conodont biofacies, Utah and Colorado; in Clark, D. L. (ed.), Conodont biofacies and provincialism: Geological Society of America, Special Paper 196, pp. 233-250.
- Kaiser, D. A., 1990, Conodont biofacies analysis of the Lower to Middle Pennsylvanian (Morrowan and Atokan), south-central New Mexico and westernmost Texas: Unpublished MS thesis, University of Oklahoma, Norman, 115 pp.
- Kottlowski, F. E., 1960, Summary of Pennsylvanian sections in southwestern New Mexico and southeastern Arizona: New Mexico Bureau of Mines & Mineral Resources, Bulletin 66, 187 pp.
- Merrill, G. K., and von Bitter, P. H., 1976, Revisions of conodont carbonate biofacies nomenclature and interpretations of environmental controls in Pennsylvanian rocks of eastern and central North America: Royal Ontario Museum, Life Sciences Contributions, no. 108, 46 pp.
- Mims, R. L., 1971, Microfacies analysis of the La Tuna Formation (Morrowan), Vinton Canyon, El Paso County, Texas: Permian Basin Section, Society of Economic Paleontologists and Mineralogists, Guidebook to the Robledo and Franklin Mountains, pp. 87-106.
- Nelson, L. A., 1940, Paleozoic stratigraphy of Franklin Mountains, West Texas: American Association of Petroleum Geologists, Bulletin, v. 24, pp. 157-172.
- Osleger, D. A., 1981, Stratigraphy and microfacies analysis of the La Tuna Formation (Morrowan—Atokan), Franklin Mountains, Texas and New Mexico, and Bishop Cap, New Mexico: Unpublished MS thesis, University of Texas at El Paso, 138 pp.
- Thompson, M. L., 1942, Pennsylvanian System in New Mexico: New Mexico Bureau of Mines & Mineral Resources, Bulletin 17, 92 pp.
- Wilson, J. L. W., 1975, Carbonate facies in geologic history: Springer-Verlag, Berlin, 471 pp.

Selected conversion factors*

TO CONVERT	MULTIPLY BY	TO OBTAIN	TO CONVERT	MULTIPLY BY	TO OBTAIN
Length			Pressure, stress		
inches, in	2.540	centimeters, cm	lb in ⁻² (= lb/in ²), psi	7.03×10^{-2}	kg cm ⁻² (= kg/cm ²)
feet, ft	3.048×10^{-1}	meters, m	lb in ⁻²	6.804×10^{-2}	atmospheres, atm
yards, yds	9.144×10^{-1}	m	lb in ⁻²	6.895×10^3	newtons (N)/m ² , N m ⁻²
statute miles, mi	1.609	kilometers, km	atm	1.0333	kg cm ⁻²
fathoms	1.829	m	atm	7.6×10^2	mm of Hg (at 0° C)
angstroms, Å	1.0×10^{-8}	cm	inches of Hg (at 0° C)	3.453×10^{-2}	kg cm ⁻²
Å	1.0×10^{-4}	micrometers, μm	bars, b	1.020	kg cm ⁻²
Area			b	1.0×10^6	dynes cm ⁻²
in ²	6.452	cm ²	b	9.869×10^{-1}	atm
ft ²	9.29×10^{-2}	m ²	b	1.0×10^{-1}	megapascals, MPa
yds ²	8.361×10^{-1}	m ²	Density		
mi ²	2.590	km ²	lb in ⁻³ (= lb/in ³)	2.768×10^1	gr cm ⁻³ (= gr/cm ³)
acres	4.047×10^3	m ²	Viscosity		
acres	4.047×10^{-1}	hectares, ha	poises	1.0	gr cm ⁻¹ sec ⁻¹ or dynes cm ⁻²
Volume (wet and dry)			Discharge		
in ³	1.639×10^1	cm ³	U.S. gal min ⁻¹ , gpm	6.308×10^{-2}	l sec ⁻¹
ft ³	2.832×10^{-2}	m ³	gpm	6.308×10^{-5}	m ³ sec ⁻¹
yds ³	7.646×10^{-1}	m ³	ft ³ sec ⁻¹	2.832×10^{-2}	m ³ sec ⁻¹
fluid ounces	2.957×10^{-2}	liters, l or L	Hydraulic conductivity		
quarts	9.463×10^{-1}	l	U.S. gal day ⁻¹ ft ⁻²	4.720×10^{-7}	m sec ⁻¹
U.S. gallons, gal	3.785	l	Permeability		
U.S. gal	3.785×10^{-3}	m ³	darcies	9.870×10^{-13}	m ²
acre-ft	1.234×10^3	m ³	Transmissivity		
barrels (oil), bbl	1.589×10^{-1}	m ³	U.S. gal day ⁻¹ ft ⁻¹	1.438×10^{-7}	m ² sec ⁻¹
Weight, mass			U.S. gal min ⁻¹ ft ⁻¹	2.072×10^{-1}	l sec ⁻¹ m ⁻¹
ounces avoirdupois, avdp	2.8349×10^1	grams, gr	Magnetic field intensity		
troy ounces, oz	3.1103×10^1	gr	gausses	1.0×10^5	gammas
pounds, lb	4.536×10^{-1}	kilograms, kg	Energy, heat		
long tons	1.016	metric tons, mt	British thermal units, BTU	2.52×10^{-1}	calories, cal
short tons	9.078×10^{-1}	mt	BTU	1.0758×10^2	kilogram-meters, kgm
oz mt ⁻¹	3.43×10^1	parts per million, ppm	BTU lb ⁻¹	5.56×10^{-1}	cal kg ⁻¹
Velocity			Temperature		
ft sec ⁻¹ (= ft/sec)	3.048×10^{-1}	m sec ⁻¹ (= m/sec)	°C + 273	1.0	°K (Kelvin)
mi hr ⁻¹	1.6093	km hr ⁻¹	°C + 17.78	1.8	°F (Fahrenheit)
mi hr ⁻¹	4.470×10^{-1}	m sec ⁻¹	°F - 32	5/9	°C (Celsius)

*Divide by the factor number to reverse conversions.

Exponents: for example 4.047×10^3 (see acres) = 4,047; 9.29×10^{-2} (see ft²) = 0.0929.

Editor: Betsy Julian, Jiri Zidek

Typeface: Display heads: Spartan

Text: Times

Presswork: Miehle Single Color Offset
Harris Single Color Offset

Binding: Smyth sewn with softbound cover

Paper: Cover on 17-pt. Kivar
Text on 70-lb White Matte

Ink: Cover—PMS 320
Text—Black

Quantity: 1,000